Hydrogenation and Hydrogen Isotope Exchange: Novel, Selective Catalyst and Process Development

Richard J. Mudd

PhD Thesis

2016

Author Declaration

This thesis is the result of the author's original research. It has been composed by the author and has not been previously submitted for examination which has led to the award of a degree.

Signed: 

Date: 22-09-2016

“The only way of discovering the limits of the possible is to venture a little way into the impossible”

Arthur C. Clark

Abstract

The field of iridium(I)-mediated processes has expanded over the past 50 years, with new avenues of research constantly opening. To this end, the Kerr group has developed a series of cationic iridium(I) catalysts bearing a bulky NHC/phosphine ligand sphere that can effectively mediate mild hydrogen isotope exchange and olefin hydrogenation processes.

Having said this, with the ever-expanding scope of NHCs and the increasing ease of access to phosphines, the possibility still exists to further improve upon these complexes with lower catalyst loadings, faster reaction times, and an improved substrate scope. To this end, this thesis details some of the work achieved throughout the last 3.5 years.

Within the first chapter, progress towards more efficient olefin hydrogenation is discussed. In the first instance, highly selective hydrogenation, through the use of a directing group was targeted. Initial investigations focussed upon manipulating the counterion to the cationic iridium(I) complexes in question, and manipulating the ligand sphere through changing the nature of the phosphine and NHC. This process generated new methods for the synthesis of NHC/phosphine catalysts, and was applied to the production of a number of novel complexes. Following on from this, a highly efficient reduction process was optimised, and the selectivity therein investigated.

Following on from this, the equivalent asymmetric reaction was then studied, thus entering a new field of research within the group, and therefore, requiring the development of a completely new catalyst system. This process was guided by the non-asymmetric system, and synthesis of a number of model non-chiral complexes. After thoroughly testing the newly synthesised complexes, greater understanding was gained of the requirements for a highly enantioselective reaction, and, through this, to propose a plausible selectivity model and mechanism.

In chapter two, we discuss the development of NHC/phosphine catalysts in hydrogen isotope exchange, with a partiular focus on the selectivity of the exchange process. Following on from previous work in the group, this first targets the use of weakly

coordinating acids as a directing group, and the impact that addition of base has upon the selectivity of the reaction.

Furthermore, understanding that drug design is moving away from planar molecules, towards non-planar, sp^3-rich compounds, we also investigated the possibility of exchange at positions in a molecule other than an sp^2 aryl ring. This was initially observed when developing the hydrogenation methods discussed in chapter one, enabling selective sp^2 exchange in conjugated olefins. This new, highly selective method of labelling was examined through a combined experimental and computational investigation, leading to a thorough understanding of the mechanism and factors governing reaction selectivity. Having progressed from sp^2-aryl to sp^2-non-aryl exchange, the logical progression was to next investigate sp^3 exchange. Through a detailed study three protocols were developed, enabling exchange on a wide range of sp^3 hybridised sites, in pharmaceutically relevant systems. These new processes were investigated mechanistically and computationally to ascertain the mechanism and selectivity of exchange.

Acknowledgements

Primarily I would like to express my deepest gratitude to my supervisor and friend Prof. W. J. Kerr, for accepting me into his group, supporting and guiding my research, and granting me the opportunity to present at a myriad of different locations. I now know that it is not acceptable to wear trainers with a suit.

Secondly, the support from Dr Laura Paterson and Dr Dave Lindsay has been invaluable throughout my PhD. Although I might not have always followed it, your advice has helped to make me the researcher that I am today. I especially thank you both for the excellent work that you have done in proof reading draft papers, reports and this thesis, I know it can't have been easy.

I also acknowledge my friends in the Kerr PhD research group for the chemical and moral support. Firstly, Calum, Monks and Malky, meeting you all helped to build my character, and I am now well prepared to deal with abuse in the work place. Secondly Racheal and Goldie, with your expressive RBF and the occasional tantrum you ensured that there was never a quiet moment in the first two years of my PhD. To the Chocolate Avenger, at times you were both brilliant and annoying, but if I ever have to hear the phrase "just a simple question" again I might have a breakdown. To Marc the greatest dance-master I have ever had the pleasure of meeting, you always set the bar high and forced me to better myself, culminating in the invention of the wacky-waving-inflatable-arm-flailing-tubeman dance, for which I will always be grateful. To my PhD compatriot, pub partner and chemical sounding board Andy "volume turned up to 11" Malcolm, you have been an invaluable part of my PhD. I will never forget the Friday afternoon pub texts and I will forever have echoes of "Doug" ringing in my ears. To PKO, you were a constant source of frustration, but your joining the group meant we were never short of laughter, be it at you, or your quite simply ridiculous tales of misadventure. To John, there is never a quiet moment with you around, both your enthusiasm for chemistry and alcohol are intoxicating. To Renan and Peter, your calming influence in the lab and Hungarian stoicism, has helped me to keep what little hair remains on my head. To the diabetic twins Liam and Gary, you are a endless source of entertainment, concern and confusion, keep eating.

Throughout my time in the group these has always been undergraduate students in the laboratory, that contribute to the groups work, atmosphere and dance moves, it wouldn't of been the same without you; Tim, Amelia, Jenny, Jen, Kirsty, Olivia, Gayle, Declan, Graham, Calum, Fiona, Rory, Josh, Reka, Paul, Adele, Giorgia and Craig.

I have been lucky enough to make a great number of friends during my time at Strathclyde who have been willing to sit and listen to me, without telling me to "shut my whore mouth." In particular, those from the Watson, Jamieson and Percy research groups.

Last but not least. I am grateful for the moral and occasional monetary support provided by my parents and family, I truly could not have done it without you.

List of Publications

Stated below are the works from (or associated with) this thesis that have been accepted for publication in the literature. A number of additional publications are planned for 2016-17. Authorship is recorded alphabetically or by institution rather than by individual author contribution.

W. J. Kerr, R. J. Mudd, L. C. Paterson, J. A. Brown, *Chem Eur J.* **2014**, *20*, 14604.

W. J. Kerr, R. J. Mudd, J. A. Brown, *Chem Eur. J.* **2016**, *22*, 4738.

W. J. Kerr, R. J. Mudd, P. K. Owens, M. Reid, J. A. Brown, S. Campos, *J. Labelled Compd. Radiopharm.* **2016**, (*Accepted DOI: 10.1002/jlcr.3427*).

Contents

Abbreviations

σ	Hammett sigma parameter
µL	Microlitres
^{o}C	Degrees celsius
%BV	Percent buried volume
ADMET	Adsorption, Distribution, Metabolism, Excretion and Toxicology
BArF	Tetrakis[3,5-bis(trifluoromethyl)phenyl]borate
Bn	Benzyl
COD	Cyclooctadiene
CPME	Cyclopentyl methyl ether
Cy	Cyclohexyl
DCM	Dichloromethane
DCE	Dichloroethane
DEC	Diethyl carbonate
DMC	Dimethyl carbonate
DMF	*N*,*N*-Dimethylformamide
DMFL	Dimethylformal
DMSO	Dimethylsulfoxide
DoE	Design of experiments
EDG	Electron donating group
Et	Ethyl
EWG	Electron withdrawing group
g	Grammes
h	Hours
HIE	Hydrogen isotope exchange
Hz	Hertz

IBn	1,3-Di(benzyl)imidazol-2-ylidene
ICy	1,3-Di(cyclohexyl)imidazol-2-ylidene
IDiPP	1,3-Di(bis-2,6-di-iso-ropylphenyl)imidazol-2-ylidene
IEt	1,3-Di(ethyl)imidazol-2-ylidene
IiPr	1,3-Di(isopropyl)imidazol-2-ylidene
IMe	1,3-Di(methyl)imidazol-2-ylidene
IMes	1,3-Di(2,4,6-trimethylphenyl)imidazol-2-ylidene
i-Pr	Iso-propyl
J	Coupling constant
KIE	Kinetic isotope effect
Me	Methyl
Mes	Mesityl
mg	Milligrammes
MHz	Megahertz
min	Minutes
mL	Millilitres
mmi	Membered metallocylic intermediate
mmol	Millimoles
mol	Moles
MTBE	Methyl *tert*-butyl ether
n-Bu	*n*-Butyl
NBD	Norbornadiene
NHC	*N*-Heterocyclic carbene
NMR	Nuclear magnetic resonance
	s - singlet
	d - doublet

t - triplet

q – quartet

quin – apparent quintet

sex – apparent sextet

sep – apparent septet

oct – apparent octet

m - multiplet

br - broad

OTf ..... Triflate

Ph ..... Phenyl

PhIBn ..... 1,3-Di(benzyl)benzimidazol-2-ylidene

py ..... Pyridine

r.t. ..... Room temperature

R&D ..... Research and development

RDS ..... Rate determining step

Sol ..... Solvent

SIMes ..... 1,3-Bis(2,4,6-trimethylphenyl)imidazolidine-2-ylidene

t-Bu ..... *tert*-Butyl

TCA Tolman cone angle

Temp ..... Temperature

TEP ..... Tolman electronic parameter

tert ..... Tertiary

TFT ..... Trifluorotoluene

THF ..... Tetrahydrofuran

Chapter 1. Chemo- and Enantioselective Olefin Hydrogenation

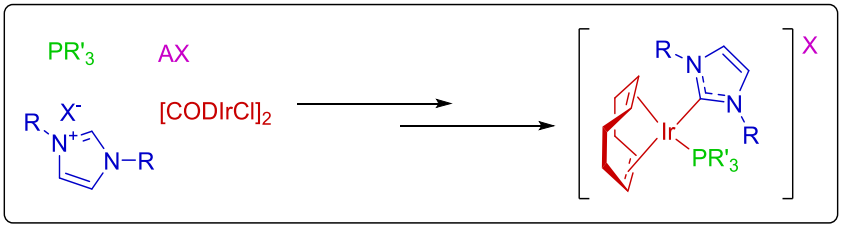

1. Introduction

The process to reduce a carbon-carbon double bond is one of the most important tools in the repertoire of the organic chemist; as such it remains an intense area of research. Within this area, transition metal catalysis is one of the most commonly used methods for either process or synthetic chemists. This has led to a wide variety of catalysts being developed, with work still ongoing to further improve their efficiency.[1]

1.1. Heterogeneous Hydrogenation

Traditional approaches to hydrogenation reaction usually apply heterogeneous catalysts.[2] Such methods utilise transition metals (commonly Rh, Pt or Pd) adsorbed onto a solid support (including carbon, silica and alumina). The mechanism of hydrogenation on a metal surface, as is used in heterogeneous catalysis, can vary with the catalyst and has yet to be fully elucidated. Having said this, one of the first and simplest mechanisms was proposed by Horuiti and Polanyi (**Scheme 1.1**).[3] Initially, a hydrogen molecule binds to the metal surface (**I**), breaking the H-H bond (**II**). Next, the substrate binds through the π-bond of the olefin, thus weakening the C=C bond (**III**). Finally, in a stepwise, fashion a molecule of hydrogen is added across the C=C bond (**IV-VI**), forming a metal alkyl intermediate (**V**), before generating the hydrogenated substrate in the final non-reversible step (**VII**).

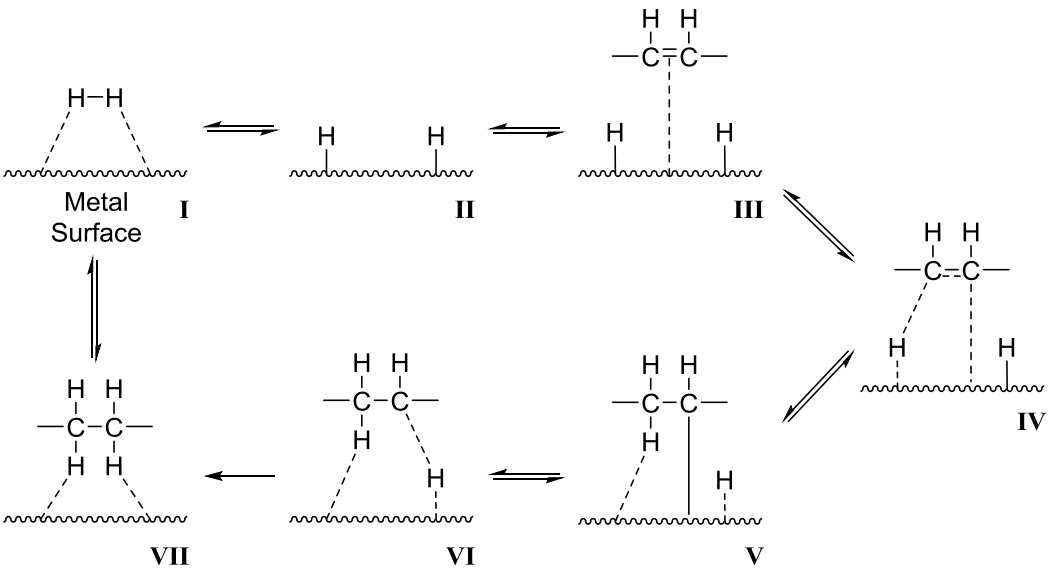

Scheme 1.1 General mechanism for homogeneous catalytic hydrogenation.

Such methods perform excellently in the hydrogenation of a wide variety of organic compounds; however, they often require elevated temperatures or pressures, and can suffer from poor selectivity. Therefore, the focus for much of the research in recent years has surrounded the production of catalysts that can facilitate mild and selective hydrogenation. In this regard, the most promising developments have arisen from the area of homogeneous transition metal catalysis, for which several advantages exist over heterogeneous catalysis. These include greater catalyst surface area, more efficient heat transfer, and most importantly the ability to tune the catalyst to a specific purpose, therefore, allowing chemo-, regio-, and enantioselective catalysts.

1.2. Homogeneous Hydrogenation

Homogeneous hydrogenation constitutes a large area of chemistry; the developments in coordination and organometallic chemistry have allowed the preparation of a growing variety of soluble metal complexes.[4] Among this plethora of complexes there are many that show activity in the complexation and activation of olefin π-bonds. These complexes can be further divided by the mode of hydrogenation. The first class, monohydride hydrogenation catalysts, proceed by formation of a metal hydride species which, by reaction with the substrate, forms a metal alkyl intermediate (**Scheme 1.2**).[5] This intermediate subsequently reacts with another molecule of hydrogen to regenerate the metal hydride and release the hydrogenated product.

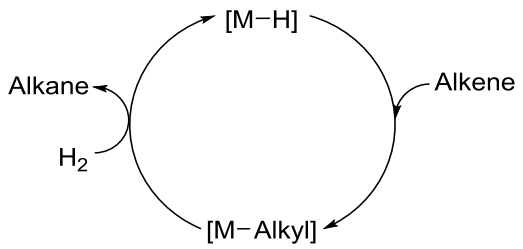

Scheme 1.2 General mechanism for monohydride reduction.

The second class, dihydride hydrogenation catalysts, do not exist as monohydride species. Instead, through reaction with hydrogen and the substrate they form a dihydride, alkene-bound metal species (**Scheme 1.3**). Migratory insertion, followed by reductive elimination of the metal alkyl species, yields the saturated alkane product.

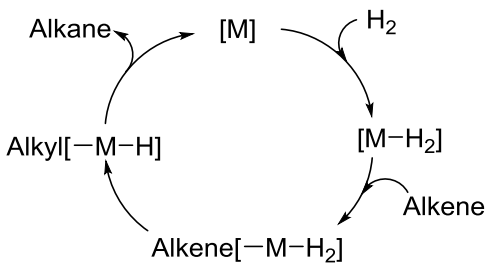

Scheme 1.3 General mechanism for dihydride reduction.

The first breakthrough in the area of homogeneous catalysis came in 1938 when Calvin and Polanyi reported the hydrogenation of unsaturated species such as *p*-benzoquinone, using quinoline solutions of copper acetate at 100 °C.[6,7] However, the potential of the area was not fully realised until more than 20 years later, when several rhodium and iridium complexes were shown to have incredible catalytic activity towards homogeneous hydrogenation processes.

1.2.1. Rhodium

In 1963, Bath and Vaska isolated a rhodium(I) hydridocarbonyl complex, [RhHCO(PPh_3)$_3$] **1** (**Scheme 1.4**).[8] A few years later,Wilkinson and co-workers proved this complex to be an efficient hydrogenation catalyst, albeit with some interesting limitations.[9] The complex could facilitate the reduction of terminal olefins such as 1-hexene **2** to hexane **3**, however it could not reduce internal olefins such as cyclohexene **4** and *cis*-4-methylpent-2-ene **5**.

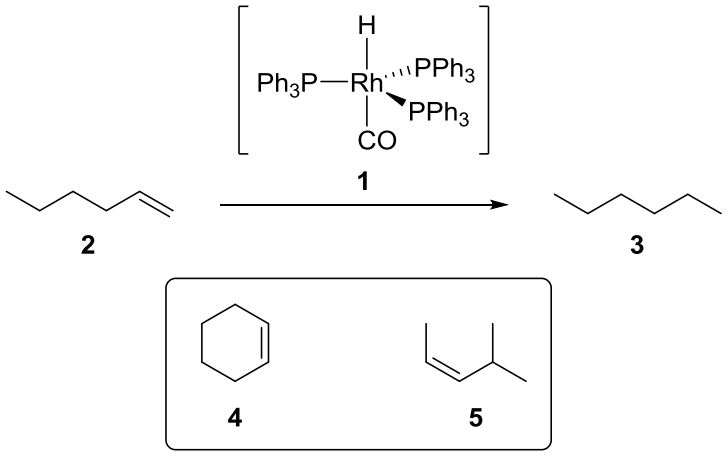

Scheme 1.4 Reduction of internal alkenes with complex **1.**

Wilkinson proposed that this selectivity must be related to the mechanism of hydrogenation for complex **1**. It was therefore proposed that the complex was in itself a precatalyst, and the dissociation of a triphenylphosphine ligand was required to form the active catalyst **6** (**Scheme 1.5**). This hydride complex could then proceed by a monohydride reduction mechanism as previously discussed (**Scheme 1.2**). The key step of this mechanism is the initial formation of the metal alkyl species. In the case of internal olefins, the metal alkyl species would incur a large steric penalty, and is therefore strongly disfavoured.

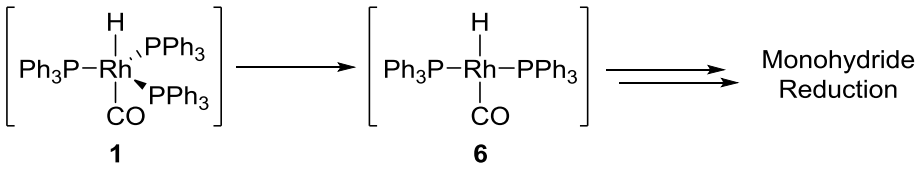

Scheme 1.5 Rh-phosphine complex activation.

One of the most important discoveries in the area of rhodium chemistry is the work performed by Wilkinson in 1965, producing the catalyst that bears his name, $[RhCl(PPh_3)_3]$ **7**.[10] This compound, easily prepared through the reaction of $RhCl_3$-$.3H_2O$ with triphenylphosphine in refluxing ethanol, was at the time of its discovery, the most active homogeneous hydrogenation catalyst and is still widely used to this day (**Scheme 1.6**).

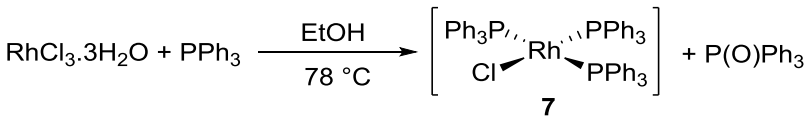

Scheme 1.6 Synthesis of Wilkinson's catalyst **7**.

The main advantage of Wilkinson's complex at the time of its development was its ability to selectively hydrogenate olefins in the presence of other reducible groups such as nitro and aldehyde, and to reduce terminal alkenes in the presence of internal olefins.[11,12,13,14] The coordination of the reducible group to the metal was shown to be important in selectivity of reduction, with terminal olefins reducing at the fastest rate, tri-substituted olefins the slowest and tetra-substituted olefins not reducing at all (**Figure 1.1**).[14]

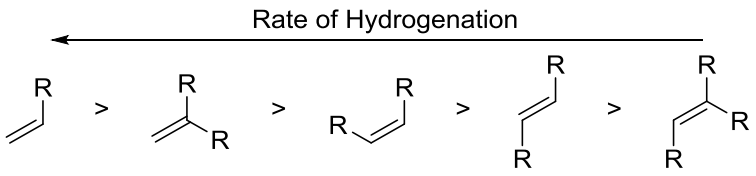

Figure 1.1 General order of alkene reactivity in hydrogenation.

Following the isolation of complex **7**, the mechanism by which hydrogenation proceeded was extensively researched. In particular, Halpern produced key mechanistic insights that finally lead to the elucidation of the mechanism.[15] It was found that the active catalyst was formed by dissociation of a phosphine unit, following which addition of hydrogen produced dihydride species **8**. Substrate coordination delivered alkene complex **9**, which was followed by migratory insertion, giving metal alkyl species **10**, which could undergo reductive elimination to release the reduced product (**Scheme 1.7**). Indeed, this pathway follows the dihydride mechanism previously discussed.

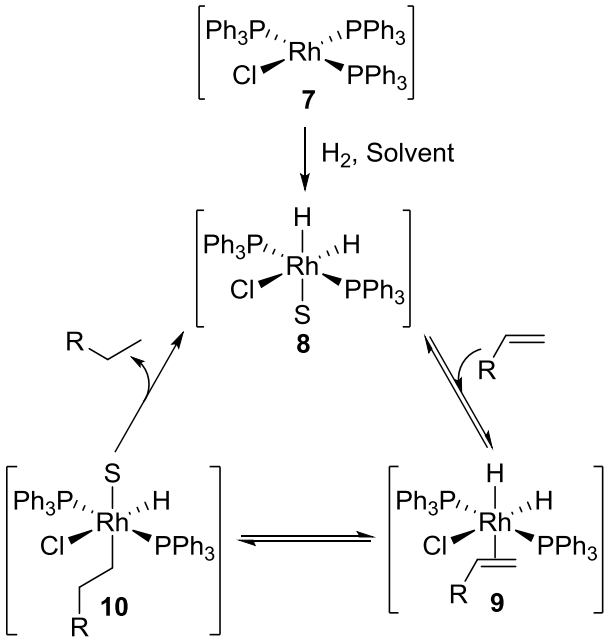

Scheme 1.7 Mechanism of hydrogenation with Wilkinson's catalyst **7**.

Further exploration in this field by Osborn and Schrock uncovered the previously unexplored area of cationic rhodium diene catalysts, such as **11** (**Scheme 1.8**).[16,17] The ligands employed in the earliest cases were a phosphine and a diene, either norbornadiene (NBD) **12** or cyclooctadiene (COD) **13**. Such catalysts, when

introduced to a hydrogen atmosphere, reduced the diene to leave a cationic rhodium(I) complex such as **14**, which was found to be active in the hydrogenation of both terminal and internal olefins.

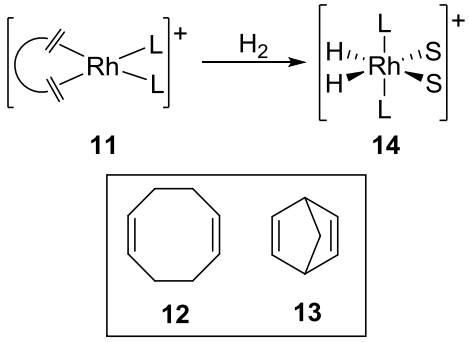

Scheme 1.8 General structure and activation of Rh-diene complexes.

1.2.2. Iridium

Although a large variety of iridium complexes are known today, their development began somewhat later than the rhodium complexes. The reasons for this late development can be explained by the comparison of Wilkinson's catalyst, **7**, with its iridium counterpart **15** (**Figure 1.2**). The former as previously discussed, is an excellent catalyst for hydrogenation processes, however the corresponding iridium complex **15** showed very little catalytic activity.[5]

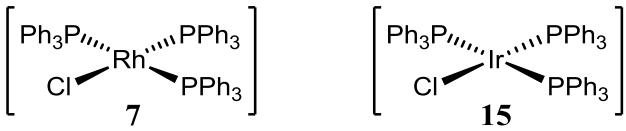

Figure 1.2 Wilkinson's catalyst **7** and the iridium analogue **15**.

This can be explained by considering the first step of the mechanism for hydrogenation with complex **7** (**Scheme 1.7**), the initial dissociation of a phosphine ligand. In the case of iridium, because it often forms stronger metal-ligand bonds than rhodium ([Cp(CO)Rh-CO], 46 kcalmol^{-1} and [Cp(CO)Ir-CO], 57 kcalmol^{-1}), this dissociation does not take place. The increased metal-ligand bond strength is also observed in the choice of solvent used with each metal. Rhodium, with its weaker metal-ligand bonds, will form reactive intermediates in polar, coordinating solvents (e.g. EtOH, acetone). However, under these conditions, iridium forms stable species that can often be

isolated, an advantage in some cases when attempting to isolate reaction intermediates and elucidate reaction mechanisms.[17]

This meant that the seminal research carried out by Vaska in 1965 with [IrCl(CO)(PPh_3)$_2$], **16**, went largely unremarked at the time due to the poor catalytic activity it showed (**Scheme 1.9**).[18] Having said this, his studies are a landmark in organometallic chemistry that provided excellent information about the oxidative addition process, now known to be a key step in many catalytic reactions. Vaska showed that in the presence of hydrogen, complex **16** would undergo a reversible reaction forming stable dihydride species, **17**, through the now generally accepted process of oxidative addition.

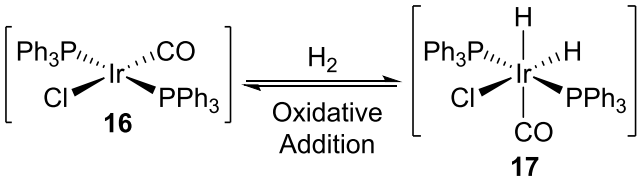

Scheme 1.9 Oxidative addition of molecular hydrogen with Vaska's complex.

In studies based upon those already performed with rhodium, Osborn and co-workers synthesised cationic iridium diene catalysts bearing two phosphine ligands, such as **18** (**Figure 1.3**).[16,19,20] However the hydrogenation process with catalysts of this type was only examined in polar solvents (MeOH or acetone) with disappointing results. Despite this, some activity was observed towards small terminal and internal alkenes, but no activity was observed with larger, more substituted substrates. Indeed, despite the isolation of hydride complex **19** in the same report, in which a solvent molecule must dissociate to allow substrate complexation, it was not until much later that the use of a non-coordinating solvent was considered.

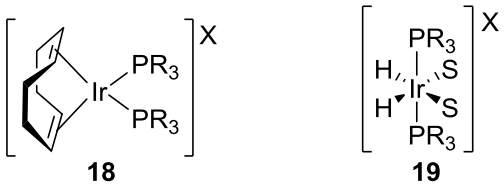

Figure 1.3 General structure and activation of Ir-diene complexes.

The most significant development in this area of chemistry was made in 1977, when Crabtree *et al.* employed the non-coordinating, halogenated solvent, DCM, with complexes such as **18**.[21,22] This solvent had long been ignored by organometallic chemists, as it was recognised that for the common Rh(I) systems, oxidative addition of the C-Cl bond was a possibility. However, due to the common resting state of Ir(III) for many of the iridium complexes, this side process was deemed unlikely. Through the application of DCM as the reaction medium, a more labile intermediate, **19**, was envisaged, in which the solvent is now the weakly bound DCM (**Figure 1.3**). Complexes of type **18** also showed improved activity towards more highly substituted olefins than had been previously observed with Wilkinson's catalyst **7**.[14] Furthermore, the use of only one phosphine ligand and a smaller pyridine ligand in complex **20**, allowed facile complexation of the substrate, shown by the improved activity over the previous bis-phosphine system, such as complex **21** (**Figure 1.4**, **Table 1.1**).[21,23]

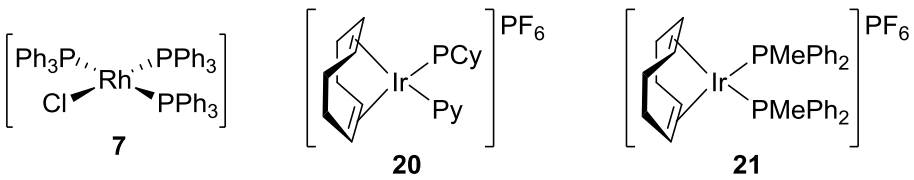

Figure 1.4

Entry	Substrate	Complex	Maximum rate ($mol_{sub}mol^{-1}_{cat}h^{1}$)
1	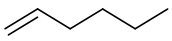 **22**	**21**	5100
2		**20**	6400
3		**7**	60
4	 **4**	**21**	3800
5		**20**	4500
6		**7**	70
7	 **23**	**21**	50
8		**20**	4000
9		**7**	0

Table 1.1 Comparative rate data for common Rh and Ir complexes in alkene hydrogenation

From this series of catalysts, **20** was identified as the most optimal, being able to facilitate all but the most hindered of substrates, **23**, at just 0.1 mol%. In further

examination of the utility of the catalyst, Crabtree *et al.* then utilised a variety of more functionalised organic compounds to good effect, despite requiring higher catalyst loading.[24] From this study, it was noticed that a coordinating group, such as a carbonyl or alcohol, could influence the hydrogenation reaction, without themselves being reduced or oxidised. To further examine this observation, Crabtree *et al.* began by studying the hydrogenation of terpinen-4-ol, **24**, with a heterogeneous palladium catalyst and with his own homogeneous catalyst, **20** (**Scheme 1.10**, **Table 1.2**).

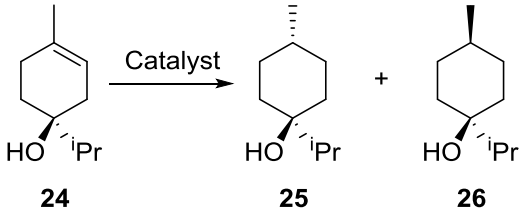

Scheme 1.10.

Entry	Catalyst	25 (%)	26 (%)
1	Pd/C	20	80
2	**20**	99.9	0.1

Table 1.2 Diastereoselective reduction of terpinen-4-ol **24**, with crabtree's catalyst **20** and heterogeneous Pd/C.

From these results it became clear that catalyst **20** coordinated to the alcohol moiety and directed the delivery of H_2 from the face bearing the alcohol functionality.[25] In efforts to confirm this idea of coordination, attempts were made to isolate the cyclometallated product of substrate **24** with catalyst **20**. Unfortunately, the labile nature of the intermediates with catalyst **20** prevented this. However, reaction of *endo*-5-norbornen-2-ol, **28**, with the less active catalyst, **27**, allowed the detection of cyclometallated species **29**, thus providing convincing evidence for the directed hydrogenation mechanism (**Scheme 1.11**).

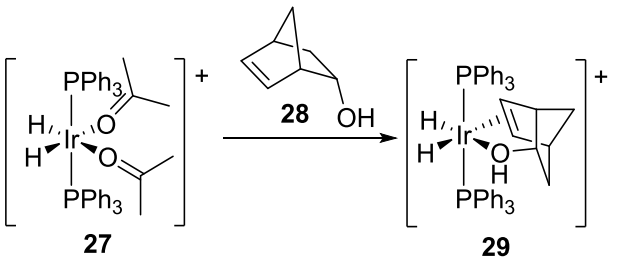

Scheme 1.11 Isolated alcohol-alkene chelate for directed hydrogenation.

At the same time, Stork and Kahne produced similar results, applying Crabtree's catalyst **20** on a much greater range of substrates to good effect.[26] It was shown that although terminal olefins **30** failed to give any selectivity, when changing to tri-substituted olefins **31**, **32** and **33**, with selectivity improved in moving from primary to tertiary alcohols (**Scheme 1.12**, **Table 1.3**). It is also worthy of note that, when protected as the acetate, none of the previous selectivity with the alcohols was observed.

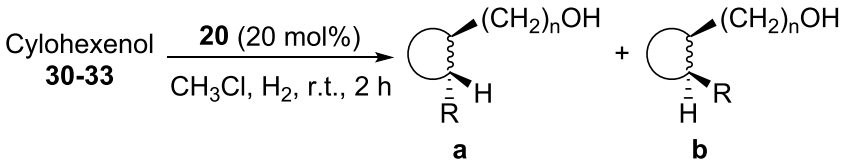

Scheme 1.12

Entry	Substrate	a/b	Yield
1	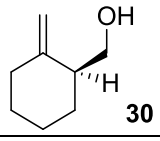 **30**	1/1	86
2	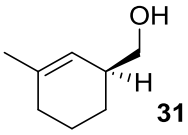 **31**	6/1	78
3	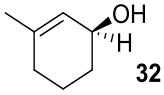 **32**	74/1	48
4	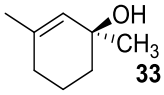 **33**	99/1	64

Table 1.3 Diastereoselective reduction of cyclohexenols with Crabtree's catalyst **20**.

Crabtree's catalyst **20** has proven to be an incredibly active catalyst, and over the last 40 years, is still the most commonly applied homogeneous hydrogenation catalyst in organic synthesis. However, there are several areas in which improvements could be made. The primary area initially targeted was the thermal stability of the complex, with its known propensity to form inactive hydride, bridged-iridium clusters such as **34** (**Figure 1.5**).[21,23,27]

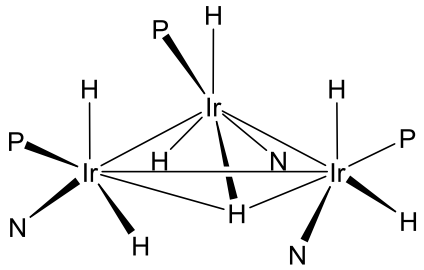

Figure 1.5 Proposed, inactive hydride bridged iridium trimer.

This has led to a large number of complexes being designed around the same structural motif, with modifications attempting to combat the low thermal stability. Notably, in 2001, Nolan *et al.* reported the synthesis of an analogue in which the phosphine was replaced by a bulky NHC ligand, envisaged to sterically disfavour the formation of any iridium clusters (**Scheme 1.13**).[28] Utilising a similar synthetic process as Crabtree, Nolan generated a bispyridine iridium(I) cationic species **36**, from the commercially available iridium cyclooctadiene chloride dimer **35**. Following reaction with the previously generated free carbene **37** (SIMes), pyridinyl/NHC complex **38** was delivered.

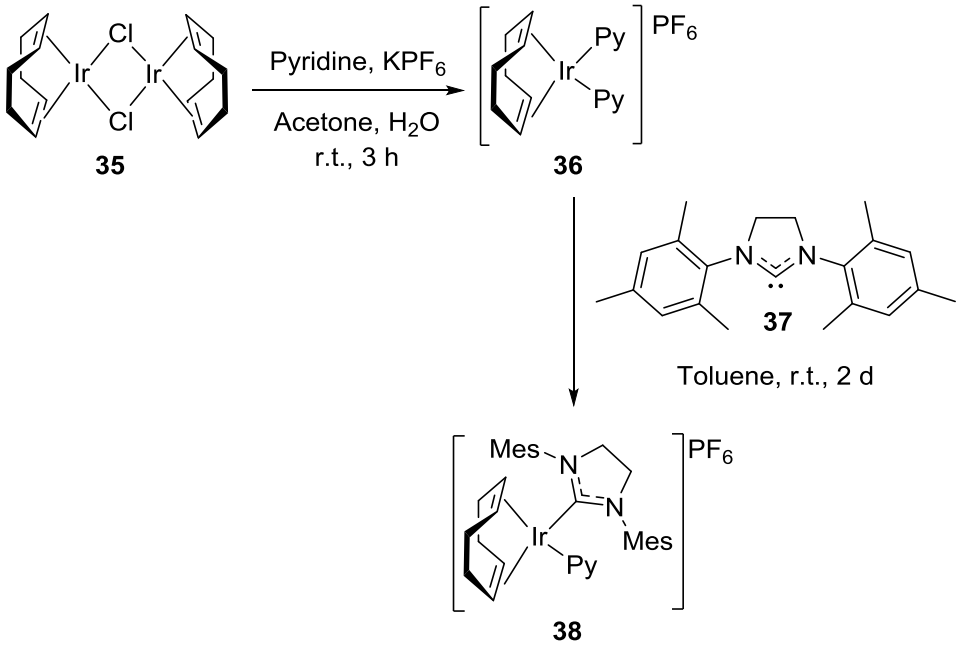

Scheme 1.13 Synthesis of NHC/pyridine iridium complex **38**.

Although the substrate scope explored by Nolan *et al*. is somewhat limited, it does highlight the apparent improved thermal stability of the new complex **38**, over Crabtree's complex **20** (**Table 1.4**). Indeed, at room temperature and with an unhindered olefin, cyclohexene **4**, both complexes reach completion. However, with a more substituted olefin, 1-methylcyclohexene **39**, at room temperature neither complex reacts effectively. Notably, with more forcing conditions complex **20** delivers a lower yield, indicating degradation of the active catalyst, while complex **39** delivers a quantitative yield.

Entry	Complex	Substrate	Time (h)	H_2 Pressure (psi)	Temperature (°C)	Yield (%)
1	**20**	 **4**	0.5	15	r.t.	100
2	**38**		2		r.t.	100
3	**20**	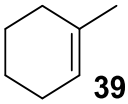 **39**	2		r.t.	65
4	**38**		3.5		r.t.	42
5	**20**		7	60	50	34
6	**38**		7		50	100

Table 1.4 Comparative alkene reduction with Crabtree's catalyst **20** and NHC/pyridine complex **38**.

At a similar time, Buriak *et al.* also developed a series of complexes based upon Crabtree's catalyst, **20**, except this time exchanging the pyridine ligand for an NHC.[29] The synthesis of each of these complexes followed the same general process; of synthesising an iridium halide/carbene intermediate from the starting dimer, followed by abstraction of the halide through use of the appropriate salt and replacement with the desired phosphine. Using this method, a series of catalysts bearing different NHC/phosphine combinations were synthesised (**Figure 1.6**).

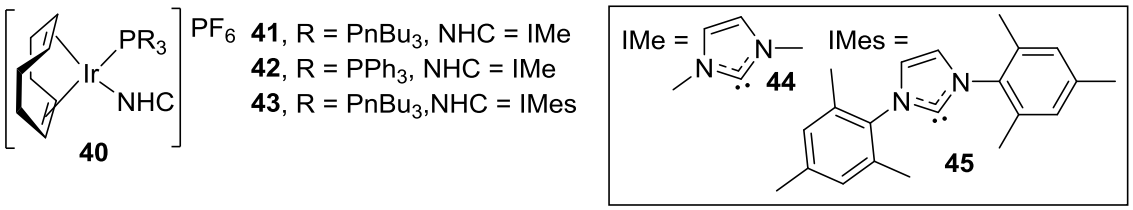

Figure 1.6 Synthesised NHC/phosphine iridium complexes.

Furthermore, each catalyst showed excellent activity for the hydrogenation of small, terminal, **22**, and di-substituted substrates, **4**, (**Table 1.5**). Moreover, the complex bearing the smallest NHC/phosphine combination, **41**, showed activity exceeding that of Crabtree's complex **20**, with even the tetra-substituted olefin **23**.

Entry	Substrate	Complex	Time (min)	Yield (%)
1	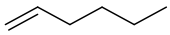 **22**	**20**	9	100
2		**41**	13	100
3	 **4**	**20**	9	100
4		**41**	15	100
5	 **23**	**20**	40	95
6		**41**	39	>99

Table 1.5 Comparative alkene reduction with Crabtree's catalyst **20** and NHC/phosphine complex **41**.

With an understanding of the ligand requirements for an optimal hydrogenation catalyst, Buriak *et al.* examined the outer sphere anionic partner to the catalyst, utilising investigations disclosed by Pfaltz *et al*. in 1998. These studies, supported the notion that larger, less coordinating counterions have a positive effect upon the rate of hydrogenation.[71] Using this as a basis, Buriak *et al.* looked to exchange the counterion,

from hexaflouro phosphate, **44**, to the much larger, less coordinating, BArF counterion, **45** (**Figure 1.7**).[72]

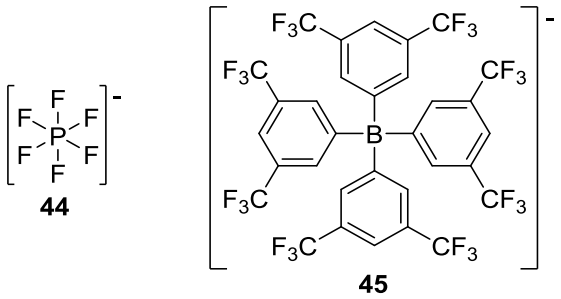

Figure 1.7 Common counterions for cationic iridium catalysts.

It was theorised that the larger anionic partner would hinder the approach of any two cationic complexes, and thereby reducing the formation of inactive clusters. Through in depth NMR spectroscopic studies, Pregosin *et al.* successfully proved that when the ionic partner is BArF, the two ions move through the solution in tandem.[30] In contrast, when PF_6 is employed, stronger solvation occurs, leaving both partners independent of the other. This gave credence to the theory that the BArF counterion could stabilise the active catalyst. Successful synthesis of BArF analogues, **46** and **47** respectively (**Figure 1.8**), allowed a comparison to the parent catalysts **41** and **20** to be drawn.

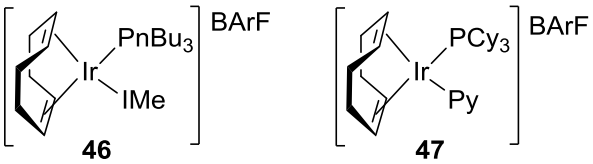

Figure 1.8 Synthesised complexes bearing the BArF counterion.

Pleasingly, both novel catalysts performed better overall than the parent catalysts **41** and **20**, with improved rates observed in the BArF analogue with both di-substituted olefin, **4**, and tetra-substituted olefin, **23** (**Table 1.6**).

Entry	Substrate	Complex	Rate (mol^{sub}/mol^{cat}/h)	Yield (%)
1	 **4**	**20**	925	100
2		**47**	1522	100
3		**41**	505	100
4		**46**	765	100
5	 **23**	**20**	208	95
6		**47**	384	>99
7		**41**	165	>99
8		**46**	217	100

Table 1.6 Comparative alkene reduction with PF_6 and BArF complexes..

As the technology for olefin hydrogenation has improved, the complexity of the substrates undergoing reduction has increased. In particularly, increasing substitution of the olefin has led to prochiral substrates being reduced. In the next section the developments in catalysis for asymmetric hydrogenation will be discussed.

1.3. Asymmetric Hydrogenation

Prior to 1968, enantioselective hydrogenation was carried out by utilising chiral auxiliaries[31] or through a heterogeneous catalyst absorbed on a chiral support.[32] However, despite the large number of catalysts and supports utilised, results varied greatly depending on the catalyst batch and the applied substrate, but generally, low to moderate selectivity was often obtained, limiting the methods application. However, the development of homogeneous asymmetric transition metal catalysts opened the door to highly selective processes.[5] Indeed, for their contribution to the area of asymmetric hydrogenation Knowles[33] and Noyori[34] shared the Nobel Prize with Sharpless[35] in 2001. Following suit from the systems previously discussed, initial asymmetric work was carried out with phosphine ligands complexed to rhodium.

1.3.1. Rhodium

The development of chiral, monodentate phosphines provided a direct approach to the preparation of asymmetric catalysts.[36] Indeed, an example of such a catalyst was reported by Knowles in 1972 for the reduction of protected *β*-dehydroamino acids, such as **48**, as a means of producing unnatural amino acids (**Scheme 1.14**). The catalyst in question was typically generated *in situ*, using a 2:1 ratio of cyclohexyl anisyl methyl phosphine (CAMP) **47** to metal and pre-hydrogenated. However, it was also shown that a pre-prepared crystalline, bisphosphine, cationic compound delivered the same results, therefore indicating a similar catalyst species as Wilkinson had previously described.[13]

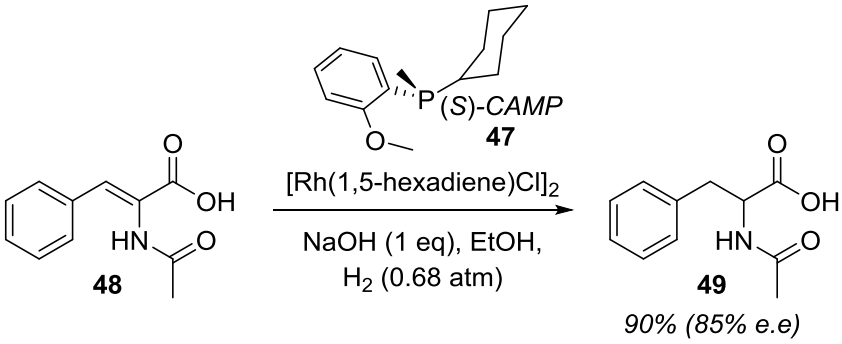

Scheme 1.14 Application of (*S*)-CAMP in alkene hydrogenation.

Despite the effectiveness of the monodentate phosphine systems, issues with the stability of the phosphines and the difficulty to prepare them in high e.e. limited their use. To combat this, C_2-symmetric, bidentate ligands were developed. Notably, the first application by Kagan, utilising the tartaric acid-derived DIOP ligand **50**, proved the effectiveness of this approach, delivering similar yields and e.e. to the monodentate systems in the reduction of **48**, but with slower reaction rates (**Figure 1.9**).[37]

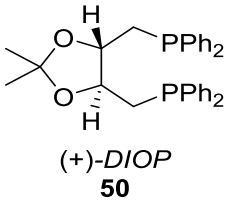

Figure 1.9 Tartaric acid-derived (+)-DIOP ligand.

However, perhaps the most notable contribution was again from Knowles, in the application of diphoshine DiPAMP **51** for the production of L-DOPA **54**, used in the treatment of Parkinson's disease (**Scheme 1.15**).[38,39,40] This synthesis went on to become the basis for the first industrial scale hydrogenation, and despite various attempts to improve upon the DiPAMP system, it still remains as one of the best catalysts within its class.

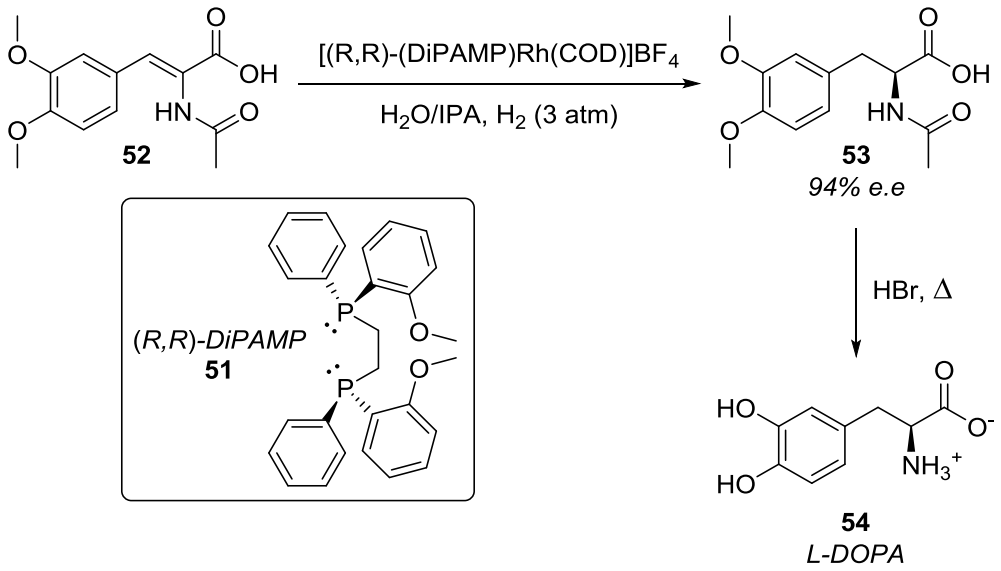

Scheme 1.15 Application of (*R*,*R*)-DiPAMP in the synthesis of *L*-DOPA.

A key issue with ligands that are chiral at phosphorus is the often long synthetic sequence required for their production. Therefore, a wide number of phosphine ligands have been investigated that bear chirality adjacent to the phosphine,[41] as described by Kagan with the DIOP system. However, a contribution that significantly elevated this class of ligand came from Burk, with the introduction of DuPhos **55** in the phospholane ligand class (**Scheme 1.16**).[42] Notably, this ligand was easily synthesised in just 2 steps from enantiopure, homochiral 1,4-diols. The catalyst was tested with similar substrates as had been previously utilised with competing systems, and performed admirably even at just 0.1 mol% loading, proving the reactivity and selectivity of the new ligand class.

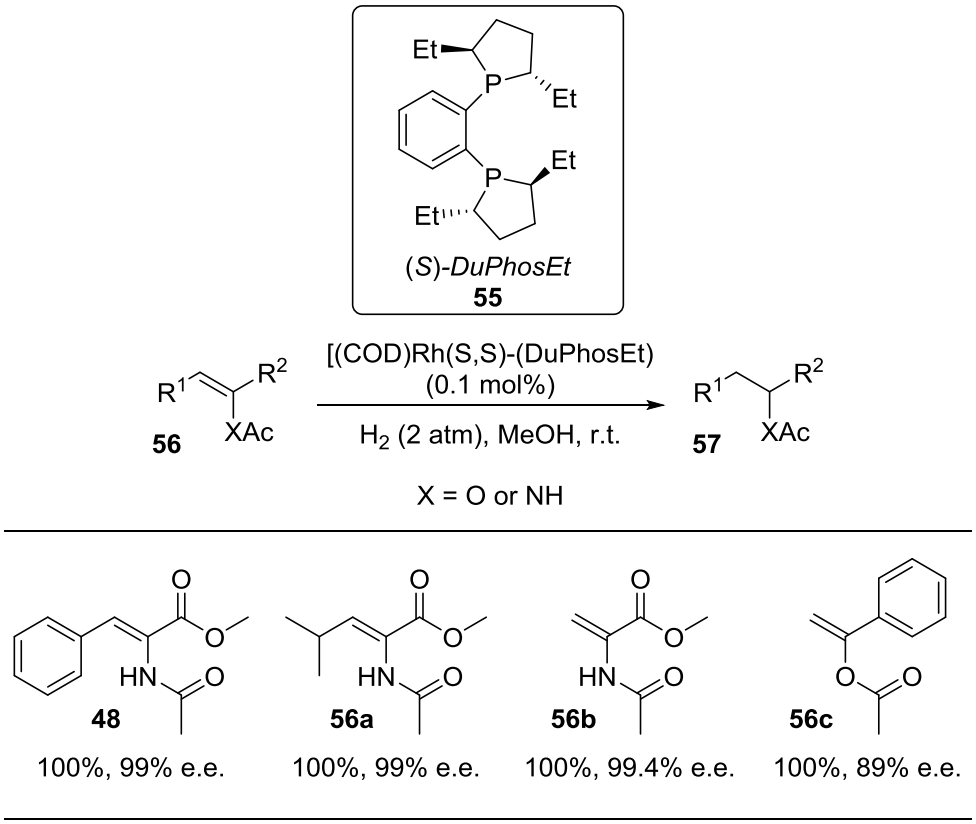

Scheme 1.16 Application of (*S*)-DuPhosEt ligand in alkene hydrogenation.

Moving further from DiPAMP, unsymmetrical diphosphine ligands have been developed. In particular, the use of ferrocene as a means of imparting chirality has been of interest since its discovery. Perhaps most importantly for hydrogenation chemistry was Togni's introduction of Josiphos **55**, capable of highly selective and expedient reduction of a range of olefins (**Scheme 1.17**).[43]

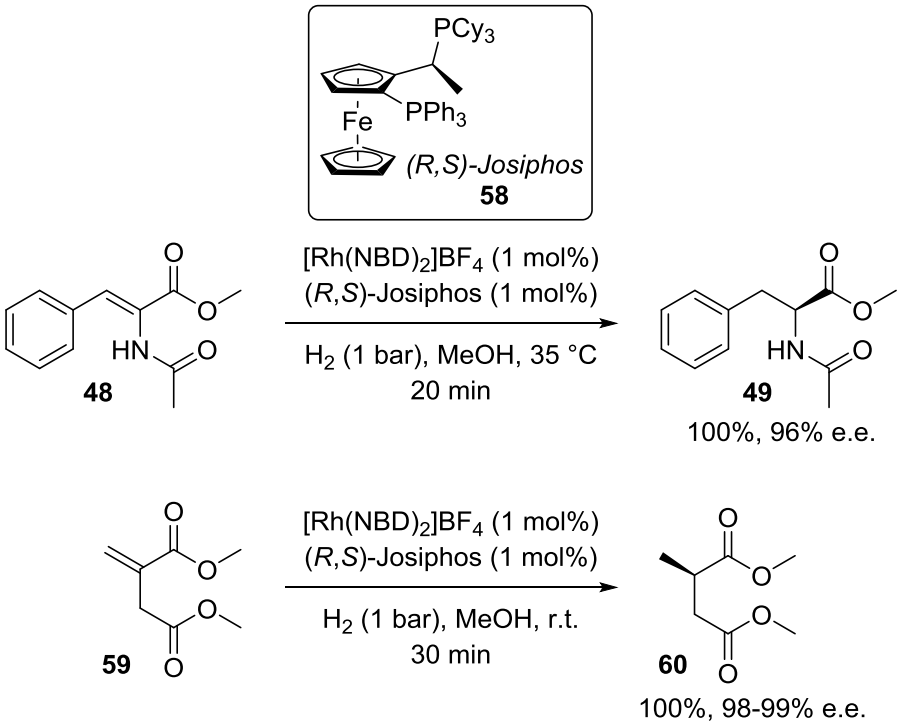

Scheme 1.17 Application of (*R,S*)-Josiphos ligand in alkene hydrogenation.

Although, the catalysts discussed above are only a fraction of those reported within the literature, they represent the degree of diversity now available. It is important to note that the substrates that are typically utilised with rhodium catalysts are functionalised with a coordinating group. Secondly, many of the complexes that facilitate olefin reduction are the same systems that reduce carbonyl groups, for example, the work that earned Noyori part of the Nobel prize,[34] and Togni's applications of Josiphos.[43] For this reason attention more recently has turned to iridium-based catalysts, to permit more selective reduction of non-functionalised olefins.

1.3.2. Iridium

As would be expected based on the non-chiral iridium hydrogenation catalysts, most of the recent developments in asymmetric iridium hydrogenation catalysts have centred around Crabtree-type systems.[44,45,46,47] Arguably, the most important breakthrough in this area came from Pfaltz *et al* with the application of chiral oxazoline-phosphine chelating complexes, such as **61**, commonly recognized under the abbreviation PHOX (**Scheme 1.18**).[48] This complex represents the first catalyst to deliver high enantioselectivities with high conversions on substrates that do not

contain a coordinating functional group, including trisubstituted and tetrasubstituted olefins. Further to this, work carried out by Pfaltz led to the widespread introduction of the BArF counterion to improve the catalyst stability.[30] Following these ground-breaking discoveries, a vast array of similar ligands have been developed and extensively reviewed.[49,50,51]

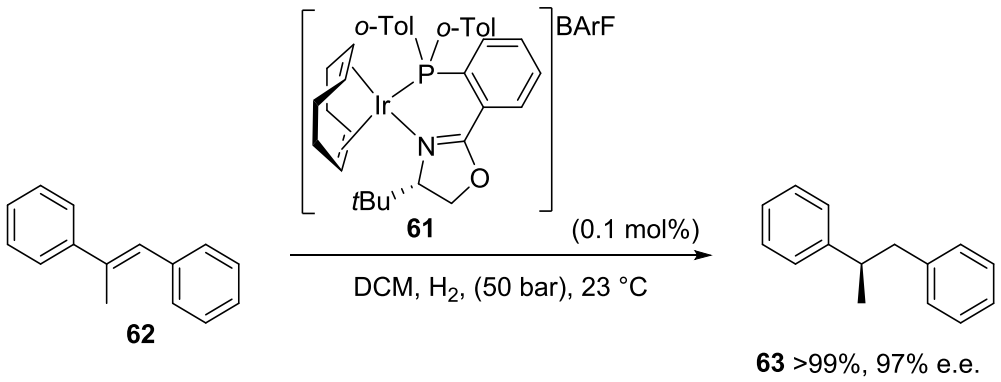

Scheme 1.18 Application of a Phox ligand in alkene hydrogenation.

Indeed, within this the series of ligands there exists two key classes; the first, with chirality within the tether, e.g. **64a**, and the second with chirality external to the tether e.g. **65a** (**Figure 1.10**). Further studies have delivered a variety of substitution patterns based on these two primary designs. Such designs commonly manipulate the phosphine-oxazoline tether, as with arylated **64b**, phosphinite linked **65b** and ferrocene derived **65c**.

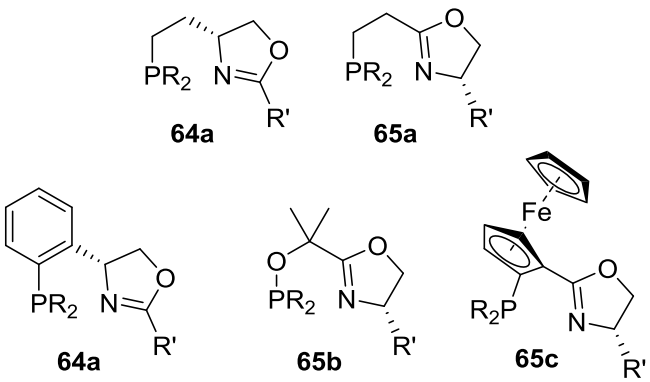

Figure 1.10 Different types of Phox derived ligands for alkene hydrogenation.

Following the initial report of PHOX ligands in hydrogenation, manipulation of the chelating group came to the forefront of the ligand design process. Certainly, the most common modifications are those that closely mimic Crabtree's catalyst **20**, such as

chiral chelating phosphine-pyridine complexes **66a-b**, initially introduced by Knochel (**Figure 1.11**).[52] Furthermore, other *N*-heterocyclic donor groups have been tested including imidazole **66c**,[53] thiazole **66d**[54] and pyrazole **66e**.[55] As the field began to move away from P-N donor ligands, an array of different donor atoms underwent testing. Most commonly, the inclusion of a N-heterocyclic carbine in place of the phosphine, as in **66f**,[56] or the oxazoline, as in **66g**.[57]

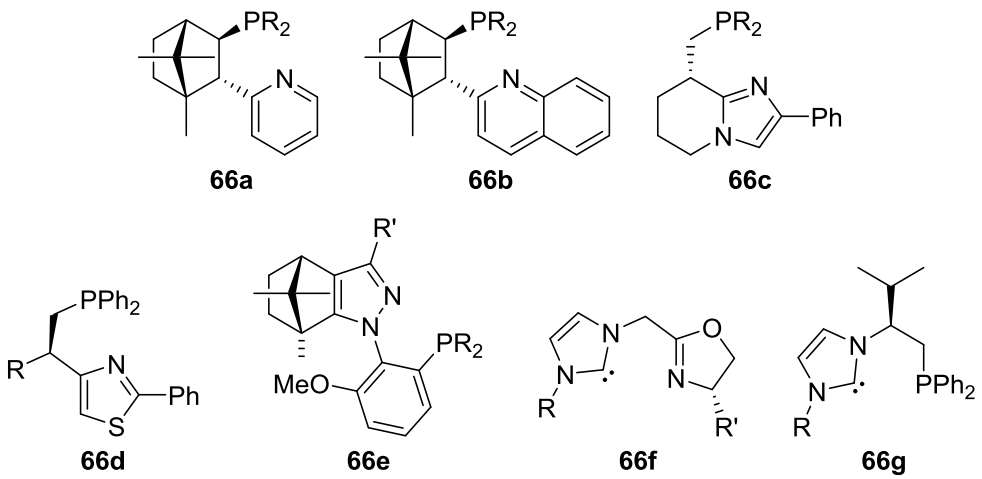

Figure 1.11 Different chelating ligands for alkene hydrogenation.

Such complexes have been widely applied, however, conditions used for hydrogenation vary widely among them. Therefore, the enantioselectivity alone is the common factor used in comparing the efficacy of each catalyst. However, perhaps the most successful in the hydrogenation of non-coordinating, tri- and tetrasubstituted alkenes, are still those reported by Pfaltz. With this in mind, a number of examples are displayed below that relate to the NeoPHOX catalyst structure **67**, in which it can clearly be observed that small variations in the catalyst and substrate greatly impact upon the enantioselectivity (**Scheme 1.19**).[58] Certainly, with model substrate **69a**, both ligand structures **67a-b** perform admirably. However, in substrate **69b** the small change between phenyl **67a** and *o*-tolyl **67b** in the ligand structure has a marked effect upon the enantioselectivity. However, by simply changing the geometry of the alkene, as in **69c**, this difference is mostly eliminated. Finally, moving to disubstituted, terminal alkene **69d**, conveys a significant decrease in the enantioselectivity. However, it has been well established that the requirements for high selectivity in terminal alkene hydrogenation are significantly different than for the more common trisubstituted systems.[47] Indeed, in a separate investigation, ThrePHOX ligand **68**, delivered a high

enantioselectivity in this substrate class.[59] Certainly, considering the vast array of catalysts currently available, the substrate scope is much wider than discussed here. Indeed, it has progressed to include; enols, enamides, allylic and homoallylic alcohols and unsaturated carbonyls, and alkenes bearing phosphorous, boron, fluorine and silicon.[49.50.51]

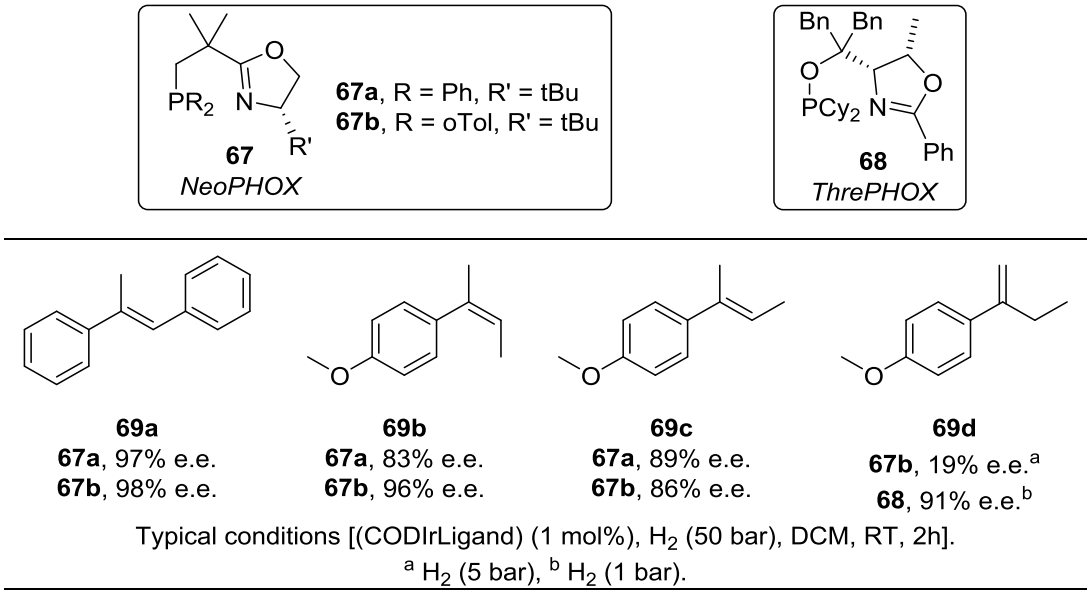

Scheme 1.19 Highlighting the substrate specificity of alkene hydrogenation catalysts.

Before discussing the origins of the enantioselectivity with iridium-based catalysts, it is first important to understand the catalyst structure and mechanism, and this has been well explored with P-N donor ligands (**Scheme 1.20**).[60] It is well recognised that upon addition of hydrogen, the typical, square planar iridium(I) species **A**, undergoes cyclooctadiene reduction and oxidative H_2 addition. This generates the octahedral iridum(III) solvated species **B**, in which the bidentate ligand is orientated *cis*-, with a hydride equatorial and *trans*- to the N-donor and a second axial and *trans*- to a solvent molecule. This intermediate is then ready to accept a molecule of hydrogen at the axial position, and the substrate alkene *trans*- to the P-donor. Furthermore, in forming intermediate **C**, the stereoselectivity of the reaction is controlled by the orientation of the alkene with respect to the ligand. Following this, oxidative addition of hydrogen and consequent migratory insertion permit the transient formation of iridium(V) intermediate **D**, calculated to be the rate determining step of the reaction. Ensuing rapid reductive elimination then completes the hydrogenation process **E**, at which point the

product molecule is released and replaced by 2 solvent molecules prior to the cycle restarting.

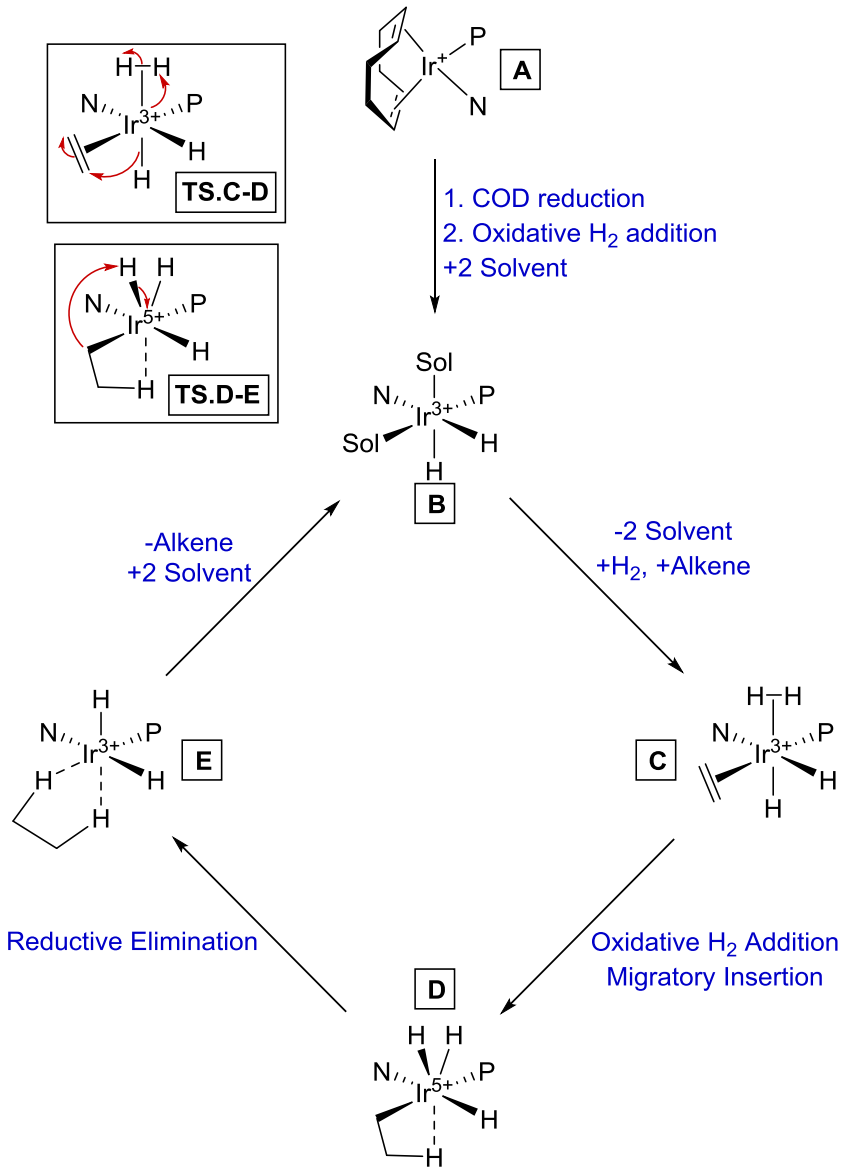

Scheme 1.20 Mechanism for alkene hydrogenation with P-N chelating ligands.

Through consideration of the previous mechanistic investigations, it is now understood that the selectivity is determined during alkene coordination and subsequent migratory insertion. Furthermore, the approach of the alkene is largely controlled by the ligand steric environment. With this knowledge, it has been possible to develop a general model to predict the outcome of an asymmetric hydrogenation process (**Scheme 1.21**).[51] Firstly, the ligand structure when coordinated to iridium is defined, either experimentally or computationally as for intermediates **II** and **III**. Then, through

orientating the structure to be viewed along the axis of alkene coordination, in the *N*-Ir-P plane, it is possible to generate a steric map relating to four quadrants **IV** and **V**, each of which represents space for an alkene substituent to occupy.

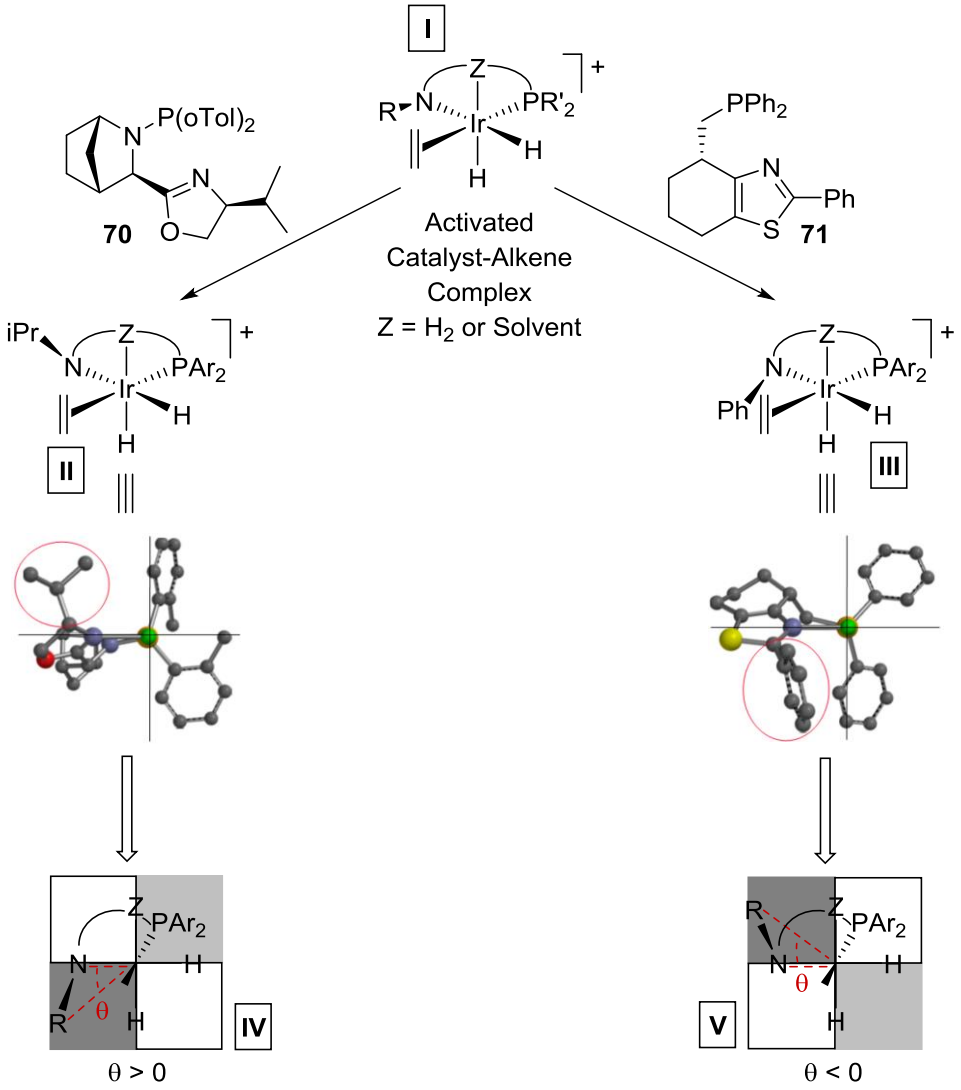

Scheme 1.21 Model for predicting the absolute stereochemistry of assymetric hydrogenation with a chelating iridium complex.

Moreover, through the application of this model, it has become clear that the angle between the substituent adjacent to the N-donor and the N-Ir-P plane dictates which quadrant model is appropriate (**Scheme 1.22**). Therefore, in conjugation with the alkene configuration the model can be used to predict the absolute stereochemistry of the product from the catalyst structure. Firstly, the smallest substituent is situated in the most hindered quadrant. This is easily achieved in a model trisubstituted alkene, as the hydrogen substituent is always smallest. Importantly, the alkene is always

orientated *anti*- to the plane of the ligand, because the migrating hydrogen originates at an axial position. Then, the hydrogen is delivered to the opposite face of the diagram (the face in which the catalyst is situated), allowing us to fully predict the stereochemical outcome of the reaction.

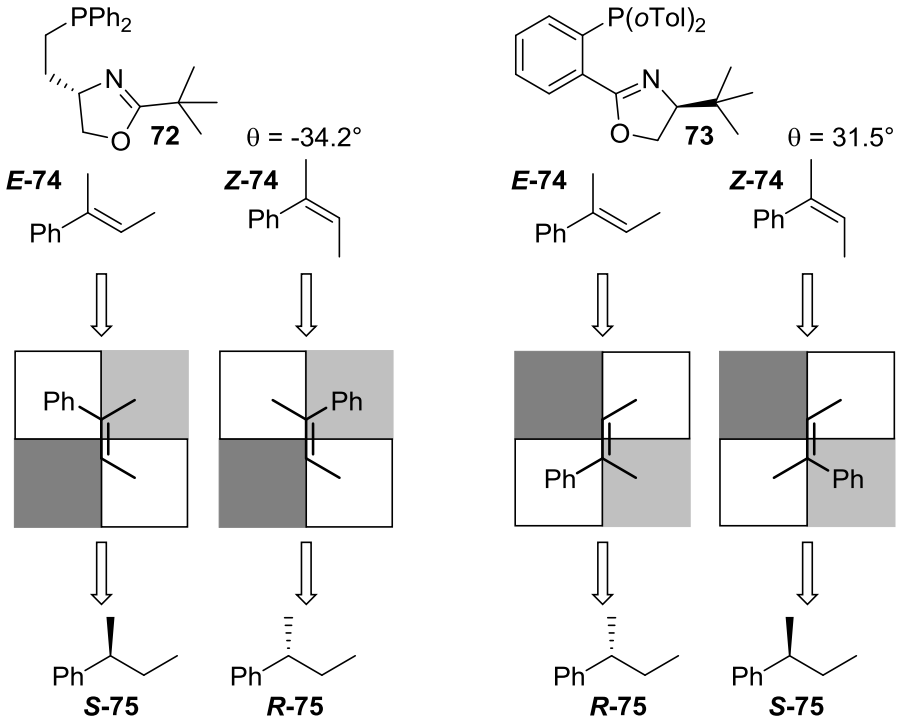

Scheme 1.22 Application of the predictive model.

Such a model provides insight as to why with many catalysts of this type are poor with regards to terminal alkenes (**Scheme 1.23**). Certainly, the catalyst must now be capable of sterically distinguishing the two groups which are situated in the least sterically encumbered quadrants. Secondly, the substrates in question are often capable of undergoing alkene isomerisation, the product of which would not deliver the same enantiomer following hydrogenation.

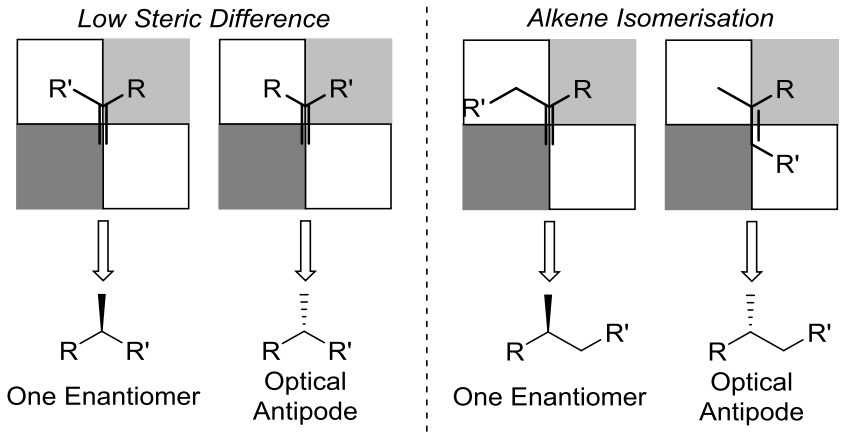

Scheme 1.23 Reasoning for low enantioselectivity in terminal alkene hydrogenation.

The impact of each ligand within this discussion can be understood through carefully parameterising the electronic and steric contributions each donor atom makes to the overall complex. Although many methods are available, in the following sections the common devices that are appropriate to the work carried out within this thesis are discussed.

1.4. Phosphines as ligands

Phosphines are one of the prominent ligand classes in homogeneous metal catalysis. This is mostly due to the remarkable electronic and steric tunability possible *via* variation of the substituents around the phosphine. Interestingly, phosphines very rarely directly interact in a metal catalysed process, instead they modulate the electronic and steric properties of the metal centre. In binding to a metal centre, phosphines form a dative bond by donation from the lone pair on the phosphorous into an empty d-orbital on the metal. Second to this, however, is the ability of the phosphine to undergo π-back donation from a filled metal *d*-orbital, into the σ*-orbital of a P-R bond (**Figure 1.12**).[61]

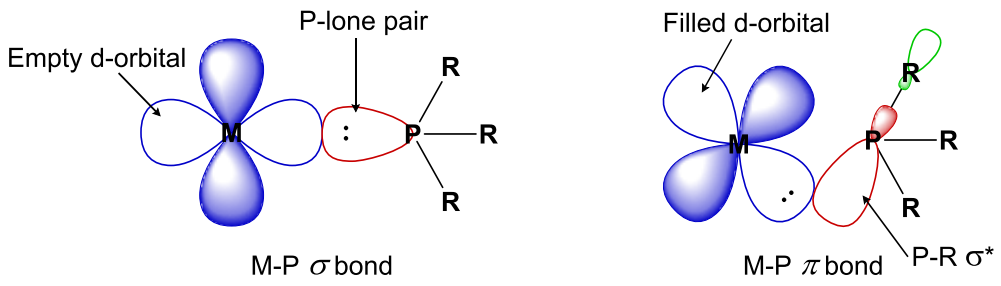

Figure 1.12 Metal-phosphine bonding.

In general, the extent of back bonding, and hence the π-acidity, of a given phosphine is dictated by the electron-withdrawing capability of the surrounding groups; the general scale of which is given below (**Figure 1.13**).

Increasing π acidity →

$PAlkyl_3$ < $PAryl_3$ < $P(OAlkyl)_3$ < $P(OAryl)_3$ < PCl_3 < CO

← Increasing σ donation

Figure 1.13 Order of phosphine π-acidity and σ-donation.

Pioneering work by Tolman in 1970, produced a series of methods for quantifying the electronic and steric effects of a phosphine ligand, that are still commonly in use today.[62,63] Firstly, to assess electronics, Tolman synthesised a series of $[Ni(CO)_3PR_3]$ complexes. Tolman realised that the donor capabilities of the phosphine ligand would be directly responsible for the amount of electron density on the nickel centre, and hence the amount of donation from the filled metal d-orbitals into the π*-orbital of the C≡O ligands This back donation weakens the C≡O bond, to such an extent that, within the IR spectrum, the CO stretch wavenumber decreases. This has since been described as the Tolman Electronic Parameter (TEP). Recently, Nolan, Cavallo *et al.* have expanded this technique to include measurements for complexes of the type $[Ir(CO)_2LCl]$, allowing comparison to other ligand classes directly.[64]

In addition to the above, Tolman also proposed a tool for quantifying the steric bulk of a given phosphine. The tool he proposed utilised the idea of a cone angle for the ligand, based on a metal-phosphine distance of 2.28 Å, and is described as the apex angle set out by three identical groups on the phosphorous atom (**Figure 1.14**). Therefore, greater steric bulk leads to a larger cone angle, as can be seen in the short series below.

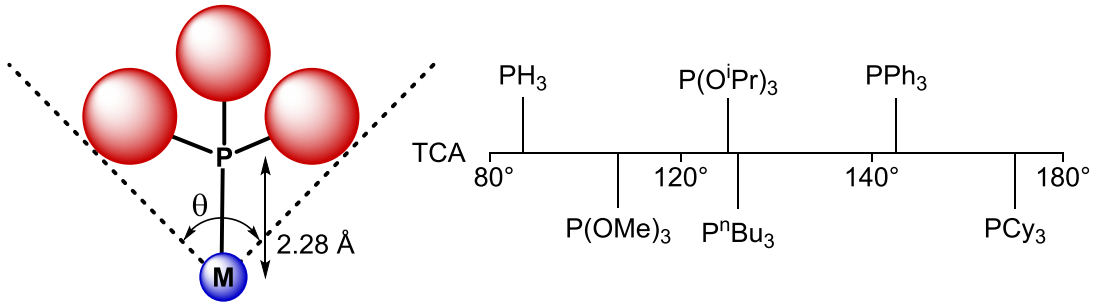

Figure 1.14 Tolman cone angle for common phosphines.

Despite the utility of phosphines as ligands in homogeneous catalysis, the propensity for the oxidation of electron rich phosphines creates challenges in their synthesis and shortens their lifetime as reagents. As such, the recent advance in the use of *N*-heterocyclic carbenes as ligands offers an alternative strategy in transition metal complex design.

1.5. *N*-Heterocyclic Carbenes as Ligands

In the past 2 decades, *N*-heterocyclic carbenes (NHCs) have been developed from little known chemical entites, to one of the most versatile and applied ligand classes in transition- and f-block metal, homogeneous catalysis.[65] Each species of this type contains a two-coordinate carbon atom, for which the singlet state is stabilised by donation of electron density from the surrounding nitrogen atoms into the empty 2p orbital (**Scheme 1.24**).

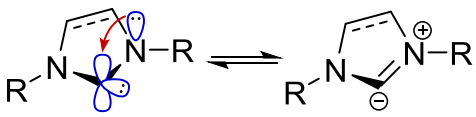

Scheme 1.24 Stabilisation of the singlet carbene by a nitrogen lone pair.

In a similar fashion to phosphines, π-back donation from a filled metal d-orbital into the empty 2p-orbital could be imagined. However, computational studies have shown that the π-donation from the nitrogen lone pairs is sufficient to almost completely fill the 2p orbital. [66] Despite this, some studies suggest that up to 15% of a metal carbene bond maybe considered to have π-character. This value while small indicates that the back donation into the carbene cannot be ignored.[67] The first crystalline NHC, **77**, was isolated by Arduengo *et al.* in 1991, through deprotonation of the parent imidazolium salt **76** (**Scheme 1.25**).[68]

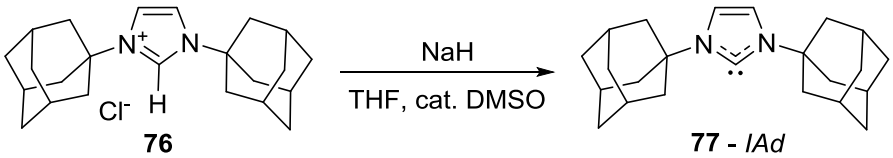

Scheme 1.25 Arduengo's isolation of a free carbene.

Following on from this work, a vast array of NHCs have been synthesised and, similarly to phosphines, it was envisaged that the electronic and steric properties of such structures would be tuneable by changing the nature of the substitution of the nitrogen atoms. As such, Nolan *et al.* synthesised iridium complexes with the general structure [$Ir(CO)_2NHCCl$], and from these the IR frequency for the CO stretch was measured to give a quantitative value for the electronic properties of the given NHC.[65] To this end, a huge range of NHCs have now been classified, and it can now be observed that the NHC ligand is even more electron-donating than the most Lewis basic phosphines (**Figure 1.15**). Interestingly, it was also noticed that only a small change in σ-donor capability was obtained through changing the nature of the nitrogen substituent.

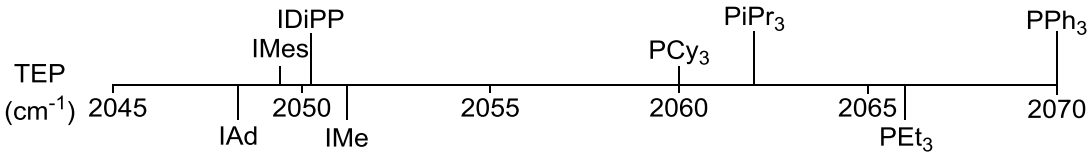

Figure 1.15 Comparison of NHC and phosphine Tolman electronic parameters.

In a similar fashion to phosphines, the steric properties of NHCs were also deemed to be of great importance, however, due to the planar nature of the NHCs, the Tolman cone angle was not deemed a viable approach for NHCs. As such, Nolan and Cavallo *et al* developed the key methodology known as percentage buried volume (%BV). Alternative methods do exist to quantify the steric properties of NHCs, however % BV is by far the widest utilised.[69,70] This method applies either the crystal structure or DFT optimised structure to generate coordinates for a given complex. The metal to ligand distance is set to R, within a sphere radius of d (**Figure 1.16**). This allows a sphere of a given volume to be drawn, centred on the metal of the complex; from this, the %BV is the volume of the sphere occupied by the ligand as a percentage of the overall sphere

volume. One of the biggest advantages to this method is that it allows direct comparisons of all ligand classes, not just NHCs.[70]

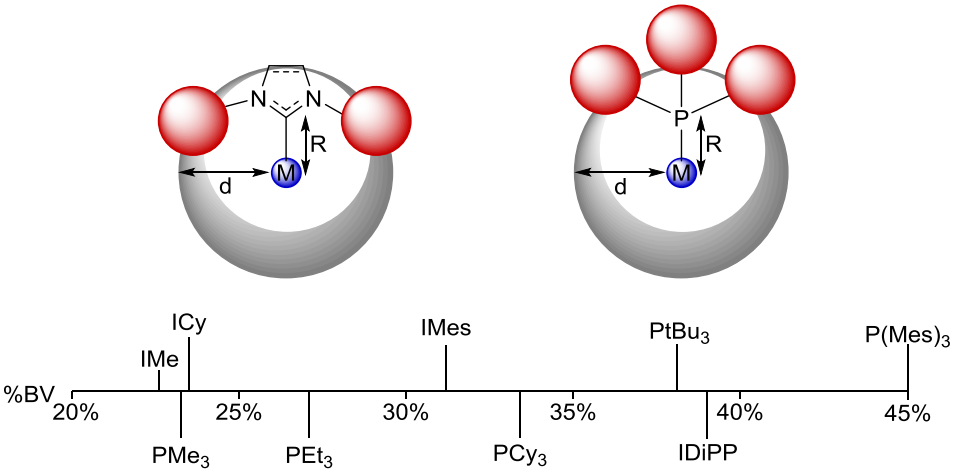

Figure 1.16 Buried volume as a method of defining steric bulk.

The discussed developments in NHC chemistry now allow access to a broad range of metal NHC complexes. Importantly, the synthesis of many NHC salts are trivial, and with the imidazolium salt typically being air stable and easily stored, they provide an accessible source of the desired carbene.

1.6.Previous Developments from Within the Kerr Group

Having recognised the developments made by the likes of Nolan[28] and Buriak,[29] and advances in synthetic organometallic strategy Kerr *et al.* gained expedient access to complex **78a**. Furthermore, they utilised the same general procedure to synthesise a range of novel complexes bearing different phosphine ligands, including complexes of $P(Me)_2Ph$ and PBn_3 yielding **78b** and **78c**, respectively (**Figure 1.17**).[71] With these complexes in hand they were quick to recognise there potential in olefin hydrogenation.

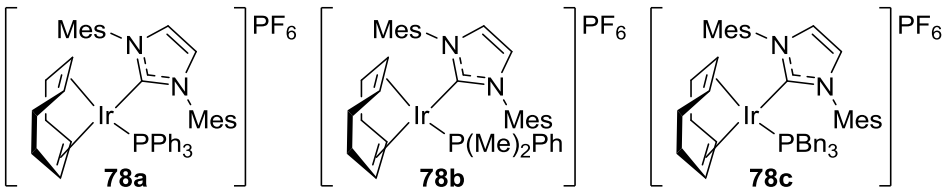

Figure 1.17 The first series of NHC/phosphine complexes sythesised by Kerr *et al*.

Each of these complexes was tested for activity in hydrogenation processes with a range of different substrates (**Table 1.7**). Pleasingly, each complex showed high activity in the reduction of simple terminal styrene, **79**. However, when moving to the more challenging tetrasubstituted substrate, **23**, the complex bearing the smallest phosphine, **78b**, proved to have the highest activity; although, extended reaction time and a higher catalyst loading was required.[72]

Entry	*Substrate*	*Complex*	*Time (h)*	*Catalyst Loading (mol%)*	*Yield*
1	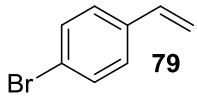 **79**	**78a**	1	0.5	100
2		**78b**	1	0.5	100
3		**78c**	1	0.5	100
4	 **23**	**78a**	16	1.0	5
5		**78c**	16	2.5	15
6		**78b**	16	7.0	84

Table 1.7 application of NHC/phosphine complexes in alkene hydrogenation.

In addition to the above, it was also observed that the hydrogenation of simple alkyne, **80**, to the corresponding alkane, **81a**, could be readily achieved through utilisation of complex **78c** (**Scheme 1.26**).

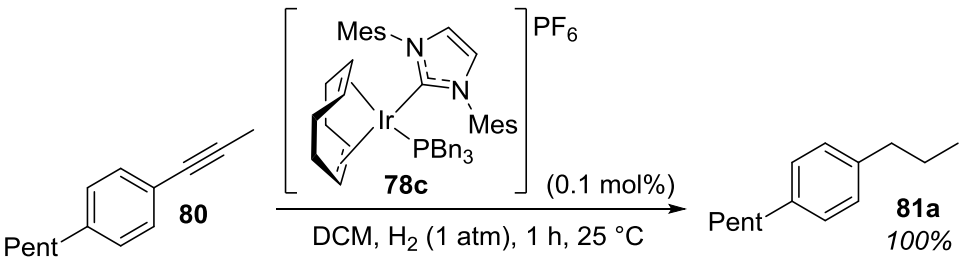

Scheme 1.26 Alkyne reduction with NHC/phosphine complex **78c**.

It was also reported, that through the use of a coordinating catalyst poison such as benzamide, this process could be controlled to selectively hydrogenate alkyne **80**, furnishing, in a *Z*-selective manner alkene **81b** in a good yield (**Scheme 1.27**).

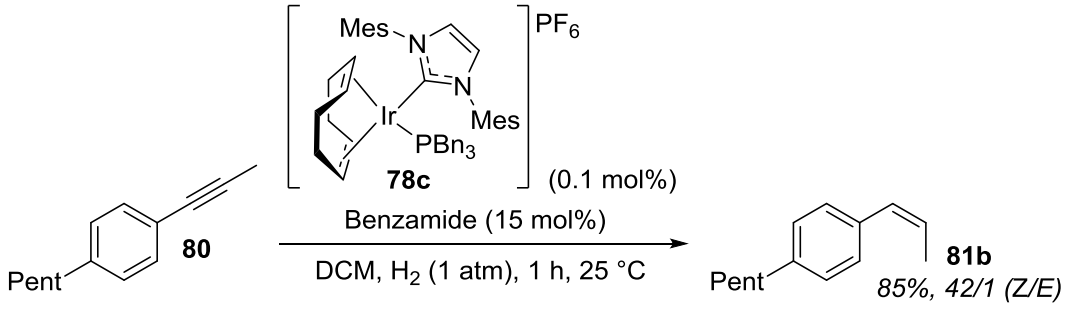

Scheme 1.27 Partial alkyne reduction with NHC/phosphine complex **78c** and benzamide.

Beyond this initial foray into hydrogenation chemistry, Kerr *et al* also looked to access a new range of complexes bearing the same ligand structure as **78a**, but with a different anionic partner.[73] Application of a newly developed protocol allowed access to complexes bearing a range of different counterions, and testing was carried out with a simple HIE reaction, but not hydrogenation (**Figure 1.18**).

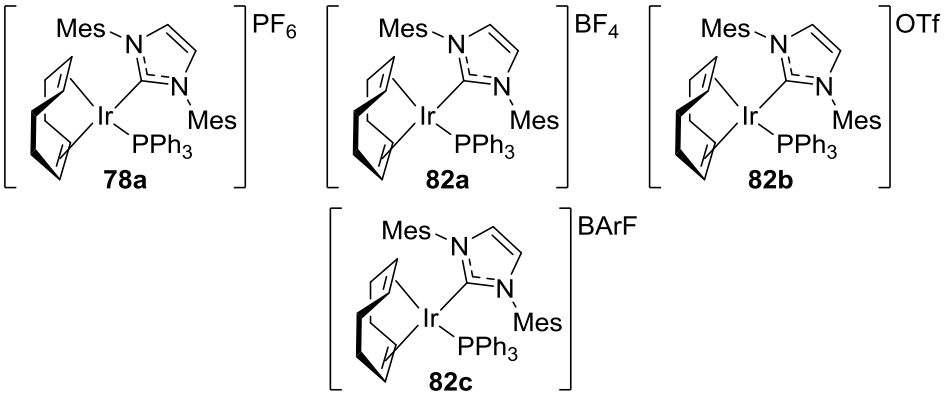

Figure 1.18 Series of counterion complexes synthesised and tested by Kerr *et al* in HIE.

2. Proposed Work

As previously discussed, research within the Kerr group has applied catalysts **78a**, **78b** and **78c** to catalytic hydrogenation processes with good success but, with a limited substrate range.[72] The primary goal of this project is the development of new complexes that can perform highly selective hydrogenation processes. Certainly, the first phase to this is consistent with work carried out in our own group,[73] and among others,[29,30] to investigate the impact of the anionic partner to the cationic catalyst complex (**Figure 1.19**).

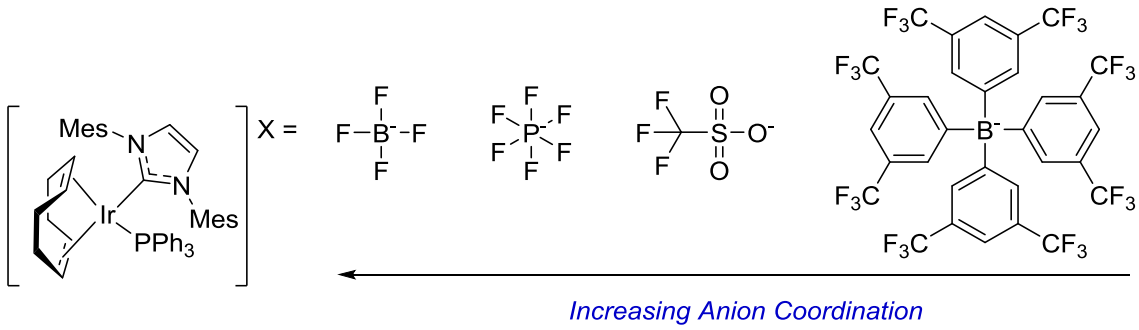

Figure 1.19 Anion affects in alkene hydrogenation.

Our next goal is to access a broad range of complexes bearing different ligand structures, in an effort to better understand the role that each ligand plays in the hydrogenation process (**Figure 1.20**). To achieve this, new, efficient methods for the production of NHC/phosphine complexes will be developed, with each complex characterised both sterically and electronically, prior to testing with several model substrates.

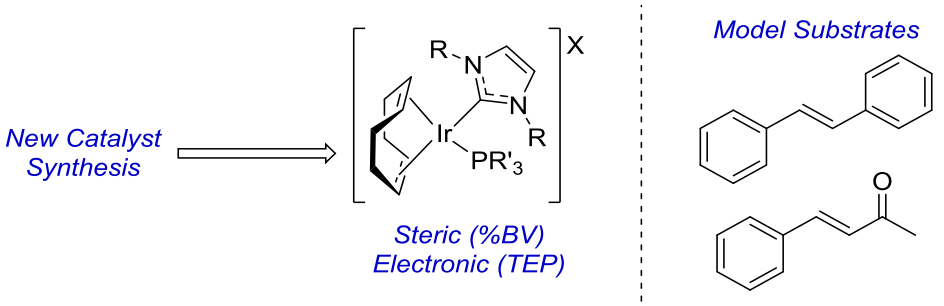

Figure 1.20 Synthesis and characterisation of new NHC/phosphine complexes for application in alkene hydrogenation.

Keeping in mind that the catalysts above have been developed and tested extensively in HIE,[71,73,74] the initial application targeted will be through a directing group assisted process, primarily, to control the site of hydrogenation (**Figure 1.21**). This will give us an opportunity to fully explore the new complexes developed in the previous sections and introduce new methods for performing regio-, chemo- and diastereoselective hydrogenation with iridium NHC/phosphine catalysts.

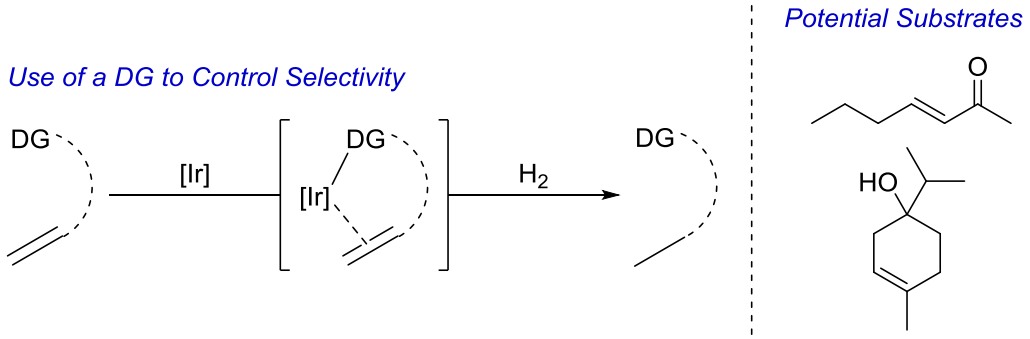

Figure 1.21 Directing group assisted hydrogenation.

Finally, the development of NHC/phosphine complexes that bear a chiral ligand should be investigated. The developments in NHC technology over the past two decades has meant that chiral carbenes have found widespread application in both organocatalysis[75] and transition metal catalysis.[76,77] With this in mind, alongside the previously discussed difficulties in synthesising chiral monodentante phosphines, our efforts would focus upon the synthesis of novel, monodentate chiral-NHC, phosphine bound complexes (**Scheme 1.28**). Considering the known propensity for such complexes to form a *trans*-geometry under a hydrogen atmosphere, we can expect a markedly different chiral environment to that of the more common chelating chiral complexes. This could allow access to a different range of hydrogenation processes, or new modes of catalytic activity as yet unexplored.

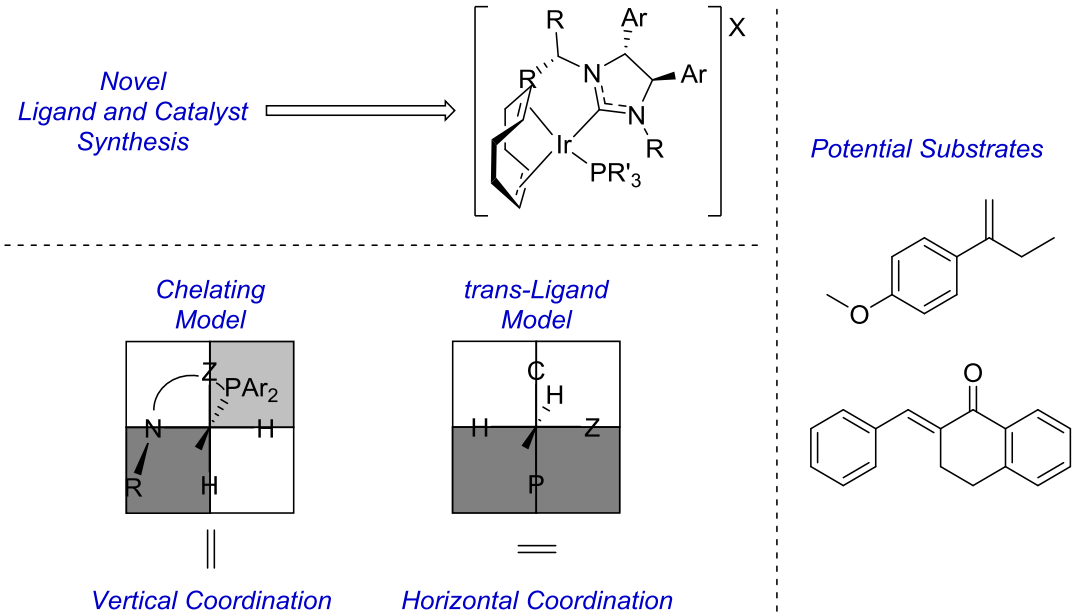

Scheme 1.28 Assymetric hydrogenation with chiral NHC/phosphine complexes.

3. Results and Discussion

3.1. Catalyst Synthesis and Initial Findings

Within previous studies, the Kerr group have developed access to a range of different counterion complexes, and investigated their reactivity in HIE.[73] Indeed, through such findings they were able to improve the complex reactivity for HIE. Furthermore, a range of counterions could be utilised in a wide array of solvents. As such, only a limited examination of phosphine/NHC complexes in hydrogenation was deemed necessary. The study was initiated with a range of alkene reductions performed with four complexes, each bearing a different anion (**Scheme 1.29**). Each anion was chosen for its proven synthetic accessibilty and reported difference in cation pairing.[30,73] The study was initiated with simple mono- or di-substituted alkenes **79**, **83a-b**, and it was found that under normal hydrogenation conditions, each complex delivered excellent high conversion in under 30 minutes.

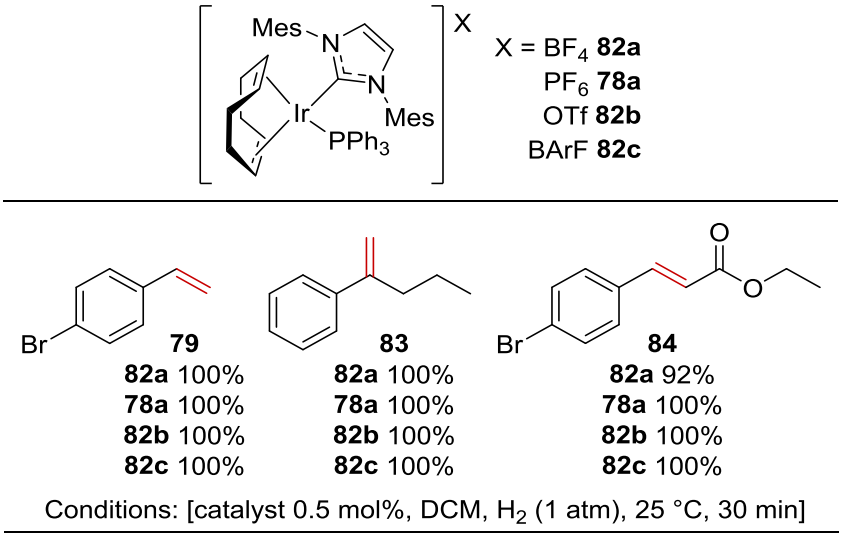

Scheme 1.29 Initial hydrogenation of mono- and bisubstituted alkenes.

In an effort to better assess the effect that the anion was having, the reaction of **84** with each complex was followed at a lowered catalyst loading (0.25 mol%) (**Graph 1.1**). In doing so, it quickly became clear that the complex bearing the non-coordinating counterions OTf, **82b**, and BArF, **82c**, delivered improved reaction rates, and the complex bearing the smaller, more coordinating counterion tetrafluoroborate, **82a**, the reverse, in line with our previous findings in HIE.[73]

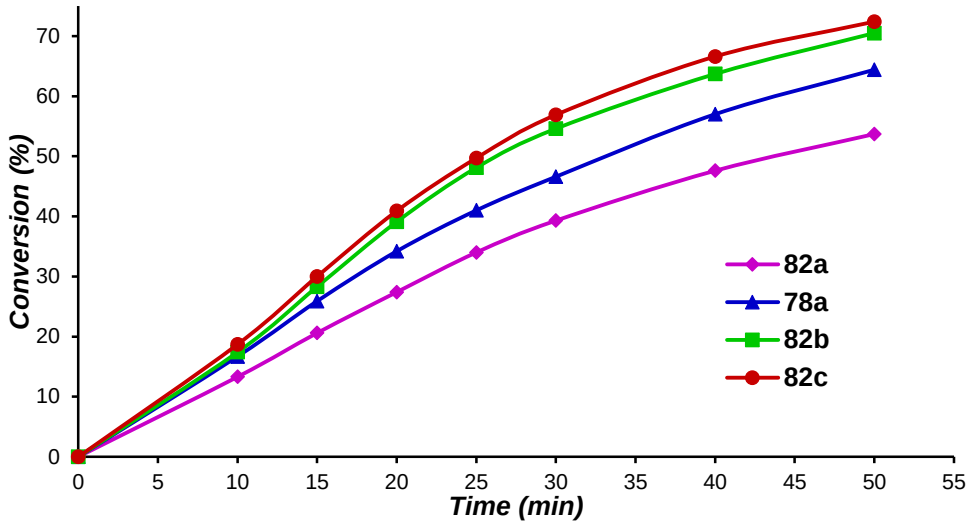

Graph 1.1 Monitored hydrogenation of conjugated ester **84**.

Finally, by studying the reaction of enone **85** with complexes **78a**, **82a-c** at varying catalyst loadings, the efficacy of each complex was assessed (**Scheme 1.30**, **Graph 1.2**). This study showed that complex **82c**, bearing the non-coordinating BArF counterion, encounters the maximum rate of the reaction at just 1.0 mol%, whereas 1.5 mol% is required for tetrafluoroborate complex **82a**. Indeed, the limiting of the rate despite increasing catalyst loading could indicate the mass transport limit of H_2 into the solution as the rate limiting factor for this substrate.

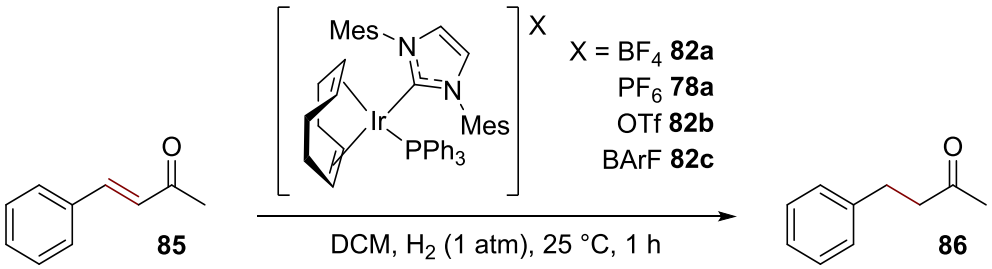

Scheme 1.30 Hydrogenation of enone **85** with different counteroin complexes.

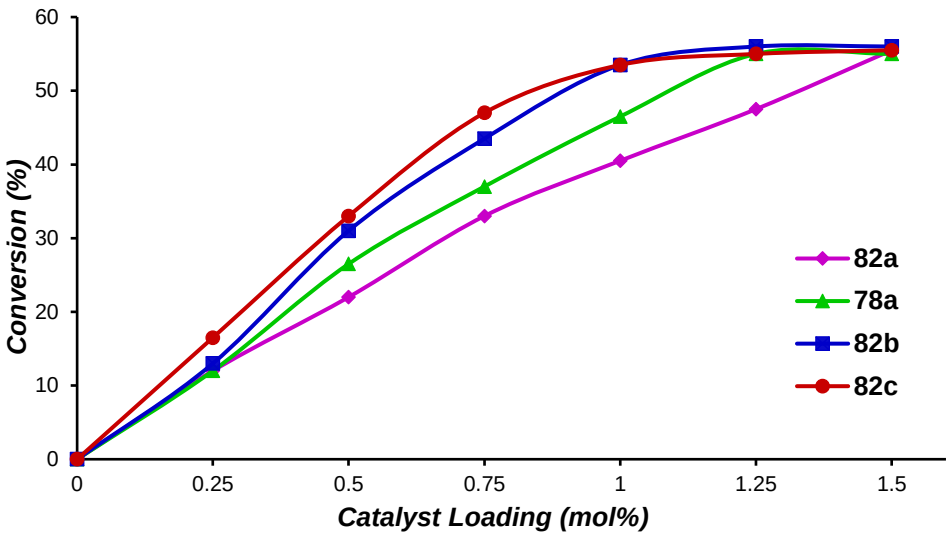

Graph 1.2 Hydrogenation of enone **85** at different catalyst loadings.

These findings clearly match those found with other iridium hydrogenation catalysts,[29,30] and indeed the same complexes in HIE.[73] With this in mind, further investigations regarding the impact that manipulating the ligand sphere could have upon the hydrogenation reaction were commenced. However, before commencing investigations into the hydrogenation reaction the synthesis of NHC/phosphine complexes, and there steric and electronic parameters were investigated.

We wished to shorten the current synthesis, and, importantly, avoid the use of strong base, highly reactive silver salts, and the highly moisture- and air-sensitive argon filtration step, commonly utilised in the synthesis of NHC/phosphine complexes.[73] Certainly, it is well known that Ir-NHC/chloride complexes can be obtained through transmetalation of the NHC from silver.[78] Furthermore, such complexes have been used in tandem with mild halide abstractors such as sodium and potassium salts, in the production of NHC/phosphine complexes.[79] However, both processes required isolation of each intermediate and required a solvent exchange from DCM to THF. However, we believed that both processes were viable in DCM, and that any by-products from the early steps would be inert in the following reactions. Therefore, we attempted a one-pot, three-step synthesis of known NHC/phosphine complex **90a** (**Scheme 1.31**). Firstly, the silver-NHC complex **88** was generated from the NHC halide salt and silver oxide, and we were pleased to observe the expected black to clear/grey colour change in just one hour, allowing us to proceed to the second step

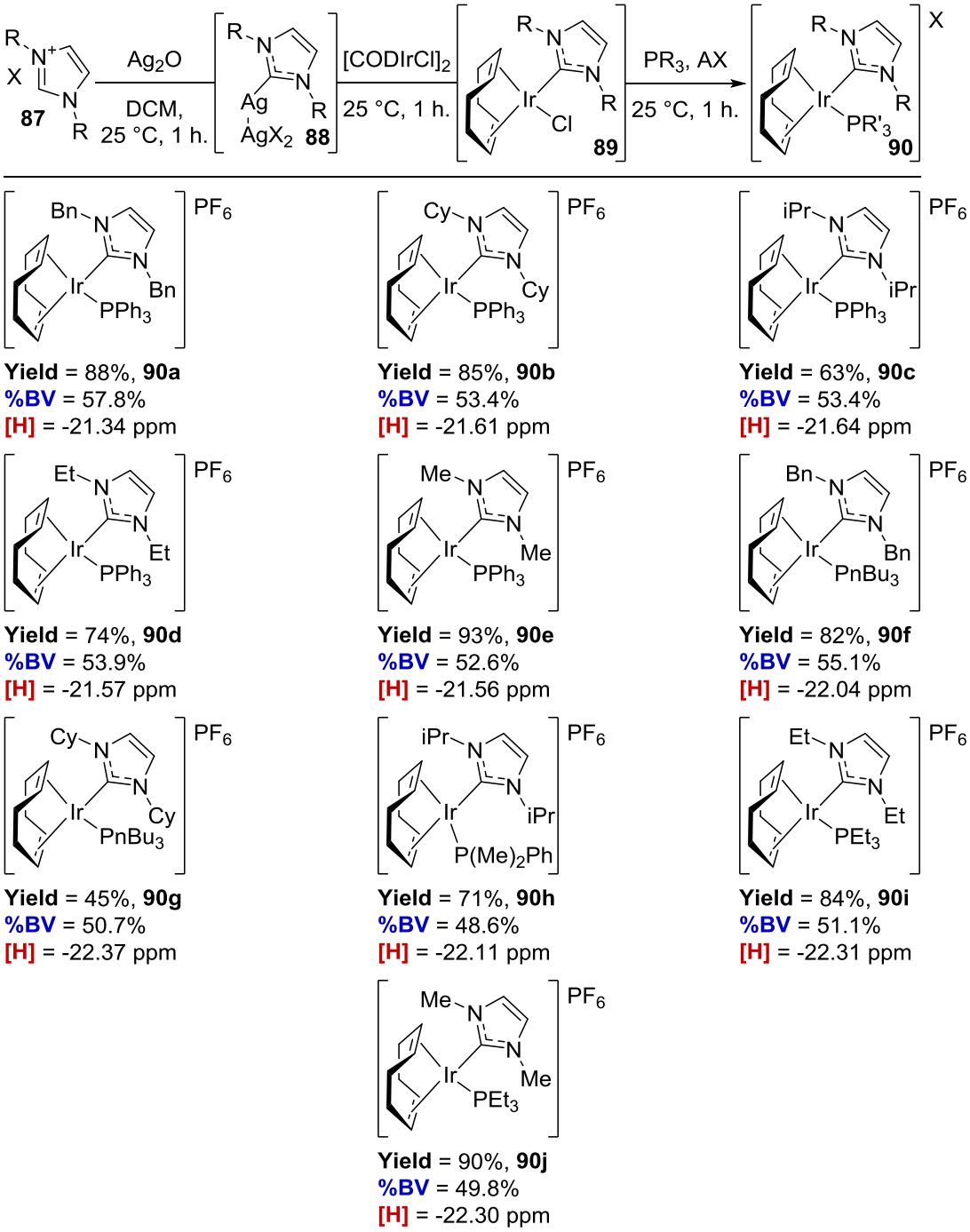

Scheme 1.31 One-pot synthesis of alkyl-NHC/phosphine complexes.

and introduce the iridium cyclooctadiene chloride dimer. Immediately, a grey to yellow colour change was observed, indicating the generation of a NHC/chloride complex **89**. Finally, we introduced the phosphine, swiftly followed by the halide abstractor, potassium hexafluorophosphate, which initiated a familiar yellow to red/orange colour change indicative of NHC/phosphine complex formation.

Pleasingly, the complex was obtained in a high yield following isolation, an improvement upon performing each step individually, thus validating the use of a one-pot protocol.[80]

To further test this new procedure and examine other NHC/phosphine complexes in alkene hydrogenation, ten further complexes were synthesised. In each case, the yields were mostly excellent, with only complex **90g** being formed in a moderate yield due to a difficult isolation. Thus, we had validated our new one-pot method with a range of alkyl-substituted NHCs **90a-e**, and with a range of aryl and alkyl phosphines **90f-j**. In an effort to parameterise these new complexes the combined percentage buried volume of each ligand from the X-ray structure of a linear metal complex was combined,[70] to generate a single term reflecting the steric bulk of the overall complex. Importantly, the steric parameter calculated from two independent complexes, is in good agreement with that found experimentally from the X-ray structure of trigonal bipyramidal iridium complex **92** bearing both NHC and phosphine ligands (**92** 55.6% versus, **78b**, 56.3%) (**Figure 1.22**).[80] Secondly, the ^{1}H NMR shift of the hydrides from the *in situ* generated octahedral iridium(III) dihydride-diacetonitrile complex were utilised to parameterise the overall complex electronics.[80]

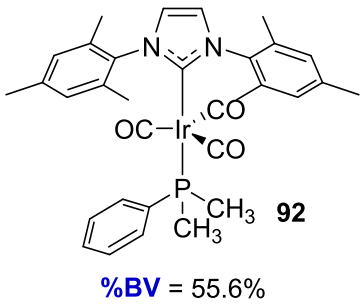

Figure 1.22 Buried volume from the X-ray crystal structure of **92**.

Following our previous success with the non-coordinating counterion BArF, we wished to further examine this new method with NaBArF in place of potassium hexafluorophosphate (**Scheme 1.32**). Furthermore, the method proved applicable in the synthesis of analogous complexes bearing the BArF counterion, **90k-n**, in excellent yields. Recognising that the counterion would only have a minimal effect upon the complex electronic parameter, and would be independent of the steric parameter, these parameters

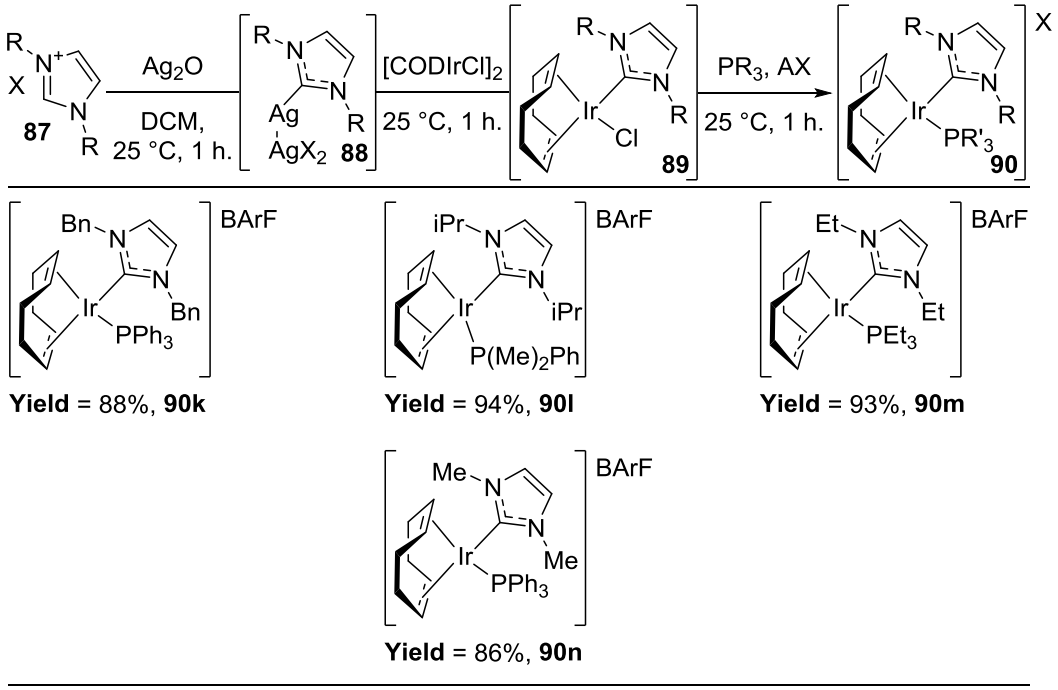

Scheme 1.32 One-pot synthesis of alkyl-NHC/phosphine BArF complexes.

were not reassessed for each counterion. However, despite all efforts to apply this new method to the synthesis of larger NHCs (i.e. IMes), with different phosphines we were unable to access the final complex. This is assumed to be due to the poor formation of the silver carbene complex and subsequent slow transmetallation to iridium. However, when applying a modified method, following the literature preparation and isolation of IMes/Cl complex **89a**,[73] we successfully synthesised a range of complexes bearing small/electron rich phosphines. This new procedure, although not one-pot, mitigates the use of highly reactive silver salts and the moisture- and air-sensitive argon atmosphere filtration (**Scheme 1.33**). However, the yields in which KPF_6 was used for the synthesis of **78c**, **91a-b** and **78b** were below those achieved with alternative methods.[80] However, when using the stronger halide abstractor NaBArF, **91c-f** were formed in excellent yields, indicating that the sequestration of the halide is important for reaction progress. Furthermore, the steric and electronic parameters were assessed for the PF_6 counterion catalysts for comparison with the previously synthesised complexes. Finally, despite extensive testing of our new methods, both failed to permit the synthesis of triphenylphosphine/IMes complexes **78a** or **82c**, presumably due to the weaker nucleophilicity of triphenyl phosphine, combined with the greater steric bulk of IMes.

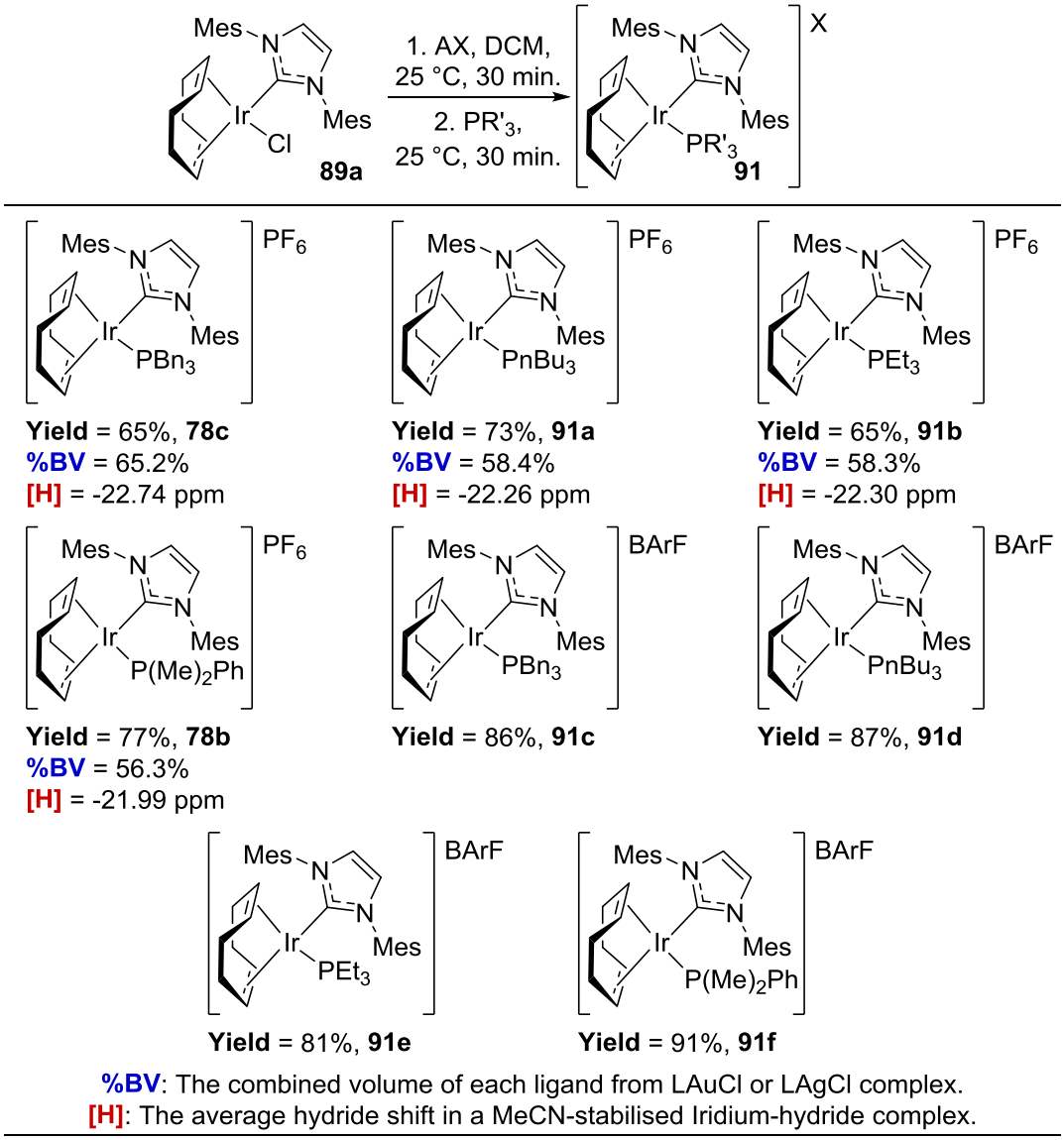

Scheme 1.33 New, efficient method for accessing IMes/alkyl-phosphine complexes.

Following the successful introduction of two new methods permitting expedient access to a range of different NHC/Phosphine complexes, we wished to investigate their efficiency in hydrogenation. To do this two alkenes were utilised, one solely coordinating through the alkene, **93**, the other bearing a potential coordinating functional group, **85** (**Scheme 1.34**). For clarity, only the results with complexes bearing the PF_6 counterion are displayed, and the results for the corresponding BArF complexes are tabulated in the Experimental Section. It became apparent very quickly through testing, that alkyl substituted NHCs paired with triphenylphosphine were not efficient in performing the hydrogenation of **90a-e**. However, by substituting triphenyl

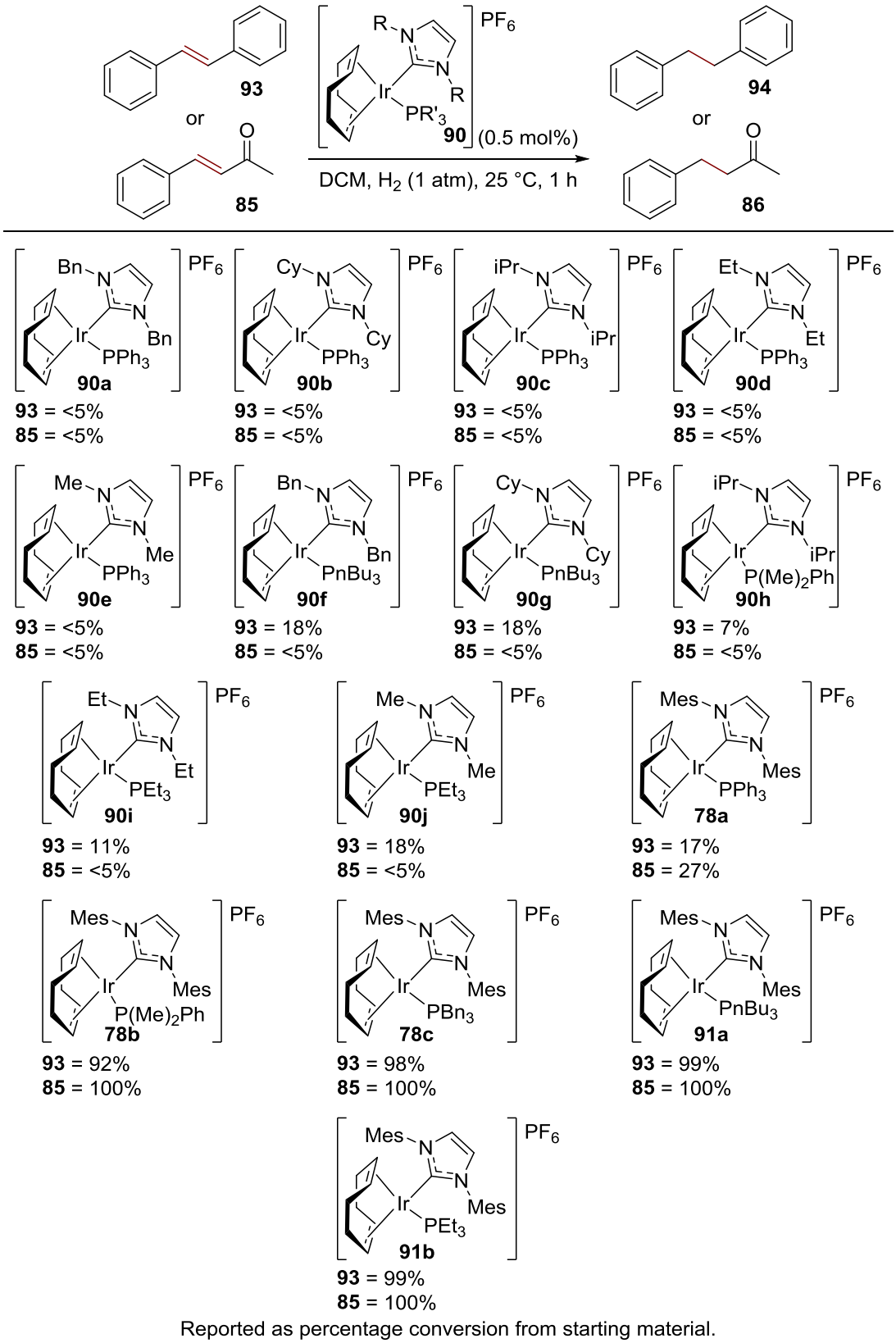

Scheme 1.34 Initial testing with new NHC/phosphine catalysts.

phosphine with a more electron donating phosphine complexes **90f-I**, low conversion was achieved with stilbene **93**, and, only trace levels of conversion were attained with

enone **85**. However, in line with our previous studies, improved conversion was obtained when switching to IMes as the NHC, with **78a**, and, moreover, to a more electron donating phosphine, in complexes **78b-c** and **91a-b**.[72] These results indicate that reaction efficiency is not solely controlled by the steric or electronic parameters we have investigated, and in fact, the catalyst structure plays a major role.[81] In the case of IMes, this could be envisaged as a C-H insertion between the aryl methyl group and the iridium centre, as in proposed structure **95** (**Figure 1.23**).

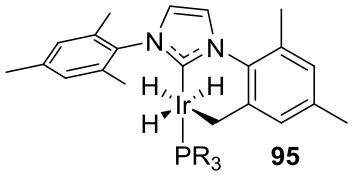

95

Figure 1.23 A plausible, stable, off-cycle intermediate.

Having introduced new methods for the synthesis of NHC/phosphine complexes and investigated their steric and electronic parameters, followed by initial testing in alkene hydrogenation, we can conclude that efficient hydrogenation is best achieved with a complex bearing IMes and an electron rich phosphine, paired with a non-coordinating counterion, such as BArF. Our following studies focussed upon the application of these highly active catalysts in regio- and chemoselective hydrogenation.

3.2.Directing Group Assisted Olefin Hydrogenation

It is well recognised within the hydrogenation literature that the chemoselectivity of alkene hydrogenation is dominated by the degree of double bond substitution. However, it has also been observed that catalysts capable of performing hydrogenation reactions can undergo directing group-assisted, hydrogen isotope exchange *via* C-H insertion.[71,72] Furthermore, a non-coordinating counterion is also known to allow improved exchange in a wide array of solvents when compared to the parent PF_6 complex.[73] With all this in mind, we looked to develop a regioselective, directing group-assisted, hydrogenation process capable of performing alkene reduction in a wide array of industrially aligned solvents.

From consideration of our earlier results, we chose to first apply enone substrate **85**, in a comparative study with another common iridium hydrogenation catalyst, by applying Crabtree's complex for the chosen process along with a range of our NHC/phosphine complexes (**Scheme 1.35**). Pleasingly, both the PF_6 **78b** and BArF **91f** NHC/phosphine complexes chosen for examination delivered complete conversion, whereas, Crabtree's complex **20** and its BArF analogue **96** delivered incomplete conversion (28% and 25%, respectively). Therefore, convinced we had a viable catalyst system in complex **91f**, we moved to optimise the reaction conditions and to further explore this reaction process through investigation of different substrates and by varying the reaction medium.

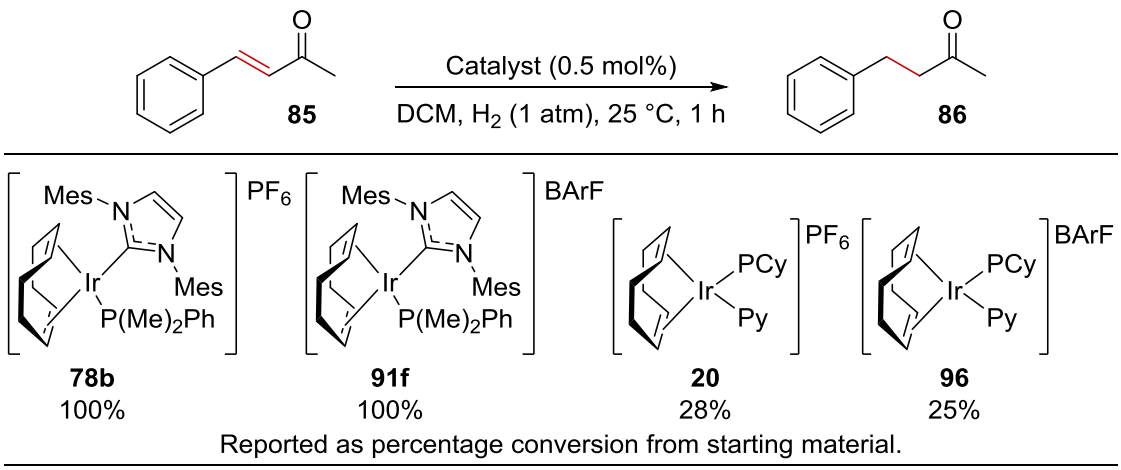

Scheme 1.35 Comparison with Crabtree's catalyst.

In an effort to improve our reaction protocol, we applied experimental design, utilising a 3-factor, 2-level design investigating catalyst loading, reaction time and substrate concentration. Through this study it was discovered that increasing catalyst loading and reaction time improved the reaction conversion, as expected. However, it was discovered that increasing substrate concentration, reduced the reaction conversion. Presumably, this indicates an inhibitory process related to a non-productive catalyst-substrate or catalyst-product complex.[5] Therefore, our optimised conditions did not greatly change from our earlier studies. However, a reduction in solvent volume was deemed appropriate (8 mL to 4 mL), necessitating an increase in reaction time.

Following on from this experimental design process, we applied the optimised conditions [**91f** (0.5 mol%), DCM (0.1 M), H_2 (1 atm), 25 °C, 2 h], to a broad range of unsaturated substrates (**Scheme 1.36**). After the initial success in the reduction of **85**, further enone substrates **97a-c** all performed well, with no hindrance to the reduction by *para*-, *meta*- or *ortho*-substitution of the aromatic ring. Increasing the steric bulk adjacent to the donor group also resulted in full conversion in **97d**. Pleasingly, alkyl-substituted enones **97e** and **97f** also readily underwent hydrogenation, however the increased steric bulk in **97f** required moderately increased catalyst loading and extended reaction time (1 mol% and 16 h) for complete conversion. In contrast, the standard, optimised conditions proved effective in the hydrogenation of chalcone derivative **97g**. More challenging α-substituted enones **97h** and **97i** required both higher catalyst loading and longer reaction times (1 mol% and 16 h), but, notably, complete conversion was still achieved at 1 atm of H_2 pressure. Furthermore, β-disubstituted enone **97j** initially proved problematic under the optimised conditions, but a modest increase in temperature, along with catalyst loading and reaction time (2 mol%, 35 °C, 40 h) delivered quantitative conversion to the reduced product.

Following the selective reduction of a range of ketones, we next investigated a range of alternative directing groups. Notably, the sensitive carbonate group in **97k** remained intact under the standard reaction conditions, delivering an excellent yield of reduced olefin, and both cinnamic acid **97l** and its *p*-brominated ethyl ester derivative, **84**, proceeded to complete conversion in excellent yields under the optimised conditions.

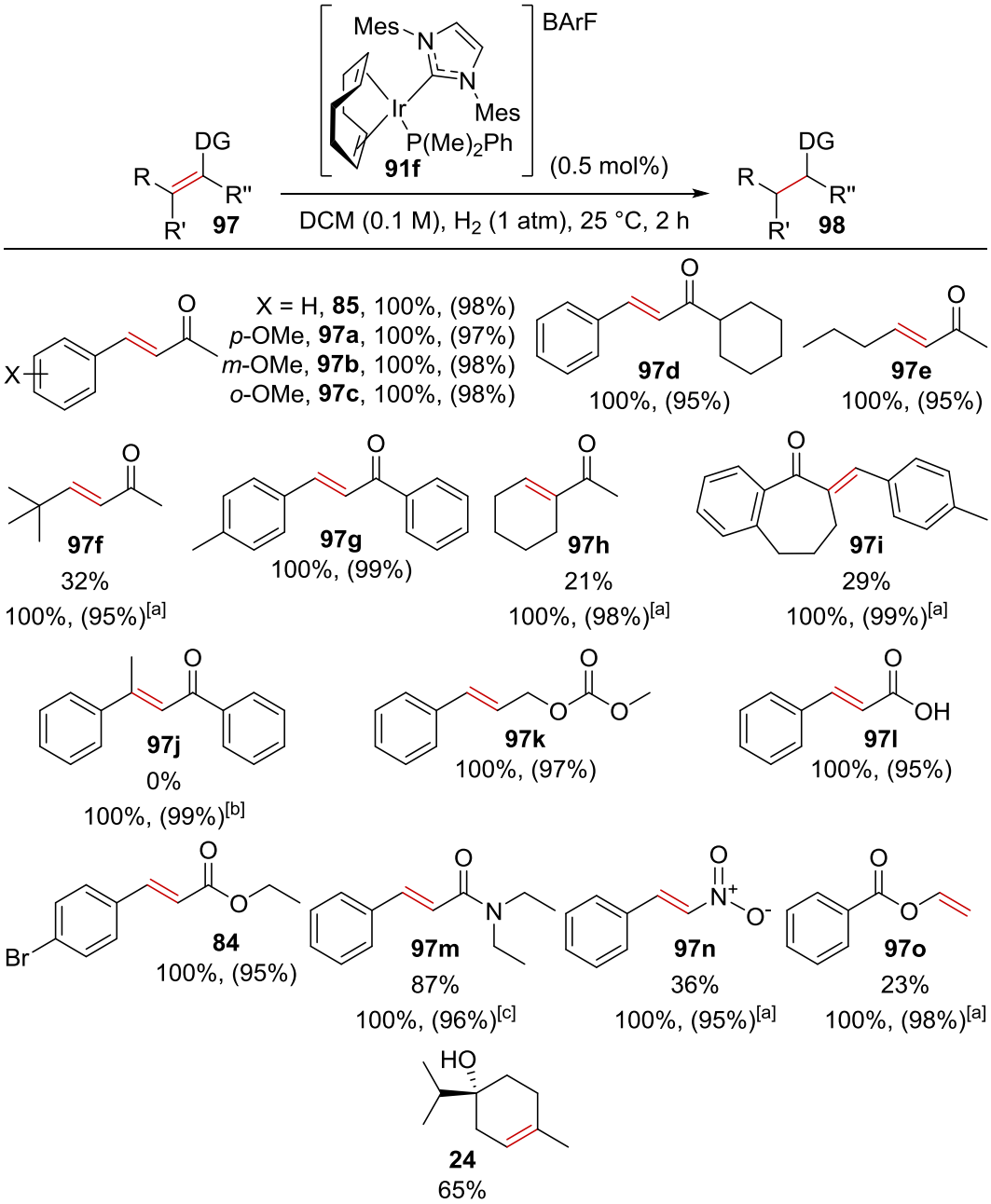

Scheme 1.36 Directing group assisted hydrogenation of further substrates.

The presence of a strongly coordinating amide donor group in **97m**, however, required a slightly elevated catalyst loading of 1 mol%, again indicating that decomplexation of the substrate from the catalyst is of key importance in catalyst turnover. The hydrogenation of the less coordinating, nitro-containing compound **97n** required an extended reaction time and moderately increased catalyst loading (1 mol%, 16 h), but still proceeded without any observed NO_2 reduction. We have shown in a separate

study that a competing C-H insertion at the *β*-position of the olefin can also occur with this compound **97n**,[82] plausibly reducing the rate of hydrogenation. Similarly, vinyl benzoate **97o** can undergo a competing *ortho*-aryl-C-H activation,[83] again reducing the rate of hydrogenation, although reduction still proceeds effectively with only 1 mol% catalyst loading. Finally, the reduction of (-)-terpinen-4-ol **24** proceeded with moderate conversion, however we felt that further investigation was required due to the diastereoselective nature of the reaction.[24]

We commenced by re-examining the catalyst choice for the reaction (**Scheme 1.37**), with the aim of reaching 100% conversion to allow assessment of the diastereoselectivity. This was achieved through using the active series of catalysts from the earlier screen. Pleasingly, the most electron-poor complex, **78a** delivered complete conversion with a remarkable 99:1 d.r. favouring the product formed *via* alcohol-directed hydrogenation, with more electron rich complexes **78b-c** and **91a-b** failing to achieve complete consumption of the starting material **24**. For clarity, only the results with complexes bearing the PF_6 counterion are displayed, and the results for the corresponding BArF complexes are tabulated in the Experimental Section.

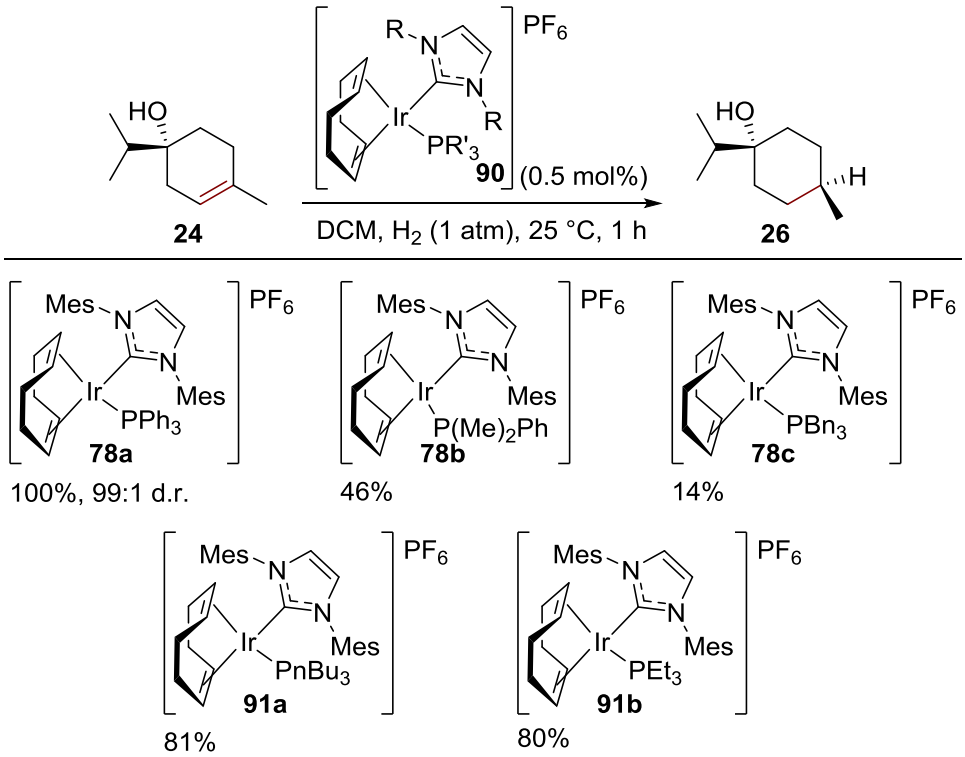

Scheme 1.37 Further investigations of the diastereoselective hydrogenation.

With a good substrate scope established, we next turned our attention to a key parameter that limits many hydrogenation methods: the narrow scope of applicable solvents.[84,85] Our recent work in the area of hydrogen isotope exchange has shown that the catalysts featuring the more non-coordinating BArF counterion can perform in a much broader range of solvents than the parent PF_6 complexes.[73] Therefore, to extend and improve the solvent scope in the present study, the hydrogenation of **85** was performed under our optimised protocol in 17 different solvents (including chlorinated, aromatic, cyclic ether, non-cyclic ether, ester, alcohol, and carbonate-based solvents) with both complex **91f** and **78b** and, for comparison, the widely-used Crabtree's catalyst **20**, and its BArF counterion analogue **96**[86] (**Scheme 1.38**, **Graph 1.3**). We were pleased to find that in every case, our newly developed catalyst system **91f** outperformed the parent PF_6 analogue **78b**, and both Crabtree's catalyst **20** and the BArF counterion analogue **96**. Secondly, and more importantly, under the optimised conditions, complete conversion was achieved by using catalyst **91f** in a practically appealing, and broad range of solvents. Notably, the solvents which gave the most effective reduction process are always the larger, less coordinating variant in each given class (e.g., t-amylOH>EtOH; i-PrOAc>EtOAc; and CPME>Et_2O). This trend indicates that complexation and decomplexation of the solvent is also an important factor,[87] and the more non-coordinating the solvent, the higher the catalyst activity.

Having previously established a different catalyst was necessary for the diastereoselective hydrogenation of **24**, we also hypothesised that a different solvent dependence was likely and, indeed, that the choice of solvent could impact upon the diastereoselectivity. Therefore, the same range of solvents was assessed for the hydrogenation of **24** with BArF complex **82c** (**Scheme 1.39**, **Graph 1.4**). We were again pleased to find a broad range of solvents capable of delivering excellent conversion and high diastereoselectivity. Only two solvents (PhMe and EtOH) out of those tested proved ineffective, with conversions below 40% and a significant decrease in diastereoselectivity. In the case of ethanol, this can be attributed to solvent versus substrate competition in binding to the catalyst, with the reverse being true of toluene.

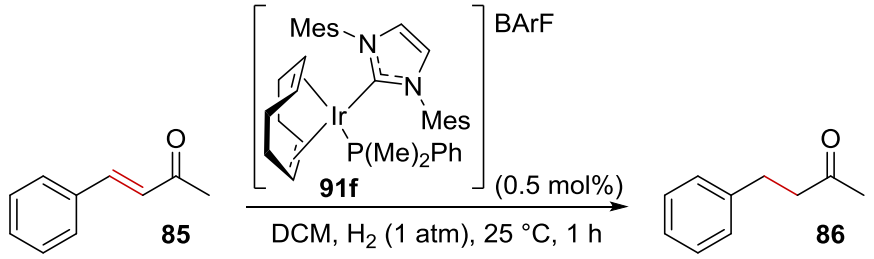

Scheme 1.38

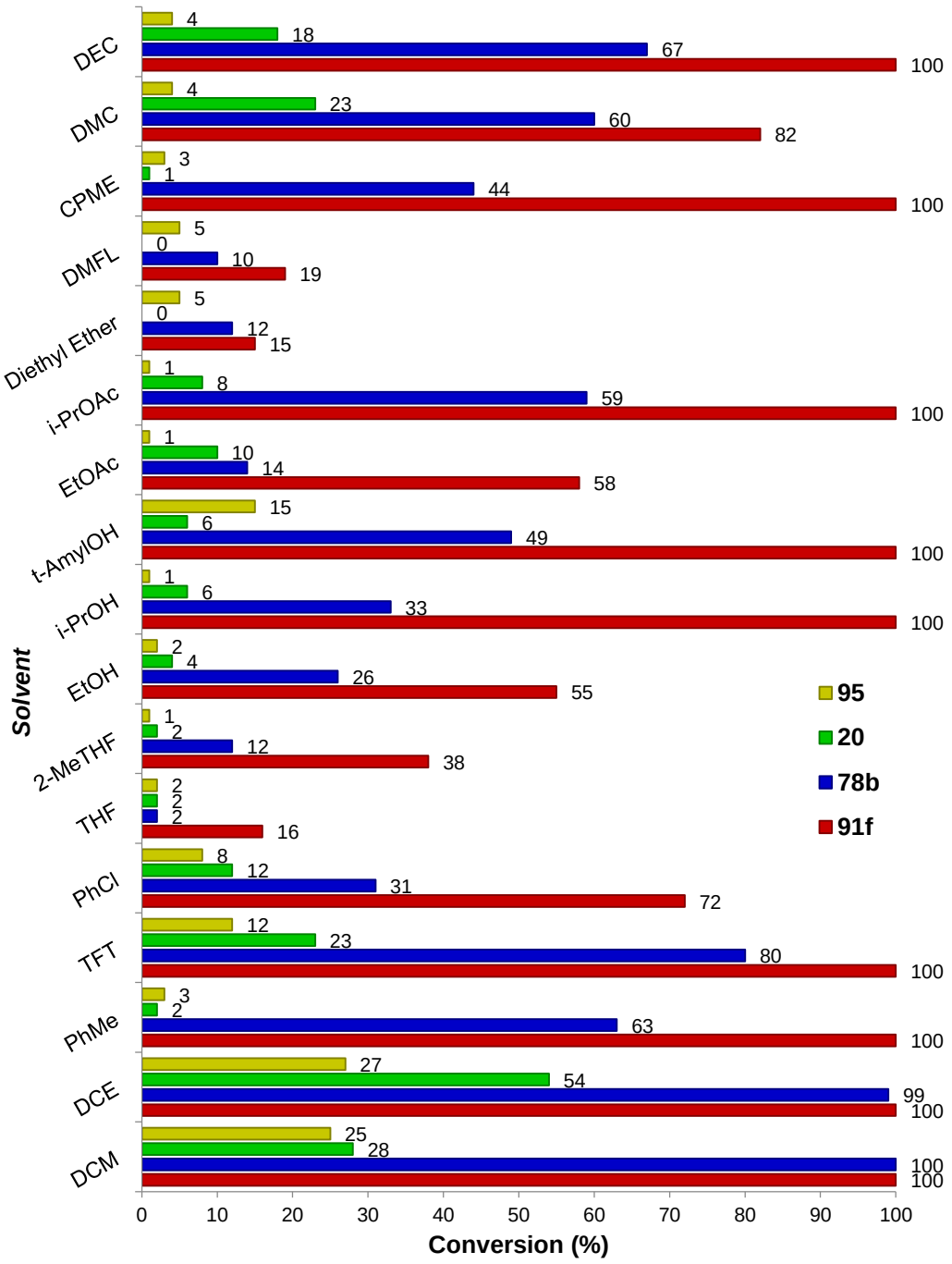

Graph 1.3 Solvent diversity in directing group assisted hydrogenation.

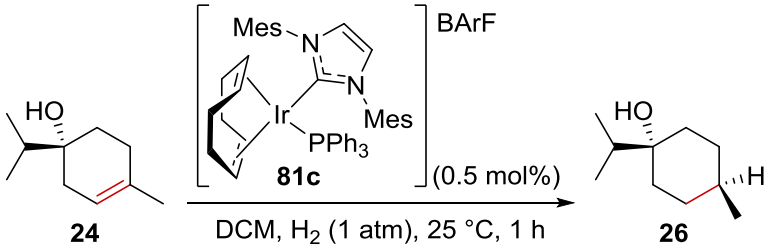

Scheme 1.39

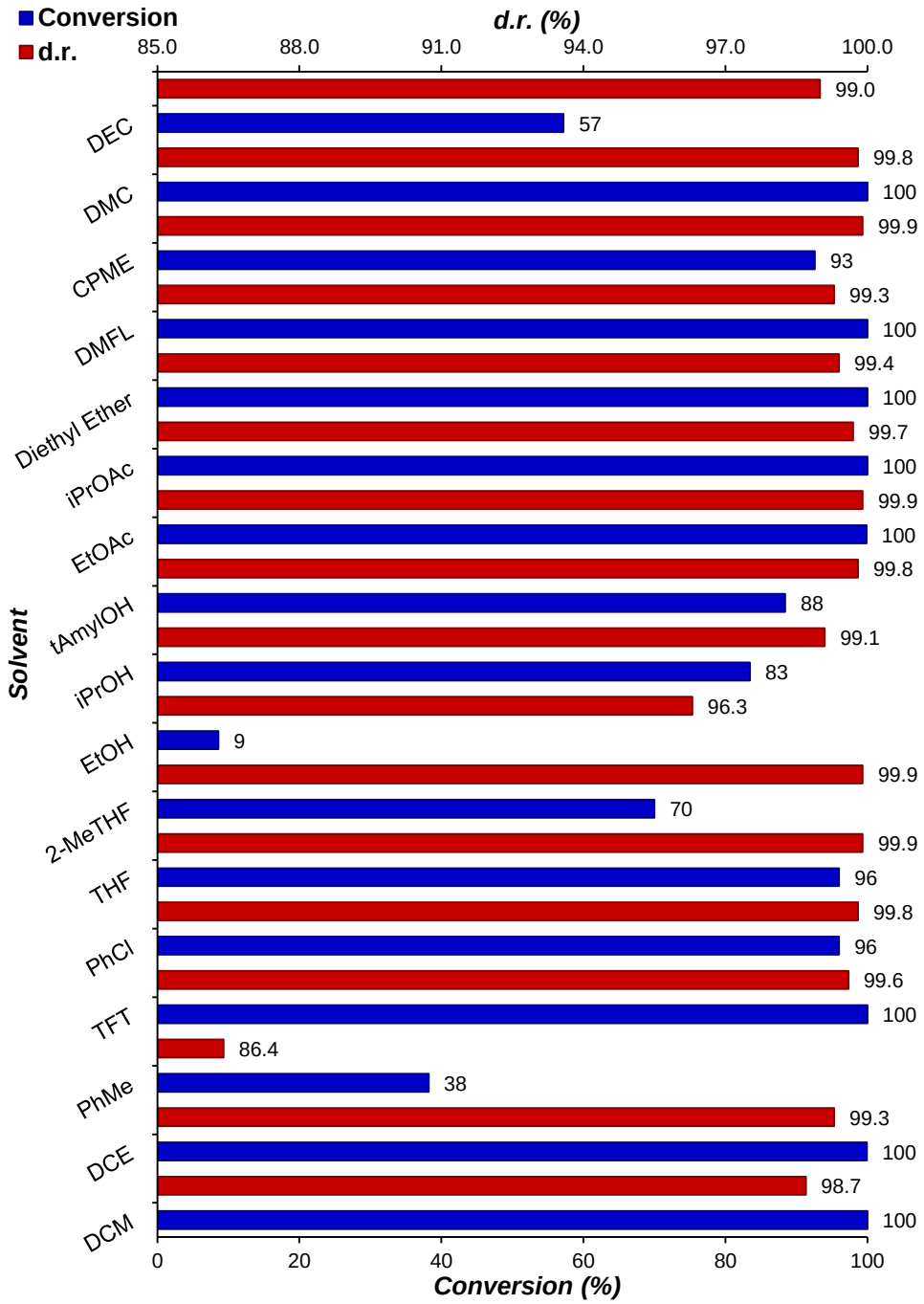

Graph 1.4 Solvent diversity in diastereoselective hydrogenation.

Having established a catalyst system that can mediate the efficient, selective hydrogenation of olefins, we turned our attention to investigating the wider chemoselectivity of this process. To ascertain the level of effectiveness in this regard, a series of competition reactions were performed utilising (*E*)-stilbene **93**, as an olefin without a directing group, against unsaturated compounds **84**, **85**, **97e**, **97g**, and **97l-n**, possessing a range of directing groups (**Table 1.8**). Our first comparison resulted in a high level of selectivity for reduction of the olefin within enone **85**. The smaller and more electron-rich enone **97e** improved upon this selectivity, with only very small amounts of **94** observed. Utilising related chalcone **97g** resulted in a decrease in selectivity, potentially due to a weaker directing group complexation. The weakly-coordinating acid **97l** showed a moderate selectivity, while the related ester **84** delivered a reverse in selectivity to favour the reduction of **93**. This reverse in selectivity can be attributed to the lack of coordination by the ester donor group in directing the hydrogenation process, with the selectivity being determined solely by the more electron-rich olefin **93** reacting preferentially. The strongly-coordinating amide donor group was found to give excellent selectivity for the hydrogenation of **97m** over **93**, whereas the poorly coordinating nitro group in **97n** gave only a moderate selectivity for the directed hydrogenation process.

The breadth of directing group scope studied within this series of competition reactions allowed us to develop the hypothesis that coordination of the substrate to the catalyst is critical in determining the observed selectivity. Based on this proposal, we postulated that this selectivity could be manipulated through the choice of solvent. To test this hypothesis, a second set of competition reactions were performed, employing a series of alcohol solvents with increasing coordinating abilities, in the order *t*-amylOH, i-PrOH, and EtOH. In the hydrogenation of **85** vs **93**, a moderate selectivity was observed in t-amylOH. This selectivity was, however, improved upon moving to the more coordinating i-PrOH; pleasingly, the best selectivity was observed with the most coordinating solvent, EtOH. This series of results suggests that the ability of a substrate to undergo hydrogenation is dependent upon displacement of the ligated solvent. Furthermore, this solvent displacement is more readily achieved by a coordinating directing group than a more weakly coordinating olefin. However, further studies with a broader range of solvents showed that non-coordinating solvents, such as toluene, can also improve the chemoselectivity, and this appears contrary to our

hypothesis of solvent co-ordinating ability. We therefore propose that a low dielectric constant partially contributes to the selectivity in the absence of a co-ordinating group in the solvent, as indicated by the lower dielectric constant of toluene (DCM: 9.14, EtOH: 25.3, and toluene 2.385).[88]

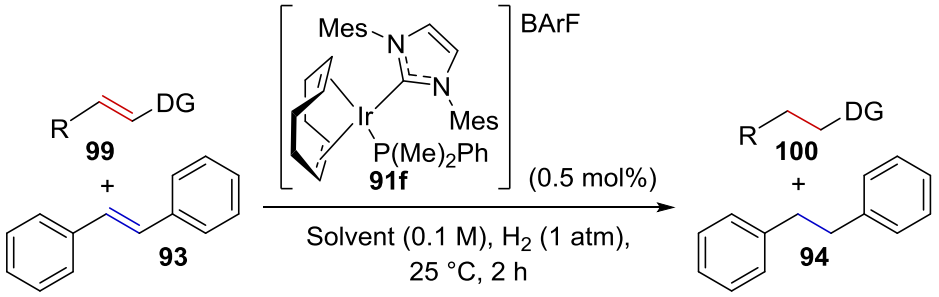

Substrate	*Solvent*	*R*	*DG*	*Selectivity (100:94)*
85	DCM	Ph	COMe	87:13
97e	DCM	n-Pr	COMe	98:2
97g	DCM	p-Tol	COPh	84:16
97l	DCM	Ph	CO_2H	76:24
84	DCM	p-BrC_6H_4	CO_2Et	7:93
97m	DCM	Ph	$CONEt_2$	96:4
97n	DCM	Ph	NO_2	66:34
85	t-AmylOH	Ph	COMe	81:19
85	i-PrOH	Ph	COMe	86:14
85	EtOH	Ph	COMe	95:5
85	PhMe	Ph	COMe	94:6
97g	PhMe	p-Tol	COPh	93:7
97n	PhMe	Ph	NO_2	77:23
Selectivity calculated from GCMS analysis of crude reaction mixture.				

Table 1.8 Chemoselectivity investigations; the effect of different directing groups and solvents.

A thorough investigation of our NHC phosphine catalysts in directing group assisted hydrogenation has delivered an efficient protocol that was applied with a variety of substrates and reaction solvents to good effect. Furthermore, the study has indicated that the directing group and the solvent both play a major role in deciding hydrogenation selectivity. With this in mind, we wished to exploit the increasing number of chiral NHCs to synthesise a complex capable of performing asymmetric hydrogenation reactions.

3.3.Asymmetric Hydrogenation

Within the field of iridium hydrogenation catalysts, there are, to our knowledge no examples of chiral-NHC/phosphine complexes where the two ligands are separate, as opposed to a chelate. Indeed, there is but a single example by Herrmann, of a C_2-symmetric monodentate NHC/chloride iridium complex in hydrogenation, and which delivers only moderate reactivity and enantioselectivity.[89] However, from our previous studies, we recognised the increased activity of NHC/phosphine complexes over NHC/Cl complexes in HIE,[71,90] and as such, we envisaged a new series of catalysts developed around this same principle.

Prior to commencing the synthesis of a chiral NHC complex, we wished to further investigate further the *N*-subsituent effect in imidazole derived NHC's. It was already understood that di-(alkyl) NHC/phosphine complexes delivered poor reactivity, necessitating the use of IMes instead. However, could we substitute only one arm of the NHC with an alkyl unit and still maintain reactivity? To answer this question, we applied a series of unsymmetrical imidazolium halides **101** to our one-pot conditions, generating a seires unsymmetrical NHC/phosphine complex **104a-f** (**Scheme 1.40**). Pleasingly, each imidazolium salt, bearing methyl, iso-propyl or benzyl, was obtained in an excellent yield when combined with triphenylphosphine, generating complexes

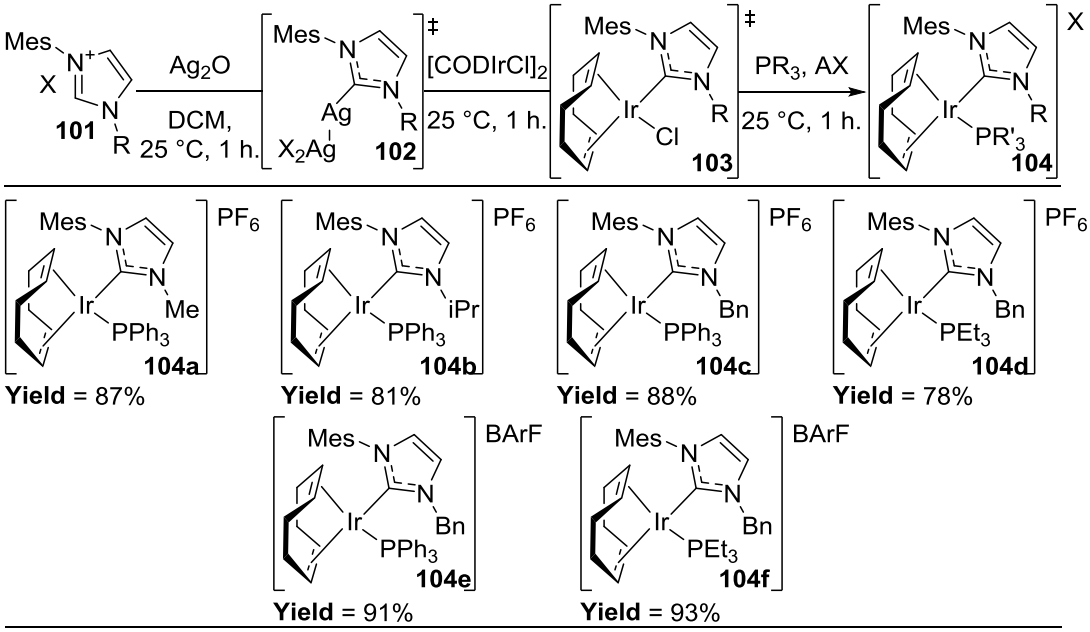

Scheme 1.40 Synthesis of novel, unssymmetrical NHC/phosphine complexes.

104a-c. Moreover, the combination of a more electron rich phosphine in **104d**, different counterion, **104e**, or both, **104f**, delivered similar yields.

However, in a similar fashion as for IMes itself, when testing the synthesis with imidazolium halide **105**, our one-pot procedure failed (**Scheme 1.41**). Instead, reverting to the previous method, and isolating the NHC/chloride complex **106** prior to halide abstraction by $AgPF_6$ and argon filtration to install the phosphine, delivered complex **104g** in good yields.

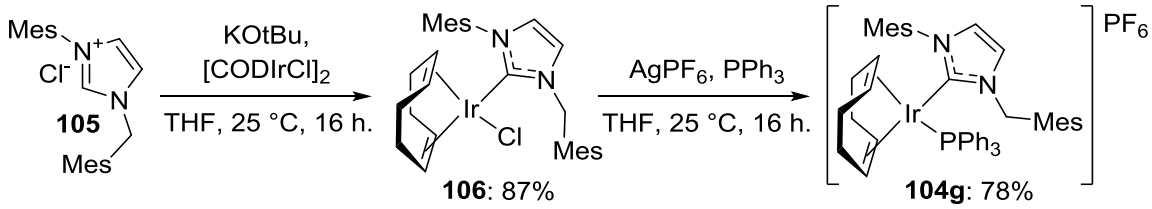

Scheme 1.41 Two step synthesis of bulky, unsymmetrical NHC/phosphine complex **104g**.

To allow comparisons to be drawn from our previous findings, the same two model alkenes were applied in hydrogenation with our new complexes **104a-g** (**Scheme 1.42**). In comparing the different NHCs, it is clear that reactivity is intermediate between a alkyl NHC and IMes. Furthermore, the mesityl-benzyl NHC complex **104c** is the most reactive, compared with the smaller, **104a-b**, or larger, **104g**, complexes. However, the greatest improvement in the hydrogenation of **93** is through application of a smaller, more electron rich phosphine complex **104d**, further reflected in the use of BArF counterion complex, **104f**. However, the hydrogenation of **85** is limited to ~30% with **104c**, with no improvement upon application of BArF complex **104e**. This indicates that a larger NHC, such as IMes, is required for complete conversion, as in the previous application of complex **91f**. Despite this, we progressed to the synthesis of a chiral NHC.

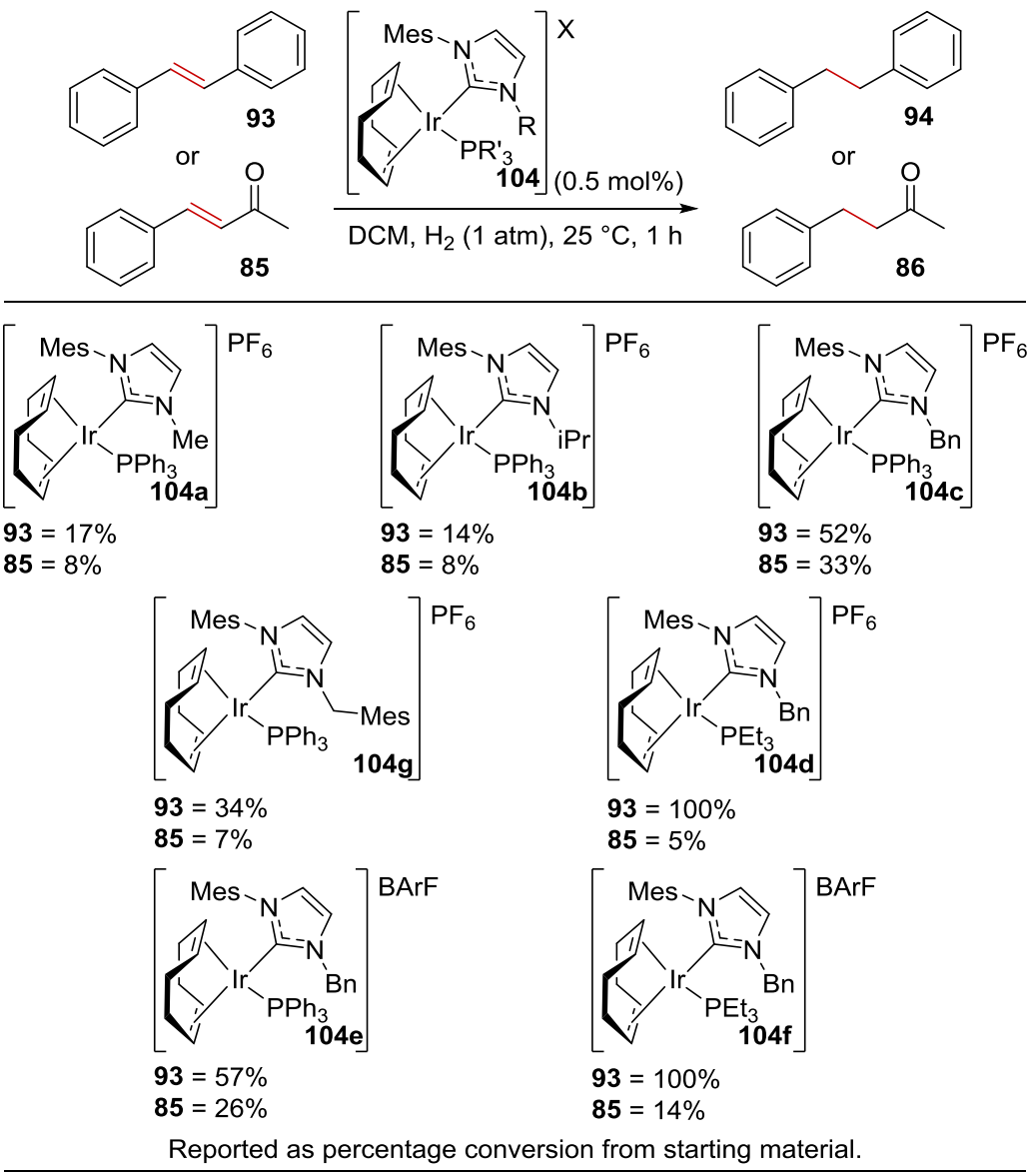

Scheme 1.42 Investigating non-chiral, unsymmetrical NHCs in alkene hydrogenation.

Recognising that our ideal chiral-NHC must bear an *N*-mesityl group, we explored the vast array of chiral imidazolium salts available within the literature.[76,77] Through this, we arrived at a series first reported by Glorius *et al.* in the enantioselective arylation of amides.[91] The reported ligand contained the required *N*-mesityl group, with a fused imidazole/oxazolidine system bearing the chiral arm, derived from readily available amino acids. Furthermore, when comparing the steric map of IMes **45**, with the free NHC **105**, it showed a good steric bias, as required for a highly enantioselective processes (**Figure 1.24**).[92] Moreover, the uniform bulk delivered from the *N*-mesityl group was largely unchanged when compared to the parent ligand.

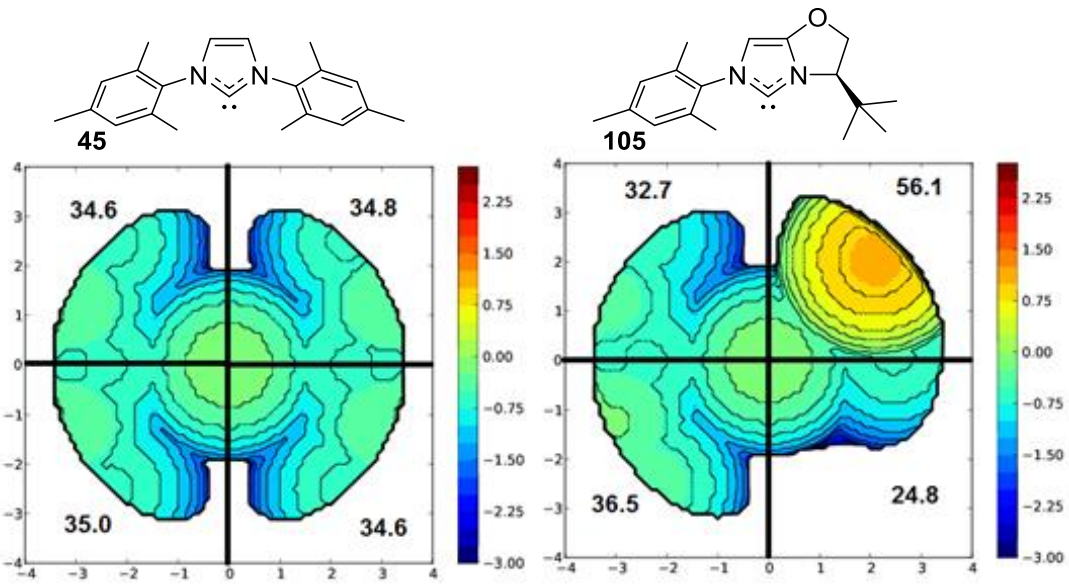

Figure 1.24 Comparision of the steric map of IMes **45** and chiral NHC **105**.

Convinced that we had chosen an appropriate ligand, we followed a modified literature procedure to synthesise imidazolium triflates **112** and **113**,[91,93] derived from valine **106** and *tert*-leucine **107**, respectively (**Scheme 1.43**). The synthesis began with a quantitative, lithium aluminium hydride reduction of the amino acids **106** and **107** to amino alcohols **108** and **109**. Next, the thermal cyclisation to form hydroxymethyl oxazolines **110** and **111** was observed to proceed best with the greater steric bulk of amino alcohol **109**. Following distillation of **110** and **111**, subsequent oxidation to the aldehyde, imine formation with mesitylamine and cyclisation, provided imidazolium triflates **112** and **113** in good yields, over three steps carried out in succession due to the low stability of the aldehyde and difficulties in isolation of the imine.

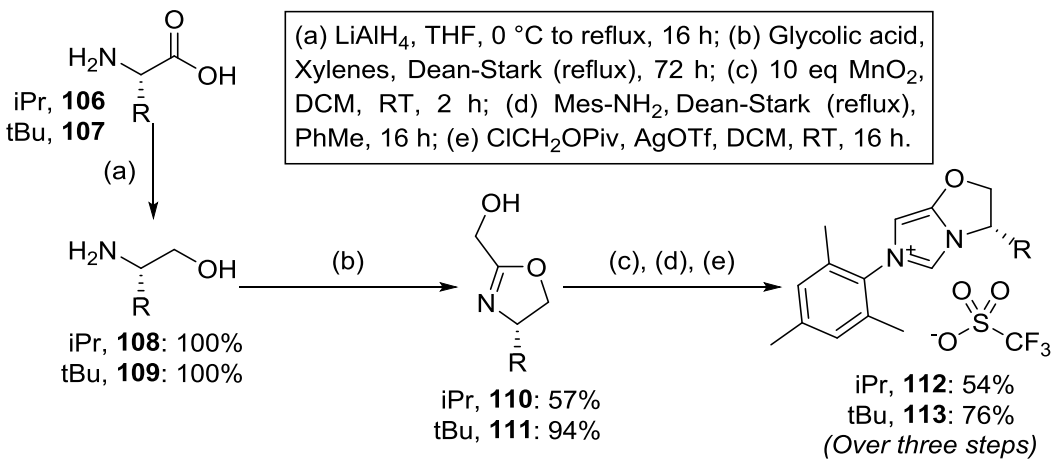

Scheme 1.43 Synthesis of chiral imidazolium triflates **112** and **113**.

Following the formation of imidazolium salts **112** and **113**, the synthesis of the complete NHC/phosphine complex **118a-e** and **119a-e** was attempted (**Scheme 1.44**). However, realising that the triflate anion was incompatible with our one-pot method, we instead applied the *in situ* generation of the free carbene through application of KO*t*Bu, to generate the novel NHC/chloride complexes **114** and **115** in good yields. This then permitted the use of our second new protocol, avoiding the need for a silver

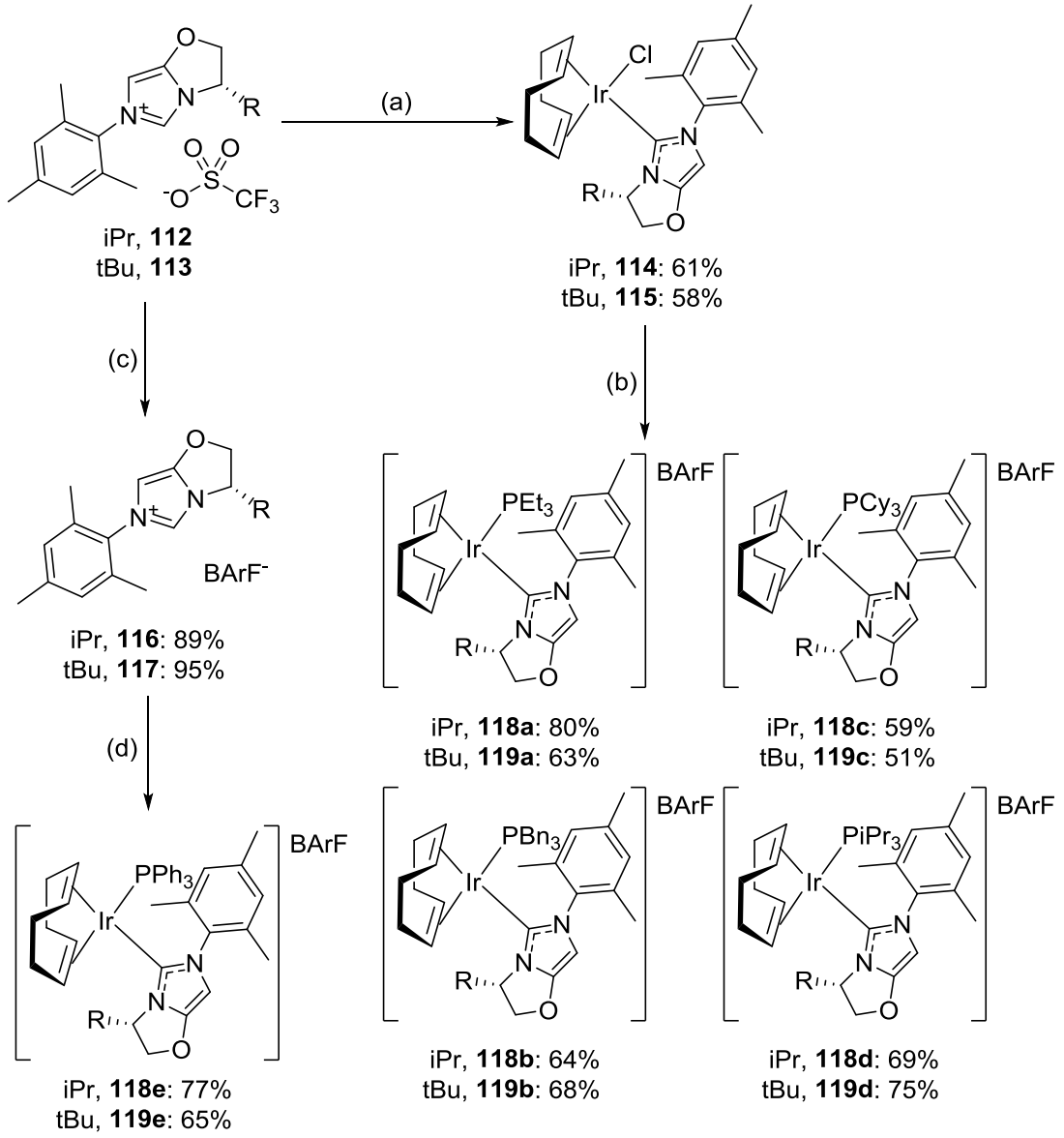

Scheme 1.44 Synthesis of chiral-NHC/phosphine complexes **118a-e** and **119a-e**.

NHC/phosphine complexes **118a-d** and **119a-d**. Furthermore, wishing to access the triphenylphosphine analogues, we synthesised the BArF imidazolium salts **116** and **117**, for use in the previously reported one-pot procedure,[73] subsequently generating complexes **118e** and **119e** in excellent yields. Each complex was delivered as a mixture of diastereomers, believed to arise from the restricted rotation of the metal-ligand bonds. However, *in-situ* transformation to a octahedral hydride complex to allow

rotation of the metal-ligand bonds delivered a single compound, confirming our hypothesis and the catalyst purity.

Pleased that we had gained access to ten new, chiral NHC/phosphine complexes **118a-e** and **119a-e** and two novel, chiral NHC/chloride complexes **114** and **115**, we applied them in asymmetric hydrogenation. In the first instance, we investigated the hydrogenation of model terminal alkene **69d** (**Scheme 1.45**). Unsurprisingly, given our previous investigations, NHC/chloride complexes **114** and **115** failed to react. However, application of NHC/phosphine complexes **118a**,**c-e** delivered complete conversion to production **120**. Promisingly, moderate enantioselectivity was also observed, to a maximum of 51% e.e. with tricyclohexylphosphine-containing complex **118d**. However, we were then somewhat surprised to find that the selectivity decreased with the application of the bulkier *t*Bu-NHC complexes **119a**,**c-e**.

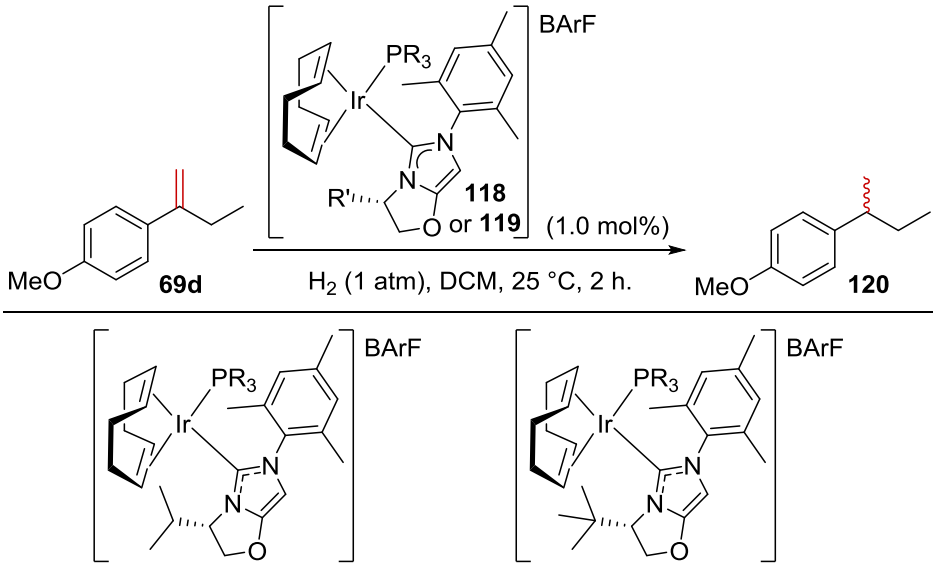

Cl, **114**: <5%, N/A
PEt_3, **118a:** >99%, 37% e.e.
PPh_3, **118e:** >99%, 36% e.e.
PCy_3, **118c:** >99%, 51% e.e.
$PiPr_3$, **118d:** >99%, 13% e.e.

Cl, **115**: <5%, N/A
PEt_3, **119a:** >99%, -12% e.e.
PPh_3, **119e:** >99%, -4% e.e.
PCy_3, **119c:** >99%, 2% e.e.
$PiPr_3$, **119d:** >99%, 8% e.e.

Reported as percentage conversion from ^{1}H NMR and e.e. from HPLC.

Scheme 1.45 Asymmetric hydrogenation of terminal alkene **69d**.

Considering the large variation in selectivity, and the seeming lack of trend in the ligand structure, we hypothesised that an alkene isomerisation maybe occurring which would decrease the selectivity. However, by performing the reaction under a deuterium

atmosphere, we detected no isotopic incorporation at positions other than those associated with hydrogenation of the terminal alkene **69d** (**Scheme 1.46**). With this in mind, we must conclude that our new catalyst structure does not contain the correct steric environment for highly enantioselective terminal alkene hydrogenation, and further catalyst design is required.

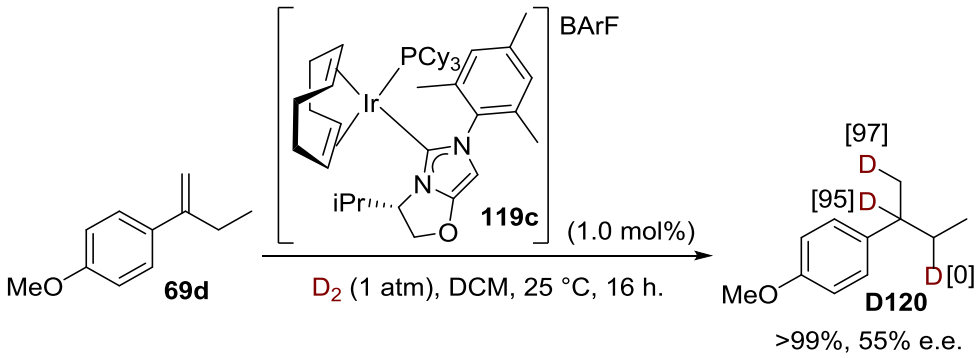

Scheme 1.46 Probing the hydrogenation reaction of terminal alkenes to discount isomerisation.

In further investigations, we tested our new catalyst system on substrates containing an appropriate group to direct the hydrogenation. Indeed, from our previous studies, we had successfully carried out the hydrogenation of a trisubstituted enone, and, as such, began this next investigation with the asymmetric hydrogenation of **121** (**Scheme 1.47**). Initial results with triethylphosphine complex **118a** delivered minimal enantioselectivity, but proved the reactivity of our catalyst system by proceeding to full conversion. Additionally, when applying complexes **118b-e** we clearly observed a reverse in enantioselectivity, indicating that the smaller phosphine of **118a**, favours the opposite enantiomer. In addition, an increase in selectivity was noted, upon the increase in phosphine buried volume, up to a promising 76% e.e. with tri-iso-propylphosphine complex **118d**. The notable outlier from this trend is tribenzylphosphine complex **118b**, which can be attributed to the flexible nature of this phosphine, not reflected in its buried volume. Similarly, with complexes **119a-e**, the influence of increasing phosphine size delivered improved selectivity, up to an impressive 91% e.e. with complex **119d**. However, this complex also incurred a reduction in conversion, spurring us to further investigate the conditions for this highly selective asymmetric hydrogenation process.

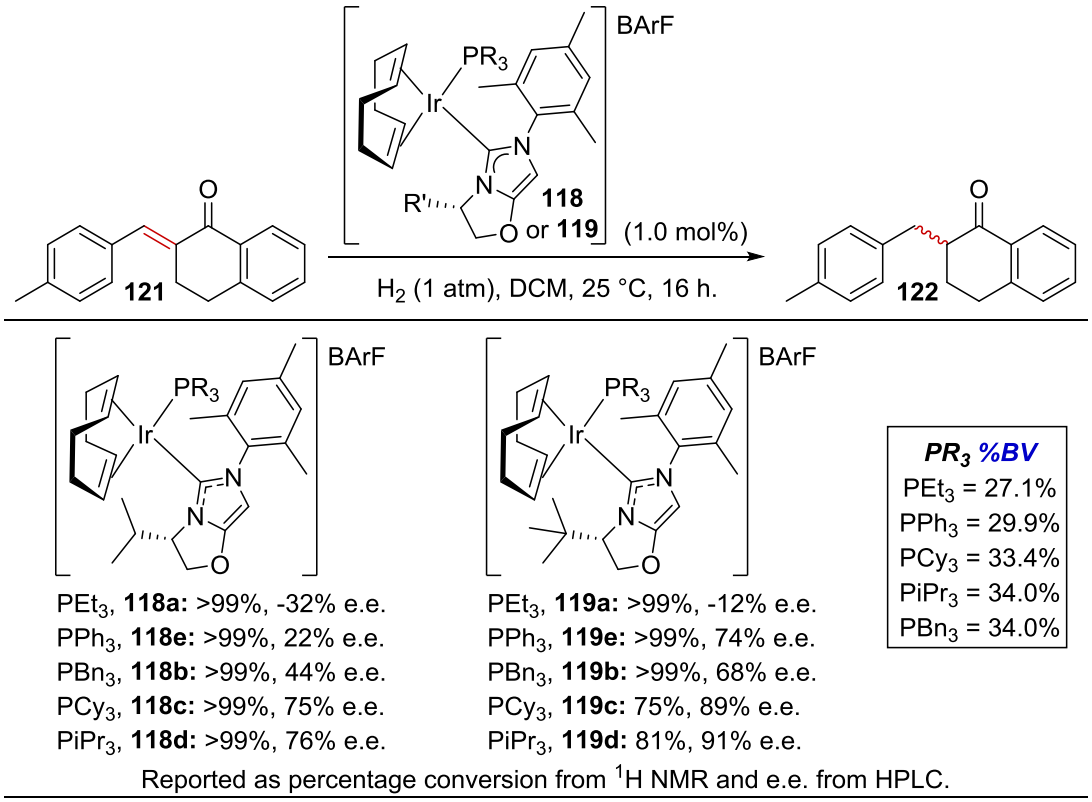

Scheme 1.47 Asymmetric hydrogenation of enone **121**.

We began by investigating the effect that the reaction medium had upon the conversion and selectivity (**Scheme 1.48**, **Graph 1.5**). The study indicated that DCM was the solvent of choice, but could be replaced if necessary with either MTBE, PhCl or t-amylOH with only small decreases in conversion and selectivty. However, i-PrOAc and DMC were not suitable candidates for hydrogenation, delivering low conversion.

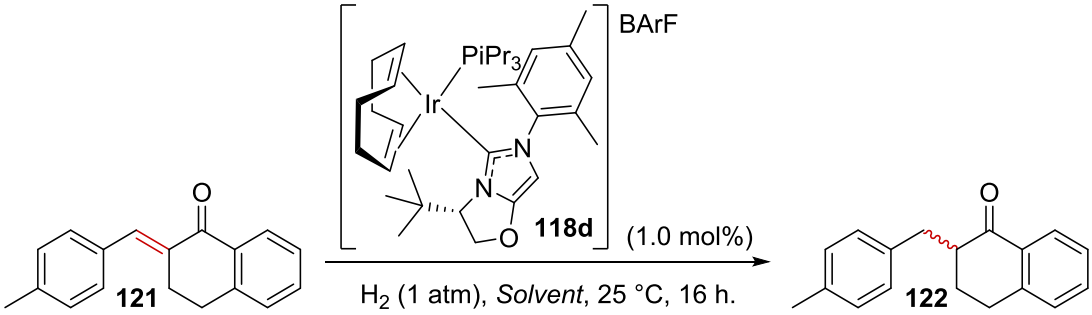

Scheme 1.48

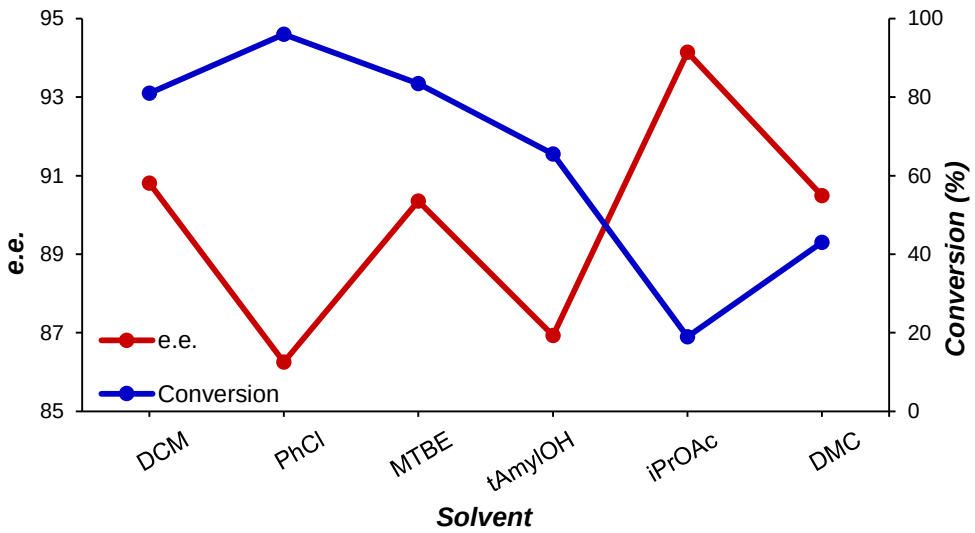

Graph 1.5 Investigating the solvent effect in assymetric hydrogenation.

Continuing in DCM, we next explored the reaction at various times to assess the rate (**Scheme 1.49**, **Graph 1.6**). After just one hour we observed an increased selectivity of 94% e.e. at our typical conversion of ~80%. Furthermore, between 2 and 16 hours, a small but significant degradation of the enantioselectivity is observed, with only a minor increase in conversion. Presumably, this indicates that the catalyst degrades after ~1 hour, generating a complex that has low activity in the reduction of **121**, and generates the opposite enantiomer or racemic product. However, although this indicates a low catalyst turnover number, the turnover frequency is significantly higher than previously expected.

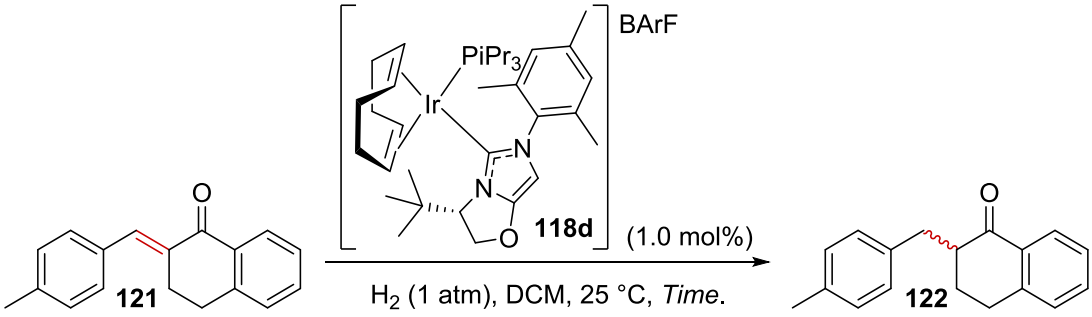

Scheme 1.49

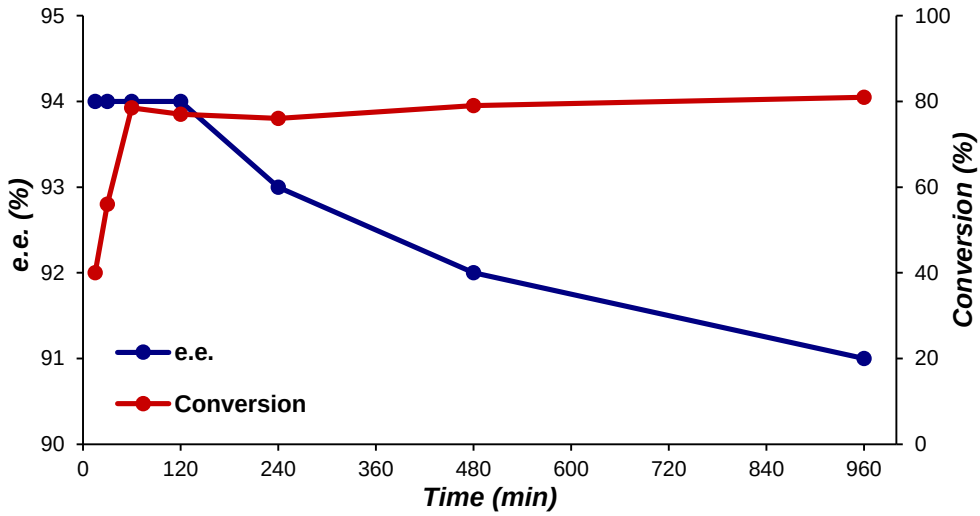

Graph 1.6 Investigating the reaction time for asymmetric hydrogenation.

As such, we next sought to investigate the catalyst loading to bring the reaction to completion (**Scheme 1.50**, **Graph 1.7**). Understandably, increasing the catalyst loading, also elevated the reaction conversion. Furthermore, in agreement with our proposal of a non-selective reduction after catalyst decomposition, increased catalyst loading also improved the selectivity up to 94% e.e.

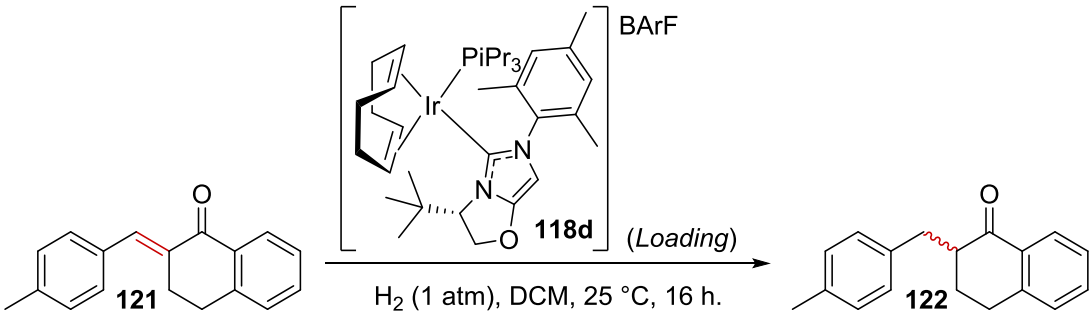

Scheme 1.50

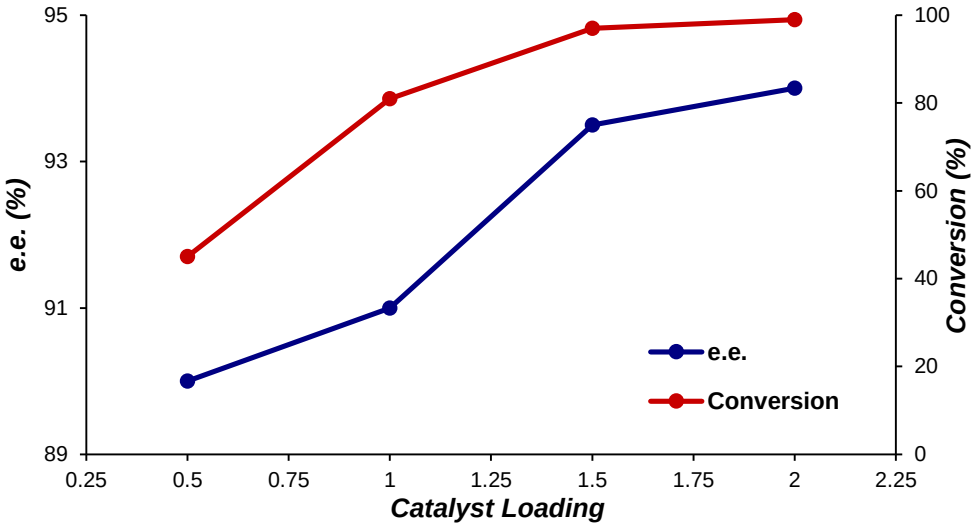

Graph 1.7 Probing the impact of catalyst loading.

Recognising that the reactions could be performed at an increased catalyst loading (2 mol%), and reduced reaction time (2 h) allowed us to better asses the effect temperature had upon the reaction (**Scheme 1.51**, **Graph 1.8**). Pleasingly, reducing the temperature to 0 °C did not impact the reaction conversion, but it did increase the selectivity to 96% e.e. Further reduction in temperature gradually reduced the reaction conversion, however the improvement in selectivity continued up to 99% e.e. at -30 °C, albeit with just an 11% conversion.

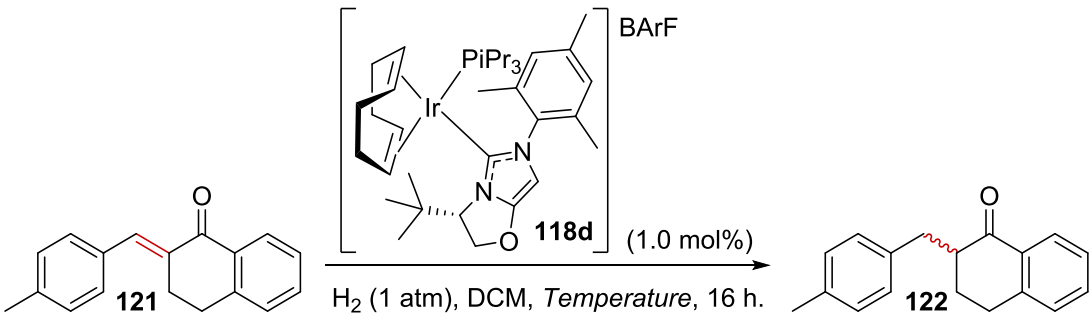

Scheme 1.51

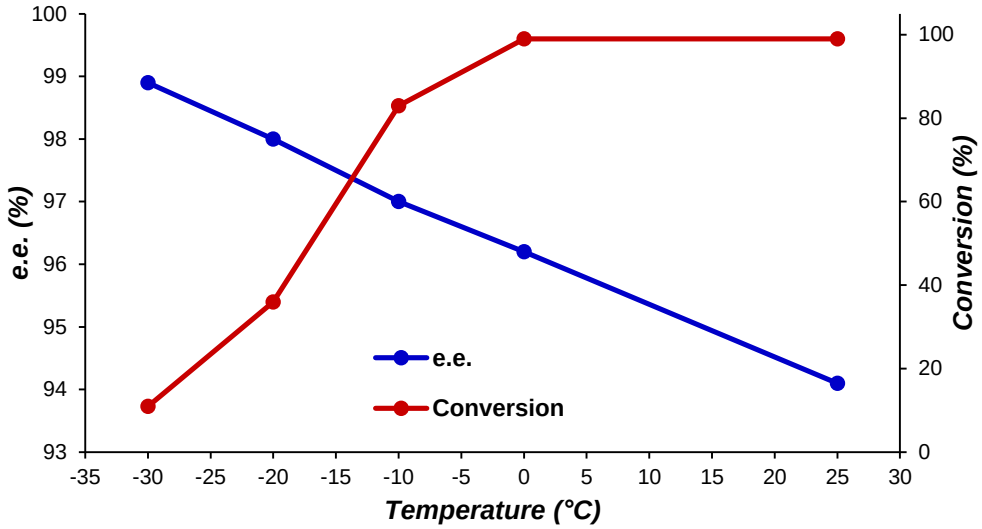

Graph 1.8 Investigating the reaction temperature dependence.

Having developed the conditions to perform an effective asymmetric hydrogenation [**119d** (2.0 mol%), H_2 (1 atm), DCM, 25 °C, 2 h], and recognising that decreasing temperature would increase the selectivity, we next wished to assess modifications to the model substrate (**Scheme 1.52**). Due to time constraints, the study only consisted of variations *β*- to the ketone. However, we were pleased to find that substitution with an electron rich aromatic **123a**, delivered an improvement in selectivity over the model substrate **121**, with the same high conversion. The trend continued with less electron rich aromatics in **123b-123e**. Indeed, with the very electron deficient aryl in **123e**, increased catalyst loading was also required to generate complete conversion. Noticing the dependence upon the substrate electronics, the e.e. was plotted against the Hammett sigma value of each aryl substituent (**Graph 1.9**). The plot clearly indicates the reaction selectivity is not solely controlled by the steric interaction between substrate and ligands, albeit the magnitude of the gradient indicates substrate electronics only plays a minor role. In contrast, steric encumbrance plays a major role, as *ortho*-substituted aryl **123f** and cyclohexyl substituted **123g** were unreactive.

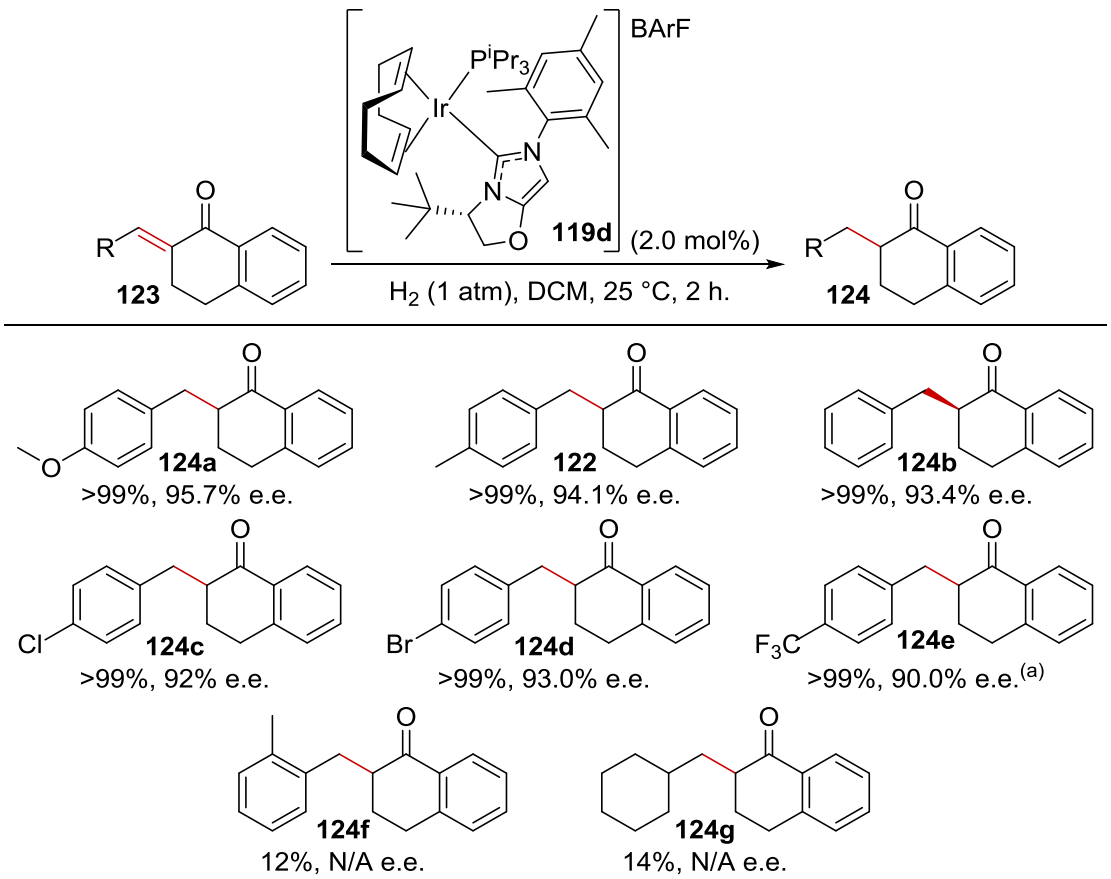

Scheme 1.52 New substrates for asymmetric hydrogenation.

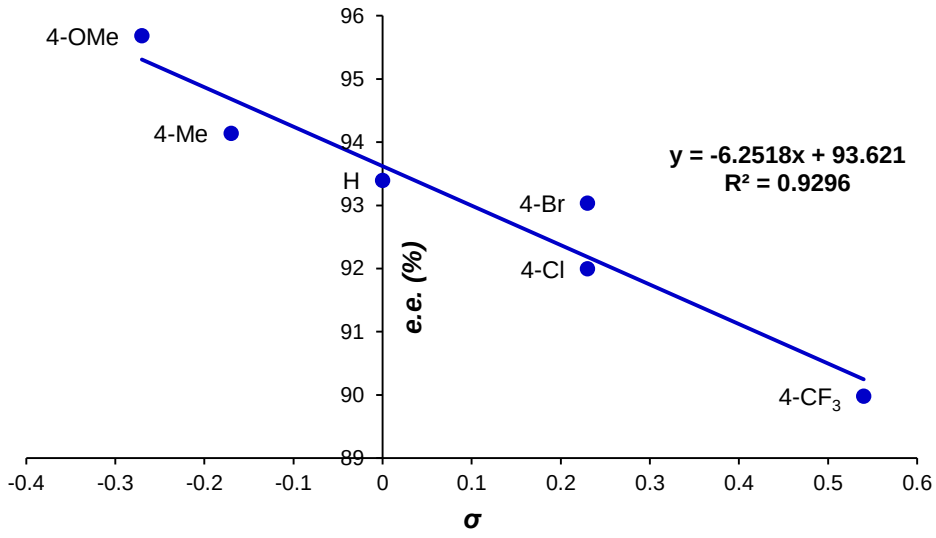

Graph 1.9 Electronic effect of the substrate aryl ring upon enatioselectivty.

With the information garnered through the application of our novel chiral NHC/phosphine complexes and the conditions for asymmetric hydrogenation, we

wished to generate a model explaining the selectivity, and furthermore, use it to predict how new substrates would perform. Our first consideration in doing this was to propose a reasonable mechanism for directing group-assisted hydrogenation (**Scheme 1.53**). Following activation with hydrogen and loss of cyclooctadiene through reduction, substrate complexation delivers octahedral iridium(III) intermediate **A**. Within this intermediate, the two ligands are *trans*-, two hydrides are coordinated equatorially, and the substrate, **85**, twists to occupy the remaining coordination sites with the ketone and alkene. Next, a hydride is transferred to the electronically favoured *β*-position, generating an iridium enolate intermediate, and leaving a free site to be occupied by a solvent molecule, giving **B**. A second molecule of hydrogen displaces the solvent to generate intermediate **C**. Subsequent α-hydride transfer reforms the carbonyl group in **D**, having fully reduced the alkene. The reduced product can then exchange with another substrate molecule to restart the cycle.

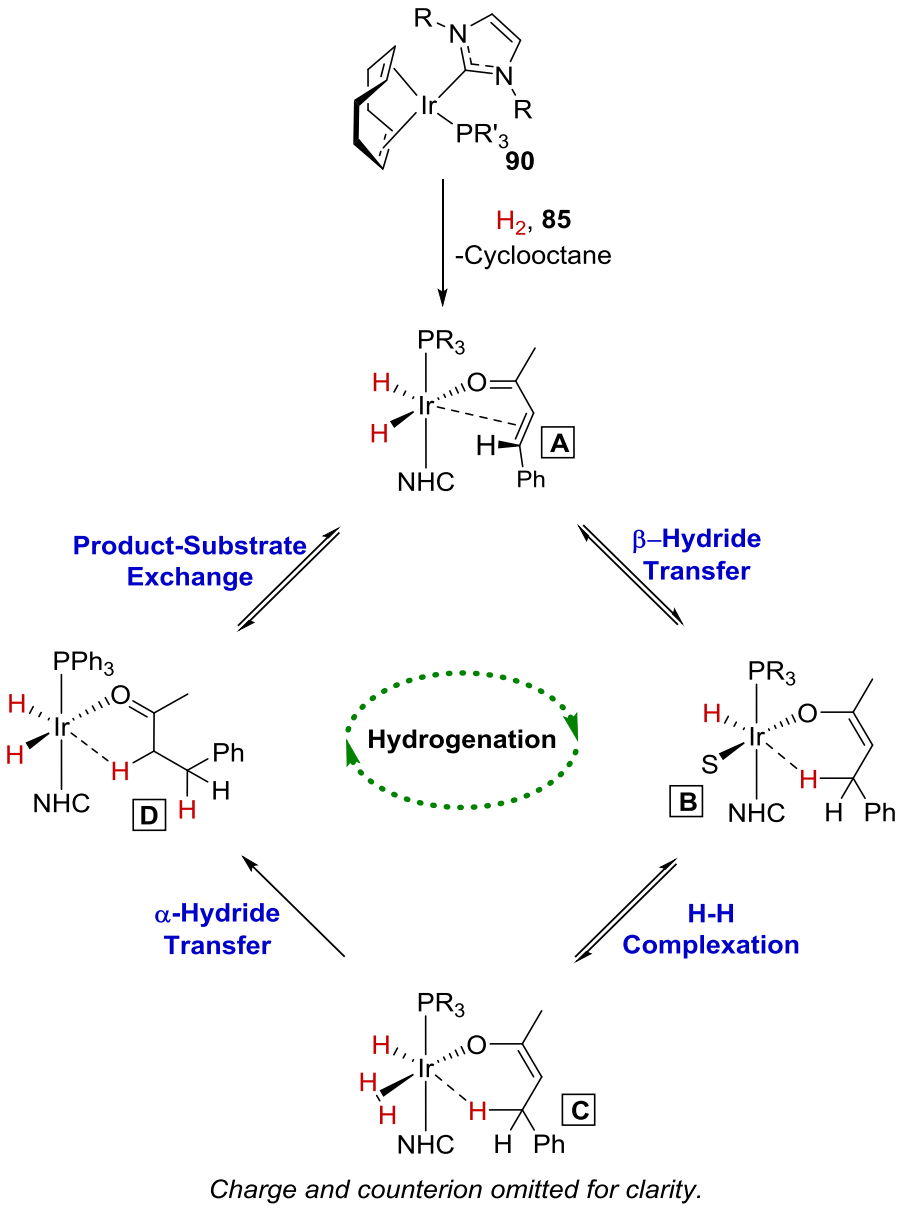

Scheme 1.53 Plausible mechanism for directing group assisted hydrogenation.

Next, if we consider both potential, productive, diasteromeric substrate-catalyst conformers (**A**), to each product enantiomer to be the same in energy and rapidly interchangeable, we can assume the reaction to be under Curtin-Hammett control. Therefore, we can calculate the difference in transition state energies for each respective pathway, using the results of our previous temperature study. Indeed, this difference in transition state energy is calculated to be 2.3 ± 0.2 kcalmol^{-1}. However, we have yet to ascertain if the reaction is under Curtin-Hammett control. Indeed, if the two productive binding isomers are significantly different in energy, the product distribution would be determined by the equilibrium between these conformers.

From the gathered evidence we can apply a similar quadrant model to that used in chelating chiral iridium complexes, controlled by the substrate coordination (**Scheme 1.54**). The new quadrant model is designed based upon a number of factors. Firstly, coordination in the face of the bulky *tert*-butyl group would be disfavoured, suggesting coordination would preferentially occur on the opposite face of the NHC. Furthermore, considering the expected *trans*- structure, and the improvement in selectivity with increasing phosphine size, the two quadrants associated with the phosphine must be sterically encumbered. Finally, coordination adjacent to the *N*-mesityl group is disfavoured over the oxazolidine, as suggested by the buried volume map. Using this model, we can then apply substrate **121** and find the favoured conformer, in which the 4-substituent occupies the least hindered quadrant. This is due to the hydride being delivered to the *β*-position, and therefore that position will be more closely associated with the metal. Following hydrogenation, this conformer would deliver the (*S*) enantiomer **123b**, which matches our experimental findings by comparison of the $[\alpha]_D$.

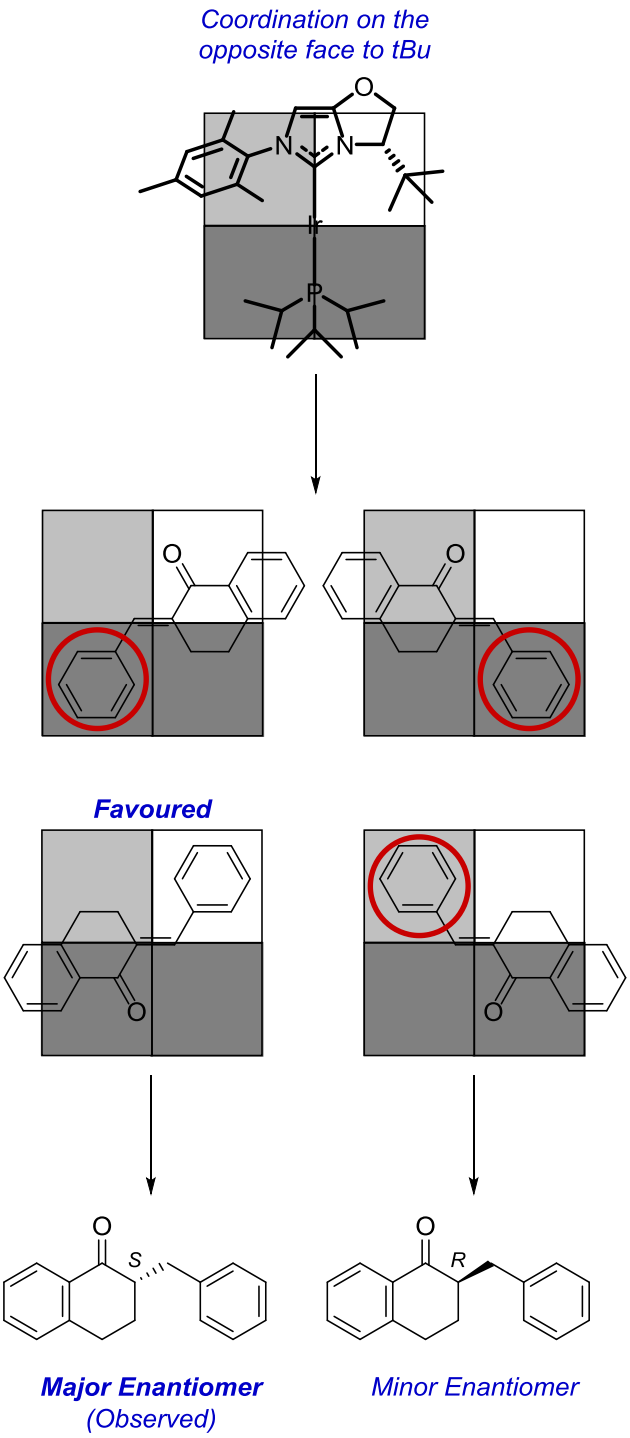

Scheme 1.54 Model for predicting the absolute stereochemistry of assymetric hydrogenation with a NHC/phosphine iridium complex.

4. Conclusions

Throughout this chapter, we have endeavoured to synthesise and test new NHC/phosphine complexes in alkene hydrogenation. In doing so we have developed new organometallic synthetic strategies, and used a range of experimental techniques to improve reaction efficiency and selectivity.

Firstly, we confirmed that the application of a more non-coordinating counterion in hydrogenation engenders an increase in reaction rate, and allowed reactions to be performed at a lower catalyst loading.

Secondly, we developed two new methods for synthesising NHC/phosphine complexes, both of which avoid the use of reactive silver salts, and the highly air- and moisture-sensitive argon atmosphere filtration (**Scheme 1.55**). These new methods proved versatile in allowing a range of NHCs, phosphines and counterions to be combined in the preparation of twenty-two different complexes. Furthermore, each complex was parameterised sterically and electronically, prior to testing in several model hydrogenation reactions. This allowed us to conclude that more electron rich phosphines paired with IMes were optimal, and in fact necessary, for successful alkene hydrogenation.

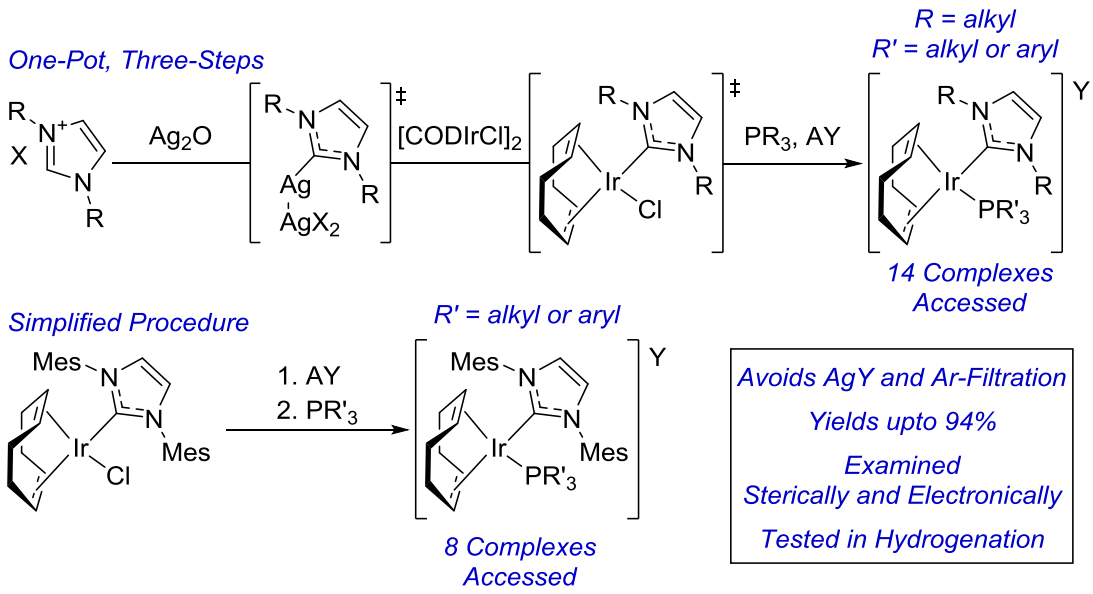

Scheme 1.55 Improved catalyst synthesis, delivering novel complexes.

Through the development of new catalysts, we improved our understanding of the hydrogenation process. This allowed us to design an effective method of directing-group assisted alkene hydrogenation (**Scheme 1.56**). The newly developed process can be performed effectively in a wide array of solvents, and upon a range of alkene substrates. Additionally, the chemoselectivity of the process was investigated and understood to be controlled by both the directing group and the reaction solvent.

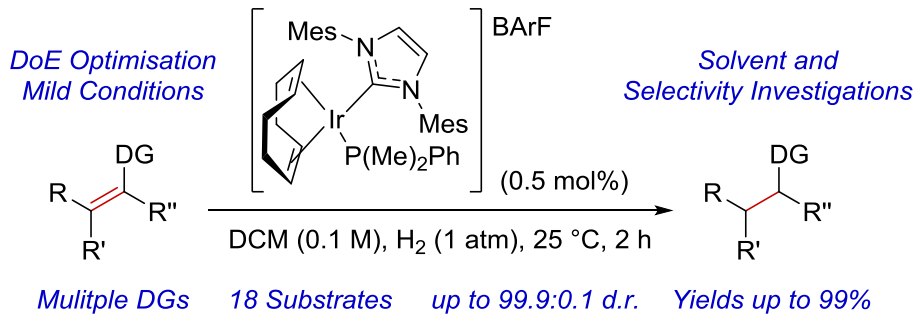

Scheme 1.56 Directing group assisted hydrogenation.

Finally, we applied the new insight gained through the development of new complexes and hydrogenation methods, to synthesise and apply a novel class of chiral-NHC/phosphine complex in asymmetric hydrogenation (**Scheme 1.57**). Development began with the synthesis and testing of a small series of novel, non-chiral, unsymmetrical NHC/phosphine complexes. With the understanding garnered from this study we were able to select an appropriate chiral NHC and design the synthesis of ten new, chiral NHC/phosphine complexes. Furthermore, through extensive experimental investigation, we developed the application of our new catalyst system, delivering a highly selective, directing group assisted, asymmetric hydrogenation process. Finally, our understanding of the hydrogenation process and the proposed mechanism enabled the design of a plausible model for predicting the absolute stereochemistry of this new hydrogenation protocol.

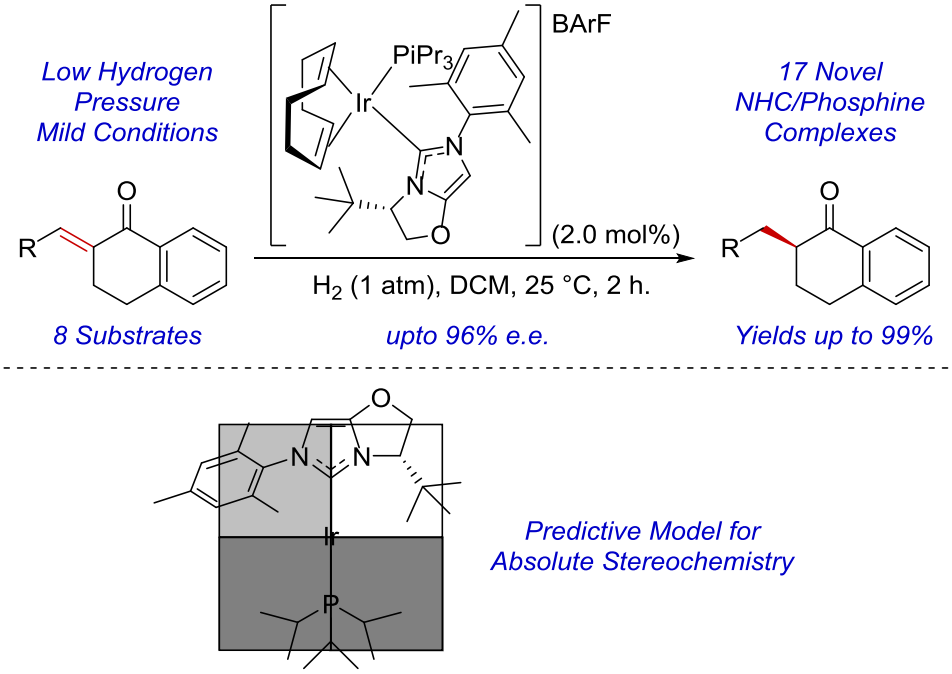

Scheme 1.57 Assymetric hydrogenation.

5. Future Work

Throughout this chapter, the challenge of developing new synthetic strategies for the production of NHC/phosphine complexes was addressed. Furthermore, there has been success in applying them in several different areas of alkene hydrogenation. With this, and our previous work in the area in mind, we now propose a number of potential avenues for further investigation.

Through the development of our directing group-assisted hydrogenation process, we noticed a distinct change in reactivity with allylic alcohols (**Scheme 1.58**). Indeed, they instead underwent the recognised redox isomerisation to generate the corresponding carbonyl, but they could also undergo ether formation, presumably through allylic substitution. As such, further investigation of this new area of reactivity for NHC/phosphine complexes should be explored.

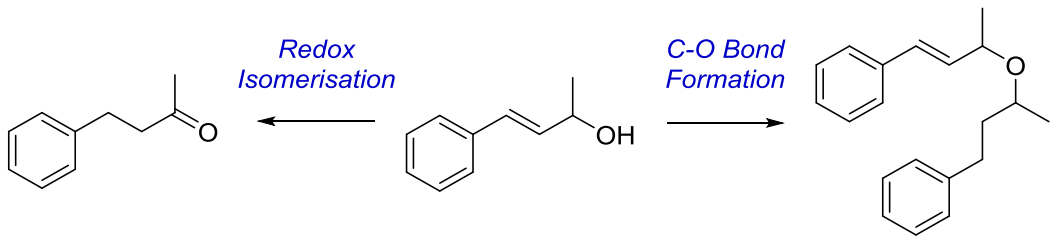

Scheme 1.58 New avenues towards isomerisation and C-X bond formation.

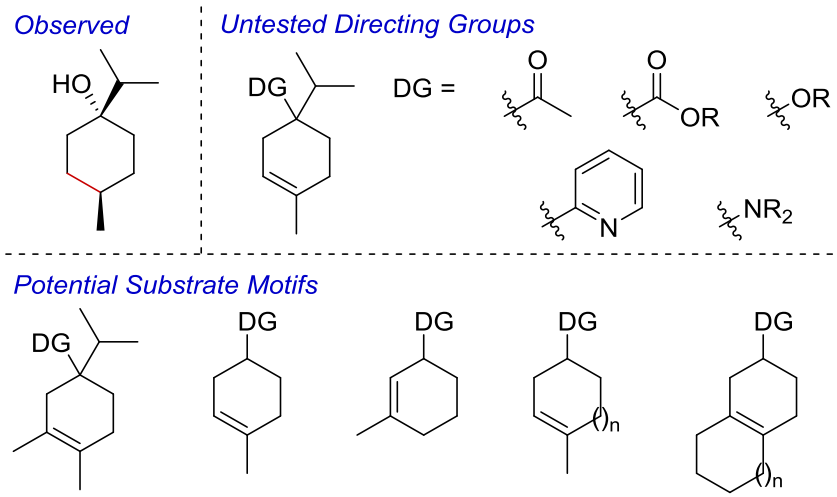

Scheme 1.59 New areas in diastereselective hydrogenation to be investigated.

Secondly, although briefly explored herein, a full examination of the potential application of NHC/phosphine complexes for diastereoselective hydrogenation could

be be explored (**Scheme 1.59**). Such investigation should focus initially on the potential of different directing groups, and expanding the substrate structure away from the model terpinen-4-ol.

In a similar fashion, with the development of our novel chiral NHC/phosphine complexes, we have only just started to scratch the surface of potential applications. Our first concern is the moderate turnover number of the complex, and initial focus should be on understanding the catalyst decomposition and improving catalyst stability (**Scheme 1.60**). Beyond this goal, work should focus upon expanding the potential substrate scope for the new directing group-assisted, asymmetric process, testing the reliability of our proposed mechanism and predictive model (**Scheme 1.61**). Furthermore, the different steric parameters inherent to these complexes, when compared to the more common chelating systems may allow improvements in substrate applicability.

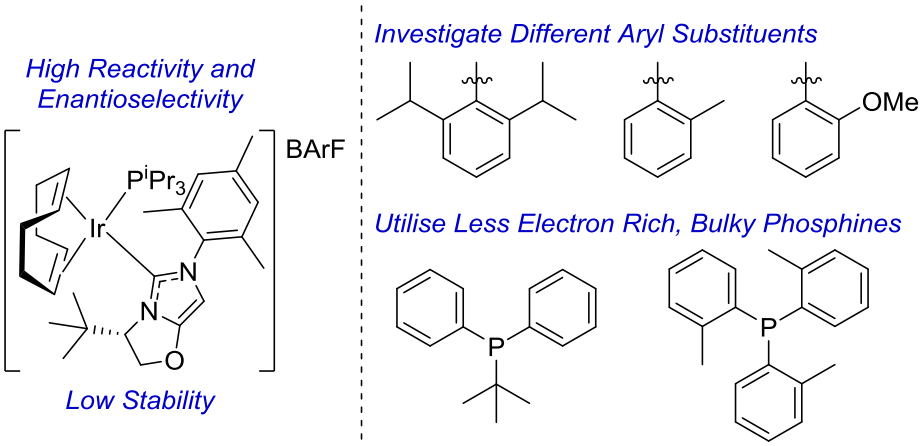

Scheme 1.60 Further work on the structure of chiral NHC/phosphine iridium complexes.

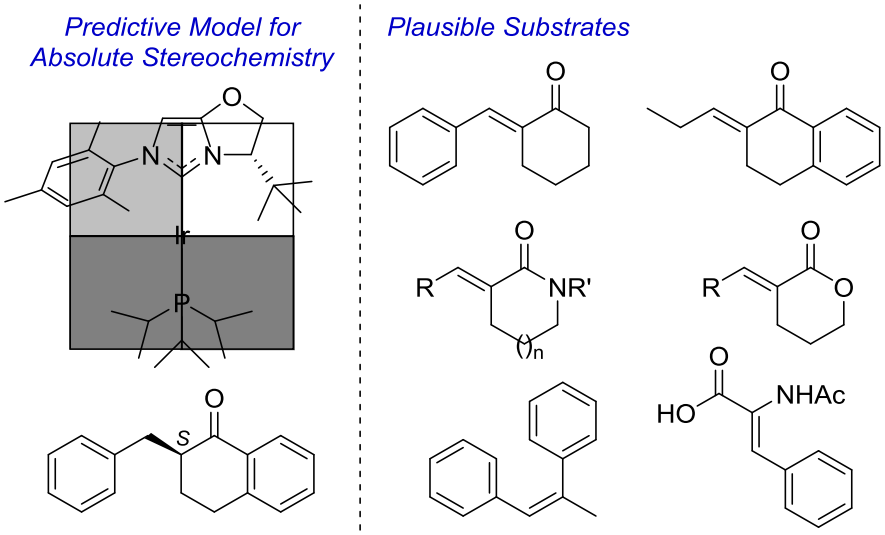

Scheme 1.61 Applications in asymetric hydrogenation.

Finally, with the majority of currently chelating, chiral NHC/phosphine complexes, which bear chirality in the tether, performing poorly in hydrogenation, there is an opportunity for new chelating catalyst structures (**Scheme 1.62**). Indeed, a plausible route to prepare a chelating chiral system modelled upon our new catalysts is proposed below.

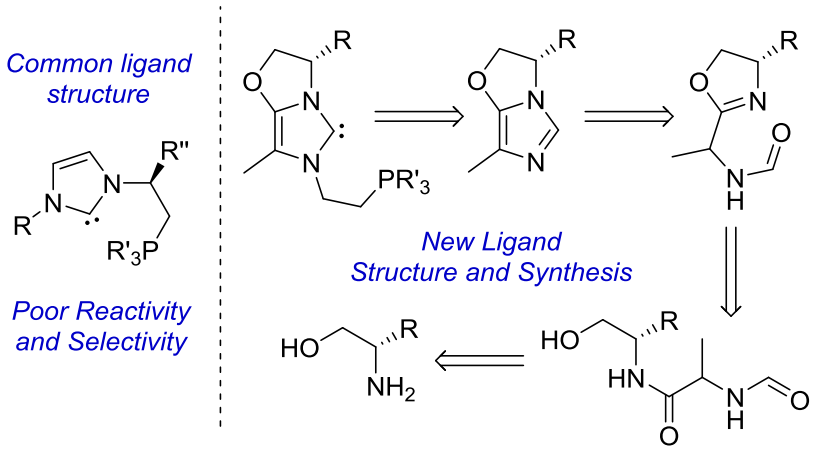

Scheme 1.62 Plausible synthesis of novel, chelating, chiral NHC-phosphine ligands.

6. Experimental

6.1. General Experimental Details

All reagents were obtained from commercial suppliers and used without further purification unless stated otherwise. Purification was carried out according to standard laboratory methods.[94]

Complexes **78a** and **82a-c** were synthesised according to literature procedures.[73]

Hydrogenation reactions were carried out on a Radley's Carousel 12 Plus Reaction Station (**Figure E1.1**).

Figure E1.1

Monitored exchange reactions were carried out using a two-neck round-bottom flask (100 mL) fitted with a double oblique stopcock connected to the manifold and deuterium balloon, and a suba seal.

^{1}H (400 MHz), ^{13}C (101 MHz) ^{31}P (162 MHz,), ^{19}F (376 MHz) and ^{11}B (128 MHz) *NMR* spectra were obtained on Bruker spectrometers in the solvents indicated. Chemical shifts are reported in ppm. Coupling constants are reported in Hz and refer to $^{3}J_{H\text{-}H}$ couplings, unless otherwise stated.

IR spectra were obtained on a Shimadzu IRAffinity-1 Spectrophotometer machine and are reported in cm^{-1} unless stated otherwise.

Thin layer chromatography was carried out using Camlab silica plates coated with fluorescent indicator UV_{254}, and were analysed using a Mineralight UVGL-25 lamp or developed using vanillin, $KMnO_4$ or Ninhydrin solution.

Flash column chromatography was carried out using Prolabo silica gel (230-400 mesh).

Gas chromatography/mass spectrometry was carried out on an instrument fitted with a DB5-type column running a 40-320 ^{o}C temperature program, ramp rate 20 ^{o}C/min with a helium carrier gas flow at 1 cm^3/min. Chemical ionisation (CI) (Methane) mass spectra was recorded on an Agilent Technologies 5975c mass spectrometer.

Gas Chromatograph-FID was carried out on a Hewlett-Packard 5890 Series II instrument fitted with a Varian Capillary Column (CP-Sil 19 CB) column running at 70-220 °C temperature program, ramp rate 12 °C/min with a hydrogen carrier gas pressure of 40 kPa. The flame ionisation detector was set to 220 °C.

Chiral HPLC was carried out on a Gilson model 302 pump, fitted with either a Chiracel OJ or OD-H column, with a flow rate of 1 mL/min eluting with hexane:isopropanol, and analysing with a Milton Roy spctromonitor 3100 UV-detector set at 256 nm or 210 nm.

Mass spectrometry data were acquired from EPSRC National Mass Spectrometry Centre, Swansea University.

General Experimental Procedures

General procedure A *Hydrogenation reactions using Radley's Carousel 12 Plus Reaction Station.*

The Radley's Carousel 12 Plus Reaction Station was evacuated and filled with argon, and the water condenser turned on. To a carousel tube was added the substrate of choice, and iridium catalyst (and additive where appropriate). The desired solvent was added, rinsing the inner walls of the tube. The tube was then sealed at the screw cap (with the gas inlet left open) under argon, and the stirring and the temperature set. The

flask was evacuated and refilled with hydrogen *via* a balloon and this process repeated a one further time. The gas inlet tube was then closed, creating a sealed atmosphere of hydrogen, the timer was initiated and a rapid red/orange to clear/yellow colour change was observed. The reaction mixture was stirred for the allotted time before removing excess hydrogen and replacing with air. The yellow solution was then prepared for analysis by ^{1}H NMR spectroscopy. Following assessment of reaction conversion, if necessary, the product was isolated by column chromatography.

General procedure B *Monitored hydrogenation reactions carried out in a round bottom flask.*

A flame-dried, 100 mL, two-neck round-bottom flask under an argon atmosphere, bearing a double oblique stopcock adaptor and a suba seal, was charged with the desired substrate, catalyst and solvent. Under argon, the flask was cooled to -78 ^{o}C in a dry ice/acetone bath. The flask was evacuated and flushed with hydrogen from a balloon and this process repeated a further two times. After the final flush, the stopcock was left open to the hydrogen balloon and the flask immersed in an oil bath at the desired temperature. The reaction solution was observed to change from a pale orange to clear within 5 min. At predefined time intervals an aliquot (~0.5 mL) was drawn from the reaction *via* syringe, and placed in a ½ dram screw cap vial prefilled with Et_2O (~1 mL). Following removal of the solvent *in vacuo*, the recovered residue was prepared for analysis by ^{1}H NMR spectroscopy.

General Procedure C *One-pot preparation of alkyl-NHC/Phosphine complexes.*

To a flame-dried, argon-cooled schlenk-tube was added silver oxide, imidazolium halide and dry DCM, the mixture was observed to change from black to a clear/grey solution after 1 h. Iridium cyclooctadiene chloride dimer was added and the reaction progressed to a bright yellow colour. After 1 h, the phosphine was added followed by addition of the salt, initiating a yellow to bright red/orange colour change. After stirring for 1 h, the reaction solution was filtered through celite to remove silver waste, washing the celite with DCM until no red colour remained. The solvent was removed

in vacuo, resulting in a red oily solid. For PF_6 complexes; addition of solvent (~5 mL) resulted in precipitation of the product as a bright red solid, which was collected by filtration and washed with petroleum ether and EtOH. For BArF complexes; the residue was purified by flash column chromatography, eluting with DCM/petroluem ether 40-60 °C (50/50). The isolated catalyst was dried in a vacuum oven (40 ^{o}C, 1 mbar) for 24 h before use.

General Procedure D *In situ preparation of MeCN-stabilised hydride complexes.*

In an oven-dried NMR tube was added ~10 mg of the desired iridium complex, ~0.5 mL of CD_2Cl_2 and the tube sealed with a Norrell septum cap. The septum was pierced with a needle to provide a gas outlet, and with a long needle attached to a hydrogen balloon with a valve to control the hydrogen flow. The hydrogen needle was immersed in the solution and hydrogen slowly bubbled through. After 5 min the outlet needle, swiftly followed by the hydrogen needle, were removed and the cap sealed with parafilm. The tube was then submitted for NMR spectroscopic analysis.

General Procedure E *Preparation of mesityl containing NHC/Phosphine complexes.*

To a flame dried, argon cooled schlenk tube was added mesityl-NHC/chloride complex **89**, dry DCM and NaBArF. After stirring at 25 °C for 30 min, the selected phosphine was added slowly, initiating an orange to red colour change. Following a further 30 min stirring, the solvent was removed *in vacuo* leaving a red oily solid. For PF_6 complexes; addition of solvent (~5 mL) resulted in precipitation of the product as a bright red solid, which was collected by filtration and washed with petroleum ether and EtOH. For BArF complexes; the residue was purified by flash column chromatography, eluting with DCM/petroluem ether 40-60 °C (50/50). The isolated catalyst was dried in a vacuum oven (40 ^{o}C, 1 mbar) for 24 h before use.

General Procedure F *Preparation of NHC/chloride complexes, with KOtBu.*

To a flame-dried Schlenk tube was added (η4-cycloocta-1,5-diene)iridium(I) chloride dimer and KO*t*Bu. After stirring the solid mixture under high vacuum for 10 min, dry

THF was added under an argon atmosphere, and the resultant red-black solution stirred at r.t. for a further 10 min. Subsequently, the imidazolium salt was added in one portion, causing a dark red to dark yellow colour change, and the reaction mixture stirred for 16 h. The THF was then removed *in vacuo* and the residue purified directly by flash column chromatography, eluting the yellow fraction with a 1:1 mixture of EtOAc and petroleum ether. After removal of the solvent *in vacuo*, the product was isolated as a bright yellow powder.

General Procedure G *Preparation of imidazolium BArF salts.*

In a 100 mL round-bottom flask, the imidazolium salt and NaBArF were dissolved in DCM and water (1/1) and stirred for 16 h at 25 ^{o}C. The biphasic solution was diluted with a further 10 mL of DCM. The aqueous phase was washed with DCM (10 mL) and the combined organic layers washed with H_2O (10 mL) and brine (10 mL). After drying with Na_2SO_4, the solvent was removed *in vacuo*, and the collected solid was dried in a vacuum oven (40 ^{o}C, 1 mbar) for 24 h, yielding the imidazolium BArF salt.

General Procedure H *Preparation of mesityl containing NHC/triphenylphosphine complexes.*

The iridium dimer was dissolved in dry THF in a previously flame-dried Schlenck round-bottom flask under argon. Through a flow of argon, triphenylphosphine was added, initiating a orange to yellow colour change. After stirring for 5 min, the imidazolium BArF salt was added. After stirring for a further 5 min, KO*t*Bu was added, causing an orange to red colour change that darkened over time. After 3 h, the solvent was removed *in vacuo*, resulting in a oily red residue which was purified by flash column chromatography, eluting with DCM/petroleum ether (50/50). The combined fractions were concentrated *in vacuo* and triturated with petroleum ether. The isolated complex was dried in a vacuum oven (40 ^{o}C, 1 mbar) for 24 h prior to use.

6.2. Catalyst Synthesis and Initial Findings

Scheme 1.29 *Initial Hydrogenation of mono- and bisubstituted alkenes.*

Reactions were carried out using general procedure A and analysed by ^{1}H NMR spectroscopy to calculate the reaction conversion, and are tabulated in **Table E1.1**. Catalyst separation was carried out through a pipette of silica eluting with Et_2O/petroleum ether (30/70).

Solvent	***Temperature (°C)***	***Time (min)***
DCM (8 mL)	25	30
	Substrate	
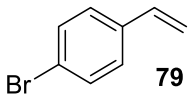 **79** (73 mg, 0.4 mmol)	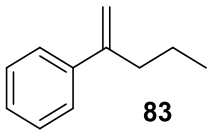 **83** (58 mg, 0.4 mmol)	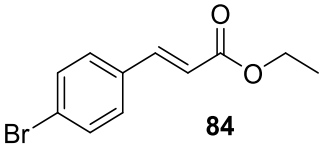 **84** (102 mg, 0.4 mmol)
Product	***Data***[72,95]	
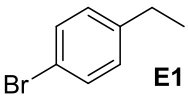 **E1**	**I.R.** (cm^{-1}): 2967, 1497. **^{1}H NMR** (400 MHz, $CDCl_3$): δ 7.43-7.33 (2H, m, Ar-H), 7.10-7.00 (2H, m, Ar-H), 2.58 (2H, q *J* = 7.6 Hz, Ar-CH_2-CH_3), 1.20 (3H, t *J* = 7.6 Hz, CH_2-CH_3). **^{13}C NMR** (101 MHz, $CDCl_3$): δ 143.2, 131.3, 129.6, 119.3, 28.3, 15.4.	
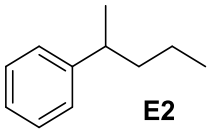 **E2**	**I.R.** (cm^{-1}): 3026, 2957, 1493. **^{1}H NMR** (400 MHz, $CDCl_3$): δ 7.35-7.20 (2H, m, Ar-H), 7.20-7.10 (3H, m, Ar-H), 2.67 (1H, se *J* = 7.1 Hz, Ar-CH), 1.62-1.44 (2H, m, CH_2), 1.33-1.10 (5H, m, CH_2 & CH-CH_3), 0.85 (3H, t *J* = 7.1 Hz, CH_2-CH_3). **^{13}C NMR** (101 MHz, $CDCl_3$): δ 148.2, 128.5, 127.2, 125.9, 40.9, 39.9, 22.5, 21.0, 14.3.	
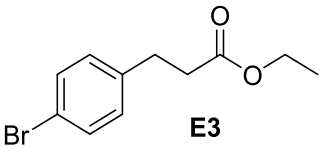 **E3**	**I.R.** (cm^{-1}): 2978, 1730, 1490. **^{1}H NMR** (400 MHz, $CDCl_3$): δ 7.42-7.35 (2H, m, Ar-H), 7.08-7.03 (2H, m, Ar-H), 4.10 (2H, q *J* = 7.2 Hz, O-CH_2-CH_3), 2.88 (2H, t *J* = 7.2 Hz, CH_2), 2.61-2.54 (2H, m, CH_2), 1.21 (3H, t *J* = 7.2 Hz, CH_2-CH_3). **^{13}C NMR** (101 MHz, $CDCl_3$): δ 172.1, 139.1, 131.0, 129.6, 119.5, 60.0, 35.2, 29.9, 13.7.	

Complex	***Conversion (%)***								
	79			***83***			***84***		
	Run		***Ave***	***Run***		***Ave***	***Run***		***Ave***
	1	***2***		***1***	***2***		***1***	***2***	
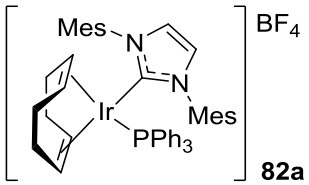 **82a** (1.9 mg, 2.0 μmol)	100	100	100	100	100	100	94	90	92
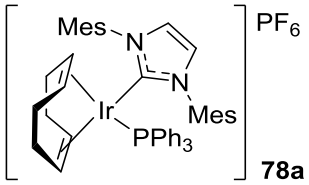 **78a** (2.0 mg, 2.0 μmol)	100	100	100	100	100	100	100	100	100
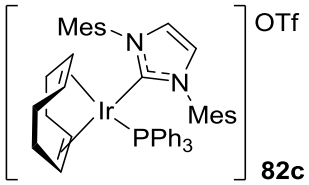 **82c** (2.0 mg, 2.0 μmol)	100	100	100	100	100	100	100	100	100
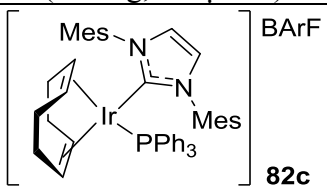 **82c** (3.5 mg, 2.0 μmol)	100	100	100	100	100	100	100	100	100

Table E1.1

Graph 1.1 *Monitored hydrogenation of conjugated ester **84**.*

Reactions were carried out using general procedure B and analysed by ^{1}H NMR specroscopy to calculate the reaction conversion. Catalyst separation was carried out through a pipette of silica eluting with Et_2O/petroleum ether (30/70).

Substrate	***Solvent***	***Temperature (°C)***
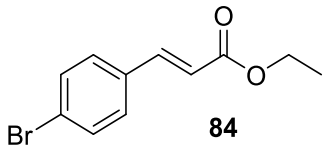 **84** (510 mg, 2.0 mmol)	DCM (40 mL)	25
Product	***Data***[72]	
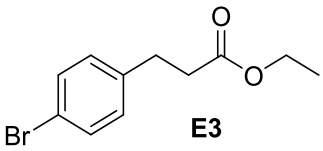 **E3**	**I.R.** (cm^{-1}): 2978, 1730, 1490. **^{1}H NMR** (400 MHz, $CDCl_3$): δ 7.42-7.35 (2H, m, Ar-H), 7.08-7.03 (2H, m, Ar-H), 4.10 (2H, q *J* = 7.2 Hz, O-CH_2-CH_3), 2.88 (2H, t *J* = 7.2 Hz, CH_2), 2.61-2.54 (2H, m, CH_2), 1.21 (3H, t *J* = 7.2 Hz, CH_2-CH_3). **^{13}C NMR** (101 MHz, $CDCl_3$): δ 172.1, 139.1, 131.0, 129.6, 119.5, 60.0, 35.2, 29.9, 13.7.	

Complex	***Time (min)***	***Conversion (%)***
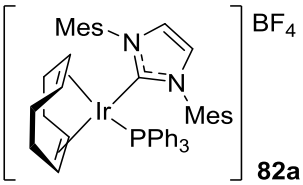 **82a** (4.8 mg, 5.0 μmol)	0	0
	10	13
	15	21
	20	27
	25	34
	30	39
	40	48
	50	54

Complex	*Time (min)*	*Conversion (%)*
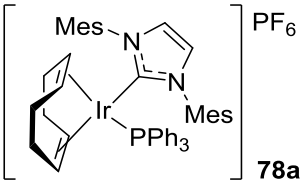 (5.1 mg, 5.0 µmol)	0	0
	10	17
	15	26
	20	34
	25	41
	30	47
	40	57
	50	64

Complex	*Time (min)*	*Conversion (%)*
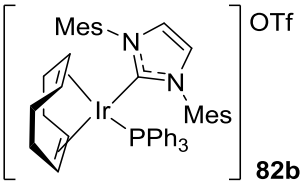 (5.1 mg, 5.0 µmol)	0	0
	10	17
	15	28
	20	39
	25	48
	30	55
	40	64
	50	71

Complex	*Time (min)*	*Conversion (%)*
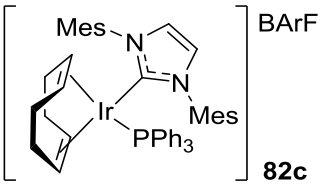 (8.8 mg, 5.0 µmol)	0	0
	10	19
	15	30
	20	41
	25	50
	30	57
	40	67
	50	72

Graph 1.2 *Hydrogenation of enone **85** at different catalyst loadings.*

Reactions were carried out using general procedure A and analysed by ^{1}H NMR spectroscopy to calculate the reaction conversion. Catalyst separation was carried out through a pipette of silica eluting with Et_2O/petroleum ether (30/70).

Substrate	***Solvent***	***Temperature (°C)***
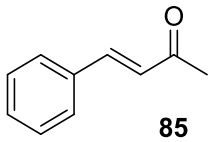 **85** (58 mg, 0.4 mmol)	DCM (8 mL)	25
Product	***Data***[72]	
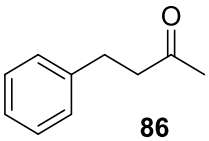 **86**	**I.R.** (cm^{-1}): 3063, 2924, 1715. **^{1}H NMR** (400 MHz, $CDCl_3$): δ 7.30-7.23 (2H, m, Ar-H), 7.20-7.14 (3H, m, Ar-H), 2.92-2.85 (2H, m, CH_2), 2.78-7.71 (2H, m, CH_2), 2.12 (3H, s, CO-CH_3). **^{13}C NMR** (101 MHz, $CDCl_3$): δ 208.0, 131.2, 128.7, 128.5, 126.3, 45.4, 30.3, 30.0.	

Complex	***Catalyst Loading (mol%)***	***Conversion (%)***		
		Run		***Ave***
		1	***2***	
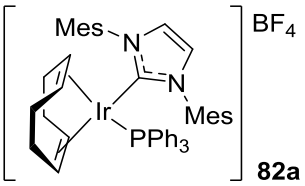 **82a**	0.25 (1.0 mg, 1.0 μmol)	14	10	12
	0.50 (1.9 mg, 2.0 μmol)	20	24	22
	0.75 (2.9 mg, 3.0 μmol)	30	36	33
	1.00 (3.8 mg, 4.0 μmol)	43	38	41
	1.25 (4.8 mg, 5.0 μmol)	44	51	48
	1.50 (5.7 mg, 6.0 μmol)	55	56	56

Complex	*Catalyst Loading (mol%)*	*Conversion (%)*		
		Run		*Ave*
		1	*2*	
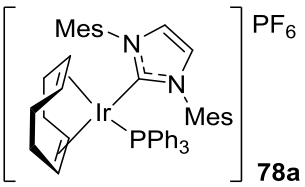 **78a**	0.25 (1.0 mg, 1.0 μmol)	13	11	12
	0.50 (2.0 mg, 2.0 μmol)	26	27	27
	0.75 (3.0 mg, 3.0 μmol)	38	36	37
	1.00 (4.0 mg, 4.0 μmol)	48	45	47
	1.25 (5.1 mg, 5.0 μmol)	53	57	55
	1.50 (6.1 mg, 6.0 μmol)	56	54	55

Complex	*Catalyst Loading (mol%)*	*Conversion (%)*		
		Run		*Ave*
		1	*2*	
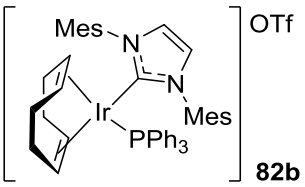 **82b**	0.25 (1.0 mg, 1.0 μmol)	12	14	13
	0.50 (2.0 mg, 2.0 μmol)	33	29	31
	0.75 (3.0 mg, 3.0 μmol)	44	43	44
	1.00 (4.1 mg, 4.0 μmol)	52	55	54
	1.25 (5.1 mg, 5.0 μmol)	54	58	56
	1.50 (6.1 mg, 6.0 μmol)	57	55	56

Complex	***Catalyst Loading (mol%)***	***Conversion (%)***		
		Run		***Ave***
		1	***2***	
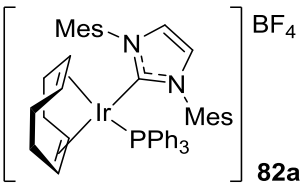 **82a**	0.25 (1.8 mg, 1.0 μmol)	16	17	17
	0.50 (3.5 mg, 2.0 μmol)	34	32	33
	0.75 (5.3 mg, 3.0 μmol)	44	50	47
	1.00 (7.0 mg, 4.0 μmol)	54	53	54
	1.25 (8.8 mg, 5.0 μmol)	54	56	55
	1.50 (10.6 mg, 6.0 μmol)	53	58	56

Scheme 1.31 *One-pot synthesis of alkyl-NHC/phosphine PF_6 complexes.*

Reactions were carried out using general procedure C. Percentage buried volumes were calculated using literature data,[70] with the equation below. The *in situ* generation of MeCN-stabilised hydride complexes was carried using general procedure D, and results are tabulated as the hydride- and corresponding phosphorous shifts (excluding ligands and counterions).

$$\%BV_{total} = \%BV_{PR_3} + \%BV_{NHC}$$

Ag_2O	***[CODIrCl]$_2$***	***AX***	***Solvent***	***Temperature (°C)***	***Time (h)***
(58 mg, 0.25 mmol)	(168 mg, 0.25 mmol)	KPF_6 (92 mg, 0.5 mmol)	DCM (10 mL)	25	3 (1+1+1)

Imidazolium Halide	***Phosphine***	***Isolation***
 **E4** (164.6 mg, 0.5 mmol)	PPh_3 (131 mg, 0.5 mmol)	Trituration from Et_2O with EtOH

Product	***Data***
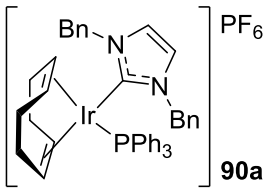 **90a** **Yield** = 421 mg, 88% **%BV** = 27.9 + 29.9 = 57.8% **[H]** = -21.34 ppm	**Appearance**: red powder. **Melting Point** (°C): >200 (dec). **IR** (cm^{-1}): 3058, 2991. **^{1}H NMR** (400 MHz, $CDCl_3$): δ 7.55-7.40 (9H, m, Ar-H), 7.36-7.26 (12H, m, Ar-H), 7.00-6.92 (4H, m, Ar-H), 6.77 (2H, s, N-CH=CH-N), 5.49 (2H, d, ^2J = 15.0 Hz, N-CH_2-Ph), 4.51 (2H, d, ^2J = 14.9 Hz, N-CH_2-Ph), 4.45-4.42 (2H, m, COD CH), 3.89-3.78 (2H, m, COD CH), 2.32-2.16 (2H, m, COD CH_2), 2.16 -2.32 (2H, m, COD CH_2), 2.02-1.89 (4H, m, COD CH_2).

^{13}C NMR (101 MHz, $CDCl_3$): δ 187.0 (d $^2J_{C-P}$ = 9.2 Hz), 134.6, 134.0, 133.9, 131.7, 131.6, 130.6, 130.1, 129.5, 129.5, 129.4, 128.9, 127.9, 122.8, 87.1, 87.0, 80.7, 54.6, 30.3, 30.9, 30.8.

^{31}P NMR (162 MHz, $CDCl_3$): δ 18.2 (PPh_3), -144.3 (sep $^1J_{F-P}$ = 710 Hz, PF_6).

^{19}F NMR (376 MHz, $CDCl_3$): δ -73.5 (d $^1J_{P-F}$ = 710 Hz, PF_6).

HRMS (NSI): m/z calculated for $C_{43}H_{43}IrN_2P$ $[M-PF_6]^+$: 809.2764; found: 809.2764.

MeCN Hydride Complex

^{1}H NMR (400 MHz, CD_3CN): -21.34 (d $^2J_{H-P}$ = 16.1 Hz).

^{31}P NMR (162 MHz, CD_3CN): δ 16.7 (t $^2J_{P-H}$ = 16.1 Hz, PPh_3).

Imidazolium Halide	*Phosphine*	*Isolation*
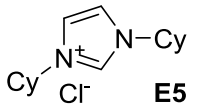 **E5** (134 mg, 0.5 mmol)	PPh_3 (131 mg, 0.5 mmol)	Trituration with EtOAc
Product	***Data***	
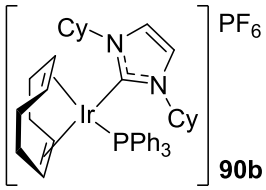 **90b** **Yield** = 400 mg, 85% **%BV** = 23.5 + 29.9 = 53.4% **[H]** = -21.61 ppm	**Appearance**: red powder. **Melting Point** (°C): >160 (dec). **IR** (cm^{-1}): 2932, 1435, 1232. **^{1}H NMR** (400 MHz, $CDCl_3$): δ 7.47-7.37 (9H, m, Ar-H), 7.14-7.10 (8H, m, Ar-H & N-CH=CH-N), 4.51 (2H, tt, *J* = 12.0 Hz, 3.3 Hz, N-CH), 4.41-4.39 (2H, m, COD-CH), 3.59-3.57 (2H, m, COD-CH), 2.49-2.32 (4H, m, COD-CH_2), 2.15-2.11 (2H, m, COD-CH_2), 1.97-1.93 (6H, m, Cy-CH_2 & COD-CH_2), 1.69-1.52 (8H, m, Cy-CH_2), 1.44-1.33 (2H, m, Cy-CH_2), 1.25-1.11 (4H, m, Cy-CH_2), 1.07-0.99 (2H, m, Cy-CH_2).	

^{13}C NMR (101 MHz, $CDCl_3$): δ 169.2 (d $^2J_{C-P}$ = 9.4 Hz), 133.6, 133.5, 131.4, 130.6, 130.1, 129.2, 129.1, 120.0, 85.4, 85.2, 79.4, 61.2, 35.4, 32.0, 31.3, 30.5, 30.4, 26.0, 25.8, 24.8.

^{31}P NMR (162 MHz, $CDCl_3$): δ 18.5 (PPh_3), -144.3 (sep $^1J_{F-P}$ = 713 Hz, PF_6).

^{19}F NMR (376 MHz, $CDCl_3$): δ -73.5 (d $^1J_{P-F}$ = 713 Hz, PF_6).

HRMS (NSI): m/z calculated for $C_{41}H_{51}IrN_2P$ $[M-PF_6]+$: 793.3390; found: 793.3390.

MeCN Hydride Complex

^{1}H NMR (400 MHz, CD_3CN): -21.61 (d $^2J_{H-P}$ = 16.7 Hz).

^{31}P NMR (162 MHz, CD_3CN): δ 17.1 (t $^2J_{P-H}$ = 16.7 Hz, PPh_3).

Imidazolium Halide	***Phosphine***	***Isolation***
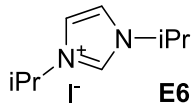 **E6** (140 mg, 0.5 mmol)	PPh_3 (131 mg, 0.5 mmol)	Trituration from petroleum ether (30-40)
Product	***Data***	
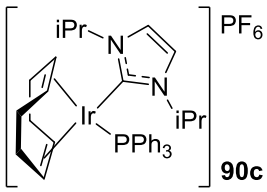 **90c** **Yield** = 271 mg, 63% **%BV** = 23.5 + 29.9 = 53.4% **[H]** = -21.64 ppm	**Appearance**: red powder. **Melting Point** (°C): >220 (dec). **IR** (cm^{-1}): 2980, 2883, 1435, 1209. **^{1}H NMR** (400 MHz, $CDCl_3$): δ 7.49-7.41 (9H, m, Ar-H), 7.21-7.16 (8H, m Ar-H & N-CH=CH-N), 5.00 (2H, septet, J = 6.7 Hz, N-CH-$(CH_3)_2$), 4.49-4.47 (2H, m, COD-CH), 3.68-3.66 (2H, m, COD-CH), 2.43-2.33 (4H, m, COD-CH_2), 2.18-2.13 (2H, m, COD-CH_2), 2.02-1.96 (2H, m, COD-CH_2), 1.50 (6H, d J = 6.7 Hz, CH-$(CH_3)_2$), 0.62 (6H, d, J = 6.7 Hz, CH-$(CH_3)_2$).	

^{13}C NMR (101MHz, $CDCl_3$): δ 169.8 (d $^2J_{C-P}$ = 9.0 Hz), 133.8, 133.7, 132.2, 132.1, 131.4, 130.6, 130.2, 129.15, 129.08, 119.3, 85.5, 85.4, 79.5, 53.3, 31.1, 30.45, 30.42, 24.7, 20.4.

^{31}P NMR (162 MHz, $CDCl_3$): δ 18.2 (PPh_3), -144.3 (sep $^1J_{F-P}$ = 712 Hz, PF_6).

^{19}F NMR (376 MHz, $CDCl_3$): δ -73.4 (d, $^1J_{P-F}$ = 712 Hz, PF_6).

HRMS (NSI): m/z calculated for $C_{35}H_{43}IrN_2P$ $[M-PF_6]^+$: 715.2789; found: 715.2791.

MeCN-Hydride Complex

^{1}H NMR (400 MHz, CD_3CN): -21.64 (d $^2J_{H-P}$ = 16.9 Hz).

^{31}P NMR (162 MHz, CD_3CN): δ 16.9 (t $^2J_{P-H}$ = 16.9 Hz, PPh_3).

Imidazolium Halide	*Phosphine*	*Isolation*
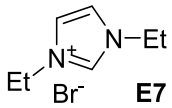 **E7** (103 mg, 0.5 mmol)	PPh_3 (131 mg, 0.5 mmol)	Trituration from petroleum ether (30-40)
Product	***Data***	
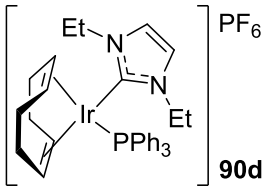 **90d** **Yield** = 308 mg, 74% **%BV** = 24.0 + 29.9 = 53.9% **[H]** = -21.57 ppm	**Appearance**: red powder. **Melting Point** (°C): >200 (dec). **IR** (cm^{-1}): 2990, 1435. **^{1}H NMR** (400 MHz, $CDCl_3$): δ 7.48-7.44 (3H, m, Ar-H), 7.41-7.38 (6H, m, Ar-H), 7.23-7.18 (6H, m, Ar-H), 6.98 (2H, s, N-CH=CH-N), 4.35-4.32 (2H, m, COD-CH), 4.16 (2H, dq, ^2J = 13.5 Hz, J = 7.3 Hz, CH_2-CH_3), 3.73-3.71 (2H, m, COD-CH), 3.64 (2H, dq, ^2J = 13.5Hz, J = 7.3 Hz, CH_2-CH_3), 2.34-2.27 (4H, m, COD-CH_2), 2.13-1.96 (4H, m, COD-CH_2), 1.07 (6H, t, J = 7.3 Hz, CH_2-CH_3).	

^{13}C NMR (101 MHz, $CDCl_3$): δ 171.9 (d $^2J_{C-P}$ = 10.6 Hz), 133.2, 133.1, 130.80, 130.77, 129.8, 129.3, 128.6, 128.4, 120.7, 85.7, 85.6, 79.2, 44.9, 30.6, 30.2, 30.1, 14.2.

^{31}P NMR (162 MHz, $CDCl_3$): δ 18.5 (PPh_3), -144.3 (sep $^1J_{P-F}$ = 711 Hz, PF_6).

^{19}F NMR (376 MHz, $CDCl_3$): δ -73.6 (d $^1J_{F-P}$ = 711 Hz, PF_6).

HRMS (NSI): m/z calculated for $C_{33}H_{39}IrN_2P$ $[M-PF_6]^+$: 687.2476; found: 687.2476.

MeCN-Hydride Complex

^{1}H NMR (400 MHz, CD_3CN): -21.57 (d $^2J_{H-P}$ = 17.1 Hz).

^{31}P NMR (162 MHz, CD_3CN): δ 17.0 (t $^2J_{P-H}$ = 17.1 Hz, PPh_3).

Imidazolium Halide	***Phosphine***	***Isolation***
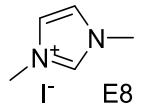 (112 mg, 0.5 mmol)	PPh_3 (131 mg, 0.5 mmol)	Trituration from petroleum ether (30-40)
Product	***Data***[29]	
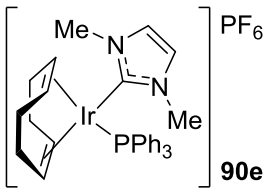 **Yield** = 374 mg, 93% **%BV** = 22.7 + 29.9 = 52.6% **[H]** = -21.56 ppm	**Appearance**: red powder. **Melting Point** (°C): >190 (dec). **IR** (cm^{-1}): 2980, 2889, 1435, 1227. **^{1}H NMR** (400 MHz, $CDCl_3$): δ 7.50-7.37 (9H, m, Ar-H), 7.28-7.23 (6H, m, Ar-H), 6.84 (2H, s, N-CH=CH-N), 4.37-4.34 (2H, m, COD-CH), 3.78-3.76 (2H, m, COD-CH), 3.47 (6H, s, N-CH_3), 2.39-2.22 (4H, m, COD-CH_2), 2.14-1.96 (4H, m, COD-CH_2).	

^{13}C NMR (101 MHz, $CDCl_3$): δ 174.2 (d $^2J_{C-P}$ = 9.6 Hz), 133.6, 133.5, 131.3, 130.5, 130.1, 129.0, 128.9, 86.2, 86.1, 80.2, 68.0, 37.16, 31.2, 30.7, 30.7.

^{31}P NMR (162 MHz, $CDCl_3$): δ 18.3 (PPh_3), -144.3 (sep $^1J_{P-F}$ = 713 Hz, PF_6).

^{19}F NMR (376 MHz, $CDCl_3$): δ -73.1 (d $^1J_{F-P}$ = 713 Hz, PF_6).

MeCN Hydride Complex

^{1}H NMR (400 MHz, CD_3CN): -21.56 (d $^2J_{H-P}$ = 17.0 Hz).

^{31}P NMR (162 MHz, CD_3CN): δ 17.04 (t $^2J_{P-H}$ = 17.0 Hz, PPh_3).

Imidazolium Halide	*Phosphine*	*Isolation*
 **E4** (164.6 mg, 0.5 mmol)	$PnBu_3$ (101 mg, 123 µL, 0.5 mmol)	Trituration from petroleum ether (30-40)
Product	***Data***	
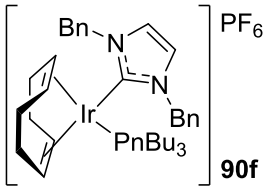 **90f** **Yield** = 367 mg, 82% **%BV** = 27.9 + 27.2 = 55.1% **[H]** = -22.04 ppm	**Appearance**: red powder. **Melting Point** (°C): 100-102. **IR** (cm^{-1}): 2959, 2930, 2872, 1447, 1234. **^{1}H NMR** (400 MHz, $CDCl_3$): δ 7.41-7.34 (6H, m, Ar-H), 7.20-7.17 (4H, m, Ar-H), 7.10 (2H, s, N-CH=CH-N), 5.65 (2H, d ^2J = 15.6 Hz, N-CH_2-Ph), 5.29 (2H, d, ^2J = 15.6 Hz, N-CH_2-Ph), 4.11-4.10 (4H, m, COD-CH), 2.18-2.12 (2H, m, COD-CH_2), 1.99-1.79 (6H, m, COD-CH_2), 1.58-1.54 (6H, m, PnBu-CH_2), 1.38-1.35 (12H, m, PnBu-CH_2), 0.89 (9H, t, J = 6.9 Hz, PnBu-CH_3).	

^{13}C NMR (101 MHz, $CDCl_3$): δ 176.7 (d, $^2J_{C-P}$ = 9.4 Hz), 134.7, 128.8, 128.0, 126.4, 122.4, 84.8, 84.7, 53.6, 30.88, 30.85, 30.16, 25.9, 23.8, 23.7, 23.6, 23.3, 13.2.

^{31}P NMR (162 MHz, $CDCl_3$): δ 0.9 ($PnBu_3$), -144.3 (sep $^1J_{P-F}$ = 712 Hz, PF_6).

^{19}F NMR (376 MHz, $CDCl_3$): δ -73.2 (d $^1J_{F-P}$ = 712 Hz, PF_6).

HRMS (NSI): m/z calculated for $C_{37}H_{55}IrN_2P$ $[M-PF_6]^+$: 749.3703; found: 749.3693.

MeCN Hydride Complex

^{1}H NMR (400 MHz, CD_3CN): -22.04 (d $^2J_{H-P}$ = 17.8 Hz).

^{31}P NMR (162 MHz, CD_3CN): δ -11.2 (t $^2J_{P-H}$ = 17.8 Hz, $PnBu_3$).

Imidazolium Halide	***Phosphine***	***Isolation***
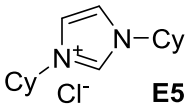 **E5** (134 mg, 0.5 mmol)	$PnBu_3$ (101 mg, 123 µL, 0.5 mmol)	Trituration from petroleum ether (30-40)
Product	***Data***	
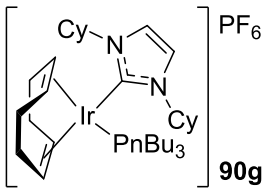 **90g** **Yield** = 198 mg, 45% **%BV** = 23.5 + 27.2 = 50.7% **[H]** = -22.37 ppm	**Appearance**: red powder. **Melting Point** (°C): 178-181. **IR** (cm^{-1}): 2933, 2872, 1452, 1238. **^{1}H NMR** (400 MHz, $CDCl_3$): δ 7.22 (2H, s, N-C<u>H</u>=C<u>H</u>-N), 4.5 (2H, tt *J* = 11.9, 3.5 Hz, N-C<u>H</u>), 4.30-4.27 (2H, m, COD-C<u>H</u>), 4.06-4.03 (2H, m, COD-C<u>H</u>), 2.24-2.14 (4H, m, COD-C<u>H</u>$_2$), 2.12-1.96 (10H, m, COD-C<u>H</u>$_2$ & C<u>H</u>$_2$), 1.89-1.68 (8H, m, C<u>H</u>$_2$), 1.59-1.55 (6H, m, C<u>H</u>$_2$), 1.43-1.35 (18H, m, C<u>H</u>$_2$), 0.94 (9H, t *J* = 7.0 Hz, P^{n}Bu$_3$-C<u>H</u>$_3$).	

^{13}C NMR (101 MHz, $CDCl_3$): δ 171.2 (d $^2J_{C\text{-}P}$ = 9.5 Hz), 119.7, 85.0, 84.9, 75.5, 60.8, 35.9, 33.8, 31.7, 31.6, 31.1, 26.6, 26.2, 25.9, 25.0, 24.7, 24.5, 24.3, 13.9.

^{31}P NMR (162 MHz, $CDCl_3$): δ 1.3 ($PnBu_3$), -144.3 (sep $^1J_{F\text{-}P}$ = 713 Hz, PF_6).

^{19}F NMR (376 MHz, $CDCl_3$): δ -73.5 (d $^1J_{P\text{-}F}$ = 713 Hz, PF_6).

HRMS (NSI): m/z calculated for $C_{35}H_{63}IrN_2P$ $[M\text{-}PF_6]^+$: 733.4329; found 733.4332.

MeCN Hydride Complex

^{1}H NMR (400 MHz, CD_3CN): -22.37 (d $^2J_{H\text{-}P}$ = 17.7 Hz).

^{31}P NMR (162 MHz, CD_3CN): δ -10.7 (t $^2J_{P\text{-}H}$ = 17.7 Hz, $PnBu_3$).

Imidazolium Halide	*Phosphine*	*Isolation*
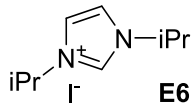 **E6** (140 mg, 0.5 mmol)	$P(Me)_2Ph$ (69 mg, 71 µL 0.5 mmol)	Trituration from petroleum ether (30-40)

Product	*Data*
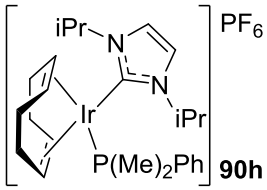 **90h** **Yield** = 261 mg, 71% **%BV** = 23.5 + 25.1 = 48.6% **[H]** = -22.11 ppm	**Appearance**: red powder. **Melting Point** (°C): >190 (dec). **IR** (cm^{-1}): 2980, 2880, 1418, 1207. **^{1}H NMR** (400 MHz, $CDCl_3$): δ 7.69-7.65 (2H, m, Ar-H), 7.51-7.45 (3H, m, Ar-H), 7.10 (2H, s, N-CH=CH-N) 4.95 (2H, septet J = 6.7 Hz, N-CH-$(CH_3)_2$), 4.41-4.38 (2H, m, COD-CH), 4.00-3.98 (2H, m, COC-CH), 2.33-2.25 (4H, m, COD-CH_2), 2.07-2.01 (4H, m, COD-CH_2), 1.57 (3H, s, P-CH_3), 1.54 (3H, s, P-CH_3), 1.47 (6H, d, J = 6.8 Hz, CH-$(CH_3)_2$), 1.21 (6H, d J = 6.8 Hz, CH-$(CH_3)_2$).

^{13}C NMR (101 MHz, $CDCl_3$): δ 171.5 (d, $^2J_{C-P}$ = 10.6 Hz), 133.8, 133.3, 130.73, 130.70, 130.65, 130.5, 128.9, 128.8, 118.2, 85.9, 85.8, 52.5, 30.6, 30.5, 30.41, 30.39, 24.0, 22.6, 14.7, 14.3.

^{31}P NMR (162 MHz, $CDCl_3$): δ -12.0 ($P(Me)_2Ph$), -144.3 (sep $^1J_{F-P}$ = 712 Hz, PF_6).

^{19}F NMR (376 MHz, $CDCl_3$): δ -73.3 (d $^1J_{P-F}$ = 711 Hz, PF_6).

HRMS (NSI): m/z calculated for $C_{25}H_{39}IrN_2P$ $[M-PF_6]^+$: 591.2476; found: 591.2475.

MeCN Hydride Complex

^{1}H NMR (400 MHz, CD_3CN): -22.11 (d $^2J_{H-P}$ = 18.5 Hz).

^{31}P NMR (162 MHz, CD_3CN): δ -27.9 (t $^2J_{P-H}$ = 18.5 Hz, $P(Me)_2Ph$).

Imidazolium Halide	*Phosphine*	*Isolation*
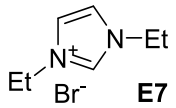 **E7** (103 mg, 0.5 mmol)	PEt_3 (59 mg, 74 µL, 0.5 mmol)	Trituration from petroleum ether (30-40)
Product	***Data***	
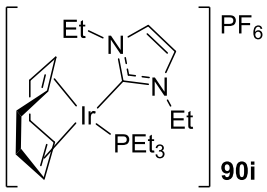 **90i** **Yield** = 289 mg, 84% **%BV** = 24.0 + 27.1 = 51.1% **[H]** = -22.31 ppm	**Appearance**: red powder. **Melting Point** (°C): 151-154. **IR** (cm^{-1}): 2980, 2887, 1463. **^{1}H NMR** (400 MHz, $CDCl_3$): δ 7.16 (2H, s, N-C<u>H</u>=C<u>H</u>-N), 4.32 (2H, dq ^2J = 13.5 Hz, J = 7.3 Hz, N-C<u>H</u>$_2$-CH$_3$), 4.17-4.02 (6H, m, COD-C<u>H</u> & N-C<u>H</u>$_2$-CH$_3$), 2.27-2.12 (4H, m, COD-C<u>H</u>$_2$), 2.06-1.94 (4H, m, COD-C<u>H</u>$_2$) 1.57 (6H, quin J = 7.7 Hz, P-C<u>H</u>$_2$-CH$_3$), 1.47 (6H, t J = 7.3 Hz, CH$_2$-C<u>H</u>$_3$), 1.05 (9H, *app.* dt J = 15.8 Hz, J = 7.6 Hz, CH$_2$-C<u>H</u>$_3$).	

^{13}C NMR (101 MHz, $CDCl_3$): δ 174.1 (d $^2J_{C-P}$ = 10.6 Hz), 121.3, 84.8, 84.7, 76.1, 45.5, 31.7, 31.6, 30.9, 16.6, 16.3, 15.7, 8.22, 8.20.

^{31}P NMR (162 MHz, $CDCl_3$): δ 7.4 (PEt_3), -144.4 (sep $^1J_{P-F}$ = 713 Hz, PF_6).

^{19}F NMR (376 MHz, $CDCl_3$): δ -73.5 (d $^1J_{F-P}$ = 711 Hz, PF_6).

HRMS (NSI): m/z calculated for $C_{21}H_{39}IrN_2P$ $[M-PF_6]^+$: 541.2451; found: 541.2445.

MeCN Hydride Complex

^{1}H NMR (400 MHz, CD_3CN): -22.31(d $^2J_{H-P}$ = 17.6 Hz).

^{31}P NMR (162 MHz, CD_3CN): δ -3.6 (t $^2J_{P-H}$ = 17.6 Hz, PEt_3).

Imidazolium Halide	***Phosphine***	***Isolation***
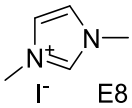 (112 mg, 0.5 mmol)	PEt_3 (59 mg, 74 μL, 0.5 mmol)	Trituration from petroleum ether (30-40)
Product	***Data***	
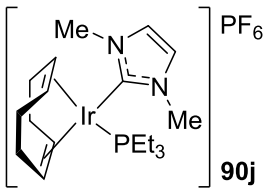 **90j** **Yield** = 297 mg, 90% **%BV** = 22.7 + 27.1 = 49.8% **[H]** = -22.30 ppm	**Appearance**: Red Powder. **Melting Point** (°C): >190 (dec). **IR** (cm^{-1}): 2978, 1558, 1458, 1385. **^{1}H NMR** (400 MHz, $CDCl_3$): δ 7.09 (2H, s, N-C<u>H</u>=C<u>H</u>-N), 4.16-4.12 (4H, m, COD-C<u>H</u>), 3.80 (6H, s, N-C<u>H$_3$</u>), 2.27-2.14 (4H, m, COD-C<u>H$_2$</u>), 2.07-1.96 (4H, m, COD-C<u>H$_2$</u>), 1.59 (6H, quin *J* = 7.8 Hz, P-C<u>H$_2$</u>-CH_3), 1.07 (9H, *app.* dt *J* = 16.0 Hz, *J* = 7.8 Hz, CH_2-C<u>H$_3$</u>).	

^{13}C NMR (101 MHz, $CDCl_3$): δ 175.6 (d $^2J_{C-P}$ = 10.7 Hz), 123.8, 85.0, 84.9, 76.4, 37.5, 31.7, 31.7, 30.9, 16.7, 16.4, 8.34, 8.32.

^{31}P NMR (162 MHz, $CDCl_3$): δ 8.0 (PEt_3), -144.4 (sep $^1J_{P-F}$ = 712 Hz, PF_6).

^{19}F NMR (376 MHz, $CDCl_3$): δ -73.4 (d $^1J_{F-P}$ = 711 Hz, PF_6).

HRMS (NSI): m/z calculated for $C_{19}H_{35}IrN_2P$ $[M-PF_6]^+$: 515.2162; found: 515.2150.

MeCN Hydride Complex

^{1}H NMR (400 MHz, CD_3CN): -22.30 (d $^2J_{H-P}$ = 17.6 Hz).

^{31}P NMR (162 MHz, CD_3CN): δ -3.5 (t $^2J_{P-H}$ = 17.6 Hz, PEt_3).

Scheme 1.32 *One-pot synthesis of alkyl-NHC/phosphine BArF complexes.*

Reactions were carried out using general procedure C.

Ag_2O	***$[CODIrCl]_2$***	***AX***	***Solvent***	***Temperature (°C)***	***Time (h)***
(58 mg, 0.25 mmol)	(168 mg, 0.25 mmol)	NaBArF (443 mg, 0.5 mmol)	DCM (10 mL)	25	3 (1+1+1)

Imidazolium Halide	***Phosphine***
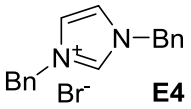 **E4** (164.6 mg, 0.5 mmol)	PPh_3 (131 mg, 0.5 mmol)
Product	***Data***
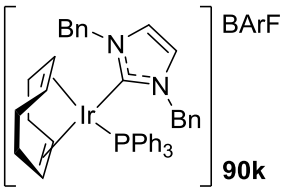 **90k** **Yield** = 737 mg, 88%	**Appearance**: red powder. **Melting Point** (°C): 185-188. **IR** (cm^{-1}): 2981, 1611, 1354, 1275, 1115. **^{1}H NMR** (400 MHz, $CDCl_3$): δ 7.74 (8H, t ^4J = 2.4 Hz, Ar-H), 7.53-7.50 (7H, m, Ar-H &), 7.46-7.42 (6H, m, Ar-H), 7.37-7.30 (12H, m, Ar-H), 6.92-6.89 (4H, m, Ar-H), 6.67 (2H, s, N-CH=CH-N), 5.52 (2H, d ^2J = 14.5 Hz, N-CH_2-Ar), 4.44 (2H, ^2J = 14.5 Hz, N-CH_2-Ar), 4.41-4.38 (2H, m, COD-CH), 3.93-3.91 (2H, m, COD-CH), 2.26-2.22 (2H, m, COD-CH_2), 2.14-2.00 (6H, m, COD-CH_2).

^{13}C NMR (101 MHz, $CDCl_3$): δ 175.0 (d $^2J_{C-P}$ = 10.7 Hz), 161.2 (q $^1J_{C-B}$ = 49.9 Hz), 134.3, 133.2, 133.10, 133.06, 131.15, 131.11, 129.7, 129.2, 129.0, 128.8, 128.7, 128.6, 128.4 (q $^2J_{C-F}$ = 31.2 Hz), 127.1, 124.1 (q $^1J_{C-F}$ = 273 Hz), 121.5, 116.9, 85.9, 85.7, 80.9, 54.0, 30.5, 30.1.

^{31}P NMR (162 MHz, $CDCl_3$): δ 18.4 (PPh_3).

^{19}F NMR (376 MHz, $CDCl_3$): δ -62.4 (BArF).

^{11}B NMR (128 MHz, $CDCl_3$): δ -6.6 (BArF).

HRMS (NSI): m/z calculated for $C_{43}H_{43}IrN_2P$ $[M-PF_6]^+$: 809.2764; found: 809.2766.

Imidazolium Halide	***Phosphine***
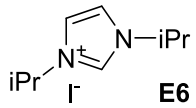 **E6** (140 mg, 0.5 mmol)	$P(Me)_2Ph$ (69 mg, 71 µL 0.5 mmol)
Product	***Data***
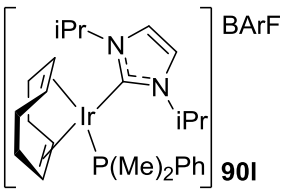 **90I** **Yield** = 683 mg, 94%	**Appearance**: red powder. **Melting Point** (°C): 180-182. **IR** (cm^{-1}): 2962, 2880, 2361, 1611, 1422. **^{1}H NMR** (400 MHz, $CDCl_3$): δ 7.68 (8H t ^4J = 2.4 Hz, Ar-H), 7.58-7.52 (2H, m, Ar-H), 7.50 (4H, s, Ar-H), 7.47-7.42 (3H, m, Ar-H), 6.94 (2H, s, N-CH), 4.88 (2H, sept J = 6.7 Hz, N-CH-$(CH_3)_2$), 4.42-4.36 (2H, m, COD-CH), 3.91-3.85 (2H, m, COD-CH), 2.24-2.15 (4H, m, COD-CH_2), 2.10-1.96 (4H, m, COD-CH_2), 1.47 (3H, s, P-CH_3), 1.45 (3H, s, P-CH_3), 1.39 (6H, d J = 6.7 Hz, CH-$(CH_3)_2$), 1.13 (6H, d J = 6.8 Hz, CH-$(CH_3)_2$).

^{13}C NMR (101 MHz, $CDCl_3$): δ 171.8 (d $^2J_{C-P}$ = 10.9 Hz), 161.2 (q, $^1J_{C-B}$ = 49.8 Hz), 134.3, 131.1, 130.2, 130.1, 128.9, 128.8, 128.4 (q $^2J_{C-F}$ = 31.5 Hz), 124.1 (q $^1J_{C-F}$ = 273 Hz), 117.9, 117.0, 86.7, 86.6, 76.4, 52.4, 30.5, 30.3, 23.7, 22.4, 14.8, 14.5.

^{31}P NMR (162 MHz, $CDCl_3$): δ -12.7 ($P(Me)_2Ph$).

^{19}F NMR (376 MHz, $CDCl_3$): δ -62.4 (BArF).

^{11}B NMR (128 MHz, $CDCl_3$): δ -6.6 (BArF).

HRMS (NSI): m/z calculated for $C_{25}H_{39}IrN_2P$ $[M\text{-}BArF]^+$: 589.2451; found: 589.2540.

Imidazolium Halide	***Phosphine***
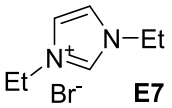 **E7** (103 mg, 0.5 mmol)	PEt_3 (59 mg, 74 µL, 0.5 mmol)

Product	***Data***
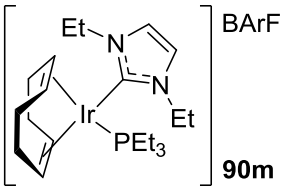 **90m** **Yield** = 654 mg, 93%	**Appearance**: red powder. **Melting Point** (°C): 208-210. **IR** (cm^{-1}): 2980, 1610, 1352, 1271, 1117. **^{1}H NMR** (400 MHz, $CDCl_3$): δ 7.68 (8H, t ^4J = 2.5 Hz, Ar-H), 7.51 (4H, s, Ar-H) 6.92 (2H, s, N-CH=CH-N), 4.27 (2H, dq ^2J = 13.4 Hz, J = 7.4 Hz, N-CH_2-CH_3), 4.13-4.10 (4H, m, COD-CH), 3.96 (2H, dq ^2J = 13.4 Hz, J = 7.4 Hz, N-CH_2-CH_3), 2.21-1.94 (8H, m, COD-CH_2), 1.50 (6H, quin J = 7.8 Hz, P-CH_2-CH_3), 1.39 (6H, t J = 7.4 Hz, CH_2-CH_3), 0.98 (9H, *app.* dt J = 16.0 Hz, J = 7.6 Hz, CH_2-CH_3).

^{13}C NMR (101 MHz, $CDCl_3$): δ 174.3 (d $^2J_{C\text{-}P}$ = 8.7 Hz), 161.2 (q $^1J_{C\text{-}B}$ = 49.4 Hz), 134.3, 128.4 (q $^2J_{C\text{-}F}$ = 33.3 Hz), 124.0 (q $^1J_{C\text{-}F}$ = 273 Hz), 120.0, 116.9, 84.8, 84.6, 44.8, 30.9, 30.8, 30.1, 16.0, 15.7, 14.6, 7.3.

^{31}P NMR (162 MHz, $CDCl_3$): δ 7.4 (PEt_3).

^{19}F NMR (376 MHz, $CDCl_3$): δ -62.45 (BArF).

^{11}B NMR (128 MHz, $CDCl_3$): δ -6.62 (BArF).

HRMS (NSI): m/z calculated for $C_{21}H_{39}IrN_2P$ $[M\text{-}BArF]^+$: 543.2476; found: 543.2470.

Imidazolium Halide	***Phosphine***
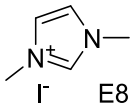 E8 (112 mg, 0.5 mmol)	PPh_3 (131 mg, 0.5 mmol)
Product	***Data***
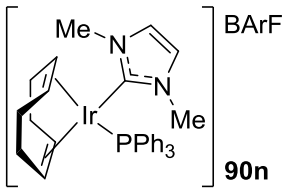 **Yield** = 654 mg, 86%	**Appearance**: red powder. **Melting Point** (°C): 175-177. **IR** (cm^{-1}): 2976, 2361, 2330, 1609, 1437. **^{1}H NMR** (400 MHz, $CDCl_3$): δ 7.75 (8H, t ^4J = 2.3 Hz, Ar-H), 7.55 (4H, s, Ar-H), 7.51-7.45 (3H, m, Ar-H), 7.43-7.37 (6H, m, Ar-H), 7.29-7.21 (6H, m, Ar-H), 6.63 (2H, s, N-CH), 4.33-4.24 (2H, m, COD-CH), 3.91-3.84 (2H, m, COD-CH), 3.41 (6H, s, N-CH_3), 2.33-2.21 (4H, m, COD-CH_2), 2.18-2.00 (4H, m, COD-CH_2).

^{13}C NMR (101 MHz, $CDCl_3$): δ 175.5 (d $^2J_{C-P}$ = 9.8 Hz), 161.9 (q $^1J_{C-B}$ = 49.6 Hz), 135.0, 133.7, 133.6, 131.6, 130.5, 130.0, 129.22, 129.15 (q $^2J_{C-F}$ = 32.7 Hz), 129.1, 124.8 (q $^1J_{C-F}$ = 273 Hz), 123.2, 117.7, 86.0, 85.9, 81.3, 37.1, 31.3, 30.8.

^{31}P NMR (162 MHz, $CDCl_3$): δ 18.35 (PPh_3).

^{19}F NMR (376 MHz, $CDCl_3$): δ -62.42 (BArF).

^{11}B NMR (128 MHz, $CDCl_3$): δ -6.65 (BArF).

HRMS (NSI): m/z calculated for $C_{31}H_{35}IrN_2P$ $[M\text{-}BArF]^+$: 657.2138; found: 657.2118.

Scheme 1.33 *New, efficient method for accessing IMes/alkyl-phosphine complexes.*

Reactions were carried out using general procedure E. Percentage buried volumes were calculated using literature data,[70] with the equation below. The *in-situ* generation of MeCN-stabilised hydride complexes were obtained using general procedure D, and tabulated as the hydride and corresponding phosphorous shifts (excluding ligands and counterions).

$$\%BV_{total} = \%BV_{PR_3} + \%BV_{NHC}$$

Solvent	***Temperature (°C)***	***Time (h)***	***IMes/Cl***
DCM (10 mL)	25	1 (0.5+0.5)	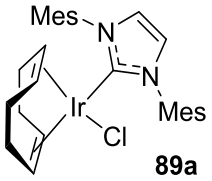 **89a** (320 mg, 0.5 mmol)

Phosphine	***AX***	***Isolation***
PBn_3 (152 mg, 0.5 mmol)	PF_6 (92 mg, 0.5 mmol)	Trituration from EtOAc

Product	***Data***[71]
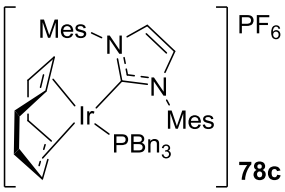 **78c** **Yield** = 343 mg, 65% **%BV** = 31.2 + 34.0 = 65.2% **[H]** = -22.74 ppm	**Appearance**: red powder. **Melting Point** (°C): >185 (dec). **IR** (cm^{-1}): 2980, 2959. **^{1}H NMR** (400 MHz, $CDCl_3$): δ 7.35 (2H, s, N-C<u>H</u>=C<u>H</u>-N), 7.28-7.17 (11H, m, Ar-<u>H</u>), 7.14-7.09 (2H, m, Ar-<u>H</u>), 6.85-6.79 (6H, m, Ar-<u>H</u>), 4.64 (2H, m, COD C<u>H</u>), 3.17-3.10 (2H, m, COD C<u>H</u>), 2.80 (6H, d ^2J = 8.8 Hz, P-C<u>H$_2$</u>-Ph), 2.47 (6H, s, Ar-C<u>H$_3$</u>), 2.42 (6H, s, Ar-C<u>H$_3$</u>), 2.25 (6H, s, Ar-C<u>H$_3$</u>), 1.80-1.67 (2H, m, COD C<u>H$_2$</u>), 1.58-1.40 (4H, m, COD C<u>H$_2$</u>), 1.35-1.18 (2H, m, COD C<u>H$_2$</u>).

^{13}C NMR (101 MHz, $CDCl_3$): δ 174.9 (d $^2J_{C-P}$ = 9.2 Hz), 141.1, 137.6, 137.1, 136.2, 134.4, 131.2, 130.8, 129.5, 128.5, 127.9, 127.8, 87.1, 76.1, 32.1, 31.1, 31.0, 21.0, 20.5, 19.9.

^{31}P NMR (162 MHz, $CDCl_3$): δ -6.9 (PBn_3), -144.5 (sep $^1J_{F-P}$ = 713 Hz, PF_6).

^{19}F NMR (376 MHz, $CDCl_3$): δ -73.5 (d ^1J = 713 Hz, PF_6).

MeCN Hydride Complex

^{1}H NMR (400 MHz, CD_3CN): -22.74 (d $^2J_{H-P}$ = 17.2 Hz).

^{31}P NMR (162 MHz, CD_3CN): δ -11.5 (t $^2J_{P-H}$ = 17.2 Hz, PBn_3).

Phosphine	***AX***	***Isolation***
$PnBu_3$ (101 mg, 123 µL, 0.5 mmol)	PF_6 (92 mg, 0.5 mmol)	Trituration from EtOAc
Product	***Data***[29]	
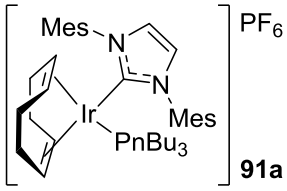 **91a** **Yield** = 348 mg, 73% **%BV** = 31.2 + 27.2 = 58.4% **[H]** = -22.26 ppm	**Appearance**: red powder. **Melting Point** (°C): 162-164. **IR** (cm^{-1}): 2949, 2870. **^{1}H NMR** (400 MHz, $CDCl_3$): δ 7.23 (2H, s, N-C<u>H</u>=C<u>H</u>-N), 7.04 (2H, br s, Ar-H), 6.96 (2H, br s, Ar-H), 4.16-4.09 (2H, m, COD-C<u>H</u>), 3.68-3.62 (2H, m, COD-C<u>H</u>), 2.34 (6H, s, Ar-C<u>H</u>$_3$), 2.28 (6H, s, Ar-C<u>H</u>$_3$), 2.17 (6H, s, Ar-C<u>H</u>$_3$), 1.91-1.81 (2H, m, COD-C<u>H</u>$_2$), 1.72-1.61 (2H, m, COD-C<u>H</u>$_2$), 1.51-1.37 (10H, m, COD-C<u>H</u>$_2$ & P^{n}Bu$_3$-C<u>H</u>$_2$), 1.26 (6H, *app.* sextet, J = 7.2 Hz, P^{n}Bu$_3$-CH$_2$-C<u>H</u>$_2$-CH$_3$), 1.15-1.06 (6H, m, P^{n}Bu$_3$-C<u>H</u>$_2$), 0.86 (9H, t, J = 7.3 Hz, P^{n}Bu$_3$-CH$_2$-C<u>H</u>$_3$).	

^{13}C NMR (101 MHz, $CDCl_3$): δ 175.5 (d $^2J_{C\text{-}P}$ = 9.1 Hz), 133.9, 129.3, 129.2, 125.6, 81.5, 81.4, 73.2, 30.8, 30.41, 30.39, 26.13, 26.10, 23.9, 23.8, 23.7, 23.4, 20.5, 19.8, 18.9, 13.2.

^{31}P NMR (162 MHz, $CDCl_3$): δ -2.6 ($PnBu_3$), -144.4 (sep $^1J_{P\text{-}F}$ = 711 Hz, PF_6).

^{19}F NMR (376 MHz, $CDCl_3$): δ -73.8 (d $^1J_{F\text{-}P}$ = 711 Hz, PF_6).

MeCN Hydride Complex

^{1}H NMR (400 MHz, CD_3CN): -22.26 (d $^2J_{H\text{-}P}$ = 18.4 Hz).

^{31}P NMR (162 MHz, CD_3CN): δ -10.1 (t $^2J_{P\text{-}H}$ = 18.4 Hz, $PnBu_3$).

Phosphine	***AX***	***Isolation***
PEt_3 (59 mg, 74 µL, 0.5 mmol)	PF_6 (92 mg, 0.5 mmol)	Trituration from EtOAc
Product	***Data***	
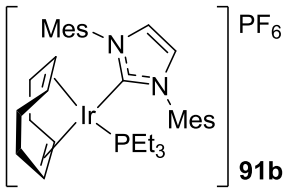 **91b** **Yield** = 282 mg, 65% **%BV** = 31.2 + 27.1 = 58.3% **[H]** = -22.30 ppm	**Appearance**: red powder. **Melting Point** (°C): >170 (dec). **IR** (cm^{-1}): 2989, 2862. **^{1}H NMR** (400 MHz, $CDCl_3$): δ 7.20 (2H, s, N-C<u>H</u>=C<u>H</u>-N), 7.05 (2H, br s, Ar-H), 6.98 (2H, br s, Ar-H), 4.16-4.10 (2H, m, COD-C<u>H</u>), 3.73-7.67 (2H, m, COD-C<u>H</u>), 2.33 (6H, s, Ar-C<u>H</u>$_3$), 2.27 (6H, s, Ar-CH_3), 2.20 (6H, s, Ar-C<u>H</u>$_3$), 1.92-1.82 (2H, m, COD-C<u>H</u>$_2$), 1.70-1.60 (2H, m, COD-C<u>H</u>$_2$), 1.57-1.45 (4H, m, COD-C<u>H</u>$_2$), 1.39 (6H, quin J = 7.7 Hz, P-C<u>H</u>$_2$-CH_3), 0.84 (9H, *app.* dt J = 15.1 Hz, J = 7.5 Hz, CH_2-C<u>H</u>$_3$).	

^{13}C NMR (101 MHz, $CDCl_3$): δ 176.9 (d $^2J_{C-P}$ = 8.1 Hz), 140.2, 136.0, 135.7, 134.6, 130.03, 129.98, 126.2, 83.8, 83.7, 73.6, 31.2, 31.01, 30.97, 21.1, 20.3, 19.7, 16.9, 16.6, 8.69, 8.67.

^{31}P NMR (162 MHz, $CDCl_3$): δ 2.2 (PEt_3), -144.4 (sep $^1J_{P-F}$ = 712 Hz, PF_6).

^{19}F NMR (376 MHz, $CDCl_3$): δ -73.7 (d $^1J_{F-P}$ = 711 Hz, PF_6).

HRMS (NSI): m/z calculated for $C_{35}H_{51}Ir^{191}N_2P$ $[M\text{-}BArF]^+$: 721.3386; found: 721.3390.

MeCN Hydride Complex

^{1}H NMR (400 MHz, CD_3CN): -22.30 (d $^2J_{H-P}$ = 16.9 Hz).

^{31}P NMR (162 MHz, CD_3CN): δ -3.6 (t $^2J_{P-H}$ = 16.9 Hz, PEt_3).

Phosphine	***AX***	***Isolation***
$P(Me)_2Ph$ (69 mg, 71 µL 0.5 mmol)	PF_6 (92 mg, 0.5 mmol)	Trituration from EtOAc
Product	***Data***[71]	
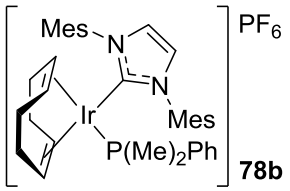 **78b** **Yield** = 342 mg, 77% **%BV** = 31.2 + 25.1 = 56.3% **[H]** = -21.99 ppm	**Appearance**: red powder. **Melting Point** (°C): >195 (dec). **IR** (cm^{-1}): 2982, 2951. **^{1}H NMR** (400 MHz, $CDCl_3$): δ 7.42-7.32 (3H, m, Ar-H) 7.28-7.21 (4H, m, Ar-H & m, N-CH=CH-N), 7.06-7.00 (2H, m, Ar-H), 6.93-6.87 (2H, m, Ar-H), 4.34-4.22 (2H, m, COD CH), 3.50-3.36 (2H, m, COD CH), 2.36 (6H, s, Ar-CH_3), 2.19 (6H, s, Ar-CH_3), 2.12 (6H, s, Ar-CH_3), 1.78-1.41 (8H, m, COD CH_2), 1.49 (3H, s, P-CH_3), 1.47 (3H, s, P-CH_3).	

^{13}C NMR (101 MHz, $CDCl_3$): δ 177.6 (d $^2J_{C-P}$ = 6.9 Hz), 139.3, 135.1, 134.2, 131.2, 130.5, 129.6, 129.3, 128.1, 125.3, 83.5, 82.6, 76.2, 75.2, 30.9, 29.9, 21.2, 20.5, 18.7, 16.5, 15.3.

^{31}P NMR (162 MHz, $CDCl_3$): δ -14.1 (PMe_2Ph), -145.1 (sep $^1J_{P-F}$ = 711 Hz, PF_6).

^{19}F NMR (376 MHz, $CDCl_3$): δ -73.9 (d $^1J_{F-P}$ = 711 Hz, PF_6).

MeCN-Hydride Complex

^{1}H NMR (400 MHz, CD_3CN): -21.99 (d $^2J_{H-P}$ = 18.5 Hz).

^{31}P NMR (162 MHz, CD_3CN): δ -26.0 (t $^2J_{P-H}$ = 18.5 Hz, PEt_3).

Phosphine	***AX***
PBn_3 (152 mg, 0.5 mmol)	NaBArF (443 mg, 0.5 mmol)
Product	***Data***
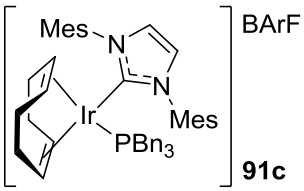 **91c** **Yield** = 762 mg, 86%	**Appearance**: red powder. **Melting Point** (°C): >175 (dec). **IR** (cm^{-1}): 2978, 2361, 1495. **^{1}H NMR** (400 MHz, $CDCl_3$): δ 7.79 (8H, t ^4J = 2.3 Hz, Ar-H), 7.58 (4H, s, Ar-H), 7.37-7.27 (13H, m, Ar-H), 7.25-7.21 (2H, m, Ar-H), 6.92-6.87 (6H, m, N-CH and Ar-H), 4.66-4.61 (2H, m, COD-CH), 3.31-3.27 (2H, m, COD-CH), 2.90 (6H, d ^2J = 8.7 Hz, P-CH_2-Ar), 2.51 (6H, s, Ar-CH_3), 2.50 (6H, s, Ar-CH_3), 2.33 (6H, s, Ar-CH_3), 1.86-1.73 (2H, m, COD-CH_2), 1.65-1.49 (4H, m, COD-CH_2), 1.43-1.32 (2H, m, COD-CH_2).

^{13}C NMR (101 MHz, $CDCl_3$): δ 176.5 (d $^2J_{C-P}$ = 7.7 Hz), 161.2 (q $^1J_{C-B}$ = 49.5 Hz), 140.4, 135.6, 135.3, 134.3, 134.2, 132.2, 132.1, 130,0, 129.5, 129.33, 129.28, 128.4 (q $^2J_{C-F}$ = 32.9 Hz), 128.3, 127.1, 125.7, 124.1 (q $^1J_{C-F}$ = 269 Hz), 116.9, 86.1, 85.9, 75.5, 31.3, 31.0, 30, 29.7, 20.5, 19.6, 19.0.

^{31}P NMR (162 MHz, $CDCl_3$): δ -7.98 (PBn_3).

^{19}F NMR (376 MHz, $CDCl_3$): δ -62.42 (BArF).

^{11}B NMR (128 MHz, $CDCl_3$): δ -6.65 (BArF).

HRMS (NSI): m/z calculated for $C_{50}H_{57}IrN_2P$ $[M\text{-}BArF]^+$: 607.3867; found: 607.3860.

Phosphine	***AX***
$PnBu_3$ (101 mg, 123 µL, 0.5 mmol)	NaBArF (443 mg, 0.5 mmol)

Product	***Data***
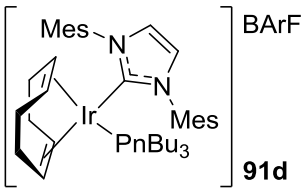 **Yield** = 727 mg, 87%	**Appearance**: red powder. **Melting Point** (°C): 162-164. **IR** (cm^{-1}): 2965, 2932, 2878, 2359, 2328, 1483, 1466. **^{1}H NMR** (400 MHz, $CDCl_3$): δ 7.73 (8H, t ^4J = 2.2 Hz, Ar-H), 7.54 (4H, s, Ar-H), 7.11 (2H, s, N-CH), 7.06 (2H, s, Ar-H), 7.02 (2H, s, Ar-H), 4.18-4.12 (2H, m, COD-CH_2), 3.74-3.68 (2H, m, COD-CH_2), 2.36 (6H, s, Ar-CH_3), 2.29 (6H, s, Ar-CH_3), 2.19 (6H, s, Ar-CH_3), 1.95-1.84 (2H, m, COD-CH_2), 1.72-1.64 (2H, m, COD-CH_2), 1.58-1.38 (10H, m, COD-CH_2 & CH_2-CH_2-CH_2), 1.28 (6H, sex J = 7.2 Hz, CH_2-CH_2-CH_3), 1.20-1.08 (6H, m, P-CH_2-CH_2), 0.87 (9H, t J = 7.2 Hz, CH_2-CH_3).

^{13}C NMR (101 MHz, $CDCl_3$): δ 176.7 (d $^2J_{C\text{-}P}$ = 8.8 Hz), 161.2 (q $^1J_{C\text{-}B}$ = 49.9 Hz), 139.9, 135.2, 135.0, 134.3, 133.5, 129.5, 129.3, 128.4 (q $^2J_{C\text{-}F}$ = 31.8 Hz), 124.9, 124.1 (q $^1J_{C\text{-}F}$ = 273 Hz), 116.9, 91.6, 81.5, 73.8, 30.7, 30.3, 26.1, 23.9, 23.7, 23.4, 20.3, 13.6, 18.8, 13.0.

^{31}P NMR (162 MHz, $CDCl_3$): δ -2.48 ($PnBu_3$).

^{19}F NMR (376 MHz, $CDCl_3$): δ -62.43 (BArF).

^{11}B NMR (128 MHz, $CDCl_3$): δ -6.65 (BArF).

HRMS (ESI): m/z calculated for $C_{41}H_{63}IrN_2P$ $[M\text{-}BArF]^+$: 807.4355; found: 807.4358.

Phosphine	***AX***
PEt_3 (59 mg, 74 µL, 0.5 mmol)	NaBArF (443 mg, 0.5 mmol)
Product	***Data***
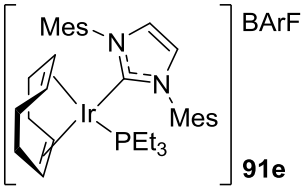 **Yield** = 642 mg, 81%	**Appearance**: red powder. **Melting Point** (°C): >170 (dec). **IR** (cm^{-1}): 2978, 2901, 2357, 1495 **^{1}H NMR** (400 MHz, $CDCl_3$): δ 7.71 (8H, s, Ar-H), 7.53 (4H, s, Ar-H), 7.10 (2H, s, N-CH), 7.05 (2H, s, Ar-H), 7.01 (2H, s, Ar-H), 4.19-4.13 (2H, m, COD-CH), 3.75-3.70 (2H, m, COD-CH), 2.34 (6H, s, Ar-CH_3), 2.28 (6H, s, Ar-CH_3), 2.18 (6H, s, Ar-CH_3), 1.93-1.81 (2H, m, COD-CH_2), 1.72-1.61 (2H, m, COD-CH_2), 1.60-1.47 (4H, m, COD-CH_2), 1.37 (6H, quin J = 7.6 Hz, P-CH_2-CH_3), 0.82 (9H, *app.* dt J = 16.0 Hz, J = 7.6 Hz, CH_2-CH_3).

^{13}C NMR (101 MHz, $CDCl_3$): δ 176.9 (d $^2J_{C\text{-}P}$ = 8.0 Hz), 161.2 (q $^1J_{C\text{-}B}$ = 49.9 Hz), 140.6, 135.8, 135.6, 135.0, 134.3, 130.2, 130.0, 128.4 (q $^2J_{C\text{-}F}$ = 33.1 Hz), 125.6, 122.0 (q $^1J_{C\text{-}F}$ = 273 Hz), 117.6, 84.2, 84.1, 73.9, 31.1, 30.93, 30.90, 21.0, 20.2, 19.6, 16.9, 16.6, 8.55, 8.51.

^{31}P NMR (162 MHz, $CDCl_3$): δ 2.1 (PEt_3).

^{19}F NMR (376 MHz, $CDCl_3$): δ -62.4 (BArF).

^{11}B NMR (128 MHz, $CDCl_3$): δ -6.65 (BArF).

HRMS (NSI): m/z calculated for $C_{35}H_{51}IrN_2P$ $[M\text{-}BArF]^+$: 721.3386; found: 721.3390.

Phosphine	***AX***
$P(Me)_2Ph$ (69 mg, 71 µL 0.5 mmol)	NaBArF (443 mg, 0.5 mmol)
Product	***Data***
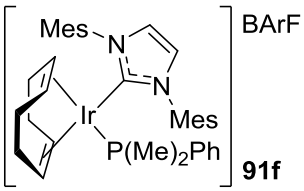 **91f** **Yield** = 731 mg, 91%	**Appearance**: red powder. **Melting Point** (°C): 146-149. **I.R.** (cm^{-1}): 2980, 2884, 1609, 1352, 1275, 1117. **^{1}H NMR** (400 MHz, $CDCl_3$): δ 7.73 (8H, t ^4J = 2.4 Hz, Ar-H), 7.53 (4H, s, Ar-H), 7.44-7.40 (1H, m, Ar-H), 7.35-7.26 (4H, m, Ar-H), 7.18 (2H, s, N-CH=CH-N), 7.08 (2H, s, Ar-H), 6.92 (2H, s, Ar-H), 4.33-4.30 (2H, m, COD-CH), 3.46-3.44 (2H, m, COD-CH), 2.39 (6H, s, Ar-CH_3), 2.21 (6H, s, Ar-CH_3), 2.11 (6H, s, Ar-CH_3), 1.78-1.48 (8H, m, COD-CH_2), 1.46 (3H, s, P-CH_3), 1.44 (3H, s, P-CH_3).

^{13}C NMR (101 MHz, $CDCl_3$): δ 178.0 (d $^2J_{C-P}$ = 8.7 Hz), 161.7 (q $^1J_{C-B}$ = 50.3 Hz), 140.3, 135.3, 135.2, 134.8, 134.1, 131.5, 131.4, 130.93, 130.90, 128.9, 128.8, 128.7 (q $^2J_{C-F}$ = 33.0 Hz), 125.4, 124.5 (q $^1J_{C-F}$ = 273 Hz), 117.4, 83.7, 83.6, 76.3, 31.3, 30.34, 30.31, 20.8, 20.0, 19.0, 16.5, 16.1.

^{31}P NMR (162 MHz, $CDCl_3$): δ -14.44 ($P(Me)_2Ph$).

^{19}F NMR (376 MHz, $CDCl_3$): δ -62.40 (BArF).

^{11}B NMR (128 MHz, $CDCl_3$): δ -6.62 (BArF).

HRMS (NSI): m/z calculated for $C_{37}H_{47}Ir^{191}N_2P$ $[M\text{-}BArF]^+$: 741.3077; found: 741.3075.

Although synthesised using a different method[73] complex **78a** was paramterised to complete the series.

Product	***Data***[71]
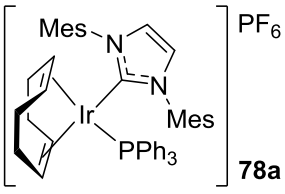 **78a** **%BV** = 31.2 + 29.9 = 61.1% **[H]** = -21.56 ppm	***MeCN-Hydride Complex*** **^{1}H NMR** (400 MHz, CD_3CN): -21.56 (d $^2J_{H-P}$ = 16.1 Hz). **^{31}P NMR** (162 MHz, CD_3CN): δ 18.6 (t $^2J_{P-H}$ = 16.1 Hz, PEt_3).

Scheme 1.34 *Initial testing with new NHC/phosphine catalysts.*

Reactions were carried out using general procedure A and analysed by ^{1}H NMR spectroscopy to calculate the reaction conversion, and the results are tabulated in **Table E1.2**. Catalyst separation was carried out by filtration through a pipette of silica, eluting with Et_2O/petroleum ether (30/70).

Solvent	***Temperature (°C)***	***Time (min)***
DCM (8 mL)	25	30
	Substrate	
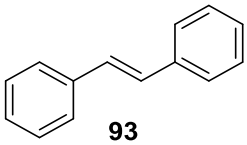 **93** (73 mg, 0.4 mmol)	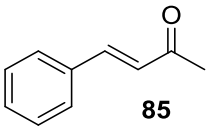 **85** (58 mg, 0.4 mmol)	
Product	***Data***[96,72]	
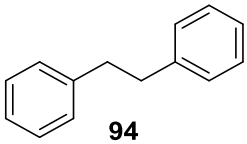 **94**	**Melting Point** (°C): 50-51. **IR** (cm^{-1}): 3057, 3026, 2916, 2855. **^{1}H NMR** (400 MHz, $CDCl_3$): δ 7.33-7.29 (4H, m, Ar-H), 7.25-7.21 (6H, m, Ar-H), 2.95 (4H, s, Ar-CH_2). **^{13}C NMR** (101 MHz, $CDCl_3$): δ 141.3, 130.0, 125.4, 37.5 (2 signals overlap).	
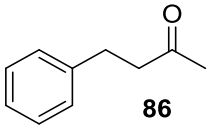 **86**	Data was consistent with that reported on page 88.	

Complex	***Conversion (%)***					
	93			***85***		
	Run		***Ave***	***Run***		***Ave***
	1	***2***		***1***	***2***	
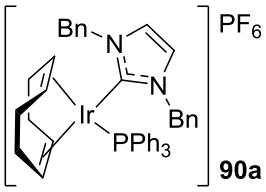 **90a** (1.9 mg, 2.0 μmol)	<5	<5	<5	<5	<5	<5
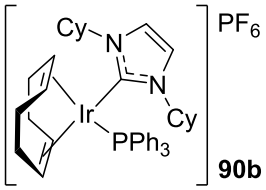 **90b** (1.9 mg, 2.0 μmol)	<5	<5	<5	<5	<5	<5
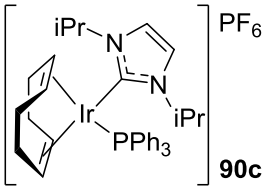 **90c** (1.7 mg, 2.0 μmol)	<5	<5	<5	<5	<5	<5
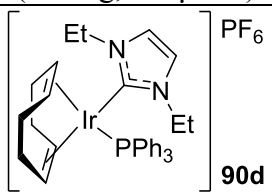 **90d** (1.7 mg, 2.0 μmol)	<5	<5	<5	<5	<5	<5
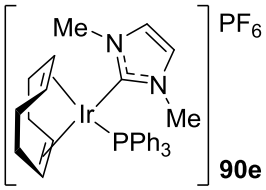 **90e** (1.6 mg, 2.0 μmol)	<5	<5	<5	<5	<5	<5
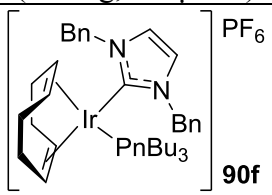 **90f** (1.8 mg, 2.0 μmol)	18	17	18	<5	<5	<5
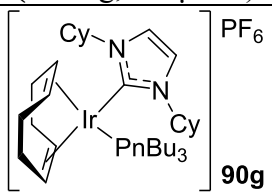 **90g** (1.8 mg, 2.0 μmol)	18	18	18	<5	<5	<5

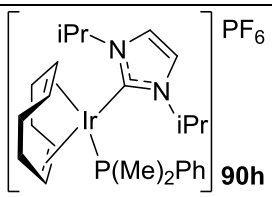 **90h** (1.5 mg, 2.0 μmol)	8	5	7	<5	<5	<5
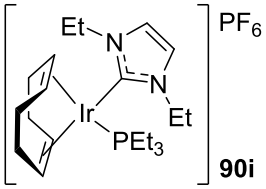 **90i** (1.4 mg, 2.0 μmol)	13	8	11	<5	<5	<5
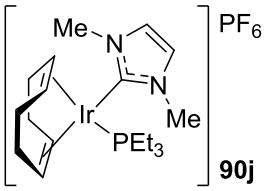 **90j** (1.3 mg, 2.0 μmol)	19	16	18	<5	<5	<5
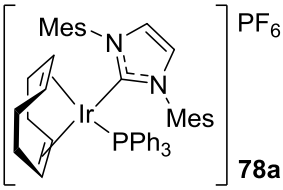 **78a** (2.0 mg, 2.0 μmol)	18	16	17	26	27	27
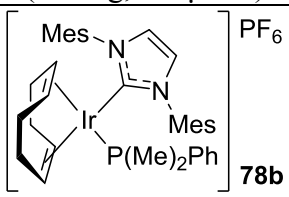 **78b** (1.8 mg, 2.0 μmol)	95	89	92	100	100	100
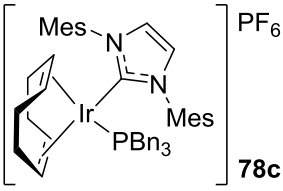 **78c** (2.1 mg, 2.0 μmol)	100	95	98	100	100	100
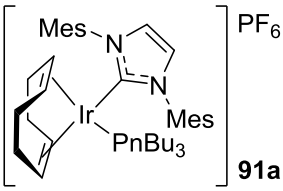 **91a** (1.9 mg, 2.0 μmol)	97	100	99	100	100	100
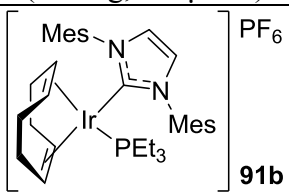 **91b** (1.7 mg, 2.0 μmol)	100	98	99	100	100	100

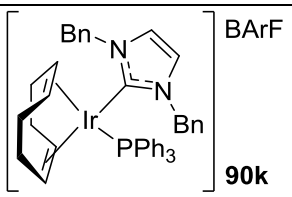 (3.3 mg, 2.0 μmol)	<5	<5	<5	<5	<5	<5
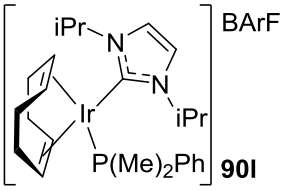 (2.9 mg, 2.0 μmol)	5	6	6	<5	<5	<5
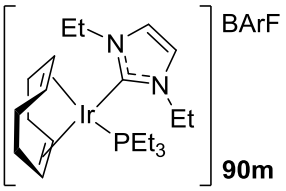 (2.8 mg, 2.0 μmol)	8	8	8	<5	<5	<5
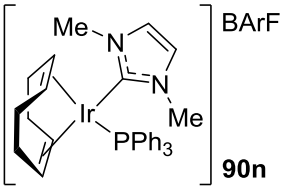 (3.0 mg, 2.0 μmol)	<5	<5	<5	<5	<5	<5
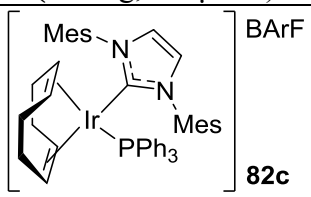 (3.5 mg, 2.0 μmol)	49	54	52	34	32	33
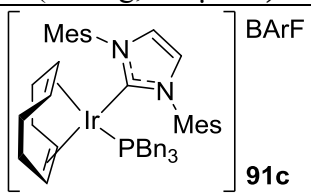 (3.5 mg, 2.0 μmol)	96	94	95	100	100	100
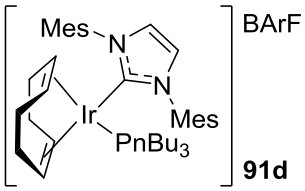 (3.3 mg, 2.0 μmol)	98	100	99	100	100	100

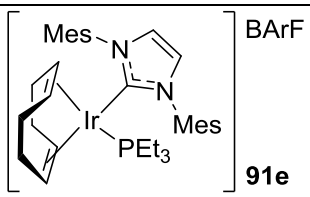 **91e** (3.2 mg, 2.0 μmol)	100	98	99	100	100	100
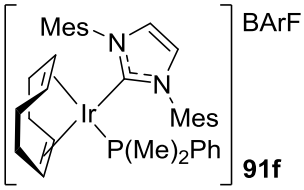 **91f** (3.2 mg, 2.0 μmol)	92	95	94	100	100	100

Table E1.2

6.3. Directing Group Assisted Olefin Hydrogenation

Scheme 1.35 *Comparison with Crabtee's catalyst.*

Reactions were carried out using general procedure A and analysed by ^{1}H NMR spectroscopy to calculate the reaction conversion, and are tabulated in **Table E1.3**. Catalyst separation was carried out by filtration through a pipette of silica, eluting with Et_2O/petroleum ether (30/70).

Substrate	***Solvent***	***Temperature (°C)***	***Time (min)***
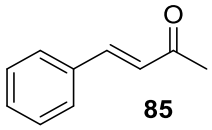 **85** (58 mg, 0.4 mmol)	DCM (8 mL)	25	30
Product	***Data***[72]		
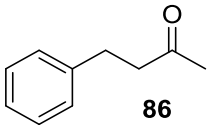 **86**	Data was consistent with that reported on page 88.		

Complex	***Conversion (%)***		
	Run		***Ave***
	1	***2***	
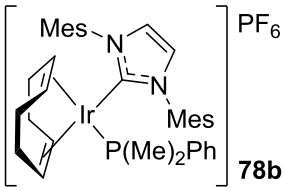 (1.8 mg, 2.0 μmol)	100	100	100
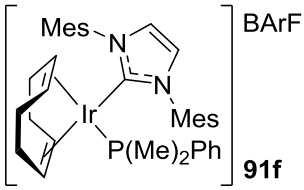 (3.2 mg, 2.0 μmol)	100	100	100
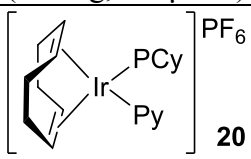 (1.5 mg, 2.0 μmol)	26	30	28
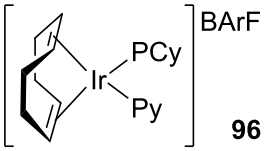 (2.7 mg, 2.0 μmol)	27	23	25

Table E1.3

Experimental design to identify optimised conditions for directing group assisted hydrogenation.

Experimental design was used to assess the effect of varying the catalyst loading, reaction time and reaction concentration. As such, 'high' and 'low' values for each of the three variables were chosen. To generate a series of experiments to study optimal conditions within the variable ranges chosen, Design Expert™ software v10.0 (Stat_Ease Inc., minneappolis, Mn) was used. This generated a *two-level, three-factorial* design containing three centre points, giving 11 experiments in total. The conversion of **85** was used as the response. The reactions were carried out according to general procedure A and analysed by ^{1}H NMR spectroscopy. (**Table E1.4**).

Complex	***Substrate***	***Solvent***	***Temperature (°C)***
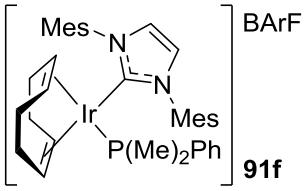 **91f**	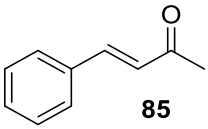 **85** (146 mg, 1.0 mmol)	DCM	25
Product	***Data***[72]		
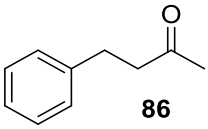 **86**	Data was consistent with that reported on page 88.		

Run[a]	*Variable A: Catalyst Loading* **(mol%)**	*91f (mg, µmol)*	*Variable B: Reaction Concentration (molL^{-1})*	*DCM (mL)*	*Variable C: Reaction Time* **(min)**	*Response: Incorporation* **(%D)**
1 (+--)	0.5	8.0, 5.0	0.05	20	0.5	75
2 (***)	0.3	4.8, 3.0	0.225	4.4	1.75	53
3 (--+)	0.1	1.6, 1.0	0.05	20	3	35
4 (***)	0.3	4.8, 3.0	0.225	4.4	1.75	52
5 (---)	0.1	1.6, 1.0	0.05	20	0.5	10
6 (++-)	0.5	8.0, 5.0	0.4	2.5	0.5	22
7 (+++)	0.5	8.0, 5.0	0.4	2.5	3	100
8 (***)	0.3	4.8, 3.0	0.225	4.4	1.75	52
9 (+-+)	0.5	8.0, 5.0	0.05	20	3	100
10 (-+-)	0.1	1.6, 1.0	0.4	2.5	0.5	7
11 (-++)	0.1	1.6, 1.0	0.4	2.5	3	12

[a] symbol in parentheses indicate points in the design; + high, * mid and – low.

Table E1.4

Run 2, 4 and 8 represent the centre points of the design. These are employed in order to:

(i) Assess any curvature in the response of incorporation changes in the variables; and

(ii) Assess the repeatability of the hydrogen isotope exchange reaction.

A response surface was created in the same design program. This generated a half-normal plot inferring that increasing the catalyst loading and reaction time had a positive impact upon the hydrogenatin reaction, with increasing reaction concentration having a negative impact. Furthermore, it indicated the order of significance of each factor; Catalyst Loading > Reaction Time > Substrate Concentration (**Graph E1.1**).

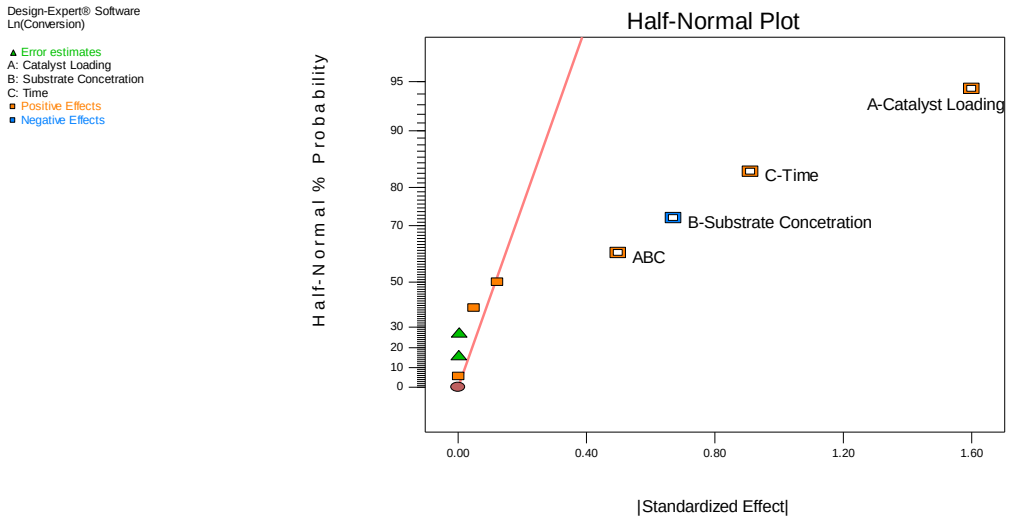

Graph E1.1

Further implementation of the design software generated **Graph E1.2**. By plotting reaction time and catalyst loading at the fixed optimal reaction concentration (0.1 molL^{-1}), it can be seen that moderately elevated catalyst loading and reaction time leads to the optimised conditions (0.5 mol%, 0.1 molL^{-1}, 2 h).

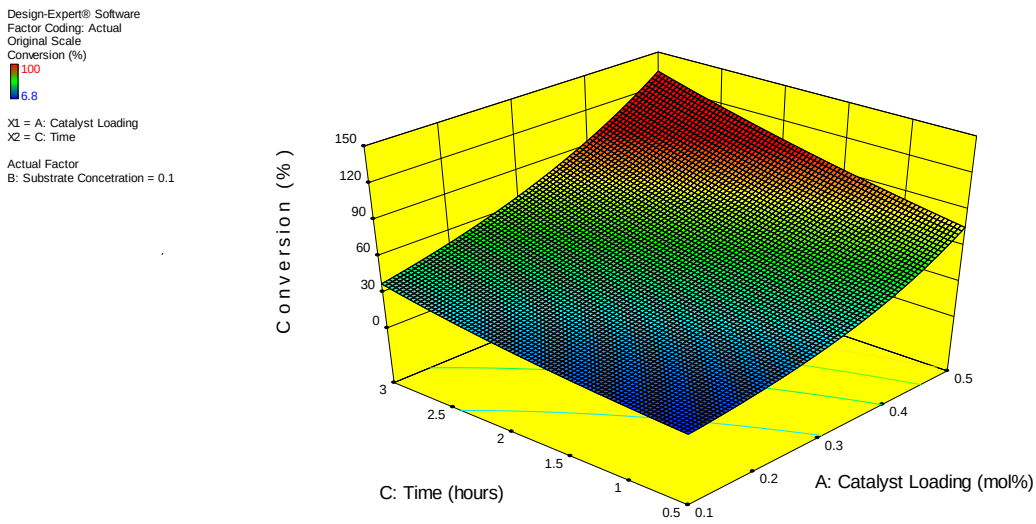

Graph E1.2

Finally, provided below is a graph of Residuals versus Predicted plot. This is a plot of the residuals versus the ascending predicted response values (low incorporation to high incorporation), and tests the assumption of constant variance in the data (**Graph E1.3**).

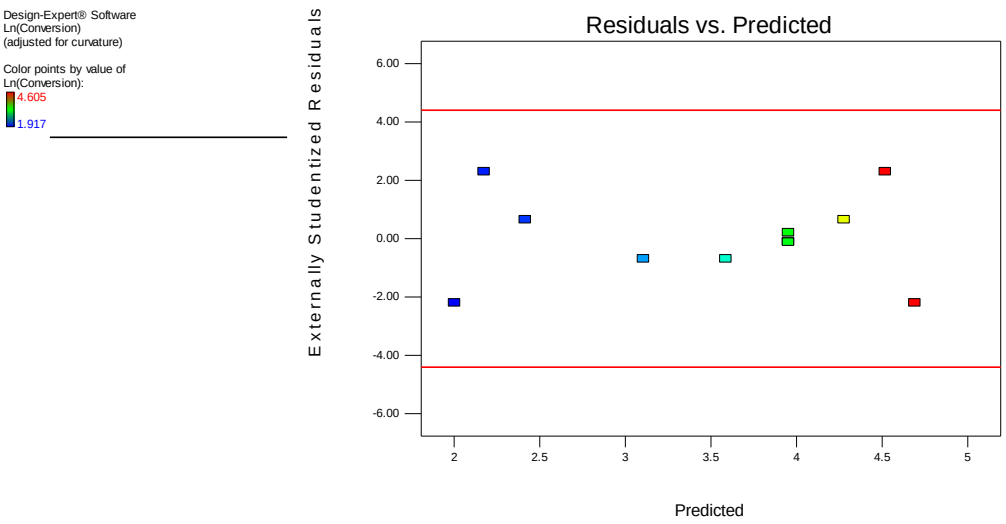
Design-Expert® Software
Ln(Conversion)
(adjusted for curvature)
Color points by value of
Ln(Conversion):
4.605
1.917
Residuals vs. Predicted
Externally Studentized Residuals
6.00
4.00
2.00
0.00
-2.00
-4.00
-6.00
2
2.5
3
3.5
4
4.5
5
Predicted

Graph E1.3

Scheme 1.36 *Directing group assisted hydrogenation of further substrates.*

Reactions were carried out using general procedure A and analysed by ^{1}H NMR spectroscopy to calculate the reaction conversion. Isolation of each reaction was carried by flash column chromatography under the given conditions.

Complex	***Solvent***	***Temperature (°C)***	***Time (h)***
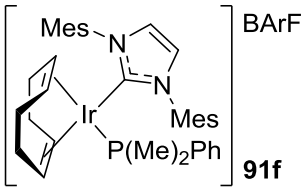 **91f** (3.2 mg, 2.0 μmol)	DCM (4 mL)	25	2

Substrate
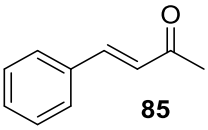 **85** (58 mg, 0.4 mmol)

Product	***Data***[72]
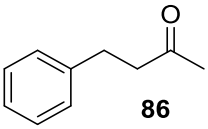 **86**	Data was consistent with that reported on page 88.

Conversion (%)	***Chromatography Conditions***	***Yield (mg, %)***
100	(Et_2O/Pet Ether, 10/90)	58.1 mg, 98%

Substrate
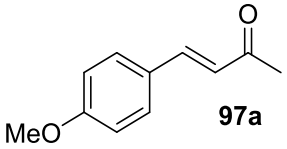 **97a** (70 mg, 0.4 mmol)

Product	***Data***[97]
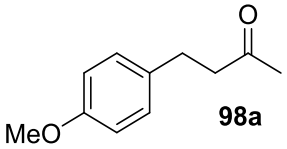 **98a**	**IR** (cm^{-1}): 3049, 2958, 1677. **^{1}H NMR** (400 MHz, $CDCl_3$): δ 7.11-7.02 (2H, m, Ar-H), 6.83-6.76 (2H, m, Ar-H), 3.75 (3H, s, O-CH_3), 2.85-2.77 (2H, m, CH_2), 2.74-2.61 (2H, m, CH_2), 2.10 (3H, s, CO-CH_3). **^{13}C NMR** (101 MHz, $CDCl_3$): δ 208.2, 158.1, 133.1, 129.3, 114.0, 55.3, 45.6, 30.2, 29.0.

Conversion (%)	***Chromatography Conditions***	***Yield (mg, %)***
100	(Et_2O/Pet Ether, 10/90)	69.2, 97

Substrate
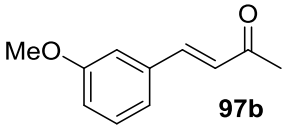 **97b** (70 mg, 0.4 mmol)

Product	***Data***[98]
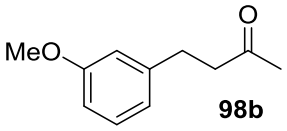 **98b**	**IR** (cm^{-1}): 3021, 2849, 1707. **^{1}H NMR** (400 MHz, $CDCl_3$): δ 7.19-7.15 (1H, m, Ar-H), 6.76-6.71 (3H, m, Ar-H), 3.76 (3H, s, O-CH_3), 2.86-2.83 (2H, m, CH_2), 2.75-2.71 (2H, m, CH_2), 2.11 (3H, s, CO-CH_3). **^{13}C NMR** (101 MHz, $CDCl_3$): δ 207.9, 159.9, 142.8, 129.6, 120.7, 114.2, 111.5, 55.2, 45.2, 30.1, 29.9.

Conversion (%)	***Chromatography Conditions***	***Yield (mg, %)***
100	(Et_2O/Pet Ether, 10/90)	69.9, 98

Substrate
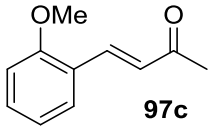 **97c** (70 mg, 0.4 mmol)

Product	***Data***[98]
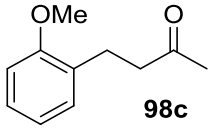 **98c**	**IR** (cm^{-1}): 3025, 2987, 1690. **^{1}H NMR** (400 MHz, $CDCl_3$): δ 7.23-7.14 (2H, m, Ar-H), 6.91-6.85 (2H, m, Ar-H) 3.84 (3H, s, O-CH_3) 2.92-2.89 (2H, m, CH_2), 2.76-2.73 (2H, m, CH_2), 2.15 (3H, s, CO-CH_3). **^{13}C NMR** (101 MHz, $CDCl_3$): δ 208.7, 157.5, 130.0, 129.4, 127.6, 120.6, 110.3, 55.3, 43.8, 30.0, 25.1.

Conversion (%)	***Chromatography Conditions***	***Yield (mg, %)***
100	(Et_2O/Pet Ether, 10/90)	69.8, 98

Substrate
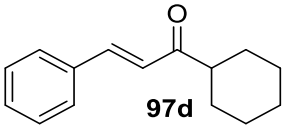 **97d** (86 mg, 0.4 mmol)

Product	***Data***[99]
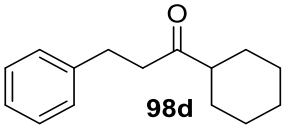 **98d**	**IR** (cm^{-1}): 3026, 2927, 2852, 1705. **^{1}H NMR** (400 MHz, $CDCl_3$): δ 7.31-7.27 (2H, m, Ar-H), 7.20-7.17 (3H, m, Ar-H), 2.90-2.87 (2H, m, CH_2), 2.78-2.75 (2H, m, CH_2), 2.35-2.90 (1H, m, Cy-CH), 1.82-1.76 (4H, m, Cy-CH_2), 1.68-1.65 (1H, m, Cy-CH), 1.36-1.15 (5H, m, Cy-CH_2 & Cy-CH). **^{13}C NMR** (101 MHz, $CDCl_3$): δ 213.1, 141.4, 128.4, 128.3, 126.0, 51.0, 42.2, 29.8, 28.4, 25.9, 25.7.

Conversion (%)	***Chromatography Conditions***	***Yield (mg, %)***
100	(Et_2O/Pet Ether, 10/90)	82.2, 95

Substrate
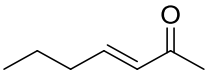 **97e** (45 mg, 0.4 mmol)

Product	***Data***[100]
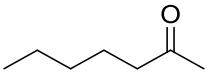 **98e**	**IR** (cm^{-1}): 3029, 2934, 2874, 1692. **^{1}H NMR** (400 MHz, $CDCl_3$): δ 2.40 (2H, t, *J* = 7.4 Hz, CO-C<u>H</u>$_2$-CH$_2$), 2.12 (3H, s, CO-C<u>H</u>$_3$), 1.56 (2H, quin *J* = 7.4 Hz, CH$_2$-C<u>H</u>$_2$-CH$_2$), 1.34-1.23 (4H, m, C<u>H</u>$_2$), 0.88 (3H, t *J* = 7.1 Hz, CH$_2$-C<u>H</u>$_3$). **^{13}C NMR** (101 MHz, $CDCl_3$): δ 209.3, 43.8, 31.4, 29.8, 23.5, 22.4, 13.9.

Conversion (%)	***Chromatography Conditions***	***Yield (mg, %)***
100	(Et_2O/Pet Ether, 10/90)	43.4, 95

Substrate
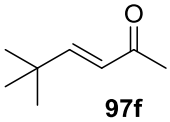 **97f** (50 mg, 0.4 mmol)

Product	***Data***[101]
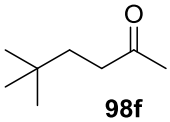 **98f**	**IR** (cm^{-1}): 3042, 2963, 2905, 1712. **^{1}H NMR** (400 MHz, $CDCl_3$): δ 2.44-2.40 (2H, m, C<u>H</u>$_2$), 2.18 (3H, s, CO-C<u>H</u>$_3$), 1.52-1.48 (2H, m, CH$_2$), 0.91 (9H, s, C-(C<u>H</u>$_3$)$_3$). **^{13}C NMR** (101 MHz, $CDCl_3$): δ 209.2, 39.1, 37.0, 29.5, 29.1, 28.8.

Time (h)	***Conversion (%)***	***Chromatography Conditions***	***Yield (mg, %)***
2	32	N/A	N/A
16	100	(Et_2O/Pet Ether, 10/90)	48.7, 95

Substrate	
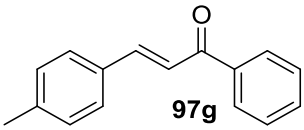 (89 mg, 0.4 mmol)	
Product	***Data***[102]
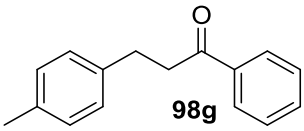	**IR** (cm^{-1}): 3049, 3020, 2922, 2864. **^{1}H NMR** (400 MHz, $CDCl_3$): δ 8.00-7.97 (2H, m, Ar-H), 7.60-7.56 (1H, m, Ar-H), 7.50-7.46 (2H, m, Ar-H), 7.19-7.12 (4H, m, Ar-H), 3.33-3.29 (2H, m, CH_2), 3.08-3.04 (2H, m, Ar-H), 2.35 (3H, m, Ar-CH_3). **^{13}C NMR** (101 MHz, $CDCl_3$): δ 198.8, 137.7, 136.4, 135.1, 132.5, 128.7, 128.1, 127.8, 127.5, 40.1, 29.2, 20.5.

Conversion (%)	***Chromatography Conditions***	***Yield (mg, %)***
100	(Et_2O/Pet Ether, 10/90)	88.8, 99

Substrate
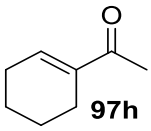 (50 mg, 0.4 mmol)

Product	***Data***[103]
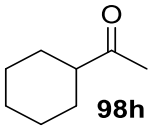	**IR** (cm^{-1}): 2932, 2961, 1683. **^{1}H NMR** (400 MHz, $CDCl_3$): δ 2.37-2.30 (1H, m, Cy-CH), 2.14 (3H, s, CO-CH_3), 1.90-1.84 (2H, m, Cy-CH_2), 1.82-1.77 (2H, m, Cy-CH_2), 1.71-1.66 (1H, m, Cy-CH), 1.39-1.19 (5H, m, Cy-CH_2 & Cy-CH). **^{13}C NMR** (101 MHz, $CDCl_3$): δ 212.2, 51.0, 28.0, 27.3, 25.4, 25.1.

91f (mg, µmol)	***Time (h)***	***Conversion (%)***	***Chromatography Conditions***	***Yield (mg, %)***
(3.2 mg, 2.0 µmol)	2	21	N/A	N/A
(6.4 mg, 4.0 µmol)	16	100	(Et_2O/Pet Ether, 10/90)	49.5, 98

Substrate
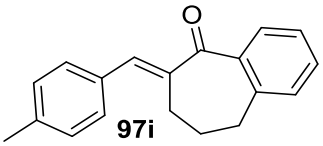 **97i** (105 mg, 0.4 mmol)

Product	***Data***
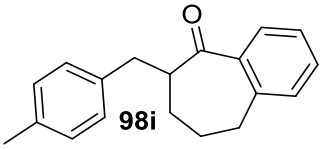 **98i**	**IR** (cm^{-1}): 3019, 2926, 2860, 1680. **^{1}H NMR** (400 MHz, $CDCl_3$): δ 7.64 (1H, dd, J = 7.6 Hz, ^{4}J = 1.6 Hz, Ar-H), 7.39 (1H, td, J = 7.5 Hz, ^{4}J = 1.5 Hz, Ar-H), 7.30-7.27 (1H, m, Ar-H), 7.23-7.21 (1H, m, Ar-H), 7.09 (4H, s, Ar-H), 3.28 (1H, dd, ^{2}J = 13.7 Hz, ^{3}J = 5.5 Hz, Ar-CH), 3.18-3.10 (1H, m, CH), 3.05-2.91 (2H, m, CH_2), 2.73 (1H, dd, ^{2}J = 13.7 Hz, ^{3}J = 7.1 Hz, Ar-CH), 2.33 (3H, s, Ar-CH_3), 2.05-2.02 (1H, m, CH), 1.94-1.88 (1H, m, CH), 1.72-1.58 (2H, m, CH_2). **^{13}C NMR** (101 MHz, $CDCl_3$): δ 197.9, 141.5, 139.5, 136.6, 135.0, 130.7, 129.3, 128.50, 128.46, 127.8, 125.9, 51.1, 36.0, 33.2, 29.9, 25.0, 20.5. **HRMS** (APCI): m/z calculated for $C_{19}H_{21}O$ $[M+H]^+$: 265.1587; found: 265.1585.

91f (mg, µmol)	***Time (h)***	***Conversion (%)***	***Chromatography Conditions***	***Yield (mg, %)***
(3.2 mg, 2.0 µmol)	2	29	N/A	N/A
(6.4 mg, 4.0 µmol)	16	100	(Et_2O/Pet Ether, 10/90)	104.7, 99

Substrate
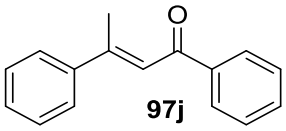 **97j** (89 mg, 0.4 mmol)

Product	***Data***[104]
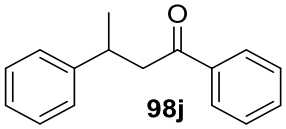 **98j**	**IR** (cm^{-1}): 3050, 2980, 2965, 1682. **^{1}H NMR** (400 MHz, $CDCl_3$): δ 7.97-7.94 (2H, m, Ar-H), 7.57-7.55 (1H, m, Ar-H), 7.49-7.45 (2H, m, Ar-H), 7.33-7.29 (4H, m, Ar-H), 7.24-7.20 (1H, m, Ar-H), 3.58-3.50 (1H, m, Ar-CH), 3.33 (1H, dd, ^2J = 16.4 Hz, ^3J = 5.7 Hz, CO-CH), 3.21 (1H, dd, ^2J = 16.4 Hz, ^3J = 8.2 Hz, CO-CH) 1.37 (3H, d, J = 7.0 Hz, CH-CH_3). **^{13}C NMR** (101 MHz, $CDCl_3$): δ 198.6, 146.1, 136.8, 132.5, 128.1, 128.0, 127.6, 126.4, 125.8, 46.6, 35.1, 21.4.

91f (mg, µmol)	***Temperature (°C)***	***Time (h)***	***Conversion (%)***	***Chromatography Conditions***	***Yield (mg, %)***
(3.2 mg, 2.0 µmol)	25	2	0	N/A	N/A
(12.8 mg, 8.0 µmol)	35	40	100	(Et_2O/Pet Ether, 10/90)	88.8 99

Substrate
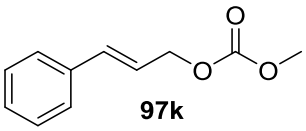 **97k** (77 mg, 0.4 mmol)

Product	***Data***[105]
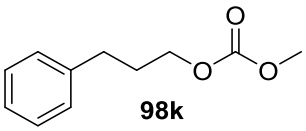 **98k**	**IR** (cm^{-1}): 3026, 2957, 1746, 1260. **^{1}H NMR** (400 MHz, $CDCl_3$): δ 7.34-7.29 (2H, m, Ar-H), 7.24-7.20 (3H, m, Ar-H), 4.19 (2H, t, J = 6.6 Hz, O-CH_2-CH_2), 3.81 (3H, s, O-CH_3), 2.76-2.72 (2H, m, Ar-CH_2-CH_2), 2.06-1.99 (2H, m, CH_2-CH_2-CH_2). **^{13}C NMR** (101 MHz, $CDCl_3$): δ 155.3, 140.5, 128.0, 127.9, 125.6, 66.9, 54.2, 31.4, 29.8.

Conversion (%)	***Chromatography Conditions***	***Yield (mg, %)***
100	(Et_2O/Pet Ether, 10/90)	75.4, 97

Substrate
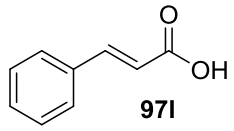 **97l** (59 mg, 0.4 mmol)

Product	***Data***[106]
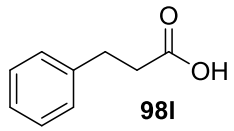 **98l**	**I.R.** (cm^{-1}): 3086 (br), 2934, 1695. **^{1}H NMR** (400 MHz, $CDCl_3$): δ 7.33-7.30 (2H, m, Ar-H), 7.24-7.22 (3H, m, Ar-H), 3.00-2.96 (2H, m, CH_2), 2.72-2.69 (2H, m, CH_2). **^{13}C NMR** (101 MHz, $CDCl_3$): δ 178.7, 140.4, 128.8, 128.5, 126.6, 35.7, 30.8.

Conversion (%)	***Chromatography Conditions***	***Yield (mg, %)***
100	(Et_2O/Pet Ether, 10/90)	57.1, 95

Substrate
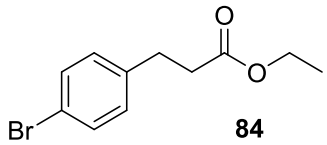 **84** (102 mg, 0.4 mmol)

Product	***Data***[72]
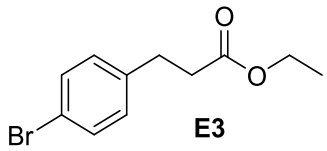 **E3**	**IR** (cm^{-1}): 2978, 1730, 1490. **^{1}H NMR** (400 MHz, $CDCl_3$): δ 7.42-7.35 (2H, m, Ar-H), 7.08-7.03 (2H, m, Ar-H), 4.10 (2H, q *J* = 7.2 Hz, O-CH_2-CH_3), 2.88 (2H, t *J* = 7.2 Hz, CH_2), 2.61-2.54 (2H, m, CH_2), 1.21 (3H, t *J* = 7.2 Hz, CH_2-CH_3). **^{13}C NMR** (101 MHz, $CDCl_3$): δ 172.1, 139.1, 131.0, 129.6, 119.5, 60.0, 35.2, 29.9, 13.7.

Conversion (%)	***Chromatography Conditions***	***Yield (mg, %)***
100	(Et_2O/Pet Ether, 10/90)	97.7, 95

Substrate
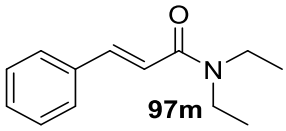 **97m** (81 mg, 0.4 mmol)

Product	***Data***[107]
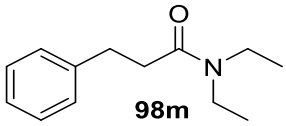 **98m**	**IR** (cm^{-1}): 3026, 2972, 2932, 2874, 1636, 1452, 1429. **^{1}H NMR** (400 MHz, $CDCl_3$): δ 7.33-7.29 (2H, m, Ar-H),7.26-7.20 (3H, m, Ar-H), 3.40 (2H, q *J* = 7.2 Hz, N-CH_2-CH_3), 3.25 (2H, q *J* = 7.2 Hz, N-CH_2-CH_3), 3.03-2.99 (2H, m, CH_2), 2.64-2.60 (2H, m, CH_2), 1.14 (3H, t *J* = 7.2 Hz, CH_2-CH_3), 1.13 (3H, t *J* = 7.2 Hz, CH_2-CH_3). **^{13}C NMR** (101 MHz, $CDCl_3$): δ 208.7, 157.5, 130.0, 129.4, 127.6, 120.6, 110.3, 55.3, 43.8, 30.0, 25.1.

91f (mg, µmol)	***Conversion (%)***	***Chromatography Conditions***	***Yield (mg, %)***
(3.2 mg, 2.0 µmol)	87	N/A	N/A
(6.4 mg, 4.0 µmol)	100	(Et_2O/Pet Ether, 10/90)	78.8, 99

Substrate
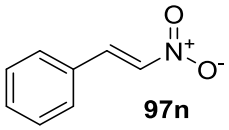 **97n** (60 mg, 0.4 mmol)

Product	***Data***[108]
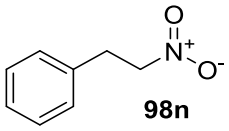 **98n**	**IR** (cm^{-1}): 3028, 2918, 1547. **^{1}H NMR** (400 MHz, $CDCl_3$): δ 7.38-7.27 (3H, m, Ar-H), 7.25-7.23 (2H, m, Ar-H), 4.64 (2H, t, *J* = 7.4 Hz, CH_2), 3.35 (2H, t, *J* = 7.4 Hz, CH_2). **^{13}C NMR** (101 MHz, $CDCl_3$): δ 135.1, 128.5, 128.1, 126.9, 75.8, 33.0.

91f (mg, µmol)	***Time (h)***	***Conversion (%)***	***Chromatography Conditions***	***Yield (mg, %)***
(3.2 mg, 2.0 µmol)	2	36	N/A	N/A
(6.4 mg, 4.0 µmol)	16	100	(Et_2O/Pet Ether, 10/90)	57.4, 95

Substrate
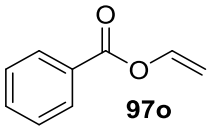 **97o** (59 mg, 0.4 mmol)

Product	***Data***[109]
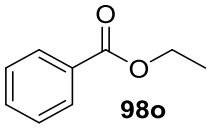 **98o**	**IR** (cm^{-1}): 2982, 1715, 1269. **^{1}H NMR** (400 MHz, $CDCl_3$): δ 8.04-8.02 (2H, m, Ar-H), 7.55-7.51 (1H, m, Ar-H), 7.44-7.39 (2H, m, Ar-H), 4.36 (2H, q, *J* = 7.1 Hz, O-CH_2-CH_3), 1.38 (3H, t, *J* = 7.1 Hz, CH_2-CH_3). **^{13}C NMR** (101 MHz, $CDCl_3$): δ 166.1, 132.3, 130.0, 129.0, 127.8, 60.4, 13.8.

91f (mg, µmol)	***Time (h)***	***Conversion (%)***	***Chromatography Conditions***	***Yield (mg, %)***
(3.2 mg, 2.0 µmol)	2	23	N/A	N/A
(6.4 mg, 4.0 µmol)	16	100	(Et_2O/Pet Ether, 10/90)	58.9, 98

Substrate
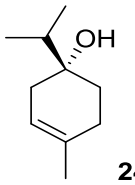 **24** (62 mg, 0.4 mmol)

Product	***Data***[25,110]
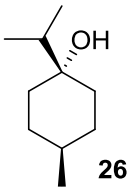 **26**	**IR** (cm^{-1}): 3102 (br), 3024, 2976. **^{1}H NMR** (400 MHz, $CDCl_3$): δ 1.90-1.77 (3H, m, CH_2 & CH-$(CH_3)_2$), 1.69-1.61 (2H, m, CH_2), 1.59-1.50 (1H, m, CH-CH_3), 1.33-1.25 (2H, m, CH_2), 1.12-1.03 (2H, m, CH_2), 0.90 (3H, d *J* = 6.6 Hz, CH-CH_3), 0.88 (6H, d *J* = 6.9 Hz, CH-$(CH_3)_2$). **^{13}C NMR** (101 MHz, $CDCl_3$): δ 72.6, 38.6, 33.7, 32.4, 30.4, 20.4, 16.9.

Conversion (%)
65

Scheme 1.37 *Further investigations of diastereoselective hydrogenation.*

Reactions were carried out using general procedure A and analysed by ^{1}H NMR to attain the reaction conversion, and are tabulated in **Table E1.5**. Catalyst separation was carried out through a pipette of silica eluting with Et_2O/petroleum ether (30/70). The degree of diastereoselective was assessed by GC-FID.

Substrate	***Solvent***	***Temperature (°C)***	***Time (h)***
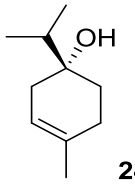 **24** (62 mg, 0.4 mmol)	DCM (8 mL)	25	1
Product	***Data***[25,110]		
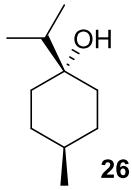 **26**	**IR** (cm^{-1}): 3102 (br), 3024, 2976. **^{1}H NMR** (400 MHz, $CDCl_3$): δ 1.90-1.77 (3H, m, C<u>H</u>$_2$ & C<u>H</u>-(CH_3)$_2$), 1.69-1.61 (2H, m, C<u>H</u>$_2$), 1.59-1.50 (1H, m, C<u>H</u>-CH_3), 1.33-1.25 (2H, m, C<u>H</u>$_2$), 1.12-1.03 (2H, m, C<u>H</u>$_2$), 0.90 (3H, d *J* = 6.6 Hz, CH-C<u>H</u>$_3$), 0.88 (6H, d *J* = 6.9 Hz, CH-(C<u>H</u>$_3$)$_2$). **^{13}C NMR** (101 MHz, $CDCl_3$): δ 72.6, 38.6, 33.7, 32.4, 30.4, 20.4, 16.9. **GC** (FID): **25** (minor diastereomers) 4.42, **26** (major diastereomer) 4.58, **24** (starting material) 4.78.		

Complex	***Conversion (%) (d.r.)***		
	Run		***Ave***
	1	***2***	
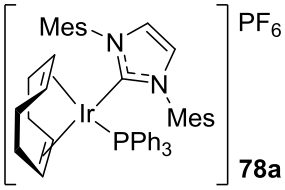 (2.0 mg, 2.0 μmol)	100 (99:1)	100 (99:1)	100 (99:1)
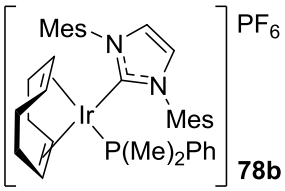 (1.8 mg, 2.0 μmol)	48	44	46
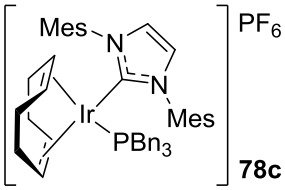 (2.1 mg, 2.0 μmol)	12	16	14
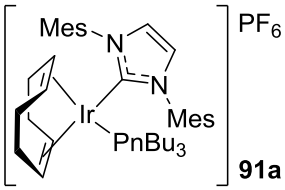 (1.9 mg, 2.0 μmol)	81	81	81
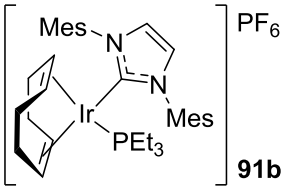 (1.7 mg, 2.0 μmol)	77	83	80
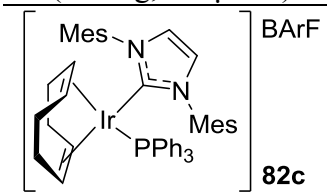 (3.5 mg, 2.0 μmol)	100 (99:1)	100 (99:1)	100 (99:1)
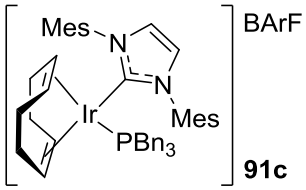 (3.5 mg, 2.0 μmol)	45	55	50

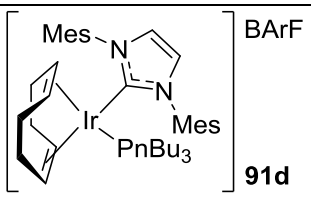 **91d** (3.3 mg, 2.0 μmol)	25	28	27
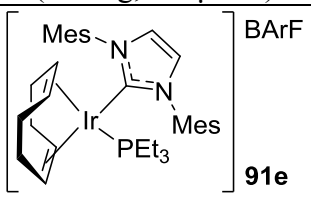 **91e** (3.2 mg, 2.0 μmol)	92	92	92
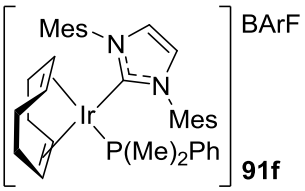 **91f** (3.2 mg, 2.0 μmol)	88	84	86

Table E1.5

Graph 1.3 *Solvent diversity in directing group assisted hydrogenation catalysts.*

Reactions were carried out using general procedure A and were analysed by ^{1}H NMR spectroscopy to calculate the reaction conversion and are tabulated in **Table E1.6**. Catalyst separation was carried out by filtration through a pipette of silica eluting with Et_2O/petroleum ether (30/70).

Substrate	***Solvent***	***Temperature (°C)***	***Time (h)***
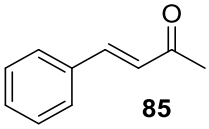 **85** (58 mg, 0.4 mmol)	DCM (4 mL)	25	2
Product		***Data***[72]	
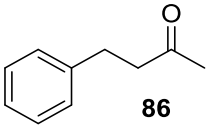 **86**	Data was consistent with that reported on page 88.		

Complex	***Solvent***	***Conversion (%)***		
		Run		***Ave***
		1	***2***	
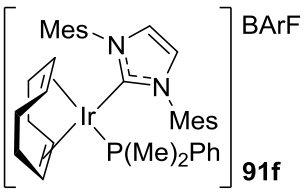 **91f** (3.2 mg, 2.0 μmol)	DCM	100	100	100
	DCE	100	100	100
	PhMe	100	100	100
	TFT	100	100	100
	PhCl	70	74	72
	THF	8	23	16
	2-MeTHF	31	45	38
	EtOH	56	53	55
	iPrOH	100	100	100
	tAmylOH	100	100	100
	EtOAc	52	64	58
	iPrOAc	100	100	100
	Diethyl Ether	17	12	15
	DMFL	18	20	19
	CPME	100	100	100
	DMC	74	90	82
	DEC	100	100	100

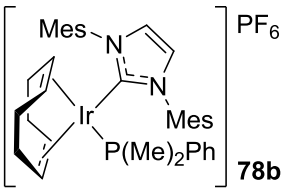 (1.8 mg, 2.0 μmol)	DCM	100	100	100
	DCE	100	98	99
	PhMe	64	62	63
	TFT	78	82	80
	PhCl	32	30	31
	THF	1	2	2
	2-MeTHF	11	13	12
	EtOH	25	26	26
	iPrOH	32	34	33
	tAmylOH	45	52	49
	EtOAc	11	16	14
	iPrOAc	56	62	59
	Diethyl Ether	11	12	12
	DMFL	9	10	10
	CPME	45	42	44
	DMC	58	62	60
	DEC	66	67	67
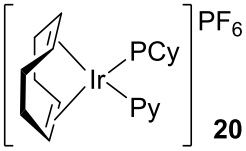 (1.5 mg, 2.0 μmol)	DCM	27	28	28
	DCE	58	49	54
	PhMe	1	2	2
	TFT	32	13	23
	PhCl	15	8	12
	THF	2	2	2
	2-MeTHF	2	2	2
	EtOH	3	5	4
	iPrOH	5	7	6
	tAmylOH	5	7	6
	EtOAc	7	12	10
	iPrOAc	9	6	8
	Diethyl Ether	0	0	0
	DMFL	0	0	0
	CPME	0	1	1
	DMC	20	26	23
	DEC	20	15	18

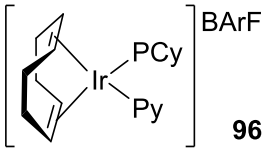 **96** (2.7 mg, 2.0 μmol)	DCM	24	26	25
	DCE	26	27	27
	PhMe	2	3	3
	TFT	11	12	12
	PhCl	8	8	8
	THF	2	2	2
	2-MeTHF	1	1	1
	EtOH	2	2	2
	iPrOH	1	1	1
	tAmylOH	14	15	15
	EtOAc	1	1	1
	iPrOAc	1	1	1
	Diethyl Ether	4	5	5
	DMFL	6	3	5
	CPME	2	3	3
	DMC	4	4	4
	DEC	3	4	4

Table E1.6

Graph 1.4 *Solvent diversity in diastereoselective hydrogenation.*

Reactions were carried out using general procedure A and analysed by ^{1}H NMR spectroscopy to calculate the reaction conversion and results are tabulated in **Table E1.7**. Catalyst separation was carried out by filtration through a pipette of silica eluting with Et_2O/petroleum ether (30/70). The degree of diastereoselective was assessed by GC-FID.

Substrate	***Complex***	***Solvent***	***Temperature (°C)***	***Time (h)***
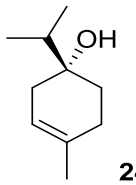 **24** (62 mg, 0.4 mmol)	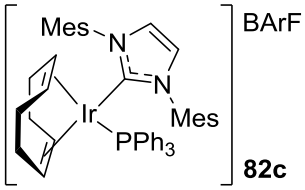 **82c** (3.5 mg, 2.0 μmol)	DCM (4 mL)	25	2
Product	***Data***[25,110]			
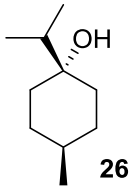 **26**	Data was consistent with that reported on page 134.			

Solvent	***Conversion (%)***			***d.r.***		
	Run		***Ave***	***Run***		***Ave***
	1	***2***		***1***	***2***	
DCM	100	100	100	98.5	99.0	98.7
DCE	100	100	100	98.7	99.9	99.3
PhMe	42	34	38	89.1	83.6	86.4
TFT	100	100	100	99.5	99.7	99.6
PhCl	95	98	96	99.9	99.7	99.8
THF	97	95	96	99.9	99.9	99.9
2-MeTHF	66	74	70	99.9	99.9	99.9
EtOH	11	6	9	94.5	98.1	96.3
iPrOH	86	80	83	98.9	99.4	99.1
tAmylOH	88	88	88	99.8	99.8	99.8
EtOAc	100	100	100	99.9	99.9	99.9
iPrOAc	100	100	100	99.5	99.9	99.7
Diethyl Ether	100	100	100	99.4	99.7	99.4
DMFL	100	100	100	99.6	99.0	99.3
CPME	90	96	93	99.9	99.9	99.9
DMC	100	100	100	99.8	99.8	99.8
DEC	59	56	57	99.0	99.0	99.0

Table E1.7

Table 1.8 *Chemoselectivity investigations; the effect of different directing groups and solvents.*

Reactions were carried out using general procedure A and analysed by GCMS to establish the reaction conversions used to calculate the selectivity. Catalyst separation was carried out by filtration through a pipette of silica eluting with Et_2O/petroleum ether (30/70).

Complex	***Solvent***	***Temperature (°C)***	***Time (h)***
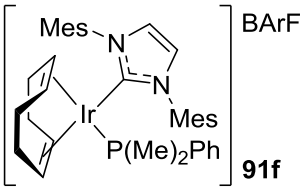 **91f** (3.2 mg, 2.0 μmol)	(4 mL)	25	1

Additive	***Product***
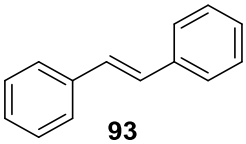 **93** (73 mg, 0.4 mmol)	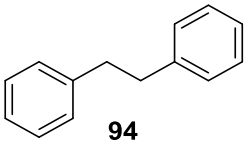 **94**

Retention time (min)	
13.28	12.12

Substrate	***Product***
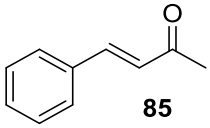 **85** (58 mg, 0.4 mmol)	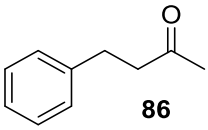 **86**
Retention time (min)	
11.01	10.21

Solvent (Dielectric constant)	***Conversion (%)***		***Selectivity***
	Substrate	***Additive***	
DCM (9.14)	82.9	12.3	87.1:12.9
tAmylOH (15.8)	100	24.1	80.6:19.4
iPrOH (20.18)	98.5	15.8	86.2:13.8
EtOH (25.30)	63.5	3.7	94.6:5.4
PhMe (2.29)	61.4	3.7	94.3:5.7
PhCl (5.69)	64.7	7.3	90:10
Diethyl Ether (4.27)	17.6	1.5	92:8
DMFL (2.64)	38.0	1.9	95:5

Substrate	***Product***
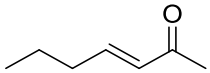 **97e** (45 mg, 0.4 mmol)	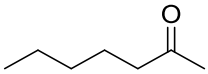 **98e**
Retention time (min)	
7.32	6.74

Solvent (Dielectric constant)	***Conversion (%)***		***Selectivity***
	Substrate	***Additive***	
DCM (9.14)	41.6	1.1	97.6:2.4

Substrate	***Product***
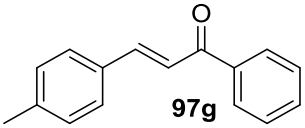 **97g** (89 mg, 0.4 mmol)	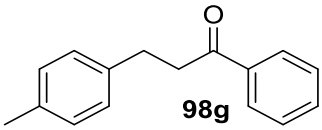 **98g**
Retention time (min)	
15.38	14.55

Solvent (Dielectric constant)	***Conversion (%)***		***Selectivity***
	Substrate	***Additive***	
DCM (9.14)	39.4	7.3	84.4:15.6
PhMe (2.29)	52.3	4.0	92.9:7.1

Substrate	***Product***
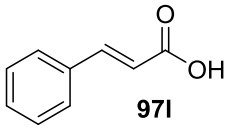 **97l** (59 mg, 0.4 mmol)	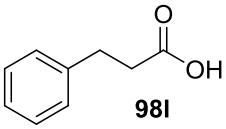 **98l**
Retention time (min)	
11.51	11.91

Solvent (Dielectric constant)	***Conversion (%)***		***Selectivity***
	Substrate	***Additive***	
DCM (9.14)	100	32.0	75.8:24.2

Substrate	***Product***
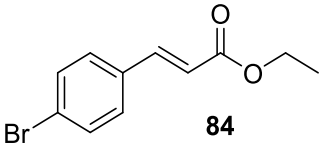 **84** (102 mg, 0.4 mmol)	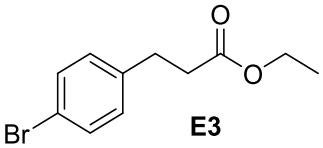 **E3**
Retention time (min)	
12.80	12.14

Solvent (Dielectric constant)	***Conversion (%)***		***Selectivity***
	Substrate	***Additive***	
DCM (9.14)	3.5	49.2	6.6:93.6

Substrate	***Product***
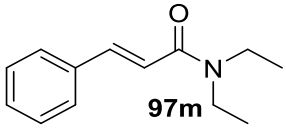 **97m** (81 mg, 0.4 mmol)	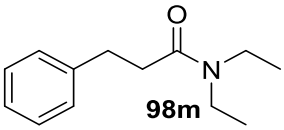 **98m**
Retention time (min)	
13.96	13.15

Solvent (Dielectric constant)	***Conversion (%)***		***Selectivity***
	Substrate	***Additive***	
DCM (9.14)	53.2	2.4	95.7:4.3

Substrate	***Product***
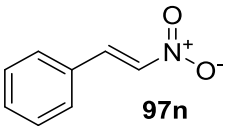 **97n** (60 mg, 0.4 mmol)	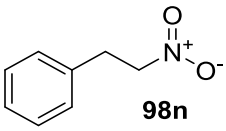 **98n**
Retention time (min)	
7.32	6.74

Solvent (Dielectric constant)	***Conversion (%)***		***Selectivity***
	Substrate	***Additive***	
DCM (9.14)	23.6	12.1	66.1:33.9
PhMe (2.29)	25.3	7.5	77.0:23.0

6.4. Asymmetric Hydrogenation

Scheme 1.40 *Synthesis of novel, non-symmetrical NHC/phosphine complexes.*

Reactions were carried out using general procedure C. The *in situ* generation of MeCN-stabilised hydride complexes carried out using general procedure D, and data are tabulated as the hydride and corresponding phosphorous shifts (excluding ligands and counterions).

Ag_2O	***$[CODIrCl]_2$***	***AX***	***Solvent***	***Temperature (°C)***	***Time (h)***
(58 mg, 0.25 mmol)	(168 mg, 0.25 mmol)	KPF_6 (92 mg, 0.5 mmol) or NaBArF (443 mg, 0.5 mmol)	DCM (10 mL)	25	3 (1+1+1)

Imidazolium Halide	***Phosphine***	***Isolation***
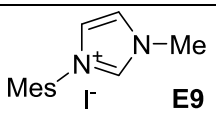 **E9** (164.1 mg, 0.5 mmol)	PPh_3 (131 mg, 0.5 mmol)	Trituration from EtOAc

Product	***Data***
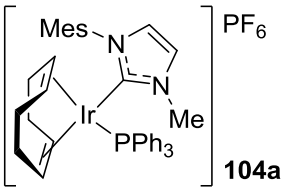 **104a** **Yield** = 395 mg, 87%	**Appearance**: red powder. **Melting Point** (°C): >175 (dec). **IR** (cm^{-1}): 2986, 2922, 1740, 1568, 1479. **^{1}H NMR** (400 MHz, $CDCl_3$): δ 7.72-7.08 (16H, m, Ar-H & N-CH), 6.97 (1H, d, J = 1.9 Hz, N-CH), 6.94 (1H, s, Ar-H), 6.82 (1H, s, Ar-H), 4.75-4.65 (1H, m, COD-CH), 4.04-3.94 (1H, m, COD-CH), 3.76-3.70 (1H, m, COD-CH), 3.55 (3H, s, N-CH_3), 3.38-3.29 (1H, m, COD-CH), 2.53-2.37 (1H, m, COD-CH_2), 2.35 (3H, s, Ar-CH_3), 2.18-2.06 (1H, m, COD-CH_2), 2.00-1.87 (3H, m, COD-CH_2), 1.85 (3H, s, Ar-CH_3), 1.58 (3H, s, Ar-CH_3), 1.51-1.35 (3H, m, COD-CH_2).

^{13}C NMR (101 MHz, $CDCl_3$): δ 173.6 (d $^2J_{C-P}$ = 9.3 Hz), 139.12, 135.5, 134.7, 130.9, 129.1, 128.7, 128.5, 128.4, 125.7, 124.0, 84.8, 84.7, 81.0, 80.9, 78.7, 48.0, 37.9, 34.0, 27.9, 27.3, 20.6, 19.6, 17.6.

^{31}P NMR (162 MHz, $CDCl_3$): δ 17.6 (PPh_3), -144.4 (sep $^1J_{F-P}$ = 713 Hz, PF_6).

^{19}F NMR (376 MHz, $CDCl_3$): δ -73.5 (d $^1J_{P-F}$ = 713 Hz, PF_6).

HRMS (NSI): m/z calculated for $C_{39}H_{43}IrN_2P$ $[M-PF_6]^+$: 761.2764; found: 761.2768.

MeCN Hydride Complex

^{1}H NMR (400 MHz, CD_3CN): -21.66 (d $^2J_{H-P}$ = 17.4 Hz).

^{31}P NMR (162 MHz, CD_3CN): δ 23.4 (t $^2J_{P-H}$ = 17.4 Hz, PPh_3).

Imidazolium Halide	*Phosphine*	*Isolation*
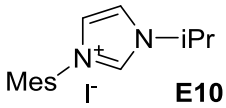 **E10** (178 mg, 0.5 mmol)	PPh_3 (131 mg, 0.5 mmol)	Trituration from EtOAc
Product	***Data***	
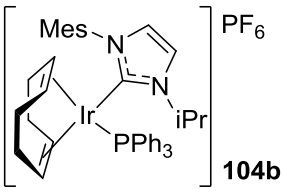 **104b** **Yield** = 379 mg, 81%	**Appearance**: red powder. **Melting Point** (°C): >160 (dec). **IR** (cm^{-1}): 3167, 2992, 2835, 1479. **^{1}H NMR** (400 MHz, $CDCl_3$): δ 7.70-7.19 (16H, m, Ar-H & N-C<u>H</u>), 7.12 (1H, d *J* = 2.1 Hz, N-C<u>H</u>), 6.94 (1H, s, Ar-<u>H</u>), 6.84 (1H, s, Ar-<u>H</u>), 5.12 (1H, sep *J* = 6.6 Hz, N-C<u>H</u>-$(CH_3)_2$), 4.55-4.45 (1H, m, COD-C<u>H</u>), 4.30-4.19 (1H, m, COD-C<u>H</u>), 3.55-3.46 (1H, m, COD-C<u>H</u>), 3.41-3.32 (1H, m, COD-C<u>H</u>), 2.35 (3H, s, Ar-C<u>H</u>$_3$), 3.34-3.25 (1H, m, COD-C<u>H</u>$_2$), 2.17-2.05 (1H, m, COD-C<u>H</u>$_2$), 2.02 (3H, s, Ar-C<u>H</u>$_3$), 2.01-1.84 (3H, m, COD-C<u>H</u>$_2$), 1.81 (3H, s, Ar-C<u>H</u>$_3$), 1.59-1.52 (2H, m, COD-C<u>H</u>$_2$), 1.50 (3H, d *J* = 6.5 Hz, CH-C<u>H</u>$_3$), 1.48-1.39 (1H, m, COD-C<u>H</u>$_2$), 0.59 (3H, d *J* = 6.6 Hz, CH-C<u>H</u>$_3$).	

^{13}C NMR (101 MHz, $CDCl_3$): δ 173.7 (d $^2J_{C-P}$ = 8.5 Hz), 139.2, 135.4, 134.7, 130.9, 129.1, 129.7, 128.5, 128.4, 125.7, 123.9, 84.7, 84.6, 81.0, 80.9, 78.7, 78.2, 37.9, 34.0, 32.5, 32.4, 27.9, 27.3, 20.5, 19.6, 17.6.

^{31}P NMR (162 MHz, $CDCl_3$): δ 18.1 (PPh_3), -144.3 (sep $^1J_{F-P}$ = 713 Hz, PF_6).

^{19}F NMR (376 MHz, $CDCl_3$): δ -73.5 (d $^1J_{P-F}$ = 713 Hz, PF_6).

HRMS (NSI): m/z calculated for $C_{41}H_{47}Ir^{191}N_2P$ $[M-PF_6]^+$: 789.3077; found: 789.3098.

MeCN-Hydride Complex

^{1}H NMR (400 MHz, CD_3CN): -21.70 (d $^2J_{H-P}$ = 17.7 Hz).

^{31}P NMR (162 MHz, CD_3CN): δ 23.5 (t $^2J_{P-H}$ = 17.7 Hz, PPh_3).

Imidazolium Halide	*Phosphine*	*Isolation*
 **E11** (179 mg, 0.5 mmol)	PPh_3 (131 mg, 0.5 mmol)	Trituration from EtOAc
Product	***Data***	
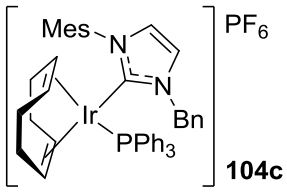 **104c** **Yield** = 433 mg, 88%	**Appearance**: red powder. **Melting Point** (°C): >190 (dec). **IR** (cm^{-1}): 2920, 2887, 2833, 2361, 1607, 1479. **^{1}H NMR** (400 MHz, $CDCl_3$): δ 7.66-7.31 (18H, m, Ar-H), 7.20 (1H, d *J* = 2.0 Hz, N-CH), 7.17 (1H, d *J* = 2.0 Hz, N-CH), 7.04-7.01 (2H, m, Ar-H), 7.00 (1H, s, Ar-H), 6.91 (1H, s, Ar-H), 5.72 (1H, d ^2J = 15 Hz, N-CH_2-Ar), 4.50-4.44 (1H, m, COD-CH), 4.20-4.07 (2H, m, N-CH_2-Ar & COD-CH), 3.83-3.72 (1H, m, COD-CH), 3.45-3.35 (1H, m, COD-CH), 2.40 (3H, s, Ar-CH_3), 2.00-1.86 (7H, m, Ar-CH_3 & COD-CH_2), 1.86-1.75 (1H, m, COD-CH_2), 1.72 (3H, s, Ar-CH_3), 1.54-1.46 (2H, m, COD-CH_2), 1.46-1.36 (1H, m, COD-CH_2).	

^{13}C NMR (101 MHz, $CDCl_3$): δ 174.9 (d $^2J_{C-P}$ = 140.1, 136.0, 135.5, 135.3, 135.2, 131.8, 130.0, 129.6, 129.4, 129.3, 128.8, 127.24, 127.20, 123.5, 85.3, 85.2, 82.9, 82.8, 79.7, 78.9, 55.1, 33.8, 32.59, 32.56, 29.2, 28.2, 21.2, 20.4, 18.2.

^{31}P NMR (162 MHz, $CDCl_3$): δ 17.7 (PPh_3), -144.3 (sep $^1J_{F-P}$ = 713 Hz, PF_6).

^{19}F NMR (376 MHz, $CDCl_3$): δ -73.5 (d $^1J_{P-F}$ = 713 Hz, PF_6).

HRMS (NSI): m/z calculated for $C_{45}H_{47}Ir^{191}N_2P$ $[M-PF_6]^+$: 837.3077; found: 837.3072.

MeCN-Hydride Complex

^{1}H NMR (400 MHz, CD_3CN): -21.55 (d $^2J_{H-P}$ = 17.3 Hz).

^{31}P NMR (162 MHz, CD_3CN): δ 23.3 (t $^2J_{P-H}$ = 17.3 Hz, PPh_3).

Imidazolium Halide	***Phosphine***	***Isolation***
 **E11** (179 mg, 0.5 mmol)	PEt_3 (59 mg, 74 µL, 0.5 mmol)	Trituration from EtOAc
Product	***Data***	
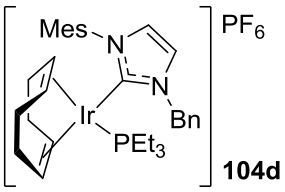 **104d** **Yield** = 328 mg, 78%	**Appearance**: red powder. **Melting Point** (°C): 165-167. **IR** (cm^{-1}): 2990, 2885, 2359, 1483. **^{1}H NMR** (400 MHz, $CDCl_3$): δ 7.41-7.29 (4H, m, Ar-H), 7.21-7.15 (2H, m, Ar-H), 7.00 (1H, s, Ar-H), 6.98 (1H, d *J* = 1.9 Hz, N-CH), 6.94 (1H, s, Ar-H), 5.87 (1H, d ^2J = 14.9 Hz, N-CH_2-Ar), 5.39 (1H, d ^2J = 14.9 Hz, N-CH_2-Ar), 4.27-4.18 (1H, m, COD-CH), 4.07-3.99 (1H, m, COD-CH), 3.84-3.74 (2H, m, COD-CH), 2.34 (3H, s, Ar-CH_3), 2.56 (3H, s, Ar-CH_3), 1.88 (3H, s, Ar-CH_3), 1.87-1.64 (11H, m, COD-CH_2 & P-CH_2-CH_3), 1.59-1.49 (1H, m, COD-CH_2), 1.48-1.36 (1H, m, COD-CH_2), 1.35-1.24 (1H, m, COD-CH_2), 1.14 (9H, *app.* dt *J* = 15.4 Hz, 7.5 Hz, Ch_2-CH_3).	

^{13}C NMR (101 MHz, $CDCl_3$): δ 176.3 (d ^2J = 9.5 Hz), 139.2, 135.7, 134.9, 134.8, 134.4, 128.8, 128.8, 127.8, 126.1, 125.7, 122.9, 84.0, 83.9, 81.5, 81.4, 75.5, 73.9, 54.4, 32.14, 32.1, 28.9, 28.5, 20.5, 19.9, 17.5, 17.0, 16.7, 8.34, 8.33.

^{31}P NMR (162 MHz, $CDCl_3$): δ 2.6 (PEt_3), -144.3 (sep $^1J_{F-P}$ = 713 Hz, PF_6).

^{19}F NMR (376 MHz, $CDCl_3$): δ -73.2 (d $^1J_{P-F}$ = 713 Hz, PF_6).

HRMS (NSI): m/z calculated for $C_{33}H_{47}Ir^{191}N_2P$ $[M-PF_6]^+$: 693.3077; found: 693.3071.

MeCN-Hydride Complex

^{1}H NMR (400 MHz, CD_3CN): -22.22 (d $^2J_{H-P}$ = 18.1 Hz).

^{31}P NMR (162 MHz, CD_3CN): δ 2.2 (t $^2J_{P-H}$ = 18.1 Hz, PEt_3).

Imidazolium Halide	***Phosphine***
 **E11** (179 mg, 0.5 mmol)	PPh_3 (131 mg, 0.5 mmol)
Product	***Data***
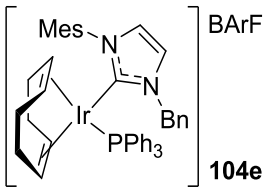 **104e** **Yield** = 785 mg, 91%	**Appearance**: Red Powder. **Melting Point** (°C): >185 (dec). **IR** (cm^{-1}): 2980, 2887, 2367, 1485, 1435. **^{1}H NMR** (400 MHz, $CDCl_3$): δ 7.69 (8H, t ^4J = 2.4 Hz, Ar-H), 7.59-7.14 (22H, m, Ar-H & Ar-H), 7.00 (1H, d J = 2.0 Hz, N-CH), 6.96 (1H, m, Ar-H), 6.93-6.89 (2H, m, Ar-H & N-CH), 6.87 (1H, s, Ar-H), 5.79 (1H, d ^2J = 14.7 Hz, N-CH_2-Ar), 4.50-4.42 (1H, m, COD-CH), 4.16-4.05 (1H, m, COD-CH), 3.92 (1H, d ^2J = 14.7 Hz, N-CH_2-Ar), 3.83-3.74 (1H, m, COD-CH), 3.45-3.35 (1H, m, COD-CH), 2.33 (3H, s, Ar-CH_3), 2.03-1.88 (4H, m, COD-CH_2), 1.86 (3H, s, Ar-CH_3), 1.81-1.70 (1H, m, COD-CH_2), 1.67 (3H, s, Ar-CH_3), 1.56-1.43 (2H, m, COD-CH_2), 1.42-1.30 (1H, m, COD-CH_2).

^{13}C NMR (101 MHz, $CDCl_3$): δ 175.2 (d $^2J_{C-P}$ = 7.7 Hz), 161.2 (q $^1J_{C-B}$ = 49.5 Hz), 139.9, 134.6, 134.3, 133.8, 133.6, 131.2, 131.0, 129.4, 129.0, 128.9, 128.64, 128.56, 128.4 (q $^2J_{C-F}$ = 30.1 Hz), 126.5, 126.1, 124.1, (q $^1J_{C-F}$ = 273 Hz), 116.9, 84.5, 84.4, 82.5, 82.4, 80.0, 78.6, 84.6, 33.2, 32.0, 31.9, 28.3, 27.4, 20.4, 19.6, 17.4.

^{31}P NMR (162 MHz, $CDCl_3$): δ 17.9 (PPh_3).

^{19}F NMR (376 MHz, $CDCl_3$): δ -62.4 (BArF).

^{11}B NMR (128 MHz, $CDCl_3$): δ -6.7 (BArF).

HRMS (NSI): m/z calculated for $C_{45}H_{47}Ir^{191}N_2P$ $[M\text{-}BArF]^+$: 837.3077; found: 837.3077.

Imidazolium Halide	***Phosphine***
 **E11** (179 mg, 0.5 mmol)	PEt_3 (59 mg, 74 µL, 0.5 mmol)

Product	***Data***
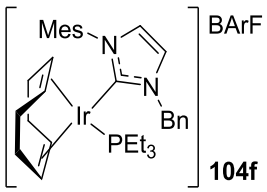 **104f** **Yield** = 735 mg, 93%	**Appearance**: Red Powder. **Melting Point** (°C): >150 (dec). **I.R.** (cm^{-1}): 2980, 2887, 2361, 1609, 1462. **^{1}H NMR** (400 MHz, $CDCl_3$): δ 7.64 (8H, t ^4J = 2.2 Hz, Ar-H), 7.59 (4H, br s, Ar-H), 7.41-7.29 (4H, m, Ar-H), 7.21-7.15 (2H, m, Ar-H), 7.00 (1H, s, Ar-H), 6.98 (1H, d J = 1.9 Hz, N-CH), 6.94 (1H, s, Ar-H), 5.87 (1H, d ^2J = 14.9 Hz, N-CH_2-Ar), 5.39 (1H, d ^2J = 14.9 Hz, N-CH_2-Ar), 4.27-4.18 (1H, m, COD-CH), 4.07-3.99 (1H, m, COD-CH), 3.84-3.74 (2H, m, COD-CH), 2.34 (3H, s, Ar-CH_3), 2.56 (3H, s, Ar-CH_3), 1.88 (3H, s, Ar-CH_3), 1.87-1.64 (11H, m, COD-CH_2 & P-CH_2-CH_3), 1.59-1.49 (1H, m, COD-CH_2), 1.48-1.36 (1H, m, COD-CH_2), 1.35-1.24 (1H, m, COD-CH_2), 1.14 (9H, *app.* dt J = 15.4 Hz, 7.5 Hz, CH_2-CH_3).

^{13}C NMR (101 MHz, $CDCl_3$): δ 177.4 (d $^2J_{C-P}$ = 9.2 Hz), 161.2 (q $^1J_{C-B}$ = 50.7 Hz), 139.8, 134.6, 134.3, 133.9, 129.1, 129.00, 128.97, 128.5, 128.4 (q $^2J_{C-F}$ = 31.2 Hz), 126.0, 125.8, 124.1 (q $^1J_{C-F}$ = 273 Hz), 121.3, 116.9, 84.9, 84.8, 82.8, 82.6, 76.3, 74.9, 54.6, 32.1, 32.04, 32.00, 28.7, 28.2, 20.3, 19.6, 17.4, 17.0, 16.7, 8.0.

^{31}P NMR (162 MHz, $CDCl_3$): δ 3.0 (PEt_3).

^{19}F NMR (376 MHz, $CDCl_3$): δ -62.41 (BArF).

^{11}B NMR (128 MHz, $CDCl_3$): δ -6.7 (BArF).

HRMS (NSI): m/z calculated for $C_{33}H_{47}Ir^{191}N_2P$ $[M\text{-}BArF]^+$: 693.3077; found: 693.3068.

Scheme 1.41 *Two-step synthesis of bulky, unsymmetrical NHC/phosphine complex* ***104g***.

Firstly, by following general procedure F the NHC/chloride complex **106** was prepared.

Imidazolium Halide	*Iridium dimer*	*KOtBu*	*THF*
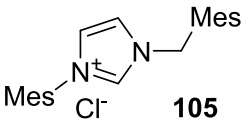 **105** (354 mg, 1.0 mmol)	(336 mg, 0.5 mmol)	(122 mg, 1.0 mmol)	(20 mL)

Product	*Data*
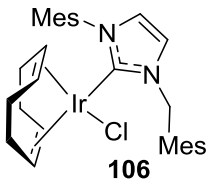 **106** **Yield** = 570 mg, 87%.	**Appearance**: Yellow powder. **Melting Point** (°C): 162-164. **I.R.** (cm^{-1}): 2978, 1916, 2361, 1609, 1487. **^{1}H NMR** (400 MHz, $CDCl_3$): δ 7.06 (1H, s, Ar-H), 6.97 (2H, s, Ar-H), 6.92 (1H, s, Ar-H), 6.65 (1H, d *J* = 2.0 Hz, N-CH), 6.47 (1H, d *J* = 2.0 Hz, N-CH), 5.84 (1H, d ^2J = 14.6 Hz, N-CH_2-Ar), 5.69 (1H, d ^2J = 14.6 Hz, N-CH_2-Ar), 4.57-4.45 (2H, m, COD-CH), 3.26 (1H, td *J* = 7.1 Hz, 2.2 Hz, COD-CH), 2.77 (1H, td *J* = 7.5 Hz, 3.4 Hz, COD-CH), 2.40 (3H, s, Ar-CH_3), 2.39 (3H, s, Ar-CH_3), 2.37 (6H, s, Ar-CH_3), 2.34 (3H, s, Ar-CH_3), 2.28-2.17 (1H, m, COD-CH_2), 2.16-2.06 (1H, m, COD-CH_2), 1.90 (3H, s, Ar-CH_3), 1.88-1.81 (1H, s, COD-CH_2), 1.67-1.58 (3H, m, COD-CH_2), 1.56-1.37 (2H, m, COD-CH_2).

^{13}C NMR (101 MHz, $CDCl_3$): δ 179.8, 138.8, 138.6, 137.2, 136.3, 134.6, 129.6, 129.0, 128.1, 122.4, 113.2, 83.5, 83.4, 51.45, 51.38, 34.8, 32.9, 29.8, 29.1, 21.31, 2.27, 20.1, 19.9, 17.9.

HRMS (NSI): m/z calculated for $C_{30}H_{38}Ir^{191}N_2$ $[M-Cl]^+$: 617.2635; found: 617.2622.

To a flame-dried, argon-cooled Schlenk round-bottom flask was added NHC/chloride **106** (327 mg, 0.5 mmol), and dry THF (10 mL). After all solids had dissolved, $AgPF_6$ (126 mg, 0.5 mmol), was added, affording a yellow to opaque orange colour change on formation of a precipitate. The reaction mixture was stirred for 15 min at r.t. before carrying out filtration through celite under an argon atmosphere using the necessary

flame-dried glassware. Addition of triphenylphosphine (131 mg, 0.5 mmol) to the clear orange solution resulted in the immediate appearance of a bright red colour. After stirring the solution for 3 h at r.t. the solvent was evaporated under reduced pressure. The red residue was redissolved in DCM (~10 mL) and filtered through celite in air, washing the celite with DCM to remove the red colour. The clear red filtrate was concentrated *in vacuo* to reveal a red, oily solid. Addition of ethyl acetate (~5 mL) resulted in the precipitation of NHC/phosphine complex **104g**, which was collected by filtration and washed with ethyl acetate and hexanes to give the product as a bright red solid. The isolated catalyst was dried in a vacuum oven (40 °C, 1 mbar) for 24 h before use.

Product	***Data***
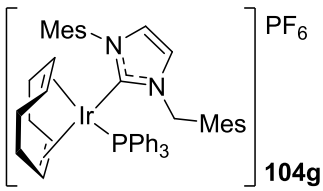 **104g** **Yield** = 400 mg, 78%	**Appearance**: red powder. **Melting Point** (°C): >180 (dec). **I.R.** (cm^{-1}): 2978, 2922, 2837, 2357, 1736, 1479. **^{1}H NMR** (400 MHz, $CDCl_3$): δ 7.62-7.24 (13H, m, Ar-H), 7.05 (1H, d *J* = 2.0 Hz, N-CH), 6.96 (1H, s, Ar-H), 6.93-6.85 (3H, m, Ar-H), 6.85-6.62 (2H, m, Ar-H), 6.58 (1H, d *J* = 2.1 Hz, N-CH), 5.69 (1H, d ^2J = 13.7 Hz, N-CH_2-Ar), 4.66-4.56 (1H, m, COD-CH), 4.43 (1H, d ^2J = 13.7 Hz, N-CH_2-Ar), 4.38-4.28 (1H, m, COD-CH), 3.62-3.48 (2H, m, COD-CH), 2.36 (3H, s, Ar-CH_3), 2.34-2.28 (1H, m, COD-CH_2), 2.67 (3H, s, Ar-CH_3), 2.11-2.00 (2H, m, COD-CH_2), 2.00-1.90 (1H, m, COD-CH_2), 1.84 (6H, s, Ar-CH_3), 1.83 (3H, s, Ar-CH_3), 1.81-1.74 (1H, m, COD-CH_2), 1.71 (3H, s, Ar-CH_3), 1.70-1.57 (3H, m, COD-CH_2).

^{13}C NMR (101 MHz, $CDCl_3$): δ 173.7 (d ^2J = 8.9 Hz), 140.3, 139.8, 138.0, 136.2, 135.6, 135.3, 134.0, 132.7, 131.9, 130.2, 129.9, 129.4, 129.2, 126.7, 129.5, 121.3, 85.1, 85.0, 82.4, 82.3, 81.2, 77.5, 49.9, 32.5, 31.3, 30.9, 30.8, 30.2, 21.2, 30.6, 19.6, 18.0.

^{31}P NMR (162 MHz, $CDCl_3$): δ 17.2 (PPh_3), -144.4 (sep $^1J_{F-P}$ = 713 Hz, PF_6).

^{19}F NMR (376 MHz, $CDCl_3$): δ -73.9 (d $^1J_{P-F}$ = 713 Hz, PF_6).

HRMS (NSI): m/z calculated for $C_{48}H_{53}Ir^{191}N_2P$ $[M-PF_6]^+$: 879.3547; found: 879.3568.

MeCN-Hydride Complex

^{1}H NMR (400 MHz, CD_3CN): -21.48 (d $^2J_{H-P}$ = 18.1 Hz).

^{31}P NMR (162 MHz, CD_3CN): δ 23.2 (t $^2J_{P-H}$ = 18.1 Hz, PPh_3).

Scheme 1.42 *Investigating non-chiral, unsymmetrical NHCs in alkene hydrogenation.*

Reactions were carried out using general procedure A and analysed by ^{1}H NMR spectroscopy to calculate the reaction conversion, and are tabulated in **Table E1.8**. Catalyst separation was carried out by filtration through a pipette of silica eluting with Et_2O/petroleum ether (30/70).

Solvent	***Temperature (°C)***	***Time (min)***
DCM (8 mL)	25	30
	Substrate	
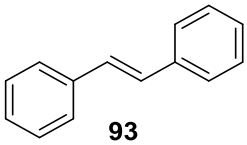 **93** (73 mg, 0.4 mmol)	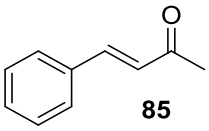 **85** (58 mg, 0.4 mmol)	
Product	***Data***[72,96]	
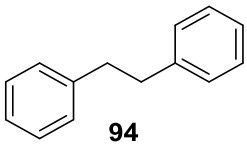 **94**	Data was consistent with that reported on page 113.	
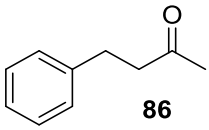 **86**	Data was consistent with that reported on page 88.	

Complex	***Conversion (%)***					
	93			***85***		
	Run		***Ave***	***Run***		***Ave***
	1	***2***		***1***	***2***	
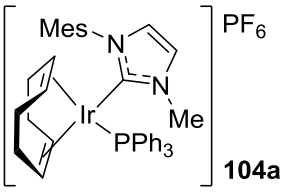 **104a** (1.8 mg, 2.0 μmol)	18	15	17	8	7	8
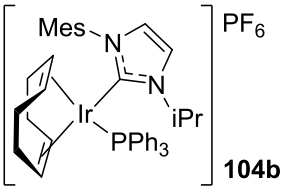 **104b** (1.9 mg, 2.0 μmol)	15	13	14	6	9	8
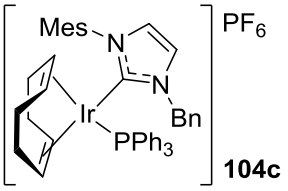 **104c** (2.0 mg, 2.0 μmol)	49	54	52	32	34	33
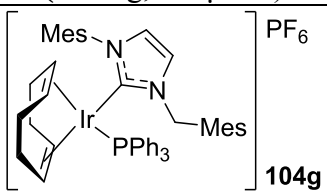 **104g** (2.1 mg, 2.0 μmol)	34	34	34	6	8	7
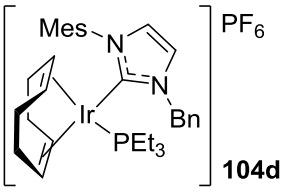 **104d** (1.7 mg, 2.0 μmol)	100	100	100	4	6	5
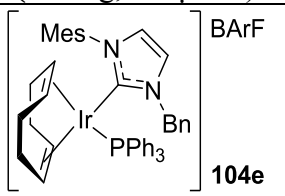 **104e** (3.4 mg, 2.0 μmol)	56	58	57	27	25	26
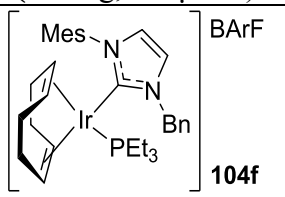 **104f** (3.1 mg, 2.0 μmol)	100	100	100	13	14	14

Table E1.8

Scheme 1.43 *Synthesis of chiral imidazolium triflates **112** and **113**.*[91,93]

To a two-neck, flame-dried, 1L round-bottom flask, equipped with a reflux condenser was added lithium aluminium hydride (13.0 g, 34.2 mmol) and dry THF (350 mL). The reaction slurry was then cooled to 0 °C in an ice bath. The amino acid (**106** 20 g, 17.1 mmol; **107** 22.4 g, 17.1 mmol) was added in small portions over the course of 2 h, before heating to reflux (80 °C) for 16 h. The following day the reaction was cooled to 0 °C with an ice bath, and a saturated solution of sodium sulfate was carefully, added dropwise until no gas was released, and the reaction mixture was then stirred for a further 2 h. The white reaction mixture was then filtered, and the residual THF removed *in vacuo*. The recovered yellow oil was purified via *via* kugelrohr distillation (3 mbar, 120 °C for both) delivering the pure amino alcohol as a clear oil, which solidified upon standing (**108** 17.5 g, 100%; **109** 19.9 g, 100%)

Product	***Data***[111,112]
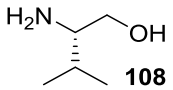 **108**	**Appearance**: Low melting, crystalline solid. **Melting Point** (°C): 29-32. **IR** (cm^{-1}): 3268 (br), 3120 (br), 2974. **^{1}H NMR** (400 MHz, $CDCl_3$): δ 3.61 (1H, dd, J = 10.4 Hz, ^2J = 4.1 Hz, C$\underline{H}_2$-OH), 3.25 (1H, dd, J = 10.4 Hz, 8.8 Hz, C$\underline{H}$-NH_2), 2.52 (1H, ddd, J = 8.8 Hz, 6.4 Hz, ^2J = 4.0 Hz, C$\underline{H}_2$-OH), 1.74 (3H, br s, N$\underline{H}_2$ & O$\underline{H}$), 1.60-1.46 (1H, m, C$\underline{H}$-$(CH_3)_2$), 0.89 (6H, m, CH-(C$\underline{H}_3$)$_2$). **^{13}C NMR** (101 MHz, $CDCl_3$): δ 65.0, 58.7, 31.9, 19.5, 18.6.
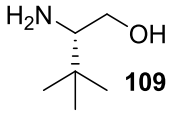 **109**	**Appearance**: Low melting, crystalline solid. **Melting Point** (°C): 28-30. **IR** (cm^{-1}): 3247 (br), 3134 (br), 2981. **^{1}H NMR** (400 MHz, $CDCl_3$): δ 3.72 (1H, dd, J = 10.4 Hz, ^2J = 3.7 Hz, C$\underline{H}_2$-OH), 3.24 (1H, t, J = 10.2 Hz, C$\underline{H}$-NH_2), 2.53 (1H, dd, J = 10.0 Hz, ^2J = 3.7 Hz, C$\underline{H}_2$-OH), 2.40 (3H, br-s, N$\underline{H}_2$ & O$\underline{H}$) 0.89 (9H, s, C-(C$\underline{H}_3$)$_3$). **^{13}C NMR** (101 MHz, $CDCl_3$): δ 62.5, 61.9, 33.4, 26.5.

In a flame dried, 100 mL, round-bottom flask, equipped with Dean-Stark apparatus, was placed glycolic acid (4.06 g, 53.4 mmol), amino alcohol (**108** 5 g, 48.5 mmol; **109** 5.68 g, 48.5 mmol) and dry xylenes (60 mL). The reaction was heated to 160 °C, and wrapped with cotton-wool and aluminium foil to ensure a steady reflux. After 72 h the

reaction was allowed to cool to remove temperature before the solvent was removed *in vacuo*. The residual oil was distilled by kugelrohr distillation (1 mbar, 140 °C for both), delivering the hydroxyl methyl oxazoline as a pale yellow oil, which solidified upon standing (**110** 3.96 g, 57%; **111** 7.26 g, 94%)

Product	***Data***[93]
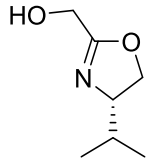 **110**	**Appearance**: Low melting, crystalline solid. **Melting Point** (°C): 44-45. **I.R.** (cm^{-1}): 3120 (br), 2974. **^{1}H NMR** (400 MHz, $CDCl_3$): δ 4.33 (1H, dd J = 9.6 Hz, ^2J = 8.4 Hz, C<u>H</u>$_2$-O), 4.21 (2H, s, C<u>H</u>$_2$-OH), 4.03 1H, t, J = 8.2 Hz, CH_2-O), 3.94-3.86 (1H, m, C<u>H</u>-N), 1.73 (1H, m, C<u>H</u>-$(CH_3)_2$), 0.96 (3H, d J = 6.7 Hz, CH-(C<u>H</u>$_3$)$_2$), 0.87 (3H, d, J = 6.8 Hz, CH-(C<u>H</u>$_3$)$_2$).
^{13}C NMR (101 MHz, $CDCl_3$): δ 167.0, 71.0, 70.7, 56.7, 32.0, 18.2, 17.6.	
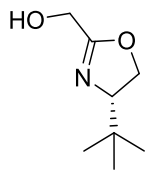 **111**	**Appearance**: Low melting, crystalline solid. **Melting Point** (°C): 48-51. **I.R.** (cm^{-1}): 3134 (br), 2981. **^{1}H NMR** (400 MHz, $CDCl_3$): δ 4.26 (1H, dd J = 10.1 Hz, ^2J = 8.4 Hz, C<u>H</u>$_2$-O), 4.24-4.20 (2H, m, C<u>H</u>$_2$-OH), 4.13 (1H, dd J = 8.2 Hz, ^2J = 8.4 Hz, C<u>H</u>$_2$-O), 3.87 (1H, m, N-C<u>H</u>), 0.90 (9H, s, C-(C<u>H</u>$_3$)$_3$).
^{13}C NMR (101 MHz, $CDCl_3$): δ 169.1, 76.2, 70.7, 57.4, 64.3, 26.2. **HRMS** (APCI): m/z calculated for $C_8H_{16}NO_2$ $[M+H]^+$: 144.1014; found: 144.1026.	

To a 25 mL round-bottom flask was added hydroxylmethyl oxazoline (**110** 1 g, 6.98 mmol; **111** 1.10 g, 6.98 mmol), DCM (10 mL) and manganese dioxide (6.06 g, 69.8 mmol).[113] The resulting suspension was stirred at room temperature for 2 h, and then filtered through celite to remove manganese impurities. The solvent was removed *in vacuo*, delivering the unstable aldehyde (**E12** or **E13**) intermediate, which was used in the following step without further purification.

During the optimisation of the oxidation, the product aldehyde (**E12** and **E13**) from hydroxyl methyl oxazoline (**110** and **111**) were found to be unstable, and only identified by ^{1}H NMR spectroscopy.

Product	***Data***
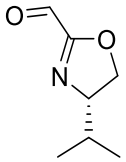 **E12**	**^{1}H NMR** (400 MHz, $CDCl_3$): δ 9.54 (1H, s, C<u>H</u>=O), 4.43-4.35 (1H, m, C<u>H$_2$</u>-O), 4.13-4.06 (2H, m, C<u>H$_2$</u>-O & N-C<u>H</u>), 1.85-1.76 (1H, m, C<u>H</u>-$(CH_3)_2$), 0.96 (3H, d, *J* = 6.7 Hz, CH-(C<u>H$_3$</u>)$_2$), 0.88 (3H, d *J* = 6.7 Hz, CH-(C<u>H$_3$</u>)$_2$).
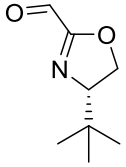 **E13**	**^{1}H NMR** (400 MHz, $CDCl_3$): δ 9.59 (1H, s, C<u>H</u>=O), 4.37 (1H, dd ^2J = 10.4 Hz, *J* = 8.9 Hz, O-C<u>H$_2$</u>), 4.22 (1H, t *J* = 8.9 Hz, N-C<u>H</u>), 4.11 (1H, dd ^2J = 10.4 Hz, *J* = 8.9 Hz, O-C<u>H$_2$</u>), 0.93 (9H, s, C-(C<u>H$_3$</u>)$_3$).

In a 100 mL round-bottom flask, equipped with Dean-Stark apparatus was placed the prepared aldehyde (**E12** or **E13**), dry toluene (60 mL) and mesityl amine (944 mg, 980 µL, 6.98 mmol). The reaction was heated to 140 °C and wrapped with cotton-wool and aluminium foil to ensure a steady reflux. After 3 h the reaction was cooled to room temperature and the solvent removed *in vacuo*, delivering the imine (**E14** or **E15**), which was used in the following step without further purification.

During the optimisation of the oxidation, the product imines (**E14** and **E15**) from aldehydes (**E12** and **E13**) could not be fully purified from the aniline starting material, and were only identified by ^{1}H NMR spectroscopy.

Product	***Data***
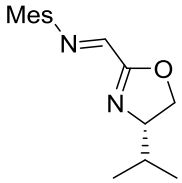 **E14**	**^{1}H NMR** (400 MHz, $CDCl_3$): δ 7.89 (1H, s, N=C<u>H</u>), 6.89 (2H, s, Ar-<u>H</u>), 4.53 (1H, dd *J* = 9.1 Hz, ^2J = 7.9 Hz, C<u>H$_2$</u>-O), 4.26-4.13 (2H, m, C<u>H$_2$</u>-O & N-C<u>H</u>), 2.29 (3H, s, *p*-Ar-C<u>H$_3$</u>), 2.13 (6H, s, *o*-Ar-C<u>H$_3$</u>), 1.98-1.85 (1H, m, C<u>H</u>-$(CH_3)_2$), 1.09 (3H, d *J* = 6.7 Hz, CH-(C<u>H$_3$</u>)$_2$), 0.99 (3H, d *J* = 6.8 Hz, CH-(C<u>H$_3$</u>)$_2$).
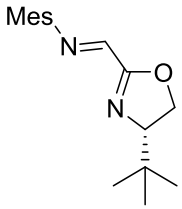 **E15**	**^{1}H NMR** (400 MHz, $CDCl_3$): δ 7.92 (1H, s, N=C<u>H</u>), 6.95 (2H, s, Ar-<u>H</u>), 4.41 (1H, dd ^2J = 10.1 Hz, *J* = 8.7 Hz, O-C<u>H$_2$</u>), 4.27 (1H, t *J* = 8.7 Hz, N-C<u>H</u>), 4.13 (1H, dd ^2J = 10.1 Hz, *J* = 8.7 Hz, O-C<u>H$_2$</u>), 2.35 (3H, s, *p*-Ar-C<u>H$_3$</u>), 2.17 (6H, s, *o*-Ar-C<u>H$_3$</u>), 0.94 (9H, s, C-(C<u>H$_3$</u>)$_3$).

In a Schlenk tube, was placed chloromethyl pivalate (1.02 g, 0.98 µL, 6.98 mmol), dry DCM (10 mL) and silver triflate (1.75 g, 6.98 mmol). The prepared imine (**E14** or **E15**) was added dropwise in a solution of dry DCM (5 mL) initiating a bright orange

colour change. The reaction was then stirred at room temperature for 16 h. The resulting solution was filtered through celite to remove silver impurities and purified by flash column chromatography with EtOAc and DCM/MeOH (95:5) successively, delivering the product imidazolium triflate (**112** 54%, 1.54 g; **113** 76%, 2.25 g) with a small amount (~5%) of pivalic acid, which further purification attempts did not eliminate.

Product	***Data***
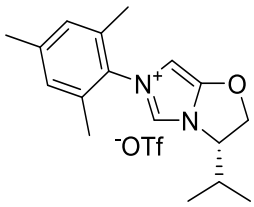 **112**	**Appearance**: yellow/brown oil. **IR** (cm^{-1}): 3074, 2964, 2867. **^{1}H NMR** (400 MHz, $CDCl_3$): δ 8.83 (1H, d, ^4J = 1.6 Hz, N-C<u>H</u>=N), 7.05 (1H, s, Ar-<u>H</u>), 7.02 (1H, s, Ar-<u>H</u>), 6.32 (1H, d, ^4J = 1.6 Hz, N-C<u>H</u>-C), 5.47-5.41 (1H, m, C<u>H</u>$_2$-O), 5.31 (1H, dd, J = 9.2 Hz, 8.2 Hz, C<u>H</u>-N), 5.02 (1H, dd, J = 9.2 Hz, ^2J = 3.7 Hz, C<u>H</u>$_2$-O), 2.59-2.48 (1H, m, C<u>H</u>-(CH$_3$)$_2$), 2.37 (3H, s, Ar-C<u>H</u>$_3$), 2.19 (3H, s, Ar-C<u>H</u>$_3$), 2.09 (3H, s, Ar-C<u>H</u>$_3$), 1.07 (3H, d, J = 6.9 Hz, CH-(C<u>H</u>$_3$)$_2$), 1.00 (3H, d, J = 6.9 Hz, CH-(C<u>H</u>$_3$)$_2$).. **^{13}C NMR** (101 MHz, $CDCl_3$): δ 151.2, 141.2, 135.4, 133.7, 132.0, 131.2, 129.6, 127.8, 120.7 (q, $^1J_{C-F}$ = 312 Hz, CF_3), 94.6, 79.2, 63.0, 31.0, 21.5, 17.5, 17.4, 16.5. **^{19}F NMR** (376 MHz, $CDCl_3$): δ -78.5 ($^-$OTf). **$[\alpha]_{20}^{D}$**: +30.1, (c 1.0, $CHCl_3$). **HRMS** (NSI): m/z calculated for $C_{17}H_{23}N_2O$ $[M\text{-}OTf]^+$: 271.1805; found: 271.1805.
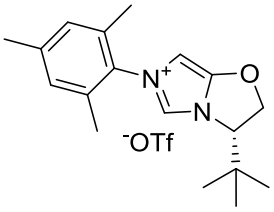 **113**	**Appearance**: Tan solid. **Melting Point** (°C): 112-114. **I.R.** (cm^{-1}): 3085, 2975, 2866. **^{1}H NMR** (400 MHz, $CDCl_3$): δ 8.65 (1H, d ^4J = 1.5 Hz, N-C<u>H</u>-N), 7.03 (1H, br s, Ar-<u>H</u>), 7.01 (1H, br-s, Ar-<u>H</u>), 6.36 (1H, d ^4J = 1.5 Hz, N-C<u>H</u>), 5.32 (1H, dd ^2J = 9.3 Hz, 8.0 Hz, N-C<u>H</u>), 5.20 (1H, dd ^2J = 9.3 Hz, 2.8 Hz, O-C<u>H</u>$_2$), 5.01 (1H, dd J = 8.0 Hz, 2.8 Hz, N-C<u>H</u>$_2$), 2.35 (3H, s, Ar-C<u>H</u>$_3$), 2.19 (3H, s, Ar-C<u>H</u>$_3$), 2.08 (3H, s, Ar-C<u>H</u>$_3$), 1.08 (9H, s, C-(C<u>H</u>$_3$)$_3$). **^{13}C NMR** (101 MHz, $CDCl_3$): δ 151.1, 141.0, 134.7, 133.3, 131.0, 129.6, 128.9, 127.6, 120.1 (q, $^1J_{C-F}$ = 312 Hz, CF_3), 95.1, 79.1, 66.7, 33.6, 26.6, 26.3, 24.8, 20.6, 16.7, 16.6. **^{19}F NMR** (376 MHz, $CDCl_3$): δ -78.5 ($^-$OTf). **$[\alpha]_{20}^{D}$**: +19.7, (c 1.0, $CHCl_3$). **HRMS** (NSI): m/z calculated for $C_{18}H_{25}N_2O$ $[M\text{-}OTf]^+$: 285.1961; found: 285.1960.

Scheme 1.44 *Synthesis of chiral-NHC/phosphine complexes* ***118a-e*** *and* ***119a-e****.*

Firstly, by following general procedure F the chiral NHC/chloride complexes were prepared.

Iridium dimer	***KOtBu***	***THF***	***Temperature***
(336 mg, 0.5 mmol)	(122 mg, 1.0 mmol)	(20 mL)	25 °C

Imidazolium Halide
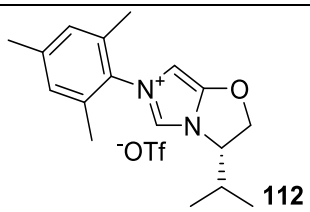 (420 mg, 1.0 mmol)

Product	***Data***
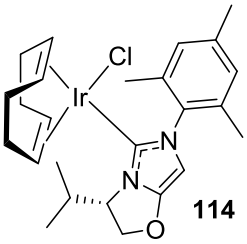 Yield = 370 mg, 61%.	**Appearance**: Yellow powder. **Melting Point** (°C): 155-157. **IR** (cm^{-1}): 2978, 2890. **^{1}H NMR** (400 MHz, $CDCl_3$): δ 7.03 (1H, s, Ar-H), 6.91 (1H, s, Ar-H), 5.92 (1H, s, N-CH), 5.20-5.11 (1H, m, N-CH), 4.97 (1H, dd, *J* = 8.5 Hz, 8.7 Hz, CH_2-O), 4.81 (1H, dd, *J* = 9.0 Hz, ^2J = 4.4 Hz, CH_2-O), 4.51-4.44 (2H, m, COD-CH), 3.66-3.54 (1H, m, CH-$(CH_3)_2$), 3.10-3.02 (1H, m, COD-CH), 2.69-2.61 (1H, m, COD-CH), 2.38 (3H, s, Ar-CH_3), 2.37 (3H, s, Ar-CH_3), 2.06-2.03 (1H, m, COD-CH_2), 2.02 (3H, s, Ar-CH_3), 1.96-1.84 (1H, m, COD-CH_2), 1.66-1.51 (4H, m, COD-CH_2), 1.50-1.39 (1H, m, COD-CH_2), 1.30-1.17 (1H, m, COD-CH_2), 1.12 (3H, d, *J* = 7.1 Hz, CH-$(CH_3)_2$), 0.94 (3H, d, *J* = 6.8 Hz, CH-$(CH_3)_2$).

^{13}C NMR (101 MHz, $CDCl_3$): δ 168.6, 150.6, 138.0, 136.4, 134.2, 128.8, 127.5, 93.8, 82.7, 82.3, 75.4, 60.1, 51.2, 51.0, 33.7, 32.5, 29.4, 28.8, 28.6, 20.6, 19.0, 18.2, 17.2, 13.7.

HRMS (APCI): m/z calculated for $C_{25}H_{33}IrN_2O_2Cl$ $[M+O-H_2]^+$:621.1852; found: 621.1850.

Imidazolium Halide
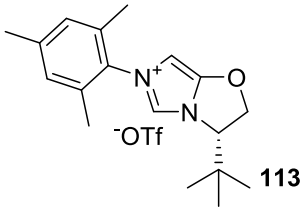 (434 mg, 1.0 mmol)

Product	***Data***
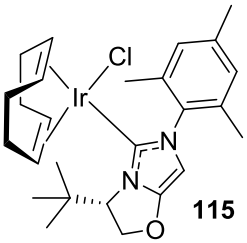 Yield = 360 mg, 58%.	**Appearance**: Yellow powder. **Melting Point** (°C): decomposes >175. **IR** (cm^{-1}): 3022, 2985, 2890. **^{1}H NMR** (400 MHz, $CDCl_3$): δ 7.05 (1H, s, Ar-H), 6.91 (1H, s, Ar-H), 5.98 (1H, s, N-CH=C), 5.20 (1H, dd, *J* = 7.1 Hz, ^2J = 2.0 Hz, CH_2-O), 4.98-4.87 (2H, m, CH_2-O & N-CH), 4.55-4.47 (1H, m, COD-CH), 4.44-4.36 (1H, m, COD-CH), 3.17-3.09 (1H, m, COD-CH), 2.47 (3H, s, Ar-CH_3), 2.46-2.41 (1H, m, COD-CH), 2.37 (3H, s, Ar-CH_3), 2.07-1.94 (5H, m, Ar-CH_3 & COD-CH_2), 1.94-1.83 (1H, m, COD-CH_2), 1.58-1.48 (1H, m, COD-CH_2), 1.44-1.38 (1H, m, COD-CH_2), 1.36-1.27 (10H, m, C-$(CH_3)_3$ & COD-CH_2), 1.14-1.03 (1H, m, COD-CH_2), 1.00-0.82 (1H, m, COD-CH_2).

^{13}C NMR (101 MHz, $CDCl_3$): δ 169.1, 151.4, 138.2, 136.9, 136.7, 134.7, 128.7, 127.3, 94.7, 81.3, 81.0, 77.7, 65.1, 52.2, 51.8, 34.0, 33.3, 32.4, 28.7, 27.9, 26.8, 20.6, 19.2, 16.9.

HRMS (APCI): m/z calculated for $C_{26}H_{37}ClIrN_2O$ $[M+H]^+$:621.2216; found: 621.2229.

Secondly, following general procedure E, the complexes bearing alkyl phosphines were synthesised.

Solvent	***NaBArF***	***Temperature (°C)***	***Time (h)***
DCM (10 mL)	(177 mg, 0.2 mmol)	25	1 (0.5+0.5)

NHC/chloride complex	***Phosphine***
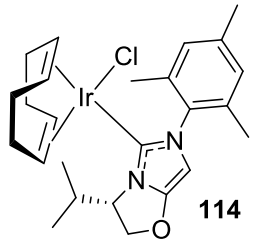 **114** (121 mg, 0.2 mmol)	PEt_3 (24 mg, 30 µL, 0.2 mmol)

Product

The compound exists as a pair of diastereomers (1:1), believed to originate from the restricted rotation of the Ir-C and Ir-P bonds, which are locked upon the synthesis of the complex, delivering two potential conformers; the data for both are give below.

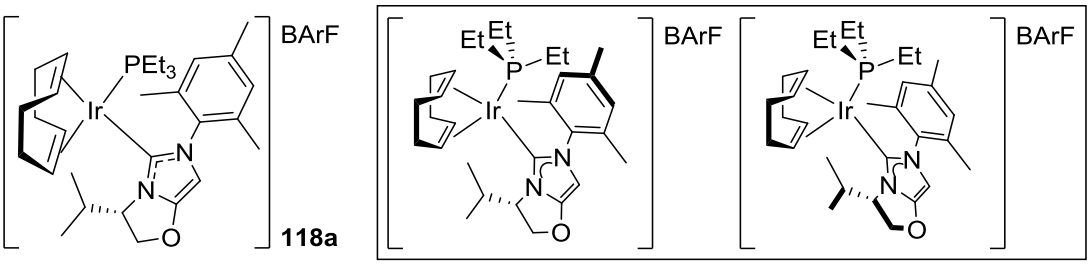

118a

Yield = 248 mg, 80%

Data

Appearance: red powder.

Melting Point (°C): >170 (dec).

IR (cm^{-1}): 3001, 2956, 2841.

^{1}H NMR (400 MHz, $CDCl_3$): δ 7.75-7.68 (8H, m, *o*-Ar-H), 7.54 (4H, s, *p*-Ar-H), 7.03-6.98 (1H, m, Ar-H), 6.97-6.91 (1H, m, Ar-H), 6.13 (0.5H, s, N-CH=C), 6.10 (0.5H, s, N-CH=C), 4.98-4.91 (0.5H, m, CH_2-O), 4.90-4.83 (1.5H, m, CH_2-O), 4.66-4.56 (1H, m, N-CH-CH_2), 4.34-4.28 (0.5H, m, COD-CH), 4.27-4.20 (0.5H, m, COD-CH), 4.19-4.12 (0.5H, m, COD-CH), 4.12-4.03 (1H, m, COD-CH), 4.00-3.92 (0.5H, m, COD-CH), 3.91-3.84 (0.5H, m, COD-CH), 3.82-3.75 (0.5H, m, COD-CH), 3.02-2.66 (0.5H, m, CH-$(CH_3)_2$), 2.66-2.54 (0.5H, m, CH-$(CH_3)_2$), 2.34 (1.5H, s, Ar-CH_3), 2.31 (1.5H, s, Ar-CH_3), 2.27 (1.5H, s, Ar-CH_3), 2.22 (1.5H, s, Ar-CH_3), 2.17-1.93 (6H, m, Ar-CH_3 & COD-CH_2), 1.91-1.78 (2H, m, COD-CH_2), 1.76-1.66 (3H, m, P-CH_2), 1.55-1.47 (2H, m, COD-CH_2), 1.47-1.36 (1H, m, COD-CH_2), 1.35-1.26 (3H, m, P-CH_2), 1.14-1.02 (6H, m, CH-$(CH_3)_2$), 0.92-0.80 (9H, m, P-CH_2-CH_3).

^{13}C NMR (101 MHz, $CDCl_3$): δ 168.8 (d, $^2J_{C-P}$ = 7.9 Hz), 161.2 (q, $^1J_{C-B}$ = 49.7 Hz), 151.3, 150.9, 139.8, 139.6, 135.3, 135.0, 134.8, 134.3, 133.9, 133.8, 129.5, 129.3, 128.9, 128.8, 128.4 (q, $^2J_{C-F}$ = 29.9 Hz), 124.1 (q, $^1J_{C-F}$ = 272.7 Hz), 116.9, 97.4, 96.8, 85.9, 85.7, 85.61, 85.56, 85.5, 85.4, 82.9, 82.8, 76.0, 74.9, 74.7, 74.3, 72.7, 62.9, 61.9, 52.9, 31.1, 30.9, 30.73, 30.71, 30.5, 30.4, 30.3, 30.0, 29.9, 20.4, 20.2, 19.3, 19.0, 18.9, 18.7, 18.6, 17.8, 17.3, 16.9, 16.6, 16.3, 16.0, 14.3, 13.4, 8.2, 7.6.

^{31}P NMR (162 MHz, $CDCl_3$): δ 5.0 (PEt_3), 4.0 (PEt_3).

^{19}F NMR (376 MHz, $CDCl_3$): δ -62.4 (BArF).
^{11}B NMR (128 MHz, $CDCl_3$): δ -6.7 (BArF).
HRMS (NSI): m/z calculated for $C_{31}H_{49}IrN_2OP$ $[M\text{-}BArF]^+$: 689.3208; found: 689.3200.

To prove the generation of a pair of diastereomers, an octahedral hydride species was formed in a solution of CD_3CN with bubbling hydrogen, in which the Ir-P and Ir-C bond would be free to rotate, thus delivering one major compound. The NMR data below supports this due to the coalescence of several key signals, following the loss of COD and the appearance of the hydride signals. This effect was also observed in all the other complexes synthesised in this series.

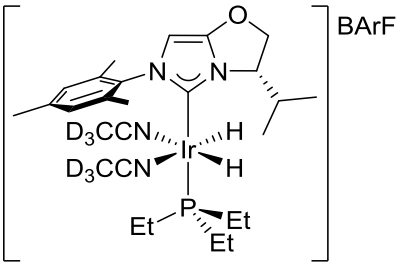

MeCN Hydride Complex
^{1}H NMR (400 MHz, CD_3CN): -22.16 (1H, dd, $^{2}J_{H\text{-}P}$ = 17.6 Hz, $^{2}J_{H\text{-}H}$ = 7.3 Hz, Ir-H), -22.26 (1H, dd, $^{2}J_{H\text{-}P}$ = 17.6 Hz, $^{2}J_{H\text{-}H}$ = 7.3 Hz, Ir-H).
^{31}P NMR (162 MHz, CD_3CN): δ -3.5 (t, $^{2}J_{P\text{-}H}$ = 17.6 Hz, PEt_3).

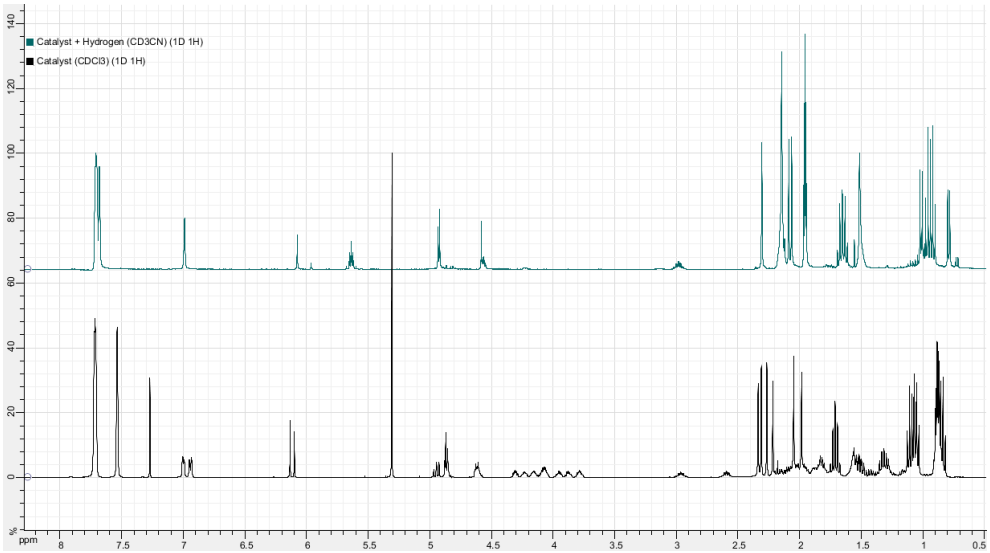

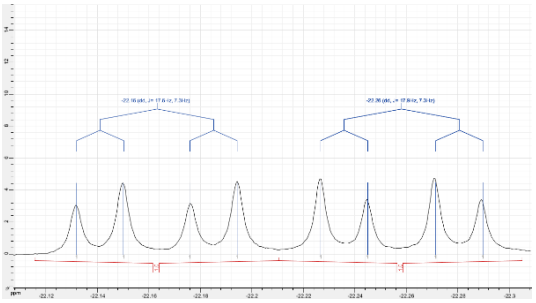

NHC/chloride complex	***Phosphine***
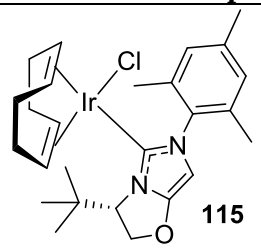 **115** (124 mg, 0.2 mmol)	PEt_3 (24 mg, 30 µL, 0.2 mmol)

Product

The compound exists as a pair of diastereomers (8:2), believed to originate from the restricted rotation of the Ir-C and Ir-P bonds, which are locked upon the synthesis of the complex, delivering two potential conformers; the data for both is given below.

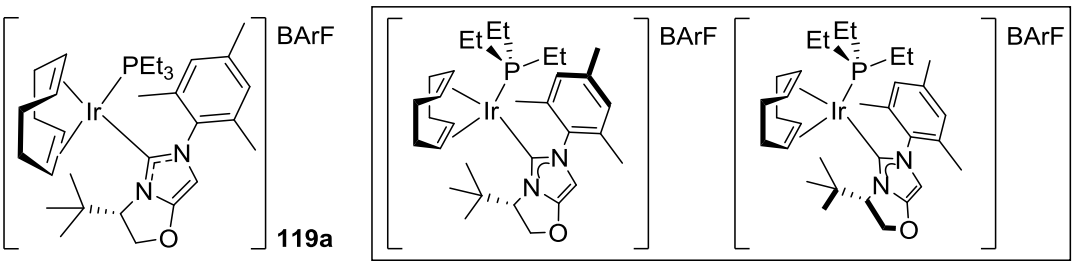

Yield = 197 mg, 63%

Data

Appearance: red powder.

Melting Point (°C): >165 (dec).

IR (cm^{-1}): 3085, 2995, 2878.

^{1}H NMR (400 MHz, $CDCl_3$): δ 7.72 (8H, br-s, Ar-H), 7.54 (4H, br-s, Ar-H), 7.06-6.99 (1H, m, Ar-H), 6.98-6.93 (1H, m, Ar-H), 6.16 (0.2H, s, N-CH=C), 6.15 (0.8H, s, N-CH=C), 5.02-4.95 (0.8H, m, O-CH_2), 4.91 (0.2H, m, O-CH_2), 4.72 (0.8H, dd ^2J = 9.6 Hz, J = 7.3 Hz, O-CH_2), 4.52 (0.2H, dd J = 7.3 Hz, 2.0 Hz, N-CH-CH_2), 4.46-4.37 (0.2H, m, COD-CH), 4.26-4.13 (1H, m, COD-CH), 4.12-3.94 (2.6H, m, COD-CH & N-CH-CH_2), 3.81-3.73 (0.2H, m, COD-CH), 3.71-3.62 (0.8H, m, COD-CH), 2.46 (0.6H, s, Ar-CH_3), 2.34 (2.4H, s, Ar-CH_3), 2.32 (0.6H, s, Ar-CH_3), 2.28 (2.4H, s, Ar-CH_3), 2.25-2.00 (2H, m, COD-CH_2), 1.97 (0.6H, s, Ar-CH_3), 1.96 (2.4H, s, Ar-CH_3), 1.95-1.77 (2H, m, COD-CH_2), 1.76-1.62 (6H, m, P-CH_2), 1.61-1.55 (1H, m, COD-CH_2), 1.53-1.25 (3H, m, COD-CH_2), 1.22 (7.2H, s, C-$(CH_3)_3$), 1.15 (1.8H, s, C-$(CH_3)_3$), 1.12-1.02 (7.2H, m, P-CH_2-CH_3), 0.90-0.80 (1.8H, m, P-CH_2-CH_3).

^{13}C NMR (101 MHz, $CDCl_3$): δ 168.7 (d $^2J_{C-P}$ = 9.4 Hz), 165.3 (d $^2J_{C-P}$ = 9.4 Hz), 161.2 (q $^2J_{C-F}$ = 49.3 Hz), 152.0, 151.6, 140.0, 139.8, 135.6, 135.5, 135.1, 134.3, 133.8, 129.8, 129.5, 128.84, 128.80, 128.40 (q $^2J_{C-B}$ = 31.0 Hz), 124.1 (q $^1J_{C-F}$ = 272.6 Hz), 116.9, 97.6, 97.5, 88.1, 88.0, 85.3, 85.1, 83.1, 83.0, 80.8, 80.7, 76.6, 76.0, 74.1, 72.4, 71.8, 68.9, 67.7, 34.9, 34.2, 31.7, 31.4, 31.3, 30.3, 29.9, 29.7, 28.7, 28.6, 26.6, 26.5, 20.3, 20.1, 19.6, 19.3, 18.6, 17.1, 16.9, 16.8, 16.2, 15.9, 8.1, 7.8.

^{31}P NMR (162 MHz, $CDCl_3$): δ 1.95 (PEt_3), 0.41 (PEt_3).

^{19}F NMR (376 MHz, $CDCl_3$): δ -62.4 (BArF).

^{11}B NMR (128 MHz, $CDCl_3$): δ -6.7 (BArF).

HRMS (NSI): m/z calculated for $C_{32}H_{51}IrN_2OP$ $[M\text{-}BArF]^+$: 703.3364; found: 703.3355.

MeCN Hydride Complex

^{1}H NMR (400 MHz, CD_3CN): -22.13 (1H, dd $^2J_{H\text{-}P}$ = 17.8 Hz, $^2J_{H\text{-}H}$ = 7.2 Hz, Ir-H), -22.29 (1H, dd $^2J_{H\text{-}P}$ = 17.8 Hz, $^2J_{H\text{-}H}$ = 7.2 Hz, Ir-H).

^{31}P NMR (162 MHz, CD_3CN): δ -3.6 (t $^2J_{P\text{-}H}$ = 17.8 Hz, PEt_3).

NHC/chloride complex	***Phosphine***
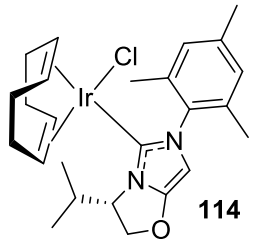 **114** (121 mg, 0.2 mmol)	PBn_3 (61 mg, 0.2 mmol)

Product

The compound exists as a pair of diastereomers (7:3), believed to originate from the restricted rotation of the Ir-C and Ir-P bonds, which are locked upon the synthesis of the complex, delivering two potential conformers; the data for both is given below.

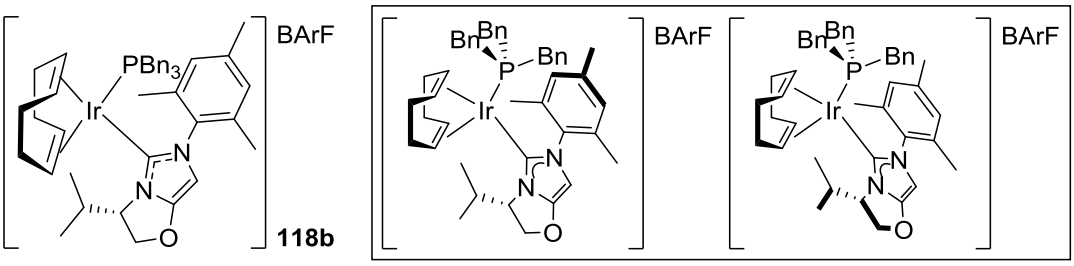

118b

Yield = 224 mg, 64%

Data

Appearance: red powder.

Melting Point (°C): >175 (dec).

IR (cm^{-1}): 3025, 2998, 2904.

^{1}H NMR (400 MHz, $CDCl_3$): δ 7.74 (8H, br s, Ar-H), 7.54 (4H, s, Ar-H), 7.35-7.24 (9H, m, Ar-H), 7.19-7.09 (2H, m, Ar-H), 7.08-7.01 (4H, m, Ar-H), 6.92-6.84 (2H, m, Ar-H), 6.29 (0.3H, s, N-CH=C), 6.22 (0.7H, s, N-CH=C), 5.05 (0.3H, m), 4.98-4.84 (2.1H, m), 4.83-4.76 (0.3H, m), 4.72-4.63 (0.3H, m), 4.59-4.54 (0.7H, m), 4.53-4.45 (0.3H, m), 4.31-4.22 (0.7H, m), 4.10-4.00 (0.7H, m), 3.79-7.68 (0.3H, m), 3.23-2.92 (6.3H, m), 2.92-2.84 (0.7H, m), 2.81-2.67 (1.3H, m), 2.49 (1H, s, Ar-CH_3), 2.46 (2H, s, Ar-CH_3), 2.44 (2H, s, Ar-CH_3), 2.33 (1H, s, Ar-CH_3), 2.31 (1H, s, Ar-CH_3),

2.09 (2H, s, Ar-C<u>H</u>$_3$), 2.06-1.93 (2H, m, COD-C<u>H</u>$_2$), 1.88-1.59 (4H, m, COD-C<u>H</u>$_2$), 1.40-1.17 (5H, m, COD-C<u>H</u>$_2$ & CH-(C<u>H</u>$_3$)$_2$), 0.97 (2H, d J = 6.8 Hz, CH-(C<u>H</u>$_3$)$_2$), 0.91 (1H, d J = 6.8 Hz, CH-(C<u>H</u>$_3$)$_2$).

^{13}C NMR (101 MHz, $CDCl_3$): δ 166.9 (d $^2J_{C\text{-}P}$ = 9.2 Hz), 165.0 (d $^2J_{C\text{-}P}$ = 9.1 Hz) 161.2 (q $^2J_{C\text{-}F}$ = 50.1 Hz), 151.7, 140.7, 140.3, 135.8, 138.6, 135.4, 135.3, 134.3, 133.7, 132.0, 131.9, 131.8, 130.2, 129.6, 129.2, 129.1, 129.0, 128.7, 128.4 (q $^1J_{C\text{-}B}$ = 31.2 Hz), 128.3, 127.5, 127.2, 124.1 (q $^1J_{C\text{-}F}$ = 272.5 Hz), 116.9, 97.8, 97.0, 88.6, 88.5, 88.4, 86.6, 86.5, 84.1, 84.0, 79.4, 78.5, 76.0, 75.3, 74.5, 63.1, 62.5, 32.1, 31.7, 31.7, 31.5, 31.3, 31.1, 30.9, 30.4, 29.6, 28.8, 28.4, 28.3, 20.5, 20.3, 19.7, 19.4, 19.2, 19.0, 18.1, 17.3, 14.2, 13.7.

^{31}P NMR (162 MHz, $CDCl_3$): δ -4.69 (PBn_3), -4.91 (PBn_3).

^{19}F NMR (376 MHz, $CDCl_3$): δ -62.4 (BArF).

^{11}B NMR (128 MHz, $CDCl_3$): δ -6.7 (BArF).

HRMS (NSI): m/z calculated for $C_{46}H_{55}IrN_2OP$ $[M\text{-}BArF]^+$: 875.3679; found: 875.3679.

MeCN Hydride Complex

^{1}H NMR (400 MHz, CD_3CN): -21.90 (1H, dd $^2J_{H\text{-}P}$ = 16.8 Hz, $^2J_{H\text{-}H}$ = 7.8 Hz, Ir-<u>H</u>), -21.95 (1H, dd $^2J_{H\text{-}P}$ = 16.8 Hz, $^2J_{H\text{-}H}$ = 7.8 Hz, Ir-<u>H</u>).

^{31}P NMR (162 MHz, CD_3CN): δ -4.0 (t $^2J_{P\text{-}H}$ = 17.6 Hz, PBn_3).

NHC/chloride complex	***Phosphine***
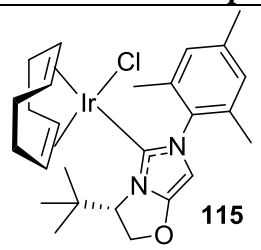 **115** (124 mg, 0.2 mmol)	PBn_3 (61 mg, 0.2 mmol)

Product

The compound exists as a pair of diastereomers (7:3), believed to originate from the restricted rotation of the Ir-C and Ir-P bonds, which are locked upon the synthesis of the complex, delivering two potential conformers; the data for both is given below.

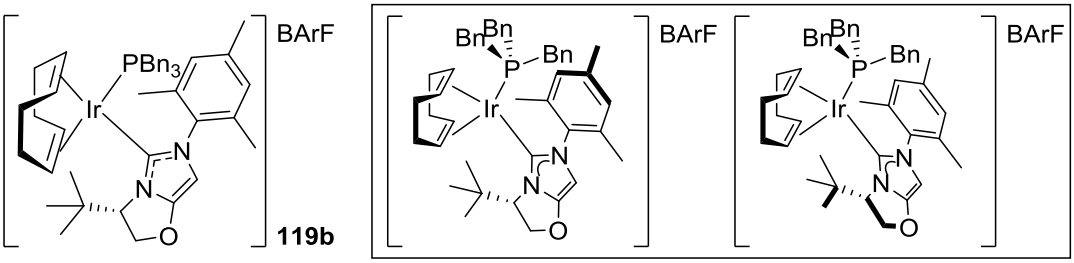

Yield = 197 mg, 63%

Data

Appearance: red powder.

Melting Point (°C): >160 (dec).

I.R. (cm^{-1}): 3064, 2986, 2888.

^{1}H NMR (400 MHz, $CDCl_3$): δ 7.77 (8H, br-s, Ar-H), 7.56 (4H, s, Ar-H), 7.40-7.20 (9.8H, m, Ar-H), 7.19-7.05 (6H, m, Ar-H), 6.97-6.86 (1.2H, m, Ar-H), 6.29 (0.3H, s, N-CH=C), 6.26 (0.7H, s, N-CH=C), 5.06-4.91 (1.4H, m), 4.87-4.89 (0.7H, m), 4.76-4.68 (0.7H, m), 4.66-4.60 (0.3H, m), 4.59-4.51 (0.3H, m), 4.50-4.36 (1.3H, m), 4.16-4.09 (0.7H, m), 3.95-3.84 (0.3H, m), 3.24-2.81 (8.3H, m), 2.72 (0.9H, s, Ar-CH_3), 2.47 (2.1H, s, Ar-CH_3), 2.44 (2.1H, s, Ar-CH_3), 2.34 (0.9H, s, Ar-CH_3), 2.25-2.19 (1H, m, COD-CH_2), 2.16 (0.9H, s, Ar-CH_3), 2.15-2.07 (0.5H, m, COD-CH_2), 2.05 (2.1H, s, Ar-CH_3), 2.02-1.91 (1H, m, COD-CH_2), 1.90-1.60 (3.5H, m, COD-CH_2), 1.54-1.34 (2H, m, COD-CH_2), 1.32 (2.7H, s, C-$(CH_3)_3$), 1.29 (6.3H, s, C-$(CH_3)_3$).

^{13}C NMR (101 MHz, $CDCl_3$): δ 167.5. (d $^2J_{C-P}$ = 8.0 Hz), 164.7 (d $^2J_{C-P}$ = 9.1 Hz) 161.3 (q $^2J_{C-F}$ = 49.8 Hz), 152.7, 152.2, 140.9, 140.4, 136.4, 136.2, 135.6, 135.5, 135.2, 134.3, 134.1, 133.4, 132.1, 132.0, 130.6, 129.9, 129.4, 129.3, 128.8, 128.4 (q $^1J_{C-B}$ = 30.6 Hz), 127.6, 127.1, 124.1 (q $^1J_{C-F}$ = 272.3 Hz), 117.0, 98.0, 97.7, 90.2, 90.1, 86.7, 86.6, 84.9, 84.8, 81.0, 80.9, 80.5, 77.5, 77.0, 76.0, 72.6, 70.0, 68.0, 35.0, 34.7, 33.7, 32.9, 32.8, 32.1, 31.8, 31.1, 30.5, 29.6, 29.0, 27.01, 26.97, 26.9, 20.5, 20.4, 19.4, 18.9, 16.9.

^{31}P NMR (162 MHz, $CDCl_3$): δ -5.10 (PBn_3), -7.60 (PBn_3)

^{19}F NMR (376 MHz, $CDCl_3$): δ -62.4 (BArF).

^{11}B NMR (128 MHz, $CDCl_3$): δ -6.7 (BArF).

HRMS (NSI): m/z calculated for $C_{47}H_{57}IrN_2OP$ $[M\text{-}BArF]^+$: 889.3835; found: 889.3830.

MeCN-Hydride Complex

^{1}H NMR (400 MHz, CD_3CN): -21.94 (1H, dd $^2J_{H-P}$ = 16.2 Hz, $^2J_{H-H}$ = 7.1 Hz, Ir-H), -21.98 (1H, dd $^2J_{H-P}$ = 16.2 Hz, $^2J_{H-H}$ = 7.1 Hz, Ir-H).

^{31}P NMR (162 MHz, CD_3CN): δ -2.8 (t $^2J_{P-H}$ = 16.2 Hz, PBn_3).

NHC/chloride complex	***Phosphine***
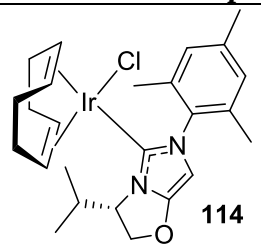 **114** (121 mg, 0.2 mmol)	PCy_3 (56 mg, 0.2 mmol)

Product

The compound exists as a pair of diastereomers (7:3), believed to originate from the restricted rotation of the Ir-C and Ir-P bonds, which are locked upon the synthesis

of the complex, delivering two potential conformers; the data for both is given below.

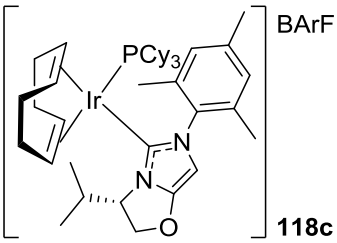

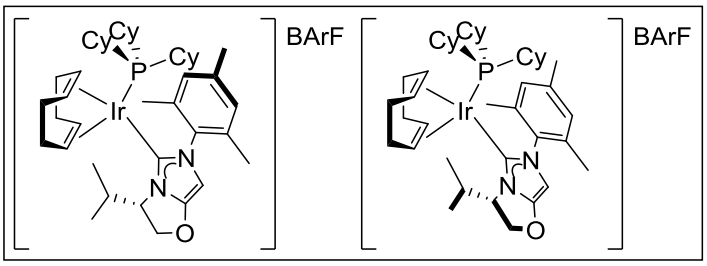

Yield = 202 mg, 59%

Data

Appearance: red powder.

Melting Point (°C): >140 (dec).

IR (cm^{-1}): 3089, 3002, 2965, 2854.

^{1}H NMR (400 MHz, $CDCl_3$): δ 7.73 (8H, br s, Ar-H), 7.55 (4H, s, Ar-H), 7.01-6.90 (2H, m, Ar-H), 6.13 (0.7H, s, N-CH=C), 6.12 (0.3H, s, N-CH=C), 4.95-4.89 (1H, m), 4.89-4.81 (0.7H, m), 4.74-4.62 (1.4H, m,), 4.59-4.52 (0.7H, m,), 4.41-4.26 (0.3H, m), 4.21-4.13 (1.3H, m), 3.89-3.79 (0.7H, 3.78-3.70 (0.3H, m), 3.32 (0.3H, m, CH-$(CH_3)_2$), 3.13-3.01 (0.7H, m, CH-$(CH_3)_2$), 2.68-2.56 (0.3H, m), 2.34 (2.1H, s, Ar-CH_3), 2.33 (0.9H, s, Ar-CH_3), 2.32 (2.1H, s, Ar-CH_3), 2.30-2.27 (0.3H, m), 2.26 (0.9H, s, Ar-CH_3), 2.01 (0.9H, s, Ar-CH_3), 1.96 (2.1H, s, Ar-CH_3), 1.94-1.05 (41H, m, COD-CH_2 & Cy-CH_2), 0.98-0.87 (6H, m, CH-$(CH_3)_2$).

^{13}C NMR (101 MHz, $CDCl_3$): δ 166.5 (d $^{2}J_{C-P}$ = 7.7 Hz), 161.3 (q $^{2}J_{C-F}$ = 49.8 Hz), 151.2, 139.7, 135.9, 135.4, 134.3, 134.0, 129.0, 128.9, 128.4 (q $^{1}J_{C-B}$ = 32.7 Hz), 128.3 124.1 (q $^{1}J_{C-F}$ = 272.3 Hz), 116.9, 98.3, 97.4, 80.4, 80.3, 77.6, 77.2, 76.7, 75.3, 75.1, 74.9, 74.4, 71.8, 69.6, 63.1, 35.6, 34.8, 32.4, 31.9, 30.7, 30.3, 30.1, 29.3, 30.0, 27.4(br), 27.2, 27.04, 26.95, 25.5 (br), 20.3, 20.0, 19.8, 19.3, 18.4, 18.0, 17.7, 14.9, 13.4.

^{31}P NMR (162 MHz, $CDCl_3$): δ 20.1 (PCy_3), 15.6 (PCy_3).

^{19}F NMR (376 MHz, $CDCl_3$): δ -62.4 (BArF).

^{11}B NMR (128 MHz, $CDCl_3$): δ -6.7 (BArF).

HRMS (NSI): major fragmentation during mass spectrometry: m/z calculated for $C_{17}H_{23}N_2O$ [M-BArF-$C_{26}H_{45}IrP]^+$: 271.1805; found: 271.1809. $C_{18}H_{33}PH$ [M-BArF-$C_{25}H_{34}IrN_2O$+H]$^+$: 281.2398; found 281.2392.

MeCN Hydride Complex

^{1}H NMR (400 MHz, CD_3CN): -22.38 (1H, dd $^{2}J_{H-P}$ = 17.0 Hz, $^{2}J_{H-H}$ = 7.2 Hz, Ir-H), -22.40 (1H, dd $^{2}J_{H-P}$ = 17.0 Hz, $^{2}J_{H-H}$ = 7.2 Hz, Ir-H).

^{31}P NMR (162 MHz, CD_3CN): δ 17.9 (t $^{2}J_{P-H}$ = 17.0 Hz, PCy_3).

NHC/chloride complex	*Phosphine*
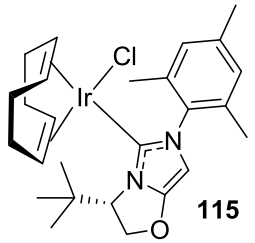 **115** (124 mg, 0.2 mmol)	PCy_3 (56 mg, 0.2 mmol)

Product	*Data*
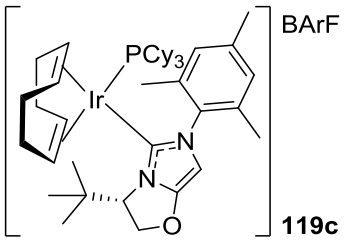 **119c** **Yield** = 176 mg, 51%	**Appearance**: red powder. **Melting Point** (°C): >135 (dec). **IR** (cm^{-1}): 3064, 2986, 2888. **^{1}H NMR** (400 MHz, $CDCl_3$): δ 7.73 (8H, br s, Ar-H), 7.55 (4H, m, Ar-H), 7.01 (1H, s, Ar-H), 6.91 (1H, s, Ar-H), 6.08 (1H, s, N-CH=C), 5.16-5.07 (1H, m), 5.06-4.96 (2H, m), 4.19-4.10 (1H, m), 3.99-3.89 (1H, m), 3.84-3.72 (1H, m), 3.71-3.59 (1H, m), 2.39 (3H, s, Ar-CH_3), 2.30 (3H, s, Ar-CH_3), 2.27-2.10 (2H, m, N-CH), 1.92 (3H, s, Ar-CH_3), 1.90-1.06 (52H, m, COD-CH_2, Cy-CH_2 & C-(CH_3)$_3$).

^{13}C NMR (101 MHz, $CDCl_3$): δ 164.9 (d $^2J_{C-P}$ = 6.2 Hz), 161.2 (q $^2J_{C-F}$ = 50.0 Hz), 151.6, 140.1, 136.3, 135.1, 134.3, 133.3, 130.4, 129.4, 129.3, 128.4 (q $^1J_{C-B}$ = 31.1 Hz), 124.1 (q $^1J_{C-F}$ = 272.3 Hz), 116.9, 97.6, 83.6, 83.5, 80.0, 76.7, 68.9, 68.7, 68.1, 65.0, 35.2, 34.2, 27.6 (br), 26.7, 26.5, 25.4 (br), 20.3, 18.9, 17.4.

^{31}P NMR (162 MHz, $CDCl_3$): δ 11.2 (PCy_3).

^{19}F NMR (376 MHz, $CDCl_3$): δ -62.4 (BArF).

^{11}B NMR (128 MHz, $CDCl_3$): δ -6.6 (BArF).

HRMS (NSI): m/z calculated for $C_{44}H_{69}IrN_2OP$ $[M\text{-}BArF]^+$: 865.4777; found: 865.4768.

MeCN Hydride Complex

^{1}H NMR (400 MHz, CD_3CN): -22.35 (1H, dd $^2J_{H-P}$ = 16.3 Hz, $^2J_{H-H}$ = 7.1 Hz, Ir-H), -22.42 (1H, dd $^2J_{H-P}$ = 16.3 Hz, $^2J_{H-H}$ = 7.1 Hz, Ir-H).

^{31}P NMR (162 MHz, CD_3CN): δ 17.4 (t $^2J_{P-H}$ = 16.3 Hz, PCy_3).

NHC/chloride complex	*Phosphine*
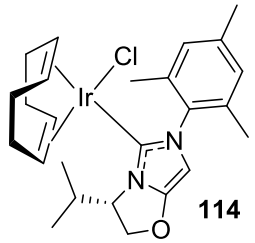 **114** (121 mg, 0.2 mmol)	$PiPr_3$ (32 mg, 38 µL 0.2 mmol)

Product

The compound exists as a pair of diastereomers (6:4), believed to originate from the restricted rotation of the Ir-C and Ir-P bonds, which are locked upon the synthesis of the complex, delivering two potential conformers; the data for both is given below.

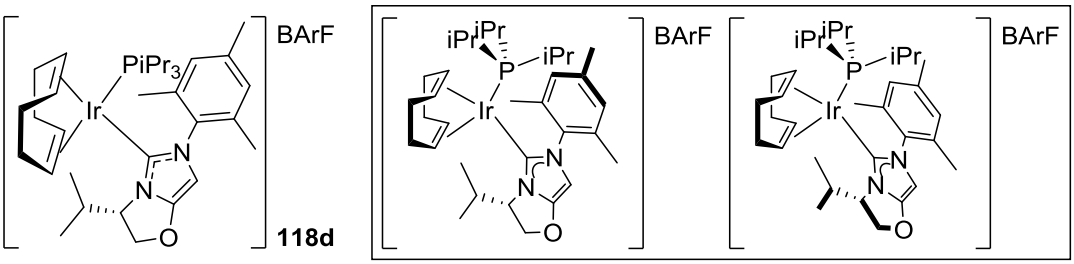

Yield = 220 mg, 69%

Data

Appearance: red powder.

Melting Point (°C): >140 (dec).

IR (cm^{-1}): 3089, 3002, 2965, 2854.

^{1}H NMR (400 MHz, $CDCl_3$): δ 7.73 (8H, br s, Ar-H), 7.55 (4H, s, Ar-H), 7.00-6.90 (2H, m, Ar-H), 6.12 (1H, s, N-CH=C), 4.98-4.86 (1.4H, m), 4.81-4.60 (2.0H, m), 4.60-4.50 (1H, m), 4.39-4.30 (0.6H, m), 4.22-4.12 (0.6H, m), 4.02-3.93 (0.4H, m), 3.86-3.75 (1H, m), 3.14-3.02 (0.6H, m, CH-$(CH_3)_2$), 2.73-2.61 (0.4H, m, CH-$(CH_3)_2$), 2.43-2.32 (3.6H, m, Ar-CH_3 & CH-$(CH_3)_2$), 2.29 (1.2H, s, Ar-CH_3), 2.25 (1.8H, s, Ar-CH_3), 2.24 (1.2H, s, Ar-CH_3), 2.23-2.04 (3.2H, m, CH-$(CH_3)_2$ & COD-CH_2), 2.01 (1.2H, s, Ar-CH_3),1.97 (1.8H, s, Ar-CH_3), 1.93-1.64 (3H, m, COD-CH_2), 1.64-1.42 (3H, m, COD-CH_2), 1.31-1.19 (12H, m, CH-$(CH_3)_2$), 1.16-1.06 (6H, m, CH-$(CH_3)_2$), 1.00-0.90 (6H, m, CH-$(CH_3)_2$).

^{13}C NMR (101 MHz, $CDCl_3$): δ 167.5 (d $^2J_{C-P}$ = 7.7 Hz), 166.1 (d $^2J_{C-P}$ = 8.2 Hz), 161.2 (q $^2J_{C-F}$ = 50.1 Hz), 151.5, 151.3, 139.9, 139.7, 135.7, 135.5, 135.4, 135.3, 134.3, 134.0, 130.4, 129.3, 129.1, 128.8 128.4 (q $^1J_{C-B}$ = 31.1 Hz), 124.1 (q $^1J_{C-F}$ = 272.3 Hz), 116.9, 98.1, 97.7, 81.3, 81.2, 90.4, 80.3, 77.9, 77.1, 75.6, 75.4, 75.1, 74.7, 74.4, 71.5, 70.0 63.1, 62.9, 33.8, 33.1, 32.7, 32.3, 30.6, 30.4, 28.8, 28.4, 26.2, 26.0, 25.9, 25.8, 20.3, 20.1, 20.0, 19.4, 19.2, 19.1, 19.0, 18.9, 18.7, 17.9, 17.6, 17.5, 14.4, 13.4.

^{31}P NMR (162 MHz, $CDCl_3$): δ 27.3 ($PiPr_3$), 23.4 ($PiPr_3$).

^{19}F NMR (376 MHz, $CDCl_3$): δ -62.4 (BArF).

^{11}B NMR (128 MHz, $CDCl_3$): δ -6.7 (BArF).

HRMS (NSI): m/z calculated for $C_{34}H_{55}IrN_2OP$ $[M\text{-}BArF]^+$: 731.3681; found: 731.3679.

MeCN Hydride Complex

^{1}H NMR (400 MHz, CD_3CN): -22.36 (1H, dd $^2J_{H\text{-}P}$ = 17.4 Hz, $^2J_{H\text{-}H}$ = 7.1 Hz, Ir-H), -22.40 (1H, dd $^2J_{H\text{-}P}$ = 17.4 Hz, $^2J_{H\text{-}H}$ = 7.1 Hz, Ir-H).

^{31}P NMR (162 MHz, CD_3CN): δ 27.4 (t $^2J_{P\text{-}H}$ = 17.4 Hz, $PiPr_3$).

NHC/chloride complex	***Phosphine***
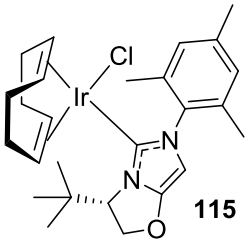 **115** (124 mg, 0.2 mmol)	$PiPr_3$ (32 mg, 38 µL 0.2 mmol)

Product

The compound exists as a pair of diastereomers (9:1), believed to originate from the restricted rotation of the Ir-C and Ir-P bonds, which are locked upon the synthesis of the complex, delivering two potential conformers; the data for both is given below.

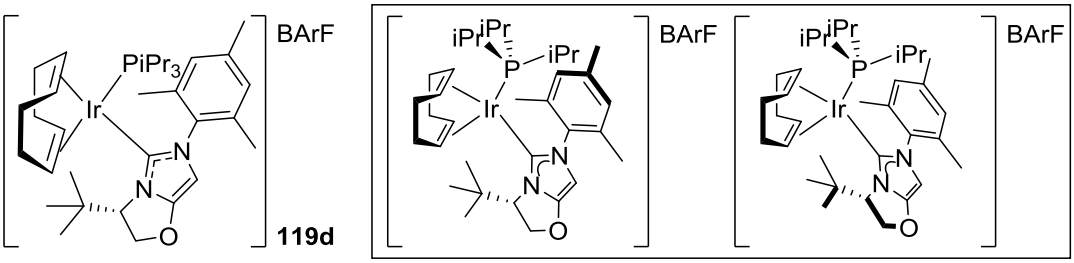

119d

Yield = 241 mg, 75%

Data

Appearance: red powder.

Melting Point (°C): >135 (dec).

IR (cm^{-1}): 3064, 2986, 2888.

^{1}H NMR (400 MHz, $CDCl_3$): δ 7.72 (8H, br s, Ar-H), 7.54 (4H, s, Ar-H), 7.01 (0.9H, s, Ar-H), 6.95 (0.1H, s, Ar-H), 6.92 (1H, s, Ar-H), 6.12 (0.9H, s, N-CH=C), 6.08 (0.1H, s, N-CH=C), 5.03-4.83 (2H, m), 4.64-4.40 (1.2H, m), 4.12-4.07 (1H, m), 4.03-3.89 (1.8H, m), 3.88-3.78 (1H, m), 2.48-2.35 (5.4H, m, CH-$(CH_3)_2$ & Ar-CH_3), 2.33 (3H, s, Ar-CH_3), 2.28 (0.3H, s, Ar-CH_3), 2.26-1.98 (2.3H, m, CH-$(CH_3)_2$ & COD-CH_2), 1.94 (0.3H, s, Ar-CH_3), 1.93 (2.7H, s, Ar-CH_3), 1.88-1.75 (2H, m, COD-CH_2), 1.67-1.57 (2H, m, COD-CH_2), 1.41-1.33 (9H, m, CH-$(CH_3)_2$), 1.32-1.27 (2H, m, COD-CH_2), 1.26-1.10 (18H, m, CH-$(CH_3)_2$ & C-$(CH_3)_3$).

^{13}C NMR (101 MHz, $CDCl_3$): δ 164.8 (d $^2J_{C\text{-}P}$ = 7.9 Hz), 161.2 (q $^2J_{C\text{-}F}$ = 49.8 Hz), 151.8, 140.0, 136.3, 135.3, 134.3, 133.5, 129.3, 129.2, 128.4 (q $^1J_{C\text{-}B}$ = 31.7 Hz), 127.9, 124.1 (q $^1J_{C\text{-}F}$ = 272.3 Hz), 116.9, 98.2, 83.72, 83.66, 78.6, 72.0, 71.9, 68.6,

66.5, 35.0, 33.4, 33.3, 27.4, 27.3, 26.5, 25.8, 25.6, 20.3, 19.8, 19.5, 19.0, 17.3, 16.9, 15.8.

^{31}P NMR (162 MHz, $CDCl_3$): δ 22.5 ($PiPr_3$), 17.8 ($PiPr_3$).

^{19}F NMR (376 MHz, $CDCl_3$): δ -62.4 (BArF).

^{11}B NMR (128 MHz, $CDCl_3$): δ -6.6 (BArF).

HRMS (NSI): m/z calculated for $C_{35}H_{57}IrN_2OP$ $[M\text{-}BArF]^+$: 745.3834; found: 745.3830.

MeCN Hydride Complex

^{1}H NMR (400 MHz, CD_3CN): -22.37 (1H, dd $^2J_{H\text{-}P}$ = 17.1 Hz, $^2J_{H\text{-}H}$ = 7.2 Hz, Ir-H), -22.40 (1H, dd $^2J_{H\text{-}P}$ = 17.1 Hz, $^2J_{H\text{-}H}$ = 7.2 Hz, Ir-H).

^{31}P NMR (162 MHz, CD_3CN): δ 27.0 (t $^2J_{P\text{-}H}$ = 17.1 Hz, $PiPr_3$).

Next, following general procedure G the imidazolium BArF salts were synthesised.

Solvent	*NaBArF*	*Temperature (°C)*	*Time (h)*
DCM/H_2O (10 mL/10 mL)	(177 mg, 1.0 mmol)	25	16 h

Imidazolium triflate
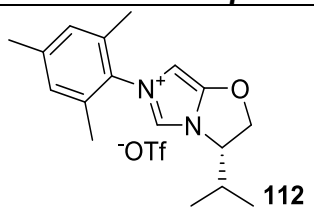 (420 mg, 1.0 mmol)

Product	*Data*
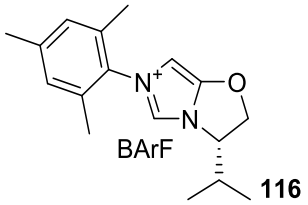 Yield = 1.01 g, 89%.	**Appearance**: tan powder. **Melting Point** (°C): 161-163. **IR** (cm^{-1}): 3033, 2997, 2980, 2865. **^{1}H NMR** (400 MHz, $CDCl_3$): δ 7.74 (1H, d ^4J = 1.7 Hz, N-CH-N), 7.73-7.66 (8H, m, Ar-H), 7.54 (4H, br s, Ar-H), 7.05 (2H, br s, Ar-H), 6.42 (1H, d ^4J = 1.5 Hz, N-CH), 5.14 (1H, dd ^2J = 9.6 Hz, J = 8.3 Hz, O-CH_2), 4.93 (1H, dd ^2J = 9.6 Hz, J = 5.0 Hz, O-CH_2), 4.71 (1H, dt J = 8.3 Hz, 5.0 Hz, N-CH), 2.37 (3H, s, Ar-CH_3), 2.26-2.14 (1H, m, CH-$(CH_3)_2$) 2.03 (3H, s, Ar-CH_3), 2.00 (3H, s, Ar-CH_3), 0.99 (3H, d J = 6.0 Hz, CH-$(CH_3)_2$), 0.97 (3H, d J = 6.0 Hz, CH-$(CH_3)_2$).

^{13}C NMR (101 MHz, $CDCl_3$): δ 161.2 (q $^1J_{C-F}$ = 50.0 Hz), 151.2, 142.3, 134.3, 133.2, 133.1, 130.2, 129.7, 129.6, 128.4 (q $^2J_{C-F}$ = 30.9 Hz), 124.1 (q $^1J_{C-F}$ = 274.1 Hz), 123.1, 117.0, 96.9, 79.4, 63.8, 30.9, 20.4, 16.7, 16.2.

^{19}F NMR (376 MHz, $CDCl_3$): δ -62.4 (BArF).

^{11}B NMR (128 MHz, $CDCl_3$): δ -6.7 (BArF).

HRMS (NSI): m/z calculated for $C_{17}H_{23}N_2O$ $[M\text{-}BArF]^+$: 271.1805; found: 271.1804.

Imidazolium triflate

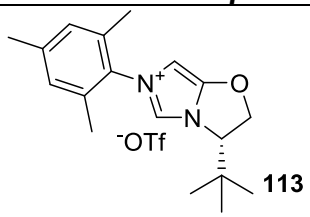

(434 mg, 1.0 mmol)

Product	***Data***
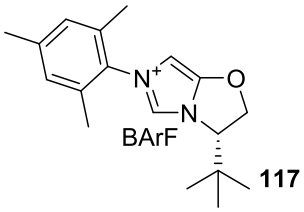 Yield = 1.09 g, 95%.	**Appearance**: tan powder. **Melting Point** (°C): decomposes >175. **IR** (cm^{-1}): 3022, 2985, 2890. **^{1}H NMR** (400 MHz, $CDCl_3$): δ 7.79 (1H, d ^4J = 1.5 Hz, N-C<u>H</u>-N), 7.71 (8H, br s, Ar-<u>H</u>), 7.53 (4H, br s, Ar-<u>H</u>), 7.04 (2H, br s, Ar-<u>H</u>), 6.42 (1H, d ^4J = 1.5 Hz, N-C<u>H</u>-C), 5.10 (1H, dd ^2J = 9.8 Hz, J = 8.2 Hz, O-C<u>H</u>$_2$), 5.03 (1H, dd ^2J = 9.8 Hz, J = 4.4 Hz, O-C<u>H</u>$_2$), 4.56 (1H, dd J = 8.2 Hz, 4.4 Hz, N-C<u>H</u>-CH$_2$), 2.36 (3H, s, Ar-C<u>H</u>$_3$), 2.04 (3H, s, Ar-C<u>H</u>$_3$), 2.00 (3H, s, Ar-C<u>H</u>$_3$) 1.01 (9H, s, C-(C<u>H</u>$_3$)$_3$).

^{13}C NMR (101 MHz, $CDCl_3$): δ 161.2 (q $^1J_{C-F}$ = 50.0 Hz), 151.2, 141.0, 134.7,133.8, 133.3, 131.0, 129.6, 128.9, 128.4 (q $^2J_{C-F}$ = 30.9 Hz), 127.6, 124.1 (q $^1J_{C-F}$ = 274.1 Hz), 120.1, 95.1, 79.1, 66.7, 33.6, 26.6, 26.3, 24.8, 20.6, 16.7, 16.6.

^{19}F NMR (376 MHz, $CDCl_3$): δ -62.4 (BArF).

^{11}B NMR (128 MHz, $CDCl_3$): δ -6.7 (BArF).

HRMS (NSI m/z calculated for $C_{18}H_{25}N_2O$ $[M\text{-}BArF]^+$: 285.1961; found: 285.1961.

Finally, following general procedure H, triphenylphosphine complexes **118e** and **119e** were synthesised.

Iridium dimer	***Solvent***	***Phosphine***	***Temperature (°C)***	***Time (h)***
(168 mg, 0.25 mmol)	THF (10 mL)	PPh_3 (131 mg, 0.5 mmol)	25	3

Imidazolium BArF

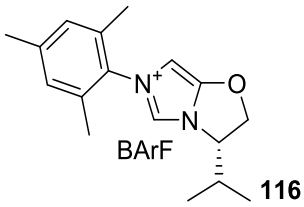

(567 mg,0.5 mmol)

Product	***Data***
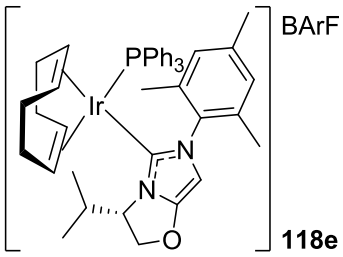 Yield = 653 mg, 77%.	**Appearance**: red powder. **Melting Point** (°C): >180 (dec) °C. **I.R.** (cm^{-1}): 3033, 2982, 2895. **^{1}H NMR** (400 MHz, $CDCl_3$): δ 7.75 (8H, br s, Ar-H), 7.55 (4H, br s, Ar-H), 7.54-7.05 (15H, m, Ar-H), 6.99 (1H, s, Ar-H), 6.97 (1H, s, Ar-H), 6.20 (1H, s, N-CH=C), 4.55-4.43 (2H, m, COD-CH & O-CH_2), 4.23-4.14 (1H, m, COD-CH), 3.74-3.62 (2H, m, COD-CH & O-CH_2), 3.56-3.42 (2H, m, COD-CH & N-CH-CH_2), 3.08-2.94 (1H, m, COD-CH), 2.37 (3H, s, Ar-CH_3), 2.23-2.03 (3H, m, COD-CH_2), 2.01 (3H, s, Ar-CH_3), 2.00 (3H, s, Ar-CH_3), 1.98-1.84 (2H, m, COD-CH_2), 1.64-1.47 (2H, COD-CH_2), 1.40-1.09 (1H, m, COD-CH_2), 0.96 (3H, d J = 6.9 Hz, CH-$(CH_3)_2$), 0.88 (3H, d J = 6.9 Hz, CH-$(CH_3)_2$).

^{13}C NMR (101 MHz, $CDCl_3$): δ 163.4 (d $^2J_{C-P}$ = 9.3 Hz), 161.2 (q $^2J_{C-F}$ = 50.0 Hz), 151.7, 139.8, 135.8, 135.3, 134.3, 133.2 (br), 131.8 (br), 131.4 (br), 130.7 (br), 129.3, 128.8, 128.6, 128.4 (q $^1J_{C-B}$ = 31.5 Hz), 124.1 (q $^1J_{C-F}$ = 272.9 Hz), 117.0, 97.1, 85.3, 85.2, 83.6, 83.7, 81.1, 77.5, 74.6, 61.4, 32.3, 31.2, 30.9, 30.8, 29.5, 28.3, 20.4, 20.1, 18.0, 17.2, 13.3.

^{31}P NMR (162 MHz, $CDCl_3$): δ 17.7 (PPh_3).

^{19}F NMR (376 MHz, $CDCl_3$): δ -62.4 (BArF).

^{11}B NMR (128 MHz, $CDCl_3$): δ -6.7 (BArF).

HRMS (NSI): m/z calculated for $C_{43}H_{49}IrN_2OP$ $[M\text{-}BArF]^+$: 833.3211; found: 833.3217.

MeCN Hydride Complex

^{1}H NMR (400 MHz, CD_3CN): -21.47 (1H, dd $^2J_{H-P}$ = 17.5 Hz, $^2J_{H-H}$ = 6.8 Hz, Ir-H), -21.59 (1H, dd $^2J_{H-P}$ = 17.7 Hz, $^2J_{H-H}$ = 6.8 Hz, Ir-H).

^{31}P NMR (162 MHz, CD_3CN): δ 17.5 (t $^2J_{P-H}$ = 17.5 Hz, PPh_3).

Imidazolium BArF

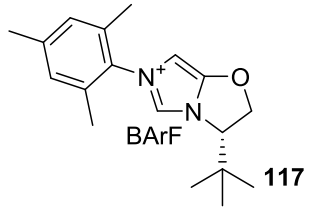

(574 mg, 0.5 mmol).

The compound exists as a pair of diastereomers (8:2), believed to originate from the restricted rotation of the Ir-C and Ir-P bonds, which are locked upon the synthesis of the complex, delivering two potential conformers; the data for both are given below.

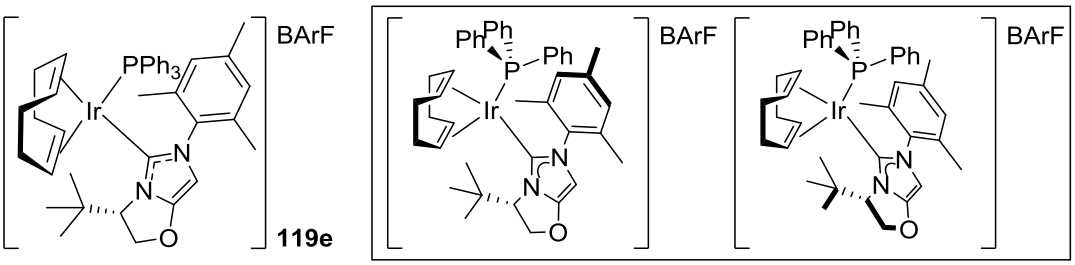

Yield = 556 mg, 65%.

Data

Appearance: red powder.

Melting Point (°C): >185 (dec).

I.R. (cm^{-1}): 3094, 3056, 2965, 2912.

^{1}H NMR (400 MHz, $CDCl_3$): δ 7.80 (8H, br s, Ar-H), 7.77-7.64 (2H, br s, Ar-H), 7.59 (4H, s, Ar-H), 7.56-7.24 (11H, br m, Ar-H), 7.17-6.90 (4H, m, Ar-H), 6.26 (0.2H, s, N-CH=C), 6.21 (0.8H, s, N-CH=C), 5.06-4.91 (0.4H, m, O-CH_2), 7.81-4.70 (0.2H, m, COD-CH), 4.56-4.51 (0.2H, m, N-CH), 4.45-4.35 (1.6H, m, COD-CH & N-CH), 4.26-4.15 (1H, m, COD-CH), 7.79-3.71 (0.2H, m, COD-CH), 3.71-3.62 (0.8H, m, COD-CH), 3.55-3.47 (0.8H, m, O-CH_2), 3.37-3.23 (1H, m, COD-CH), 3.03-2.91 (0.8H, m, O-CH_2), 2.39 (2.4H, s, Ar-CH_3), 2.36 (0.6H, s, Ar-CH_3), 2.27-2.16 (0.4H, m, COD-CH_2), 2.14 (2.4H, s, Ar-CH_3), 2.13-2.03 (3.2H, m, COD-CH_2 & Ar-CH_3), 2.01 (3H, br-s, Ar-CH_3), 2.00-1.85 (1H, m, COD-CH_2), 1.80-1.45 (4H, m, COD-CH_2), 1.24 (7.2H, s, C-$(CH_3)_3$), 1.17 (1.8H, s, C-$(CH_3)_3$).

^{13}C NMR (101 MHz, $CDCl_3$): δ 167.8 (d $^{2}J_{C-P}$ = 7.9 Hz), 162.4 (d $^{2}J_{C-P}$ = 9.1 Hz) 161.3. (q $^{2}J_{C-F}$ = 50.0 Hz), 153.4, 152.8, 140.2, 136.4, 136.2 (br), 135.7, 135.3, 135.1, 134.4, 134.0, 132.6 (br), 131.6 (br), 131.1 (br), 130.4 (br), 130.0, 129.3, 129.0, 128.50, 128.45 (q $^{1}J_{C-B}$ = 30.6 Hz), 128.2, 124.1 (q $^{1}J_{C-F}$ = 270.4 Hz), 117.0, 99.0, 97.2, 89.3, 89.2, 83.9, 79.7, 79.6, 79.4, 78.1, 78.0, 77.8, 77.4, 75.6, 75.5, 72.6, 68.4, 67.9, 34.9, 34.1, 33.7, 32.1, 31.14, 31.10, 30.8, 30.7, 30.5, 28.9, 28.4, 27.3, 26.7, 26.4, 20.4, 20.3, 19.7, 18.9, 18.2, 16.8.

^{31}P NMR (162 MHz, $CDCl_3$): δ 18.1 (PPh_3), 17.1 (PPh_3).

^{19}F NMR (376 MHz, $CDCl_3$): δ -62.4 (BArF).

^{11}B NMR (128 MHz, $CDCl_3$): δ -6.7 (BArF).

HRMS (NSI): m/z calculated for $C_{44}H_{51}IrN_2OP$ $[M\text{-}BArF]^+$: 847.3368; found: 847.3363.

MeCN Hydride Complex

^{1}H NMR (400 MHz, CD_3CN): -21.49 (1H, dd $^{2}J_{H\text{-}P}$ = 17.0 Hz, $^{2}J_{H\text{-}H}$ = 6.9 Hz, Ir-H), -21.54 (1H, dd $^{2}J_{H\text{-}P}$ = 17.0 Hz, $^{2}J_{H\text{-}H}$ = 6.9 Hz, Ir-H).

^{31}P NMR (162 MHz, CD_3CN): δ 17.5 (t $^{2}J_{P\text{-}H}$ = 17.0 Hz, PPh_3).

Scheme 1.45 *Asymmetric hydrogenation of terminal alkene **69d**.*

Reactions were carried out using general procedure A and analysed by ^{1}H NMR spectroscopy to calculate the reaction conversion, and HPLC for enantioselectivity. The results are tabulated in **Table E1.9**. Catalyst separation was carried out by filtration through a pipette of silica, eluting with Et_2O/petroleum ether (30/70).

Solvent	***Temperature (°C)***	***Time (h)***
DCM (4 mL)	25	2
	Substrate	
	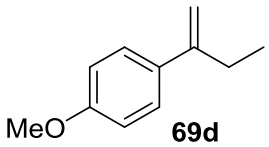 **69d** (65 mg, 0.4 mmol)	
Product	***Data***[114]	
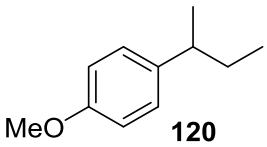 **120**	**I.R.** (cm^{-1}): 3062, 3036, 2998, 2844. **^{1}H NMR** (400 MHz, $CDCl_3$): δ 7.11 (2H, d *J* = 7.9 Hz, Ar-H), 6.81 (2H, d *J* = 7.9 Hz, Ar-H), 3.71 (3H, s, O-CH_3), 2.55 (1H, se *J* = 7.0 Hz, Ar-CH), 1.56 (2H, q *J* = 7.0 Hz, CH_2-CH_3), 1.21 (3H, d *J* = 7.0 Hz, CH_2-CH_3), 0.82 (3H, d *J* = 7.0 Hz, CH-CH_3).	
^{13}C NMR (101 MHz, $CDCl_3$): δ.158.0, 140.1, 128.3, 113.4, 55.1, 41.2, 31.6, 22.4, 12.6. **HPLC**: Column = OJ, hexane : isopropanol = 99 :1 , UV detection at λ = 256 nm, t_r = 11.00 (minor), t_r = 11.76 (major).		

Complex	***Conversion (%)***	***e.e. (%)***
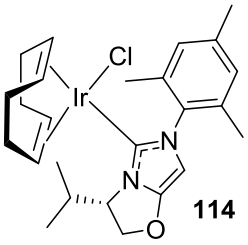 **114** (2.4 mg, 4.0 μmol)	<5	N/A
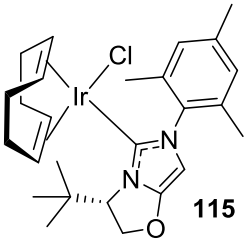 **115** (2.4 mg, 4.0 μmol)	<5	N/A

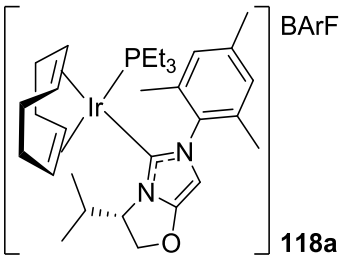 (6.2 mg, 4.0 μmol)	>99	37
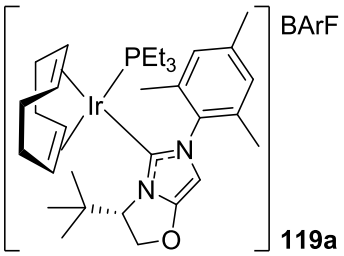 (6.2 mg, 4.0 μmol)	>99	-12
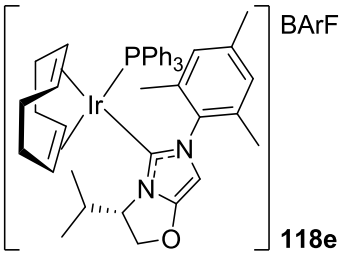 (6.8 mg, 4.0 μmol)	>99	36
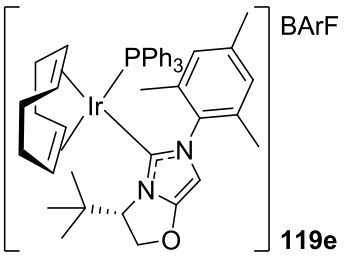 (6.8 mg, 4.0 μmol)	>99	-4
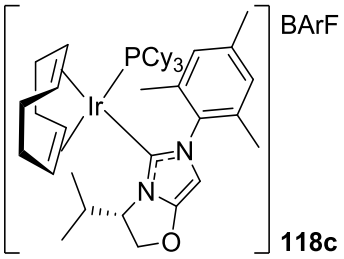 (6.8 mg, 4.0 μmol)	>99	51
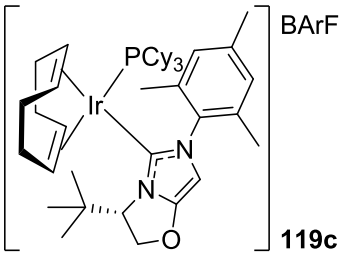 (6.8 mg, 4.0 μmol)	>99	2

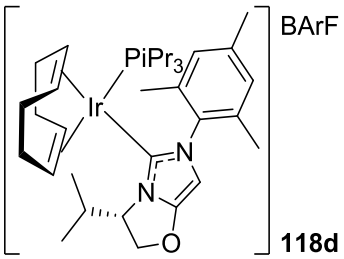 **118d** (6.4 mg, 4.0 μmol)	>99	13
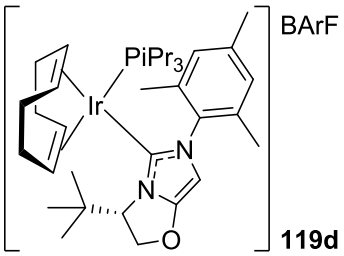 **119d** (6.4 mg, 4.0 μmol)	>99	8

Table E1.9

Scheme 1.46 *Probing the hydrogenation reaction of terminal alkenes to discount isomerisation.*

Reactions were carried out using general procedure A, except with deuterium in place of hydrogen. The reaction was analysed by ^{1}H NMR spectroscopy to calculate the reaction conversion, and HPLC for enantioselectivity. Catalyst separation was carried out by filtration through a pipette of silica, eluting with Et_2O/petroleum ether (30/70).

Solvent	***Temperature (°C)***	***Time (h)***
DCM (4 mL)	25	2

Substrate	***Complex***
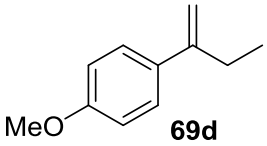 **69d** (65 mg, 0.4 mmol)	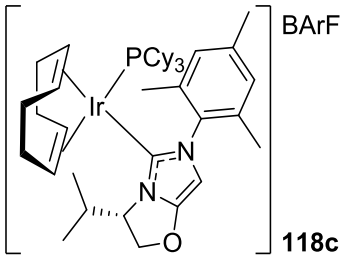 **118c** (6.8 mg, 4.0 μmol)

Product	***Data***[114]
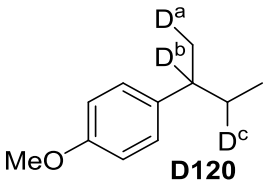 **D120** **Conversion** = >99%. **e.e.** = 55%.	**^{1}H NMR** (400 MHz, $CDCl_3$): δ 7.11 (2H, d *J* = 7.9 Hz, Ar-H), 6.81 (2H, d *J* = 7.9 Hz, Ar-H), 3.71 (3H, s, O-CH_3), 2.55 (1H, se *J* = 7.0 Hz, Ar-CH), 1.56 (2H, quin *J* = 7.0 Hz, CH_2-CH_3), 1.21 (3H, d *J* = 7.0 Hz, CH-CH_3), 0.82 (3H, t *J* = 7.0 Hz, CH_2-CH_3). Incorporation expected at δ D^a 1.21, D^b 2.55, D^c 1.56. Determined against integral at δ 3.71.

Incorporation (%)		
D^a	***D^b***	***D^c***
97	95	0

Scheme 1.47 *Asymmetric hydrogenation of enone **121**.*

Reactions were carried out using general procedure A and analysed by ^{1}H NMR spectroscopy to calculate the reaction conversion, and HPLC for enantioselectivity. The results of which are tabulated in **Table E1.10**. Catalyst separation was carried out by filtration through a pipette of silica, eluting with Et_2O/petroleum ether (30/70).

Solvent	***Temperature (°C)***	***Time (h)***
DCM (4 mL)	25	16
	Substrate	
	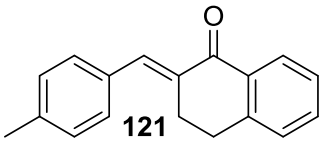 **121** (99 mg, 0.4 mmol)	
Product	***Data***[115]	
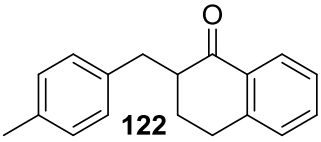 **122**	**Appearance**: White solid. **Melting point** (°C): 75-77. **IR** (cm^{-1}): 3062, 3036, 2998, 1682.	

^{1}H NMR (400 MHz, $CDCl_3$): δ 8.08 (1H, dd *J* = 7.8 Hz, ^{4}J = 1.5 Hz, Ar-H), 7.47 (1H, td *J* = 7.5 Hz, ^{4}J = 1.5 Hz, Ar-H), 7.32 (1H, t *J* = 7.5 Hz, Ar-H), 7.23 (1H, dd *J* = 7.8 Hz, ^{4}J = 1.5 Hz, Ar-H), 7.13 (4H, br-s, Ar-H), 3.46 (1H, dd *J* = 13.8 Hz, 4.0 Hz), 3.02-2.86 (2H, m), 2.79-2.69 (1H, m), 2.63 (1H, dd *J* = 13.7 Hz, 9.5 Hz), 2.34 (3H, s, Ar-CH_3), 2.13 (1H, dq *J* = 13.4 Hz, 4.5 Hz), 1.87-1.73 (1H, m).

^{13}C NMR (101 MHz, $CDCl_3$): δ.199.0, 143.6, 137.0, 135.2, 133.2, 132.0, 128.6, 128.5, 127.3, 126.4, 49.8, 35.4, 28.7, 27.9, 21.3.

HPLC: Column = OD-H, hexane : isopropanol = 99 :1 , UV detection at λ = 210 nm, t_r = 16.33 (major), t_r = 19.16 (minor).

Complex	***Conversion (%)***	***e.e. (%)***
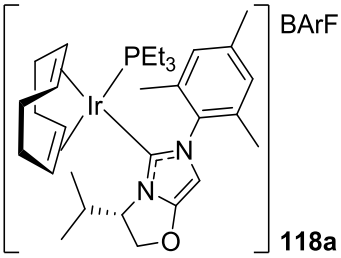 **118a** (6.2 mg, 4.0 μmol)	>99	-32

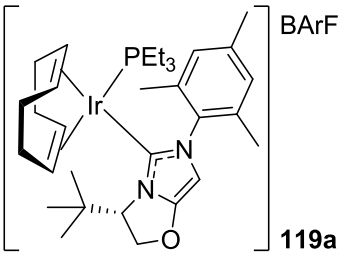 (6.2 mg, 4.0 μmol)	>99	-12
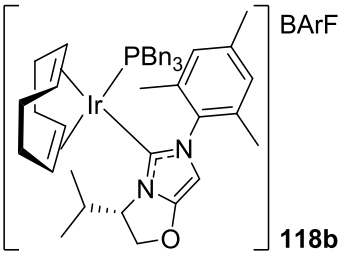 (6.8 mg, 4.0 μmol)	>99	22
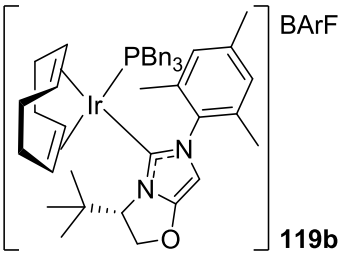 (6.8 mg, 4.0 μmol)	>99	74
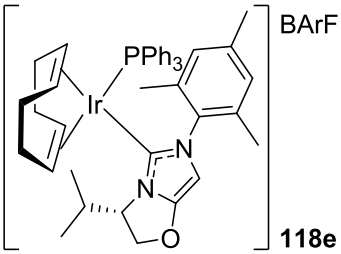 (6.8 mg, 4.0 μmol)	>99	44
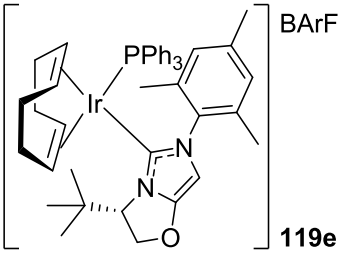 (6.8 mg, 4.0 μmol)	>99	68
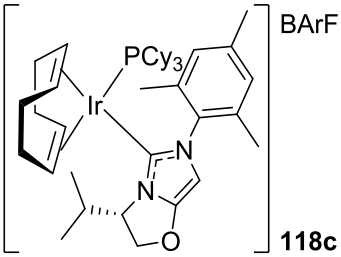 (6.8 mg, 4.0 μmol)	>99	75

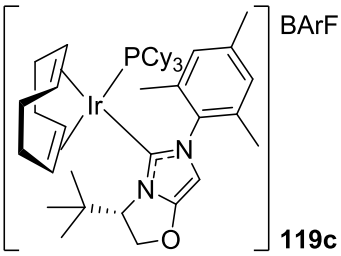 (6.8 mg, 4.0 μmol)	75	89
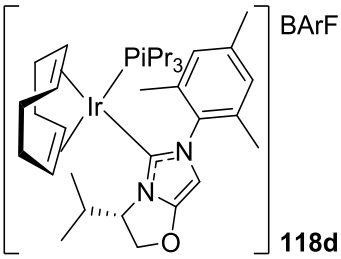 (6.4 mg, 4.0 μmol)	>99	76
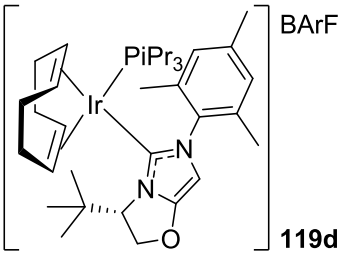 (6.4 mg, 4.0 μmol)	81	91

Table E1.10

Scheme 1.48 and **Graph 1.5** *Investigating the solvent effects in asymmetric hydrogentation.*

Reactions were carried out using general procedure A and analysed by ^{1}H NMR spectroscopy to calculate the reaction conversion, and HPLC for enantioselectivity. The results of which are tabulated in **Table E1.11**. Catalyst separation was carried out by filtration through a pipette of silica, eluting with Et_2O/petroleum ether (30/70).

Complex	***Solvent***	***Temperature (°C)***	***Time (h)***
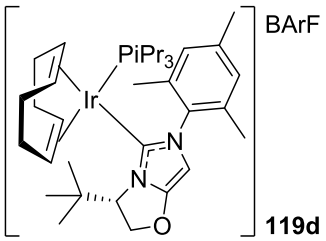 (6.4 mg, 4.0 μmol)	(4 mL)	25	16
	Substrate		
	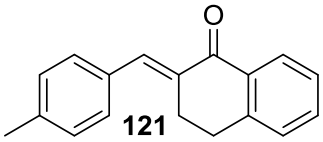 (99 mg, 0.4 mmol)		
Product	***Data***[115]		
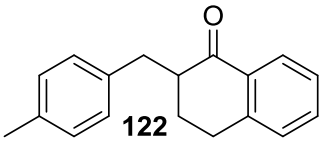	Data was consistent with that reported on page 181.		

Solvent	***Conversion (%)***	***e.e. (%)***
DCM	81	91
PhCl	96	86
MTBE	84	90
t-amylOH	66	87
i-ProAc	19	94
DMC	43	91

Table E1.11

Scheme 1.49 and **Graph 1.6** *Investigating the reaction time for asymmetric hydrogenation.*

Reactions were carried out using general procedure A and analysed by ^{1}H NMR spectroscopy to calculate the reaction conversion, and HPLC for enantioselectivity. The results of which are tabulated in **Table E1.12**. Catalyst separation was carried out by filtration through a pipette of silica, eluting with Et_2O/petroleum ether (30/70).

Complex	***Solvent***	***Temperature (°C)***
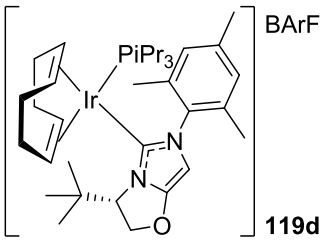 (6.4 mg, 4.0 μmol)	DCM (4 mL)	25
Substrate		
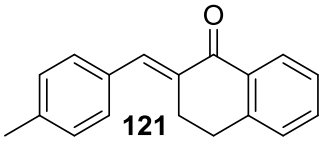 (99 mg, 0.4 mmol)		
Product	***Data***[115]	
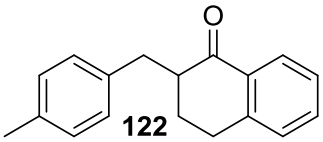	Data was consistent with that reported on page 181.	

Reaction time (min)	***Conversion (%)***	***e.e. (%)***
15	40	94
30	56	94
60	79	94
120	77	94
240	76	93
480	79	92
960	81	91

Table E1.12

Scheme 1.50 and **Graph 1.7** *Probing the impact of catalyst loading.*

Reactions were carried out using general procedure A and analysed by ^{1}H NMR spectroscopy to calculate the reaction conversion, and HPLC for enantioselectivity. The results of which are tabulated in **Table E1.13**. Catalyst separation was carried out by filtration through a pipette of silica, eluting with Et_2O/petroleum ether (30/70).

Complex	***Solvent***	***Temperature (°C)***	***Time (h)***
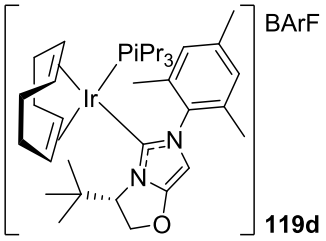 **119d**	DCM (4 mL)	25	16
Substrate			
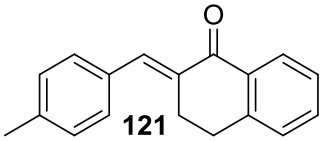 **121** (99 mg, 0.4 mmol)			
Product	***Data***[115]		
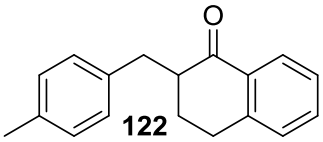 **122**	Data was consistent with that reported on page 181.		

Catalyst loading (mol%)	***Amount of 119d***	***Conversion (%)***	***e.e. (%)***
0.5	(3.2 mg, 2.0 μmol)	45	90
1.0	(6.4 mg, 4.0 μmol)	81	91
1.5	(9.6 mg, 6.0 μmol)	97	94
2.0	(12.8 mg, 8.0 μmol)	>99	94

Table E1.13

Scheme 1.51 and **Graph 1.8** *Investigating the reaction temperature dependence, and application of the Curtin-Hammett principle.*

Reactions were carried out using general procedure A and analysed by ^{1}H NMR spectroscopy to calculate the reaction conversion, and HPLC for enantioselectivity. The results of which are tabulated in **Table E1.14**. Catalyst separation was carried out by filtration through a pipette of silica, eluting with Et_2O/petroleum ether (30/70).

Complex	***Solvent***	***Time (h)***
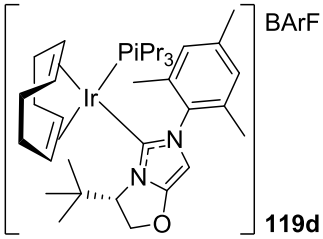 (12.8 mg, 8.0 μmol)	DCM (4 mL)	2
Substrate		
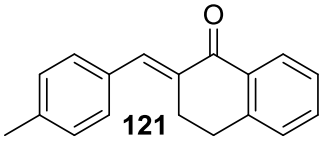 (99 mg, 0.4 mmol)		
Product	***Data***[115]	
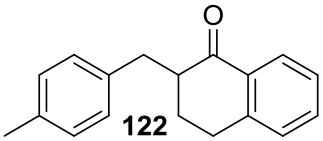	Data was consistent with that reported on page 181.	

Reaction Temperature (°C)	***Conversion (%)***	***e.e. (%)***	$\Delta\Delta G^{\ddagger}_{C\text{-}H}$ ***(kcalmol^{-1})***
25	>99	94	2.3
0	>99	96	2.1
-10	83	97	2.2
-20	36	98	2.3
-30	11	99	2.5

Table E1.14

Scheme 1.52 and Graph 1.9 *Investigating new substrates for asymmetric hydrogenation.*

Reactions were carried out using general procedure A and analysed by ^{1}H NMR spectroscopy to calculate the reaction conversion, and HPLC for enantioselectivity. Catalyst separation was carried out by filtration through a pipette of silica, eluting with Et_2O/petroleum ether (30/70).

Complex	***Solvent***	***Temperature (°C)***	***Time (h)***
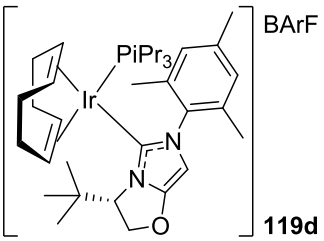 **119d** (3.2 mg, 2.0 μmol)	DCM (4 mL)	25	2

Substrate
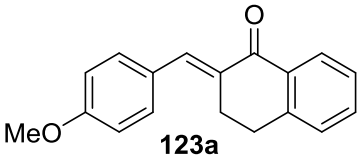 **123a** (26.4 mg, 0.1 mmol)

Product	***Data***[115]
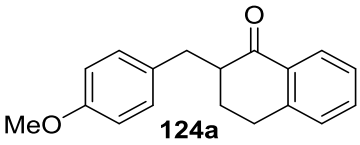 **124a**	**Appearance**: Clear oil. **IR** (cm^{-1}): 3051, 2930, 2875, 1682.

^{1}H NMR (400 MHz, $CDCl_3$): δ 8.10 (1H, dd *J* = 7.8 Hz, ^{4}J = 1.5 Hz, Ar-H), 7.48 (1H, td *J* = 7.5 Hz, ^{4}J = 1.5 Hz, Ar-H), 7.34 (1H, dd *J* = 7.8 Hz, 7.5 Hz, Ar-H), 7.24 (1H, d *J* = 7.5 Hz, Ar-H), 7.20-7.15 (2H, m, Ar-H), 6.91-6.84 (2H, m, Ar-H), 3.82 (3H, s, O-CH_3), 3.43 (1H, dd *J* = 13.6 Hz, 4.1 Hz), 3.04-2.89 (2H, m), 2.80-2.59 (2H, m), 2.14 (1H, dq *J* = 13.4 Hz, 4.5 Hz), 1.88-1.72 (1H, m).

^{13}C NMR (101 MHz, $CDCl_3$): δ 199.1, 157.8, 143.6, 133.0, 132.2, 131.7, 130.0, 128.5, 127.2, 126.4, 113.7, 55.3, 49.7, 34.1, 28.4, 27.6.

HPLC: Column = OD-H, hexane : isopropanol = 99 :1 , UV detection at λ = 210 nm, t_r = 31.28 (major), t_r = 33.88 (minor).

Conversion (%)	***e.e. (%)***	***Hammett σ***[116]
>99%	95.7%	-0.27

Substrate
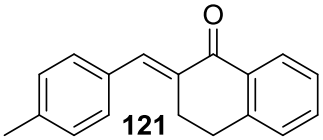 **121** (24.8 mg, 0.1 mmol)

Product	***Data***[115]
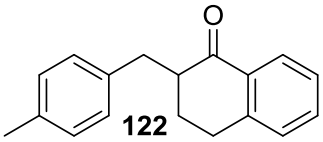 **122**	Data was consistent with that reported on page 181.

Conversion (%)	***e.e. (%)***	***Hammett σ***[116]
>99%	94.1%	-0.17

Substrate
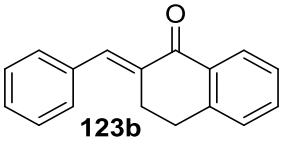 **123b** (23.4 mg, 0.1 mmol)

Product	***Data***[115]
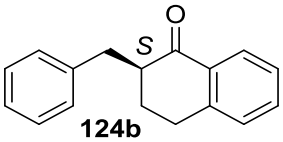 **124b**	**Appearance**: White solid. **Melting point** (°C): 51-53. **I.R.** (cm^{-1}): 3034, 2968, 1683.

^{1}H NMR (400 MHz, $CDCl_3$): δ 8.08 (1H, dd *J* = 8.0 Hz, ^4J = 1.7 Hz, Ar-H), 7.49 (1H, td *J* = 7.5 Hz, ^4J = 1.7 Hz, Ar-H), 7.35-7.30 (3H, m, Ar-H), 7.29-7.22 (4H, m, Ar-H), 3.53 (1H, dd *J* = 13.7 Hz, 4.0 Hz), 3.02-2.87 (2H, m), 2.85-2.72 (1H, m), 2.68 (1H, dd *J* = 13.7 Hz, 9.5 Hz), 2.14 (1H, dq *J* = 13.4 Hz, 4.5 Hz), 1.91-1.73 (1H, m).

^{13}C NMR (101 MHz, $CDCl_3$): δ 198.7, 143.5, 140.0, 133.0, 132.5, 128.7, 128.4, 128.2, 127.5, 126.2, 126.0, 48.9, 35.6, 28.9, 27.7.

HPLC: Column = OD-H, hexane : isopropanol = 99 :1 , UV detection at λ = 210 nm, t_r = 18.23 (major), t_r = 20.29 (minor).

$[\alpha]_D^{20}$: -21.3, (c 1.0, $CHCl_3$) [$[\alpha]_D^{20}$: +20.7, (c 1.0, $CHCl_3$) (*R*)-**124b** at 93% e.e.] [117]

Conversion (%)	***e.e. (%)***	***Hammett σ***[116]
>99%	93.4%	0

Substrate
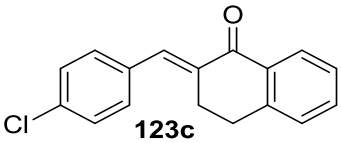 **123c**
(26.9 mg, 0.1 mmol)

Product	***Data***[115]
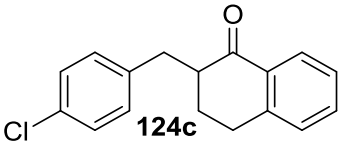 **124c**	**Appearance**: White solid. **Melting point** (°C): 85-87. **I.R.** (cm^{-1}): 3062, 2954, 1683.

^{1}H NMR (400 MHz, $CDCl_3$): δ 8.05 (1H, d *J* = 7.8 Hz, Ar-H), 7.46 (1H, td *J* = 7.5 Hz, ^{4}J = 1.4 Hz, Ar-H), 7.32 (1H, dd *J* = 7.8 Hz, 7.5 Hz, Ar-H), 7.22 (1H, d *J* = 7.5 Hz, Ar-H), 7.22-7.15 (2H, m, Ar-H), 6.99-6.88 (2H, m, Ar-H), 3.43 (1H, dd *J* = 13.6 Hz, 3.8 Hz), 3.04-2.89 (2H, m), 2.80-2.59 (2H, m), 2.14 (1H, dq *J* = 13.4 Hz, 4.0 Hz), 1.80-1.72 (1H, m).

^{13}C NMR (101 MHz, $CDCl_3$): δ 198.4, 144.0, 138.6, 133.4, 132.1, 131.8, 130.0, 129.0, 128.5, 127.4, 126.5, 49.5, 35.3, 29.0, 28.0.

HPLC: Column = OD-H, hexane : isopropanol = 99 :1 , UV detection at λ = 210 nm, t_r = 23.29 (major), t_r = 25.45 (minor).

Conversion (%)	***e.e. (%)***	***Hammett σ***[116]
>99%	92.0%	0.23

Substrate
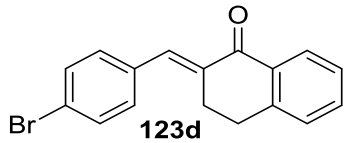 **123d**
(31.3 mg, 0.1 mmol)

Product	***Data***[118]
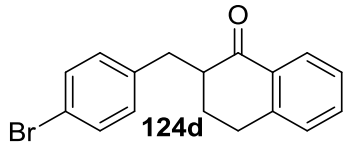 **124d**	**Appearance**: White solid. **Melting point** (°C): 78-80. **I.R.** (cm^{-1}): 3052, 2977, 1686.

^{1}H NMR (400 MHz, $CDCl_3$): δ 8.09-8.03 (1H, m, Ar-H), 7.51-7.39 (3H, m, Ar-H), 7.36-7.28 (1H, m, Ar-H), 7.25-7.19 (1H, m, Ar-H), 7.15-7.08 (2H, m, Ar-H), 3.47-3.34 (2H, m), 3.00-2.89 (1H, m), 2.77-2.60 (2H, m), 2.14-2.04 (1H, m), 1.86-1.71 (1H, m).

^{13}C NMR (101 MHz, $CDCl_3$): δ 198.9, 144.2, 139.4, 133.7, 132.6, 131.2, 131.0, 128.9, 127.9, 126.9, 120.3, 49.5, 35.3, 28.9, 28.0.

HPLC: Column = OD-H, hexane : isopropanol = 99 :1 , UV detection at λ = 210 nm, t_r = 25.39 (major), t_r = 27.71 (minor).

Conversion (%)	***e.e. (%)***	***Hammett σ***[116]
>99%	92.0%	0.23

Substrate
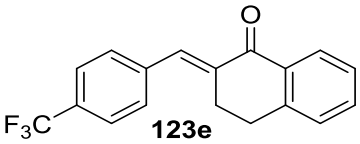 **123e** (30.2 mg, 0.1 mmol)

Product	***Data***[119]
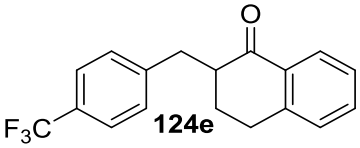 **124e**	**Appearance**: White solid. **Melting point** (°C): 56-58. **I.R.** (cm^{-1}): 3058, 2967, 1689.

^{1}H NMR (400 MHz, $CDCl_3$): δ 8.12-8.06 (1H, m, Ar-H), 7.64-7.53 (2H, m, Ar-H), 7.52-7.42 (1H, m, Ar-H), 7.41-7.30 (3H, m, Ar-H), 7.28-7.22 (1H, m, Ar-H), 3.61-3.50 (1H, m), 2.99 (1H, dd *J* = 8.0 Hz, 4.0 Hz), 2.87-2.70 (2H, m), 2.20-2.10 (2H, m), 1.95-1.76 (1H, m).

^{13}C NMR (101 MHz, $CDCl_3$): δ 198.2, 144.0, 143.9, 133.2, 132.3, 129.7, 128.9, 128.5 (br), 127.6, 126.0, 125.4 (q, $^{1}J_{C\text{-}F}$ = 268.9 Hz) 122.9, 49.3, 35.6, 29.0, 28.3.

HPLC: Column = OD-H, hexane : isopropanol = 99 :1 , UV detection at λ = 210 nm, t_r = 23.33 (major), t_r = 26.23 (minor).

Conversion (%)	***e.e. (%)***	***Hammett σ***[116]
>99%	90.0%	0.54

Substrate
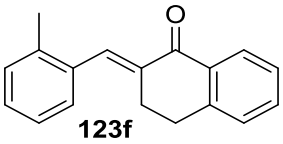 **123f** (24.8 mg, 0.1 mmol)

Product	***Data***
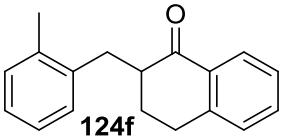 **124f**	**Product not isolated**

Conversion (%)	***e.e. (%)***
12%	N/a%

Substrate
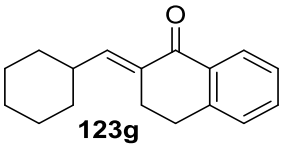 **123g**
(24.0 mg, 0.1 mmol)

Product	***Data***
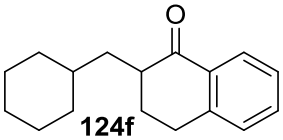 **124f**	**Product not isolated**

Conversion (%)	***e.e. (%)***
14%	N/a%

7. References

[1] P. N. Rylander, *Hydrogenation Methods*, Academic Press, **1985**.
[2] P. N. Rylander, *Catalytic Hydrogenation in Organic Syntheses*, Academic Press, **1979**.
[3] I. Horiuti, M. Polanyi, *Trans. Faraday Society*, **1934**, *30*, 1164.
[4] R. H. Crabtree, *The Organometallic Chemistry of the Transition Metals*. 4th edition, John Wiley & Sons, Inc, **2005**.
[5] J. G. de Vries, C. J. Elsevier, *Handbook of Homogeneous Hydrogenation*, Wiley-VCH, **2007**.
[6] M. Calvin, *J. Am. Chem. Soc.*, **1939**, *61*, 2230.
[7] M. Calvin, M. Polanyi, *Trans. Faraday Society*, **1938**, *34*, 1181.
[8] S. S. Bath, L. Vaska, *J. Am. Chem. Soc.*, **1963**, *85*, 3500.
[9] C. O'Connor, G. Yagupsky, D. Evans, G. Wilkinson, *Chem. Commun.*, **1968**, 420.
[10] J. F. Young, J. A. Osborn, F. H. Jardine, G. Wilkinson, *Chem. Commun.*, **1965**, 131.
[11] A. Jourdant, E. González-Zamora, J. Zhu, *J. Org. Chem.*, **2002**, *67*, 3163.
[12] F. H. Jardine, *Prog. Inorg. Chem.*, **1981**, 63.
[13] F. H. Jardine, G. Wilkinson, *J. Chem. Soc. C: Org.*, **1967**, 270.
[14] F. H. Jardine, J. A. Osborn, G. Wilkinson, *J. Chem. Soc. A: Inorg. Phys. Theo.*, **1967**, 1574.
[15] J. Halpern, *Inorg. Chim. Acta*, **1981**, *50*, 11.
[16] R. R. Schrock, J. A. Osborn, *J. Chem. Soc. D: Chem. Commun.*, **1970**, 567.
[17] R. R. Schrock, J. A. Osborn, *J. Am. Chem. Soc.*, **1976**, *98*, 2134.
[18] L. Vaska, R. E. Rhodes, *J. Am. Chem. Soc.*, **1965**, *87*, 4970.
[19] J. R. Shapley, R. R. Schrock, J. A. Osborn, *J. Am. Chem. Soc.*, **1969**, *91*, 2816.
[20] J. A. Osborn, R. R. Schrock, *J. Am. Chem. Soc.*, **1971**, *93*, 3089.
[21] R. H. Crabtree, H. Felkin, G. E. Morris, *J. Organomet. Chem.*, **1977**, *141*, 205.
[22] R. H. Crabtree, G. E. Morris, *J. Organomet. Chem.*, **1977**, *135*, 395.
[23] R. H. Crabtree, *Acc. Chem. Res.*, **1979**, *12*, 331.
[24] J. W. Suggs, S. D. Cox, R. H. Crabtree, J. M. Quirk, *Tetrahedron Lett.*, **1981**, *22*, 303.
[25] R. H. Crabtree, M. W. Davis, *Organometallics*, **1983**, *2*, 681.
[26] G. Stork, D. E. Kahne, *J. Am. Chem. Soc.*, **1983**, *105*, 1072.
[27] S.L. Regen, *J. Org. Chem.*, **1974**, *39*, 260.
[28] H.M. Lee, T. Jiang, E.D. Stevens, S.P. Nolan, *Organometallics*, **2001**, *20*, 1255.
[29] L. D. Vazquez-Serrano, B. T. Owens, J. M. Buriak, *Chem. Commun.*, **2002**, 2518.
[30] D. Drago, P. S. Pregosin, A. Pfaltz, *Chem. Commun.*, **2002**, 286.
[31] K. Harada, *Asymmetric Synthesis*, Academic Press, Orlando, USA, **1985**.
[32] E. Klabunovskii, G. V. Smith, A. Zsigmong, *Heterogeneous Enantioselective Hydrogenation: Theory and Practice*, Springer, **2006**.
[33] W. S. Knowles, *Angew. Chem. Int. Ed.* **2002**, *41*, 1998.
[34] R. Noyori, *Angew. Chem. Int. Ed.* **2002**, *41*, 2008.
[35] K. B. Sharpless, *Angew. Chem. Int. Ed.* **2002**, *41*, 2024.
[36] F. Lagasse, H. B. Kagan, *Chem. Pharm. Bull.* **2000**, *48*, 315.
[37] T. P. Dang, H. B. Kagan, *J. Chem. Soc. D* **1971**, 481.
[38] B. D. Vineyard, W. S. Knowles, M. J. Sabacky, G. L. Bachman, D. J. Weinkauff, *J. Am. Chem. Soc.* **1977**, *99*, 5946.
[39] W. S. Knowles, *Acc. Chem. Res.* **1983**, *16*, 106.
[40] W. S. Knowles, *J. Chem. Educ.* **1986**, *63*, 222.
[41] W. Tang, X. Zhang, *Chem. Rev.* **2003**, *103*, 3029.
[42] M. J. Burk, *J. Am. Chem. Soc.* **1991**, *113*, 8518.
[43] A. Togni, C. Breutel, A. Schnyder, F. Spindler, H. Landert, A. Tijani, *J. Am. Chem. Soc.* **1994**, *116*, 4062.
[44] X. Cui, K. Burgess, *Chem. Rev.* **2005**, *105*, 3272.
[45] S. J. Roseblade, A. Pfaltz, *Acc. Chem. Res.* **2007**, *40*, 1402.
[46] D. H. Woodmansee, A. Pfaltz, *Chem. Commun.* **2011**, *47*, 7912.
[47] J. J. Verendel, O. Pamies, M. Dieguez, P. G. Andersson, *Chem. Rev.* **2014**, *114*, 2130.
[48] A. Lightfoot, P. Schnider, A. Pfaltz, *Angew. Chem. Int. Ed.* **1998**, *37*, 2897.
[49] X. Cui, K. Burgess, *Chem. Rev.* **2005**, *105*, 3272.
[50] K. Kallstrom, I. Munslow, P. G. Andersson, *Chem. Eur. J.* **2006**, *12*, 3194.
[51] J. J. Verendel, O. Pamies, M. Dieguez, P. G. Andersson, *Chem. Rev.* **2014**, *114*, 2130.
[52] T. Bunlaksananusorn, K. Polborn, P. Knochel, *Angew. Chem. Int. Ed.* **2003**, *42*, 3941.

[53] P. Kaukoranta, M. Engman, C. Hedberg, J. Bergquist, P. G. Andersson, *Adv. Synth. Catal.* **2008**, *350*, 1168.
[54] P. Cheruku, A. Paptchikine, M. Ali, J.-M. Neudorfl, P. G. Andersson, *Org. Biomol. Chem.* **2008**, *6*, 366.
[55] I. Ilaldinov, D. Fatkulina, S. Bucharov, R. Jackstell, A. Spannenberg, M. Beller, R. Kadyrov, *Tetrahedron: Asymm.* **2011**, *22*, 1936.
[56] S. Nanchen, A. Pfaltz, *Chem. Eur. J.* **2006**, *12*, 4550.
[57] S. Nanchen, A. Pfaltz, *Helv. Chim. Acta* **2006**, *89*, 1559.
[58] M. G. Schrems, A. Pfaltz, *Chem. Commun.* **2009**, 6210.
[59] S. McIntyre, E. Hormann, F. Menges, S. P. Schmidt, A. Pfaltz, *Adv. Synth. Catal.* **2005**, *347*, 282.
[60] K. H. Hopmann, A. Bayer, *Organometallics* **2011**, *30*, 2483.
[61] P. Craig, *App. Organomet. Chem.*, **2010**, *24*, 667.
[62] C. A. Tolman, *J. Am. Chem. Soc.*, **1970**, *92*, 2953.
[63] C. A. Tolman, *J. Am. Chem. Soc.*, **1970**, *92*, 2956.
[64] R. A. Kelly Iii, H. Clavier, S. Giudice, N. M. Scott, E. D. Stevens, J. Bordner, I. Samardjiev, C. D. Hoff, L. Cavallo, S. P. Nolan, *Organometallics*, **2007**, *27*, 202.
[65] D. J. Nelson, S. P. Nolan, *Chem. Soc. Rev.*, **2013**, *42*, 6723.
[66] C. Boehme, G. Frenking, *Organometallics*, **1998**, *17*, 5801.
[67] X. Hu, I. Castro-Rodriguez, K. Olsen, K. Meyer, *Organometallics*, **2004**, *23*, 755.
[68] A. J. Arduengo, R. L. Harlow, M. Kline, *J. Am. Chem. Soc.*, **1991**, *113*, 361.
[69] A. Poater, B. Cosenza, A. Correa, S. Giudice, F. Ragone, V. Scarano, L. Cavallo, *Eur. J. Inorg. Chem.*, **2009**, *2009*, 1759.
[70] H. Clavier, S. P. Nolan, *Chem. Commun.*, **2010**, *46*, 841.
[71] J. A. Brown, S. Irvine, A. R. Kennedy, W. J. Kerr, S. Andersson, G. N. Nilsson, *Chem. Commun.* **2008**, 1115.
[72] L. S. Bennie, C. J. Fraser, S. Irvine, W. J. Kerr, S. Andersson, G. N. Nilsson, *Chem. Commun.*, **2011**, *47*, 11653.
[73] A. R. Kennedy, W. J. Kerr, R. Moir, M. Reid, *Org. Biomol. Chem.* **2014**, *12*, 7927.
[74] J. A. Brown, A. R. Cochrane, S. Irvine, W. J. Kerr, B. Mondal, J. A. Parkinson, L. C. Paterson, M. Reid, T. Tuttle, S. Andersson, G. N. Nilsson, *Adv. Synth. Catal.* **2014**, *356*, 3551.
[75] D. M. Flanigan, F. Romanov-Michailidis, N. A. White, T. Rovis, *Chem. Rev.* **2015**, *115*, 9307.
[76] V. Cesar, S. Bellemin-Laponnaz, L. H. Gade, *Chem. Soc. Rev.* **2004**, *33*, 619.
[77] F. Wang, L.-J. Liu, W. Wang, S. Li, M. Shi, *Coord. Chem. Rev.* **2012**, *256*, 804.
[78] A. R. Chianese, X. Li, M. C. Janzen, J. W. Faller, and R. H. Crabtree, *Organometallics*, **2003**, *22*, 1663.
[79] G. E. Dobereiner, A. Nova, N. D. Schley, N. Hazari, S. J. Miller, O. Eisenstein, R. H. Crabtree, *J. Am. Chem. Soc.* **2011**, *133*, 7547.
[80] M. Reid, *PhD Thesis*, University of Strathclyde, **2015**.
[81] R. H. Crabtree, *Chem. Rev.* **2015**, *115*, 127-150.
[82] W. J. Kerr, R. J. Mudd, L. C. Paterson, J. A. Brown, *Chem Eur J.* **2014**, *20*, 14604.
[83] J. Devlin, W. J. Kerr, D. M. Lindsay, T. J. D. McCabe, M. Reid, T. Tuttle, *Molecules* **2015**, *20*, 11676.
[84] J. L. Tucker, *Org. Proc. Res. Dev.* **2006**, *10*, 315.
[85] D. J. C. Constable, C. Jimenez-Gonzalez, R. K. Henderson, *Org. Proc. Res. Dev.* **2007**, *11*, 1623.
[86] B. Wustenberg, A. Pfaltz, *Adv. Synth. Catal.* **2008**, *350*, 174.
[87] J. A. Brown, A. R. Cochrane, S. Irvine, W. J. Kerr, B. Mondal, J. A. Parkinson, L. C. Paterson, M. Reid, T. Tuttle, S. Andersson, G. N. Nilsson, *Adv. Synth. Catal.* **2014**, *356*, 3551.
[88] J. A. Dean, *Lange's Handbook of Chemistry*, 15th edition, McCraw-Hill, **1998**.
[89] D. Baskakov, W. A. Herrmann, E. Herdtweck, S. D. Hoffmann, *Organometallics* **2007**, *26*, 626.
[90] A. R. Cochrane, S. Irvine, W. J. Kerr, M. Reid, S. Andersson, G. N. Nilsson, *J. Labelled Compd. Radiopharm.* **2013**, *56*, 451.
[91] F. Glorius, G. Altenhoff, R. Goddard, C. Lehmann, *Chem. Commun.* **2002**, 2704.
[92] A. Poater, L. Falivene, C. A. Urbina-Blanco, S. Manzini, S. P. Nolan, L. Cavallo, *Procedia Comput. Sci.* **2013**, *18*, 845.
[93] J. Seayad, P. K. Patra, Y. Zhang, J. Y. Ying, *Org. Lett.* **2008**, *10*, 953.
[94] W. L. F. Armarego, C. L. L. Chai, *Purification of Laboratory Chemicals*, 7th edition, Butterwoth-Heinemann, **2013**.
[95] M. Gerst, J. Morgenthaler, C. Rüchardt, *Chem. Ber.*, **1994**, *127*, 691.
[96] J. D. St. Denis, C. C. G. Scully, C. F. Lee, A. K. Yudin, *Org. Lett.*, **2014**, *16*, 1338.
[97] I. Peňafiel, I. M. Pastor, M. Yus, M. A. Esteruelas, M. Oliván, *Organometallics* **2012**, *31*, 6154.

[98] J.-Y. Shang, F. Li, X.-F. Bai, J.-X. Jiang, K.-F. Yang, G.-Q. Lai, L.-W. Xu, *Eur. J. Org. Chem.* **2012**, 2809.
[99] M. Chen, J. Wang, Z. Chai, C. You, A. Lei, *Adv. Synth. Catal.* **2012**, *354*, 341.
[100] . Yi, J. T. Miller, D. Y. Zemlyanov, R. Zhang, P. J. Dietrich, F. H. Ribeiro, S. Suslow, M. M. Abu-Omar, *Angew. Chem. Int. Ed.* **2014**, *53*, 833.
[101] R. Mello, J. Martínez-Ferrer, A. Alcalde-Aragonés, T. Varea, R. Acrete, M. E. González-Núňez, G. Asenio, *J. Org. Chem.* **2011**, *76*, 10129.
[102] Q. Xu, J. Chen, H. Tian, X. Yuan, S. Li, C. Zhou, J. Liu, *Angew. Chem. Int. Ed.* **2014**, *53*, 225.
[103] Y.-F. Wang, Y.-R. Gao, S. Mao, Y.-L. Zhang, D.-D. Guo, Z.-L. Yan, S.-H. Guo, Y.-Q. Wang, *Org. Lett.* **2014**, *16*, 1610.
[104] L. R. Jeffries and Silas Cook, *Tetrahedron* **2014**, *70*, 4204.
[105] M. Verdecchia, M. Feroci, L. Palombi, L. Rossi, *J. Org. Chem.* **2002**, *67*, 8287.
[106] S. Morrissey, I. Beadham, N. Gatherwood, *Green Chem.* **2009**, *11*, 466.
[107] M. Szostak, M. Spain, A. J. Eberhart and D. J. Procter, *J. Am. Chem. Soc.* **2014**, *136*, 2268.
[108] L. Greb, C.-G. Daniliuc, K. Bergander and J. Paradies, *Angew. Chem. Int. Ed.* **2013**, *52*, 5876.
[109] S. Ushijima, K. Moriyama, H. Togo, *Tetrahedron* **2012**, *68*, 4701.
[110] R.-I. Nagamatsu, S. Mitsuhashi, K. Shigetomi, M. Ubukata, *Biosci. Biotechnol. Biochem.* **2012**, *76*, 1904.
[111] C. D. Campbell, C. Concelion, A. D. Smith, *Tetrahedron: Asymm.* **2011**, *22*, 797.
[112] C. A. M. Cariou, B. M. Kariuki, J. S. Snaith, *Org. Biomol. Chem.* **2008**, *6*, 3337.
[113] Activated MnO_2 was prepared fresh following the procedure found in: *Encyclopedia of Reagents for Organic Synthesis*, 2nd edition, Wiley-VCH, **2009**.
[114] L. Li, S. Zhao, A. Joshi-Pangu, M. Diane, M. R. Biscoe, *J. Am. Chem. Soc.* **2014**, *136*, 14027.
[115] T. Ishimura, N. Shibata, T. Horikawa, N. Yasuda, S. Nakamura, T. Toru, M. Shiro, *Angew. Chem. Int. Ed.* **2008**, *47*, 4157.
[116] C. Hansch, A. Leo, *Substituent Constants for Correlation Analysis in Chemistry and Biology*, Wiley-Interscience, **1979**.
[117] X. Liu, Z. Han, Z. Wang, K. Ding, *Angew. Chem. Int. Ed.* **2014**, *53*, 1978.
[118] C. Schlepphorst, B. Maji, F. Glorius, *ACS Catal.* **2016**, *6*, 4184.
[119] B. Teng, W. Chen, S. Dong, C. W. Kee, D. A. Gandamana, L. Zong, C.-H. Tan, *J. Am. Chem. Soc.* **2016**, *138*, 9935.

Chapter 2. Hydrogen Isotope Exchange: Investigating Selectivity

1. Introduction

Within the UK, the pharmaceutical industry accounts for 20% of the total R&D spending,[1] which is clearly indicative of the constant development of new medical compounds and treatment methods. Within this R&D spending, approximately 60% of all novel molecular entities fail in pre-clinical trials, as such, a fresh initiative was developed to assess potentially interesting molecules at an earlier stage in development.[2] A key aspect of this initiative was the application of absorption, distribution, metabolism, excretion, and toxicology (ADMET) studies at an earlier stage where it can have maximum impact on later stage success.[3]

Within ADMET studies, radiolabelled compounds are extensively applied, and remain as the 'gold standard' with no other technique ensuring the detection and quantification of all drug-related signals in a complex system.[4] Having said this, recent developments in analytical techniques allow for the detection of even trace quantities of heavy isotope labelled compounds without the inconvenience of handling radioactive materials.[5] As such, it is expected that labelled compounds, containing both radioactive and heavy isotopes, will continue to play a significant role in drug discovery and development, maintaining the demand for new methods for the production of such labelled compounds.

Secondary to the pharmaceutical industry, are research chemistry laboratories which investigate chemical reaction mechanisms.[6] In such laboratories, a labelled compound can be used to trace the fate of a substrate through a proposed mechanism, or to deliver key insight into reaction kinetics.

This demand for labelled compunds has led to an increase in the development of efficient and facile methods to incorporate various isotopes into molecules. The most commonly used isotopes are carbon-13 (^{13}C) and -14 (^{14}C) and the hydrogen isotopes deuterium (^{2}H) and tritium (^{3}H).

1.1. Carbon Labelling (^{13}C & ^{14}C)

The use of carbon isotope-labelled drug molecules for testing results in several drawbacks. Primarily, the label is introduced at an early stage in the synthesis. Nevertheless, carbon labelled compounds are often synthesised and applied in drug

development. One example of ^{13}C incorporation is the synthesis of [$^{13}C_6$]primaquine **2**, a drug used to combat relapsing malaria caused by *Plasmodium vivax*. The synthesis is successfully completed from [$^{13}C_6$]anisole **1**, in seven steps (**Scheme 2.1**).[7]

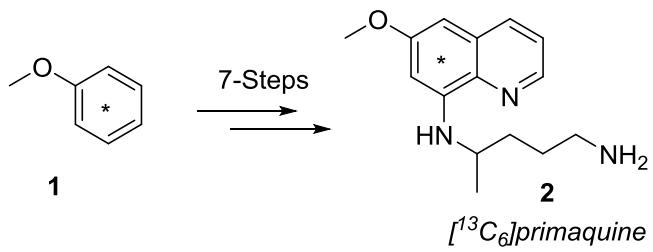

Scheme 2.1 ^{13}C labelling of *Primaquine*.

This requirement can often lead to the redesign of the synthetic route to accommodate a commercially available source of labelled starting material. This is especially troublesome in complex molecules such as natural products, which may require many steps to synthesise and a great deal of time to optimise the synthetic route.

Similarly, the incorporation of the radioactive isotope ^{14}C is introduced during synthesis. However, due to the low commercial availability of ^{14}C labelled compounds, this is often achieved by use of $^{14}CO_2$, generated from $Ba^{14}CO_3$ and concentrated sulfuric acid, ^{14}C-methyl iodide or ^{14}C-metal cyanide. In the production of [^{14}C] AZD4694 **5**, for use in positron emission tomography studies towards the treatment of Alzheimer's disease, $^{14}CO_2$ was used to introduce the radiolabel. In this 14-step synthesis, the radiolabel was introduced in the second step, requiring the handling and disposal of radioactive material for the further 12 steps (**Scheme 2.2**).[8]

Additionally, the specific radioactivity of ^{14}C is often too low to allow studies at relevant doses with highly potent drugs. In cases such as this, the application of a different radioisotope is required; this is most commonly an isotope of hydrogen.

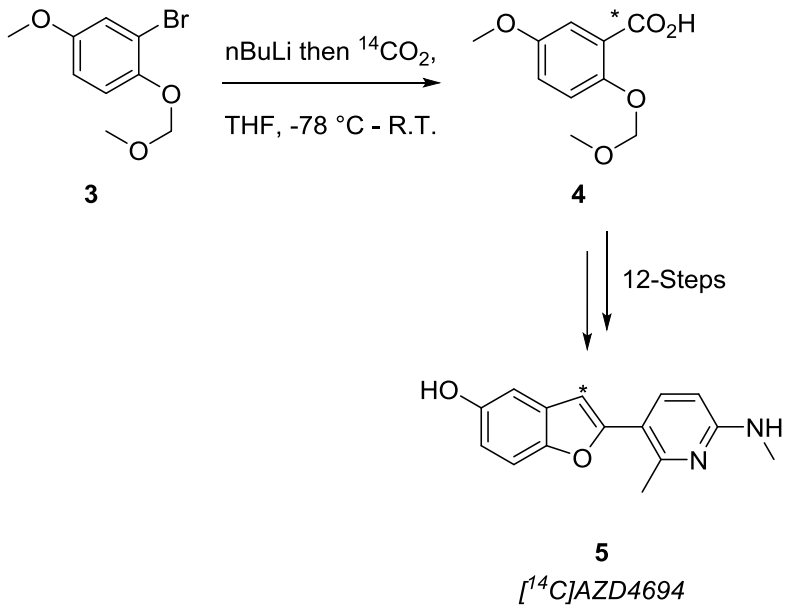

Scheme 2.2 ^{14}C labelling with by carboxylation.

1.2. Hydrogen Labelling (^{2}H & ^{3}H)

Deuterium- and tritium-labelling can be achieved by application of a variety of methods; the choice of method is dependent upon a number of factors, including regio- and chemo-selectivity, and the stability of the labelled compound to the reaction conditions. A key area of hydrogen labelling utilises a reagent/substrate containing a heavy hydrogen isotope. An example of this is *ortho*-lithiation followed by addition of an electrophilic source of the isotope.[9] An example from Beak and Brown illustrates the incorporation of deuterium into the benzamide-derived aromatic **6** leading to the lithiated intermediate **7**, which is quenched by addition of a deuterated alcohol to give deuterium labelled benzamide **8** (**Scheme 2.3**). However, this method uses strongly basic reaction conditions that may not be suitable with more complex molecules.

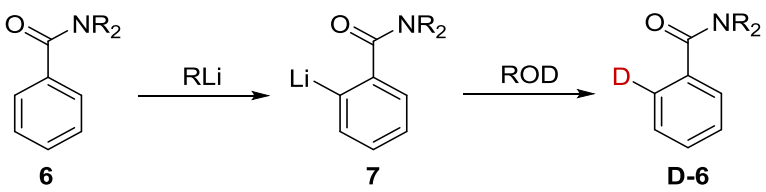

Scheme 2.3 ^{2}H labelling by deprotonation and D-quench.

Another approach used to incorporate a hydrogen isotopic label is to use a deuterated or tritiated reducing agent. A variety of methods have been applied, the most common

of which is a metal-mediated reduction of a carbon-halogen bond. A recent example takes tribrominated precursor **8** to the tritiated drug molecule [$^3H_3$](*R*,*R*)-4-methoxyfenoterol **9** using a heterogeneous palladium catalyst to facilitate the reduction (**Scheme 2.4**).[10] This method has the obvious drawback of requiring a halogen be incorporated into the molecule at some point during the synthesis, which may not always be possible and may necessitate a redesign of the molecule's synthesis.

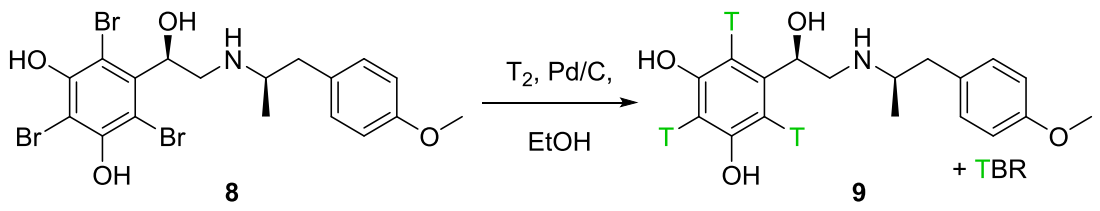

Scheme 2.4 ^{3}H labelling by dehalogenation.

Alternatively, a step already embedded in the synthesis may require the reduction of a functional group e.g. an aldehyde, alkene or ketone. An excellent example of this is the enatioselective reduction of enone **10** in the presence of a chiral ruthenium-based Noyori catalyst, using [^{3}H]formic acid as the isotope donor, leading to the tritium labelled EP4 agonist [^{3}H]**11** (**Scheme 2.5**).[11] A variety of non-transition metal based reduction methods are also available using deuterated and tritiated analogues of $NaBH_4$.[12] However, these methods all require a viable functional group for reduction.

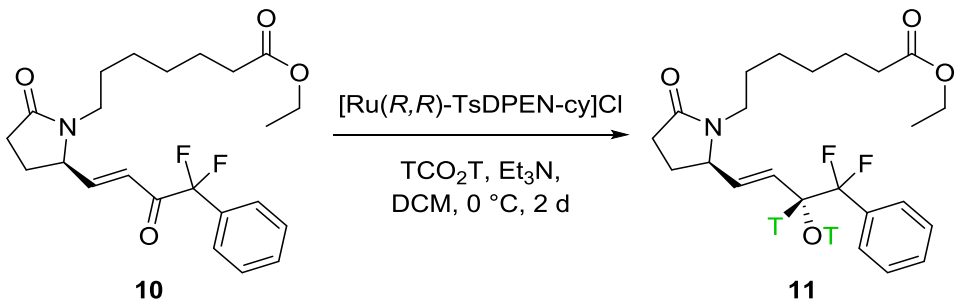

Scheme 2.5 ^{3}H labelling by asymmetric carbonyl hydrogenation.

Another method to install a hydrogen isotope is to perform direct exchange of the more abundant ^{1}H atom within a molecule for its heavy or radioactive counterpart (^{2}H-deuterium or ^{3}H-tritium), a process commonly used on fully functionalised drug molecules. The challenge is to install the hydrogen isotope only at the required position with sufficient levels of incorporation to allow utility in subsequent ADMET studies.

Two approaches are commonly used, the first of which is heterogeneous transition metal-catalysed hydrogen isotope exchange.

1.3. Heterogeneous Hydrogen Isotope Exchange

Most heterogeneous methods of isotope exchange apply widely available platinum or palladium catalysts. The benefit of simple removal of heterogeneous catalysts by filtration is countered by the high catalyst loading, temperature, and pressure that is often required for their use. Having said this, examples do exist in which such catalysts have been used to give high incorporations with some measure of regioselectivity.[13] One such example by Faigl *et al.* shows the selective deuteration of piperidine derivative **12**, where exchange proceeds exclusively at the benzylic position with high levels of incorporation (**Scheme 2.6**).[14]

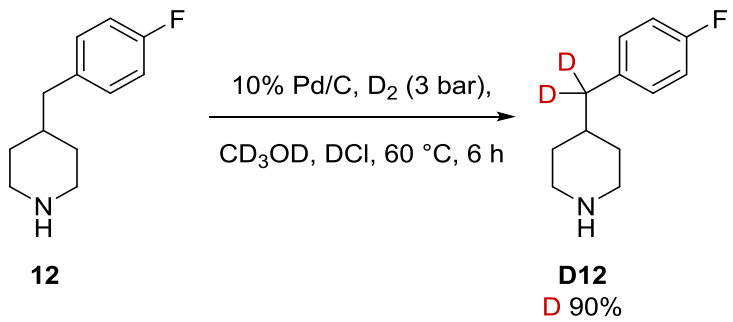

Scheme 2.6 ^{2}H labelling of benzyllic positions.

Aromatic labelling is also possible with heterogeneous catalysts as described by Sajiki *et al.*[15] However, extreme conditions are required to label efficiently on aromatic structures bearing electron withdrawing groups. This shown in the deuteration of diacid **13**, in which a temperature of 180 °C and a prolonged reaction time of 24 h is required to obtain appreciable levels of incorporation (**Scheme 2.7**).

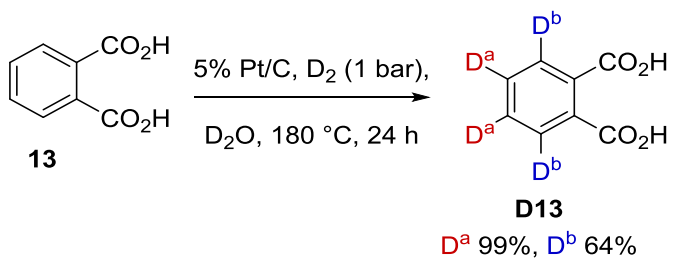

Scheme 2.7 ^{2}H labelling of electron poor aromatics.

All the above methods have their place in the modern chemical industry; however, the challenge reamains of finding a practical means to label a fully functionalised drug molecule under mild conditions and in a regioselective manner. The most imprtant development in addressing this problem has come from the area of homogeneous catalysed transition-metal hydrogen isotope exchange.

1.4. Homogeneous Hydrogen Isotope Exchange

1.4.1. Platinum & Nickel

The earliest developments in hydrogen isotope exchange (HIE) are based around the use of platinum species and, although still applied today, these techniques are non-selective.[13] One of the first examples comes from Garnett and Hodges in 1967 and applied a Pt(II) salt in acetic acid and hydrochloric acid, using heavy water as the deuterium source, to label a variety of arenes albeit with low levels of incorporation (**Scheme 2.8**).[16]

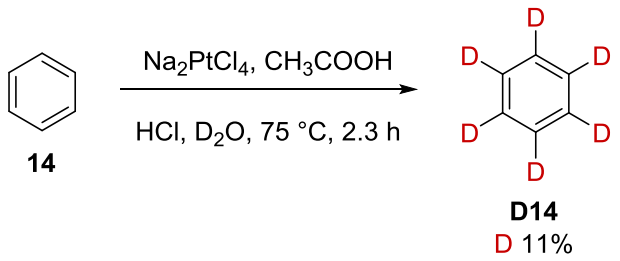

Scheme 2.8 Early example of homogeneous HIE.

More recent developments have led to higher levels of incorporation through the use of microwave irradiation; but still in a non-regioselective manner, as shown by Atzrodt and Derdau.[13] Applying similar conditions to Garnett and Hodges, a Pt(II) salt facilitated the exchange of deuterium in **15** under basic conditions with good levels of incorporation (**Scheme 2.9**).

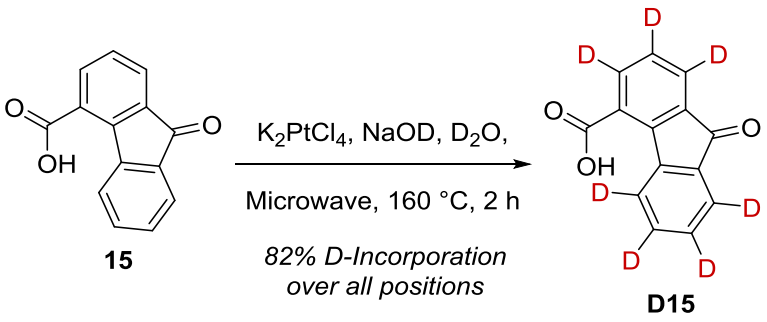

Scheme 2.9 Microwave assisted HIE.

Another transition metal used in HIE processes is nickel, which was investigated extensively throughout the 1970s and 1980s and showed some selectivity for labelling *ortho*- to aniline and phenol derivatives.[17] An example from MacDonald and Shannon used nickel embedded on kieselguhr with heavy water as the isotope source. These conditions delivered good incorporations at the *ortho*-positions in phenol, however when moving to 3,5-dimethylphenol **16**, the selectivity was eroded with significant incorporation at the *ortho* and benzylic positions (**Scheme 2.10**).[18]

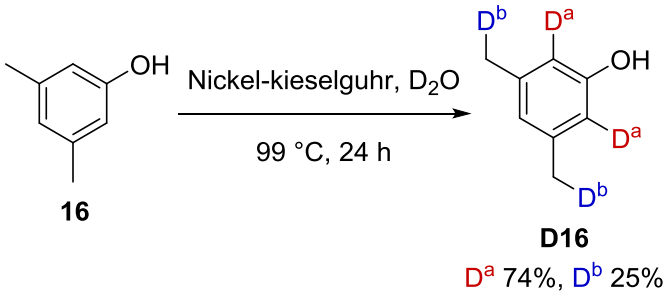

Scheme 2.10 Ortho phenol and benzyllic HIE.

One advantage to using nickel as a HIE catalyst is its ability to label regioselectively in pyridine-like structures at the α-position.[19] An example from Hesk *et al.* uses the ability to perform tritium exchange with Raney-nickel successfully in compound **17**, in which almost exclusive regioselectivity is observed (**Scheme 2.11**).[20]

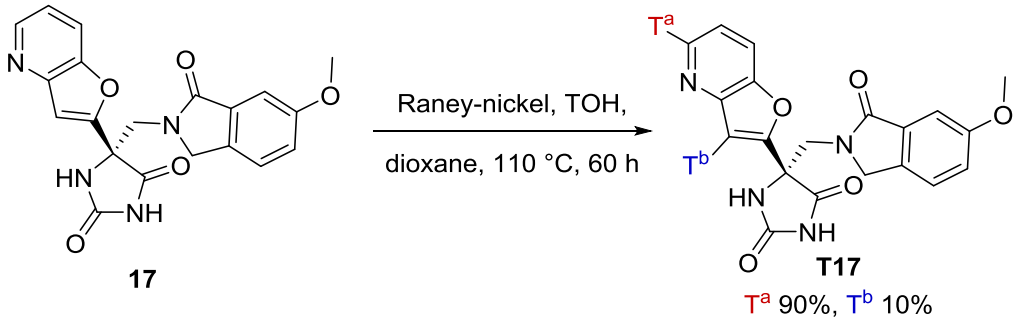

Scheme 2.11 Pyridine C-2 HIE.

1.4.2. Ruthenium & Rhodium

One of the first reported uses of ruthenium in HIE came in 1974 when Regen applied a tris(triphenylphosphine)ruthenium(II) dichloride species **18** to the labelling of primary alcohols, such as **19**, in the α-position (Error! Reference source not found.).[21] However, temperatures in excess of 150 °C were required for significant levels of incorporation, and when moving to secondary alcohols no exchange was observed.

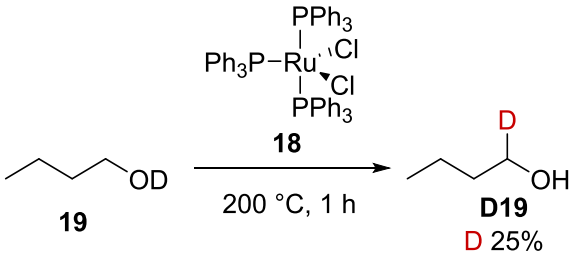

Scheme 2.12 α-HIE in an alcohol.

Following this work, labelling was successfully completed on amines, including piperidines and piperazines, which are common functionalities within drug molecules. An example is SCH66336 **20**, in which incorporation occurs selectively at the α-position of the piperidine ring, with notably, no halogen exchange observed (**Scheme 2.12**).[22]

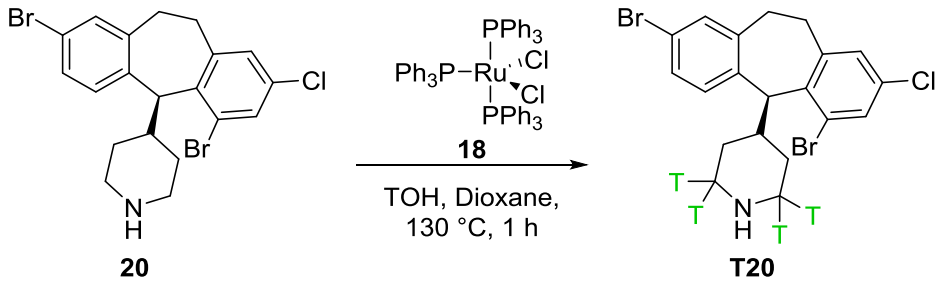

Scheme 2.13 Piperidine C-2 HIE.

The first reported use of a rhodium species in HIE processes was in 1975, when Garnett *et al.* developed a rhodium trichloride hydrate that was used as an alternative to the tetrachloroplatinate species previously employed (*vide supra*).[23] Although deuteration occurred at a slower rate, the reaction did not require a mineral acid for stabilisation, hence simplifying the experimental procedure.

Indeed, Lockley *et al.* continued to optimise this rhodium trichloride hydrate system, but it wasn't until 1982, that they reported the regioselective labelling of chromone-2-carboxylic acid **21** in DMF/D_2O at elevated temperature with excellent levels of incorporation (**Scheme 2.14**).[24]

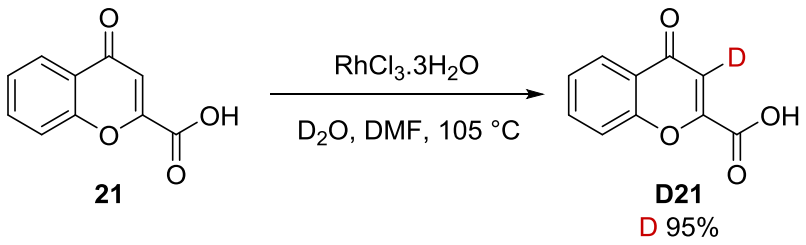

Scheme 2.14 Acid directed HIE.

Following this early success, Lockley hypothesised that the high regioselectivity for *ortho*-exchange must originate from coordination of the carboxylate to the rhodium centre, thus forming a five-membered cyclometallated intermediate **22** (**Figure 2.1**). Therefore, in the presence of deuterated water regiospecific deuterium incorporation occurred. Further studies supported this hypothesis and allowed for the incorporation of aromatic carboxylic acids,[24,25] amides,[25] amines[25] and anilines[26] as functional handles capable of directing HIE.

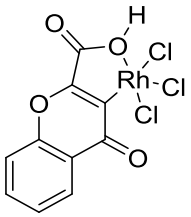

22

Figure 2.1 Proposed cyclometallated intermediate.

More recently, Li *et al.* developed a range of rhodium(III) hydride complexes such as **23**, and employed them in the deuterium labelling of benzo[h]quinoline **24**, in deuteroacetone (**Scheme 2.15**).[27] Electron donating phosphine ligands were found to be crucial for catalyst activity, the most active of which was applied in the labelling of heteroaromatic systems, presumably following a similar five-membered cyclometallated intermediate as proposed by Lockley.[24]

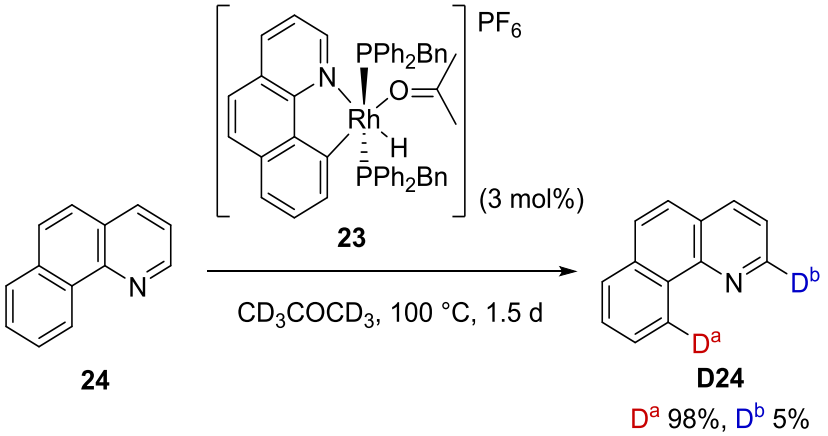

Scheme 2.15 Directed HIE in benzoquinoline.

Despite early success with ruthenium and rhodium complexes, many of these catalysts are limited by the high temperatures and prolonged reaction times associated with their use. Therefore, focus has switched to complexes with alternative metals, in particular iridium.

1.4.3. Iridium

The emergence of iridium complexes as HIE catalysts in the 1980s and 1990s revolutionised isotope exchange.[28,29] One of the earliest examples of regioselective labelling using iridium complexes was reported by Crabtree, where incorporation into the methyl groups in caffeine **26** is observed (**Scheme 2.16**).[30] The complex **25**,

previously applied in olefin hydrogenation and found to be highly active, as was discussed in Chapter 1. Importantly, this was one of the first examples of the use of a homogeneous catalyst in labelling chemistry, in which exchange occurred at room temperature, clearly indicating the activity of the complex in the HIE process.

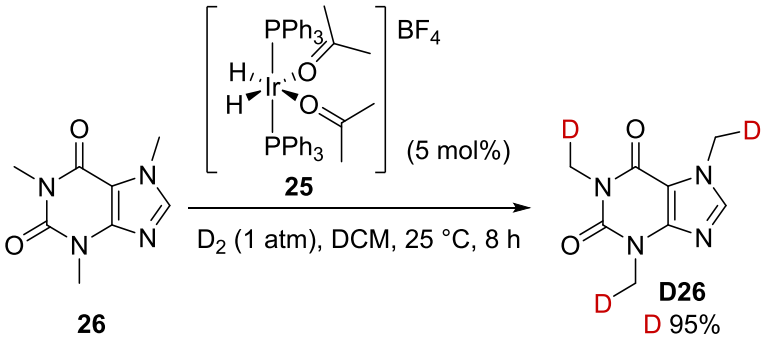

Scheme 2.16 sp^3 HIE in *Caffiene*.

Despite this result, it wasn't until 1992 that Heys employed complex **25**, already proven to activate C-H bonds, to perform regioselective *ortho*- exchange on a variety of aromatic model substrates (**Scheme 2.17**). This study expanded the scope of this labelling chemistry to include a variety of functional handles, allowing excellent *ortho*-selective exchange in substrates **D27a-e**.[31] It was also observed, that the substituent on the aromatic ring affected selectivity in the deuteration of the C-2 or C-6 positions, and importantly, that substitution at C-3 favoured incorporation at C-2, as in **D27f-g**. It is also noteworthy that the poorly coordinating nitro group **D27i** gave only low levels of incorporation. Furthermore, addition of an extra methylene unit between the aromatic ring and functional handle **D27j** caused labelling to cease completely.

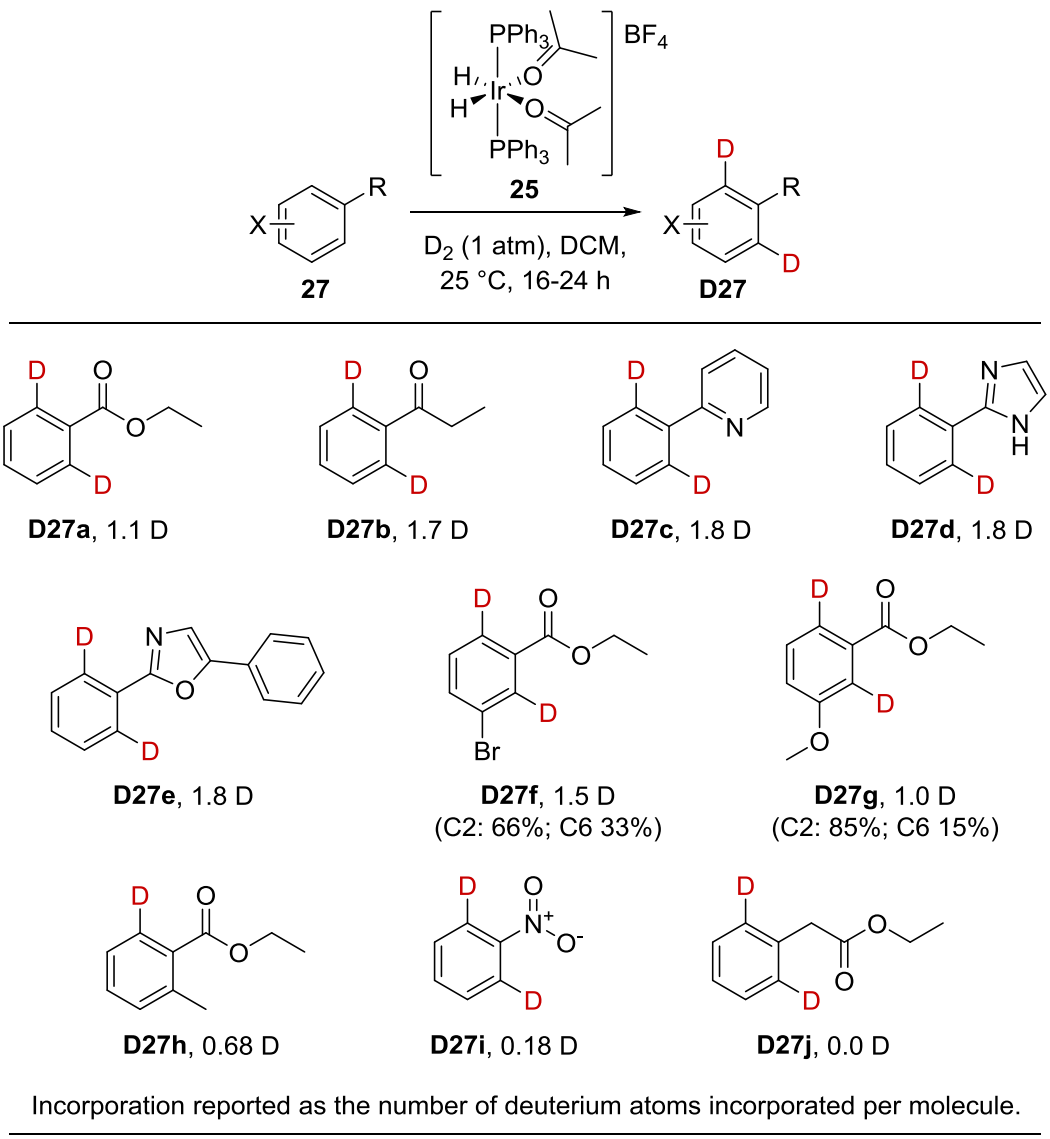

Scheme 2.17 HIE mediated by complex **25**, and different directing groups.

To further explain the efficacy of this catalyst system, in 1993 Heys reported further studies in which the rate of *ortho*-deuteration was studied (**Scheme 2.18**).[32] It was observed that substitution at the 4-position of benzoate ester **28** improved the overall level of labelling substrates (**D28a-c**), except in the case of the strongly withdrawing triflouromethyl group **D28d**, in which it was mildly diminished. Indeed, the same results were reflected in the use of dimethyl benzamides. One standout result was the failure to label any compound containing a nitrile substituent, such as **D28e**; Heys speculated that this may be due to irreversible complexation of the nitrile to the iridium centre, shutting down the catalyst.

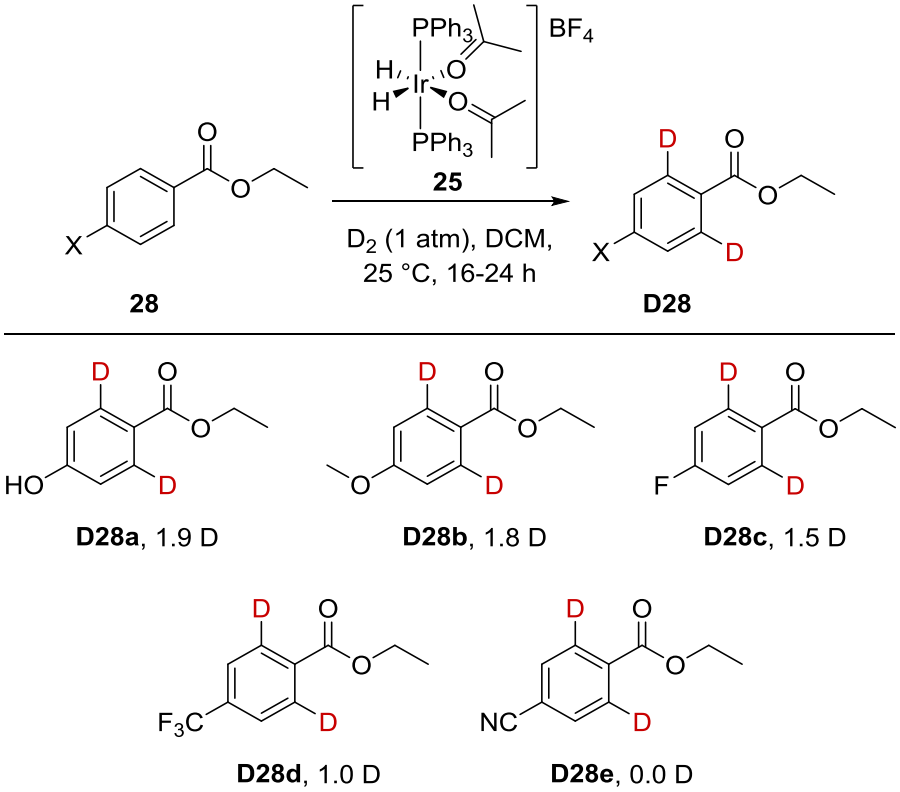

Scheme 2.18 HIE mediated by complex **25** with substituted aromatic rings.

In attempts to explain the *para*-substituent effect, Heys performed labelling experiments on substituted benzophenones, such as **29** (**Figure 2.2**), and found that the rate of deuteration was indeed faster for substituted aromatic rings (**Table 2.1**). This led to the conclusion that because complexation to the substrate is identical for

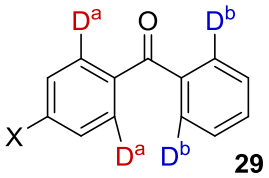

Figure 2.2

Entry	*X*	*Ratio of Da / Db(a)*		
		25 min	*55 min*	*24 h*
1	Cl	1.6	1.2	1.0
2	OMe	2.1	1.4	1.0

(a) Ratio of the average number of deuterium atoms incorporated at the given position.

Table 2.1 Comparative rate study of substituted aromatics.

labelling both aromatic rings, the rate determining step of the reaction must occur during the C-H bond breaking or C-D bond formation steps of the reaction.

In further studies, Hesk applied the commercially available catalyst, **30**, developed by Crabtree for hydrogenation processes with great success, as discussed in Chapter 1. Labelling *ortho*- to acetanilides, such as **31**, was found to proceed in a highly regioselective manner with high levels of incorporation (**Scheme 2.19**).[33]

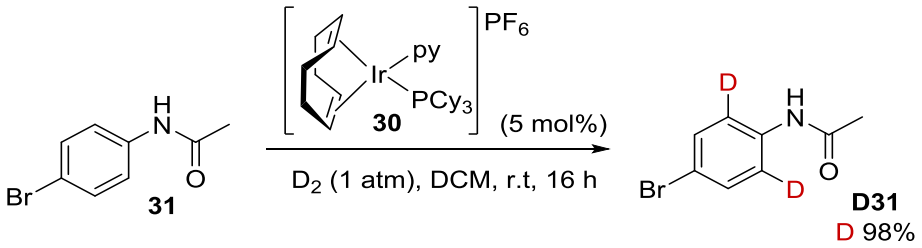

Scheme 2.19 Crabtree's catalyst **30**, in HIE.

Importantly, the work by Hesk gave examples in which the catalyst could label at a position four or five bonds distant from the site of complexation, as in acetophenone, **32**, or acetanilide, **34**, respectively. This evidence lent further support to the now generally accepted idea that the reaction could proceed *via* a five-membered metallocylic intermediate (five-mmi), **33**, or a six-mmi, **35** (**Scheme 2.20**).

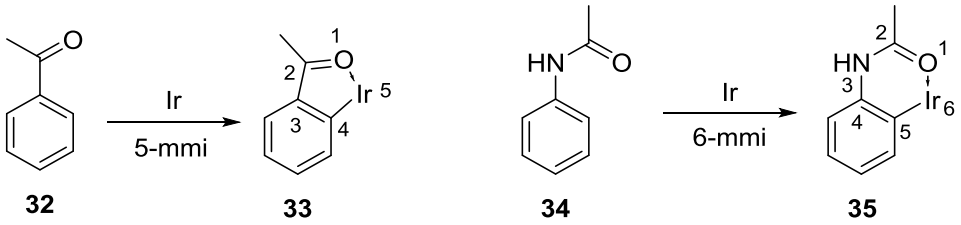

Scheme 2.20 Plausible cyclometallated intermediates.

Heys went on to produce a series of phosphine based analogues of complex **30**, including **36** and **37** in an attempt to further improve the reactivity and elucidate the mechanism behind the HIE process (**Figure 2.3**).[34]

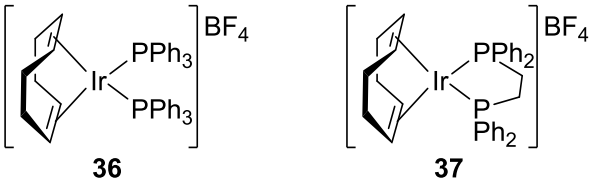

Figure 2.3 Monodentate **36** and chelating **37** phosphine complexes.

In particular, Heys *et al*. attempted to explain how a catalyst could be tuned to exclusively label via a 5-mmi as oppose to a 6-mmi. In efforts towards this, ethyl 1-napthoate **38** (a substrate which could label *via* a 5- or 6-mmi, **39** and **41** respectively) was labelled using complexes **30**, **36**, and **37** (**Scheme 2.21**). Heys observed that complexes **36** and **37** were indeed much more active than complex **30** (**Table 2.2**). More interestingly, complex **36** failed to label at the C-8 position *via* a 6-mmi, hence it was proposed that the larger ligand sphere of the two monodentate ligands hindered the formation of the larger, less planar 6-mmi, therefore favouring the smaller, and more planar 5-mmi.

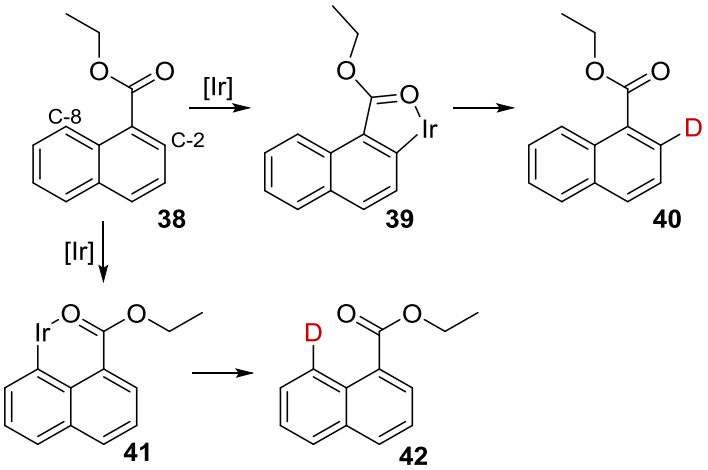

Scheme 2.21 Proposed labelling in ethyl 1-napthoate **38**.

Entry	*Complex*	*Catalyst Loading (mol%)*	*Incorporation*[a]	
			C-2	*C-8*
1	**30**	50.0	0.55	-
2	**36**	2.2	0.90	-
3	**37**	2.5	0.54	0.35

a) Average number of deuterium atoms incorporated at the given position.

Table 2.2 Comparison of complexes **30**, **36** and **37** in HIE.

From this work and the previous discoveries by Lockley and Hesk, Heys proposed a plausible catalytic cycle for complexes similar to **30** (**Scheme 2.22**). Initially, the complex **43**, now thought to be a pre-catalyst, loses the cyclooactadiene unit in forming the active catalyst **44**. Through analogy with similar structures,[35,36] Heys proposed that if a non-bidentate ligand is used, a *trans* arrangement of ligands is optimal. The extra ligands "S" are proposed to be loosely bound, and either a solvent molecule, a molecule of deuterium or a substrate molecule, allowing for coordination of the substrate **45** in a facile manner. Complexation of the coordinating functionality brings the *ortho* position of the aromatic ring close to the iridium centre as in **46**. Oxidative insertion of the iridium into the *ortho* aromatic C-H bond gives **47**. A known hydride fluxionality process was then proposed, leaving a deuteride *cis* to the iridium bound *ortho* carbon, **48**.[37] Reductive elimination, and therefore formation of the C-D bond, is now possible, forming **49**, which can undergo decomplexation to release the labelled product **50** and regenerate the catalyst **44** with another molecule of deuterium.

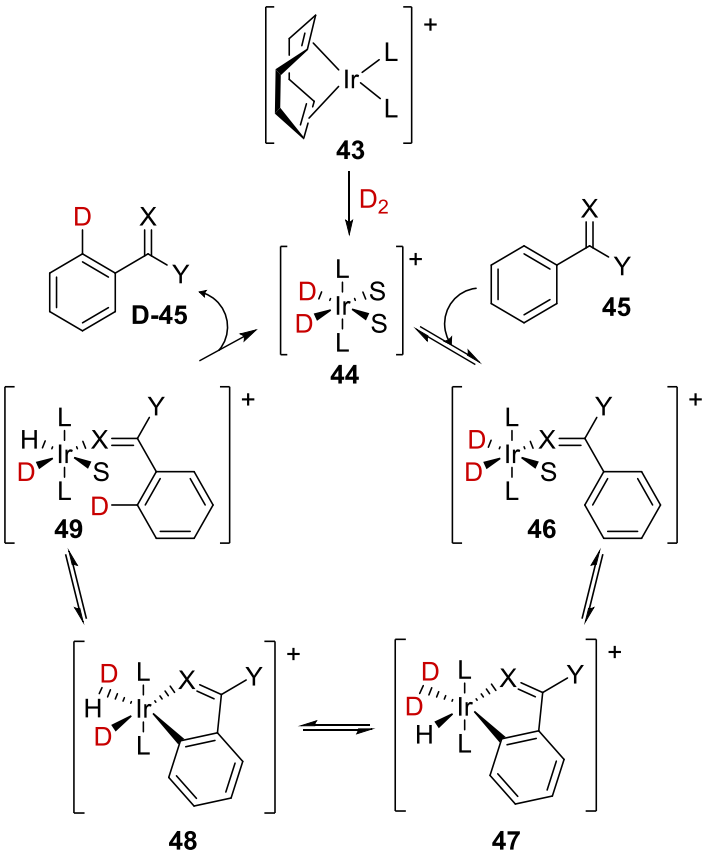

Scheme 2.22 Heys' proposed mechanism for HIE with Crabtree-like catalysts.

Despite the initial success of complex **30**, it wasn't until 2001 that Herbert fully elucidated the scope of this complex in HIE processes.[38] The study began by testing a range of esters, amides and ketones for their potential to act as a functional handle in the HIE process (**Scheme 2.23**). The esters, as had been previously reported by Hesk, performed excellently, with a *para*-substituent on the aromatic ring. Having said this, incorporation levels fell drastically with *ortho*- or *meta*-substitution. Additionally, electron withdrawing substituents hindered the deuteration process. Upon switching to an amide as the functional handle, the levels of incorporation generally improved. This is thought to be principally an electronic effect associated with the electron-

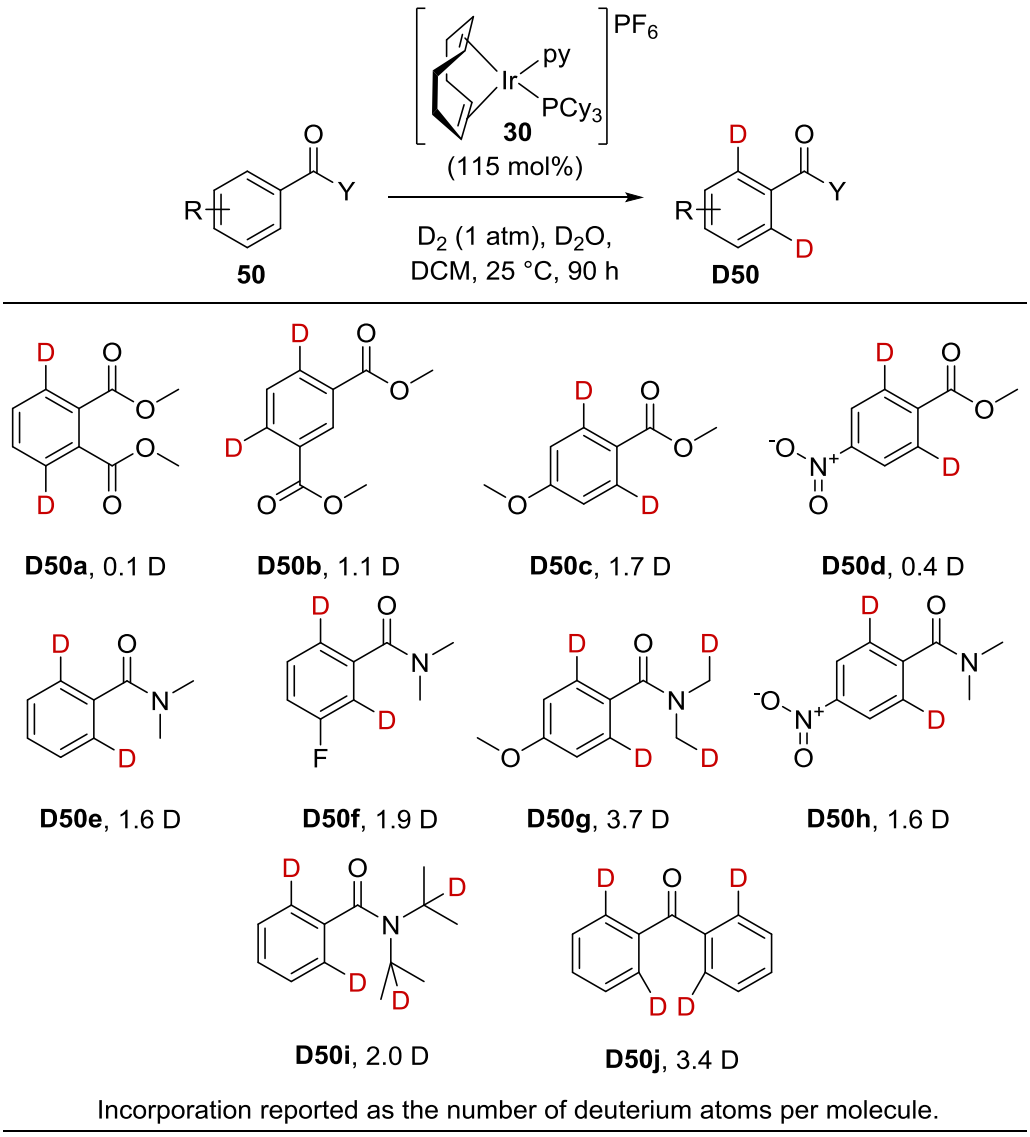

Scheme 2.23 HIE with Crabtree's catalyst, with different directing groups.

donating capabilities of the coordinating functional handle. Unlike esters, the deuteration of substituted amides remained mostly unaffected by the aryl substituent. Coordination of such amide substrates was proposed to occur primarily through the oxygen of the amide, because changing the nitrogen substituent from dimethyl to the bulky di-iso-propyl did not significantly hinder incorporation. Furthermore, ketones were shown to act as excellent coordinating functional handles, delivering similar incorporations as amide handles.

In addition to the expected incorporation, it is noteworthy that incorporation was observed in the methyl units of dimethyl benzamide **D50g** (**Scheme 2.23**). Indeed, labelling in this position is also proposed to occur *via* a 5-mmi, **52**, in which the iridium inserts into an alkyl C-H bond (**Scheme 2.24**).

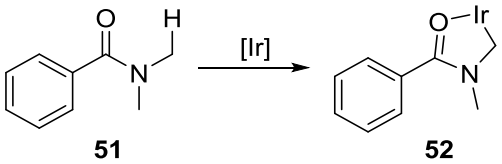

Scheme 2.24 Proposed sp^3 HIE cyclometallated intermediate.

These excellent initial results prompted Herbert to investigate the labelling of arenes bound to a heteroatom. A series of functionalities commonly found in pharmaceutical chemistry were chosen, and isotope exchange using complex **30** was attempted (**Scheme 2.25**). Studies with aniline **D53a** and phenol **D53b** systems showed no incorporation. However, by masking the amine (with either a Boc protecting group **D53c**, or as a hydrazine **D53d**) allowed labelling to be achieved, albeit with low to moderate levels of incorporation. However, the same was not true of the alcohols, which when masked as an ester **D53e** delivered no incorporation. Further work included benzylic amines **D53f** and benzylic alcohols **D53g** to allow formation of a 5-mmi. Whilst the poorly coordinating benzyl alcohol still failed to give any incorporation, moderate levels of incorporation were observed in benzylamine. Unfortunately, the directed labelling with alternative functional handles proved to be difficult, as nitro **D27i**, sulfoxide **D53h**, sulfone **D53i** and sulfonamide **D53j** groups failed to deliver any significant incorporation.

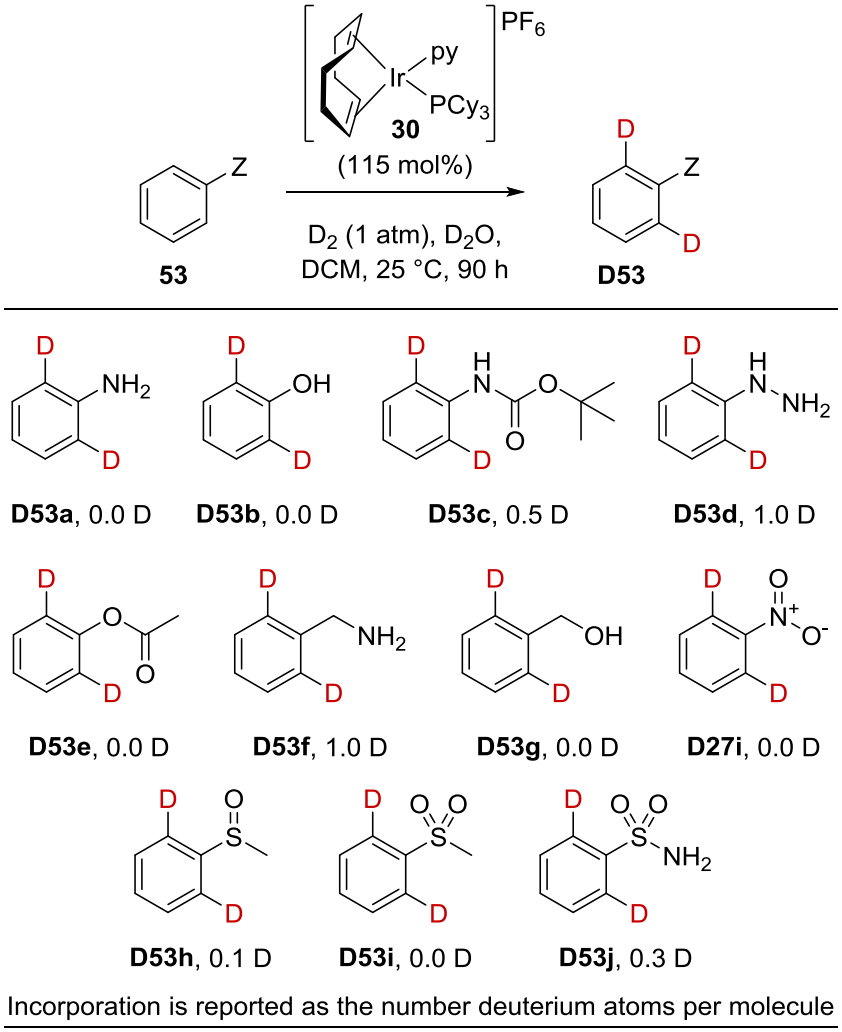

Scheme 2.25 Further challenging substrates with Crabtree's catalyst.

Efficient exchange was also observed with a variety of heterocycles including imidazoles, thiazoles, and pyridines in each case giving good levels of incorporation (**Scheme 2.26**). Notable, with select heterocycles, was the ability to label depending on the position of substitution on the heterocycle. With 1-methy-3-phenylpyrazol **D54a** labelling was achieved through the favoured 5-mmi. However, only the less reactive 6-mmi is available for 1-methy-5-phenylpyrazol **D54b**, leading to a lower overall incorporation. Also worthy of note is the change in incorporation upon changing the coordinating atom within the same molecule. For 4-phenylthiazol D**54c**, a 5-mmi coordinating through the nitrogen can be envisaged, and for phenylthiazol **D54d** a 5-mmi coordinating through the sulfur. It is observed that sulfur delivers a low incorporation compared to nitrogen. Herbert believed that this was due to the hybridisation of each coordinating atom. For the nitrogen, the lone pair resides in the

same plane as the aromatic ring to be labelled, hence allowing a facile coordination/insertion process. However, for the sulfur, the lone pairs reside above and below the plane of the aromatic ring, causing coordination to occur at a site distant from the aromatic ring hindering the insertion process.

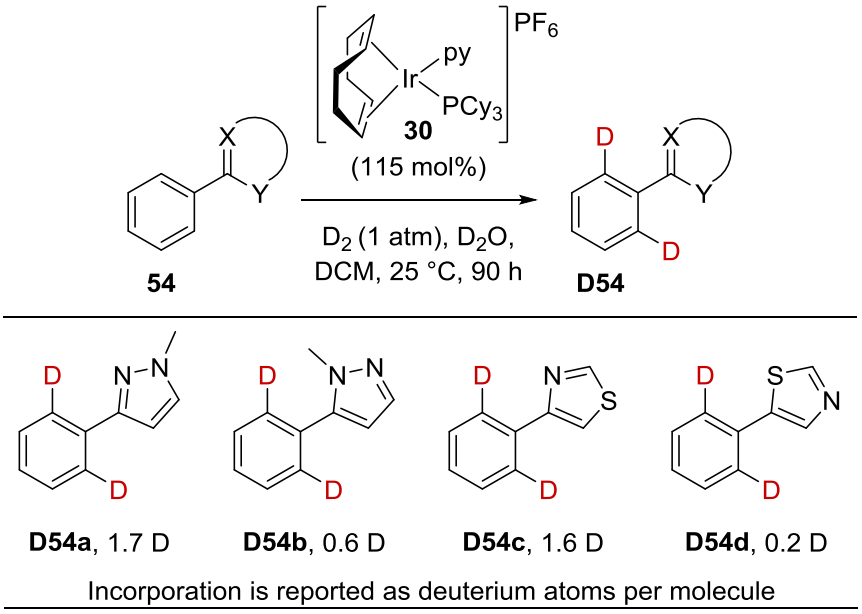

Scheme 2.26 Heterocycle directed HIE with Crabtree's catalyst.

The success of Crabtree's catalyst, **30**, in both hydrogenation and HIE processes has led to increased interest in cationic iridium(I) complexes. With further developments to the ligand sphere, the utility of such complexes could potentially be improved, allowing for a more efficient catalyst.

1.4.4. Iron

In part due to the increasing price of second and third row transition metals, in particular rhodium, iridium, platinum and palladium, there has been a significant increase in research regarding more cost effective metal catalysts.[39] Within this emerging field, Chirik and Hesk *et al*. recently disclosed a bis(arylimdazol-2-ylidene)pyridine iron bis(dinitrogen) complex **55** that can perform hydrogen isotope exchange with a range of aryl and heteroaryl molecules (**Scheme 2.27**).[40] However, in contrast to those discussed previously, these complexes deliver isotopes without the need for a directing group, making them complementary to those typically developed to date. Within the substrate scope several trends appear, for example the exchange is

always favoured at the less hindered position the aryl ring, as in **D56a**, and is biased towards less electron-rich substrates **D56c**. This trend is also apparent in a range of heteroaryl structures tested, including **D56d**. The complimentary nature of this process was displayed in the labelling at *N*,*N*-dimethylbenzamide **D56e**. Utilising iridium(I) complex **30**, exchange was observed exclusively at the *ortho*-positions, while iron complex **55** installed the label at the less hindered *meta*- and *para*-positions. Remarkably, when applying toluene **D56f** as a substrate for exchange, it was noted that there was an inverse dependence upon the deuterium pressure. The origin of this unexpected trend, has been proposed to be caused by the formation of inactive Fe(0)

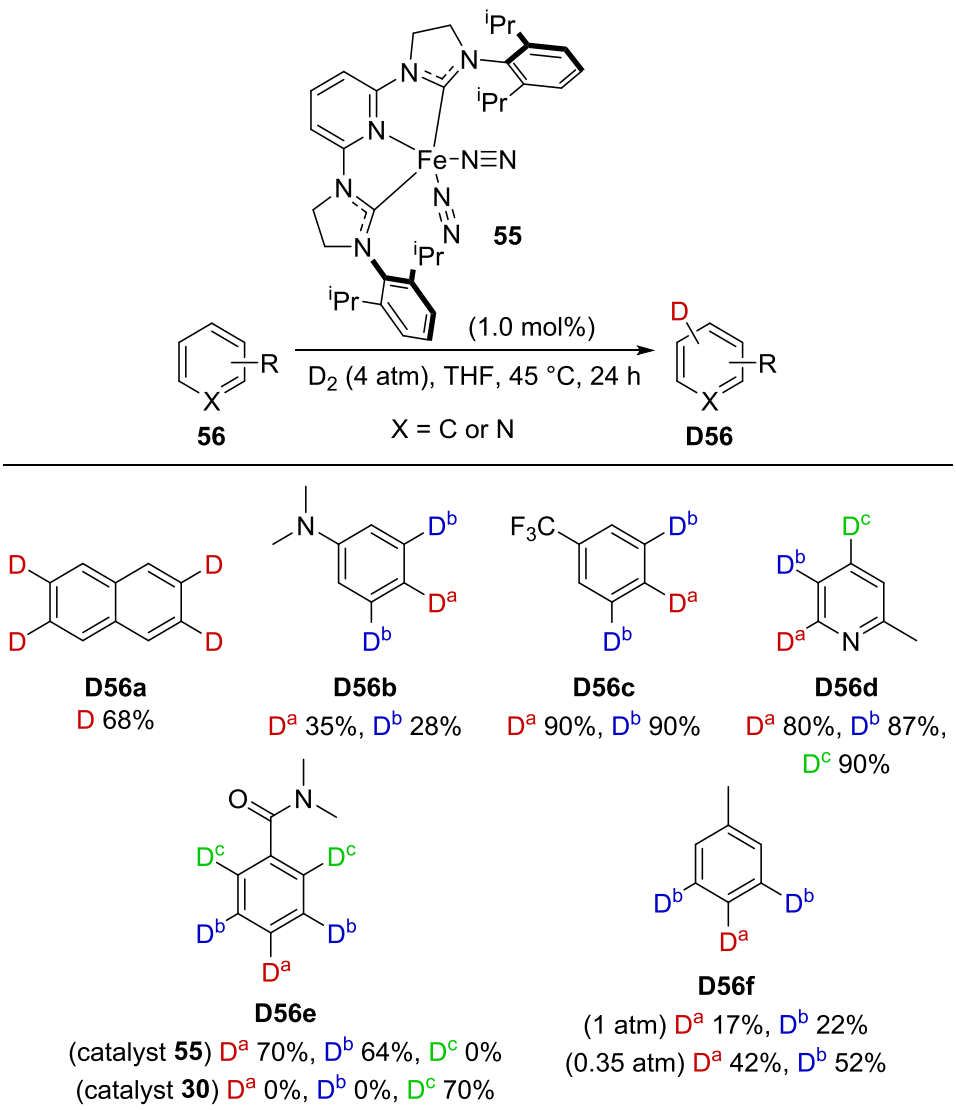

Scheme 2.27 HIE with Ir-complex **55**.

at higher deuterium/hydrogen pressures. However, detailed mechanistic investigations have yet to carried out for this process. It is also worth noting that although the complex is highly reactive, it is only usable in a glove-box, currently limiting its use within industrial laboratories.

1.5. Previous Developments from within the Kerr Group

As noted in the previous chapter, Nolan *et al*. synthesised a more stable NHC/pyridine complex **60c**, and Buriak *et al*. synthesised a series of more reactive NHC/phosphine complexes **60e** (**Scheme 2.28**), and applied them successfully in olefin hydrogenation.

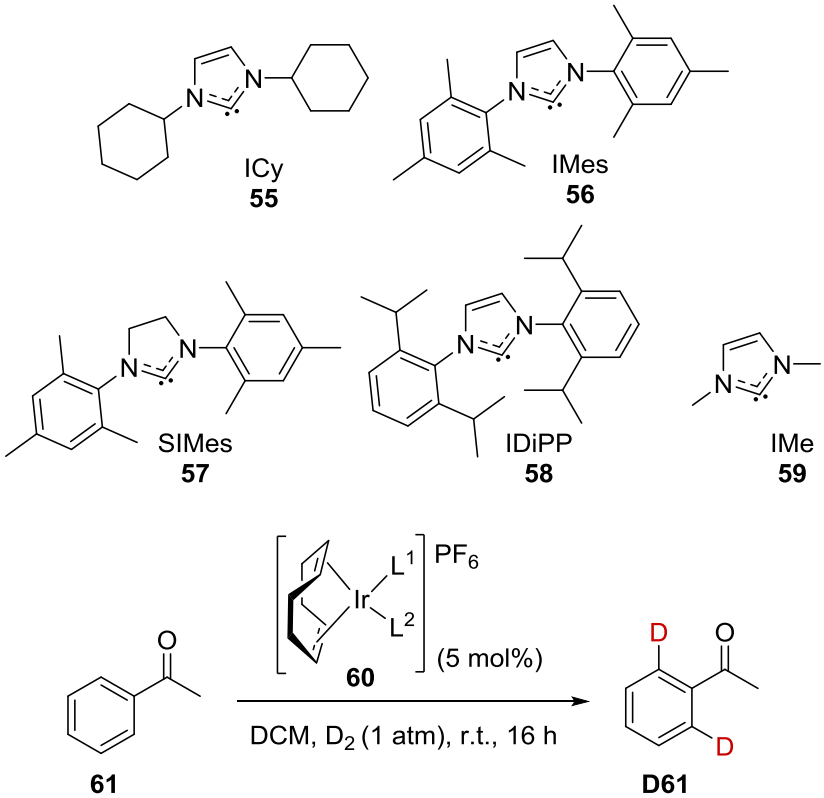

Scheme 2.28 ligands used for HIE catalysts.

Entry	*L¹*	*L²*	*Complex*	*% D-Incorporation*
1	Pyridine	ICy	**60a**	0
2	Pyridine	IMes	**60b**	89
3	Pyridine	SIMes	**60c**	94
4	Pyridine	IDiPP	**60d**	81
5	P^nBu_3	IMe	**60e**	0
6	PCy_3	Py	**30**	95

Table 2.3 Comparison of NHC/pyridine, NHC/phosphine and Crabtree's catalyst in HIE.

Noting this improvement, Kerr *et al*. were keen to expand the scope of the HIE processes with iridium catalysts, and utilised these complexes (**Table 2.3**).[41,42] Disappointingly however, the complex **59a**, bearing the smallest NHC/pyridine combination was inactive in the exchange process. The most promising NHC/pyridine complex **59c** showed similar reactivity to complex **30** in the HIE of acetophenone **61**. However, the study also revealed the same necessity for higher catalyst loading across more complex substrates. Furthermore, the small ligand sphere of NHC/phosphine complex **60e**, also delivered no reactivity.

Despite the early failure of complex **60e** to facilitate HIE processes; Kerr *et al* continued to investigate the synthesis and application of other NHC/Phosphine complexes (**Scheme 2.29**). To this end, the synthesis of complexes a combination of both bulky NHC and bulky phosphine ligands was realised,[43] despite earlier work by Buriak *et al* indicating that such complexes were inaccessible. The access to such complexes was achieved *via* a modified method initially applied by Herrmann and Köcher.[44] First, dimer **62** is reacted with sodium ethoxide, in the non-coordinating, non-polar solvent,

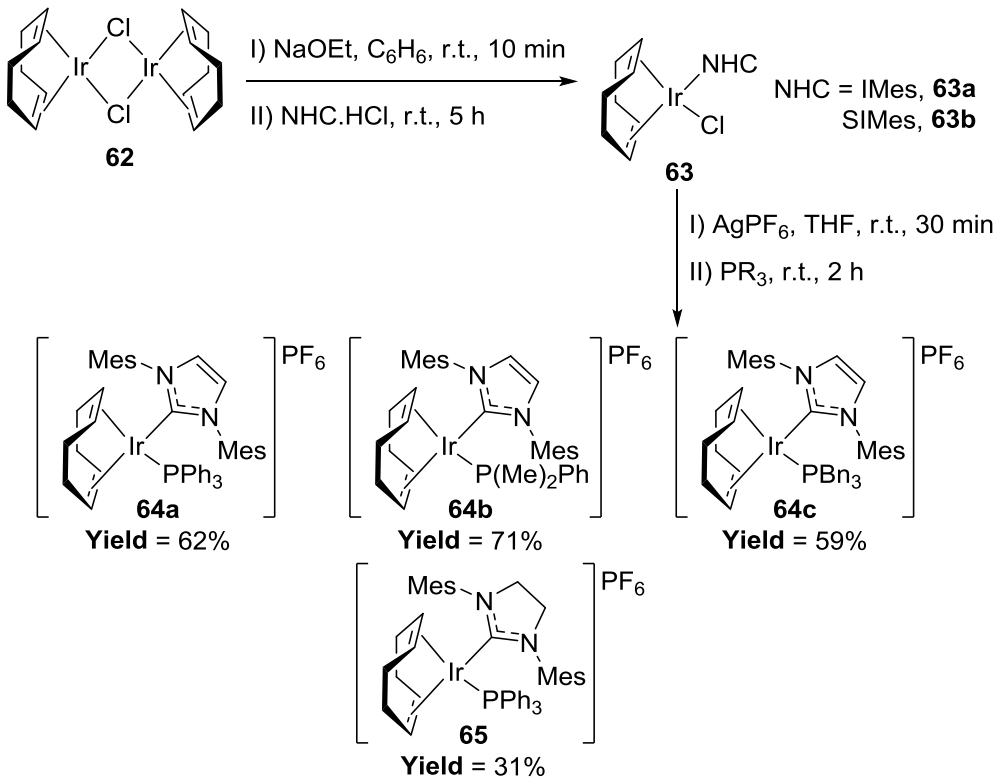

Scheme 2.29 Synthesis of bulky NHC/phosphine complexes by Kerr *et al*.

benzene. Treatment with an imidazolium salt then formed the requisite carbene *in situ* and produced intermediate **63**, which, upon treatment with silver hexafluorophosphate and a phosphine, delivered complex **64a-c** and **65** in good yields.

Following this, the complexes were then applied and were found to be highly active HIE catalysts with a range of functional handles, including ketones **D61**, amides **D66a-b**, nitro **D27i** and *N*-heterocycles **D27c**, a selection of which are shown below (**Scheme 2.30**).

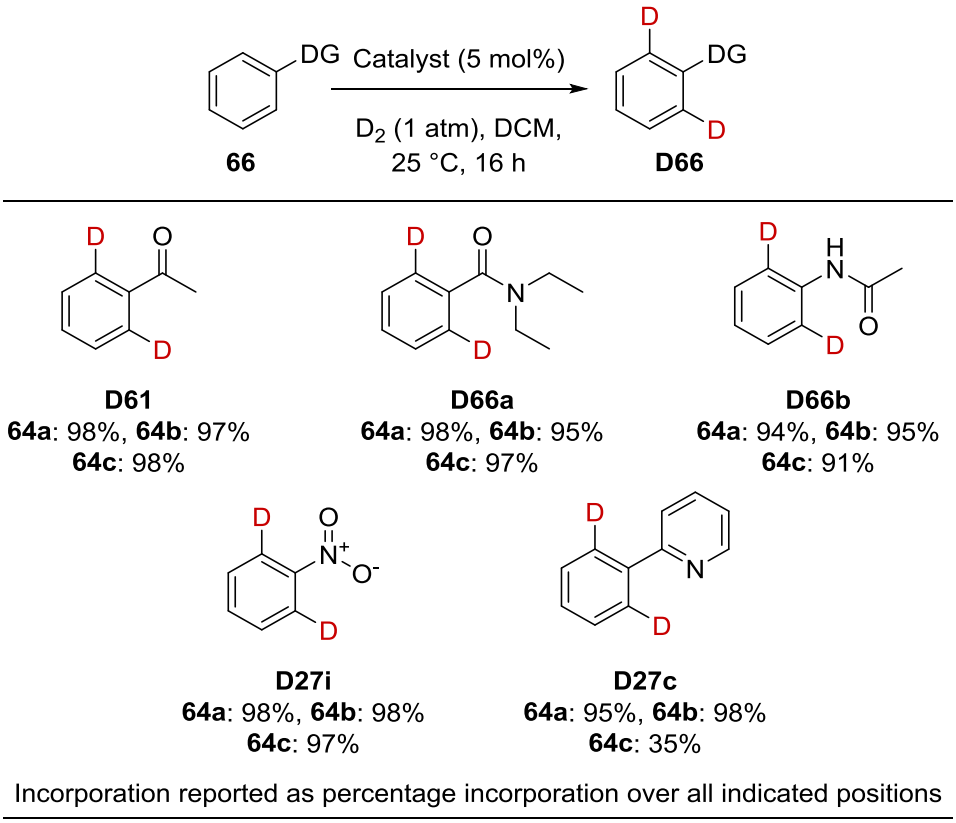

Scheme 2.30 HIE with NHC/phosphine complexes.

With regards to selectivity, amide **67**, for which both 5- and 6-mmi are possible, was chosen (**Scheme 2.31**). With the standard conditions (5 mol%, 16 h) high incorporation at both positions D^a and D^b was observed with each catalyst (**64a**, **64b** and **64c**). However, with just 0.5 mol% of complex **64b**, exclusive exchange was observed at position D^a, *via* a 5-mmi.

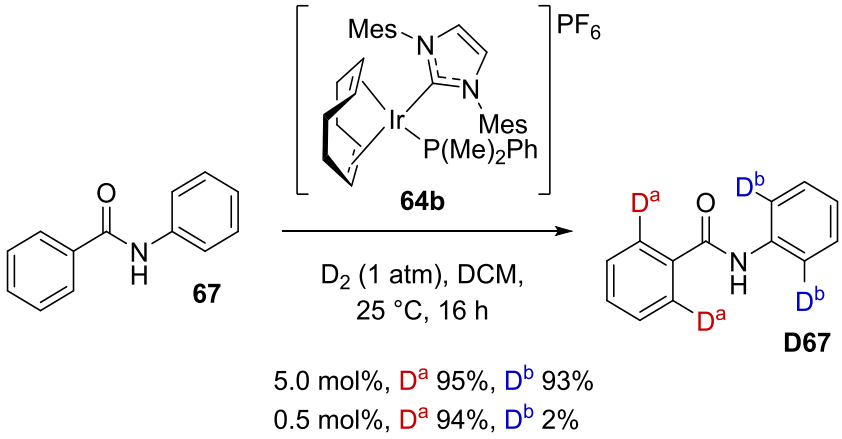

Scheme 2.31 Selective labelling of Benzanilide **67**.

Following on from the initial report of these complexes, Kerr *et al*. studied the mechanism using experimental and computational methods. The findings further supported the mechanism proposed by Heys *et al*. (**Scheme 2.22**).[34] However, one key new interaction was identified when the substrate was bound to the catalyst, an agostic interaction between iridium and the *ortho*- C-H bond being was observed (**Figure 2.4**).[45]

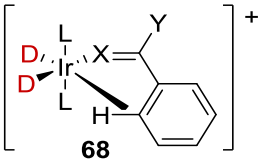

Figure 2.4 Proposed agostic interaction.

Based on this, the application of these new NHC/phosphine examples was expanded to include active pharmaceutical ingredients (**Figure 2.5**), such as *Perebron* **D69** in which incorporation is observed exclusively *ortho*- to the oxadiazole directing group. Furthermore, high incorporation was observed in *Celecoxib* **D70**, with good selectivity for the pyrazole directing group.

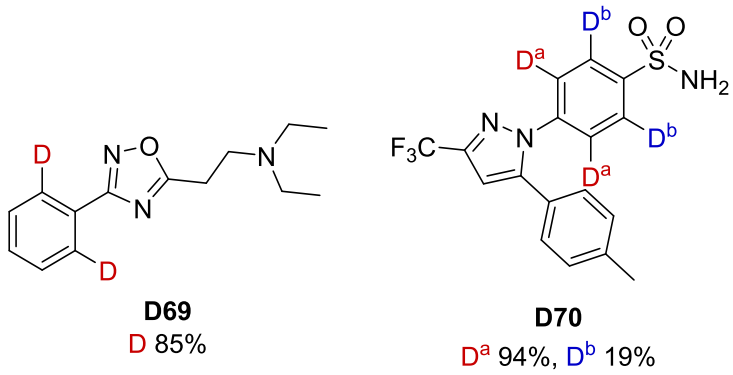

Figure 2.5 HIE on drug compounds.

Having investigated the ligand sphere, Kerr *et al*. next turned their attention to the outer sphere, and in particular the anionic partner to the cationic iridium complex, and the effect that it has upon the catalyst activity.[46] Drawing inspiration from the work of Pfaltz *et al*., Pregosin *et al*. and Buriak *et al*. as discussed in Chapter 1, a range of complexes with the same ligand architecture as complex **64a**, but bearing different anionic partners were synthesised (**Figure 2.6**). However, a modified procedure was utilised that avoided the use of a carcinogenic solvent and which elevated the yields, to deliver tetrafluoroborate **71a** and triflate **71b** counterion complexes.

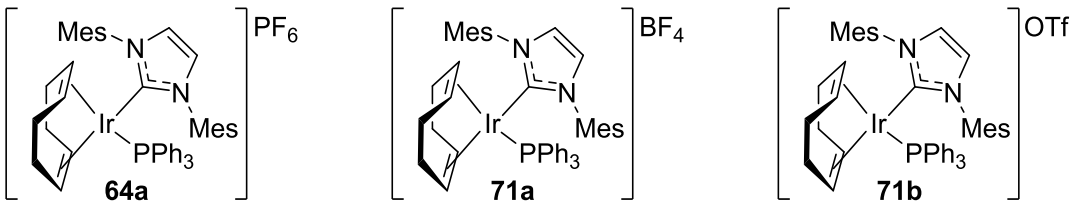

Figure 2.6 Different counterion complexes.

However, for the complex bearing the most non-coordinating counterion, tetrakis-(3,5-triflouromethylphenyl)borate (BArF) a new synthetic strategy was required (**Scheme 2.32**). Commencing from the common iridium dimer **62**, in one-pot, triphenylphosphine was added, generating the phosphine chloride intermediate **72**. Following this, addition of the imidazolium salt bearing the BArF counterion **73**, was used as a source for the counterion, with the free NHC generated *in situ* upon addition of base. Imidazolium salt **73** is readily generated from commercially available IMes.HCl **74** and NaBArF **75**.

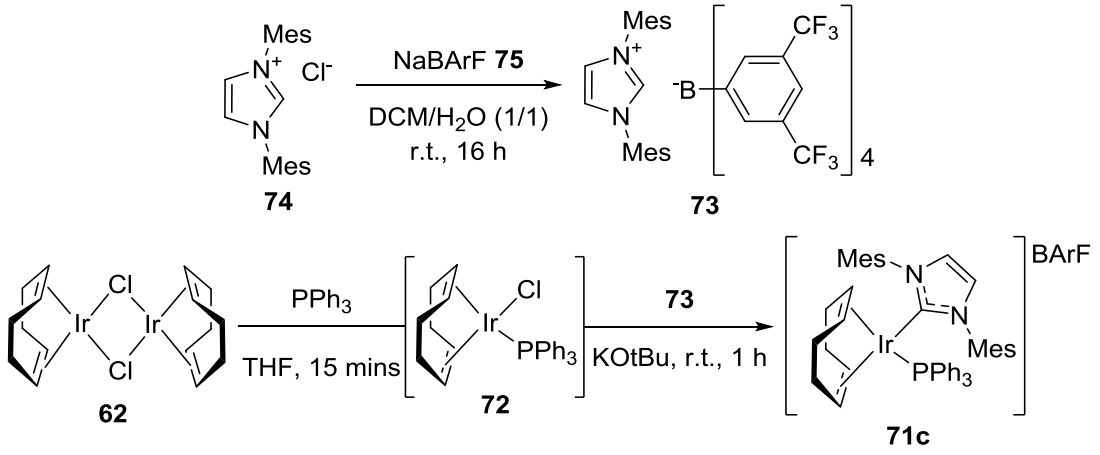

Scheme 2.32 Synthesis of BArF anion complex.

The comparison of the three new complexes with the parent PF_6 complex **64a** clearly indicated the improved reactivity of more non-coordinating counterions in hydrogen isotope exchange (**Scheme 2.33**).

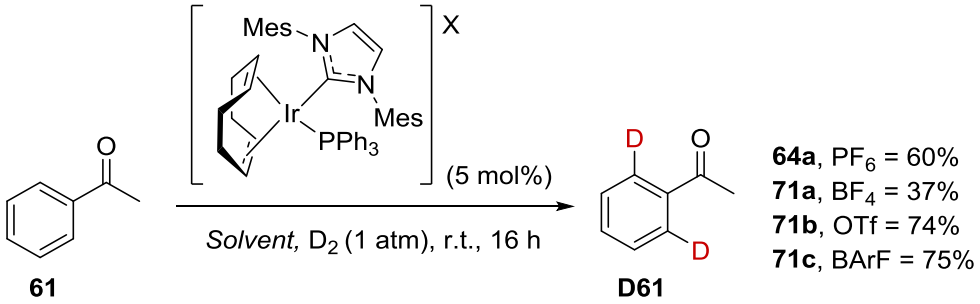

Scheme 2.33 Comparison of counterion complexes in HIE.

Furthermore, when comparing the reactivity of the most active complex **71c** for exchange on ketone **61** in a variety of different reaction solvents, it outperformed the original complex **64a** in fifteen out of sixteen cases, a selection of which are shown (**Graph 2.1**).

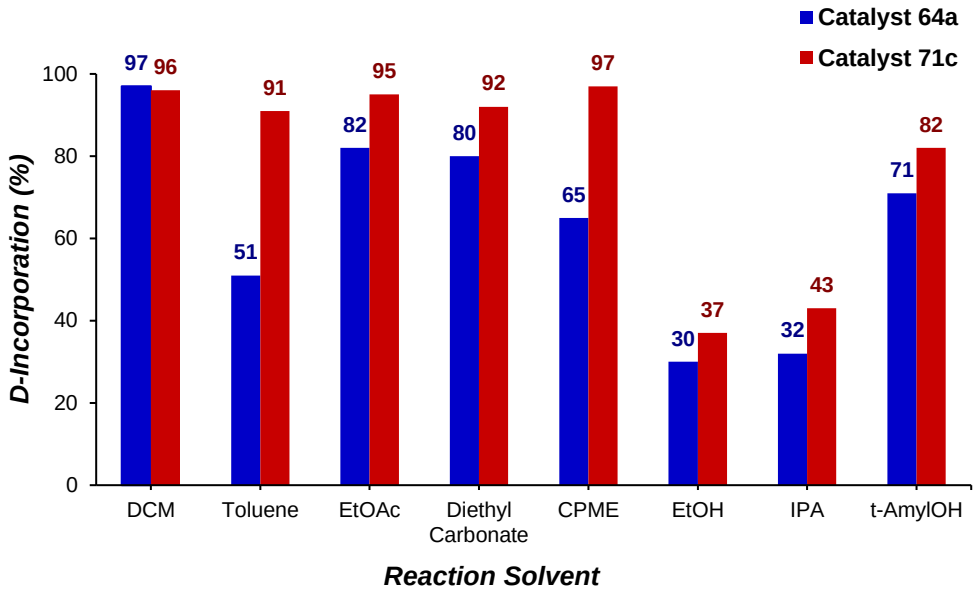

Graph 2.1 Comparision of PF_6 and BArF complexes in different solvents.

With the knowledge that the newly developed catalyst system could achieve high levels of reactivity in solvents outwith the normal chlorinated media, Kerr *et al*. could examine the labelling of systems previously inaccessible due to poor reactivity or solubility. Indeed, one of the key functional groups which remains as a challenge within directed C-H activation in general, and an important bioisostere of a carboxylic acid, the tetrazole, was targeted.[47] Pleasingly, through thorough investigative work, a method to deliver high deuterium incorporation *ortho*- to an unprotected tetrazole was developed (**Scheme 2.34**). The conditions necessary for exchange involved a mildly elevated temperature and, importantly, the inclusion of an inorganic base to produce the tetrazolium anion. The newly developed system performed excellently across a range of aryl tetrazoles, including different electronic **D76a-c** and steric parameters **D76e-f**. The formation of the tetrazolium anion is suggested through ^{19}F NMR of substrate **D76c** with and without base, and is likely necessary to stabilise the binding of the substrate to the catalyst. Moreover, the poor reactivity of both substrate **D76b** without base, and protected tetrazole **D76d**, lend strong credence to this hypothesis.

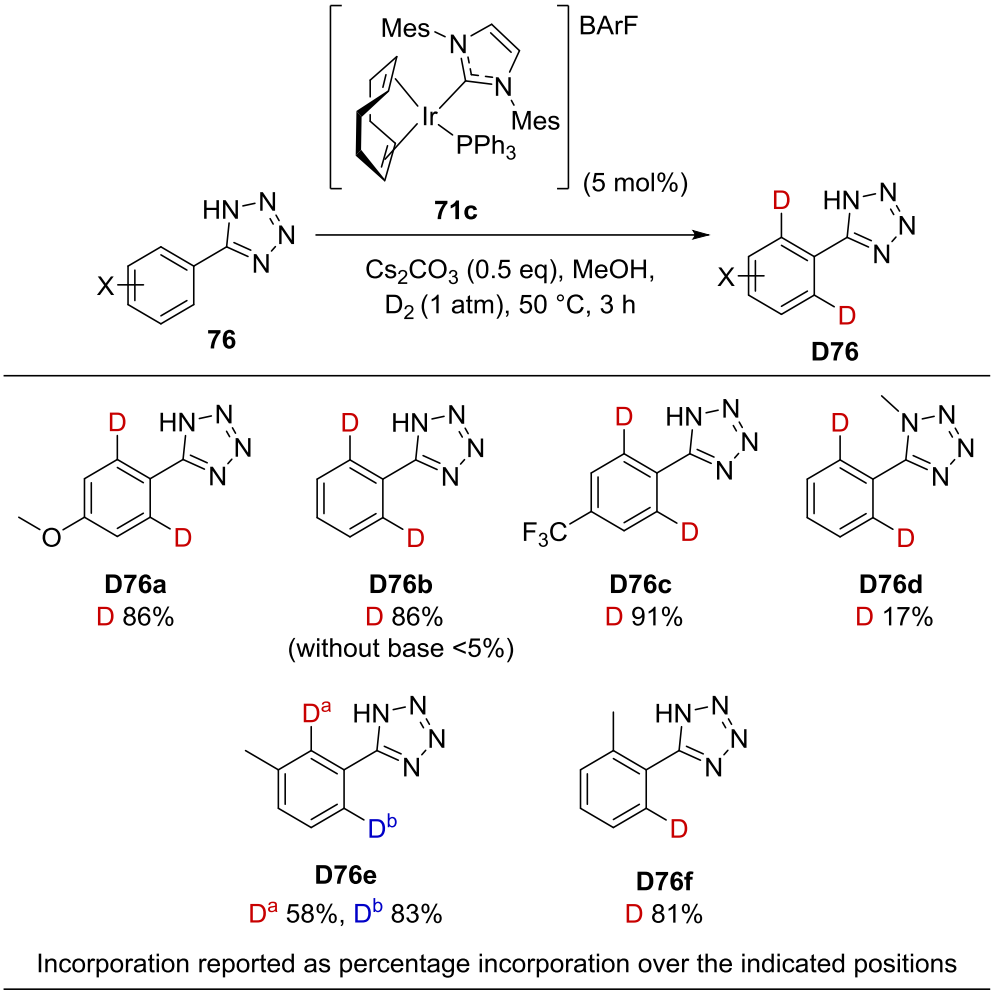

Scheme 2.34 HIE with tetrazole directing groups.

Additionally, and through the development of catalysts bearing the NHC/phosphine ligand motif, Kerr *et al.* improved the synthesis of the air stable, isolable, chloro/carbene complex **63a**, the key intermediate in the synthesis of these catalysts (**Scheme 2.35**).[46] This process then proved to be applicable to a broad number of different complexes, including **63b**, **63c**, **63d** and **63e**.[48]

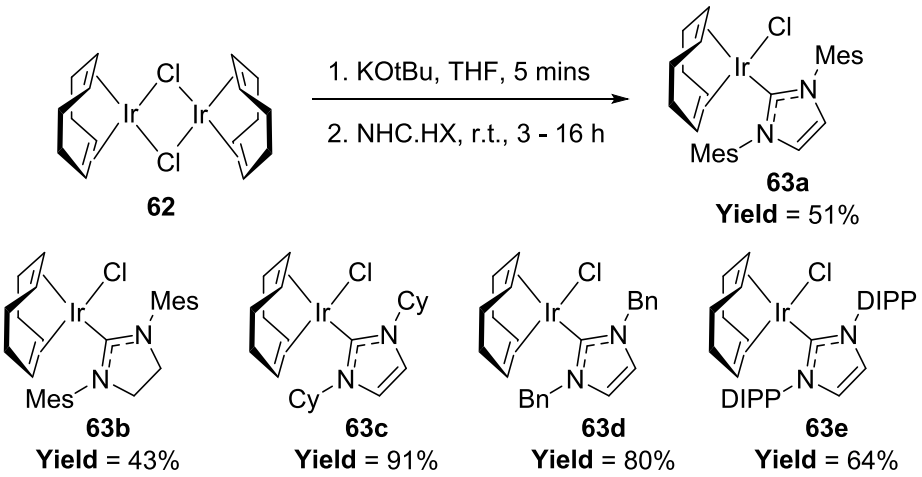

Scheme 2.35 Synthesis of NHC/chloride complexes.

With efficient access to complexes **63a-e**, Kerr *et al.* tested this simplified catalyst system for activity in HIE processes (**Scheme 2.36**). These complexes showed good activity within a limited range of substrates. Most notably, complex **63a** delivered high incorporations with ketone **D61** and pyridine **D27c** as donor groups. However, the complex did not function well with amide directing groups **D66a-b** through either a 5- or 6-mmi.

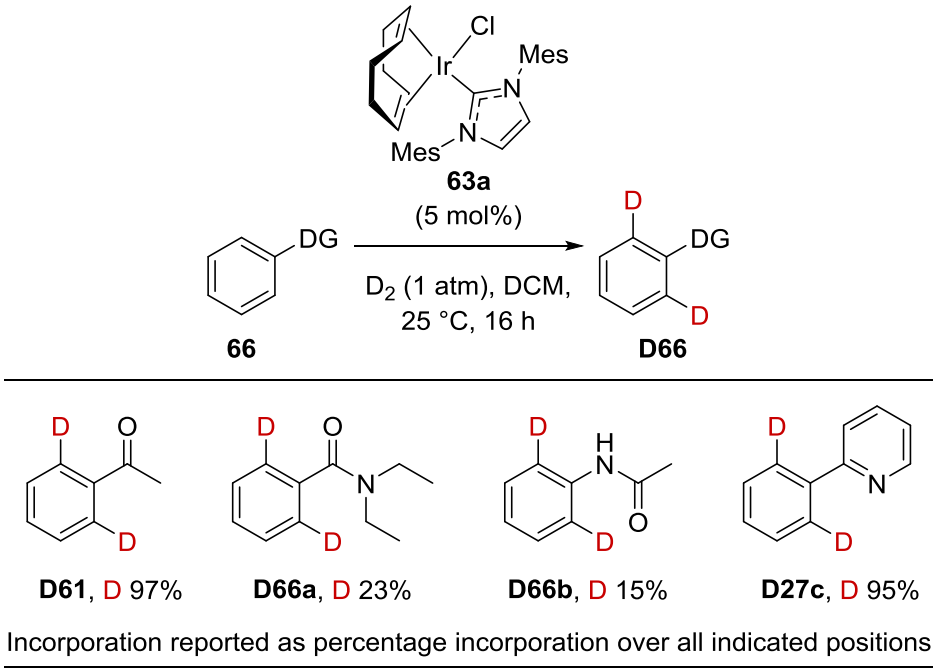

Scheme 2.36 NHC/chloride complex **63a** in HIE.

With a broad array of complexes available, to facilitate hydrogen isotope exchange with an increasing range of challenging substrates, Kerr *et al*. targeted the labelling of sulfonamides which at the time, were notable by their absence in C-H activation literature.[49] From previous work within the group, it was understood that NHC/phosphine complex was a poor choice for this functional group. However, NHC/chloride complexes were found to be highly reactive for hydrogen isotope exchange on aryl primary sulfonamides **78** (**Scheme 2.37**). In particular, complex **77** was found to possess the correct steric, and electronic parameters for high isotope incorporation. Across a range of primary sulfonamides **D78a-f**, complex **77** consistently delivered high deuterium incorporation, with only small decreases noted in electron deficient substrate **D78c** and sterically encumbered substrate **D78f**. Most notable, however, is the reverse in selectivity for *Celecoxib* **D70**, in which exchange

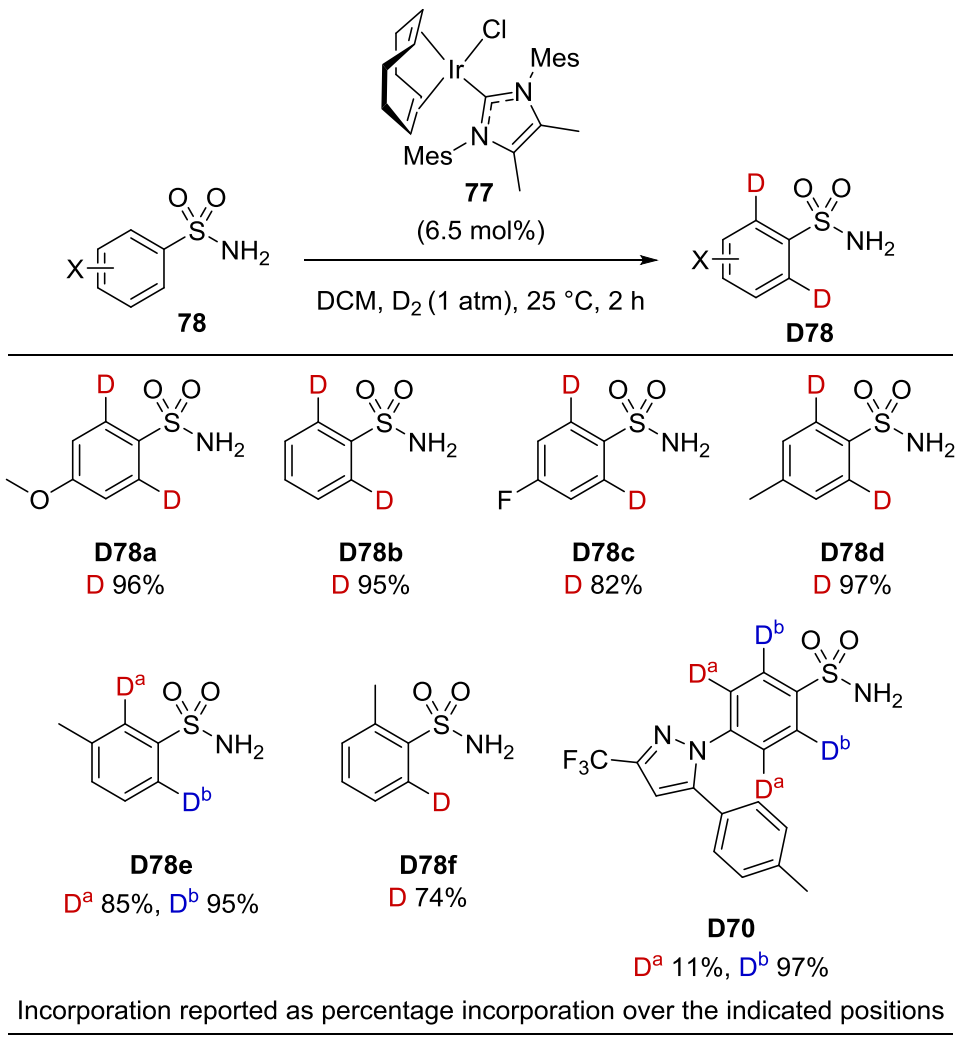

Scheme 2.37 HIE with sulfonamide directing groups.

occurs with good selectivity for the sulfonamide directed process, whereas NHC/phosphine complexes deliver selective exchange adjacent to the pyrazole (**Scheme 2.37**).

To understand the activity of this substrate with NHC/chloride complex **77** compared with NHC/phosphine complex **64a** Kerr *et al*. examined the mechanism computationally. The findings were, somewhat in contrast to the experimental observations, in that the sulfonamide-catalyst binding (**79** to **80**) was better stabilised by complex **64a**. However, the barrier to C-H activation (**80** to **81**) was lower for complex **77**, which is in general agreement with the experimental observations (**Scheme 2.38**).

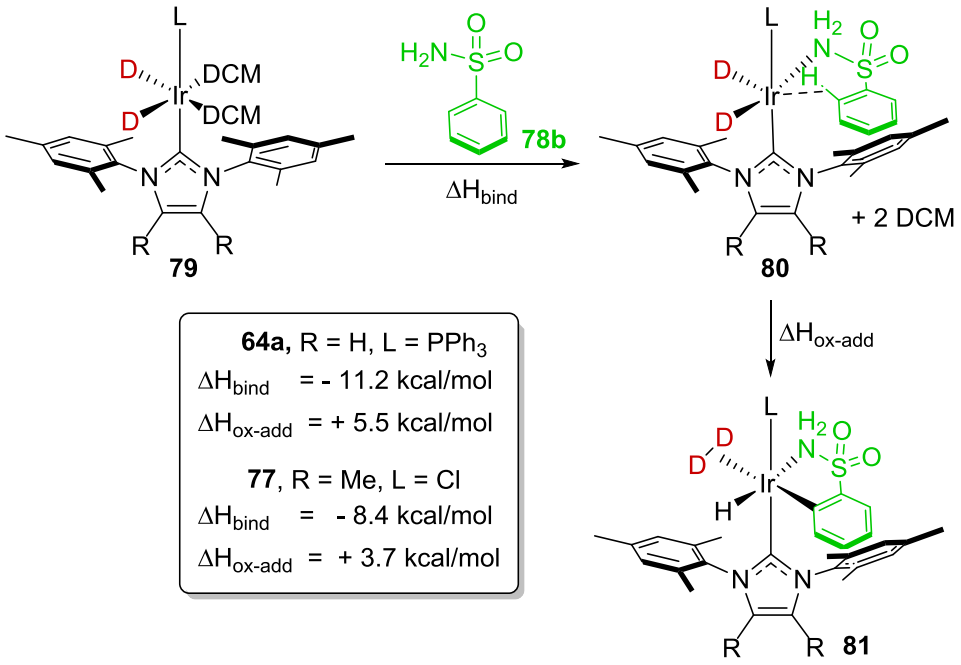

Scheme 2.38 Calculated binding and C-H insertion for sulfonamide directed HIE.

Notably, when examining the reverse selectivity in *Celecoxib* **D70**, the substrate catalyst binding was found to be key. It clearly indicated that the larger NHC/phosphine complex **64a** could more readily accommodate the planar pyrazole directing group than the tetrahedral sulfonamide, matching the previous experimental findings. Pleasingly, and in contrast, the smaller NHC/chloride complex **77** was better able to accommodate the sulfonamide in intermediate **82** and notably was observed to be stabilised by a hydrogen bond between the chloride and the amino group (**Figure 2.7**).

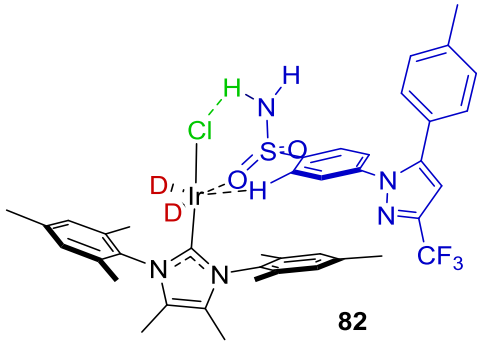

Figure 2.7 Binding of *Celecoxib*, including proposed H-bonding.

However, despite these considerable advances by Kerr *et al* in the last decade, several areas of HIE still remain unexplored. In particular, these are furthering the directing groups that can facilitate exchange, improving the diversity of positions where exchange is possible, and further understanding the selectivity within the established systems. Some of these areas are explored within this thesis, and are briefly introduced in the next section.

2. Proposed Work

Within the Kerr group, a wide variety of novel complexes bearing NHC/phosphine or NHC/chloride ligand combinations have been successfully applied in an array of HIE processes.[43,45,46,48,49] Most recently, these studies were extended to include tetrazoles **76b**, which react efficiently under basic conditions.[47] With this in mind, the first aim of this project will be to develop a means of performing HIE upon the carboxylic acids isostere, such as **83**, which still represent a challenge for iridium-catalysed HIE due to their poorly ligating nature (**Scheme 2.39**).

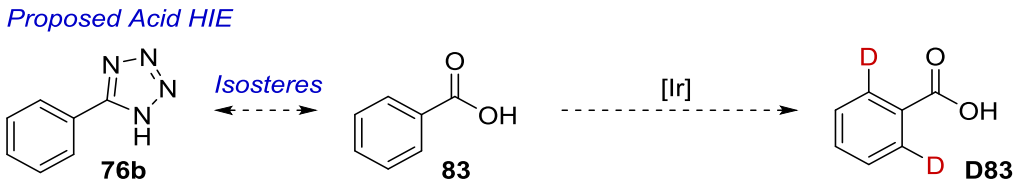

Scheme 2.39 Carboxylic acid HIE.

Moving from the challenge of new directing groups to direct exchange, it is well established that drug discovery has moved towards decreasing levels of planarity within the drug design process, as a means of increasing diversity.[50] One way in which this is being achieved is to remove aromaticity from target molecules. This poses an interesting question for the labelling chemist; how to incorporate a label in a molecule that does not contain an aryl ring? In an effort to address this, studies here would focus upon the selective labelling of non-aryl-sp^2 centres, as in **84**. Such C-H activation has been reported stoichiometrically by iridium catalysts since the late 1980s,[51] however it has yet to be realised catalytically. However, problems arise when considering that the conditions typically used for HIE are similar to those for olefin hydrogenation.[43,52] As such, it will be key to generate catalytic conditions that favour exchange over hydrogenation (**Scheme 2.40**).

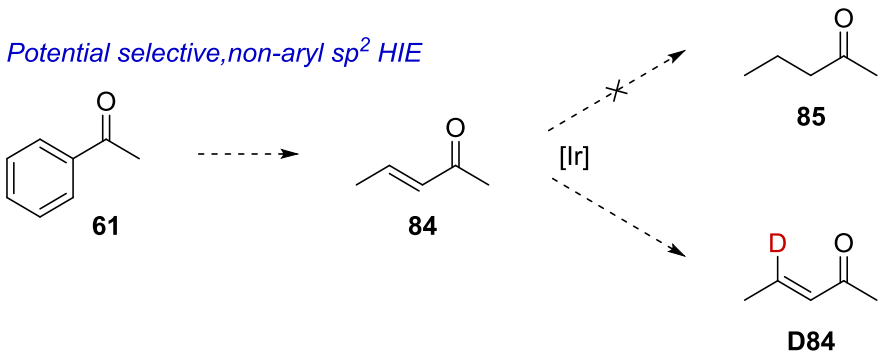

Scheme 2.40 Non-aryl sp^2 HIE.

In a complimentary fashion, the next goal would be to target the labelling of sp^3 hybridised C-H bonds, as in **85**. This truly represents the cutting edge of C-H activation technology, examples of which have already been reported in HIE with Crabtree's catalyst **30**.[30,53] However, as is typical of applications of this catalyst, high loadings are required (≥50 mol%), and only a very limited substrate scope has currently been examined. As such, a demand still exists for effective and general catalytic exchange at sp^3 centres. Indeed, the proposed first target would be to facilitate exchange at activated C-H bonds,[54] such as those adjacent to a heteroatom or electron withdrawing functionality. With this in mind, and due to their ubiquitous nature within drug design,[55] the labelling of saturated heterocycles presents an appealing opportunity (**Scheme 2.41**).

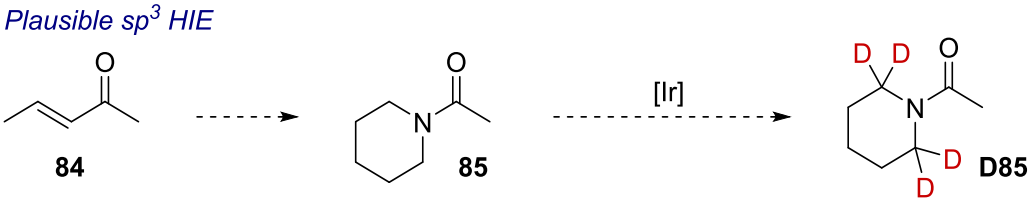

Scheme 2.41 sp^3 HIE.

Overarching each proposed project is the aim to understand the mechanism behind each new process and, any selectivity that is present within them.

3. Results and Discussion

3.1. Acid Directed HIE

In light of the chemical similarities between carboxylic acids and tetrazoles it was envisaged that the conditions for labelling tetrazoles could potentially be applied to exchange on carboxylic acids.[47] To initiate this study, carboxylic acid **86a** was chosen for its ease of analysis by LCMS, however, only low levels of incorporation were observed, and so the process required further investigation (**Scheme 2.42**).

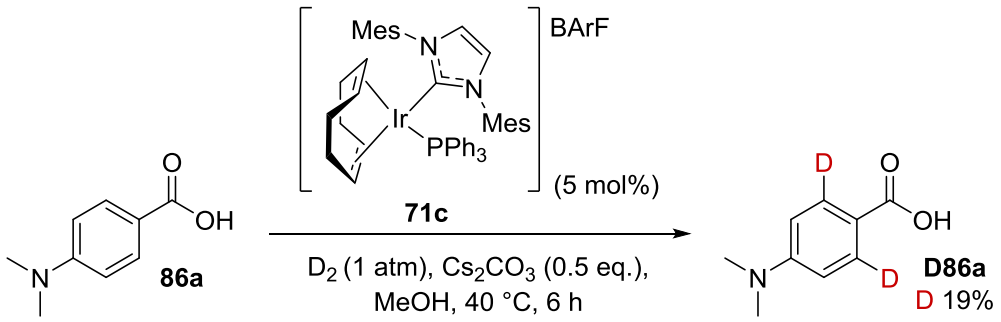

Scheme 2.42 Initial labelling of carboxylic acid **86a** under non-optimised conditions.

The first consideration in improving the reactivity of the model system was to change the base, as conceivably, a carbonate base could bind to iridium in a similar fashion to the deprotnated acid substrate. As such, in place of caesium carbonate, the non-coordinating organic base di-iso-propylethylamine (DIPEA) was utilised. Secondly, in typical HIE reactions utilising catalyst **71c**, methanol is a poor solvent, and so a range of alternative solvents were be tested, including alcohols, ethers and esters (**Scheme 2.43**, **Graph 2.2**). When utilising Cs_2CO_3 as the base, in alcoholic media, methanol and isopropanol proved to be similar, with tAmylOH somewhat worse, reflecting the solubility of Cs_2CO_3 in these solvents. Moving to ester-based solvents did not improve the incorporation, neither did ethereal solvents 2-MeTHF and CPME. However, with the more non-coordinating MTBE, moderate incorporation was observed. A more dramatic improvement, was made by changing the base to DIPEA. Despite initial indications in MeOH, the switch of base improved the incorporation in every solvent, including, most notably, MTBE. At this point it was also noted that even a small increase in temperature could have a drastic impact upon the degree of incorporation. As such, the temperature was increased to 50 °C for further testing.

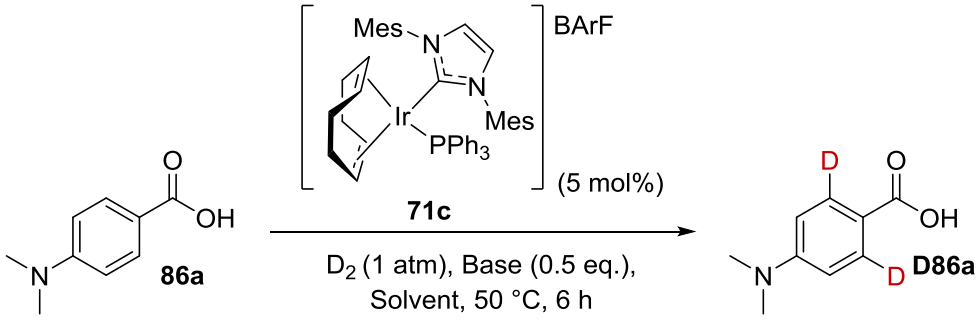

Scheme 2.43

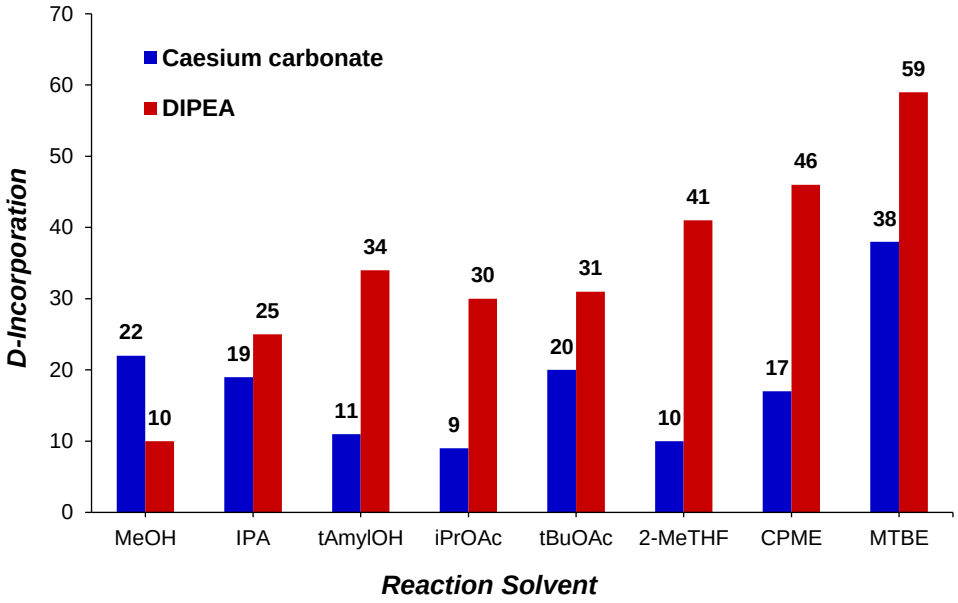

Graph 2.2 Solvent and base screen.

Having chosen MTBE as solvent and DIPEA as base for further investigations, changes in the catalyst structure were then examined in an attempt to improve the incorporation (**Scheme 2.44**). The complexes chosen were those found to be active in previously in HIE or hydrogenation. It was noted at this point that both a phosphine/NHC ligand sphere and a non-coordinating counterion were necessary for exchange to occur, as can be seen in the poor performance of complexes **63a**, **30** and **64a**. Pleasingly, all other complexes performed well, with complex **87a** delivering the highest levels of incorporation. This could perhaps be attributed to the complex bearing the flexible but bulky tribenzyl phosphine conferring the best balance of thermal stability and reactivity.

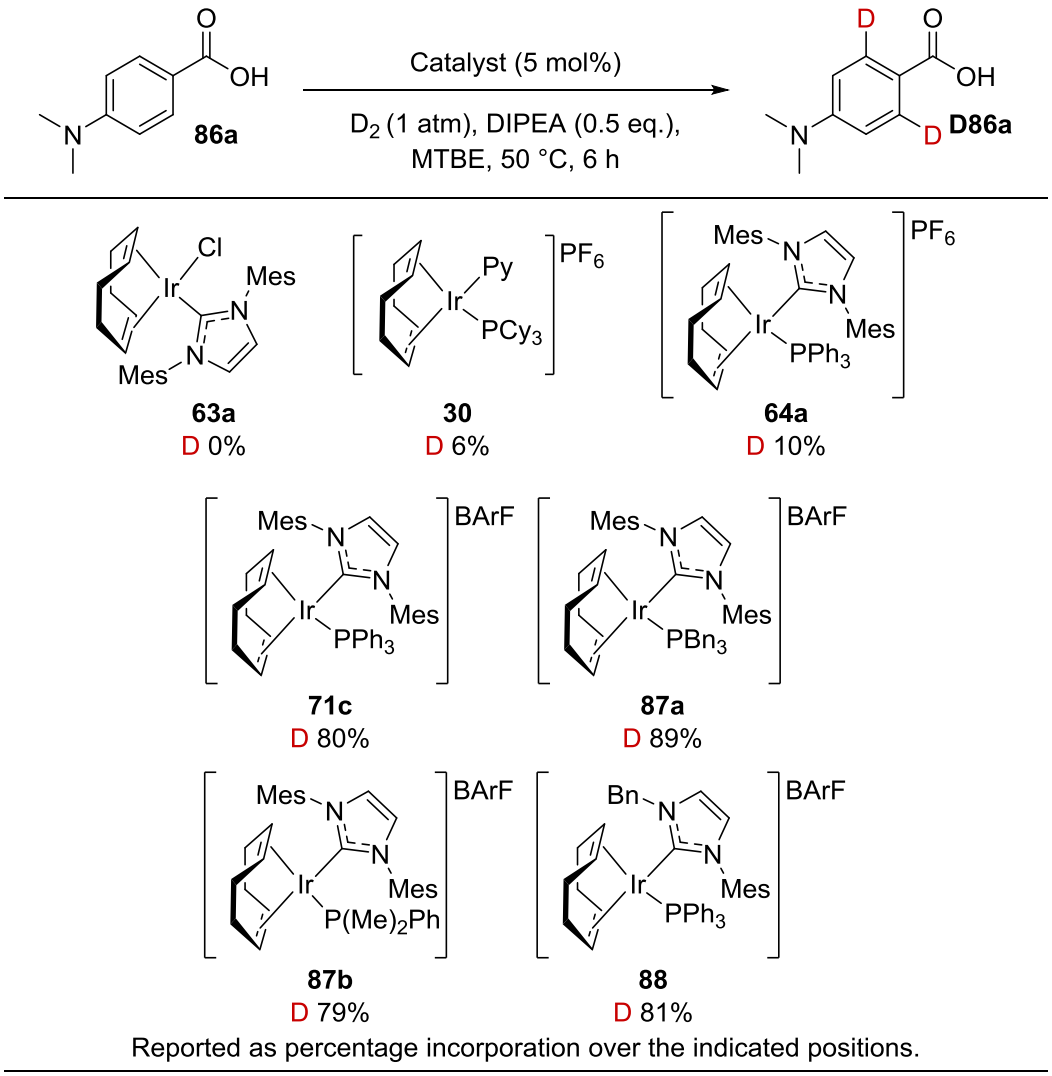

Scheme 2.44 Catalyst screen.

Having attained high levels of incorporation with catalyst **87a**, it was then decided to test further substrates under these pre-optimization conditions (**Scheme 2.45**). In part, this was due to the presene of a basic site in the model substrate. Based on this, could DIPEA be omitted from the reaction coditions and still maintain a high incorporation? Secondary to this, the change in pKa across substituted benzoic acids is well recognised in the literature and any changes in reactivity correlating to this could implicate the deprotonation within the reaction mechanism.[56] In efforts to test this hypothesis, six *p*-substituted carboxylic acids were tested both with and without DIPEA, at a slightly lower catalyst loading (2.5 mol%) so any changes in reactivity would be more apparent. The initial model substrae D**86a**, delivered an elevated incorporation without base. This trend was continued across each substrate be they

electron rich as in D**86b-c**, electron poor D**86d-f**, or unsubstituted **D86g**. These results indicated that the base plays no part in the reaction, other than to serve as a mild inhibitor.

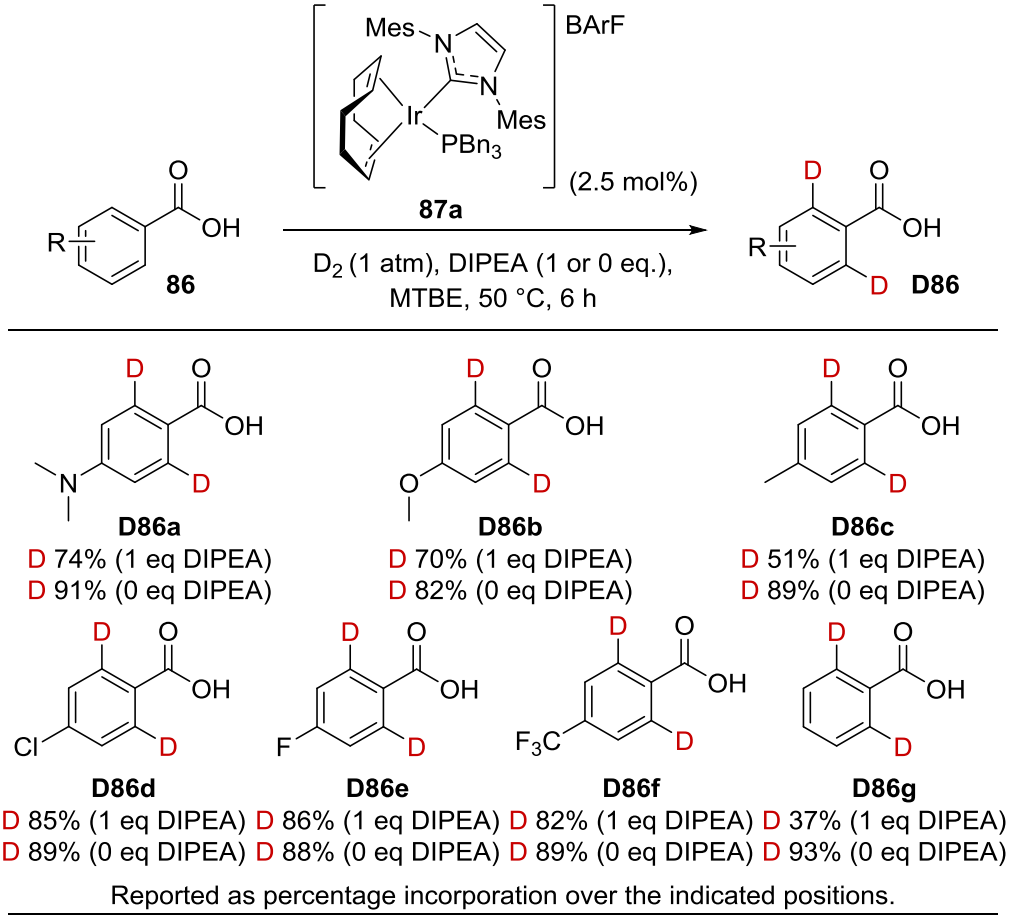

Scheme 2.45 Investigating the role of base in the reaction.

With this somewhat surprising finding, we reassessed the solvent choice for this reaction, this time omitting the base (**Scheme 2.46**, **Graph 2.3**). When the reaction was performed in methanol, this time no reactivity was observed, indicating as previously discussed in the tetrazole work, that when a base is present the reaction can progress *via* a different pathway.[47] However, in line with our other investigations both IPA and *t*AmylOH delivered some incorporation. The ester and ether based solvents each performed more effectively than when either DIPEA or Cs_2CO_3 was present, with increases noted as more sterically congested solvents were applied, leading to MTBE remaining optimal.

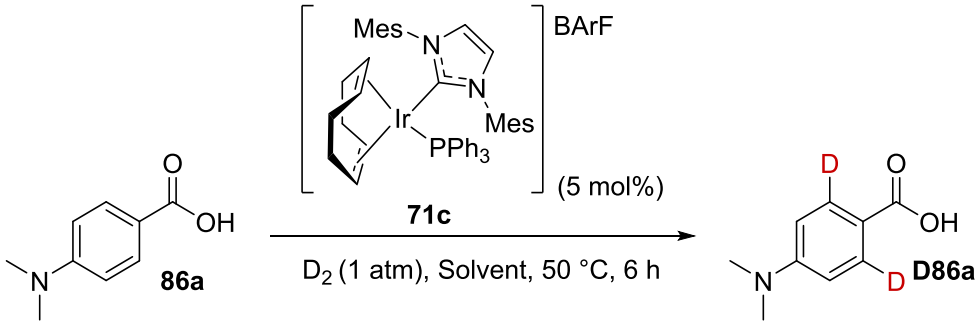

Scheme 2.46

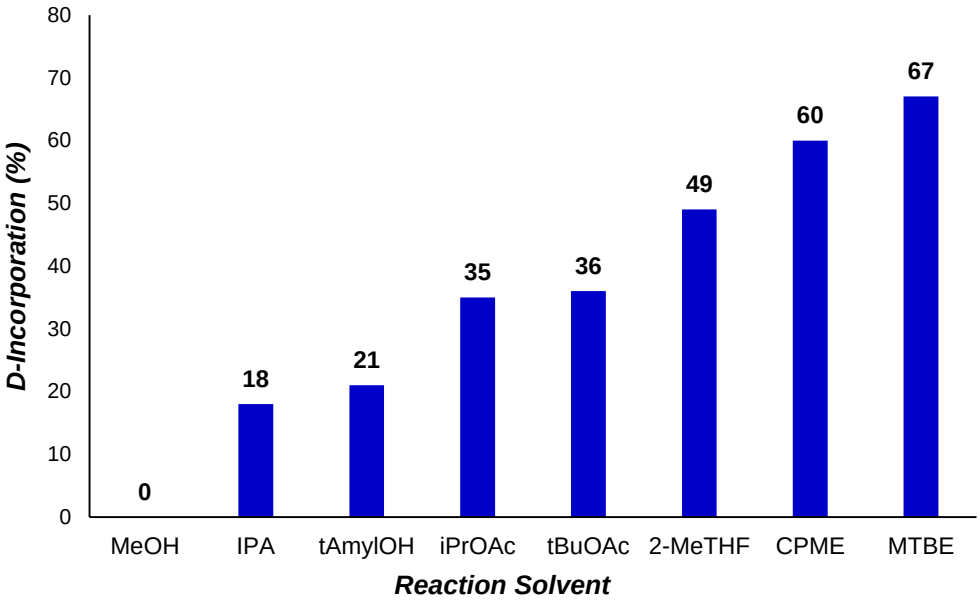

Graph 2.3 Reassessing the solvent scope without base.

Following the optimization of the solvent, catalyst and use of base, we next sought to examine the continuous variables of catalyst loading, reaction time and reaction temperature (**Scheme 2.47, Table 2.4**). To do this a three-factor, two-level design of experiment (DoE) was employed, in an effort to minimise the number of experiments while maximising the chemical space incorporated into the optimization. Notable comparisons from this study include; entry 1 vs 3, which indicates the necessity of a mildly elevated temperature, and entry 10 vs 11, indicating the need for increased catalyst loading.

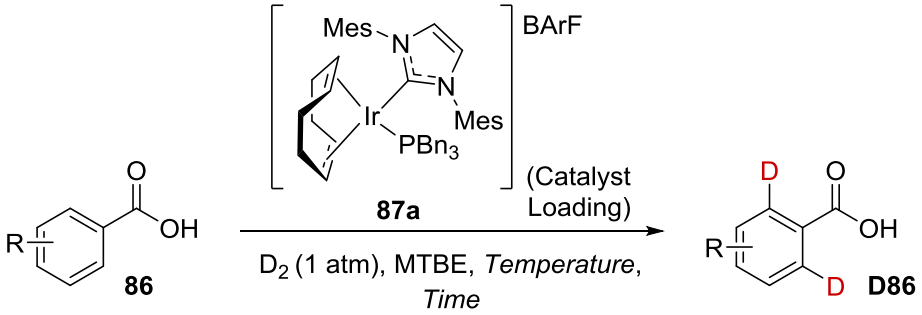

Scheme 2.47

Entry[a]	*Catalyst loading (mol%)*	*Reaction time (min)*	*Reaction Temperature (°C)*	*D-incorporation (%)*[b]
1 (+++)	7.5	240	55	90
2 (---)	2.5	120	25	39
3 (+--)	7.5	240	25	60
4 (***)	5.0	180	40	73
5 (***)	5.0	180	40	75
6 (***)	5.0	180	40	78
7 (-+-)	2.5	240	25	49
8 (-++)	2.5	240	55	87
9 (+--)	7.5	120	25	51
10 (--+)	2.5	120	55	72
11 (+-+)	7.5	120	55	87

[a] symbol in parentheses indicate points in the design; + high, * mid and – low. [b] Incorporation is measured as the percentage incorporation calculated by LCMS, over the two *ortho*-positions.

Table 2.4 Design of experiments; without base present.

Furthermore, the statistical software in use for this optimisation provides a good visual representation inferring the significance of each factor, be it positive or negative in effect, in the form of a half-normal plot (**Table 2.4**). In these plots, the most significant factors lie furthest from the line, and the least significant closest. Indeed, from this we can deduce that the most significant factor in this process is temperature. Furthermore, the catalyst loading and reaction time are less important, but still have an impact upon the reaction.

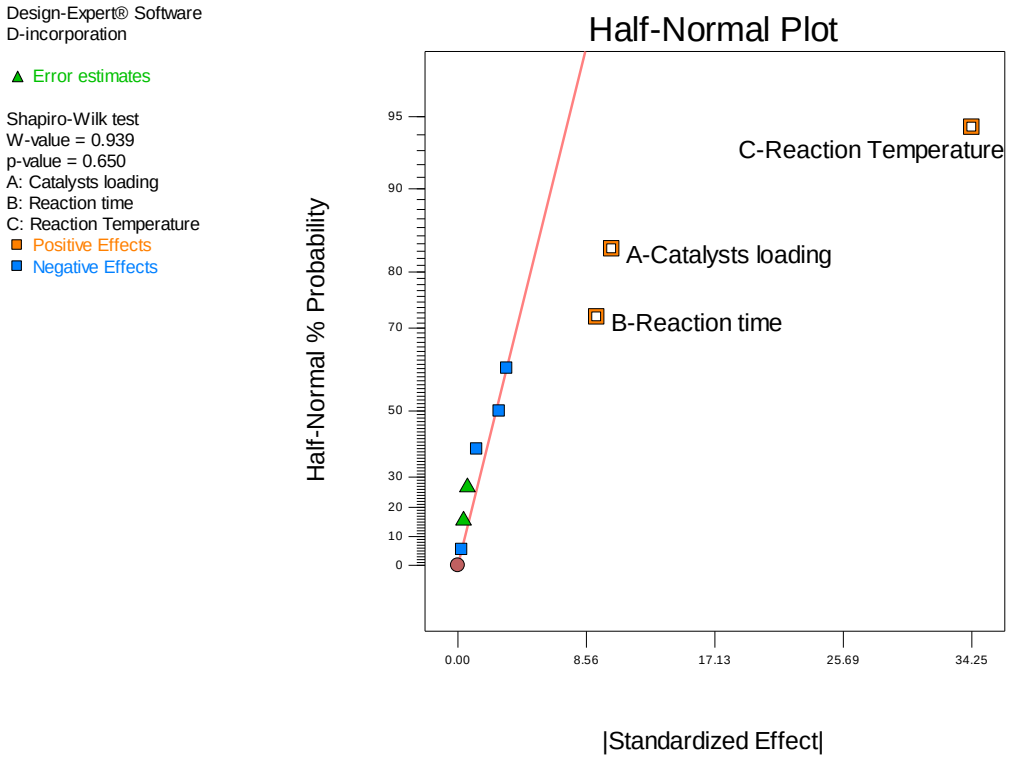

Graph 2.4 Half-normal plot.

With improved understanding of the significance of the factors chosen for optimization, conditions were next chosen to deliver high incorporation, whilst minimising the reaction time and catalyst loading. Following on from this, we investigated a range of carboxylic acids to understand the range of labelling that this new protocol could achieve. Commencing the study with a range of *p*-substituted acids (**Scheme 2.48**), it quickly became apparent that the *p*-dimethylamino group **86a** hindered the reaction slightly, despite delivering a good overall incorporation, with all substrates **86b-g** givin high levels of incorporation. Furthermore, no substrate **86a-g** showed a significant deviation in level of incorporation, indicating that there is a low dependence upon the substrate electronics for this reaction.

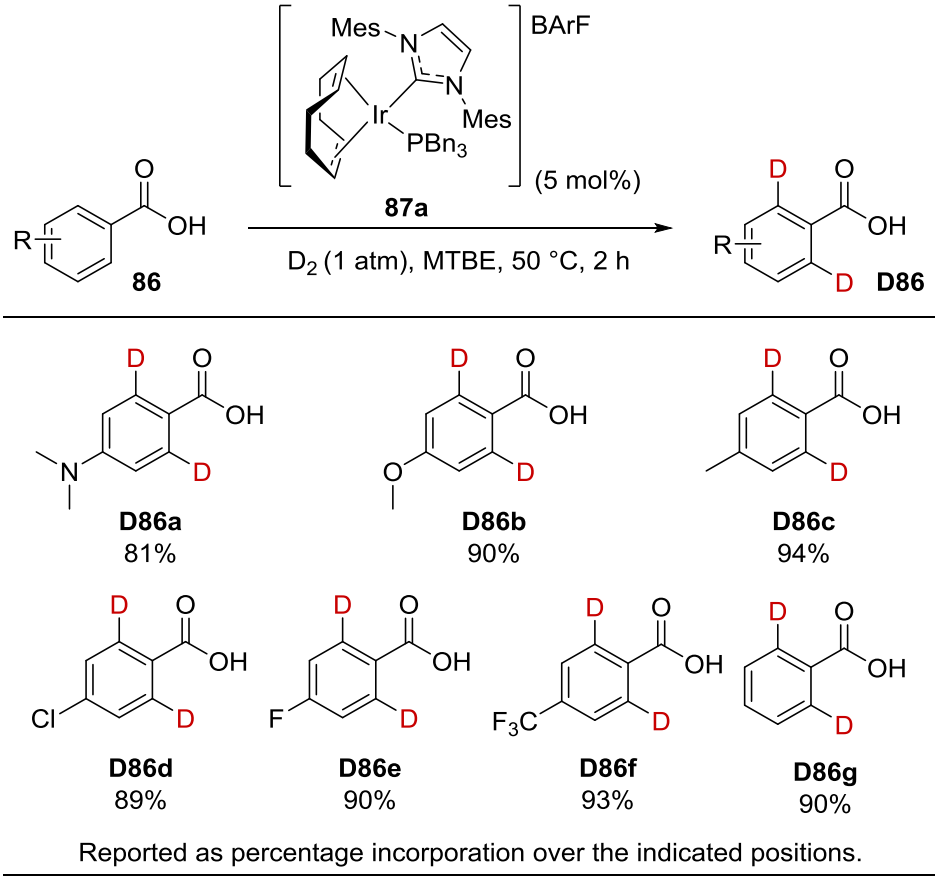

Scheme 2.48 Investigating electronic effects upon the HIE reaction.

To assess the impact of steric congestion around the labelling site and directing group further, *meta*- and *ortho*-substituted acids were eamined (**Scheme 2.49**). Continuing the previous trend, 3-(dimethylamino) benzoic acid **D86h** performed poorly, labelling to low levels at the 2-position only. This can be explained by two effects. Firstly, a pincer-type complex could be formed between the acid and amino group to form a thermodynamically stable intermediate that does not readily progress in the reaction. Secondly, the dimethyl amino group is a strongly electron-donating substituent and therefore can increase the strength of the aryl C-H bonds at positions *ortho*- and *para*- to itself. The same effect is observed to a much lesser degree in 3-methoxy benzoic acid **D86i**, in which case only a small disparity is observed between labelling sites, and there is good overall incorporation. Unfortunately, the trend could not be observed in other *meta*-substituted substrates as the signals for both *ortho*- positions overlap in both substrates **D86j-k**. However, with such high overall incorporations observed, any difference between *ortho*- positions must be small. Pleasingly, when both *meta*-positions are blocked, excellent incorporation is still observed, as in substrate **D86l**.

Progressing to *ortho*-substitution, proved to deliver the same exceptional levels of incorporation **D86m-p** as had been observed in the previous substrates. The notable exception here was salicylic acid **D86q**, which delivered a diminished level of incorporation. This can perhaps be attributed to a stable chelate being formed between the phenol and acid moieties. Unsurprisingly, 3-nicotinic acid **D86r** and its *N*-oxide **D86s** both delivered no incorporation, as these functional groups are known inhibitors in transition metal catalysis.[57]

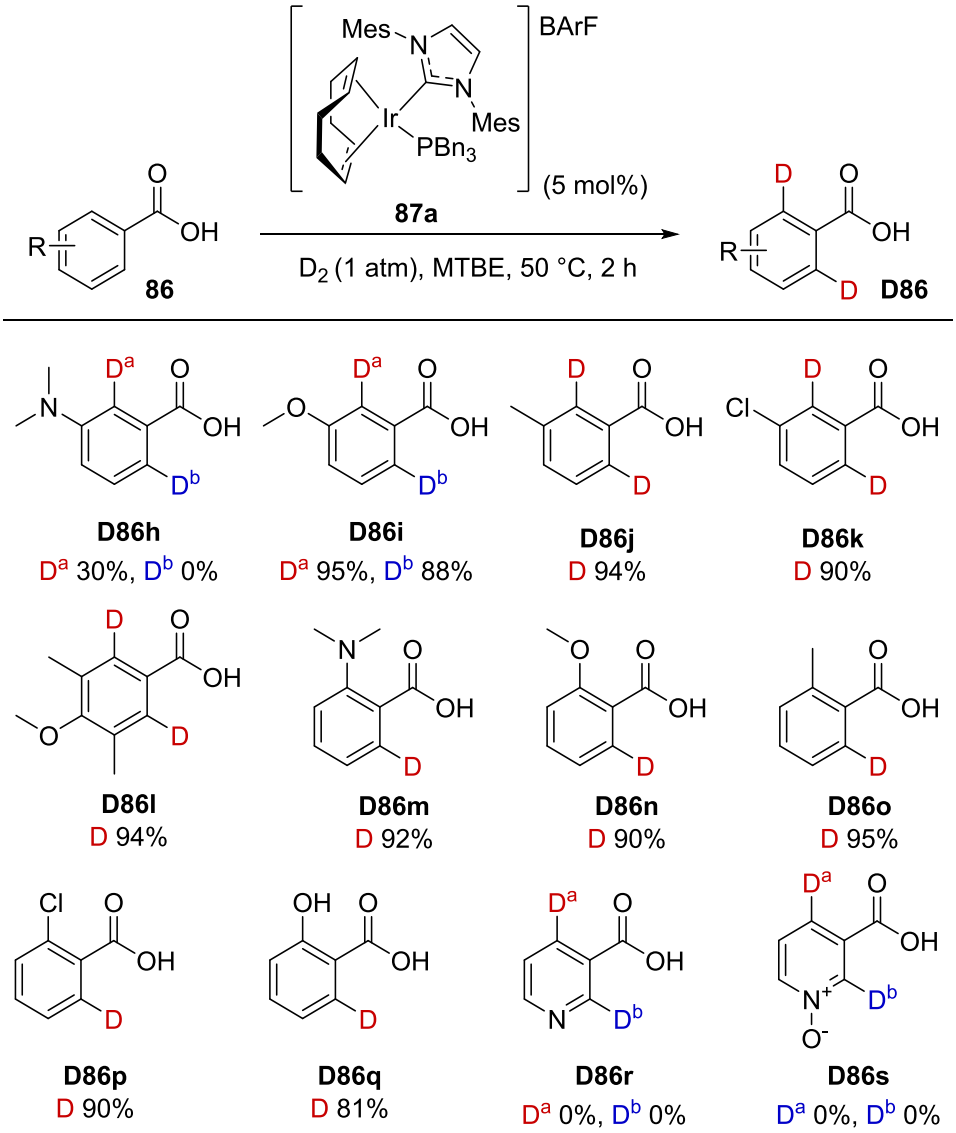

Scheme 2.49 Further substrate investigation.

Having successfully developed conditions for the HIE of benzoic acids, we next considered a small number of phenylacetic acid derivatives for testing under the same

conditions (**Scheme 2.50**). This substrate class is desirable as it is found in many common active pharmaceutical ingredients (API), such as *ibuprofen*. However, none of the chloro-substituted phenylacetic acids **D89a-c** showed any incorporation. Even when constraining the acid, as in **D86d**, so it would be appropriately orientated for exchange, no incorporation was observed. The poor reactivity of this series can therefore be attributed to the increased ring strain generated in the formation of a 6-mmi, for C-H activation of phenylacetic acids, over that of a 5-mmi, for benzoic acids.

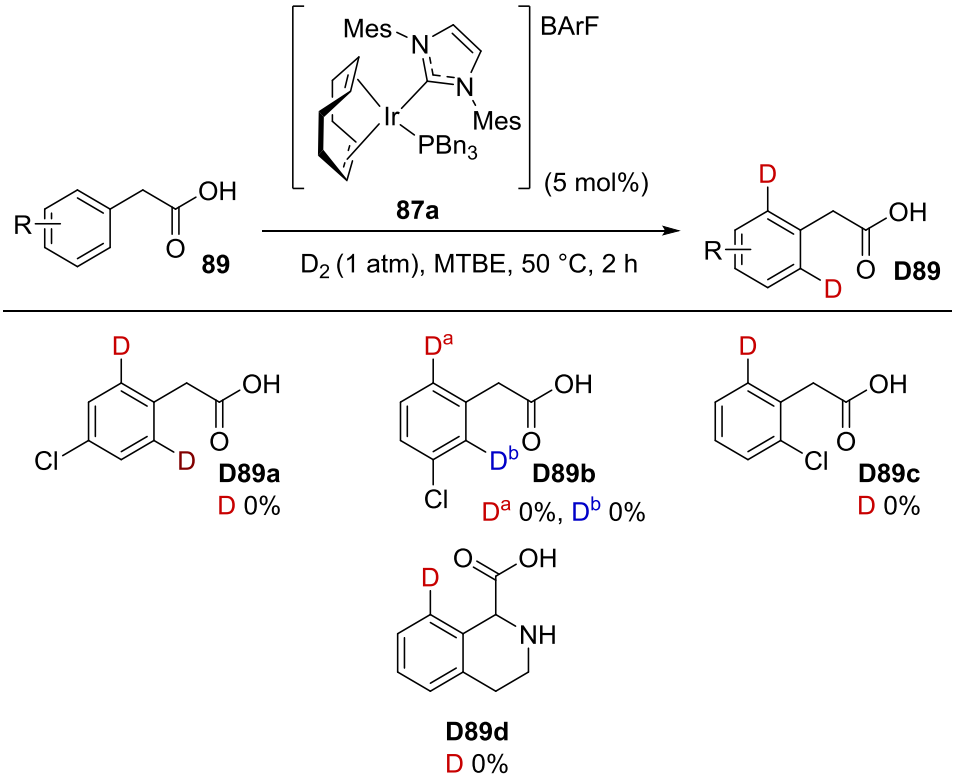

Scheme 2.50 Application of HIE conditions on arylacetit acids.

The final substrate to be assessed was 4-nitrobenzoic acid **86t**. This substrate was chosen as it has the potential to undergo exchange at two distinct *ortho*-positions (**Scheme 2.51**). However, under the conditions optimised for exchange adjacent to the acid, each of the four *ortho*-positions labelled to an equal degree.

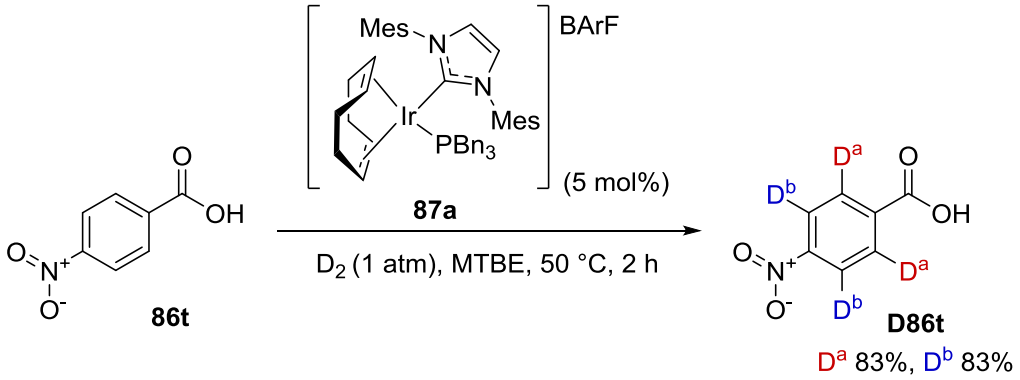

Scheme 2.51 Selectivity of HIE in substrate **D86t**.

With the competition between two directing groups delivering the same level of incorporation from both, the next question we wished to answer was; is this true of all directing groups? In an effort to answer this question we utilised a technique previously popularised by Glorius *et al.* for testing the robustness of a catalytic system.[58] This approach involves testing a model reaction by spiking it with 1 equivalent of an additive and observing the reaction outcome. Through a modified method, the study we performed can be separated into two parts: substrates which can label competitively; and additives which may participate in a side reaction or inhibit the reaction. To enable rapid analysis by LCMS, all of the substrates would contain an anisole ring. Therefore, to ascertain if this simple functional group would hinder the reaction, testing began with 4-methyl anisole **90a**, and the reaction progressed as normal, validating the use of this group within the additive. Therefore, we then turned our attention to functional groups that may participate in a side reaction or inhibit the reaction (**Table 2.5**). The first additives tested contained functional groups that could bind competitively with the substrate and inhibit the reaction. Pleasingly, in the presence of an alcohol **90b** or a phenol **90c** the reaction progressed as normal. However, with a primary primary amine **90d** or an aniline **90e**, complete inhibition of the labelling reaction was observed, notably with no reduction in the recovered yield yield. Unsurprisingly, the reaction was also halted in the presence of nitrile group **90f**, as it is well known to ligate strongly to iridium. Moving away from inhibitors and towards reactive species, we next applied boronic acid **90g** and pinacol boron **90h**, and in both cases the labelling reaction proceeded uninhibited. However, in the case of boronic acid **90g**, a decrease in yield was observed, presumably due to deborylation. As expected, aryl bromide **90i** remained intact with no sign of dehalogenation. Finally,

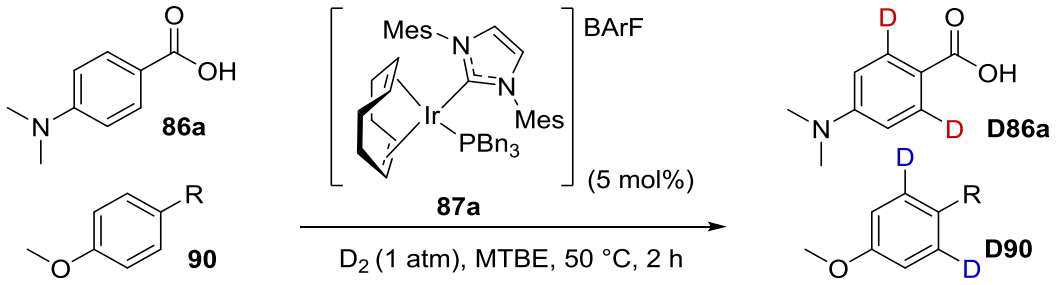

Entry[a]	R	Additive Yield (%)	Substrate 86a D-incorporation (%)	Substrate 86a Yield (%)
1	90a	92	89	99
2	90b	99	86	99
3	90c	98	78	99
4	90d	99	0	99
5	90e	94	0	99
6	90f	99	0	99
7	90g	69	83	98
8	90h	99	85	99
9	90i	99	79	99
10	90j	0	75	99
11	90k	0	69	95

[a] Incorporation and yield calculated from LCMS analysis.

Table 2.5 Competition reactions; investigating the functional group tolerance.

application of olefinic functionalities such as alkene **90j** and alkyne **90k** allowed the reaction to progress as normal. However, the olefin was completely consumed in both cases, and through careful analysis of the LCMS data it was deduced that both olefins had been reduced to the same 4-ethylanisole by-product. In summary, strongly coordinating groups inhibit the reaction, there is no noticeable reaction between the

catalyst and common coupling partners, and, finally, olefin reduction takes place alongside the labelling reaction.

We next applied a series of additives known to undergo exchange under previously optimised conditions, and which could exchange competitively with the acid (**Table 2.6**).[45,47] Pleasingly, the competition reaction with **90l** matched the incorporation previously achieved with substrate D**86t**, with near to equal labelling at each position, validating the use of competition reactions as a means of investigating substrate selectivity. Similarly, applying ketone **90m** gave similar incorporation in both substrate and additive. Differences began to emerge with a pyridine directing group

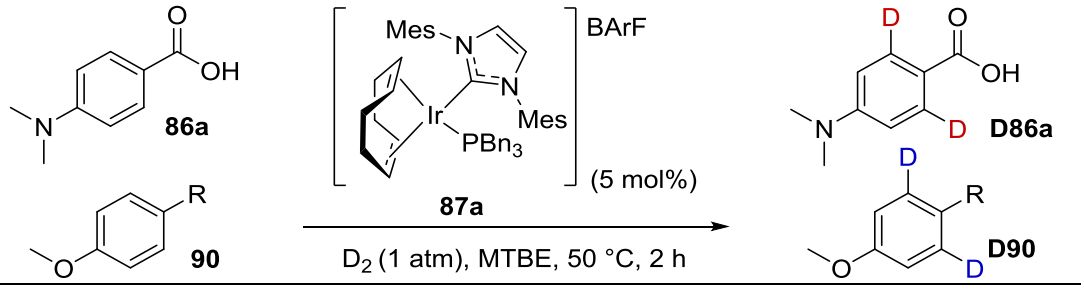

Entry[a]	R	Additive D-incorporation (%)	Additive Yield (%)	Substrate 86a D-incorporation (%)	Substrate 86a Yield (%)
1	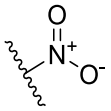 **90l**	81	95	79	95
2	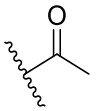 **90m**	83	92	77	99
3	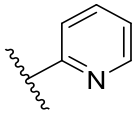 **90n**	44	98	0	91
4	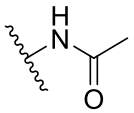 **90o**	54	99	68	99
5	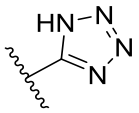 **90p**	9	94	0	99
6[b]	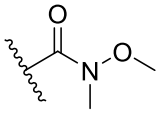 **90q**	90	99	76	90

[a] Incorporation and yield calculated from LCMS analysis; [b] Incorporation measured over the two ortho and three N-methyl positions.

Table 2.6 Competition reactions; investigating the selectivity of exchange.

90n, which favours incorporation into the additive, matching the results with substrate **D86r**.[43] When the additive contained a directing groupd that could label *via* a 6-mmi, as in acetamide **90o**, the expected favoured 5-mmi in the substrate produced the greater incorporation. Somewhat surprisingly, the addition of a tetrazole **90p** to the reaction mixture halted the exchange on the acid **86a**, and delivered only minimal exchange on the tetrazole. Finally, in applying Weinreb amide **90q**, exchange continued unhindered on the substrate **86a**. However, exchange also took place on the *ortho*- and *N*-methyl positions of the amide. Such exchange has been noted previously within other amide functionalities.[45]

From understanding gained from previous studies on tetrazoles, namely that addition of base to an acidic substrate can change the selectivity of such competition reactions, we utilised DoE again to optimise conditions employing one equivalent of DIPEA, in this case investigating catalyst loading, reaction temperature and reaction time. Similarly, this optimisation indicated that temperature was the most important factor for an affective reaction. However, it also inferred an increased dependence upon the catalyst loading, which is reflected in the chosen conditions (7.5 mol% catalyst, 55 °C and 2 h). In the same fashion as previously, we then repeated the competition reactions, and found that for many of the additives no change was evident except a mild reduction in substrate incorporation **90a-c**,**f**,**h** and **i** (**Table 2.7**). However, a notable change was observed with primary amine **90d** and aniline **90e**, in which incorporation was observed in the substrate, whereas, previously, the reaction had been completely inhibited. Additionally, the yield of the boronic acid additive **90g**, was elevated to excellent levels, indicating that the degradation could be acid catalysed. Similarly, low yield of alkene **90j** was recovered, compared with the complete hydrogenation in the absence of base. However, in contrast with this, alkyne additive **90k** completely shut down the exchange process, despite delivering a low recovered yield of additive. Noticeable from the LCMS analysis of this reaction, was the presence of alkene additive **90j**, clearly indicating an incomplete reduction, and that the order of reactivity was alkyne reduction first, followed by alkene reduction and exchange.

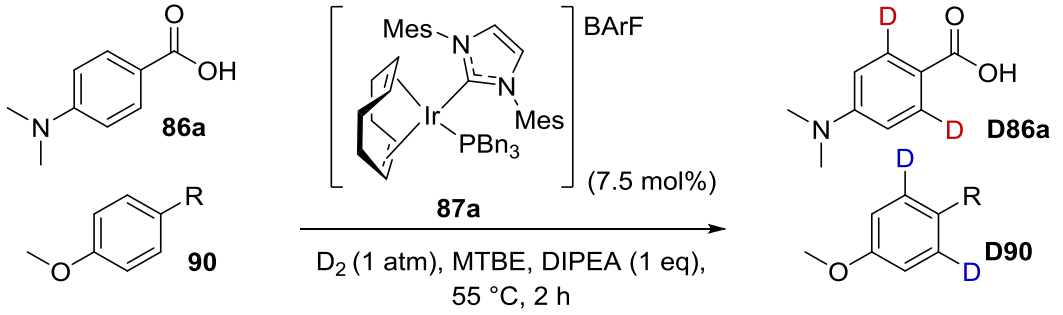

Entry[a]	R	Additive Yield (%)	Substrate 86a D-incorporation (%)	Substrate 86a Yield (%)
1	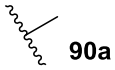 **90a**	89	80	99
2	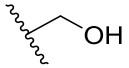 **90b**	99	79	99
3	 **90c**	99	70	99
4	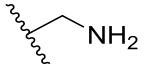 **90d**	99	20	99
5	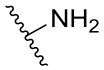 **90e**	99	66	99
6	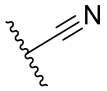 **90f**	99	0	99
7	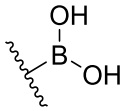 **90g**	92	84	99
8	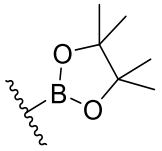 **90h**	93	77	99
9	 **90i**	99	76	99
10	 **90j**	18	81	99
11	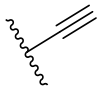 **90k**	23	0	91

[a] Incorporation and yield calculated from LCMS analysis; [b] No mass ion observed.

Table 2.7 Competition reactions; investigating the functional group tolerance (with base).

Next, we reassessed the competition between exchangeable substrates, and from the outset a marked difference was observed (**Table 2.8**). Pleasingly, reactions with both nitro **90l** and ketone **90m** substrates now strongly favoured exchange on the acid substrate. Furthermore, pyridine additive **90n** increased the incorporation within both additive and substrate. Improving upon the moderate selectivity observed without

base, substrate exchange was completely favoured over acetamide **90o**. Disappointingly, tetrazoles **90p** still completely inhibited the reaction. The most significant reversal, however, was for Weinreb amide additive **90q**, in which no label was present but a high incorporation into the acid substrate was maintained.

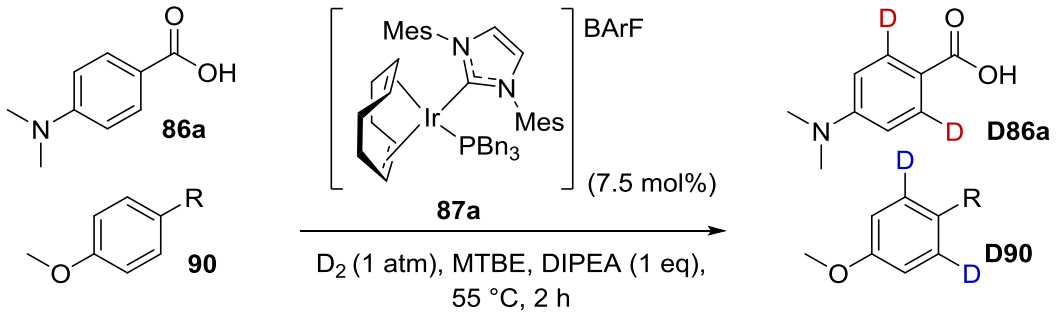

Entry[a]	*Additive*	*Additive*		*Substrate 86a*	
		D-incorporation (%)	*Yield (%)*	*D-incorporation (%)*	*Yield (%)*
1	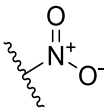 **90l**	10	91	82	99
2	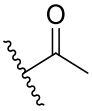 **90m**	27	95	82	94
3	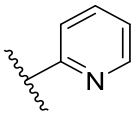 **90n**	77	94	24	99
4	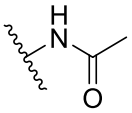 **90o**	5	99	69	99
5	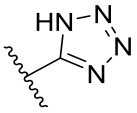 **90p**	9	99	6	99
6[b]	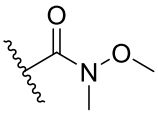 **90q**	0	99	70	99

[a] Incorporation and yield calculated from LCMS analysis; [b] Incorporation measure over the two ortho and three N-methyl positions.

Table 2.8 Competition reactions; investigating the selectivity of exchange (with base).

Pleasingly, these investigations were further validated by reapplying failed substrates **D86r-s** and non-selective 4-nitrobenzoic acid **D86t** (**Scheme 2.52**). Both 3-nicotinic acid **D86r** and its *N*-oxide **D86s** now delivered a low incorporation, in agreement with

the competition reactions. Furthermore, exchange within nitro versus acid competition substrate **D86t** was favoured *ortho*- to the carboxylic acid.

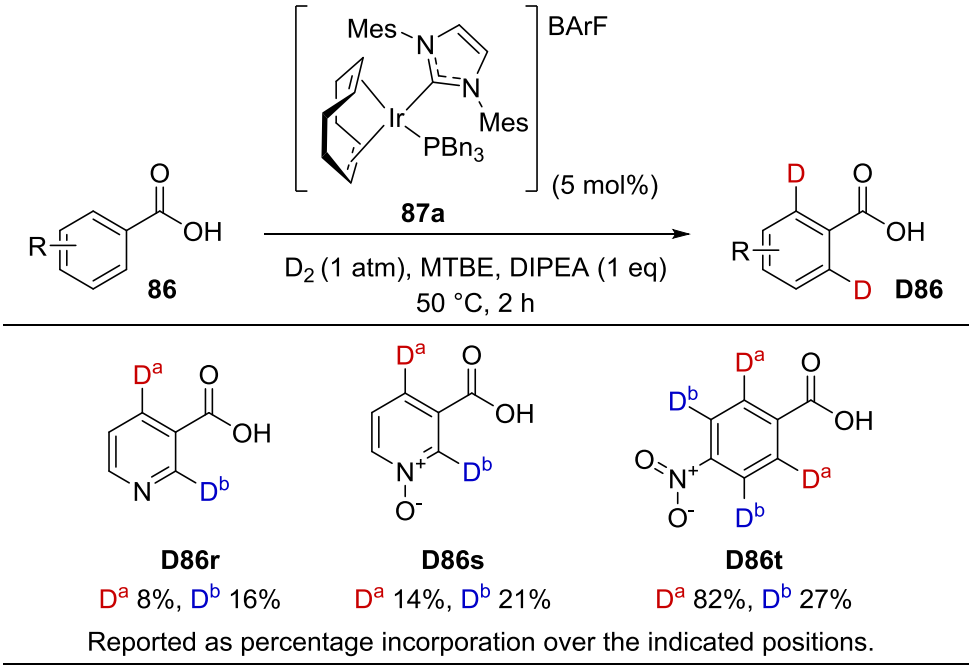

Scheme 2.52 Reassessing selected substrates under basic conditions.

Finally, to fully expand the utility of our new HIE protocol, we examined a number of drug compounds under our optimised conditions without base present (**Scheme 2.53**). Pleasingly, *Probenecid* **D91**, used in the treatment of gout, delivered high incorporation, selectively adjacent to the carboxylic acid, and with negligible incorporation adjacent to the tertiary sulfonamide. Furthermore, the common drug *Aspirin* **D92** delivered excellent levels of incorporation solely *ortho*- to the acid directing group. In addition, the anthranilic acid derivative *Mefanamic acid* **D93**, gave a hoghly incorporation but a slightly reduced in comparison to *Aspirin* **D92**. This is perhaps indicative of inhibition due to the secondary amine functionality, as has been observed in the competition reactions with primary amines.

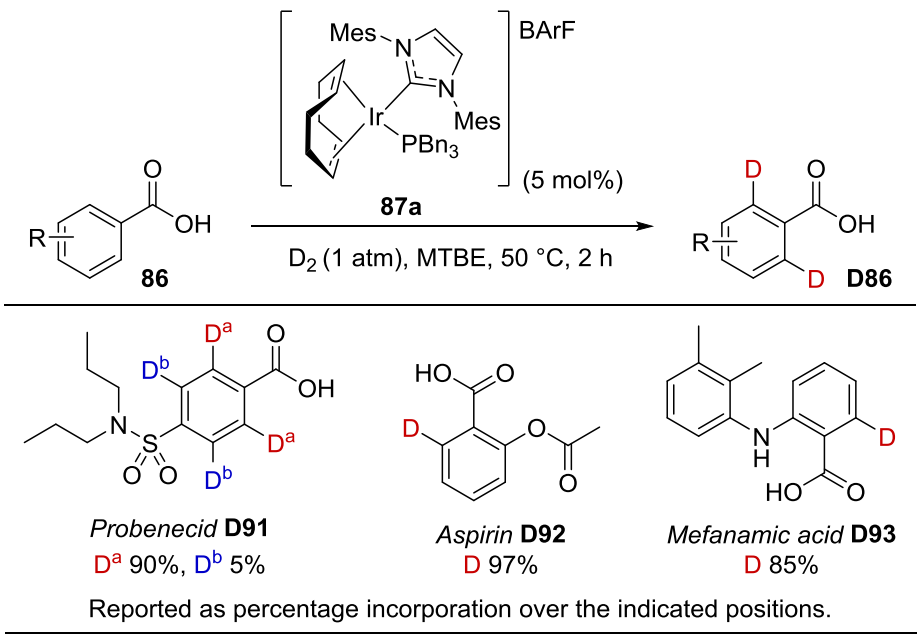

Scheme 2.53 HIE on carboxylic acid-containing drugs.

To conclude, we have developed a novel process for performing HIE on benzoic acids without the need for basic conditions, utilising our highly active iridium(I) NHC/phosphine complexes. Furthermore, we have applied the DoE-optimised conditions across a range of substrates and have thoroughly investigated the functional group tolerance of the reaction. Within this investigation, we mimicked a more complex system by utilising a series of competition reactions, and found that the addition of base can drastically change the selectivity within them. Finally, we validated the utility of the process by performing HIE on several drug compounds, all with high levels of incorporation.

3.2. Non-Aryl sp^2 HIE

Despite the wide array of functional groups that can direct iridium-catalysed HIE, a common factor is that the positions labelled are in general, aromatic. Furthermore, it is recognised that the pharmaceutical industry is striving to impart a greater degree of three-dimensionality within the drug design process in an effort to generate greater compound diversity.[50] As such, a means of introducing an isotopic label within compounds that do not contain an aryl unit is of increasing importance. Therefore, we initiated a project to investigate the potential for HIE at non-aryl positions.[59]

Through our previous investigations, we firstly recognised that planar substrates, labelling via a 5-mmi, performed excellently with our phosphine/NHC catalyst system. Secondly, it is generally recognised within the literature that as we move from aryl to alkyl positions that any C-H activation event would be more demanding, due to the decreasing π-character of the bond and increasing steric clash with the metal (**Figure 2.8**).[60] In light of this, we first targeted HIE at alkenyl positions.

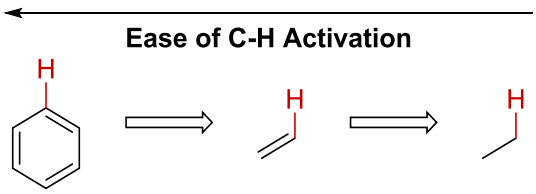

Figure 2.8 Percieved ease of C-H activation.

Remarkably, despite the widespread application of transition metal catalysts in alkenyl C-H functionalisation processes,[61,62,63,64] there remain few examples of selective HIE at alkenyl positions, with most processes focussing on allylic or vinylic systems, through double bond isomerisation.[24,65,66] As such, we initiated this study by investigating HIE of model enone **94**, which contains a similar directing group to acetophenone **61**, but is also known to undergo alkene reduction.[67] Therefore, the key aims of this project would be to minimise olefin reduction to **95**, while maximising the isotope incorporation in **D94**. Primarily, this was achieved through the choice of catalyst. Indeed, from our previous findings we had recognised that a smaller phosphine induced an increased rate of hydrogenation.[59] However, would a larger phosphine inhibit the hydrogenation? And, could a change in NHC solely deliver HIE? To answer these questions, we applied a variety of catalysts from our library (**Scheme**

2.54). It quickly became clear that any NHC other than IMes, for example **96a-b** did not deliver reactivity, a parallel with the hydrogenation process. Furthermore, low reactivity was observed with phosphite **96c** and chloride **63a** acting as the secondary ligand. Unsurprisingly, this left us with four active catalysts, **30** and **64a-c**, which have been widely applied previously. With each of these complexes, delivering different degrees of deuterium incorporation and hydrogenation, it was deemed necessary to further assess the reaction as it progressed.

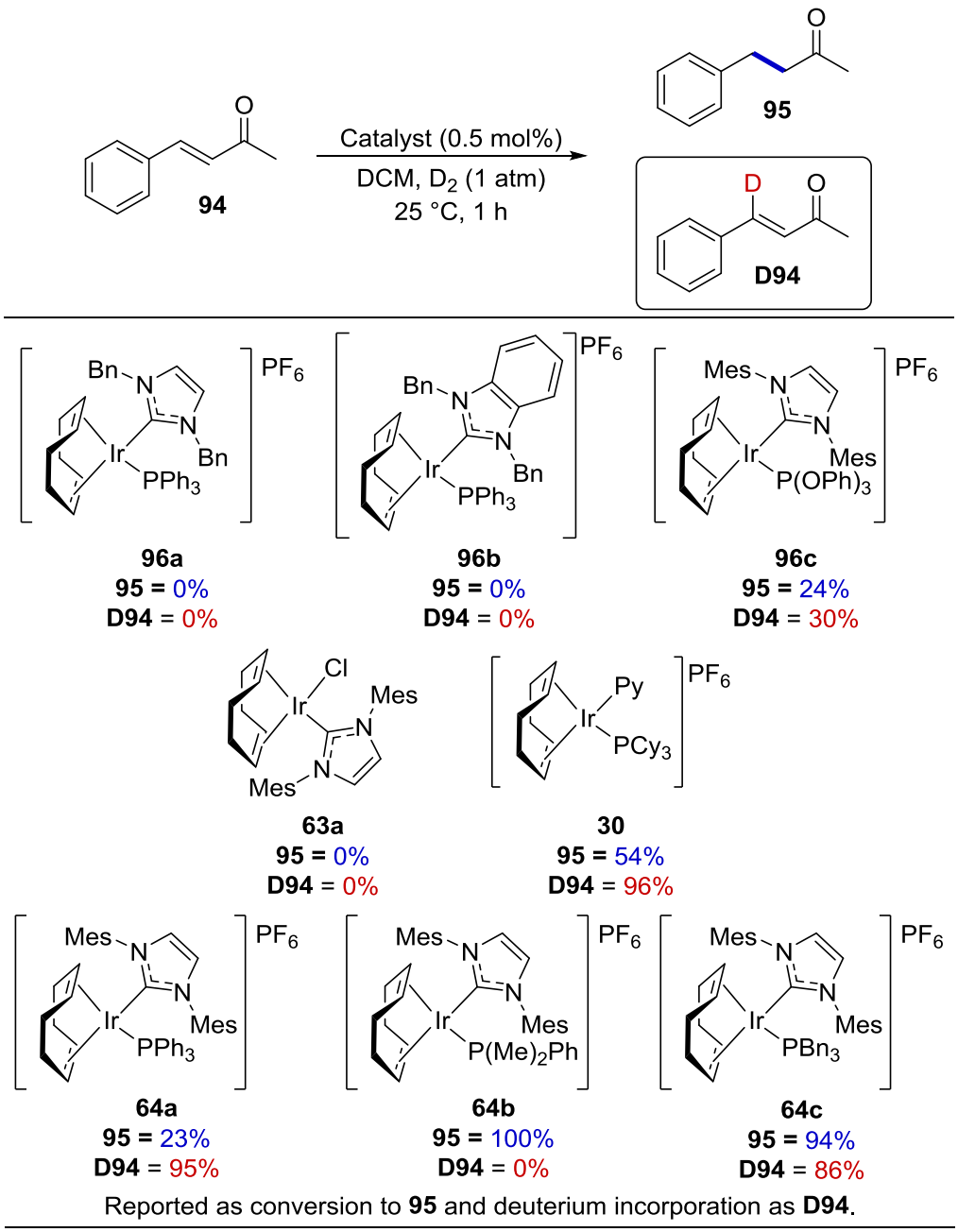

Scheme 2.54 Catalyst screen for olefinic hydrogen isotope exchange.

By following the reaction, we identified the degree of incorporation (**Graph 2.5**) alongside olefin reduction (**Graph 2.6**) over the course of a two-hour reaction, at 0.1 mol% catalyst loading. Indeed, each complex delivered excellent levels of incorporation with reduced hydrogenation at this lower catalyst loading. Furthermore, in each of the phosphine/NHC complexes **64a-c** it was clear that the HIE pathway was favoured, and would reach 80%-90% within the hour. However, Crabtree's complex **30** stalled at ~65% after one hour, perhaps indicative of the improved stability of the encumbered ligand sphere in the phosphine/NHC complexes.

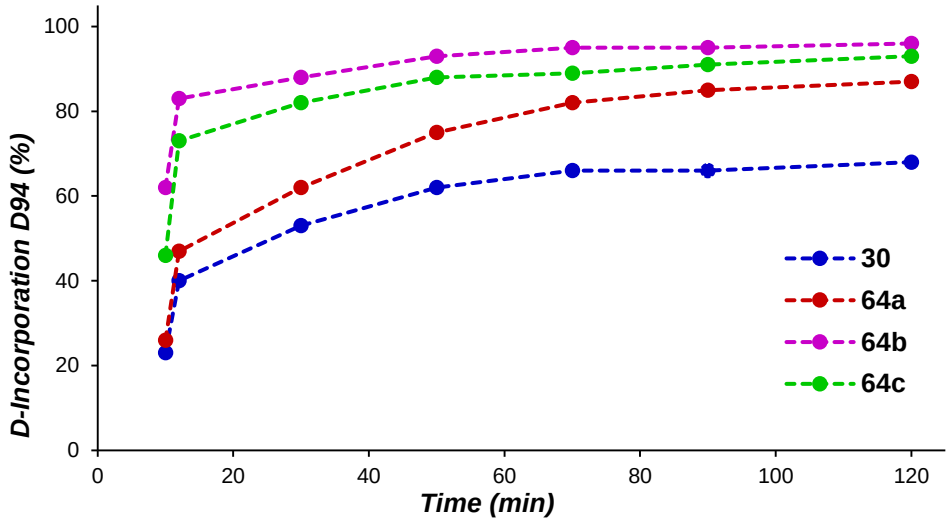

Graph 2.5 Monitored HIE.

Despite the greater rate of incorporation with catalysts **64b-c**, complex **64a** was chosen for further study because it showed the greater selectivity for HIE. Indeed, complex **64a** delivered less than 5% hydrogenation after one hour, a fifth of that generated by complex **64b**, and a third of that by complex **64c** (**Graph 2.6**).

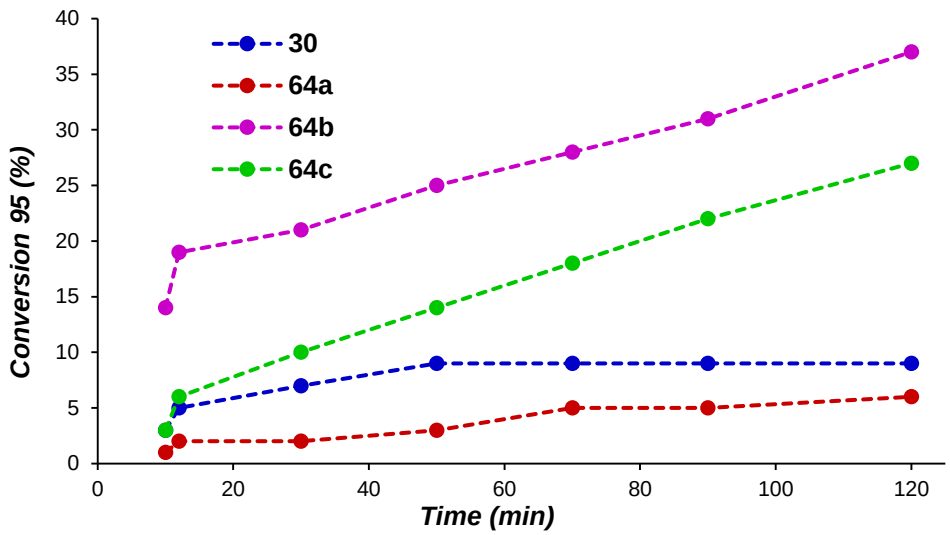

Graph 2.6 Monitored hydrogenation.

In an effort to further improve the selectivity of exchange, the effect of concentration on the reaction was assessed (**Table 2.9**). Although a small drop in incorporation was observed upon increasing the concentration, it also delivered a more significant reduction in hydrogenation, leading to optimised conditions that could be applied upon a range of substrates [**64a** (0.1 mol%), DCM (0.4 M), D_2 (1 atm), 25 °C, 1h].

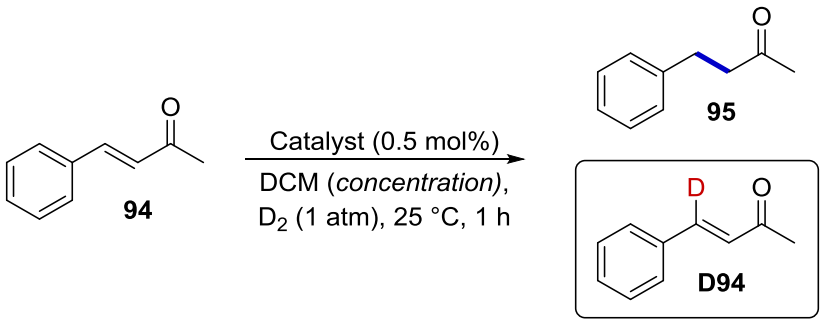

Entry	*Concentration (M)*	*D-Incorporation (%)*	*Hydrogenation (%)*
1	0.050	88	7
2	0.066	82	4
3	0.10	83	3
4	0.20	81	3
5	0.40	81	1
6	0.80	9	0

Table 2.9 Effect of concentration on HIE/hydrogenation selectivty.

In an attempt to assess the reaction scope and garner any mechanistic insight, we turned our attention to substitution of the phenyl ring (**Scheme 2.55**). Pleasingly, high

levels of deuterium incorporation were observed in each *para*- and *meta*- substituted example **D97a-i**. However, upon moving to *ortho*-substituted substrates only the strongly donating methoxy group in **D97l** delivered any incorporation, with neither bromo- or chloro substituted examples **D97j-k** reacting. Two factors could be considered accountable for this lack of reactivity. Firstly, that the *ortho*-substituent clashes with the catalyst and disfavours approach of the C-H bond to themetal centre. Secondly, the substituent could eclipse the olefin, thereby, twisting the aryl ring out of conjugation, significantly perturbing the electronics of the substrate, and no longer activating the β-position.

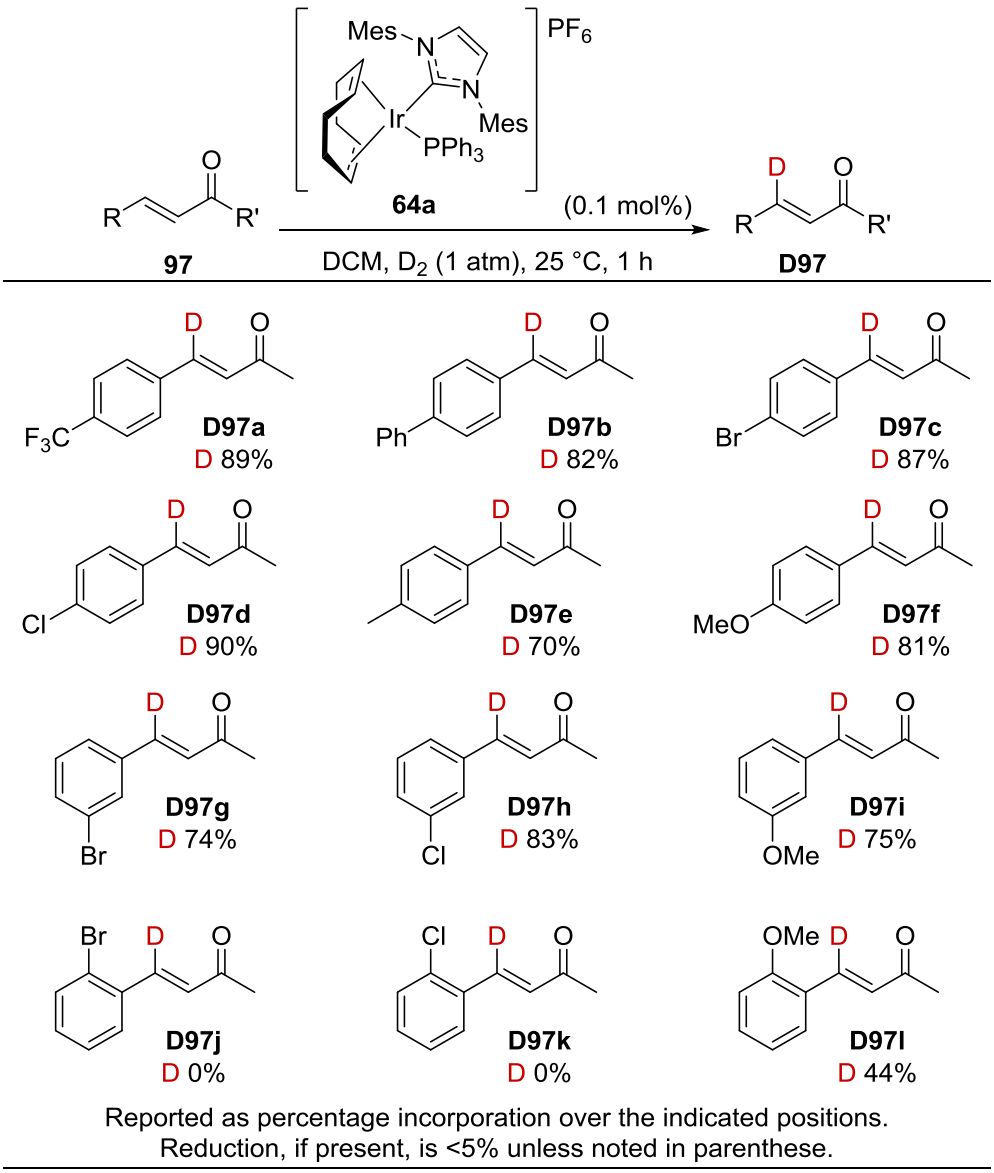

Scheme 2.55 HIE on substituted 4-phenyl butanones.

To confirm our hypothesis, we next changed the nature of the substituent at the *β*-position of the enone (**Scheme 2.56**). Changing the phenyl ring to a heterocycle delivered good results, with excellent incorporations in both furan and thiophene examples D**97m-o**. However, upon moving to pyridyl substitution, exchange was now observed *α*- to the ketone in **D97p**, indicating that the pyridine is preferentially acting as a directing group. However, when the aromatic portion is replaced bly an alkyl group, as in **D97q-r**, no reactivity towards HIE is observed. This clearly is consistent with our previous hypothesis that the aryl unit activates the *β*-position to HIE. Despite this setback, when moving to an enol ether, as in **D97s**, exchange is again observed, albeit at a slightly elevated catalyst loading of 0.5 mol%. Upon considering the reactivity of **D97p** and **D97s**, it became clear that the position of exchange must be activated by group capable of removing electron density from the olefin, and consequently the C-H bond to undergo HIE.

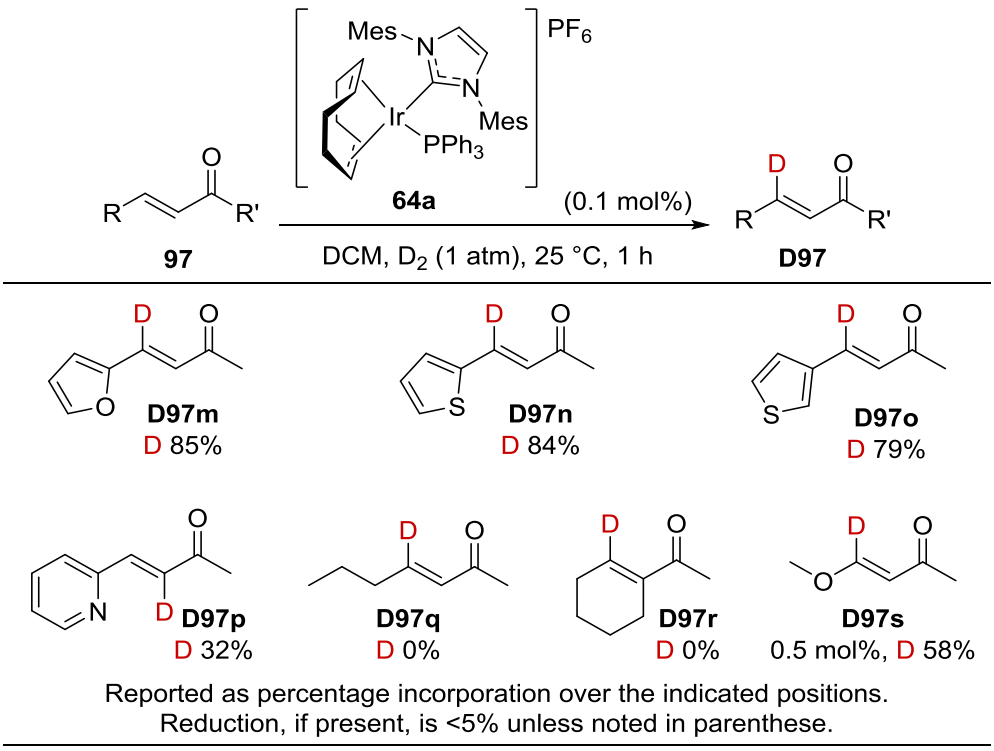

Scheme 2.56 Investigating the effect of changing the 4-substituent.

Understanding that activation of the olefin was necessary for exchange, we next turned our attention to the functional groups capable of directing the exchange (**Scheme 2.57**). Continuing with ketone directing groups, it was found that a more hindered directing group increased the rate of both HIE and hydrogenation **D97t-u**. However, the

selectivity for HIE could be regained by reducing the catalyst loading, as was proven with **D97t** at just 0.025 mol% catalyst loading. Despite this, utilising a large but planar directing group such as **D97v** generated the expected levels of incorporation and hydrogenation. This result indicates that the bulky groups if non-planar, may twist the substrate and, as such, favour hydrogenation. Furthermore, any decomplexation events would be favoured, increasing the catalyst turnover. Progressing to other carbonyl directing groups was, however, not as successful, with acid, aldehyde and ester directing groups failing to deliver any incorporation. Pleasingly, when applying the more coordinating amide directing group, high incorporation was again achieved e.g. substrates **D97z** and **D97aa**. Notably, in Weinreb amide **D97aa**, a small amount of exchange was observed in the *N*-methyl group, similarly to our previous work.[45] Finally, the nitro directing group **D97ab** also delivered high levels of incorporation with only a low level of hydrogenation.

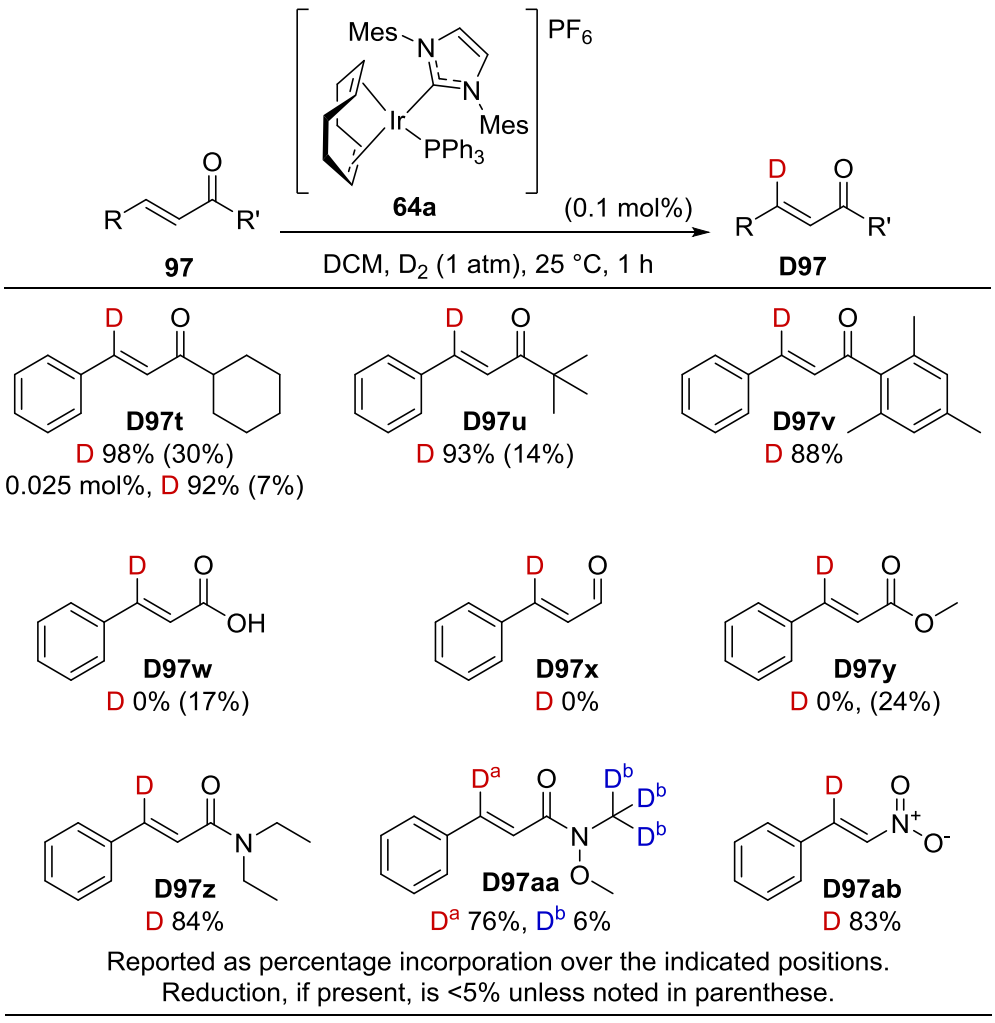

Scheme 2.57 Investigating the influence of the directing group on olefinic HIE.

In an effort to assess the effectiveness of olefinic exchange in comparison to aromatic exchange, we chose to investigate in more detail several derivatives of chalcone, a common motif within the drug design process (**Scheme 2.58**).[68,69] Pleasingly, upon application of our optimised conditions to **98a**, isotope incorporation was observed at both the *ortho*- and *β*- positions with, notably, a preference for olefinic exchange. This preference increased further upon substitution of the aryl ring connected to the alkene as in **98b-c**. However, when the substitution was reversed in **98d-e** more similar levels of exchange were achieved at both *ortho*- and *β*-positions. The same effects were observed when each aromatic ring was *meta*-substituted, **D98f-I**, or if the aromatic adjacent to the ketone was *ortho*-substituted **D98h**. Markedly, a preference for the more hindered *ortho*-position was observed, as has been previously investigated in the literature with complex **30**.[70] This evidence clearly indicates a strong dependence upon the electronic nature of the labelling position for HIE selectivity in the chalcone system.

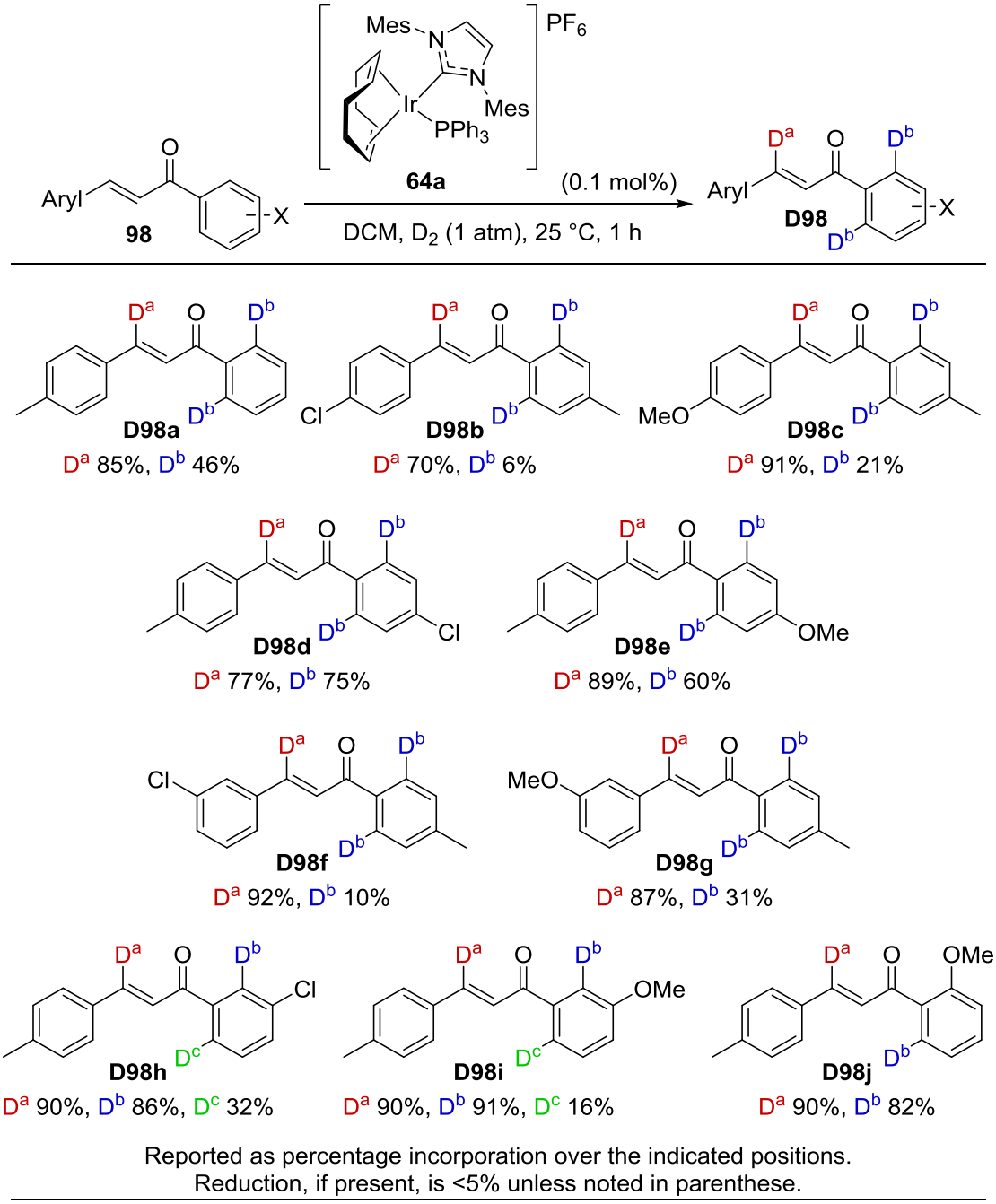

Scheme 2.58 Probing the selectivity between olefinic and aromatic HIE.

Conspicuously missing from this study so far are examples with *ortho*-substitution of the *β*-phenyl ring. When investigated, these delivered somewhat unexpected results (**Scheme 2.59**). For cases in which the *ortho*-substituent can be considered non-coordinating, as in **D98k-l**, the preference is for *ortho*-HIE. However, and in contrast to this, when the substituent can coordinate, as in **D98m-n**, HIE was favoured in the olefinic position. This can be explained by the substituent coordinating to the catalyst

and directing the exchange. Moreover, this effect could also contribute to the overall reduction in incorporation observed in **D98m-n**, if the chelate formed is thermodynamically stable, and therefore hinders the continuation of the catalytic cycle.

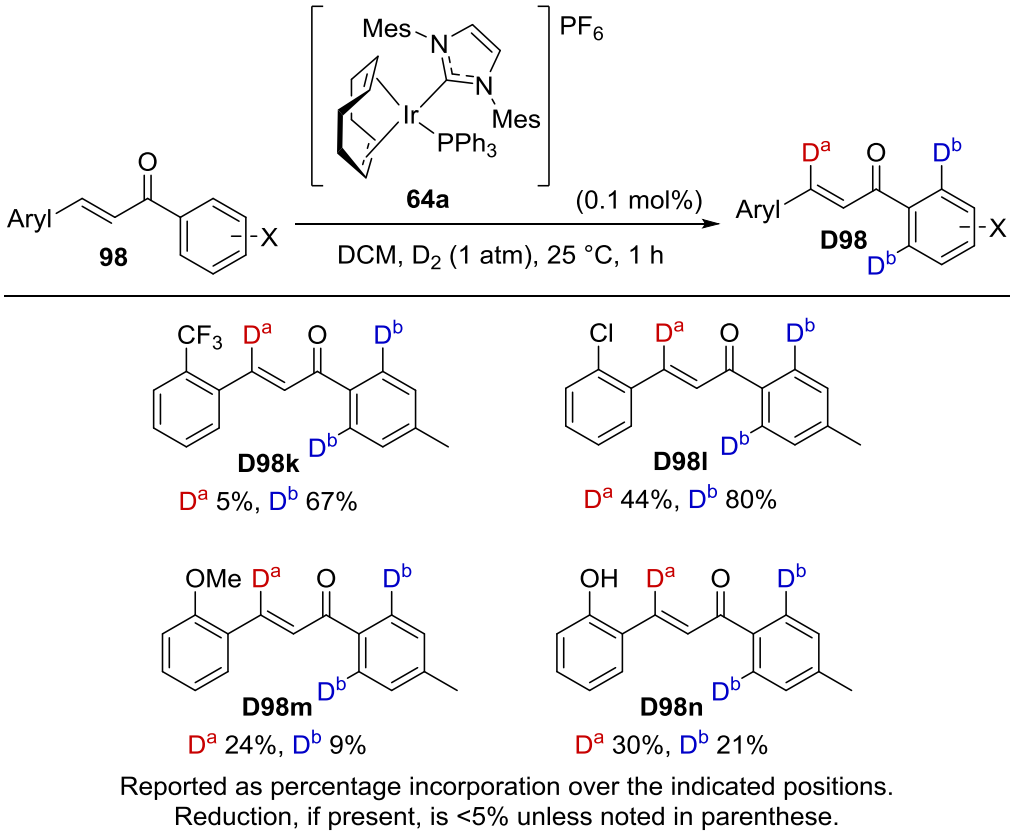

Scheme 2.59 Examining the influence of *ortho*-substituents on selectivity in olefinic HIE

To further expand the application of our new system, we turned to fused bicyclic chalcone-like structures (**Scheme 2.60**). Firstly, we were pleased to find that *α*-substitution of the enone did not hinder the olefinic exchange process. Secondly, and somewhat surprisingly, we observed a change in selectivity depending upon the size of the fused ring. Initially, with indanone-derived substrate **D98o** we observed excellent olefinic exchange with low aryl incorporation. However, the substrate derived from tetralone, **D98p**, delivered good incorporation at both olefinic and aryl sites. Furthermore, when further increasing the ring size **D98q** the selectivity for olefinic HIE was restored.

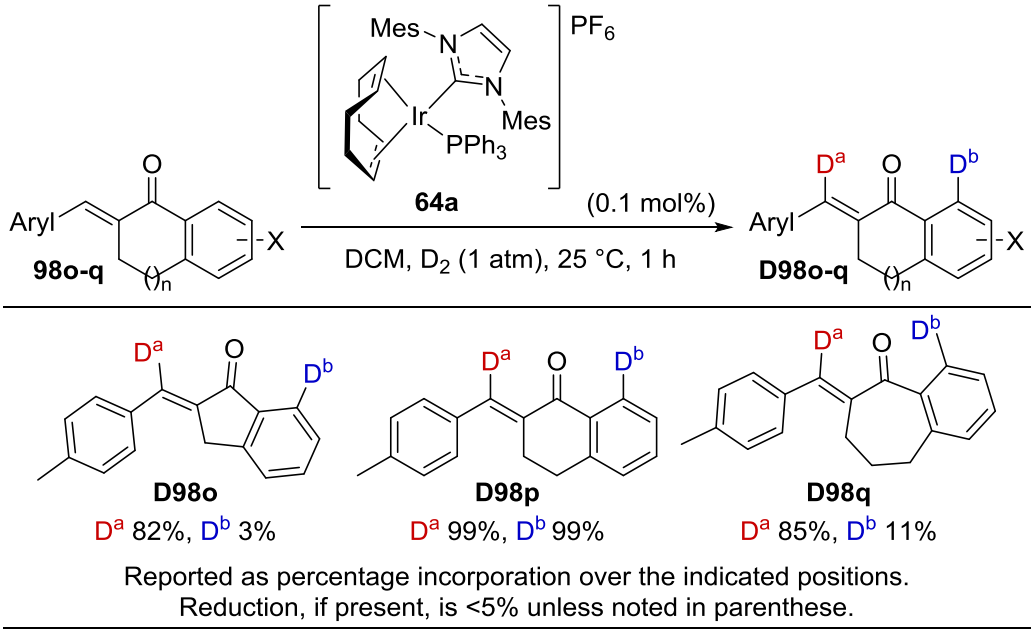

Scheme 2.60 Fused chalcone substrates for HIE.

Having established selectivity between different exchangeable sites in which the same directing group guides both exchange processes, we next posed the question; is this selectivity the same when each site has its own directing group to guide exchange? To answer this, we utilised a combination of competition reactions (**Table 2.10**), with olefinic labelling substrate **94** and a series of additives capable of undergoing HIE (**Scheme 2.61**). Firstly, the analogues competition reaction to chalcone-derived substrate **D98a**, in which substrate **94** was preferentially labelled instead of additive **D61**. The markedly different isotopic distribution between the competition reaction and substrate **D98a** indicates that the selectivity between two labelling sites with a single directing group, is different from two labelling sites each with their own directing groups. To futher advance our study we applied a range of additives to assess the variations in selectivity with different directing groups. Indeed, labelling of substrate **94** was favoured in the application of ester **D100a** and nitro **D27i** additives, which did not undergo HIE. In contrast, pyrazole **D100b** additive delivered completely selective aryl HIE, with no incorporation upon substrate **94**. However, both aryl amide **D100c** and pyridyl **D27c** additives halted all HIE processes. Finally, application of benzoic acid **D86g** additive hindered the reaction, delivering low levels of incorporation in substrate **94**.

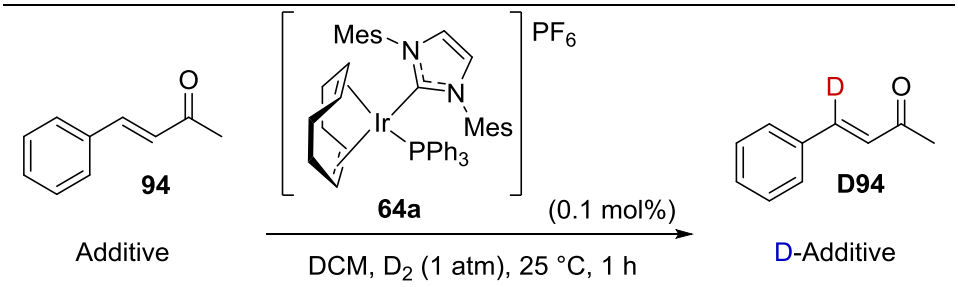

Entry	*Additive*	*D-Incorporation (%)*	
		Substrate	*Additive*
1	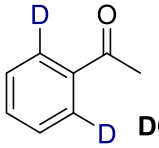 **D61**	83	5
2	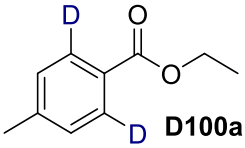 **D100a**	89	2
3	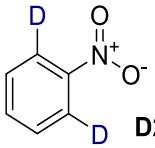 **D27i**	84	0
4	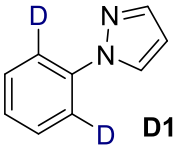 **D100b**	3	93
5	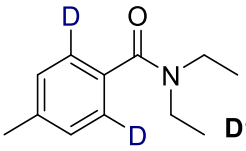 **D100c**	0	0
6	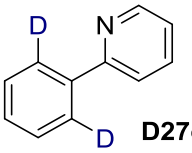 **D27c**	0	0
7	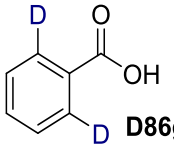 **D86g**	23	0

Reported as percentage incorporation across the indicated positions.

Table 2.10 Competition reactions between aromatic and olefinic HIE.

Following the completion of the intermolecular competition reactions, we wished to assess the same competition intramolecularly (**Scheme 2.61**). Indeed, olefinic HIE was favoured in the presence of both ester **D101a** and nitro **D101b** directing groups. Moreover, pyrazole containing substrate **D101c** exchanged solely on the aromatic

position, *ortho*- to the heterocycle. Finally, with pyridyl substrate **D101d**, no HIE was observed. Pleasingly, the inter- and intramolecular reaction were in good agreement, therefore, validating the use of a simplified substrate in an intermolecular competition reaction as a predictor for a more complex intramolecular substrate.

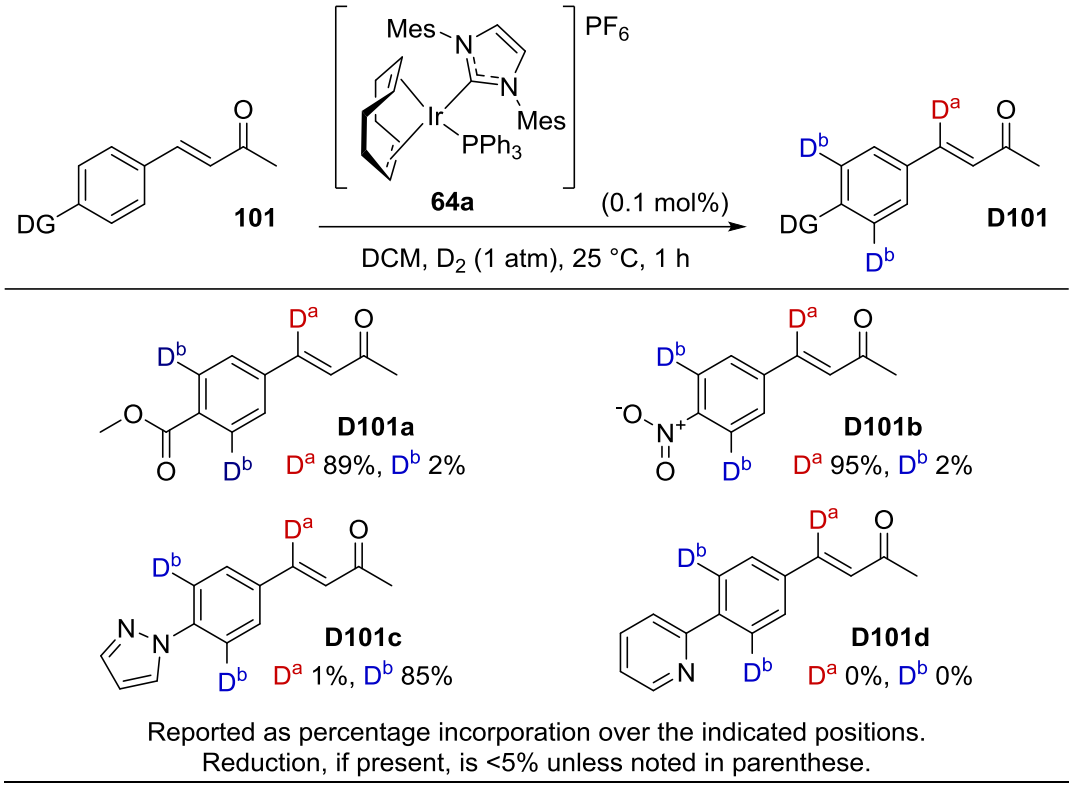

Scheme 2.61 Selectivity between aromatic and olefinic exchange in a single molecule.

So far, we have worked under the assumption that the mechanism for olefinic exchange is the same as that for aromatic exchange, i.e. pathway I (**Scheme 2.62**). However, we should also consider the possibility that a different pathway maybe in operation, for example one more akin to a conjugate addition followed by a hydride abstraction, i.e. pathway II. This pathway would commence from the same initial intermediate **A**, and would be followed by a conjugate hydride addition, to generate intermediate **E**, containing an iridium enolate in which the transferred deuteride is still associated with the metal centre. Intermediate **E** can then undergo rotation of the C-C bond, to orientate the hydride for abstraction, as in intermediate **F**. Following hydride abstraction, common intermediate **D** is formed, which can readily exchange with another unlabelled substrate molecule **94**, to continue the catalytic cycle.

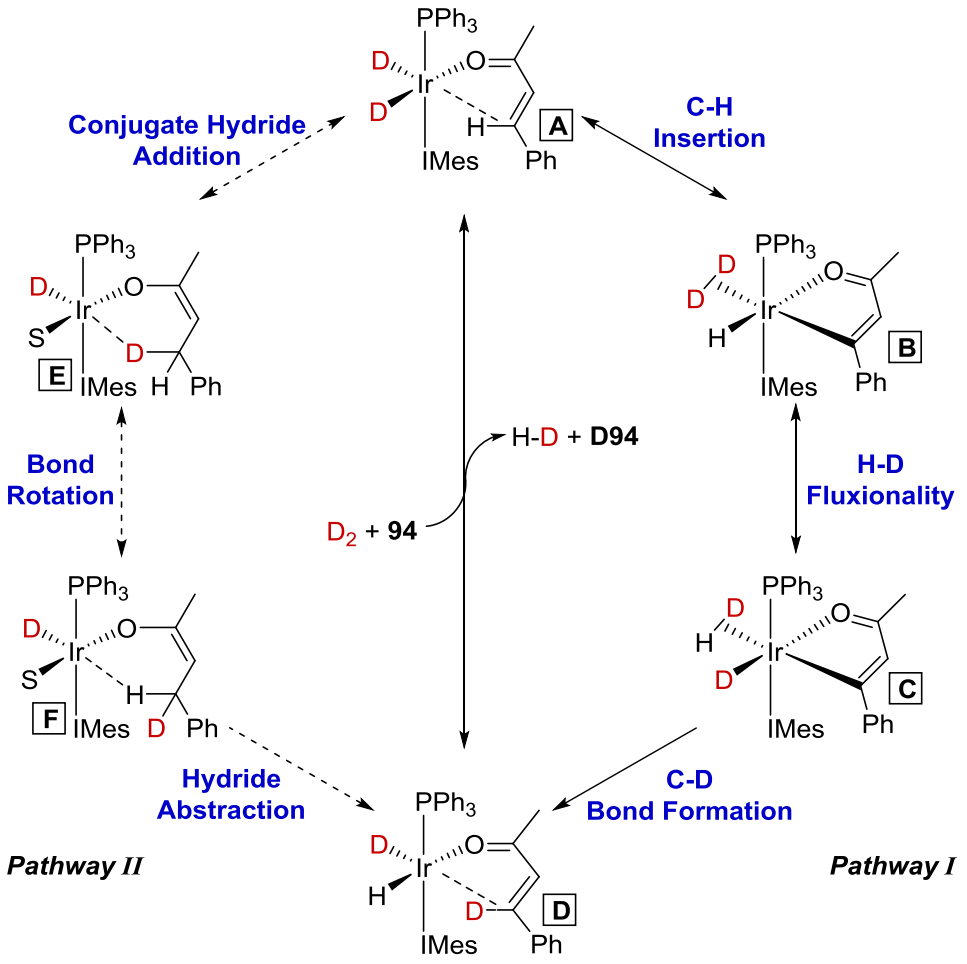

Scheme 2.62 Potential pathways for olefinic HIE to occur.

A series of experiments were conducted, in order to probe these mechanistic possibilities. The first consideration included utilising the opposite isomer of our model substrate, i.e *Z*-**94** in the HIE process (**Scheme 2.63**). This would indicate if intermediate **A** was indeed the starting point for this mechanism, or if an outer sphere pathway was more likely. In accordance with the proposed pathways, *Z*-**94** did not under go HIE, validating the proposal of an initial intermediate similar to **A**.

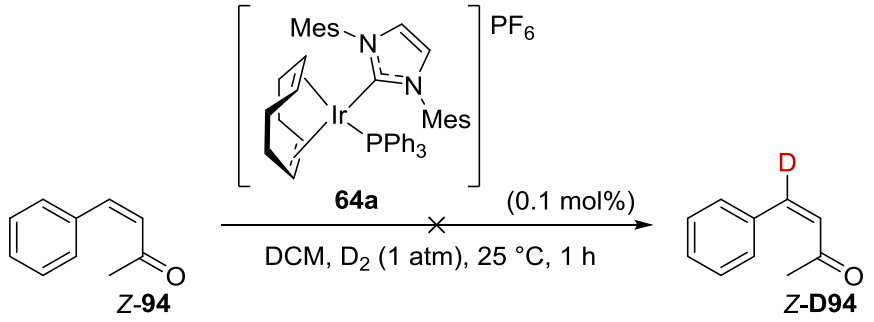

Scheme 2.63 HIE upon *Z*-enone.

Next, we considered the first step in each pathway: either conjugate hydride addition or C-H insertion. Given that conjugate addition would involve the transfer of a hydride, a build-up of charge in the transition state would be expected at the *β*-position, whereas, C-H insertion would be considered more electron neutral. With this in mind, we utilised a Hammett plot to investigate charge build-up close to or upon the aromatic ring (**Graph 2.7**). Pleasingly, the plot delivered a very small *ρ*-value (-0.0204) indicative of no significant charge build up in the transition state, suggesting that conjugate hydride addition is unlikely.

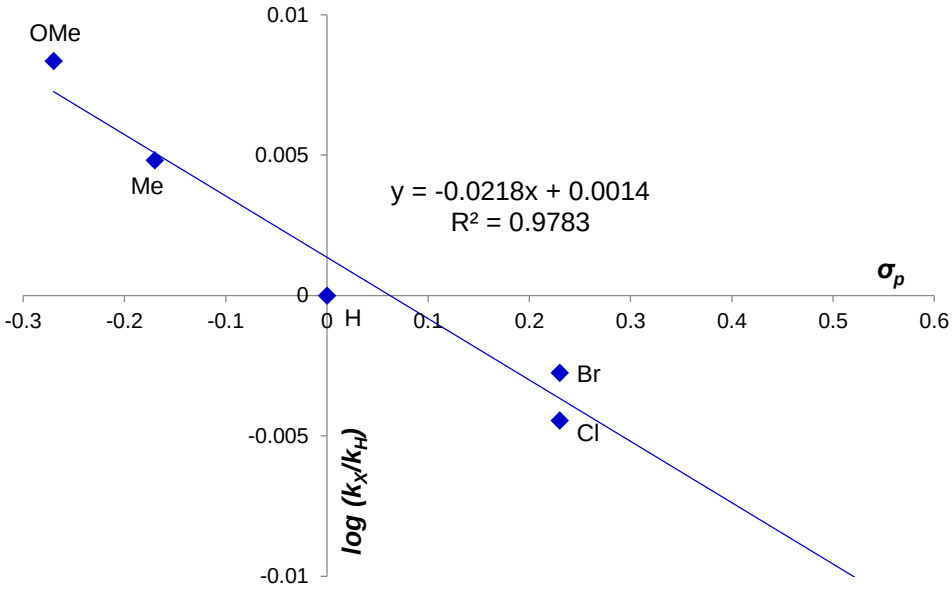

Graph 2.7 Hammett plot for olefinic HIE.

Further to this evidence, we performed a kinetic isotope effect (KIE) experiment in order to confirm the presence of a C-H insertion during the rate determining step (**Scheme 2.64**). We utilised two methods of measuring the forward reaction installing

deuterium and the reverse reaction installing hydrogen, either; running independent reactions for a given amount of time (**Graph 2.8**), or alternatively, monitoring a single reaction (**Graph 2.9**), and found that each method delivered similar KIE values 3.56 and 3.80, respectively. Indeed, when compared to other values within the literature, they strongly suggest a C-H insertion as the rate determining step.[71,45,49]

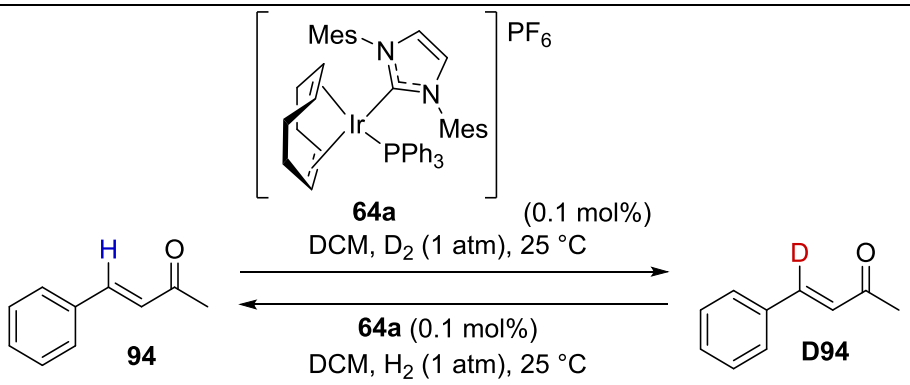

Scheme 2.64 KIE experiment for olefinic HIE.

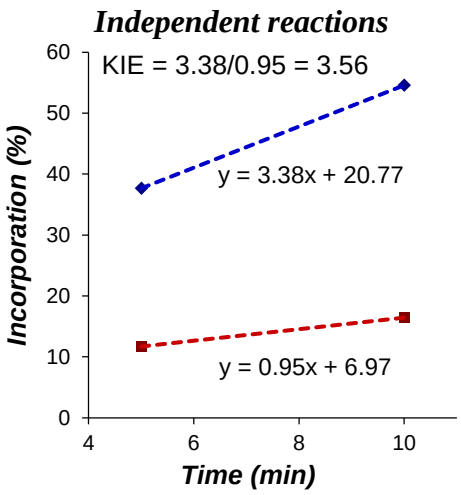

Graph 2.8

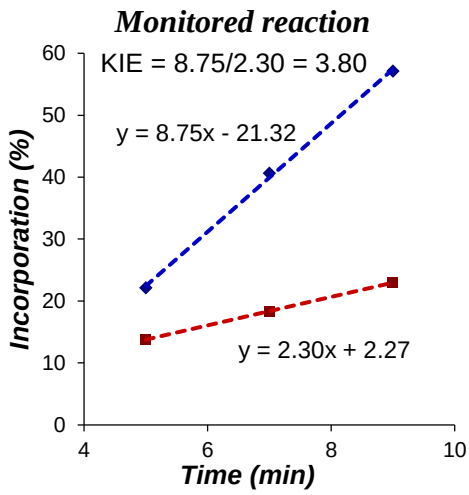

Graph 2.9

The mechanistic information generated suggests that the same reaction pathway is in operation for both olefinic and aromatic HIE. With this in mind, we turned our attention to the selectivity that we have observed for HIE over hydrogenation, initially, we sought answers in the proposed mechanism of each process (**Scheme 2.65**). In particular, the choice of catalyst with respect to each optimised process delivered key insight; a small phosphine for hydrogenation and a large phosphine for HIE. This indicated that the pathway for hydrogenation was sterically more demanding. Certainly, on considering the proposed substrate-bound intermediates for each process,

this is valid, with the substrate in **A** being planar to accommodate the agostic C-H interaction. In contrast, in intermediate **B** the substrate is twisted to allow the alkene π-system to interact with the metal, generating a steric clash between the phenyl group and one of the two ligands, and breaking the substrate conjugation. Further to this, HIE proceeds through a 5-mmi, as in **B**, known to form very effectively with minimal ring strain. Additionally, the hydrogenation proceeds via a 6-mmi, as in **F**, generating greater ring strain, and perhaps indicating a higher energy transition state.

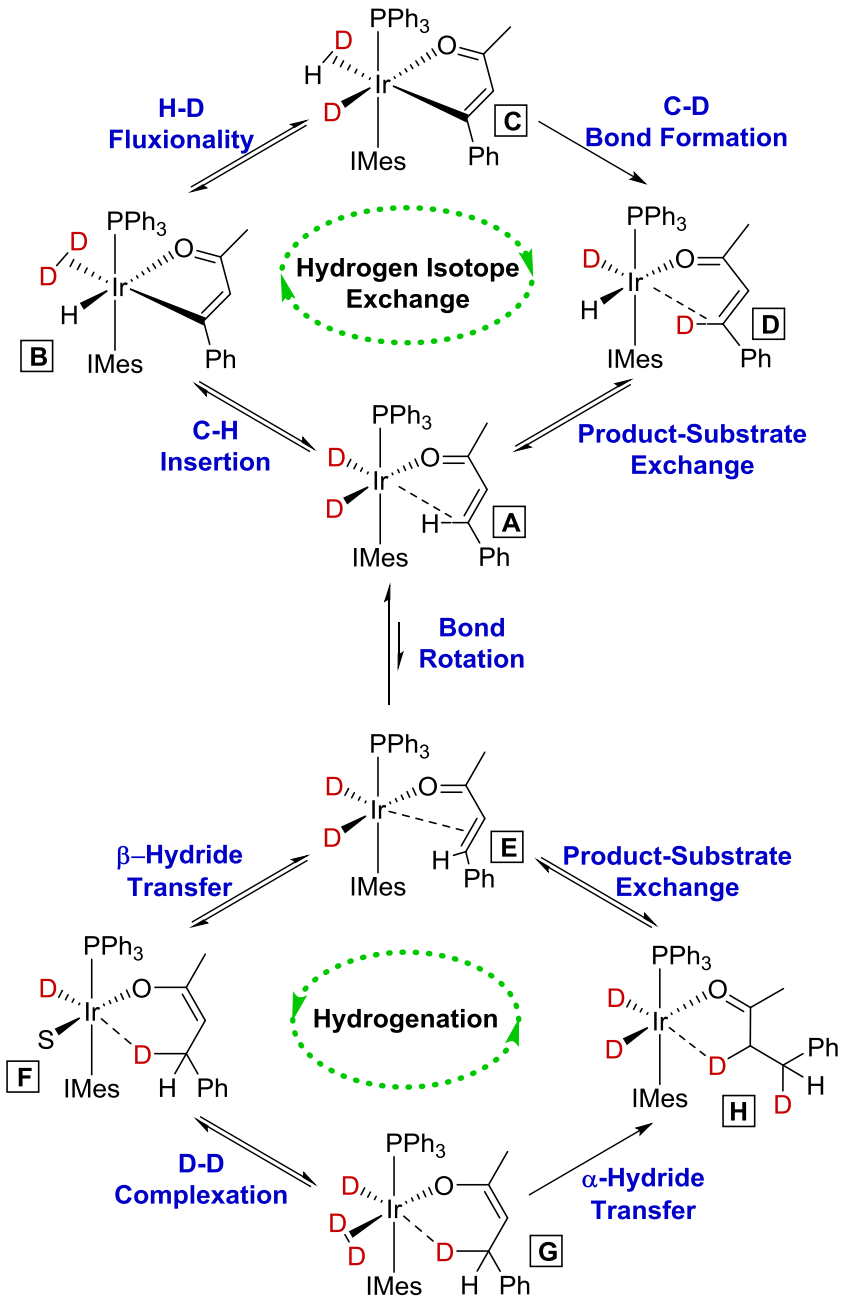

Scheme 2.65 Proposed mechanism for both HIE and hydrogenation.

Further to this, we carried out DFT-computational studies to reinforce our proposal (Carried out by Dr M. Reid). Firstly, considering the initial binding conformer for each process, we observed the planar binding of the substrate in HIE binding isomers **A-I** and **A-II**, as previously suggested (**Figure 2.9**).

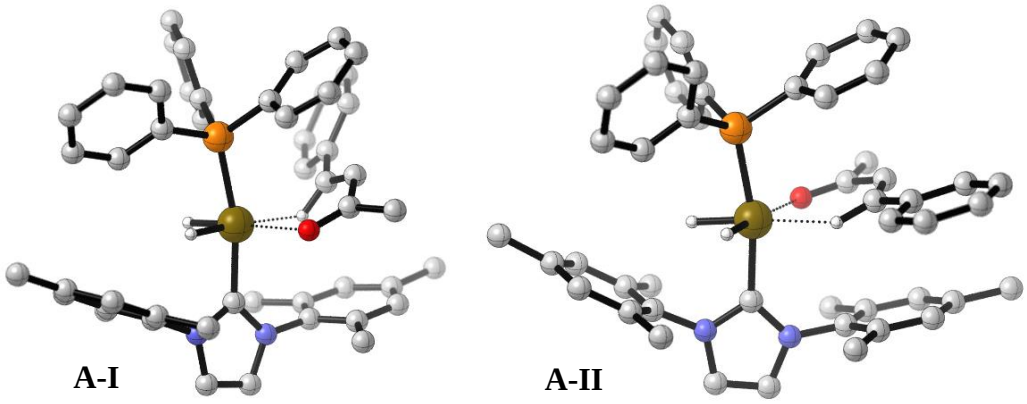

Figure 2.9 Calculated binding conformers for HIE.

Moreover, the twisting of the substrate and the increased substrate-ligand steric clash are apparent in alkene-bound isomers **E-I** and **E-II** (**Figure 2.10**).

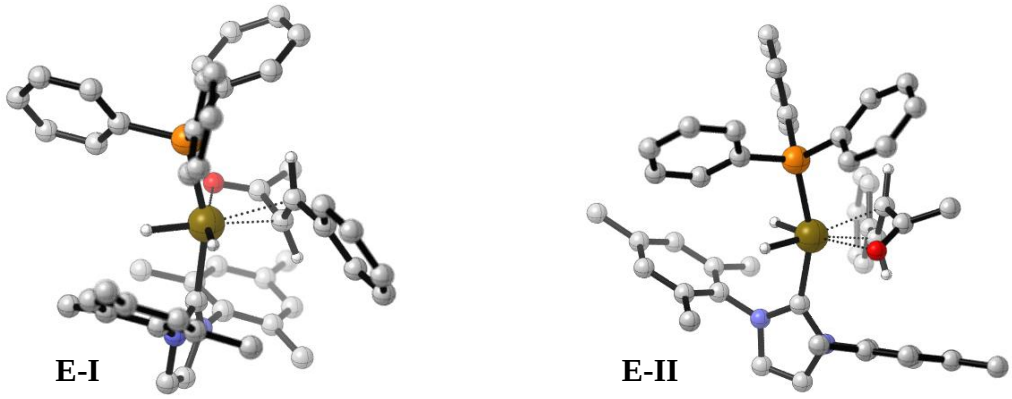

Figure 2.10 Calculated binding conformers for hydrogenation.

Secondly, we considered the intermediates following the first step of each reaction, which is the presumed rate determining step. Indeed, in the case of HIE we can observe the proposed cyclometallated intermediates **B-I** and **B-II** (**Figure 2.11**). It is worth noting at this point that in intermediate **B-I**, the aryl ring is distorted, breaking conjugation to the enone, whereas **B-II** is still fully delocalised.

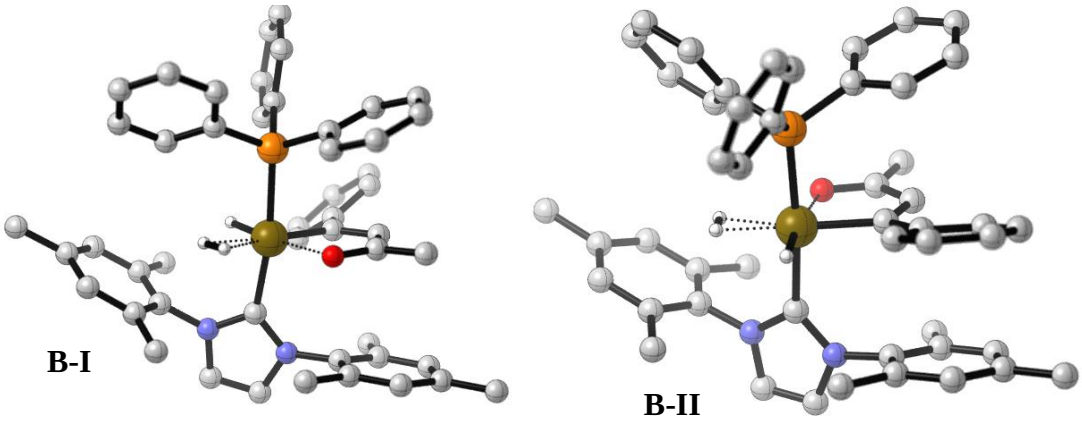

Figure 2.11 Calculated intermediates following C-H insertion.

Furthermore, when viewing the intermediates following *β*-hydride transfer, 16-electron complexes **F-I** and **F-II** were obtained (**Figure 2.12**). This indicates, as proposed in intermediates **F** and **G**, that further stabilisation by solvent or molecular hydrogen may be necessary, although this aspect has yet to be calculated.

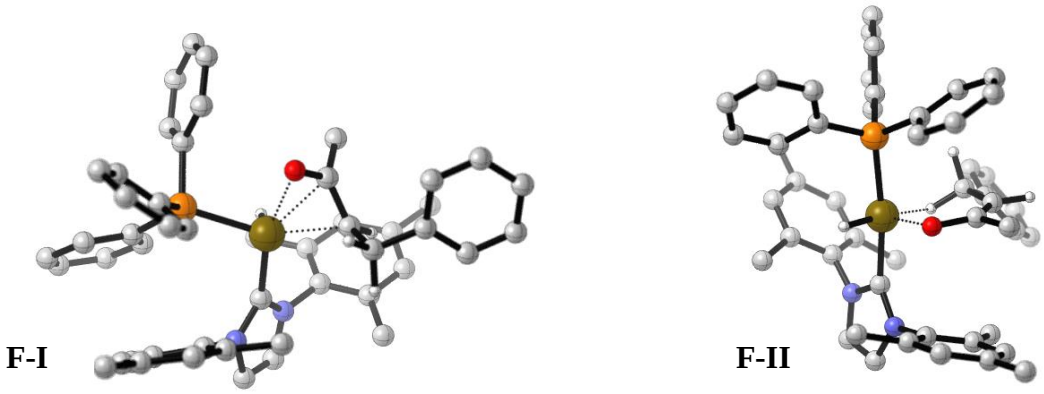

Figure 2.12 Calculated intermediates following *β*-hydride transfer.

Finally, through examination of the relative energies it quickly became clear that both the binding and the intermediate following the first step in the mechanism were lower in energy for HIE (**Graph 2.10**). Indeed, although transition states have yet to be calculated, we can assume from this that the HIE process will have a lower activation energy than hydrogenation, which in line with our experimental findings.

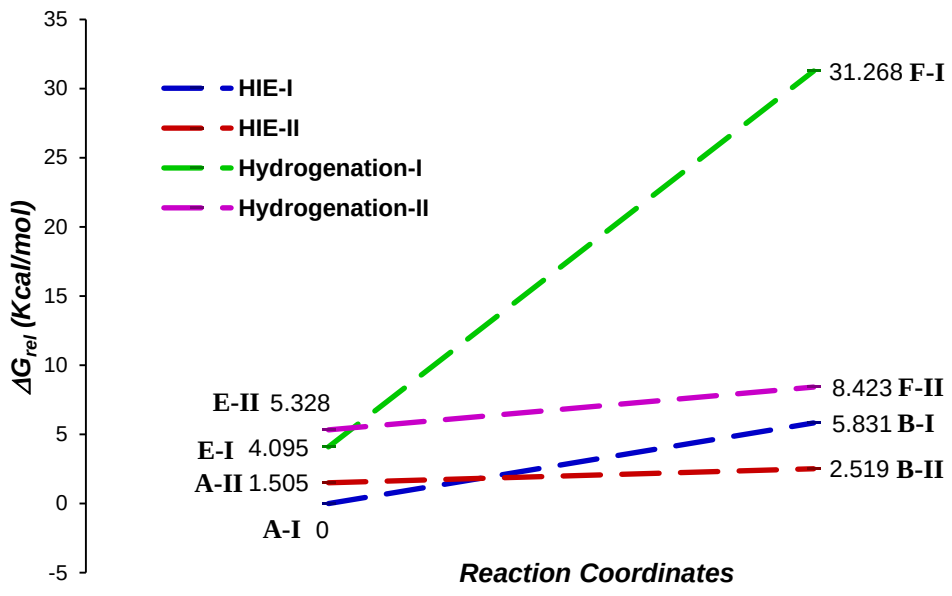

Graph 2.10 Calculated free energies relating to the proposed HIE and hydrogenation pathways.

To conclude our work in this novel area of HIE we examined several pharmaceutically relevant molecules with our new protocol (**Scheme 2.66**). Pleasingly, with slightly extended reaction times, we were able to achieve good levels of exchange at both olefinic positions in choleretic agent *Cyclovalone* **D102**. Furthermore, the application of anticonvulsant *Ilepicimide* **D103** under our optimised conditions delivered excellent levels of incorporation.

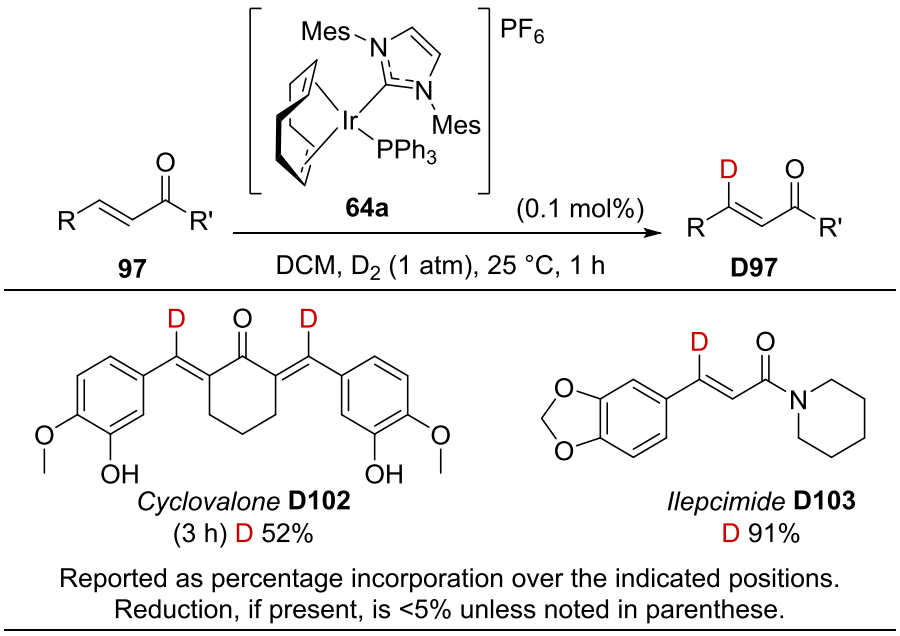

Scheme 2.66 Testing olefinic HIE on pharmaceutical agents.

In conclusion, we have developed a method to selectively incorporate an isotope into the β-position of an olefin, via a directed C-H insertion. This method has been examined in a wide variety of substrates, many of which contain competing exchange sites. Through this and further mechanistic work, we have proposed a plausible mechanism for olefinic exchange, similar to that recognised for aromatic HIE. Further to this, we have examined both mechanisms and can plausibly explain the high selectivity for HIE over the competing hydrogenation process. Finally, we applied this understanding to two pharmaceutically relevant compounds to fully validate the method.

3.3. sp^3 HIE

Following on from our successful studies into the labelling of olefinic positions through directed HIE, we next investigated the challenge of sp^3 HIE. Undeniably, it has been well recognised within the literature that sp^3 positions are the most challenging C-H positions to activate. However, if the position is adjacent to electronegative heteroatoms or electron withdrawing functional groups, then it is more readily disposed to C-H functionalisation (**Figure 2.13**).[7273] Indeed, such an effect could be related to the reduction in pK_a of the given hydrogen.

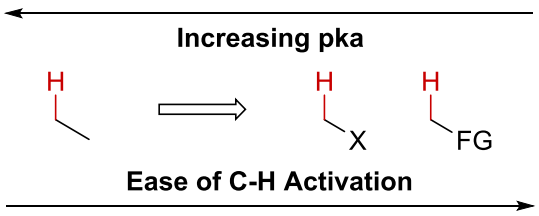

Figure 2.13 Recognised reactivity sp^3 C-H activation.

With this in mind, and recognising the high proportion of drug compounds that contain saturated heterocycles,[55] we first targeted HIE on the saturated six-membered morpholine and piperazines systems. We first utilised *N*-(pyridin-2-yl)morpholine **104**, under standard HIE conditions with a series of catalysts previously proven to be active in aromatic HIE and olefin hydrogenation (**Scheme 2.67**). Initially, the bulky NHC/phosphine combination was found to be necessary for high levels of incorporation, through the comparison of catalysts **63a**, **30** and **64a**. Further to this, elevated incorporation was achieved when a more non-coordinating counterion was utilised, as in catalyst **71c**. However, further manipulation of the ligand sphere, be it in changing of phosphine (**87a-b**) or NHC, as in **88**, delivered similar incorporations. Therefore, complex **71c** was chosen for further study, and was utilised in an effort to further explore this new process.

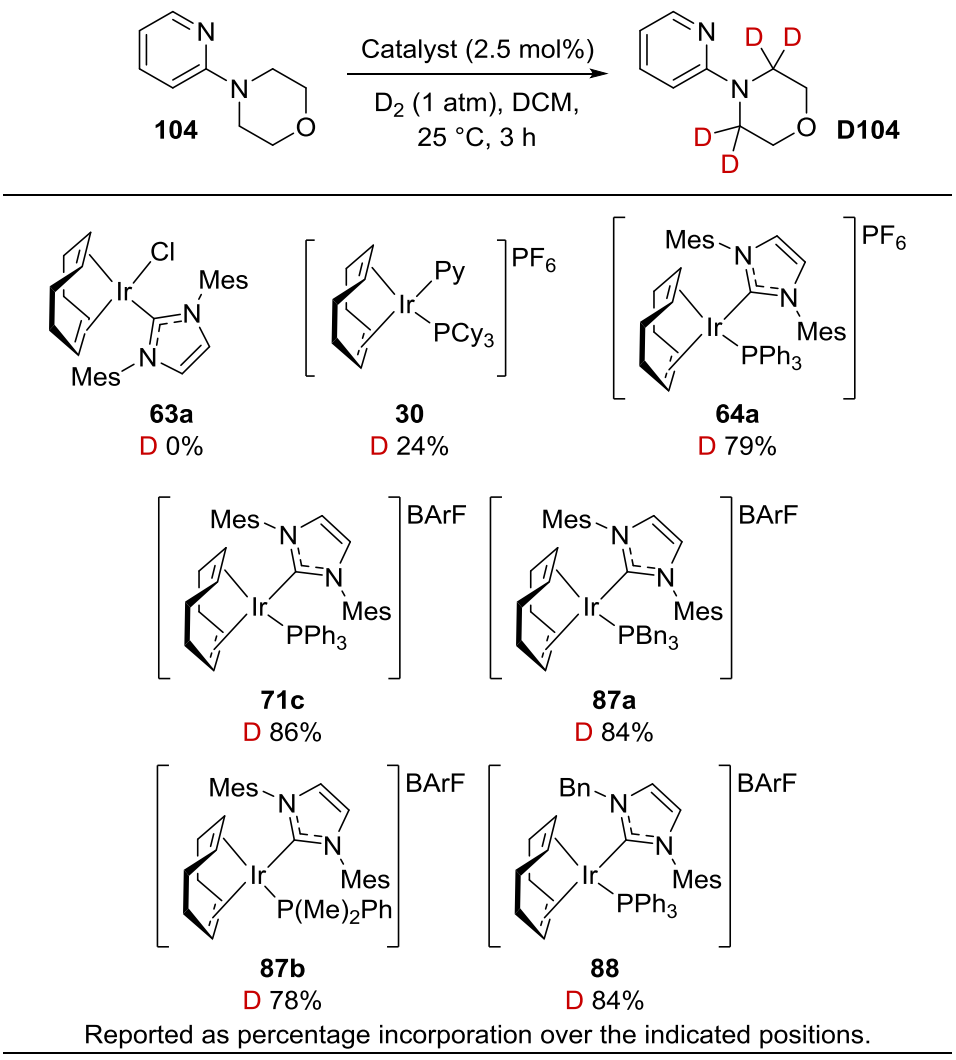

Scheme 2.67 First catalyst screen for sp^3 HIE.

Having achieved excellent levels of incorporation in DCM, we next assessed the utility of our new process in different solvents (**Scheme 2.68**, **Graph 2.11**). Initial experiments in MeOH delivered moderate levels of incorporation. However, upon increasing the steric bulk of the solvent, and, therefore, reducing its potential to coordinate with the catalyst, the incorporation increased, as can be observed in IPA and *t*amylOH. Furthermore, both ester and ether solvents reflected this same trend, indicating that catalyst solvation influences the catalyst turnover. Moreover, the most non-coordinating ester and ether solvents, *t*BuOAc and MTBE, delivered elevated incorporations compared to DCM. However, DCM was the chosen solvent for further testing due to the improved solubility in our substrate scope, with alternative solvents applied when necessary.

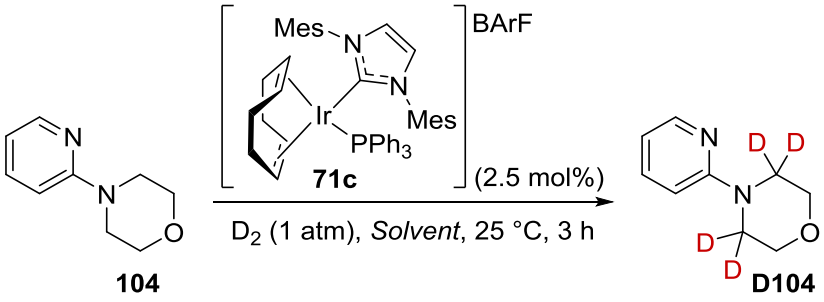

Scheme 2.68

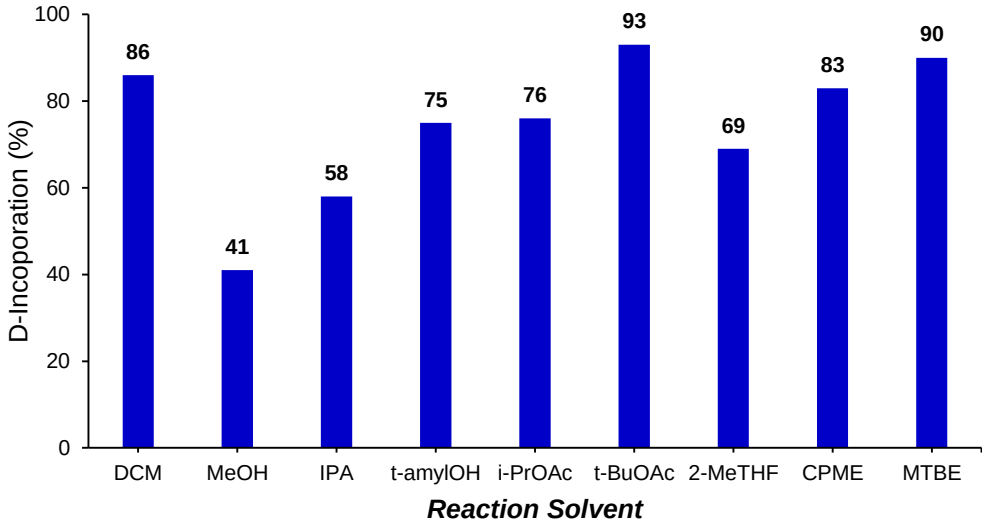

Graph 2.11 Application of different solvents for sp^3 HIE.

Prior to broadening these investigations, we wished to assess the conditions chosen for exchange. To achieve this, we utilised a *three-factor*, *two-level*, design of experiments, including; catalyst loading, reaction time and reaction concentration. The findings showed that reaction time and concentration had only a small influence upon the reaction, with catalyst loading proving much more influential. With this in mind, it was discovered that a reduction in catalyst loading and reaction time still delivered the same excellent isotope incorporation.

With optimal conditions in hand, we investigated exchange upon morpholine, piperidine and piperazine systems, engaging a variety of different directing groups and substitution patterns. Beginning the study, we probed HIE on morpholine, with a variety of directing groups (**Scheme 2.69**). Pleasingly, both model substrate **D104** and pyrimidine **D105a**, containing *N*-heterocyclic directing groups, delivered excellent levels of incorporation. Following this trend, both quinoline **D105b** and isoquinoline

D105c, proved highly effective in directing the exchange. However, amide **D105d** or carbamate **D105e** directing groups failed to deliver and isotope exchange. Indeed, given previous results with other amide groups this was somewhat expected, given that *N*-methyl amides underwent exchange, but *N*-ethyl amides did not, presumably due to the increased steric ecumbrance.[45]

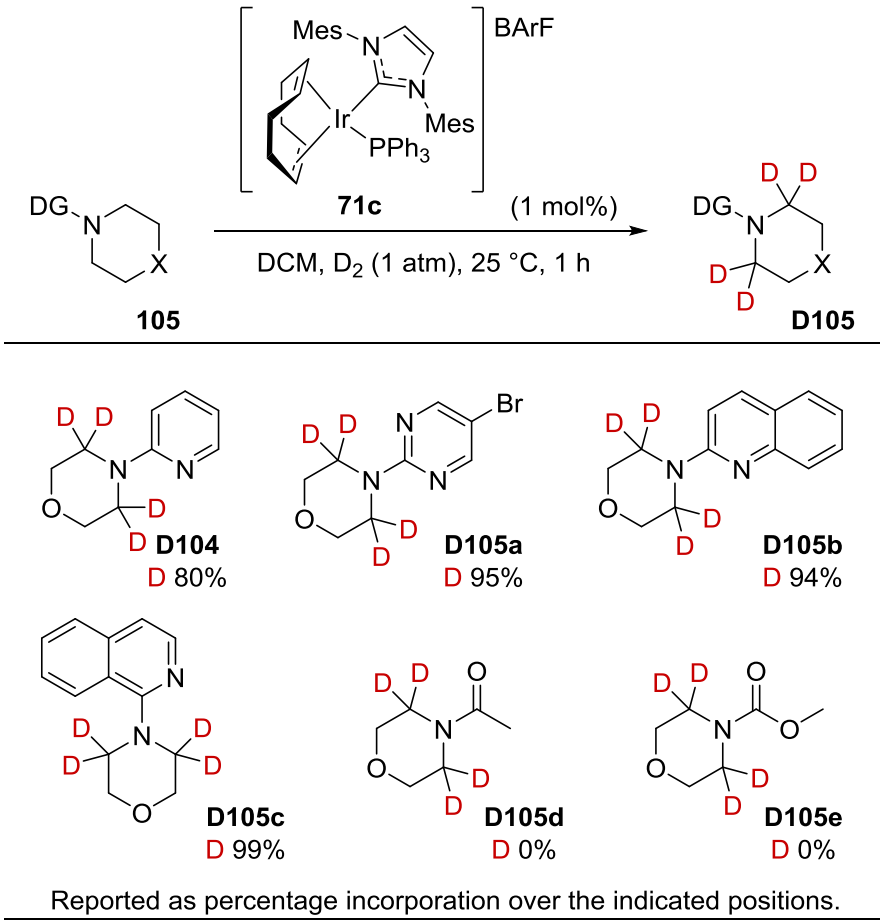

Scheme 2.69 HIE on morpholine substrates.

We next considered exchange upon piperidine *N*-heterocyles (**Scheme 2.70**). Firstly, examination of sp^3 HIE directed by a 5-membered heterocycle, as in thiazole **D105f**, delivered good levels of deuterium incorporation, albeit slightly reduced when compared to the previous 6-membered examples, such as **D104**. Secondly, by substituting the 4-position of the piperidine ring, we were able to differentiate the axial and equatorial hydrogens by ^{1}H NMR spectroscopy. Initially, with alcohol-bearing substrates **D105g-h**, excellent incorporation was delivered, however, no significant axial versus equatorial selectivity was observed. In contrast, when utilising acid-bearing substrates **D105i-j**, selectivity for the equatorial hydrogen was observed.

However, after substituting the directing unit with a -CF_3 group, any trace of selectivity was eliminated, as in **D105k**. Overall to our knowledge, this is the first example of such axial versus equatorial selectivity in donor group directed, metal-mediated, C-H activation. However, the origins of this selectivity are presently poorly understood. Presumably, however, the equatorial hydrogen is more accessible to the catalyst. Further to this, deuterium was also successfully incorporated on piperidinone **D105l** in high levels, despite the potential for a non-productive interaction with the ketone.

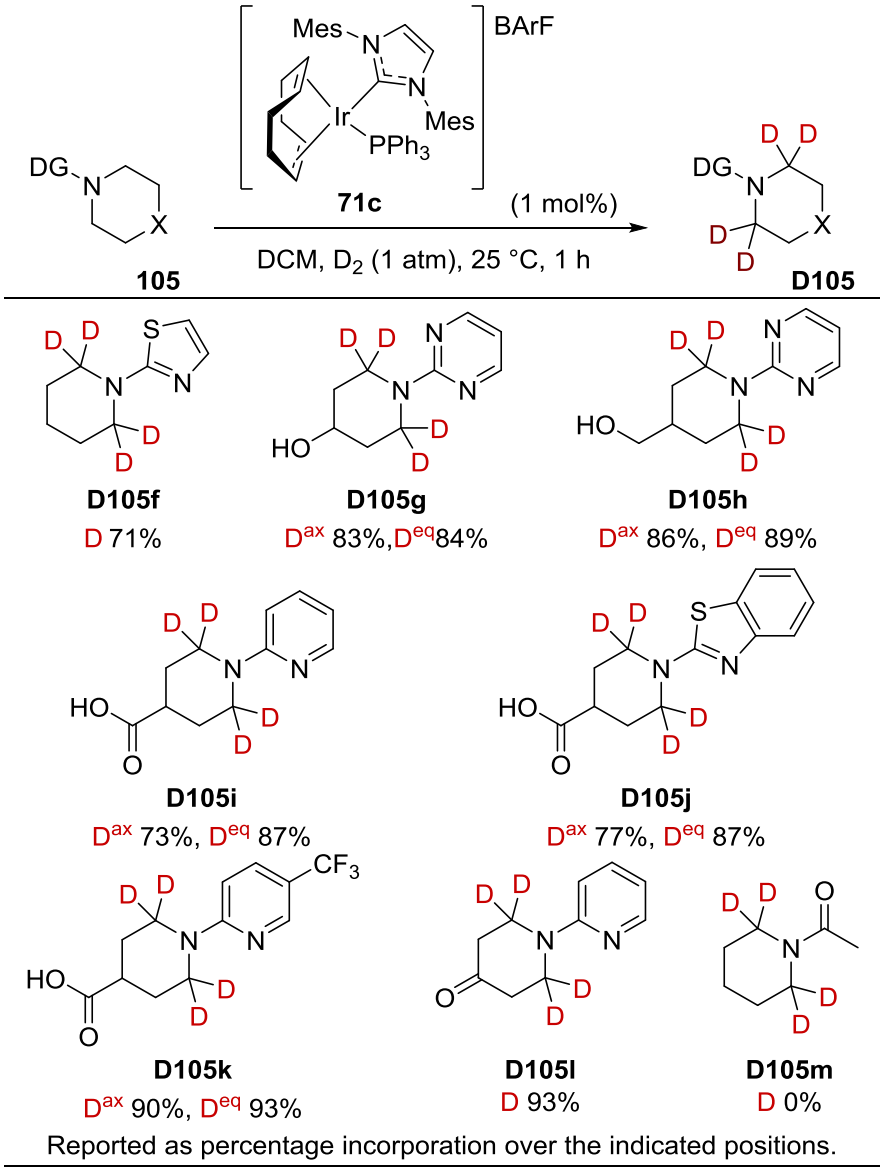

Scheme 2.70 HIE on piperidine substrates.

Finally, in a similar fashion to the morpholine examples, no exchange was observed with an amide directing group **D105m**.

We next progressed to performing exchange on piperazine, in an effort to complete the labelling of common 6-membered, saturated *N*-heterocyles (**Scheme 2.71**). However, application of the conditions previously utilised with morpholine and piperidine derivatives delivered low incorporations when the second piperazines nitrogen was unsubstituted as in **D105n-r**. However, by capping the free nitrogen, as in **D105s-u**, excellent levels of deuterium incorporations were recovered, and, in the case of **D105u**, only exchange directed by the pyridine was observed with none directed by the amide carbonyl. These first results clearly indicate a non-productive interaction between the catalyst and the free secondary amine, perhaps in a similar fashion as in transfer hydrogenation, which has been previously explored with similar catalyst structures.[74]

With this in mind, and again using experimental design techniques, we targeted a second protocol that would allow HIE on substrates containing secondary amines. We examined the same three variables as in the first design, and we were able to reassess the impact of each factor. Interestingly, the design results showed a greater time dependence than previously observed, allowing us to generate a new protocol through increasing the catalyst loading and reaction time [**71c** (5 mol%), DCM, 25 °C, 3 h]. Indeed, the new protocol delivered excellent levels of incorporation, in each of the previously troublesome substrates **D105n-r**, allowing efficient exchange on unsubstituted piperazines. Interestingly, under these new conditions, incorporation was now observed in low levels at the C5-position of pyridine in substrates **D105o-p**. Indeed, methods have previously been reported for such types of exchange, most commonly using rhodium or ruthenium catalysts.[75]

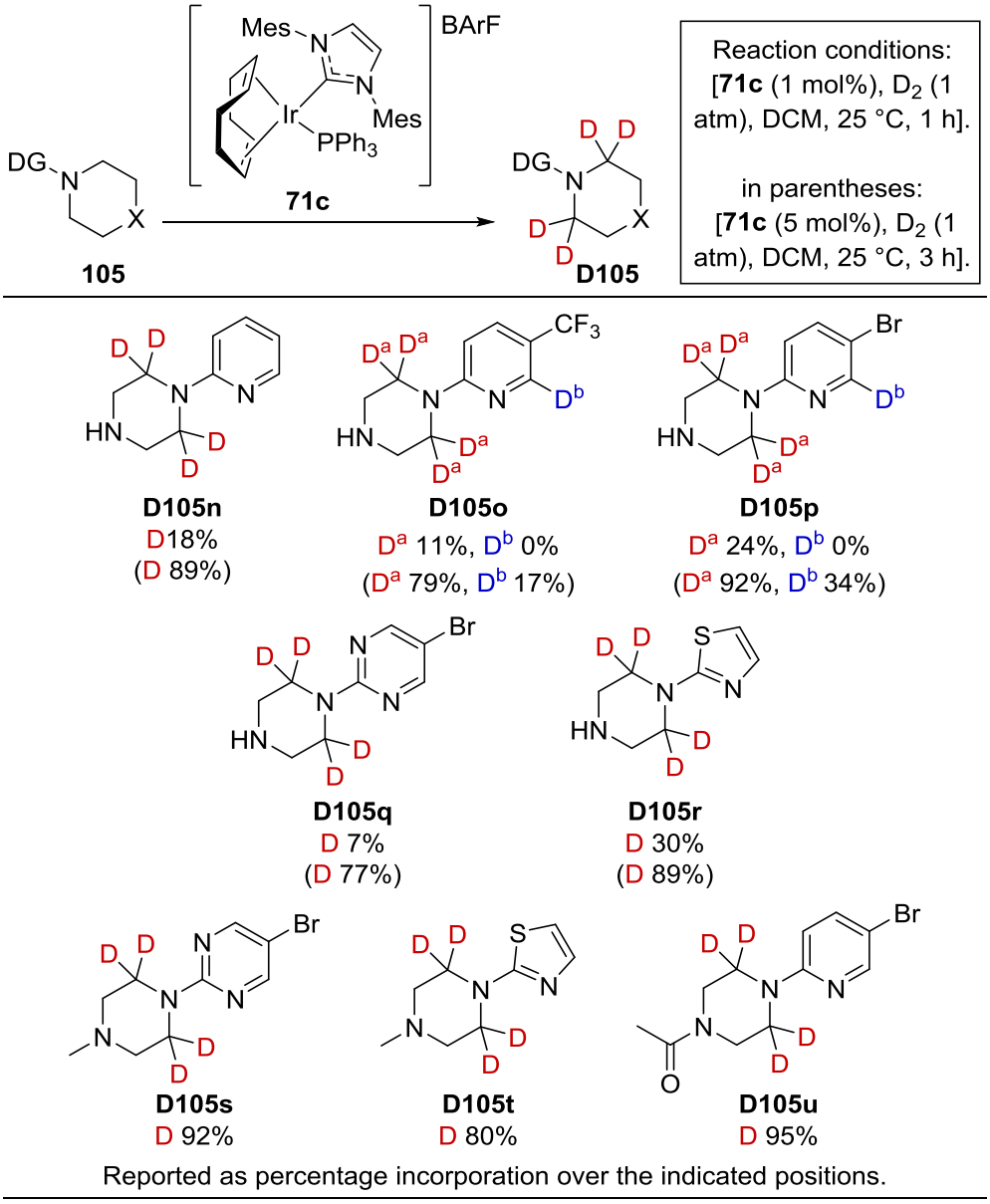

Scheme 2.71 HIE on piperazines substrates.

In an effort to understand the change in reactivity observed with unprotected, secondary amine-containing substrates, we examined the reaction mixture by ^{31}P NMR spectroscopy with piperidine substrate **105v** and piperazines substrate **105q** (**Figure 2.14**). Prior to activation, only the expected square planar complex is present (16.3 ppm) with both substrates. However, following activation with H_2, the reaction containing piperidine substrate **105v** clearly forms a single catalyst species with a chemical shift of 24.3 ppm. In contrast for the reaction **105q**, multiple signals were observed, with none in the expected region around 24 ppm. This certainly indicates that different processes are operating, which are assumed to be outside the HIE

pathway. Moreover, presumably at least one of the alternative catalyst species is formed reversibly, allowing generation of the active catalyst species, albeit at very lower concentration, to facilitate HIE at a reduced rate. Unfortunately, despite these promising initial findings, further attempts to investigate this system did not yield any useful information due to the complex mixture formed upon activating the catalyst in the presence of **105q**.

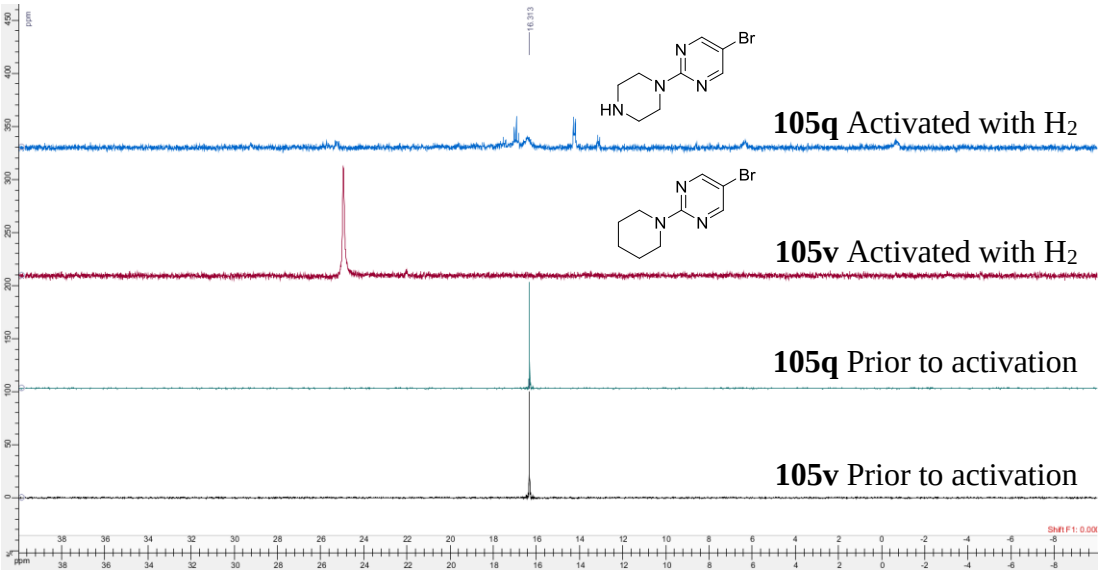

Figure 2.14 NMR studies examining the catalyst deactivation with piperazines.

Having successfully delivered excellent levels of incorporation in a wide range of six-membered, saturated heterocycles, we wished to investigate alternative ring sizes (**Scheme 2.72**). Initial results under the first set of conditions showed a clear preference for HIE on the six-membered piperidine **D105v** over seven-membered azepane **D105w** or five-membered pyrrolidine **D105x** substrates. Furthermore, four-membered azetidine **D105y** did not show any activity for HIE. In order to address this, we then applied the alternative conditions previously optimised for piperazines. In this case, excellent incorporation was observed within azepane **D105w** and pyrrolidine **D105x**, however, azetidine **D105y** still proved resistant to HIE, with only minor levels of exchange observed on the pyridine ring.

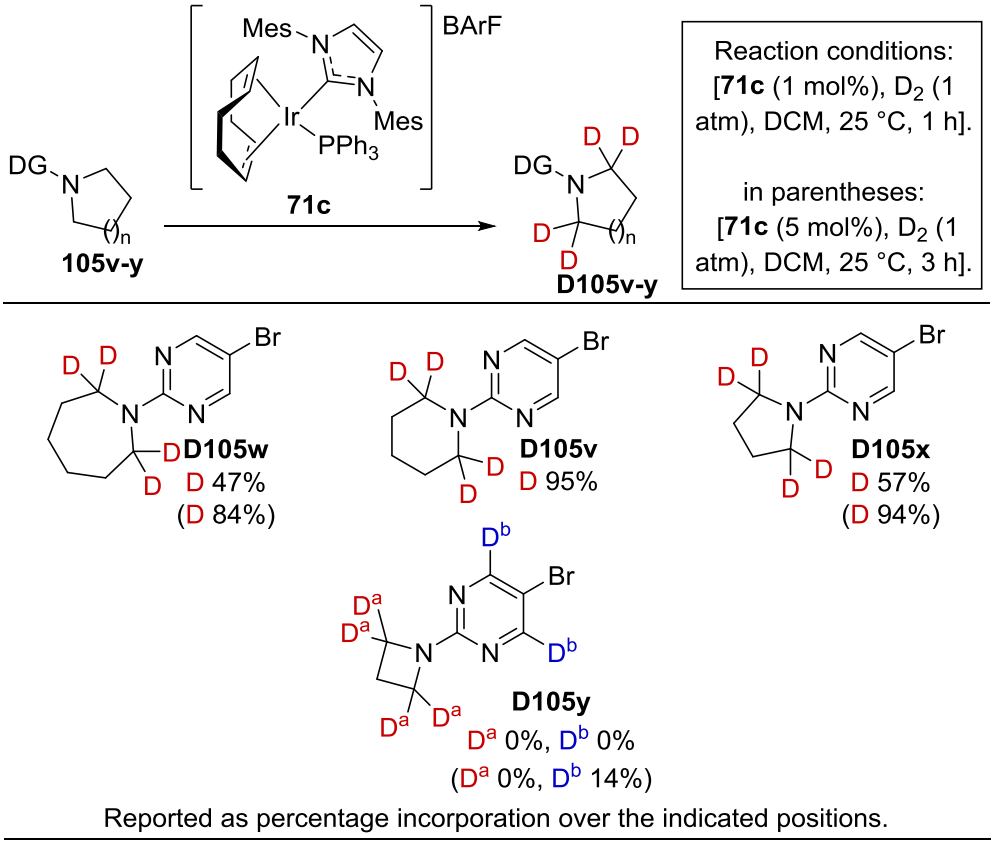

Scheme 2.72 Investigating HIE on different sized, saturated N-heterocycles.

However, despite the excellent incorporations achieved with *N*-heterocyles, their labelling could still not be accessed through carbonyl-based directing groups. To remedy this, we reassessed a range of catalysts under more forcing conditions, akin to those used in carboxylic acid HIE with substrate **105d**, utilising MTBE as the solvent to allow access to a higher reaction temperature of 50 °C, (**Scheme 2.73**). Notably, even under these more forcing conditions, complexes **63a**, **30**, **64a** and **88** did not deliver any incorporation, indicating that both a bulky NHC (i.e. IMes) and the more non-coordinating BArF counterion are necessary. Furthermore, when examining the catalysts that did deliver incorporation, **71c**, **87a-b**, it became clear that a more electron-rich phosphine was required to access high deuterium incorporations, with complex **87a** delivering excellent, near-quantitative incorporation.

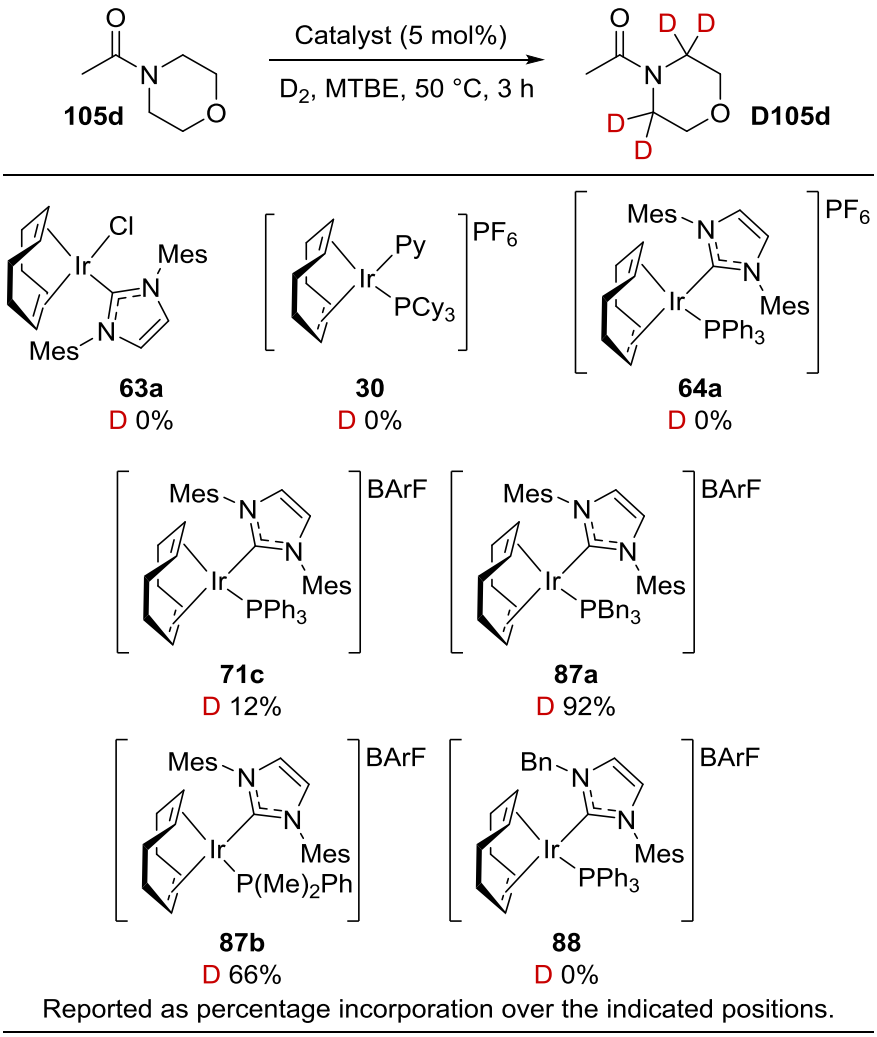

Scheme 2.73 Reassessing the catalyst choice for carbonyl directed HIE.

With the knowledge that through changing the catalyst to **87a** we could access high deuterium incorporation utilising carbonyl directing groups, we next sought to fully optimise the reaction conditions. In a similar fashion to previous protocols, we utilised design of experiments to do this, in this case examining the catalyst loading, reaction time and reaction temperature. It was found that catalyst loading and reaction temperature had a similarly positive impact upon the labelling, whereas reaction time had almost no impact over the chosen reaction time window. Through this, we were able to generate optimised conditions to apply in sp^3 HIE with carbonyl directing groups [**87a** (5 mol%), MTBE, 50 °C, 1 h] (**Scheme 2.74**). However, initial success with model substrate **D105d** and piperidine **D105l** was limited, as further substrates proved to be challenging, such as piperazine **D106a**, containing the troublesome secondary amine group. Even substitution of successful substrates appeared to inhibit

the reaction, as with the acid in **D106b** or the piperidine in **D106c**. Although our available complexes can facilitate the reaction, these results suggest a generally effective system will require further exploration.

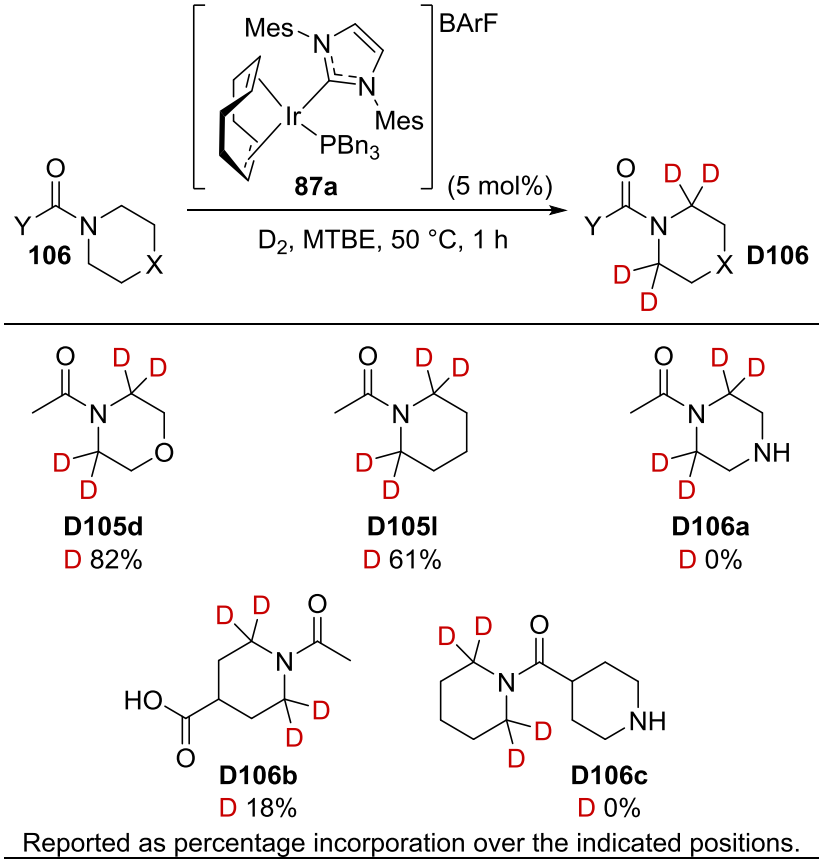

Scheme 2.74 sp^3 HIE with carbonyl directing groups.

However, these conditions did improve the level of exchange in a number of substrates that had also been unsuccessful under the earlier conditions (**Scheme 2.75**). Indeed, it also validates the solvent utility of the process that the poorly coordinating tetrazole **D107a** works excellently in *t*BuOAc. Moreover, both the poorly soluble benzimidazole **D107b**, which also contains a secondary amine, and thiazole **D107c** delivered excellent incorporation at the sp^3 and aryl positions using 2-MeTHF as solvent.

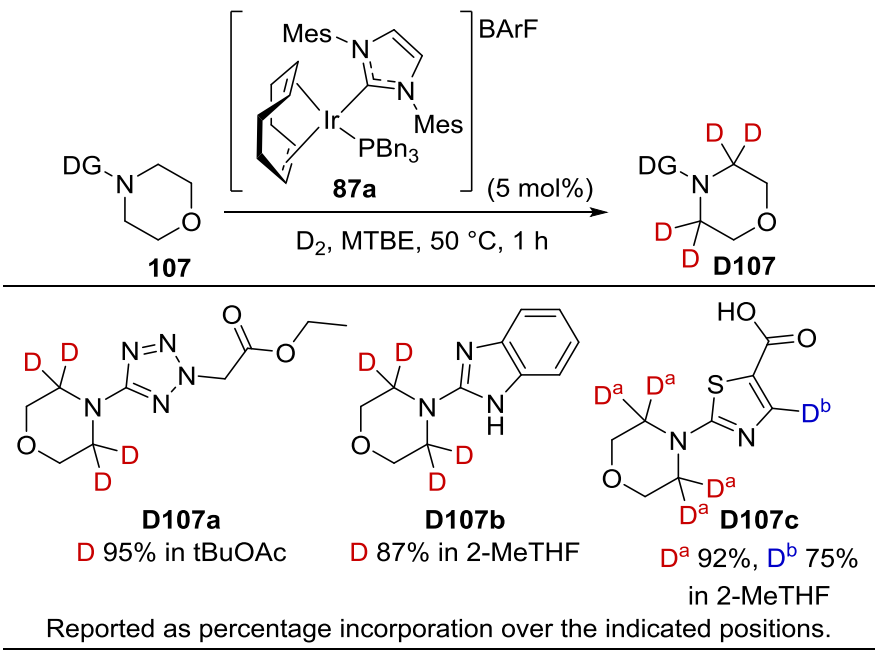

Scheme 2.75 Further solvent scope with problematic substrates.

Having accessed a wide variety of saturated heterocycles, we next turned our attention to acyclic systems in an effort to expand the utility of our new process (**Scheme 2.76**). Initial results under our first protocol indicated the increased challenge of performing HIE using substrates that can assume non-productive conformations. Indeed, only 2-methoxyquinoline **D108a** underwent HIE, delivering only low levels of incorporation. However, application of our second protocol resulted in more promising results. Firstly, **D108a** garnered excellent levels of exchange, solely at the methyl position. Next, 2-ethylmethylamino pyridine **D108b** delivered excellent incorporation across all both exchangeable positions, notably with no selectivity for CH_3 and CH_2 positions, with both proceeding *via* a 5-mmi. Further to this, upon removing the ethyl substituent from the nitrogen, as in **D108c**, a significantly lower incorporation resulted, reminiscent of the results achieved with piperazine substrates. However, through application of our third protocol, high isotope incorporation was restored. Following this, we observed the same trend for 2-(benzylamine)pyridine **D108d** in which the third protocol delivered high isotope incorporation.

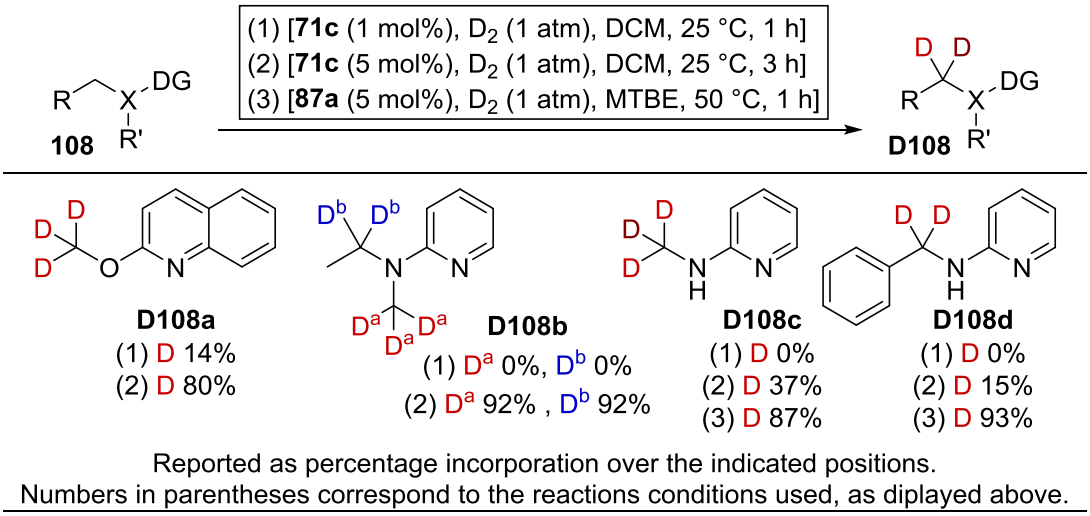

Scheme 2.76 HIE on non-cyclic substrates.

Keeping with acyclic substrates, we also wished to examine sp^3 positions activated by a functional group other than a simple ether or amine (**Scheme 2.77**). Firstly, activation by a carboxylic acid **D108e** was examined, and, although poor under our first protocol, good incorporation was achieved using protocol two. Secondly, activation was realised with an ester **D108f**. Despite the similarity carboxylic acid substrate this performed noticeably worse, perhaps indicating that a pseudo-CMD C-H insertion assisted by the carboxylate, takes place with substrate **D108e**.

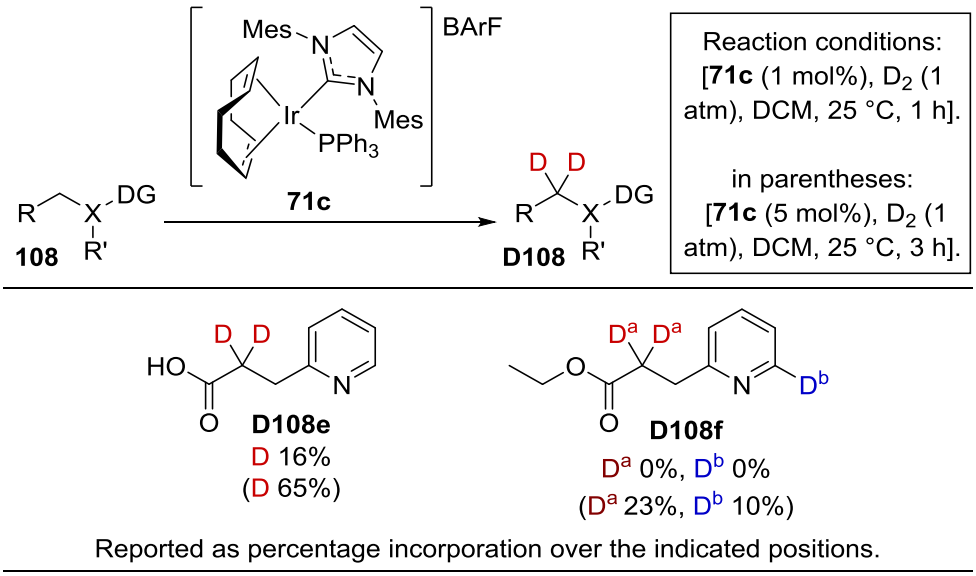

Scheme 2.77 HIE on FG-activated, non-cyclic sp^3 positions

To assess the application of these new protocols in multifunctional systems, we applied a series of competition reactions, in a similar fashion to our earlier studies (**Table 2.11**). To do this we applied model substrate **104**, under our first optimised protocol, with a single equivalent of an additive. In the first instance, the additive contained an aryl nitro functional group **90l**, in this case, the deuterium incorporation occurred

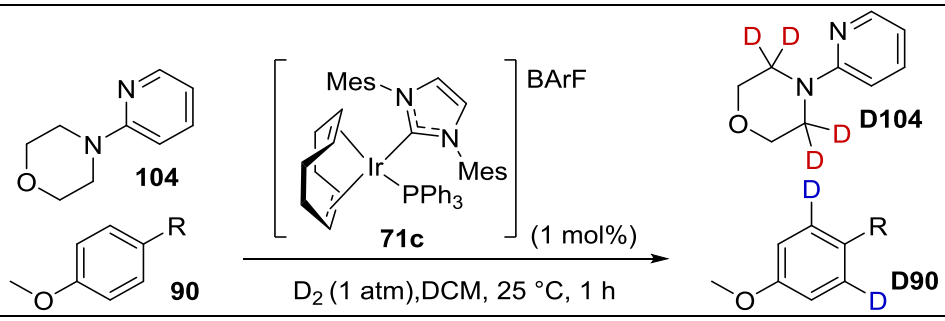

Entry[a]	*Additive*	*Additive* *D-incorporation (%)*	*Substrate 104* *D-incorporation (%)*
1	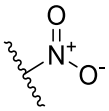 **90l**	24	94
2	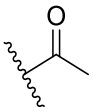 **90m**	6	94
3	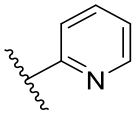 **90n**	14	0
4	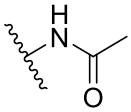 **90o**	0	82
5	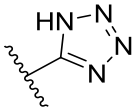 **90p**	25	0
6[b]	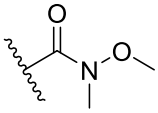 **90q**	17	92
7[c]	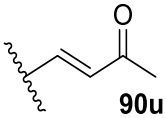 **90u**	35	88

[a] Incorporation calculated from LCMS analysis; [b] Incorporation measure over the two ortho and three N-methyl positions; [c] Incorporation measured over the one olefinic position only.

Table 2.11 Competition reactions; investigating the selectivity of HIE.

preferentially at the sp^3 position in **D104**. Similar results were obtained with aryl ketone **90m**, clearly indicating that although we may consider the aryl C-H bond to be better activated to C-H insertion, it is not the sole factor controlling HIE selectivity. In contrast to this, application of pyridinyl additive **90n** reversed the selectivity, with only low levels of incorporation observed on the aryl additive and no sp^3 incorporation. As expected in amide additive **90o**, the six-mmi was disfavoured versus the five-mmi within substrate **D104**. Surprisingly, given the typically basic conditions for HIE on tetrazoles,[47] exchange was observed solely upon the aryl tetrazoles additive **90p**, perhaps indicative of a similar interaction between the tetrazole as the secondary amine already highlighted. Consistent with our previous results, the carbonyl directing group of Weinreb amide **90q** was disfavoured over substrate **D104**. Furthermore, the olefinic exchange in **90u** was disfavoured over the sp^3 exchange in D**104**. When considering this result, it is somewhat surprising, since typical olefinic labelling proceeds at just 0.1 mol% of a very similar catalyst.

To validate our use of competition reactions, we applied our methodology to a selectin of few substrates containing multiple directing groups (**Scheme 2.78**). Firstly, ester functionalised compound **109a** delivered excellent selectivity for the sp^3 sites. However, use of nitro functionalised substrate **109b** resulted in high incorporation *ortho* to the nitro group, in poor agreement with our competition reactions. Notably, we observed a significantly higher incorporation at C2 opposed to C4, perhaps indicating a different mechanism is in operation as previously observed in other 3-substituted pyridines.[75] Alternatively, the 2- and 4-positions of pyridine are electron deficient in comparison to the anisyl ring utilised in the competition reactions, and therefore, the barrier to C-H insertion would be lower, allowing a faster exchange and delivering a different selectivity.

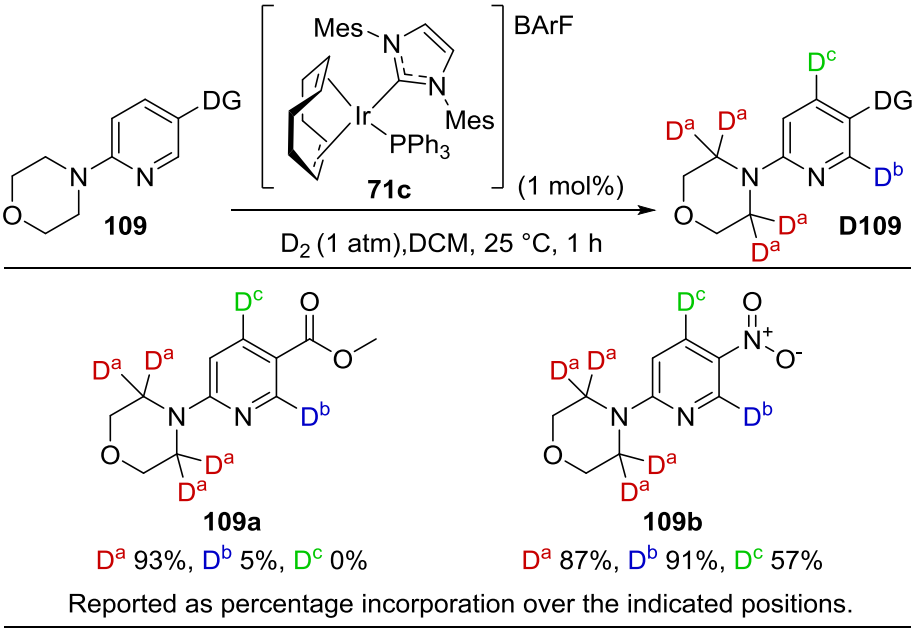

Scheme 2.78 HIE on substrates containing multiple labelling sites.

Throughout the labelling of sp^3 centres, we have worked under the assumption that the mechanism is the same as aryl- and olefinic HIE (i.e. proceeding via C-H insertion). In an effort to clarify the sp^3 labelling mechanism, we performed a KIE experiment as probe for a C-H insertion event (**Scheme 2.79**, **Graph 2.12**). This was achieved by running several reactions over different reaction times, and measuring the isotope incorporation to establish the rate of exchange. Indeed, measuring the rate for both deuterium and hydrogen independently, delivered a KIE value of 3.22, which is in good agreement with those obtained previously for similar C-H insertion events.[45,49,59] We concluded that this was strong evidence indicating the mechanism proceeded *via* the same pathway as previously discussed for aryl- and olefinic HIE. It is worth noting at this point, that although this is true of the chosen substrate **105v**, it may not be the case for exchange in alternative substrates, such as **D108a-b**. However, further examination of such substrates was outside the scope of this project.

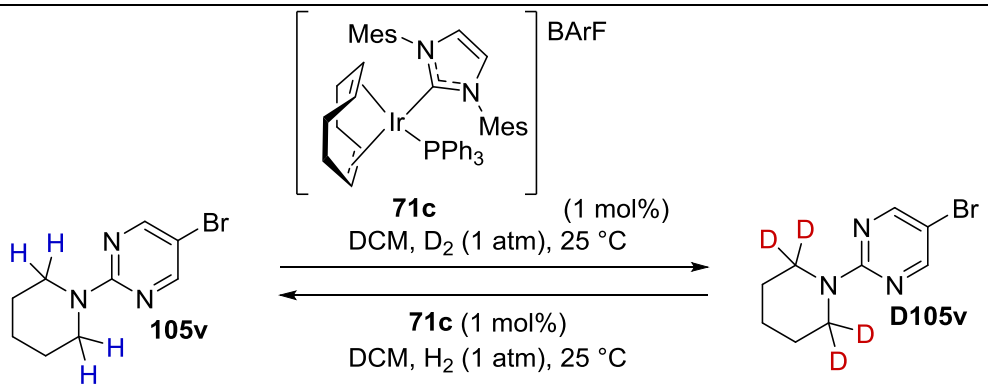

Scheme 2.79 KIE experiment for sp^3 HIE.

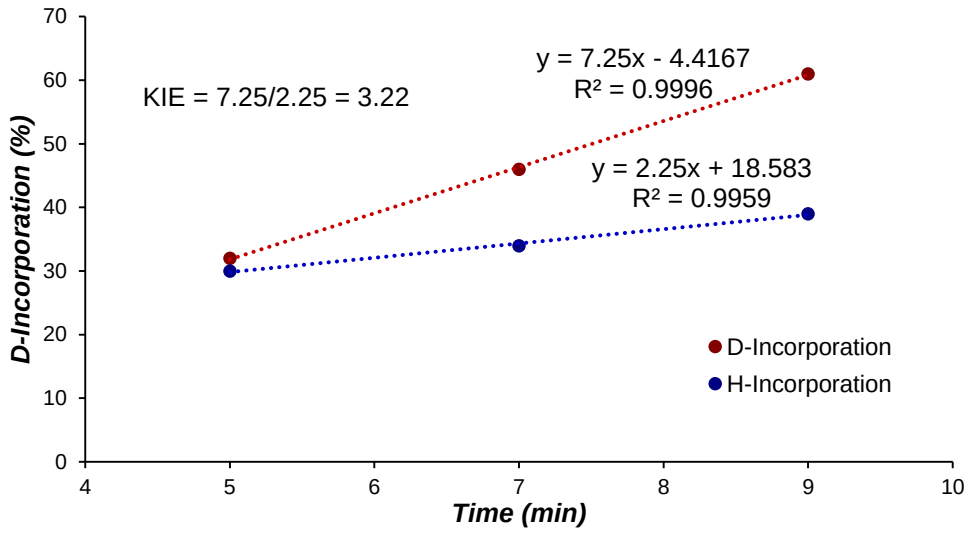

Graph 2.12

To conclude this project, and to fully evaluate the validity of our three new protocols, we applied them in HIE on several commercial drug compounds (**Scheme 2.80**). Commencing the study by exploiting our first protocol with antidepressant *Mirtazapine* **D110**, we were pleased to observe excellent deuterium incorporation solely on the piperazine ring. Furthermore, application of the tranquilizer *Azaperone* **D111** led to excellent and selective isotope incorporation again on the piperazine, with only minimal labelling observed on the arene, as predicted by our earlier studies. Submission of the stimulant *Caffeine* **D112** to our first protocol resulted in moderate incorporation, solely directed by the imidazole nitrogen. Indeed, even with excellent incorporation under our second optimised conditions, the isotope was delivered only to this at a single position. Finally, application of the antipsychotic *Clozapine* **D113** proved especially troublesome, with both the first and second protocol delivering low

incorporations. This is likely due to two factors; firstly the presence of a diphenylamine, and secondly the nature of the imine directing group. Indeed, we can consider the imine to be a midpoint between an *N*-heterocyle and a carbonyl directing group. Additionally, the presence of the adjacent arene further hinders the directing group. Despite this, our final optimised conditions delivered a good isotope incorporation solely on the piperazine heterocycle.

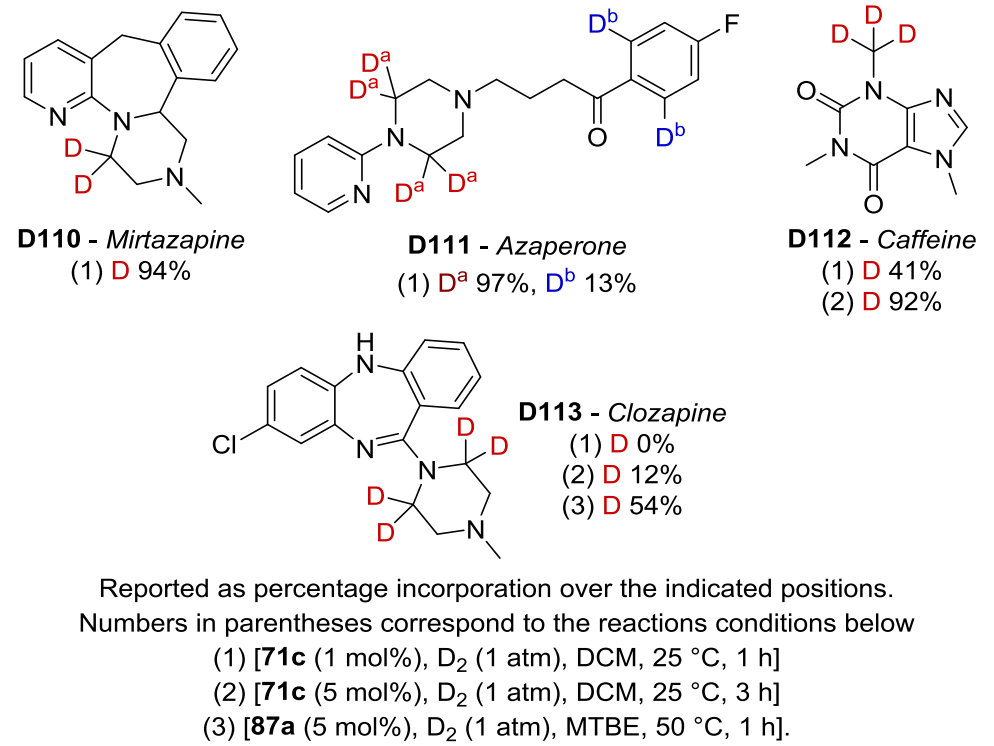

Scheme 2.80 HIE on drug substrates.

In summary, we have successfully and expediently generated three new protocols through application of experimental design, and have successfully applied them in HIE at sp^3 centres. Furthermore, these protocols allow us to impart a hydrogen isotope upon a range 5- 6- and 7- membered saturated heterocycles, through a directed exchange utilising a wide array of functional groups. Additionally, we have successfully applied these protocols within non-cyclic substrates, vastly improving the value of our new methods. Further to this, we have continued our efforts to understand the selectivity observed within HIE through the careful selection of substrates and proper application of competition reactions. Finally, the practicality of our protocol has been demonstrated through the successful labelling of four drug compounds.

3.4. Understanding Selectivity in HIE

Throughout this chapter, we have consistently explored the reaction mechanism and selectivity of each new process that we have investigated. Indeed, we conclude that each process, aryl-, olefinic- or sp^3 HIE proceeds through the same principal mechanistic pathway (**Scheme 2.81**). Furthermore, we have recognised that the rate-determining step of the mechanism is the insertion of iridium into the C-H bond undergoing exchange. However, an important question remained; what governs the selectivity of HIE? And, can it be predicted?

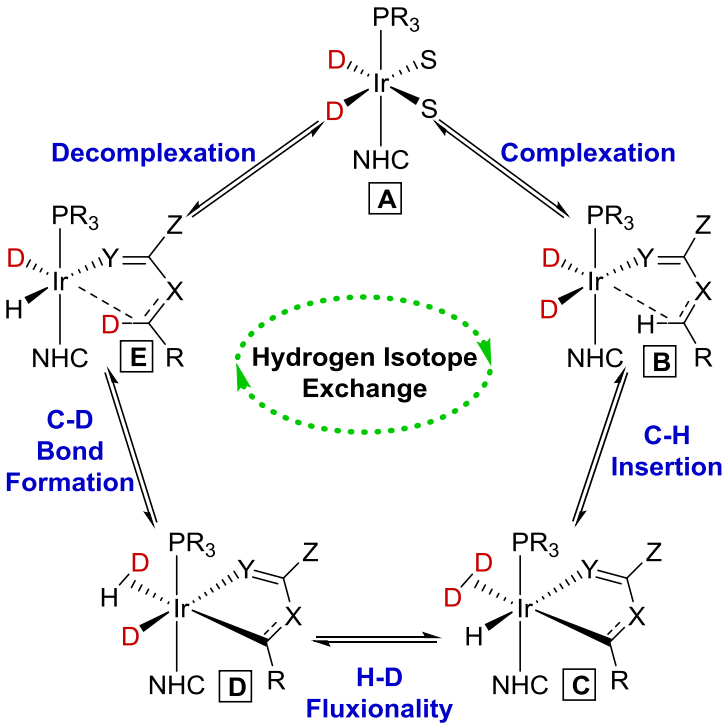

Scheme 2.81 General mechanism for Ir-catalysed HIE.

To answer these questions, we first attempted to ascertain which step of the mechanism determined the selectivity of exchange. With the knowledge that C-H insertion was rate determining, each following step was considered to be energetically less demanding, and, therefore, not involved in determining the selectivity. Therefore, we considered one of either substrate-catalyst complexation or C-H insertion to be responsible for the fate of the isotopic label in HIE. We next identified a key example to examine, in the form of chalcone derivative **98c**, which in our previous studies had delivered selective olefinic exchange over the potential aromatic exchange (Scheme 2.82). When considering the whole range of chalcone derivatives, we have previously

noted the substantial change in selectivity upon manipulation of the electronic properties of the substrate. It was considered that this would most influence the C-H activation event, as any change in the complexation would affect both aryl and olefinic positions, because since they both originate from the same directing group.

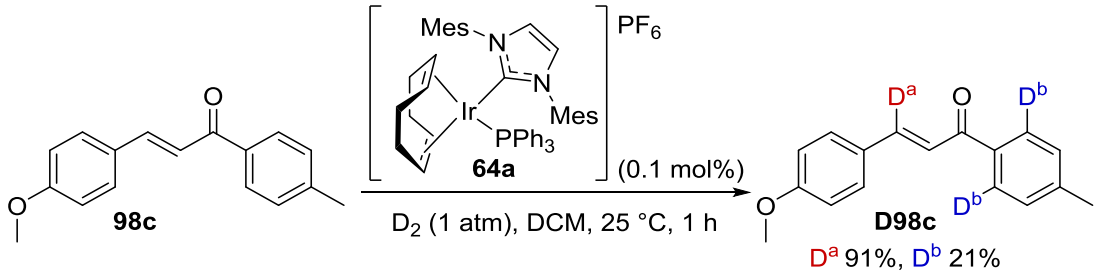

Scheme 2.82 Selectivty in chalcone-derived substrate **98c**.

To investigate the difference in C-H insertion events we utilised an Eyring-Polanyi plot to examine the activation energy of each process, respectively (**Graph 2.12**). Through careful analysis of our data, we were able to generate values representing the energetic changes through each activation process. In doing so, the major contribution to the activation energy was found to originate from the change in enthalpy, with only a small contribution from reaction entropy. Secondly, and most importantly, the activation energy for olefinic exchange was significantly lower than that of aromatic exchange, thus implying that the olefinic C-H insertion is kinetically favoured, matching our experimental findings. It is also important to note that, although higher in energy, the barrier to aromatic C-H insertion is still accessible at the normal reaction temperature, explaining the low but appreciable levels of incorporation on the aryl ring. Therefore, the case of a single directing group with two independent labelling sites, can be considered, in principle, to be controlled by the enthalpy of activation. However, we accept that this enthalpy involves a number of equilibria (e.g. catalyst-substrate and catalyst-product binding) which could in turn control the observed selectivity.

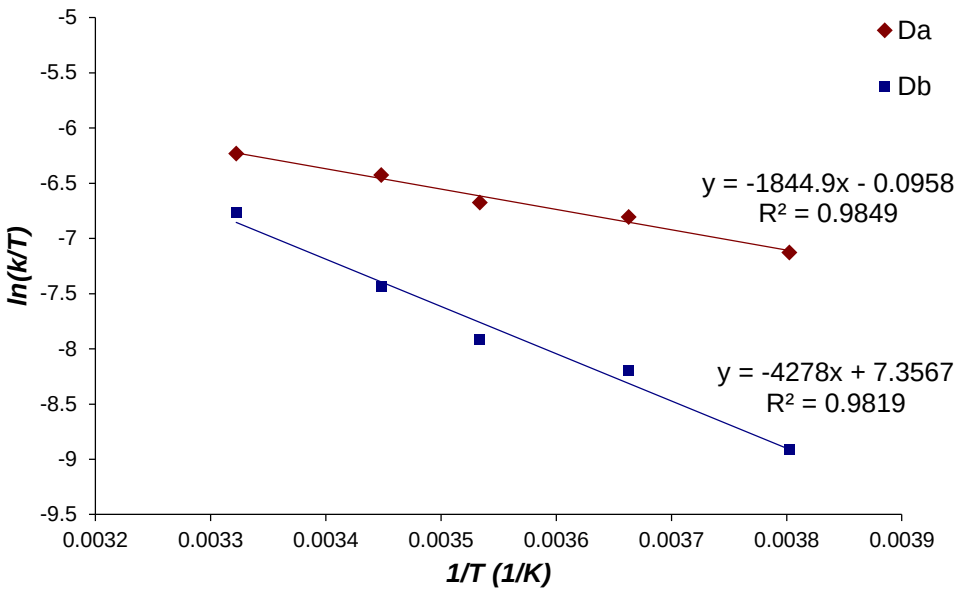

Graph 2.13 Eyring-Polanyi plot of HIE upon chalcone **98c**.

Olefinic C-H (D^a)	***Aromatic C-H (D^b)***
$\Delta H^{\ddagger}$ = 3.7 kcal mol^{-1}	$\Delta H^{\ddagger}$ = 8.5 kcal mol^{-1}
$\Delta S^{\ddagger}$ = -0.7 cal mol^{-1} K^{-1}	$\Delta S^{\ddagger}$ =-0.5 cal mol^{-1} K^{-1}
E_a = 3.9 kcal mol^{-1}	E_a = 8.6 kcal mol^{-1}

However, we had also observed in aryl-, olefinic- and sp^3 HIE that having two distinct directing groups, each associated with its own labelling site, delivered markedly different selectivity depending upon the directing group. Therefore, we next considered if the directing group was affecting the C-H insertion. To this end, we revisited selected results previously obtained within our competition studies (**Scheme 2.83**).

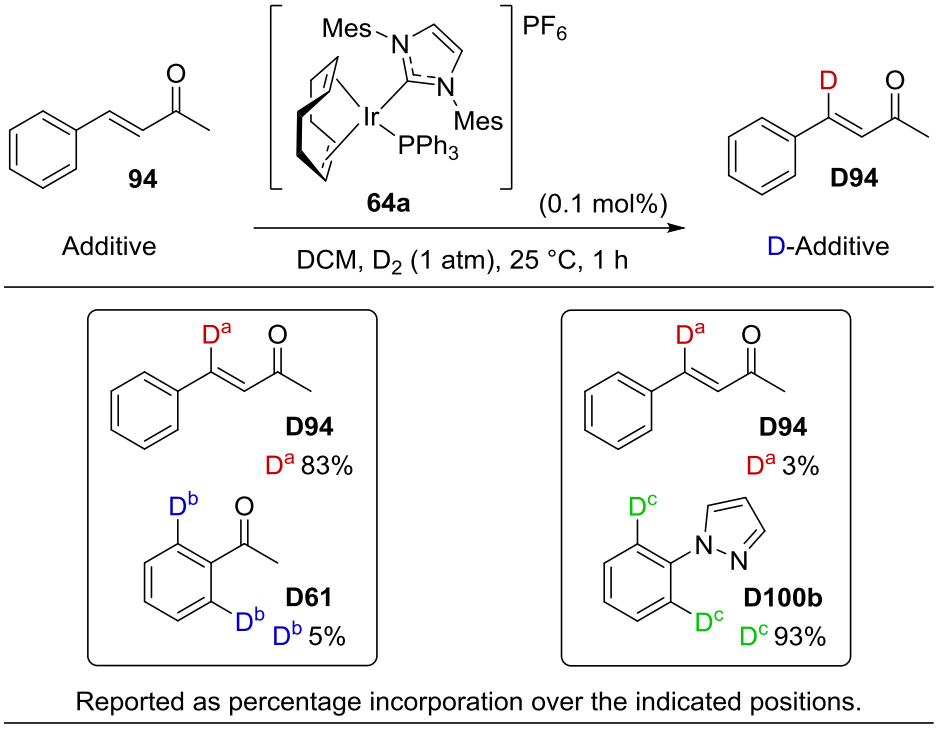

Scheme 2.83 Selectivty from the competition reactions between **94**, **61** and **100b**.

The chosen examples exhibit a reverse in selectivity through a change in directing group. If it is the C-H insertion step governing this change in selectivity, it would be reflected in the activation energy (**D61**>**D94**>**D100b**), as previously mentioned. Therefore, we again utilised an Eyring-Polanyi plot to ascertain the activation energy for each respective exchange process (**Graph 2.14**). In contrast to our previous investigation with chalcone **D98c**, the magnitude of activation energy did not match the findings from the competition reactions. In fact, the lowest activation energy was for the least favoured site of exchange, on acetophenone **D61**. With these findings in mind, we turned our attention back to the reaction mechanism, in which complexation remained as the only candidate for controlling HIE in this case.

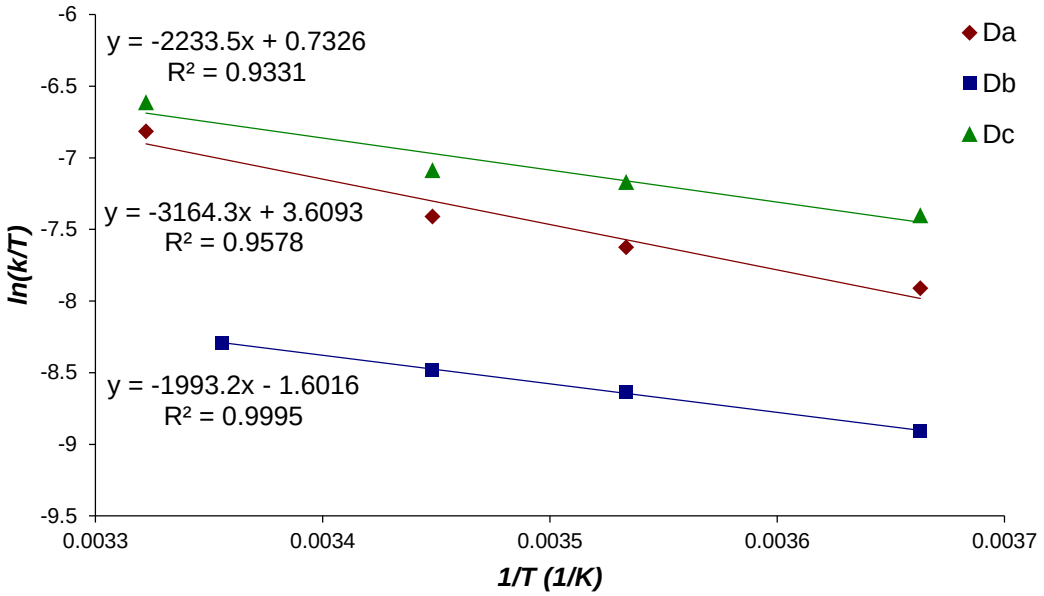

Graph 2.14 Eyring-Polanyi plot of HIE upon substrates **94**, **61** and **100b**.

94 (D^a)	***61 (D^b)***	***100b (D^c)***
$\Delta H^{\ddagger}$ = 6.3 kcal mol^{-1}	$\Delta H^{\ddagger}$ = 4.0 kcal mol^{-1}	$\Delta H^{\ddagger}$ = 4.4 kcal mol^{-1}
$\Delta S^{\ddagger}$ = -0.8 cal mol^{-1} K^{-1}	$\Delta S^{\ddagger}$ = -0.7 cal mol^{-1} K^{-1}	$\Delta S^{\ddagger}$ = -0.7 cal mol^{-1} K^{-1}
E_a = 6.5 kcal mol^{-1}	E_a = 4.2 kcal mol^{-1}	E_a = 4.2 kcal mol^{-1}

Having ascertained that the selectivity of exchange can be governed by either the C-H insertion step or substrate-catalyst complexation step of the HIE process, we next wished to assess different factors that could control the activation energy, and substrate binding energy, in an effort to predict HIE selectivity. In the first instance, we further investigated the fused chalcone structures discussed earlier (**Scheme 2.84**). Indeed, through computationally optimising the geometry of each substrate **98o-q**, we gained insight into the substrate structure and, in particular, the bond angle between the directing group and labelling site. Furthermore, when comparing this bond angle to that of a typical cyclometallated species **99**, it became clear that it reflected well the selectivity of exchange. The origins of this effect can be attributed to the increase in ring strain in the C-H insertion step when the substrate geometry is not already suited to cylcometallation. Hence, expanding the bond angle, as for *ortho*-exchange in **98o**, causes HIE to occur selectively at the *β*-position. Similarly, contracting the bond angle, as for *ortho*-exchange in **98q**, causes HIE to occur selectively at the *β*-position. Alternatively, when both bond angles are similar to that found in intermediate **99**, exchange occurs at both positions, as in **D98p**.

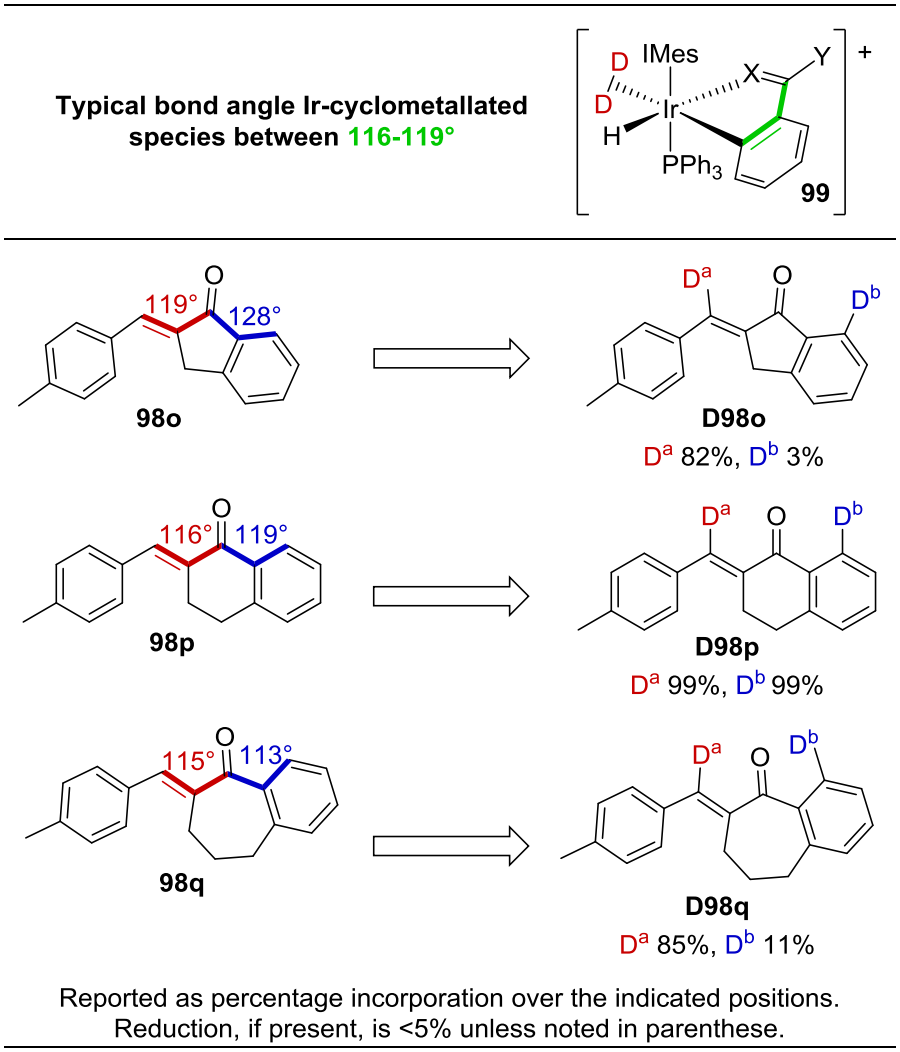

Scheme 2.84 Understanding selectivity in fused chalcone substrates.

Recognising that with a non-planar substrate, the orientation of the hydrogen to undergo exchange could significantly influence the efficiency of HIE, we can draw less information from the calculated bond angles (**Scheme 2.85**). However, relative to favoured piperidine **105v**, compression and expansion of the bond angles in **105w** and **105x**, respectively could indicate a more hindered HIE process. Furthermore, the significant expansion of the bond angle in azetidine **105y** reflects the lack of isotope incorporation. However, if we instead consider the distance between the nitrogen of the directing group and exchange site, we obtain further insight. In particular, that the shortest distance is found in piperidine **105v**, which performs excellently in HIE. Secondly, the distances in both azepane **105w** and pyrrolidine **105x** are significantly greater, and experience lower isotope incorporation. Finally, azetidine **105y** has the largest distance, correlated to its lack of activity. All of this indicates that we can use

the bond angle in sp^{2-}, and the distance in sp^3 HIE, between the directing group and the labelling site, to predict HIE selectivity.

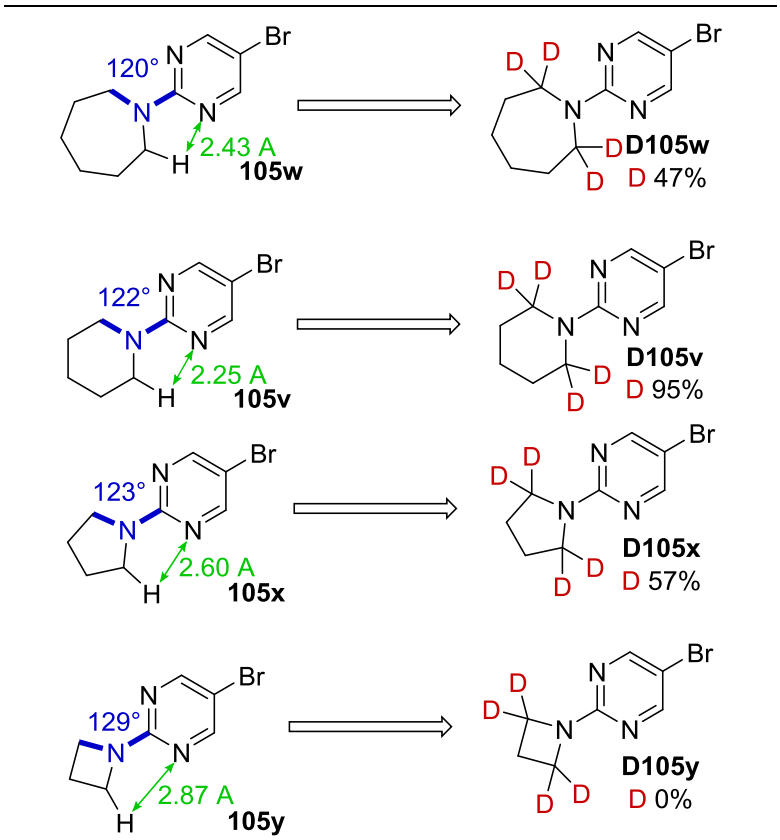

Scheme 2.85 Understanding selectivity with different ring sizes.

In an effort to test this theory we conducted several competition reactions between each substrate **105v-y**, in which we expect the substrate-catalyst complexation to control the selectivity of HIE (**Scheme 2.86**). Pleasingly, in each case the favoured substrate for exchange was that with the shortest distance between the directing group and the exchange site. Indeed, we can attribute this effect to the increased stabilisation of complexation associated with the agostic interaction between iridium and the exchangeable C-H bond. However, we can also attribute it to the increase in ring strain associated with C-H insertion, as previously mentioned. Therefore, it is clear that one cannot totally separate the substrate-catalyst complexation and C-H insertion in attempting to predict the site of HIE.

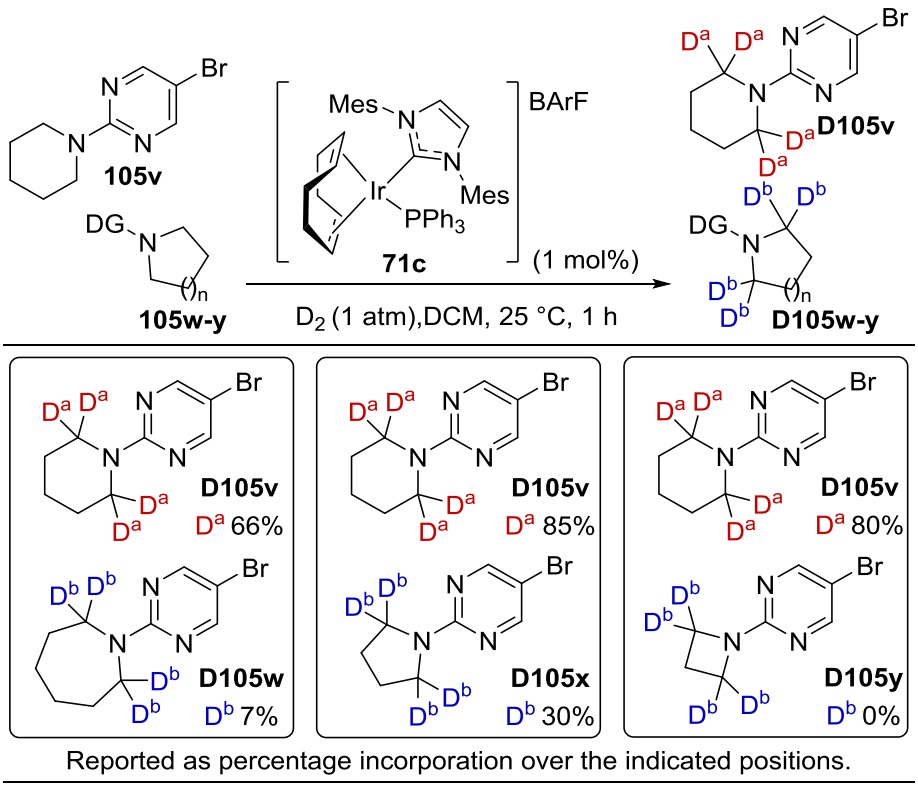

Scheme 2.86 Testing the selectivity of different ring sizes.

Despite this, through compiling the results from our investigations we have generated a five-step guide for predicting HIE, when using a phosphine/NHC catalyst. (**Scheme 2.87**). Firstly, we must consider the directing group, which has the greatest impact upon the labelling selectivity, with strongly basic *N*-heterocycles proving most favourable, and weakly basic or acidic carbonyl groups being disfavoured. Indeed, our previous findings in aryl HIE suggest that the pK_{aH} of an *N*-heterocyclic directing group is a good reflection of its selectivity in HIE.[76] However, it is important to note that a steric or electronic bias may change this ordering. Secondly, we must consider the size of each proposed cyclometallated intermediate, understanding that a 5-mmi is kinetically favoured over a 6-mmi. Thirdly, if the angle (or distance) between the directing group and labelling position are constrained or expanded from an optimal window then labelling will be disfavoured. Subsequently, if both positions exchange via similar proposed intermediates, we must consider the site of exchange. In principle, this is ordered from non-activated sp^3 to activated aromatic C-H bonds. However, it is important to note that this order may change depending upon the substitution near the exchange site. Indeed, if a secondary directing group (e.g. a functional group containing an accessible lone pair) is present, if would be favoured. Conversely, if only

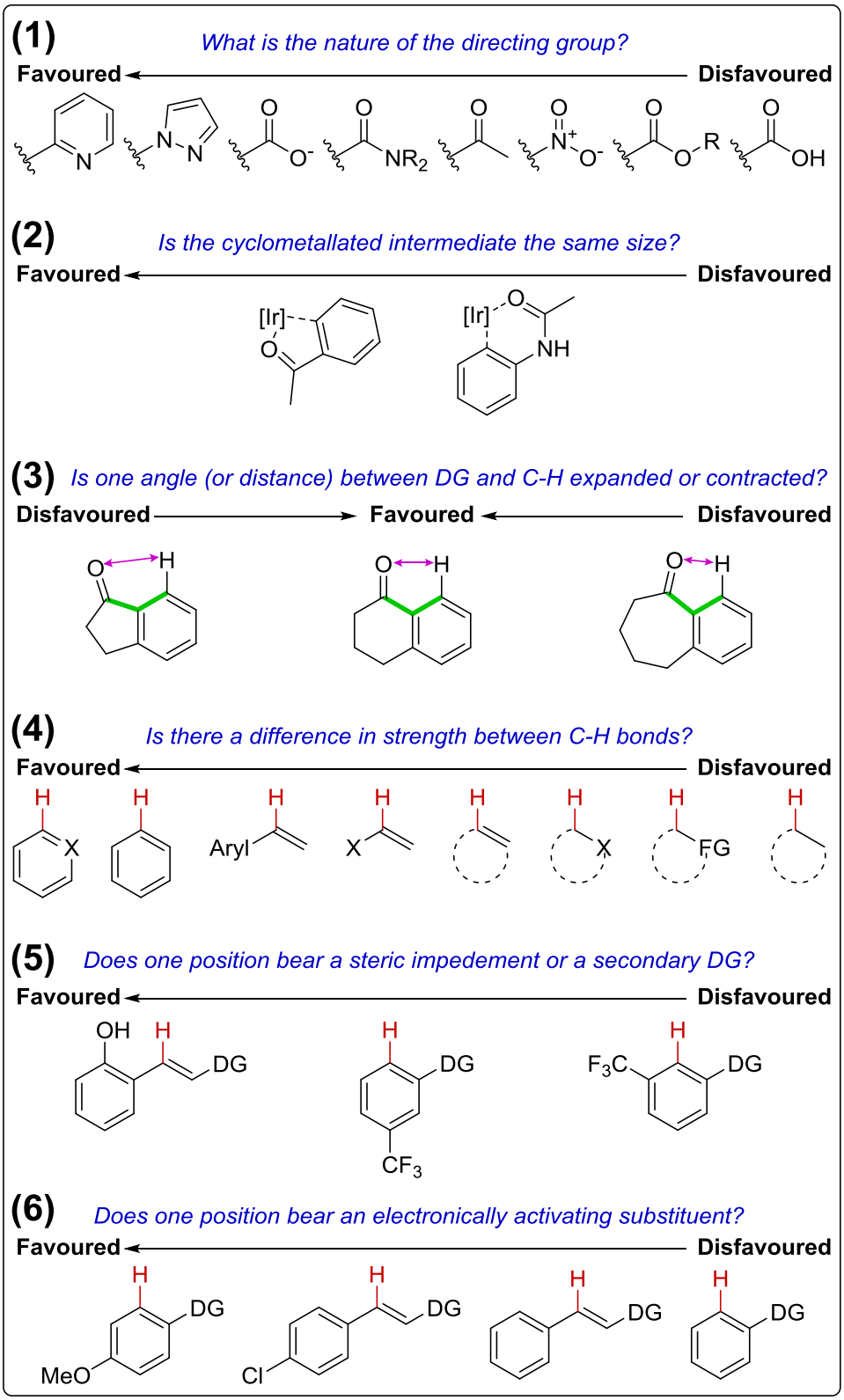

Scheme 2.87 Guide to predicting the favoured site of exchange in multifunctional pharmacueticals.

a steric interaction is expected, the site is disfavoured. Finally, substitution of the substrate as a means of perturbing the C-H bond may influence the selectivity. In

general, any substituent will activate a position to exchange over the non-substituted derivative.

Within this final section, we have explored the nature of the mechanism controlling HIE. We can conclude from the studied examples, that for two distinct potential C-H insertion events, both directed by the same functional group, the kinetically favoured process takes precedent. On the contrary, if multiple functional groups are present, the substrate-catalyst complexation selects the position of exchange. However, decisive prediction of HIE requires examination of both processes. Therefore, based upon our experimental findings, we developed a series of guidelines to aid in the prediction of HIE selectivity. With this, we believe that, when utilising our NHC/phosphine catalysts in HIE with complex, multifunctional molecules, the selectivity of exchange can be reasonably predicted.

4. Conclusions

Throughout this chapter, we have endeavoured to apply our NHC/phosphine complexes to a range of new applications in hydrogen isotope exchange. In doing this we have utilised a wide array of experimental methods, and paired them where appropriate with theoretical findings.

Our initial work focussed upon delivering an industrially friendly protocol that could replace more common high temperature methods in the labelling of aryl carboxylic acids (**Scheme 2.88**). Capitalising upon the broad range of available catalysts, and improved solvent utility of non-coordinating counterion complexes, we successfully realised a method for base-free, *ortho*-deuteration. Through this work we gained vital insight into the interaction of acidic directing groups with the catalyst, and the impact upon labelling chemo- and regioselectivity that the addition of base can impart.

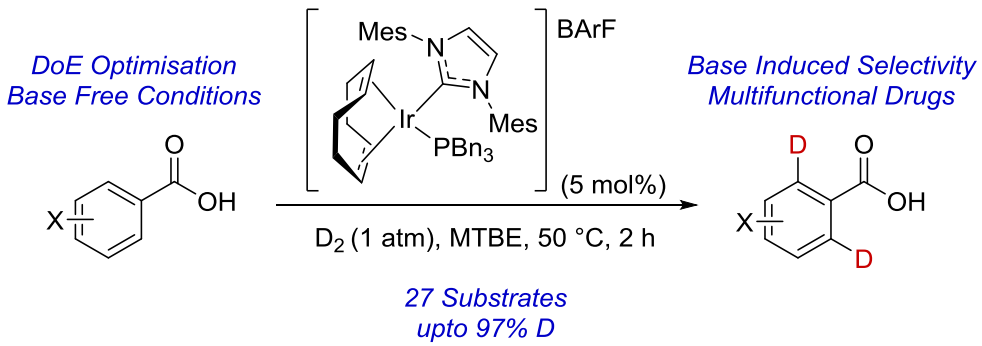

Scheme 2.88 Acid directed HIE.

In an effort to interpret the future needs of the pharmaceutical industry, we looked to examine exchange on non-aryl positions, initially through labelling of olefinic sites (**Scheme 2.89**). Successfully exploiting the insight garnered through studies examining the reduction of such species, we were able to expediently introduce an efficient method of introducing a deuterium label through a directed exchange. This allowed us to further study the mechanism of exchange, and interpret the selectivity between exchange and hydrogenation through theoretical modelling.

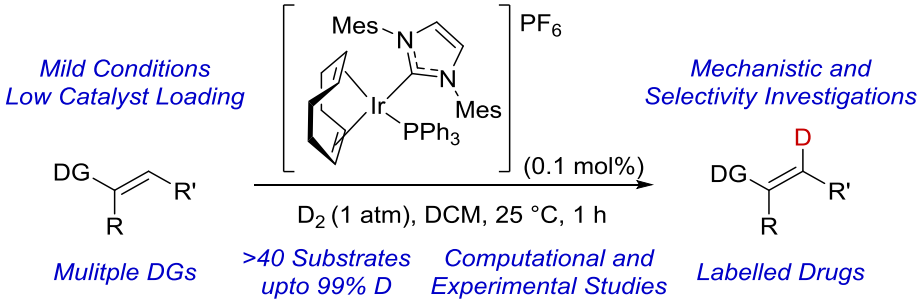

Scheme 2.89 Non-aryl sp^2 HIE

To bring the application of our NHC/phosphine complexes to the forefront of C-H activation technology, we next applied them in the deuterium labelling of sp^3 positions (**Scheme 2.90**). Exploiting our earlier investigations, we quickly applied experimental design techniques to generate three distinct protocols, allowing isotopic labelling of a wide array of cyclic and non-cyclic sp^3 sites. This in turn, allowed us to further study the mechanism and investigate the selectivity between different labelling sites.

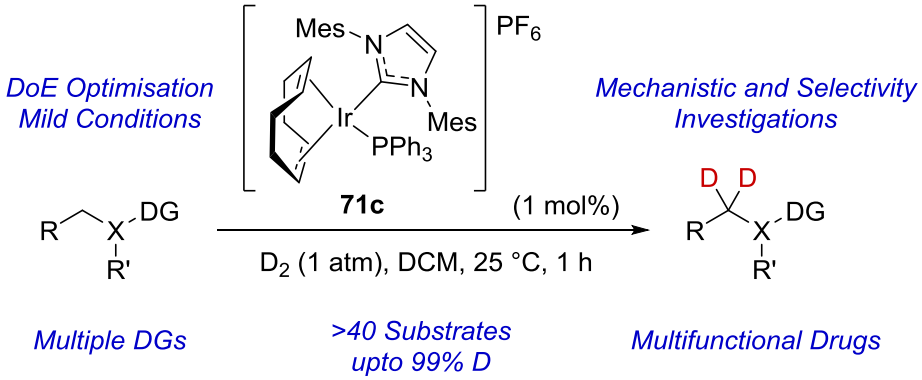

Scheme 2.90 sp^3 HIE.

Lastly, by compiling our results regarding selectivity within the hydrogen isotope exchange process, we produced a five-step guide to predicting the dominant site of exchange within multifunctional compounds (**Scheme 2.87**). Primarily, this is controlled by the nature of the directing group, then the cyclometallated intermediate or its precursor, including the agostic interaction, and, finally, the relative accessibility of the bond to undergo C-H insertion.

5. Future Work

Within this thesis we have detailed an expansion of the functionalities capable of undergoing exchange, and through this have further enhance understanding of the required catalyst structure in each case. Considering these findings and those from previous work, we have detailed below potential future projects.

Having discussed within this work the successful exchange utilising carboxylic acids, and, moreover, in previous work, tetrazole directing groups, we can next consider the potential use of further common bioisosteres of this type (**Scheme 2.91**). Indeed, when considering this, primary efforts should aim at sp^2-based directing groups which show good activity with our NHC/phosphine complexes. Indeed, this could include directing groups such as; hydroxamic acids, sulfonylureas and oxadiazolones. Furthermore, when considering tetrahedral directing groups such as, sulfonamides[49] and sulfones,[77] which have proven successful with NHC/Cl and chelating complexes respectively, we can also consider phosphonic, sulfonic and tetramic acids.

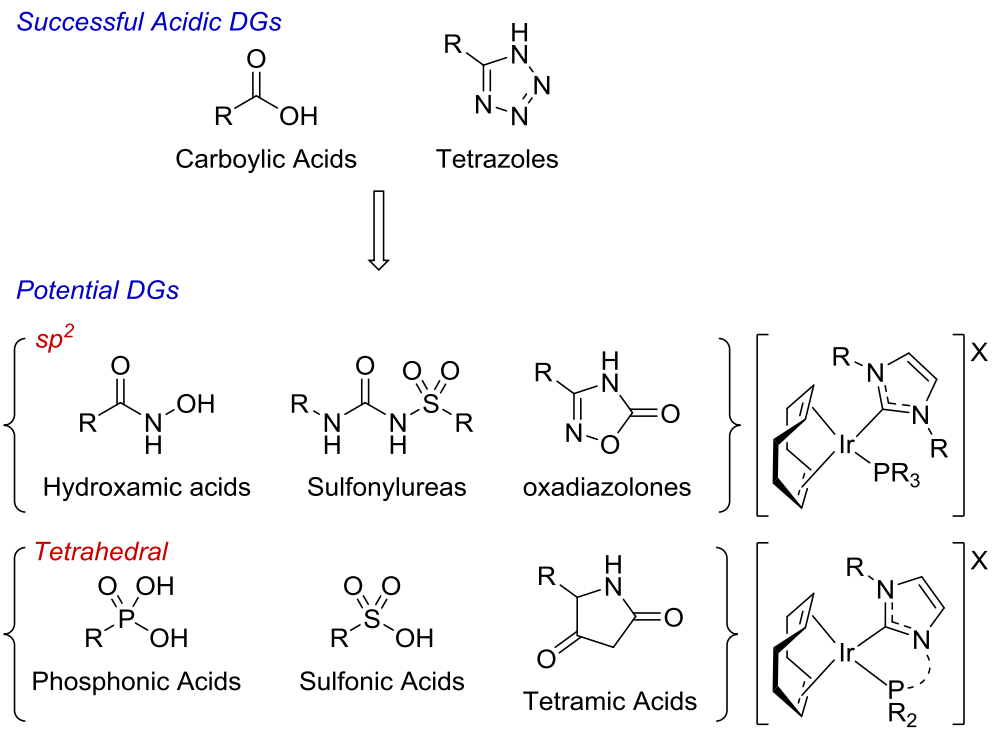

Scheme 2.91 Further labelling of acidic moieties.

Having established that C-H insertion and exchange is viable at sp^3 centres through the use of *N*-heterocyclic directing groups, we should next consider the capricious

nature of carbonyl directing groups (**Scheme 2.92**), with a view to further investigating the origins of the preference for HIE at the equatorial position of six-memebred heterocycles. Certainly, improvement in this area is especially attractive due to the potential application in isotopically labelled amino acids and peptides (**Scheme 2.93**). Such labelling methods would require a different solvent scope than currently available, with most peptides being only poorly soluble in typical labelling solvents. With this in mind, development of different counterion complexes bearing more coordinating counterions may hold the key to improving water solubility of the iridium complexes (**Scheme 2.94**).

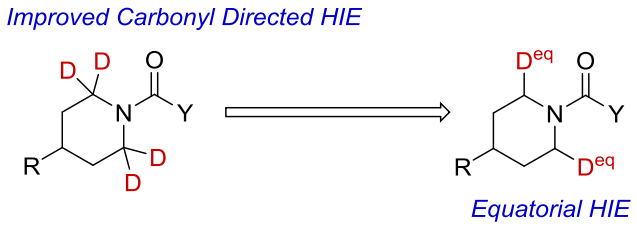

Scheme 2.92 Potential improvement in carbonyl directed sp^3 HIE.

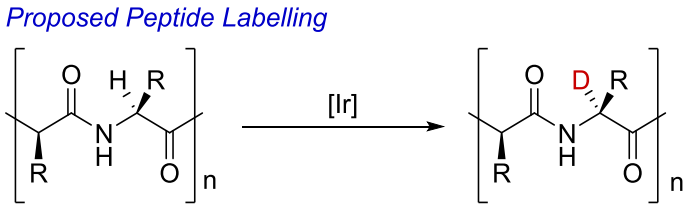

Scheme 2.93 Peptide labelling.

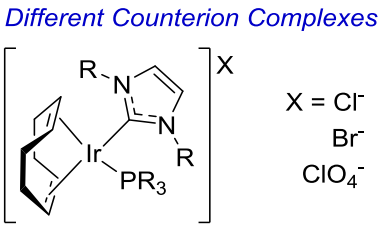

Scheme 2.94 Improved water soluble complexes.

6. Experimental

6.1. General Experimental Details

All reagents were obtained from commercial suppliers and used without further purification unless stated otherwise. Purification was carried out according to standard laboratory methods.[78]

Iridium complexes were synthesised as stated in the relevant references or Experimental Section of **Chapter 1**, **Section 5.1**.

Exchange reactions (**Sections 3.1 and 3.3**) were carried out on a Heidolph Synthesis 1 Liquid 16 device (**Figure E2.1**).

Figure E2.1

Exchange reactions (**Section 3.2**) were carried out using a round-bottom flask (25 mL) fitted with a double oblique stopcock connected to a manifold and deuterium balloon.

^{1}H (300 MHz or 400 MHz) and ^{13}C (75 MHz or 101 MHz) NMR spectra were obtained on Bruker spectrometers in the solvents indicated. Chemical shifts are reported in ppm. Coupling constants are reported in Hz and refer to $^{3}J_{\text{H-H}}$ couplings, unless otherwise stated. ^{1}H NMR spectra were obtained using a 10 second delay to allow full relaxation of all hydrogen environments (D1 = 10).

IR spectra were obtained on a Shimadzu IRAffinity-1 Spectrophotometer machine and peaks are reported in cm^{-1} unless stated otherwise.

Thin layer chromatography was carried out using Camlab silica plates coated with fluorescent indicator UV_{254}. Plates were analysed using a Mineralight UVGL-25 lamp or developed using vanillin, $KMnO_4$ or Ninhydrin solution.

Flash column chromatography was carried out using Prolabo silica gel (230-400 mesh).

Mass spectrometry data was acquired from EPSRC National Mass Spectrometry Centre, Swansea University.

The distribution of hydrogen isotopes in the products was determined by a liquid chromatography-mass spectrometry (LC-MS) system with a Symmetry Shield RP18 column, 3.9 x 150 mm, with a gradient program. LC column conditions were as follows:

mobile phase A: water (900 mL), acetonitrile (100 mL), TFA (1 mL)

mobile phase B: water (100 mL), acetonitrile (900 mL), TFA (1 mL),

Flow rate: 0.6 mL/min

Details of Computational Methods

Density functional theory[79,80] (DFT) was employed to calculate the gas-phase electronic structures and energies for all species involved in H/D exchange or hydrogenation reactions. All structures thus far have been optimised with the hybrid meta-GGA exchange correlation functional M06.[81] The M06 density functional was used in conjunction with the 6-31G(*d*)[82,83] basis set for main group non-metal atoms and the Stuttgart RSC[84] effective core potential along with the associated basis set for Ir. Harmonic vibrational frequencies were calculated at the same level of theory to characterize respective minima (reactants, intermediates, and products with no imaginary frequency). The validity of using the 6-31G(d) basis set has previously been checked by comparative single point energy calculations employing the def2-TZVP[85] basis set for all atoms on similar H/D exchange systems.[49] All calculations using the M06 functional have been performed using Gaussian 09 quantum chemistry program package (version A.02).[86]

General Experimental Procedures

General procedure A *Exchange reactions using Heidolph synthesis 1 liquid 16 device.*

The Heidolph Synthesis 1 Liquid 16 device was evacuated and filled with argon, and the water condenser turned on. To a carousel tube was added the substrate of choice (0.086 mmol), and iridium catalyst (and additive where appropriate). The desired solvent (1 mL) was added, rinsing the inner walls of the tube. The tube was then sealed at the screw cap (with the gas inlet left open) under argon. The flask was twice evacuated and refilled with deuterium *via* a balloon. The gas inlet tube was then closed, creating a sealed atmosphere of deuterium, the carousel shaking motion initiated (750 rpm) and the temperature set. After starting the device shaking motion and temperature controller, the timer was initiated and a rapid red/orange to clear/yellow colour change was observed. The reaction mixture was stirred for the allotted time before removing excess deuterium and replacing with air. The yellow solution was then analysed by LC-MS or ^{1}H NMR.

The level and regioselectivity of deuterium incorporation in the substrate can be determined by ^{1}H NMR spectroscopy. The integrals were calibrated against a peak corresponding to a position not expected to be labelled. The equation below was then used to calculate the extent of labelling.

$$\%\,Deuteration\ = 100 - [\left(\frac{residual\ integral}{number\ of\ exchangeable\ sites}\right) \times 100]$$

The incorporation of deuterium into each substrate can be verified by LCMS, by observing a shift in the isotope distribution in the starting material (M) to show M+1 (D_1), M+2 (D_2), M+3 (D_3) etc. for the labelled compound.

General procedure B *Exchange reaction carried out in a round bottom flask.*

A flame-dried 50 mL round-bottom flask under an argon atmosphere, bearing a double oblique stopcock adaptor, was charged with the desired substrate, catalyst and solvent (and additive where appropriate). The flask was cooled to -78 °C in a dry-ice/acetone slurry bath. The flask was evacuated and refilled with deuterium from a balloon, and the process repeated three times. After the final flush, the stopcock was left open to the balloon and the flask immersed in an oil bath at the desired temperature. The reaction solution was observed to change from a pale orange colour to clear within 5 min. Following the allotted reaction time, the deuterium atmosphere was released and replaced with air. The solvent was removed *in vacuo* and the reaction residue passed through a plug of silica (eluting with petroleum ether/Et_2O, 1/1).

Where appropriate, the conversion of the substrate was calculated by ^{1}H NMR. Peaks arising from both the starting material the reduced product was identified; calibration of the reduced product against the starting material and the equation below allowed calculation of the conversion.

$$\%\,Conversion = 100\ \times \left(\frac{reduced\ integral}{reduced\ integral + starting\ material\ integral}\right)$$

The level and regioselectivity of deuterium incorporation in the substrate can be determined by ^{1}H NMR spectroscopy. The integrals were calibrated against a peak corresponding to a position not expected to be labelled. The equation below was then used to calculate the extent of labelling.

$$\%\,Deuteration\ = 100 - [\left(\frac{residual\ integral}{number\ of\ exchangeable\ sites}\right) \times 100]$$

General procedure C *Monitored exchange reactions carried out in a round bottom flask.*

A flame-dried, 100 mL, two-necked round-bottom flask under an argon atmosphere, bearing a double oblique stopcock adaptor and a suba seal, was charged with the desired substrate, catalyst and solvent. The flask was cooled to -78 ^{o}C in a dry ice/acetone bath. The flask was evacuated and flushed with deuterium from a balloonand the process repeated a further two times. After the final flush, the stopcock was left open to the deuterium balloon and the flask immersed in an oil bath at the desired temperature. The reaction solution was observed to change from a pale orange colour to clear within 5 min. At predefined time intervals an aliquot (~0.5 mL) was drawn from the reaction *via* syringe, and placed in a ½ dram screw cap vial prefilled with Et_2O (~1 mL). Following removal of the solvent *in vacuo*, the recovered residue was prepared for analysis by ^{1}H NMR spectroscopy.

6.2. Acid Directed HIE

Scheme 2.42 *Initial labelling of carboxylic acid* ***86a*** *under non-optimised conditions.*

The reactions were carried out following general procedure A and analysed by LCMS and ^{1}H NMR spectroscopy to confirm the extent and position of exchange.

Complex	***Solvent***	***Temperature (°C)***	***Time (h)***	***Base***
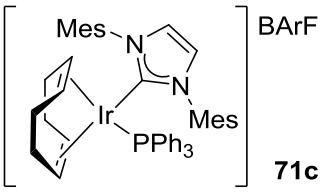 **71c** (7.4 mg, 0.043 mmol)	MeOH	40	6	Cs_2CO_3 (14.0 mg, 0.043 mmol)

Substrate	***^{1}H NMR data***[87]
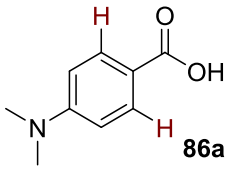 **86a** (14.2 mg)	**^{1}H NMR** (300 MHz, DMSO): δ 12.21 (1H, br s, O-H), 7.77-7.71 (2H, m, Ar-H), 6.74-6.64 (2H, m, Ar-H), 2.97 (6H, s, N-CH_3). Incorporation expected at δ 7.77-7.71. Determined against integral at δ 2.97.
	LCMS data
	Retention time: 2.23 min; Mass ion: 166.2 $(M+H)^+$

D-Incorporation (%)		
Run		***Average***
1	***2***	
18	19	19

Graph 2.2 *Solvent and base screen.*

The reactions were carried out following general procedure A and analysed by LCMS to confirm the extent of exchange. Position of exchange was confirmed through ^{1}H NMR spectroscopy of the highest incorporation result (**Table E2.1**).

Complex	***Temperature (°C)***	***Time (h)***
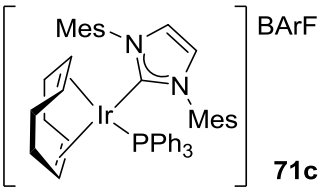 (7.4 mg, 0.043 mmol)	50	6
Substrate	***data***	
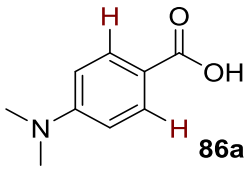 (14.2 mg, 0.086 mmol)	Data was consistent with that reported on page 308.	

Entry	***Solvent***	***Base***	***D-Incorporation (%)***		
			Run		***Average***
			1	***2***	
1	MeOH	Cs_2CO_3 (14.0 mg, 0.043 mmol)	23	21	22
2	IPA		20	17	19
3	tAmylOH		13	9	11
4	iPrOAc		9	9	9
5	tBuOAc		17	23	20
6	2-MeTHF		9	11	10
7	CPME		17	17	17
8	MTBE		37	39	38
9	MeOH	DIPEA (5.6 mg, 0.043 mmol)	8	11	10
10	IPA		24	26	25
11	tAmylOH		36	32	34
12	iPrOAc		31	28	30
13	tBuOAc		28	34	31
14	2-MeTHF		38	44	41
15	CPME		49	43	46
16	MTBE		56	61	59

Table E2.1

Scheme 2.44 *Catalyst screen.*

The reactions were carried out following general procedure A and analysed by LCMS to confirm the extent of exchange. Position of exchange was confirmed through ^{1}H NMR spectroscopy the of highest incorporation result (**Table E2.2**).

Solvent	***Temperature (°C)***	***Time (h)***	***Base***
MTBE	50	6	DIPEA (5.6 mg, 0.043 mmol)
Substrate		***data***	
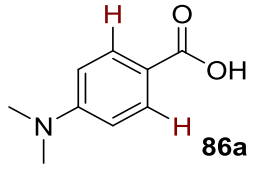 **86a** (14.2 mg, 0.086 mmol)		Data was consistent with that reported on page 308.	

Entry	***Complex***	***D-Incorporation (%)***		
		Run		***Average***
		1	***2***	
1	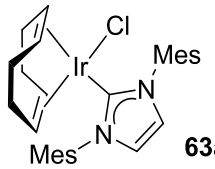 **63a** (2.8 mg, 0.0043 mmol)	0	0	0
2	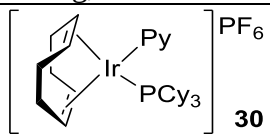 **30** (3.5 mg, 0.0043 mmol)	6	6	6
3	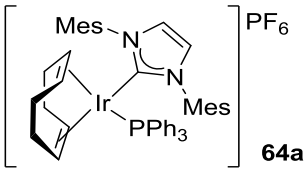 **64a** (4.4 mg, 0.0043 mmol)	10	9	10
4	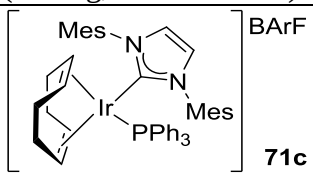 **71c** (7.4 mg, 0.0043 mmol)	76	83	80

5	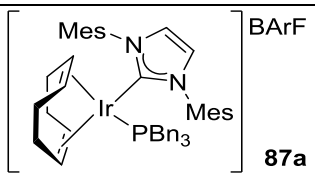 **87a** (7.6 mg, 0.0043 mmol)	91	87	89
6	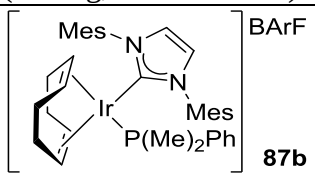 **87b** (6.9 mg, 0.0043 mmol)	72	85	79
7	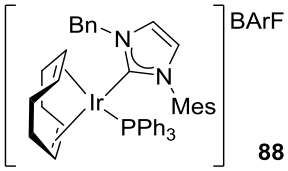 **88** (7.3 mg, 0.0043 mmol)	83	78	81

Table E2.2

Scheme 2.45 Investigating the role of base in the reaction.

The reactions were carried out following general procedure A and analysed by ^{1}H NMR spectroscopy to confirm the extent and position of exchange.

Complex	*Solvent*	*Temperature (°C)*	*Time (h)*
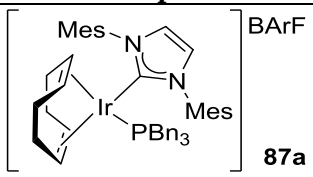 (3.8 mg, 0.002.6 mmol)	MTBE	50	6

Substrate	*Data*
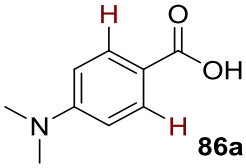 (14.2 mg, 0.086 mmol)	Data was consistent with that reported on page 308.

Entry	*Base*	*D-Incorporation (%)*		
		Run		*Average*
		1	*2*	
1	DIPEA (5.6 mg, 0.043 mmol)	74	74	74
2	N/A	90	92	91

Substrate	*^{1}H NMR data*[88]
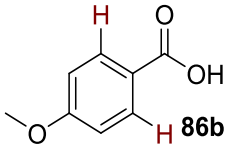 (13.1 mg, 0.086 mmol)	**^{1}H NMR** (300 MHz, DMSO): δ 12.68 (1H, br s, O-H), 7.93-7.84 (2H, m, Ar-H), 7.05-6.97 (2H, m, Ar-H), 3.81 (3H, s, O-CH_3) Incorporation expected at δ 7.93-7.84. Determined against integral at δ 3.81.

Entry	*Base*	*D-Incorporation (%)*		
		Run		*Average*
		1	*2*	
1	DIPEA (5.6 mg, 0.043 mmol)	65	74	70
2	N/A	86	78	82

Substrate	***^{1}H NMR data***[88]
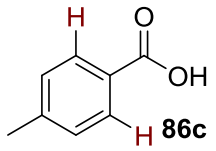 **86c** (11.7 mg, 0.086 mmol)	**^{1}H NMR** (300 MHz, DMSO): δ 12.75 (1H, br s, O-H), 7.86-7.77 (2H, m, Ar-H), 7.33-7.25 (2H, m, Ar-H), 2.36 (3H, s, Ar-CH_3). Incorporation expected at δ 7.86-7.77. Determined against integral at δ 2.36.

Entry	***Base***	***D-Incorporation (%)***		
		Run		***Average***
		1	***2***	
1	DIPEA (5.6 mg, 0.043 mmol)	58	44	51
2	N/A	90	87	89

Substrate	***^{1}H NMR data***[87]
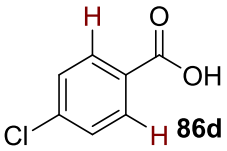 **86d** (13.5 mg, 0.086 mmol)	**^{1}H NMR** (300 MHz, DMSO): δ 13.17 (1H, br s, O-H), 7.97-7.89 (2H, m, Ar-H), 7.60-7.51 (1H, m, Ar-H). Incorporation expected at δ 7.97-7.89. Determined against integral at δ 7.60-7.51.

Entry	***Base***	***D-Incorporation (%)***		
		Run		***Average***
		1	***2***	
1	DIPEA (5.6 mg, 0.043 mmol)	84	86	85
2	N/A	90	88	89

Substrate	***^{1}H NMR data***[89]
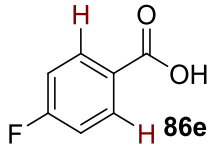 **86e** (12.0 mg, 0.086 mmol)	**^{1}H NMR** (300 MHz, DMSO): δ 13.03 (1H, br s, O-H), 8.06-7.94 (2H, m, Ar-H), 7.36-7.26 (2H, m, Ar-H). Incorporation expected at δ 8.06-7.94. Determined against integral at δ 7.36-7.26.

Entry	***Base***	***D-Incorporation (%)***		
		Run		***Average***
		1	***2***	
1	DIPEA (5.6 mg, 0.043 mmol)	86	86	86
2	N/A	88	88	88

Substrate	***^{1}H NMR data***[89]
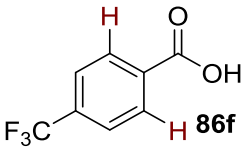 **86f** (16.4 mg, 0.086 mmol)	^{1}H NMR (300 MHz, DMSO): δ 13.47 (1H, br s, O-H), 8.18-8.07 (2H, m, Ar-H), 7.92-7.82 (2H, m, Ar-H). Incorporation expected at δ 8.18-8.07. Determined against integral at δ 7.92-7.82.

Entry	***Base***	***D-Incorporation (%)***		
		Run		***Average***
		1	***2***	
1	DIPEA (5.6 mg, 0.043 mmol)	90	74	82
2	N/A	90	88	89

Substrate	***^{1}H NMR data***[90]
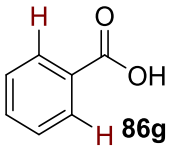 **86g** (16.4 mg, 0.086 mmol)	**^{1}H NMR** (300 MHz, DMSO): δ 12.93 (1H, br s, O-H), 8.00-7.88 (2H, m, Ar-H), 7.66-7.56 (1H, m, Ar-H), 7.55-7.44 (2H, m, Ar-H). Incorporation expected at δ 8.00-7.88. Determined against integral at δ 7.55-7.44.

Entry	***Base***	***D-Incorporation (%)***		
		Run		***Average***
		1	***2***	
1	DIPEA (5.6 mg, 0.043 mmol)	38	35	37
2	N/A	94	91	93

Graph 2.3 *Reassessing the solvent scope without base.*

The reactions were carried out following general procedure A and analysed by LCMS to confirm the extent of exchange. the position of exchange was confirmed through ^{1}H NMR spectroscopy of highest incorporation result (**Table E2.3**).

Complex	***Temperature (°C)***	***Time (h)***
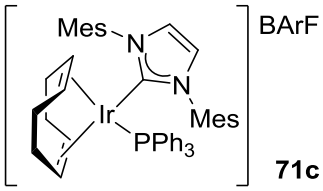 (7.4 mg, 0.0043 mmol)	50	6
Substrate	***data***	
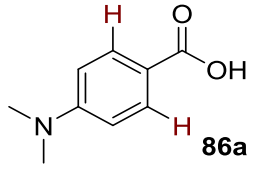 (14.2 mg, 0.086 mmol)	Data was consistent with that reported on page 308.	

Entry	***Solvent***	***D-Incorporation (%)***		
		Run		***Average***
		1	***2***	
1	MeOH	0	0	0
2	IPA	19	17	18
3	tAmylOH	21	21	21
4	iPrOAc	38	33	35
5	tBuOAc	38	34	36
6	2-MeTHF	49	49	49
7	CPME	59	61	60
8	MTBE	69	65	67

Table E2.3

Table 2.4 *Design of experiment; without base present.*

Experimental design was used to assess the effect of varying the catalyst loading, reaction time and reaction temperature. As such, 'high' and 'low' values for each of the three variables were chosen. To generate a series of experiments to study optimal conditions within the variable ranges chosen, Design Expert™ software v10.0 (Stat_Ease Inc., Minneappolis, Mn) was used. This generated a *2-level, three-factorial* design containing three centre points, giving 11 experiments in total. The deuterium incorporation of 4-dimethylamino benzoic acid **86a** was used as the response. The reactions were carried out according to general procedure A and analysed by LCMS to confirm the extent of exchange. The position of exchange was confirmed through ^{1}H NMR spectroscopy of the three centre point experiments (**Table E2.4**).

Complex	***Solvent***
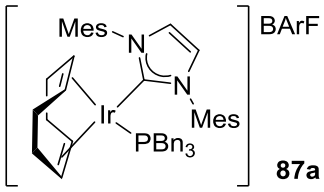 **87a**	MTBE
Substrate	***Data***
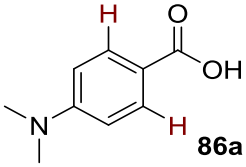 **86a** (14.2 mg, 0.086 mmol)	Data was consistent with that reported on page 306.

Run	*Variable A: Catalyst Loading (mol%)*	*Amount of 87a (mg (µmol))*	*Variable B: Reaction Time (min)*	*Variable C: Reaction Temperature (°C)*	*Response: D-Incorporati on (%)*
1 (+++)	7.5	11.4 (6.45)	240	55	90
2 (---)	2.5	3.8 (2.15)	120	25	39
3 (+--)	7.5	11.4 (6.45)	240	25	60
4 (***)	5.0	7.6 (4.30)	180	40	73
5 (***)	5.0	7.6 (4.30)	180	40	75
6 (***)	5.0	7.6 (4.30)	180	40	78
7 (-+-)	2.5	3.8 (2.15)	240	25	49
8 (-++)	2.5	3.8 (2.15)	240	55	87
9 (+--)	7.5	11.4 (6.45)	120	25	51
10 (--+)	2.5	3.8 (2.15)	120	55	72
11 (+-+)	7.5	11.4 (6.45)	120	55	87
[a] symbol in parentheses indicate points in the design; + high, * mid and – low.					

Table E2.4

Runs 4, 5 and 6 represent the centre points of the design. These are employed in order to:

(i) Assess any curvature in the response of incorporation changes in the variables; and

(ii) Assess the repeatability of the hydrogen isotope exchange reaction.

A response surface was created in the same design program. This generated a half-normal plot which inferred that increasing the reaction temperature, catalyst loading and reaction time all had a positive impact upon the HIE reaction. Furthermore, it inferred the order of significance of each factor as; Reaction Temperature >> Catalyst Loading = Reaction Time (**Graph E2.1**).

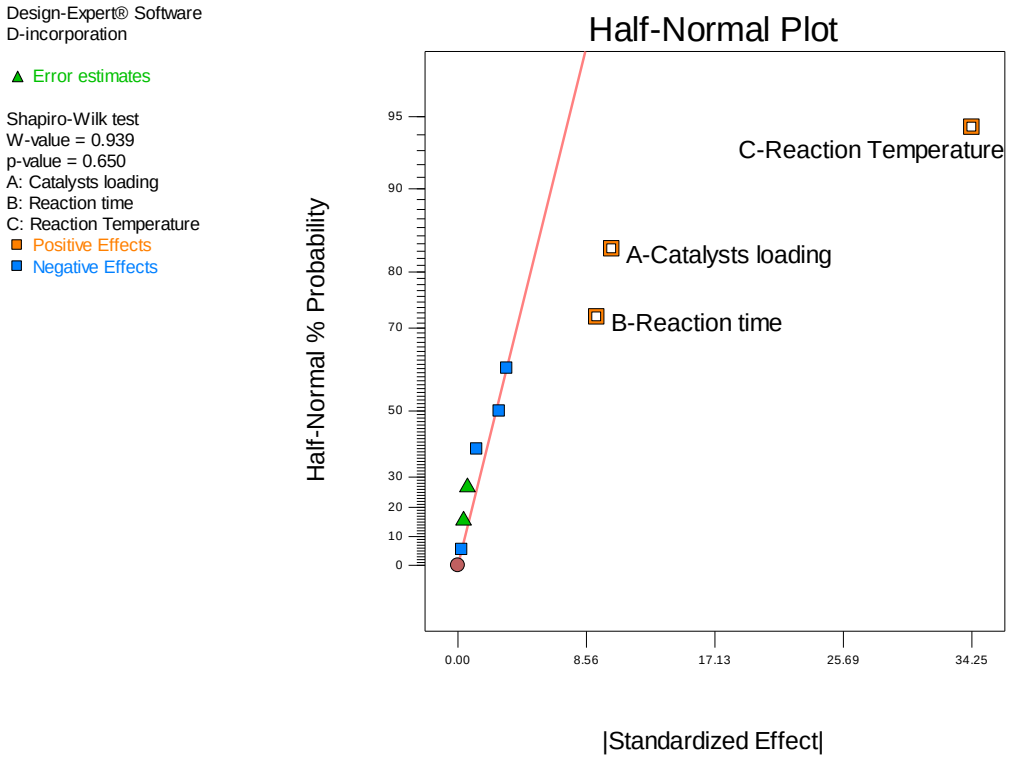

Graph E2.1

Further implementation of the design software generated **Graph E2.2**. By plotting reaction time and temperature at the fixed optimal catalyst loading (5 mol%) it can been seen that elevated temperatures and short reaction times leads to the optimised conditions (5 mol% catalyst, 50 °C, 2 h).

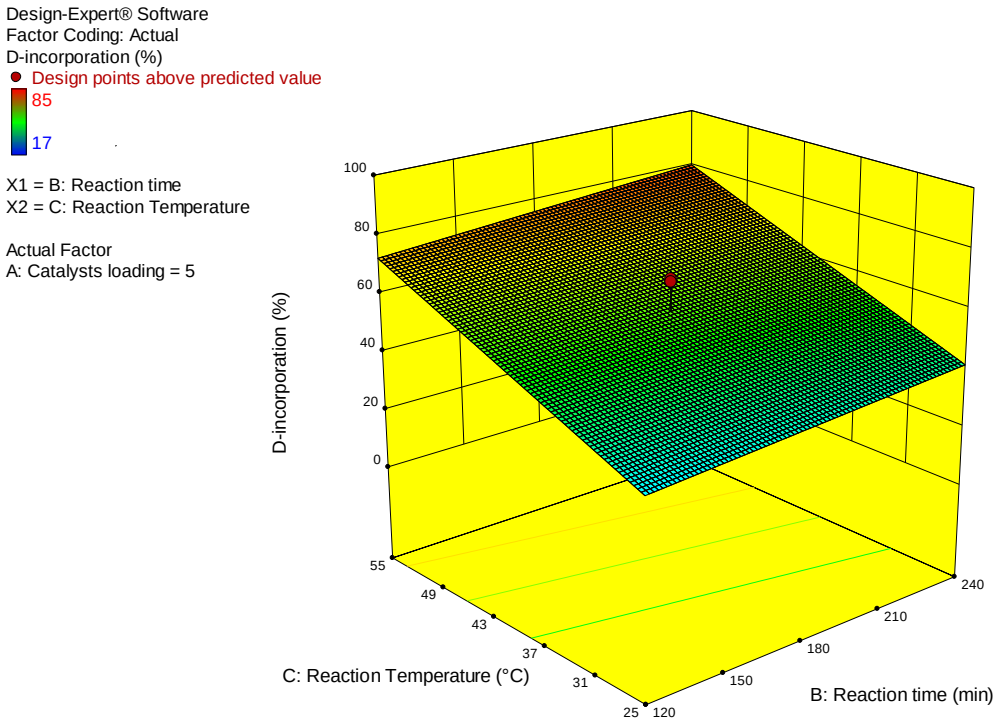

Graph E2.2

Finally, provided below is a graph of Residuals versus Predicted plot. This is a plot of the residuals versus the ascending predicted response values (low incorporation to high incorporation), and tests the assumption of constant variance in the data (**Graph E2.3**).

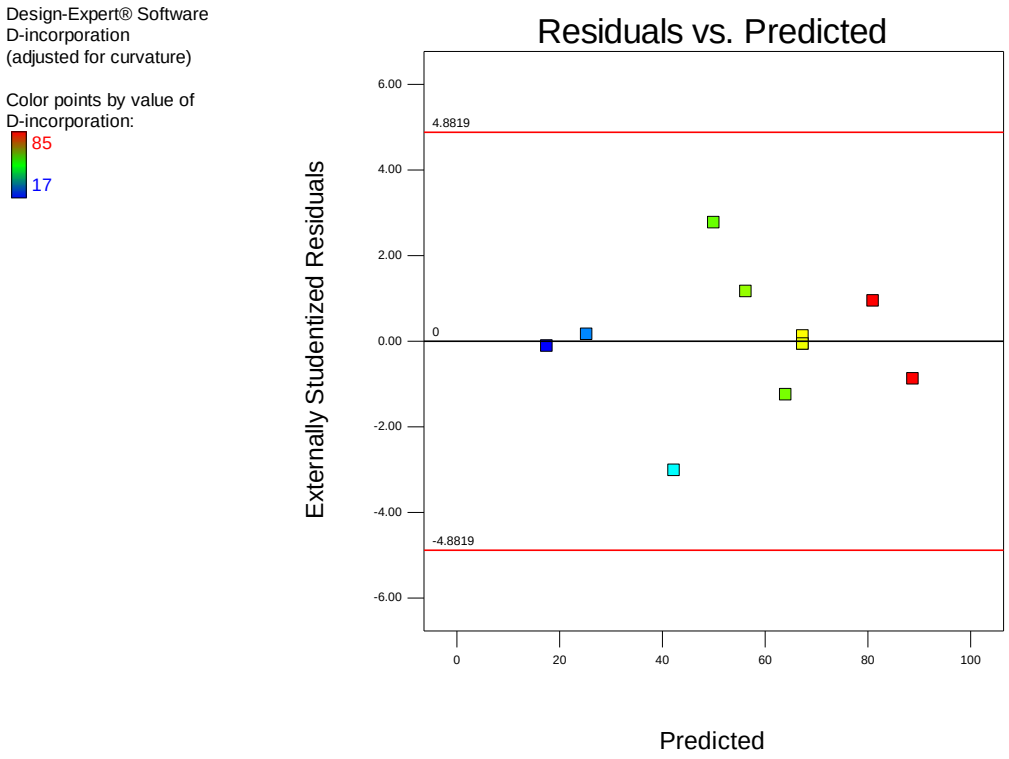
Design-Expert® Software
D-incorporation
(adjusted for curvature)
Color points by value of
D-incorporation:
85
17
Residuals vs. Predicted
Externally Studentized Residuals
6.00
4.8819
4.00
2.00
0
0.00
-2.00
-4.00
-4.8819
-6.00
0
20
40
60
80
100
Predicted

Graph E2.3

Scheme 2.48 *Investigating electronic effects upon the HIE reaction.*

The reactions were carried out following general procedure A, and analysed by ^{1}H NMR spectroscopy to confirm the extent and position of exchange.

Complex	***Solvent***	***Temperature (°C)***	***Time (h)***
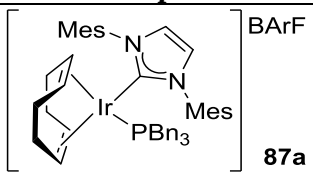 **87a** (7.6 mg, 0.0043 mmol)	MTBE	50	2

Substrate	***Data***
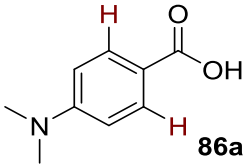 **86a** (14.2 mg, 0.086 mmol)	Data was consistent with that reported on page 308.

D-Incorporation (%)		
Run		***Average***
1	***2***	
84	78	81

Substrate	***Data***
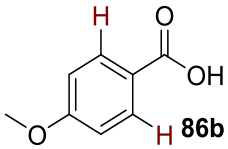 **86b** (13.1 mg, 0.086 mmol)	Data was consistent with that reported on page 312.

D-Incorporation (%)		
Run		***Average***
1	***2***	
89	90	90

Substrate	***data***
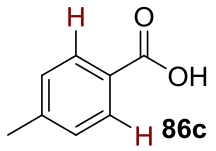 **86c** (11.7 mg, 0.086 mmol)	Data was consistent with that reported on page 313.

D-Incorporation (%)		
Run		***Average***
1	***2***	
93	95	94

Substrate	***data***
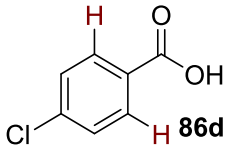 **86d** (13.5 mg, 0.086 mmol)	Data was consistent with that reported on page 313.

D-Incorporation (%)		
Run		***Average***
1	***2***	
91	87	89

Substrate	***data***
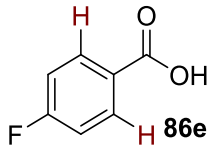 **86e** (12.0 mg, 0.086 mmol)	Data was consistent with that reported on page 313.

D-Incorporation (%)		
Run		***Average***
1	***2***	
90	90	90

Substrate	***data***
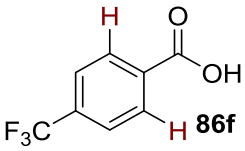 **86f** (16.4 mg, 0.086 mmol)	Data was consistent with that reported on page 314.

D-Incorporation (%)		
Run		***Average***
1	***2***	
93	93	93

Substrate	***data***
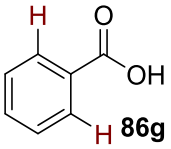 **86g** (16.4 mg, 0.086 mmol)	Data was consistent with that reported on page 314.

D-Incorporation (%)		
Run		***Average***
1	***2***	
90	89	90

Scheme 2.49 *Further substrate investigations.*

The reactions were carried out following general procedure A, and analysed by ^{1}H NMR spectroscopy to confirm the extent and position of exchange.

Complex	*Solvent*	*Temperature (°C)*	*Time (h)*
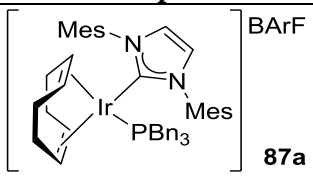 **87a** (7.6 mg, 0.0043 mmol)	MTBE	50	2

Substrate	*^{1}H NMR data*[91]
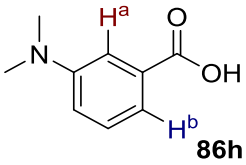 **86h** (14.2 mg, 0.086 mmol)	**^{1}H NMR** (300 MHz, DMSO): δ 12.73 (1H, br s, O-H), 7.32-7.19 (3H, m, Ar-H), 6.98-6.91 (1H, m, Ar-H), 2.92 (6H, s, N-CH_3). Incorporation expected at δ D^a 7.32-7.19 & D^b 6.98-6.91. Determined against integral at δ 2.92.

D-Incorporation (%)					
Run				*Average*	
1		*2*			
D^a	*D^b*	*D^a*	*D^b*	*D^a*	*D^b*
28	0	32	0	30	0

Substrate	*^{1}H NMR data*[87]
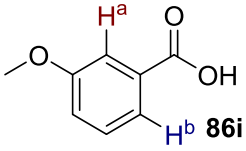 **86i** (13.1 mg, 0.086 mmol)	**^{1}H NMR** (300 MHz, DMSO): δ 12.97 (1H, br s, O-H), 7.56-7.48 (1H, m, Ar-H), 7.46-7.35 (2H, m, Ar-H), 7.22-7.13 (1H, m, Ar-H), 3.79 (3H, s, O-CH_3). Incorporation expected at δ D^b 7.46-7.35 & D^a 7.56-7.48. Determined against integral at δ 3.79.

D-Incorporation (%)					
Run				*Average*	
1		*2*			
D^a	*D^b*	*D^a*	*D^b*	*D^a*	*D^b*
94	84	96	92	95	88

Substrate	***^{1}H NMR data***[88]
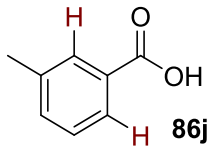 **86j** (11.7 mg, 0.086 mmol)	**^{1}H NMR** (300 MHz, DMSO): δ 12.86 (1H, br s, O-H), 7.79-7.69 (2H, m, Ar-H), 7.46-7.32 (2H, m, Ar-H), 2.35 (3H, s, Ar-CH_3). Incorporation expected at δ 7.79-7.69. Determined against integral at δ 2.35.

D-Incorporation (%)		
Run		***Average***
1	***2***	
94	94	94

Substrate	***^{1}H NMR data***[88]
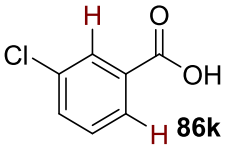 **86k** (13.5 mg, 0.086 mmol)	**^{1}H NMR** (300 MHz, DMSO): δ 13.32 (1H, br s, O-H), 7.94-7.84 (2H, m, Ar-H), 7.74-7.66 (1H, m, Ar-H), 7.57-7.49 (1H, m, Ar-H). Incorporation expected at δ 7.94-7.84. Determined against integral at δ 7.49.

D-Incorporation (%)		
Run		***Average***
1	***2***	
91	89	90

Substrate	***^{1}H NMR data***[92]
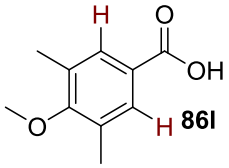 **86l** (15.5 mg, 0.086 mmol)	**^{1}H NMR** (300 MHz, DMSO): δ 12.66 (1H, br s, O-H), 7.62 (2H, s, Ar-H), 3.69 (3H, s, O-CH_3), 2.25 (6H, s, Ar-CH_3). Incorporation expected at δ 7.62. Determined against integral at δ 2.25.

D-Incorporation (%)		
Run		***Average***
1	***2***	
94	94	94

Substrate	***^{1}H NMR data***[93]
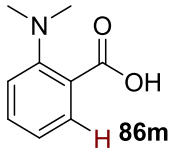 **86m** (14.2 mg, 0.086 mmol)	**^{1}H NMR** (300 MHz, DMSO): δ 7.99-7.94 (1H, m, Ar-H), 7.70-7.59 (2H, m, Ar-H), 7.39-7.31 (1H, m, Ar-H). Incorporation expected at δ 7.99-7.94. Determined against integral at δ 7.39-7.31.

D-Incorporation (%)

Run		***Average***
1	***2***	
88	95	92

Substrate	***^{1}H NMR data***[87]
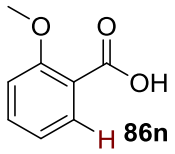 **86n** (13.1 mg, 0.086 mmol)	**^{1}H NMR** (300 MHz, DMSO): δ 12.56 (1H, br s, O-H), 7.65-7.58 (1H, m, Ar-H), 7.55-7.44 (1H, m, Ar-H), 7.15-7.07 (1H, m, Ar-H), 7.02-6.93 (1H, m, Ar-H), 3.80 (3H, s, O-CH_3). Incorporation expected at δ 7.65-7.58. Determined against integral at δ 3.80.

D-Incorporation (%)

Run		***Average***
1	***2***	
91	88	90

Substrate	***^{1}H NMR data***[88]
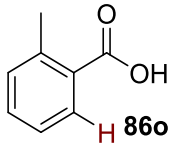 **86o** (11.7 mg, 0.086 mmol)	**^{1}H NMR** (300 MHz, DMSO): δ 12.78 (1H, br s, O-H), 7.85-7.76 (1H, m, Ar-H), 7.48-7.38 (1H, m, Ar-H), 7.32-7.21 (2H, m, Ar-H), 2.51 (3H, s, Ar-CH_3). Incorporation expected at δ 7.85-7.76. Determined against integral at δ 2.51.

D-Incorporation (%)

Run		***Average***
1	***2***	
96	94	95

Substrate	***^{1}H NMR data***[94]
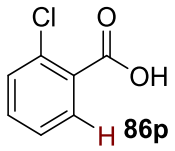 **86p** (13.5 mg, 0.086 mmol)	**^{1}H NMR** (300 MHz, DMSO): δ 13.36 (1H, br s, O-H), 7.82-7.72 (1H, m, Ar-H), 7.58-7.47 (2H, m, Ar-H), 7.45-7.37 (1H, m, Ar-H). Incorporation expected at δ 7.82-7.72. Determined against integral at δ 7.58-7.47.

D-Incorporation (%)		
Run		***Average***
1	***2***	
90	90	90

Substrate	***^{1}H NMR data***[95]
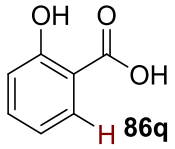 **86q** (11.9 mg, 0.086 mmol)	**^{1}H NMR** (300 MHz, DMSO): δ 7.79 (1H, dd J = 7.8 Hz, ^4J = 1.9 Hz, Ar-H), 7.55-7.45 (1H, m, Ar-H), 6.98-6.86 (2H, m, Ar-H). Incorporation expected at δ 7.79. Determined against integral at δ 6.98-6.86.

D-Incorporation (%)		
Run		***Average***
1	***2***	
85	76	81

Substrate	***^{1}H NMR data***[96]
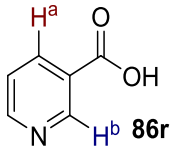 **86r** (10.6 mg, 0.086 mmol)	**^{1}H NMR** (300 MHz, DMSO): δ 13.32 (1H, br s, O-H), 9.06 (1H, d ^4J = 2.4 Hz, Ar-H), 8.78 (1H, dd J = 4.8 Hz, ^4J = 1.8 Hz, Ar-H), 8.26 (1H, dt J = 7.9 Hz, ^4J = 2.0 Hz, Ar-H), 7.53 (1H, dd, J = 7.9 Hz, 4.9 Hz, Ar-H). Incorporation expected at δ D^b 9.06 & D^a 8.78. Determined against integral at δ 7.53.

c					
Run				***Average***	
1		***2***			
D^a	***D^b***	***D^a***	***D^b***	***D^a***	***D^b***
0	0	0	0	0	0

Substrate	***^{1}H NMR data***[97]
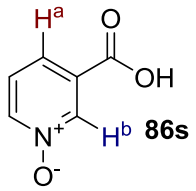 **86s** (12.0 mg, 0.086 mmol)	**^{1}H NMR** (300 MHz, DMSO): δ 13.88 (1H, br s, O-H), 8.51-8.45 (1H, m, Ar-H), 8.44-8.38 (1H, m, Ar-H), 7.79-7.72 (1H, m, Ar-H), 7.57-7.49 (1H, m, Ar-H). Incorporation expected at δ D^b 8.51-8.45 & D^a 8.44-8.38. Determined against integral at δ 7.57-7.49.

D-Incorporation (%)					
Run				***Average***	
1		***2***			
D^a	***D^b***	***D^a***	***D^b***	***D^a***	***D^b***
0	0	0	0	0	0

Scheme 2.50 *Application of HIE conditions on arylacetic acids.*

The reactions were carried out following general procedure A, and analysed by ^{1}H NMR spectroscopyto confirm the extent and position of exchange.

Complex	*Solvent*	*Temperature (°C)*	*Time (h)*
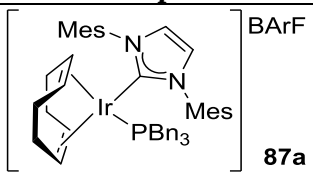 **87a** (7.6 mg, 0.0043 mmol)	MTBE	50	2

Substrate	*^{1}H NMR data*[91]
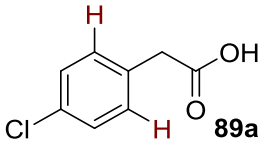 **89a** (14.7 mg, 0.086 mmol)	**^{1}H NMR** (300 MHz, DMSO): δ 12.37 (1H, br s, O-H), 7.40-7.33 (2H, m, Ar-H), 7.31-7.24 (2H, m, Ar-H), 3.57 (2H, s, Ar-CH_2). Incorporation expected at δ 7.40-7.33. Determined against integral at δ 3.57.

D-Incorporation (%)		
Run		*Average*
1	*2*	
0	0	0

Substrate	*^{1}H NMR data*[91]
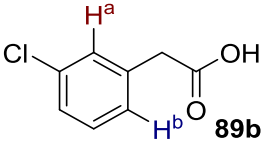 **89b** (14.7 mg, 0.086 mmol)	**^{1}H NMR** (300 MHz, DMSO): δ 12.42 (1H, br s, O-H), 7.38-7.27 (3H, m, Ar-H), 7.26-7.19 (1H, m, Ar-H), 3.60 (2H, s, Ar-CH_2). Incorporation expected at δ 7.38-7.27. Determined against integral at δ 3.60.

D-Incorporation (%)					
Run				*Average*	
1		*2*			
D^a	D^b	D^a	D^b	D^a	D^b
0	0	0	0	0	0

Substrate	***^{1}H NMR data***[98]
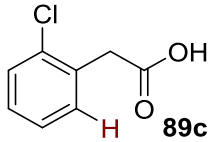 **89c** (14.7 mg, 0.086 mmol)	**^{1}H NMR** (300 MHz, DMSO): δ 12.44 (1H, br s, O-H), 7.47-7.35 (2H, m, Ar-H), 7.33-7.24 (2H, m, Ar-H), 3.70 (2H, Ar-CH_2). Incorporation expected at δ 7.33-7.24. Determined against integral at δ 3.70.

D-Incorporation (%)		
Run		***Average***
1	***2***	
0	0	0

Substrate	***^{1}H NMR data***[99]
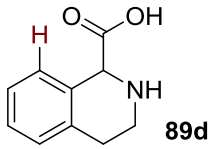 **89d** (15.2 mg, 0.086 mmol)	**^{1}H NMR** (300 MHz, DMSO): δ 7.82-7.74 (1H, m, Ar-CH-N), 7.28-7.02 (m, 3H, Ar-H), 3.39-3.27 (1H, m, CH), 2.89-2.71 (4H, m, CH_2). Incorporation expected at δ 7.28-7.02. Determined against integral at δ 3.39-3.27.

D-Incorporation (%)		
Run		***Average***
1	***2***	
0	0	0

Scheme 2.51 *Selectivity of HIE in substrate* ***D86t***

The reactions were carried out following general procedure A, and analysed by ^{1}H NMR to confirm the extent and position of exchange, using *N*-Boc morpholine **S1** as an internal standard within the sample.

Complex	***Solvent***	***Temperature (°C)***	***Time (h)***
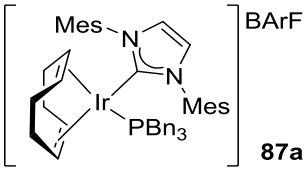 **87a** (7.6 mg, 0.0043 mmol)	MTBE	50	2
Internal Standard	***^{1}H NMR data***[100]		
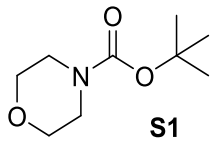 **S1** (16.1 mg, 0.086 mmol)	**^{1}H NMR** (300 MHz, DMSO): δ 3.56-3.46 (4H, m, N-C<u>H</u>$_2$), 3.30-3.22 (4H, m, O-C<u>H</u>$_2$), 1.38 (9H, s, C-(C<u>H</u>$_3$)$_3$).		

Substrate	***^{1}H NMR data***[101]
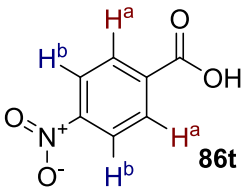 **86t** (14.2 mg, 0.086 mmol)	**^{1}H NMR** (300 MHz, DMSO): δ 13.64 (1H, br s, O-<u>H</u>), 8.34-8.26 (2H, m, Ar-<u>H</u>), 8.20-8.10 (2H, m, Ar-<u>H</u>). Incorporation expected at δ D^{a} 8.34-8.26 & D^{b} 8.20-8.10. Determined against integral of the internal standard at δ 1.38.

D-Incorporation (%)					
Run				***Average***	
1		***2***			
D^{a}	***D^{b}***	***D^{a}***	***D^{b}***	***D^{a}***	***D^{b}***
83	83	82	82	83	83

Table 2.5 *Competition reactions; investigating the functional group tolerance.*

To allow quantification of the substrate and additive remaining after the reaction, each additive **90a-k** and substrate **86a** were calibrated against an internal standard through LCMS analysis. The results are detailed below:

Internal Standard	***LCMS data***	
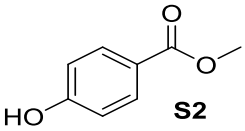 **S2** (10 mg)	***Retention time (min)***	***Mass ion***
	2.09	No mass ion observed

Additive	***LCMS data***		
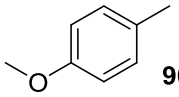 **90a**	***Retention time (min)***		***Mass ion***
	2.92		No mass ion observed
Mass (mg)	***Area***		***Additive / internal standard***
	Internal standard	***Additive***	
2.3	1100	4.0	0.00364
5.6	1200	9.9	0.00825
9.9	1400	17	0.0121
17.0	1200	22	0.0183

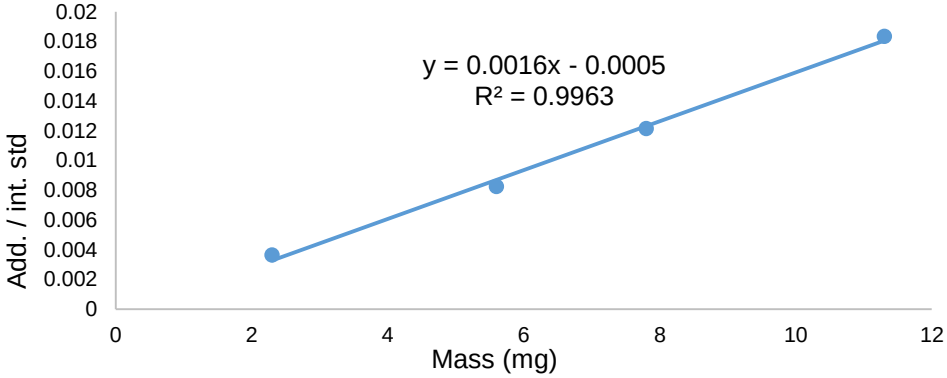

Additive	***LCMS data***		
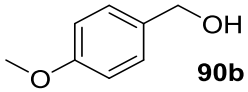 **90b**	***Retention time (min)***		***Mass ion***
	1.76		No mass ion observed
Mass (mg)	***Area***		***Additive / internal standard***
	Internal standard	***Additive***	
3.6	1800	17	0.00944
5.6	4300	72	0.0167
9.0	700	16	0.0229
16.0	720	24	0.0333

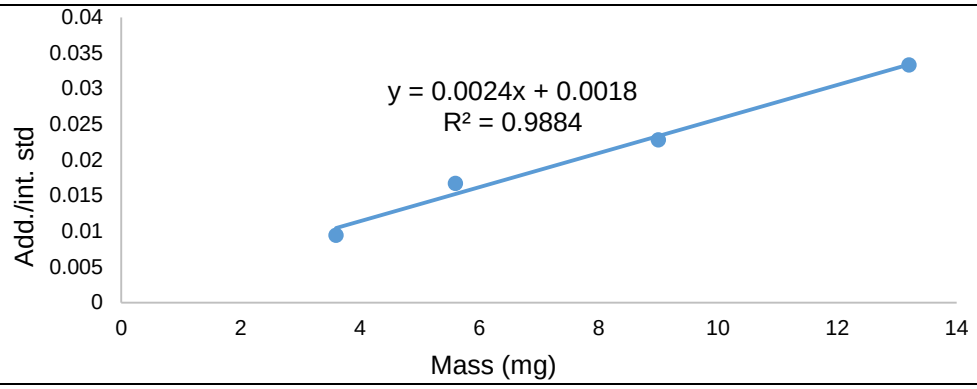

Additive	***LCMS data***		
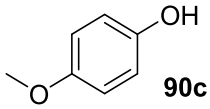 **90c**	***Retention time (min)***		***Mass ion***
	1.68		No mass ion observed
Mass (mg)	***Area***		***Additive / internal standard***
	Internal standard	***Additive***	
2.7	2500	21	0.00840
6.1	3100	43	0.0139
7.8	220	4.0	0.0182
11.8	3100	77	0.0248

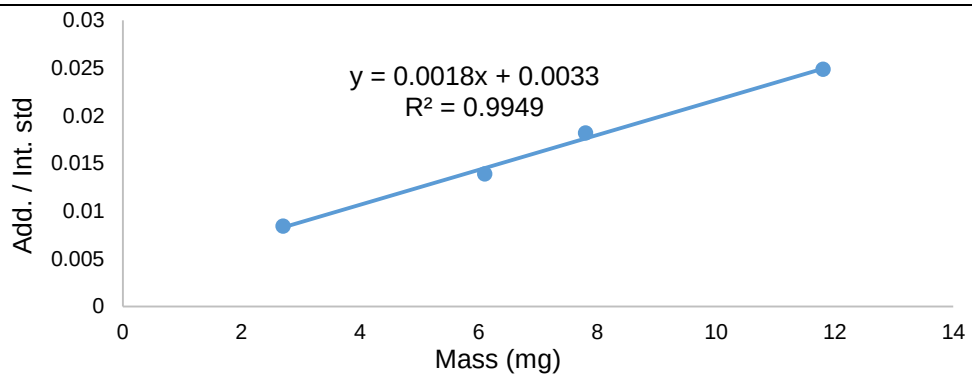

Additive	***LCMS data***		
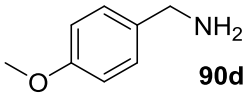 **90d**	***Retention time (min)***		***Mass ion***
	0.33		121.2 $(M-NH)^+$
Mass (mg)	***Area***		***Additive / internal standard***
	Internal standard	***Additive***	
3.1	2200	51	0.0232
6.3	2800	81	0.0289
9.3	1500	60	0.0400
11.4	3500	150	0.0429

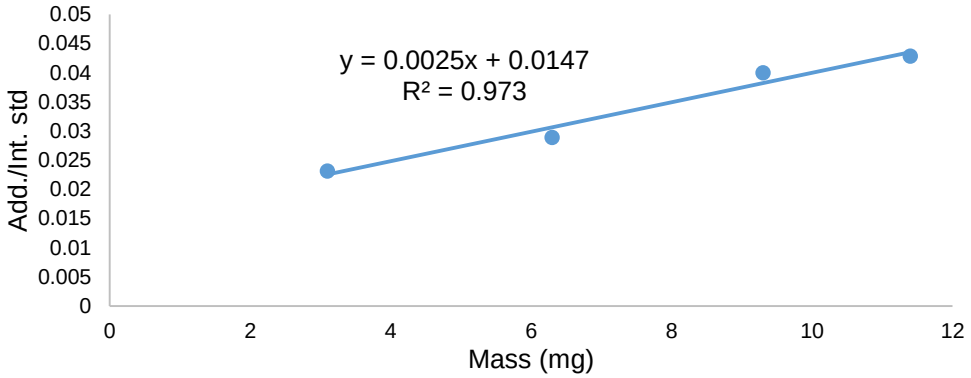

Additive	***LCMS data***		
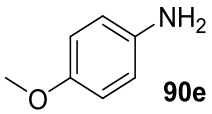 **90e**	***Retention time (min)***		***Mass ion***
	0.28		124.2 $(M+H)^+$
Mass (mg)	***Area***		***Additive / internal standard***
	Internal standard	***Additive***	
2.1	1600	55	0.0343
6.1	2500	110	0.044
7.8	1800	100	0.0556
10.2	3100	180	0.0581

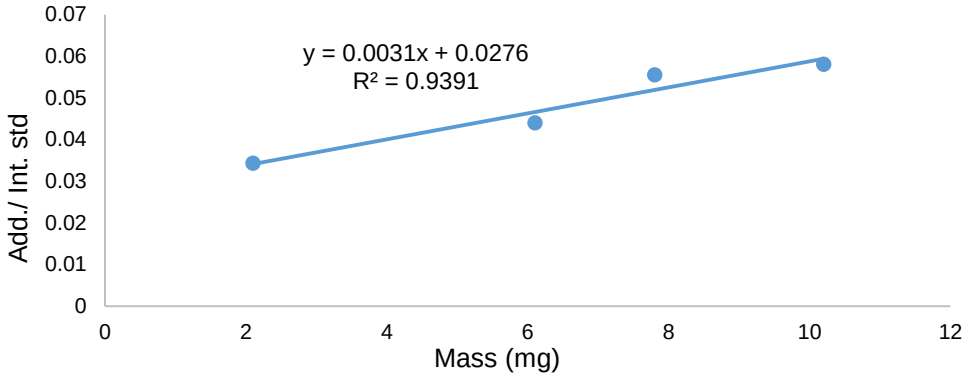

Additive	*LCMS data*	
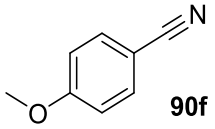 **90f**	*Retention time (min)*	*Mass ion*
	2.44	No mass ion observed

Mass (mg)	*Area*		*Additive / internal standard*
	Internal standard	*Additive*	
3.2	1300	520	0.400
6.3	2800	2100	0.750
8.9	2070	2140	1.03
11	2760	3170	1.15

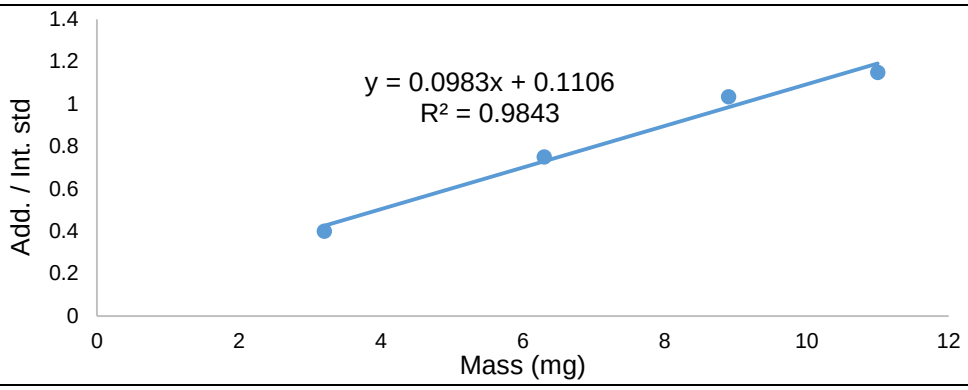

Additive	*LCMS data*	
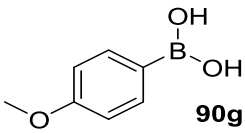 **90g**	*Retention time (min)*	*Mass ion*
	1.63	No mass ion observed

Mass (mg)	*Area*		*Additive / internal standard*
	Internal standard	*Additive*	
3.1	2700	110	0.0407
6.4	810	66	0.0815
10.1	1100	150	0.136
13.0	1800	330	0.183

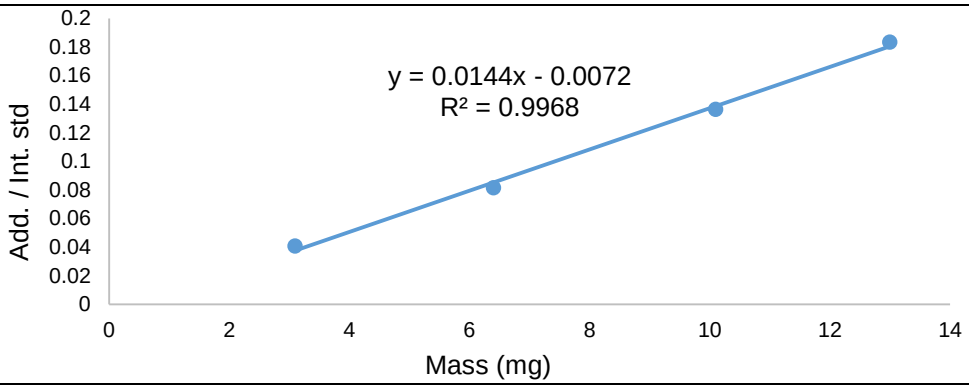

Additive	*LCMS data*	
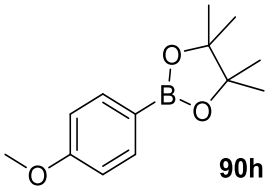 **90h**	*Retention time (min)*	*Mass ion*
	3.34	No mass ion observed

Mass (mg)	*Area*		*Additive / internal standard*
	Internal standard	*Additive*	
4.7	200	210	0.105
11	1700	420	0.247
14.9	3200	990	0.309
20.9	2200	920	0.418

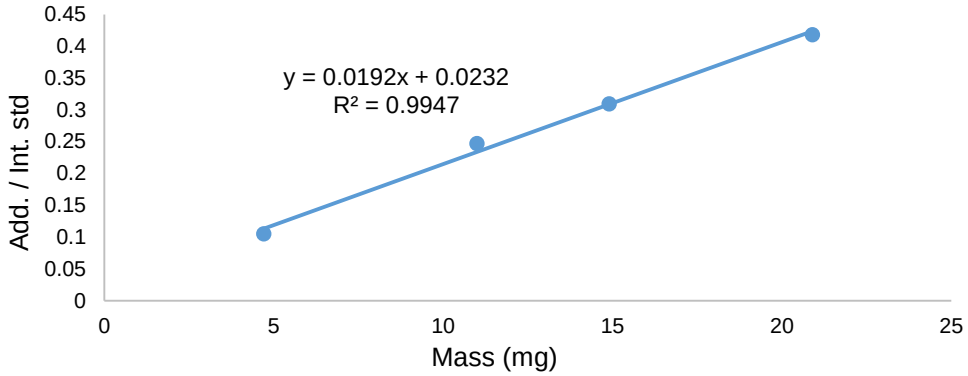

Additive	*LCMS data*	
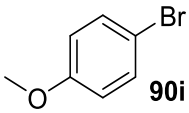 **90i**	*Retention time (min)*	*Mass ion*
	3.10	No mass ion observed

Mass (mg)	*Area*		*Additive / internal standard*
	Internal standard	*Additive*	
4.1	3700	38	0.0103
8.5	2600	49	0.0188
12.6	2800	85	0.0304
16.7	2000	78	0.0390

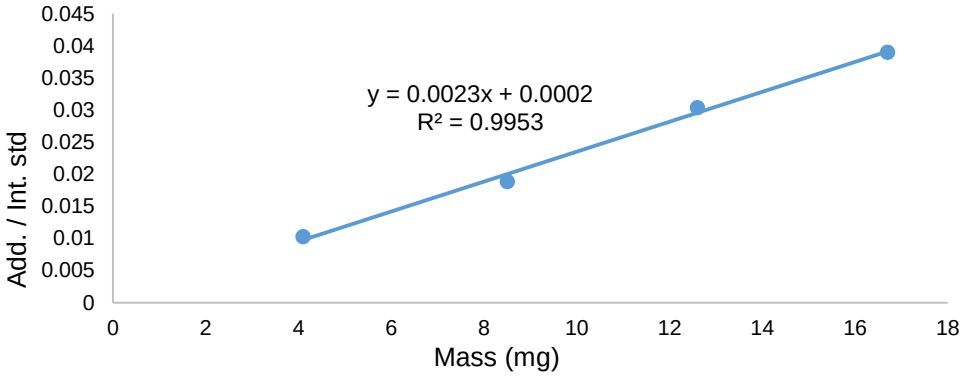

Additive	***LCMS data***		
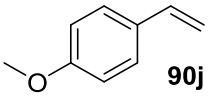 **90j**	***Retention time (min)***		***Mass ion***
	3.05		No mass ion observed
Mass (mg)	***Area***		***Additive / internal standard***
	Internal standard	***Additive***	
2.7	4200	1600	0.381
5.0	4700	3100	0.660
8.0	4800	4200	0.875
11.5	4400	4800	1.09

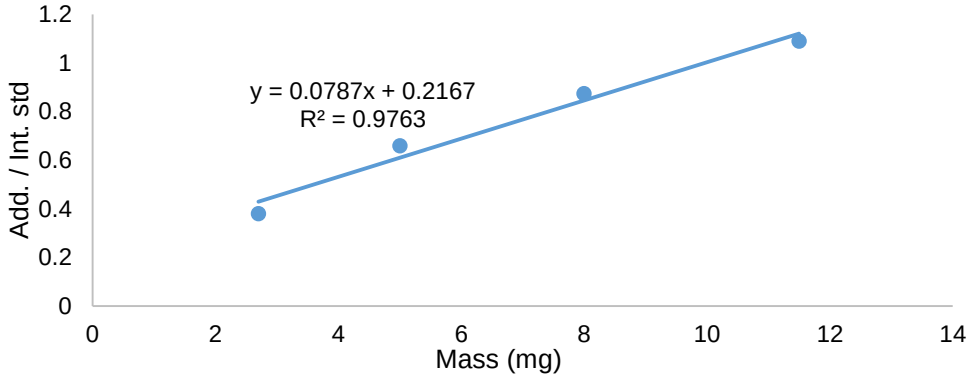

Additive	***LCMS data***		
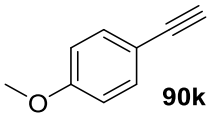 **90k**	***Retention time (min)***		***Mass ion***
	2.88		No mass ion observed
Mass (mg)	***Area***		***Additive / internal standard***
	Internal standard	***Additive***	
3.5	2500	1200	0.480
6.5	2800	2600	0.929
8.3	2800	3100	1.11
12.4	3100	4400	1.42

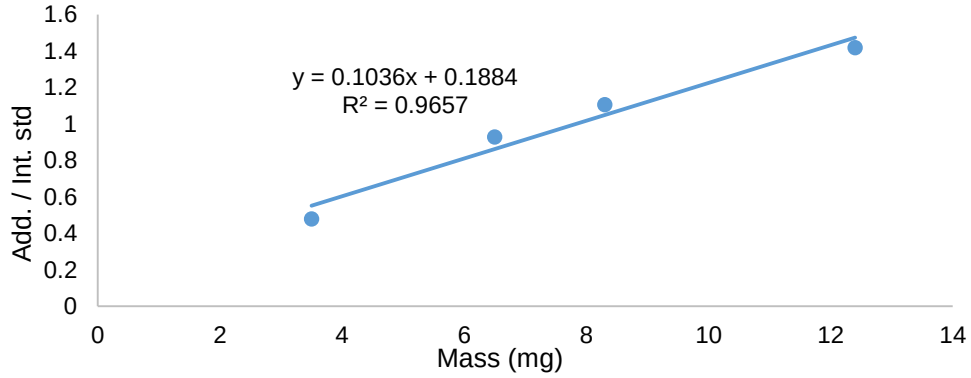

Substrate	***LCMS data***		
	Retention time (min)		***Mass ion***
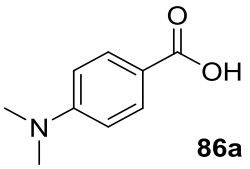 **86a**	2.23		166.2 $(M+H)^+$
Mass (mg)	***Area***		***Substrate / internal standard***
	Internal standard	***Substrate***	
4.5	2100	90	0.0429
7.7	1700	120	0.0706
10.3	3300	340	0.103
15.1	630	81	0.129

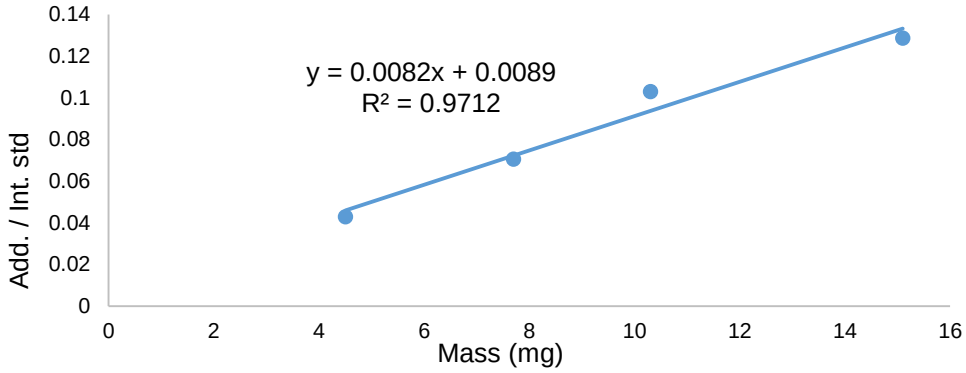

Following calibration, the reactions were carried out following general procedure A, which was modified by adding a stock solution of internal standard **S2** (1 mL of a 10 mg/mL solution) at the end of the reaction, and analysed by LCMS to confirm the extent of exchange and the amount of acid and additive remaining.

Internal Standard	***LCMS data***			
	Retention time (min)		***Mass ion***	
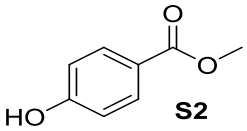 **S2** (10 mg)	2.09		No mass ion observed	
Complex	***Substrate***	***Solvent***	***Temperature (°C)***	***Time (h)***
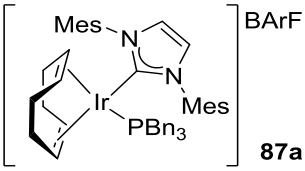 **87a** (7.6 mg, 0.0043 mmol)	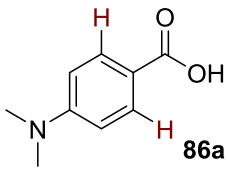 **86a** (14.2 mg, 0.086 mmol)	MTBE	50	2

Additive	*Run*	*Add. yield (%)*	*Sub. yield (%)*	*Sub. incorporation (%)*
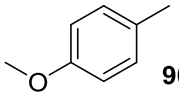 **90a** (10.6 mg, 0.086 mmol)	***1***	91	99	91
	2	92	99	87
	Average	92	99	89

Additive	*Run*	*Add. yield (%)*	*Sub. yield (%)*	*Sub. incorporation (%)*
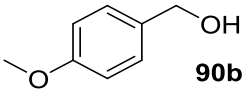 **90b** 11.9 mg (0.086 mmol)	***1***	99	99	86
	2	99	99	86
	Average	99	99	86

Additive	*Run*	*Additive yield (%)*	*Substrate yield (%)*	*Substrate incorporation (%)*
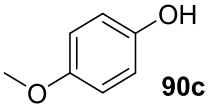 **90c** 10.7 mg (0.086 mmol)	***1***	97	99	72
	2	98	99	83
	Average	98	99	78

Additive	*Run*	*Add. yield (%)*	*Sub. yield (%)*	*Sub. incorporation (%)*
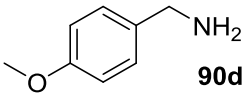 **90d** 11.8 mg (0.086 mmol)	***1***	99	99	0
	2	99	99	0
	Average	99	99	0

Additive	*Run*	*Add. yield (%)*	*Sub. yield (%)*	*Sub. incorporation (%)*
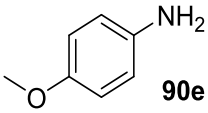 **90e** 10.6 mg (0.086 mmol)	***1***	92	99	0
	2	96	99	0
	Average	94	99	0

Additive	*Run*	*Add. yield (%)*	*Sub. yield (%)*	*Sub. incorporation (%)*
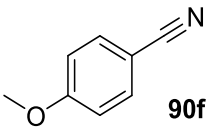 **90f** 11.5 mg (0.086 mmol)	***1***	99	99	0
	2	99	99	0
	Average	99	99	0

Additive	*Run*	*Add. yield (%)*	*Sub. yield (%)*	*Sub. incorporation (%)*
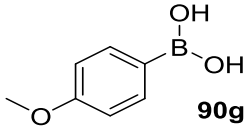 **90g** 13.2 mg (0.086 mmol)	***1***	66	97	89
	2	71	99	77
	Average	69	98	83

Additive	*Run*	*Add. yield (%)*	*Sub. yield (%)*	*Sub. incorporation (%)*
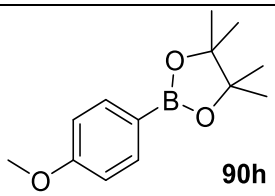 **90h** 16.2 mg (0.086 mmol)	***1***	99	99	83
	2	99	99	87
	Average	99	99	85

Additive	*Run*	*Add. yield (%)*	*Sub. yield (%)*	*Sub. incorporation (%)*
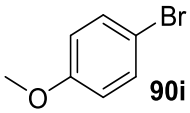 **90i** 16.1 mg (0.086 mmol)	***1***	99	99	79
	2	99	99	78
	Average	99	99	79

Additive	*Run*	*Add. yield (%)*	*Sub. yield (%)*	*Sub. incorporation (%)*
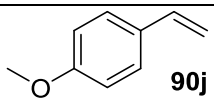 **90j** 11.5 mg (0.086 mmol)	***1***	0	99	71
	2	0	99	79
	Average	0	99	75

Additive	*Run*	*Add. yield (%)*	*Sub. yield (%)*	*Sub. incorporation (%)*
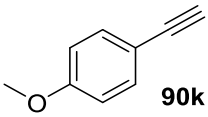 **90k** 11.4 mg (0.086 mmol)	***1***	0	90	62
	2	0	99	75
	Average	0	95	69

Table 2.6 *Competition reactions; investigating the selectivity of exchange.*

To allow quantification of the substrate and additive remaining after the reaction, each additive **90l-q** and substrate **86a** were calibrated against an internal standard through LCMS analysis. The results of which are detailed below:

Internal Standard	***LCMS data***	
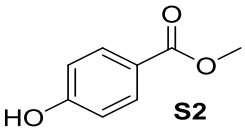 **S2** (10 mg)	***Retention time (min)***	***Mass ion***
	2.09	No mass ion observed

Additive	***LCMS data***	
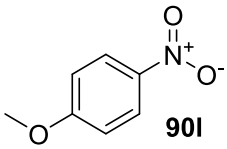 **90l**	***Retention time (min)***	***Mass ion***
	2.63	165.1 $(M+H)^+$

Mass (mg)	***Area***		***Additive / internal standard***
	Internal standard	***Additive***	
3.1	980	23	0.0234
6.2	3600	180	0.0500
9.2	810	56	0.0691
13.7	4200	520	0.124

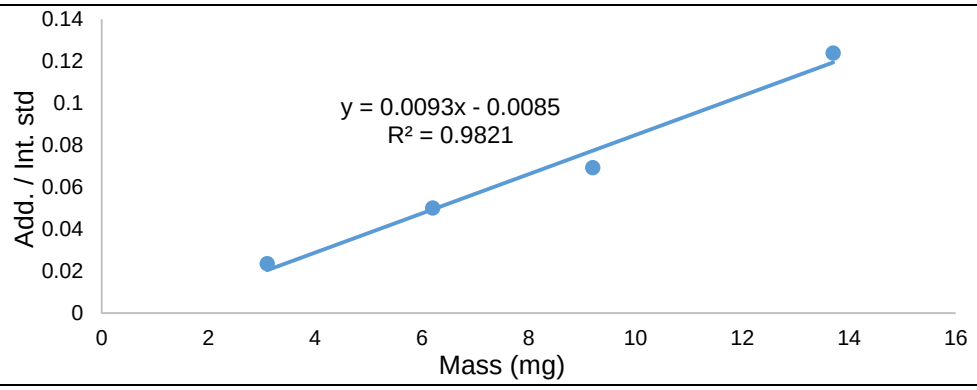

Additive	*LCMS data*		
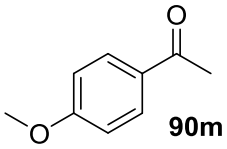 **90m**	*Retention time (min)*		*Mass ion*
	2.37		151.1 $(M+H)^+$
Mass (mg)	*Area*		*Additive / internal standard*
	Internal standard	*Additive*	
3.4	610	141	0.231
6.4	478	161	0.337
9.7	449	315	0.479
13.0	486	299	0.615

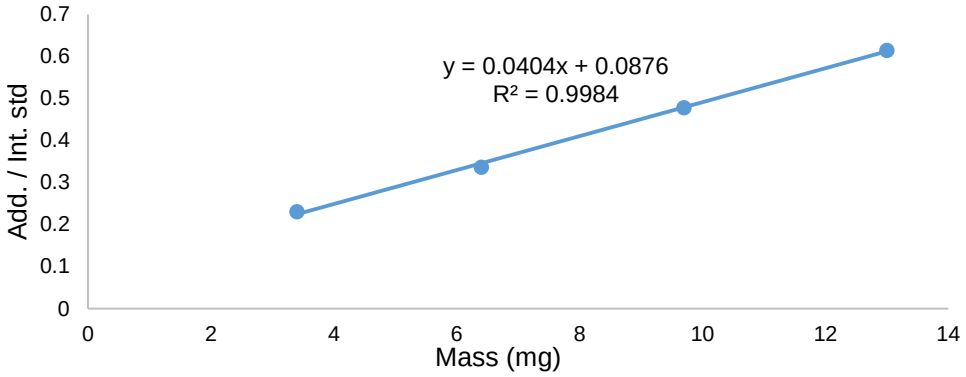

Additive	*LCMS data*		
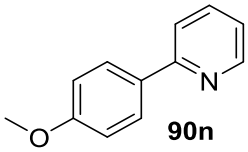 **90n**	*Retention time (min)*		*Mass ion*
	1.18		186.1 $(M+H)^+$
Mass (mg)	*Area*		*Additive / internal standard*
	Internal standard	*Additive*	
4.5	4900	1100	0.224
8.6	4100	1500	0.366
12.2	4400	2300	0.523
16.6	3970	2520	0.634

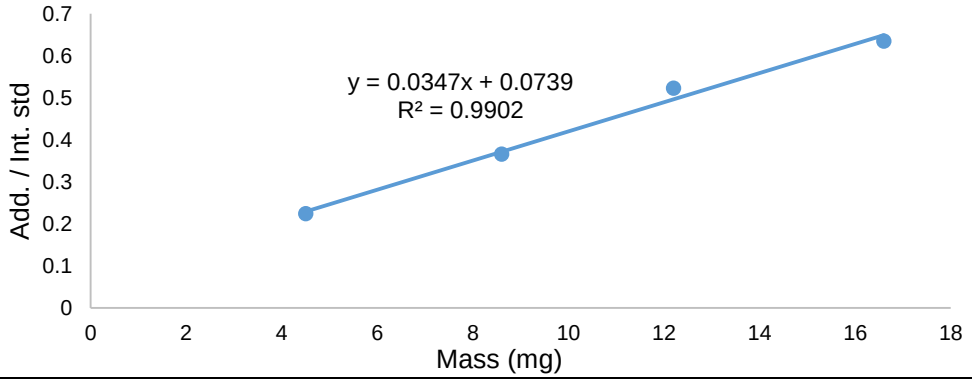

Additive	*LCMS data*		
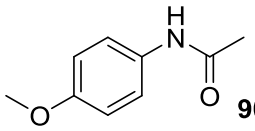 **90o**	*Retention time (min)*		*Mass ion*
	1.65		166.2 $(M+H)^+$
Mass (mg)	*Area*		*Additive / internal standard*
	Internal standard	*Additive*	
3.4	3900	990	0.254
7.1	4200	2300	0.548
10.4	3700	2600	0.703
14.0	2020	1990	0.985

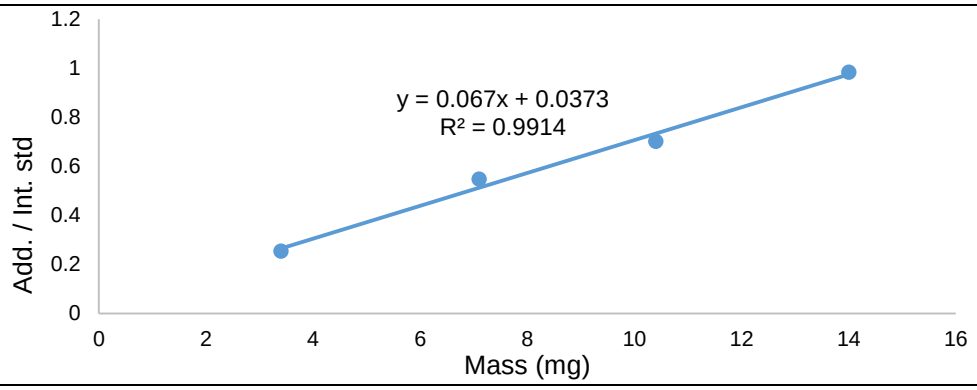

Additive	*LCMS data*		
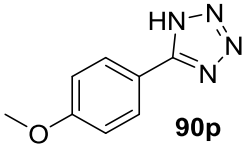 **90p**	*Retention time (min)*		*Mass ion*
	1.93		175.2 $(M-H)^-$
Mass (mg)	*Area*		*Additive / internal standard*
	Internal standard	*Additive*	
3.9	2700	1000	0.370
7.1	4100	2700	0.659
11.0	820	840	1.02
15.5	2100	3200	1.52

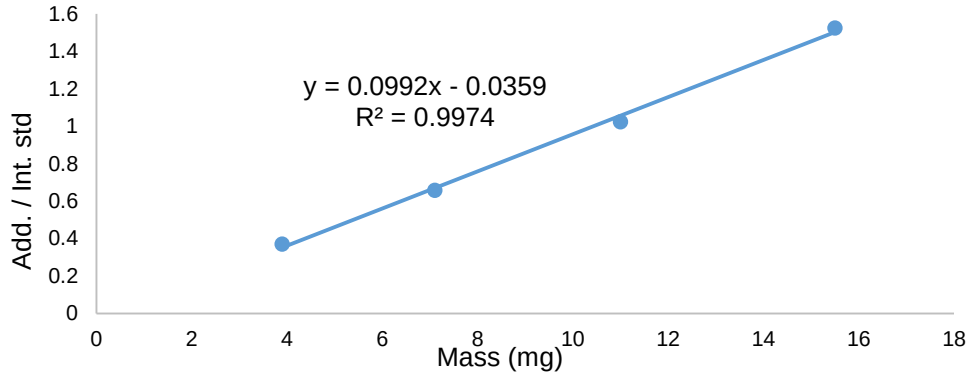

Additive	*LCMS data*		
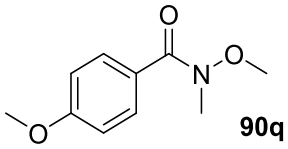 **90q**	*Retention time (min)*		*Mass ion*
	2.13		196.2 $(M+H)^+$
Mass (mg)	*Area*		*Additive / internal standard*
	Internal standard	*Additive*	
4.3	1900	330	0.174
8.8	2800	1500	0.536
12.8	1400	1100	0.787
17.5	1900	2100	1.11

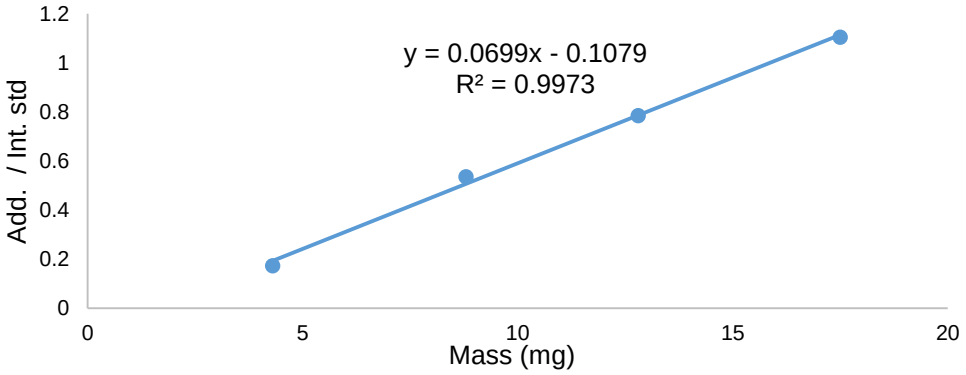

Following calibration, the reactions were carried out following general procedure A which was modified by adding a stock solution of internal standard **S2** (1 mL of a 10 mg/mL solution) at the end of the reaction, and analysed by LCMS to confirm the extent of exchange and the amount of acid and additive remaining. Position of exchange in additives is assumed from similar known compounds.[45,47]

Internal Standard	*LCMS data*			
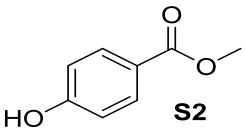 **S2** (10 mg)	*Retention time (min)*		*Mass ion*	
	2.09		No mass ion observed	
Complex	*Substrate*	*Solvent*	*Temperature (°C)*	*Time (h)*
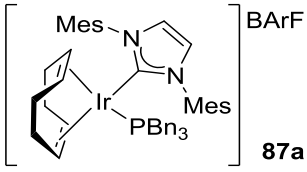 **87a** (7.6 mg, 0.0043 mmol)	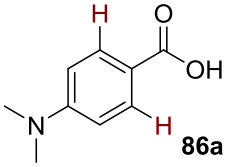 **86a** (14.2 mg, 0.086 mmol)	MTBE	50	2

Additive	*Run*	*Add. yield (%)*	*Add. incorporation (%)*	*Sub. yield (%)*	*Sub. incorporation (%)*
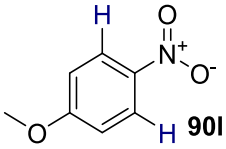 90l 13.2 mg (0.086 mmol)	***1***	96	83	99	81
	2	94	78	90	77
	Average	95	81	95	79

Additive	*Run*	*Add. yield (%)*	*Add. incorporation (%)*	*Sub. yield (%)*	*Sub. incorporation (%)*
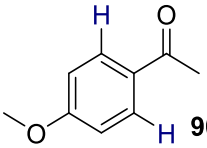 90m 12.9 mg (0.086 mmol)	***1***	96	85	99	77
	2	88	81	99	77
	Average	92	83	99	77

Additive	*Run*	*Add. yield (%)*	*Add. incorporation (%)*	*Sub. yield (%)*	*Sub. incorporation (%)*
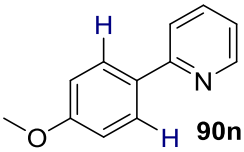 90n 15.9 mg (0.086 mmol)	***1***	99	52	95	0
	2	97	36	88	0
	Average	98	44	91	0

Additive	*Run*	*Add. yield (%)*	*Add. incorporation (%)*	*Sub. yield (%)*	*Sub. incorporation (%)*
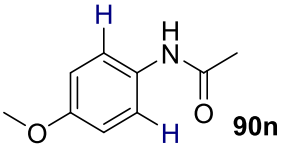 90n 14.4 mg (0.086 mmol)	***1***	99	50	99	67
	2	99	58	99	68
	Average	99	54	99	68

Additive	*Run*	*Add. yield (%)*	*Add. incorporation (%)*	*Sub. yield (%)*	*Sub. incorporation (%)*
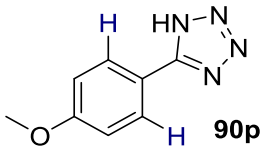 **90p** 15.2 mg (0.086 mmol)	***1***	99	9	99	0
	2	89	9	99	0
	Average	94	9	99	0

Additive	*Run*	*Add. yield (%)*	*Add. incorporation (%)*	*Sub. yield (%)*	*Sub. incorporation (%)*
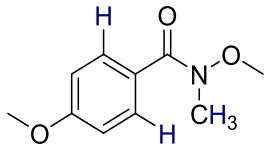 **90q** 16.8 mg (0.086 mmol)	***1***	99	89	95	77
	2	99	90	85	75
	Average	99	90	90	76

Design of experiments with 1 equivalent of DIPEA

Experimental design was used to assess the effect of varying the catalyst loading, reaction time and reaction temperature. As such 'high' and 'low' values for each of the three variables were chosen. To generate a series of experiments to study optimal conditions within the variable ranges chosen, Design Expert™ software v10.0 (Stat_Ease Inc., Minneappolis, Mn) was used. This generated a *two-level, three-factorial* design containing three centre points, giving 11 experiments in total. The deuterium incorporation of 4-(dimethylamino)benzoic acid **86a** was used as the response. The reactions were carried out according to general procedure A and analysed by LCMS to confirm the extent of exchange. The position of exchange was confirmed through ^{1}H NMR spectroscopy of the three centre point reaction products. (**Table E2.5**).

Complex	***Base***	***Solvent***
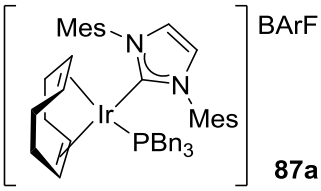	DIPEA (11.2 mg, 0.086 mmol)	MTBE
Substrate	***Data***	
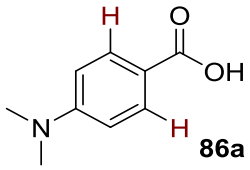 (14.2 mg, 0.086 mmol)	Data was consistent with that reported on page 308.	

Run	*Variable A: Catalyst Loading (mol%)*	*Amount of 87a (mg (µmol))*	*Variable B: Reaction Time (min)*	*Variable C: Reaction Temperature (°C)*	*Response: D-Incorporation (%)*
1 (+++)	7.5	11.4 (6.45)	240	55	85
2 (---)	2.5	3.8 (2.15)	120	25	17
3 (+--)	7.5	11.4 (6.45)	240	25	58
4 (***)	5.0	7.6 (4.30)	180	40	67
5 (***)	5.0	7.6 (4.30)	180	40	68
6 (***)	5.0	7.6 (4.30)	180	40	67
7 (-+-)	2.5	3.8 (2.15)	240	25	26
8 (-++)	2.5	3.8 (2.15)	240	55	59
9 (+--)	7.5	11.4 (6.45)	120	25	34
10 (--+)	2.5	3.8 (2.15)	120	55	61
11 (+-+)	7.5	11.4 (6.45)	120	55	85
[a] symbol in parentheses indicate points in the design; + high, * mid and – low.					

Table E2.5

Runs 4, 5 and 6 represent the centre points of the design. These are employed in order to:

(i) Assess any curvature in the response of incorporation changes in the variables; and

(ii) Assess the repeatability of the hydrogen isotope exchange reaction.

A response surface was created in the same design program. This generated a half-normal plot inferring that increasing the reaction temperature, catalyst loading and reaction time had a positive impact upon the HIE reaction. Furthermore, it indicated the order of significance of each factor; Reaction Temperature > Catalyst Loading >> Reaction Time (**Graph E2.4**).

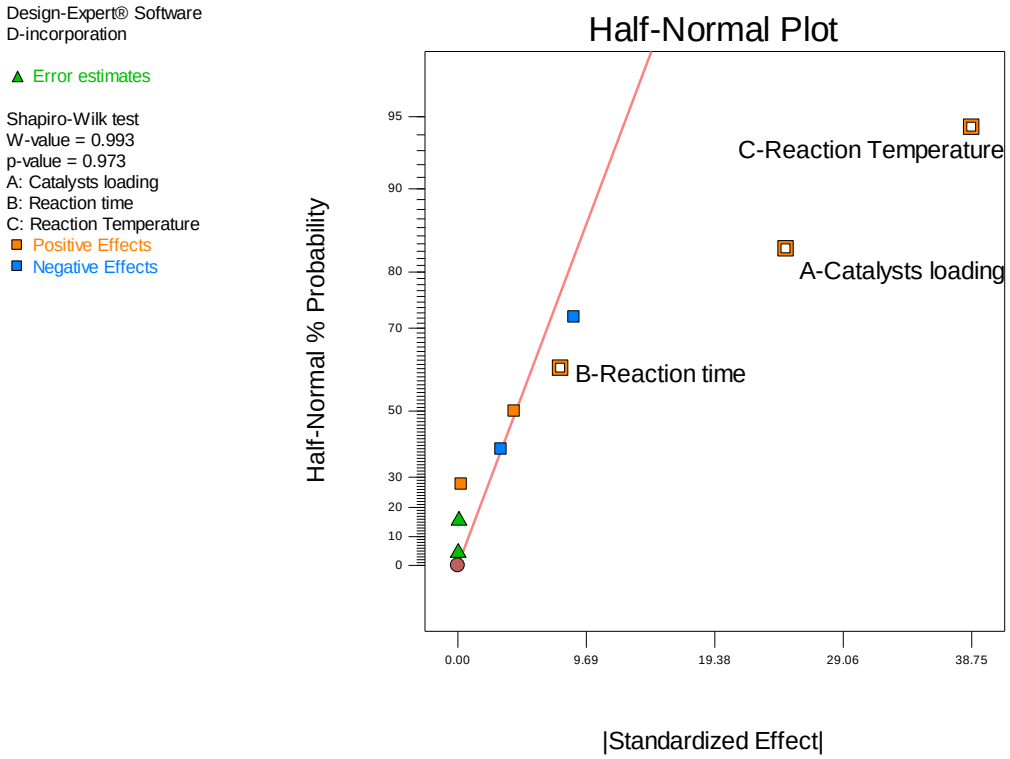

Graph E2.4

Further implementation of the design software generated **Graph E2.5**. By plotting reaction time and temperature at the fixed optimal reaction time (120 min) it can be seen that elevated temperature and increased catalyst loading leads to the optimised conditions (7.5 mol% catalyst, 55 °C, 2 h).

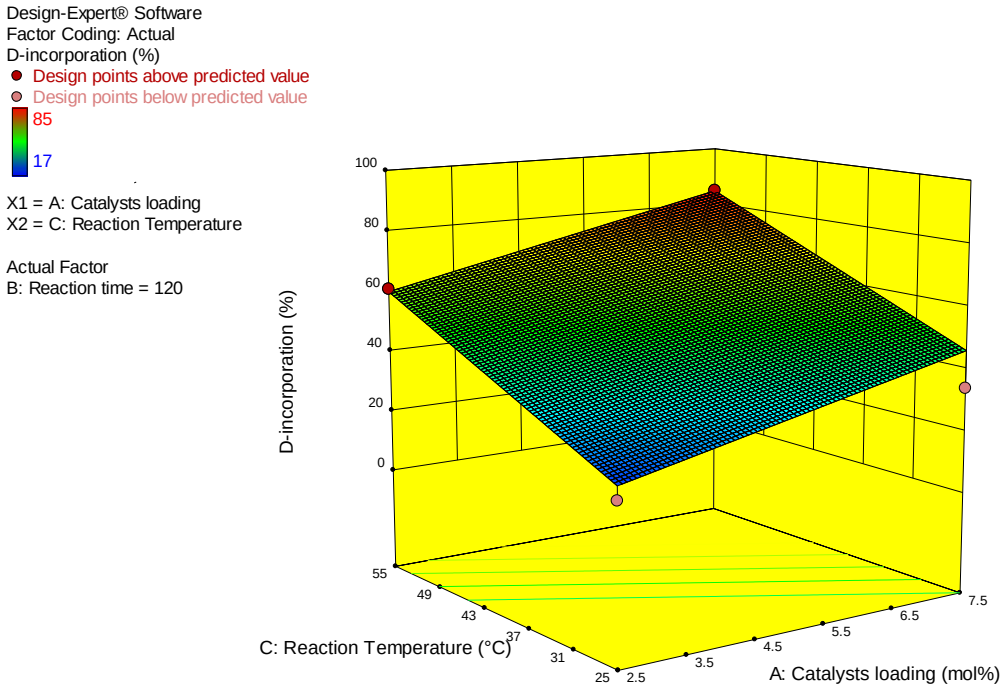

Graph E2.5

Finally, provided below is a graph of Residuals versus Predicted plot. This is a plot of the residuals versus the ascending predicted response values (low incorporation to high incorporation), and tests the assumption of constant variance in the data (**Graph E2.6**).

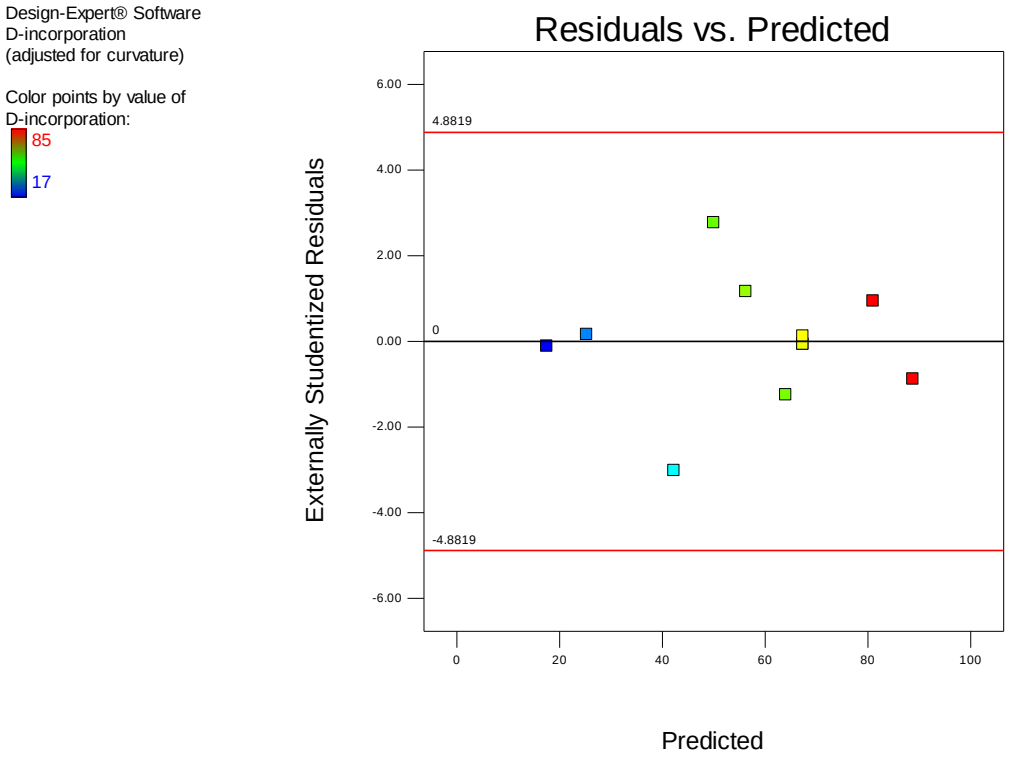
Design-Expert® Software
D-incorporation
(adjusted for curvature)
Color points by value of
D-incorporation:
85
17
Residuals vs. Predicted
Externally Studentized Residuals
6.00
4.00
2.00
0.00
-2.00
-4.00
-6.00
4.8819
0
-4.8819
0
20
40
60
80
100
Predicted

Graph E2.6

Table 2.7 *Competition reactions; investigating the functional group tolerance (with base).*

To allow quantification of the substrate and additive remaining after the reaction, each additive **90a-k** and substrate **86a** were calibrated against an internal standard through LCMS analysis, as has been previously reported *vide supra*.

Following calibration, the reactions were carried out following general procedure A, with a modified work up involving the addition of a stock solution of internal standard **S2** (1 mL of a 10 mg/mL solution in MeCN) at the end of the reaction, and analysed by LCMS to confirm the extent of exchange and the amount of acid and additive remaining.

Internal Standard	***LCMS data***			
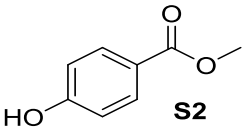 **S2** (10 mg)	***Retention time (min)***		***Mass ion***	
	2.09		No mass ion observed	
Complex	***Substrate***		***Solvent***	***Base***
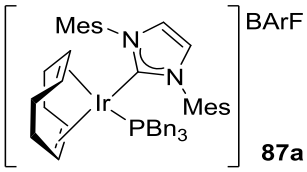 **87a** (11.4 mg, 0.0645 mmol)	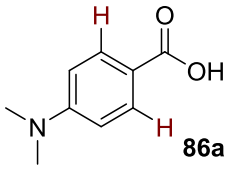 **86a** (14.2 mg, 0.086 mmol)		MTBE	DIPEA 11.2 mg (0.086 mmol)
			Temperature (°C)	***Time (h)***
			55	2

Additive	***Run***	***Add. yield (%)***	***Sub. yield (%)***	***Sub. incorporation (%)***
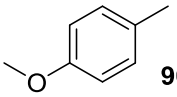 **90a** (10.6 mg, 0.086 mmol)	***1***	92	99	81
	2	86	99	78
	Average	89	99	80

Additive	***Run***	***Add. yield (%)***	***Sub. yield (%)***	***Sub. incorporation (%)***
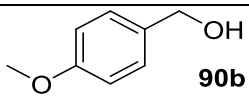 **90b** 11.9 mg (0.086 mmol)	***1***	99	99	78
	2	99	99	79
	Average	99	99	79

Additive	*Run*	*Additive yield (%)*	*Substrate yield (%)*	*Substrate incorporation (%)*
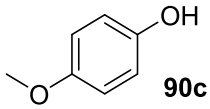 **90c** 10.7 mg (0.086 mmol)	***1***	99	99	69
	2	99	99	71
	Average	99	99	70

Additive	*Run*	*Add. yield (%)*	*Sub. yield (%)*	*Sub. incorporation (%)*
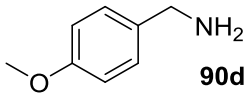 **90d** 11.8 mg (0.086 mmol)	***1***	99	99	19
	2	99	99	20
	Average	99	99	20

Additive	*Run*	*Add. yield (%)*	*Sub. yield (%)*	*Sub. incorporation (%)*
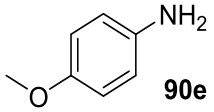 **90e** 10.6 mg (0.086 mmol)	***1***	99	99	65
	2	99	99	66
	Average	99	99	66

Additive	*Run*	*Add. yield (%)*	*Sub. yield (%)*	*Sub. incorporation (%)*
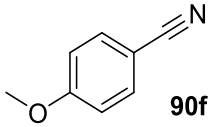 **90f** 11.5 mg (0.086 mmol)	***1***	99	99	0
	2	99	99	0
	Average	99	99	0

Additive	*Run*	*Add. yield (%)*	*Sub. yield (%)*	*Sub. incorporation (%)*
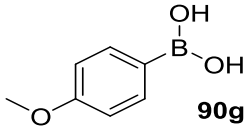 **90g** 13.2 mg (0.086 mmol)	***1***	91	99	84
	2	92	99	84
	Average	92	99	84

Additive	*Run*	*Add. yield (%)*	*Sub. yield (%)*	*Sub. incorporation (%)*
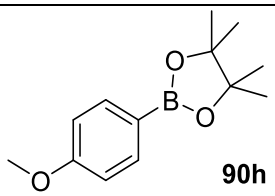 **90h** 16.2 mg (0.086 mmol)	***1***	92	99	71
	2	93	99	83
	Average	93	99	77

Additive	*Run*	*Add. yield (%)*	*Sub. yield (%)*	*Sub. incorporation (%)*
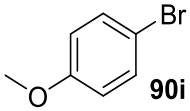 **90i** 16.1 mg (0.086 mmol)	***1***	99	99	70
	2	99	99	82
	Average	99	99	76

Additive	*Run*	*Add. yield (%)*	*Sub. yield (%)*	*Sub. incorporation (%)*
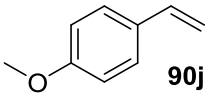 **90j** 11.5 mg (0.086 mmol)	***1***	22	99	81
	2	14	99	80
	Average	18	99	81

Additive	*Run*	*Add. yield (%)*	*Sub. yield (%)*	*Sub. incorporation (%)*
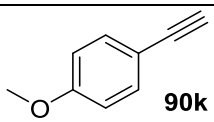 **90k** 11.4 mg (0.086 mmol)	***1***	21	96	0
	2	25	86	0
	Average	23	91	0

Table 2.8 *Competition reactions; investigating the selectivity of exchange (with base).*

To allow quantification of the substrate and additive remaining after the reaction, each additive **90l-q** and substrate **86a** were calibrated against an internal standard through LCMS analysis, as has been previously reported (*vide supra*).

Following calibration, the reactions were carried out following general procedure A, which was modified by adding a stock solution of internal standard **S2** (1 mL of a 10 mg/mL solution) at the end of the reaction, and analysed by LCMS to confirm the extent of exchange and the amount of acid and additive remaining. The position of exchange in the additives is assumed from similar known compounds.[45,47]

Internal Standard	***LCMS data***			
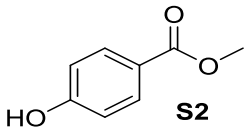 (10 mg)	***Retention time (min)***		***Mass ion***	
	2.09		No mass ion observed	
Complex	***Substrate***		***Solvent***	***Base***
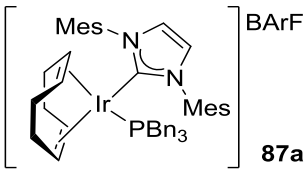 (11.4 mg, 0.0645 mmol)	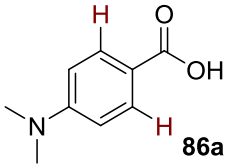 (14.2 mg, 0.086 mmol)		MTBE	DIPEA 11.2 mg (0.086 mmol)
			Temperature (°C)	***Time (h)***
			55	2

Additive	***Run***	***Add. yield (%)***	***Add. incorporation (%)***	***Sub. yield (%)***	***Sub. incorporation (%)***
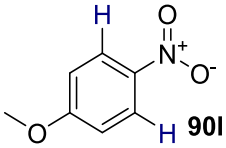 13.2 mg (0.086 mmol)	***1***	93	9	99	83
	2	88	10	99	81
	Average	91	10	99	82

Additive	*Run*	*Add. yield (%)*	*Add. incorporation (%)*	*Sub. yield (%)*	*Sub. incorporation (%)*
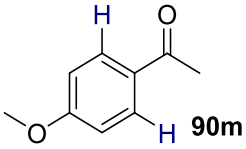 **90m** 12.9 mg (0.086 mmol)	***1***	94	24	99	82
	2	96	30	89	82
	Average	95	27	94	82

Additive	*Run*	*Add. yield (%)*	*Add. incorporation (%)*	*Sub. yield (%)*	*Sub. incorporation (%)*
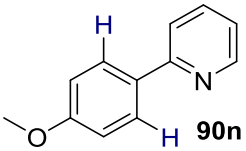 **90n** 15.9 mg (0.086 mmol)	***1***	96	77	99	25
	2	92	77	99	23
	Average	94	77	99	24

Additive	*Run*	*Add. yield (%)*	*Add. incorporation (%)*	*Sub. yield (%)*	*Sub. incorporation (%)*
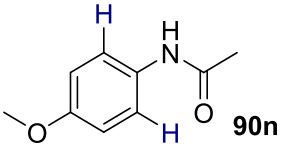 **90n** 14.4 mg (0.086 mmol)	***1***	99	4	99	68
	2	99	5	99	69
	Average	99	5	99	69

Additive	*Run*	*Add. yield (%)*	*Add. incorporation (%)*	*Sub. yield (%)*	*Sub. incorporation (%)*
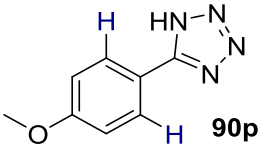 **90p** 15.2 mg (0.086 mmol)	***1***	99	9	99	5
	2	99	9	99	6
	Average	99	9	99	6

Additive	*Run*	*Add. yield (%)*	*Add. incorporation (%)*	*Sub. yield (%)*	*Sub. incorporation (%)*
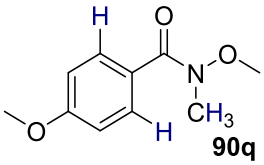 **90q** 16.8 mg (0.086 mmol)	***1***	99	0	99	68
	2	99	0	99	72
	Average	99	0	99	70

Scheme 2.52 *Reassessing selected substrates under basic conditions.*

The reactions were carried out following general procedure A, and analysed by ^{1}H NMR spectroscopy to confirm the extent and position of exchange.

Complex	*Solvent*	*Temperature (°C)*	*Time (h)*
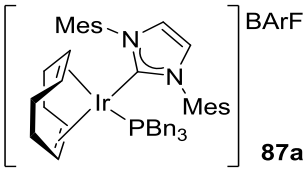 **87a** (11.4 mg, 0.0645 mmol)	MTBE	55	2

Substrate	*data*
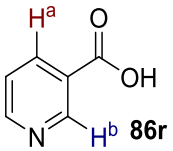 **86r** (10.6 mg, 0.086 mmol)	Data was consistent with that reported on page 327.

D-Incorporation (%)					
Run				*Average*	
1		*2*			
D^a	D^b	D^a	D^b	D^a	D^b
9	18	7	14	8	16

Substrate	*Data*
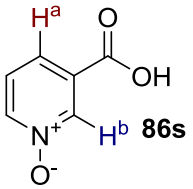 **86s** (12.0 mg, 0.086 mmol)	Data was consistent with that reported on page 328.

D-Incorporation (%)					
Run				*Average*	
1		*2*			
D^a	D^b	D^a	D^b	D^a	D^b
14	20	14	21	14	21

Internal Standard	***Data***
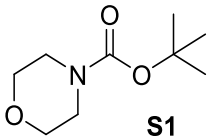 **S1** (16.1 mg, 0.086 mmol)	Data was consistent with that reported on page 331.

Substrate	***Data***
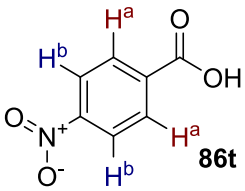 **86t** (14.2 mg, 0.086 mmol)	Data was consistent with that reported on page 331.

D-Incorporation (%)					
Run				***Average***	
1		***2***			
D^a	D^b	D^a	D^b	D^a	D^b
80	26	84	27	82	27

Scheme 2.53 *HIE on carboxylic acid-containing drugs.*

The reactions were carried out following general procedure A, and analysed by ^{1}H NMR spectroscopy to confirm the extent and position of exchange.

Complex	*Solvent*	*Temperature (°C)*	*Time (h)*
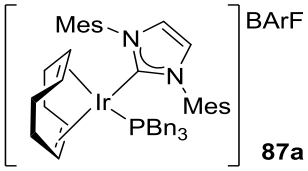 **87a** (7.6 mg, 0.0043 mmol)	MTBE	50	2

Substrate	*^{1}H NMR data*[102]
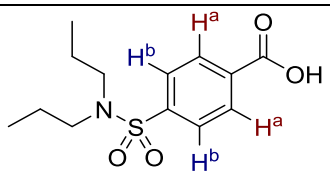 *Probenecid* - **91** (10.6 mg, 0.086 mmol)	**^{1}H NMR** (300 MHz, DMSO): δ 8.24-8.18 (2H, m, Ar-H), 7.99-7.94 (2H, m, Ar-H), 3.19-3.14 (4H, m, N-CH_2) 1.62-1.50 (4H, m, CH_2-CH_3), 0.92 (6H, t *J* = 7.6 Hz, CH_2-CH_3). Incorporation expected at δ D^a 8.24-8.18 & D^b 7.99-7.94. Determined against integral at δ 0.92.

D-Incorporation (%)					
Run				*Average*	
1		*2*			
D^a	*D^b*	*D^a*	*D^b*	*D^a*	*D^b*
92	6	88	4	90	5

Substrate	*^{1}H NMR data*[103]
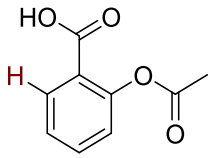 *Aspirin* - **92** (13.1 mg, 0.086 mmol)	**^{1}H NMR** (300 MHz, DMSO): δ 13.00 (1H, br s, O-H), 7.92 (1H, dd *J* = 7.8 Hz, ^{4}J = 1.8 Hz, Ar-H), 7.63 (1H, ddd *J* = 8.1 Hz, 7.4 Hz, ^{4}J = 1.8 Hz, Ar-H), 7.37 (1H, td *J* = 7.5 Hz, ^{4}J = 1.3 Hz, Ar-H), 7.18 (1H, dd *J* = 8.1 Hz, ^{4}J = 1.4 Hz, Ar-H), 2.24 (3H, s, CO-CH_3). Incorporation expected at δ 7.92. Determined against integral at δ 2.24.

D-Incorporation (%)		
Run		*Average*
1	*2*	
97	97	97

Substrate	***^{1}H NMR data***[104]
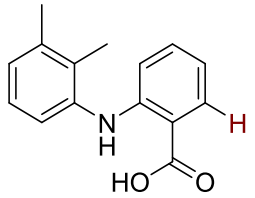 *Mefanamic acid* - **93** (13.1 mg, 0.086 mmol)	**^{1}H NMR** (300 MHz, DMSO): δ 13.00 (1H, br s, O-H), 9.45 (1H, br-s, N-H), 7.87 (1H, dd *J* = 8.2 Hz, ^4J = 1.8 Hz, Ar-H), 7.29 (1H, ddd, *J* = 8.5 Hz, 7.1 Hz, ^4J = 1.7 Hz, Ar-H), 7.14-7.06 (2H, m, Ar-H), 7.05-6.98 (1H, m, Ar-H), 6.72-6.63 (2H, m, Ar-H), 2.27 (3H, s, Ar-CH_3), 2.08 (3H, s, Ar-CH_3). Incorporation expected at δ 7.87. Determined against integral at δ 2.27.

D-Incorporation (%)		
Run		***Average***
1	***2***	
85	84	85

6.3. Non-Aryl sp^2 HIE

Scheme 2.54 *Catalyst screen for olefinic hydrogen isotope exchange.*

The reactions were carried out following general procedure B and analysed by ^{1}H NMR spectroscopy to confirm the degree of hydrogenation, and the position and degree of deuterium incorporation (**Table E2.6**).

Solvent	***Temperature (°C)***	***Time (h)***
DCM 4 mL	25	1
Substrate	***^{1}H NMR data***[105]	
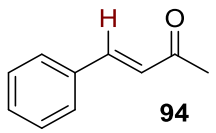 **94** (58.5 mg, 0.4 mmol)	**^{1}H NMR** (400 MHz, $CDCl_3$): δ 7.62-7.49 (3H, m, Ar-H and d, *J* = 15.9 Hz, Ar-CH=CH), 7.47-7.39 (3H, m, Ar-H), 6.75 (1H, d, *J* = 15.9 Hz, CH=CH-CO), 2.41 (3H, s, OC-CH_3). Incorporation expected at δ 7.62-7.49. Determined against integral at δ 2.41.	
Hydrogenation Product	***^{1}H NMR data***[52]	
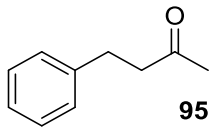 **95**	**^{1}H NMR** (400 MHz, $CDCl_3$): δ 7.30-7.23 (2H, m, Ar-H), 7.20-7.14 (3H, m, Ar-H), 2.92-2.85 (2H, m, CH_2), 2.78-7.71 (2H, m, CH_2), 2.16 (3H, s, CO-CH_3). Conversion determined using integrals at δ 2.41 (**D94**) and 2.16 (**95**).	

Entry	***Complex***	***D-Incorporation (%)***			***Hydrogenation (%)***		
		Run		***Average***	***Run***		***Average***
		1	***2***		1	2	
1	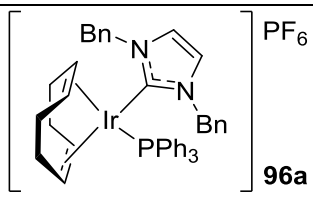 **96a** (1.9 mg, 0.002 mmol)	0	0	0	0	0	0
2	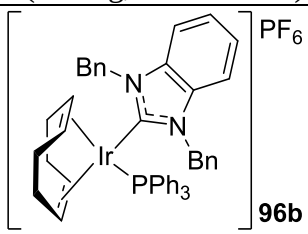 **96b** (2.0 mg, 0.002 mmol)	0	0	0	0	0	0

3	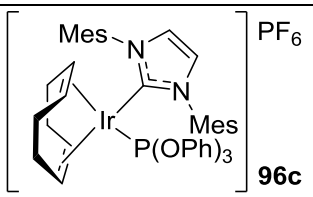 (2.1 mg, 0.002 mmol)	32	27	30	22	26	24
4	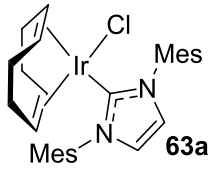 (1.3 mg, 0.002 mmol)	0	0	0	0	0	0
5	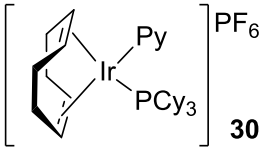 (1.6 mg, 0.002 mmol)	96	95	96	56	52	54
6	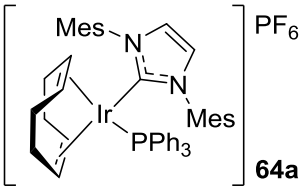 (2.0 mg, 0.002 mmol)	96	94	95	20	26	23
7	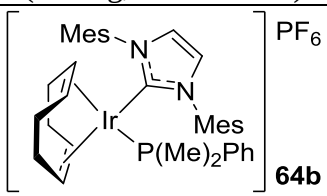 (1.8 mg, 0.002 mmol)	0	0	0	100	100	100
8	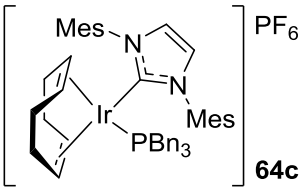 (2.1 mg, 0.002 mmol)	92	79	86	98	90	94

Table E2.6

Graph 2.5 & Graph 2.7 *Monitored HIE and hydrogenation of* ***94****.*

The reactions were carried out following general procedure C and analysed by ^{1}H NMR spectroscopy to confirm the degree of hydrogenation, and the position and degree of deuterium incorporation (**Table E2.7**).

Solvent	***Temperature (°C)***
DCM (40 mL)	25
Substrate	***Data***
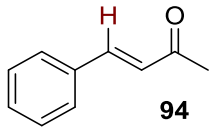 **94** (292.3 mg, 2.0 mmol)	Data was consistent with that reported on page 362.
Hydrogenation Product	***Data***
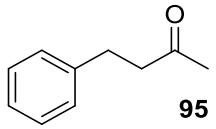 **95**	Data was consistent with that reported on page 362.

Entry	*Complex*	*Time (min)*	*D-Incorporation (%)*	*Hydrogenation (%)*
1	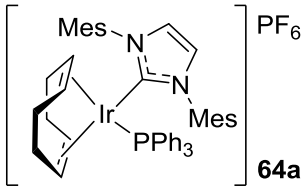 **64a** (2.0 mg, 0.002 mmol)	10	26	1
2		20	47	2
3		30	62	2
4		40	75	3
5		70	82	5
6		90	85	5
7		120	87	6
8	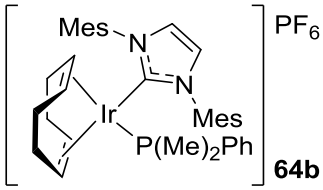 **64b** (1.8 mg, 0.002 mmol)	10	62	14
9		20	83	19
10		30	88	21
11		40	93	25
12		70	95	28
13		90	95	31
14		120	96	37
15	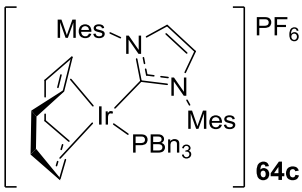 **64c** (2.1 mg, 0.002 mmol)	10	46	3
16		20	73	6
17		30	82	10
18		40	88	14
19		70	89	18
20		90	91	22
21		120	93	27
22	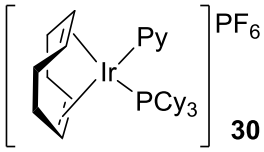 **30** (1.6 mg, 0.002 mmol)	10	23	3
23		20	40	5
24		30	53	7
25		40	62	9
26		70	66	9
27		90	66	9
28		120	68	9

Table E2.7

Table 2.9 *Effect of concentration on HIE/hydrogenation selectivity.*

The reactions were carried out following general procedure B and analysed by ^{1}H NMR spectroscopy to confirm the degree of hydrogenation, and the position and degree of deuterium incorporation (**Table E2.8**).

Complex	***Solvent***	***Time (h)***	***Temperature (°C)***
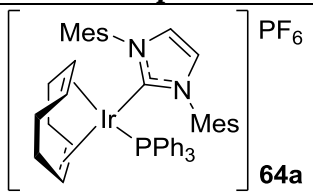 **64a** (0.4 mg, 0.0004 mmol)	DCM	1	25
Substrate		***Data***	
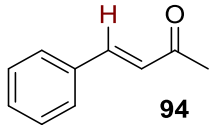 **94** (58.5 mg, 0.4 mmol)		Data was consistent with that reported on page 362.	
Hydrogenation Product		***Data***	
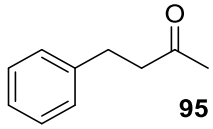 **95**		Data was consistent with that reported on page 362.	

Entry	***Concentration (M)***	***Solvent volume (mL)***	***D-Incorporation (%)***			***Hydrogenation (%)***		
			Run		***Average***	***Run***		***Average***
			1	***2***		***1***	***2***	
1	0.050	8	85	90	88	6	7	7
2	0.066	6	81	83	82	4	4	4
3	0.10	4	83	82	83	3	2	3
4	0.20	2	81	80	81	2	3	3
5	0.40	1	80	82	81	1	1	1
6	0.80	0.5	10	8	9	0	0	0

Table E2.8

Scheme 2.55 *HIE on p-substituted 4-phenyl butanones.*

The reactions were carried out following general procedure B and analysed by ^{1}H NMR spectroscopy to confirm the degree of hydrogenation, and the position and degree of deuterium incorporation.

Complex	***Solvent***	***Time (h)***	***Temperature (°C)***
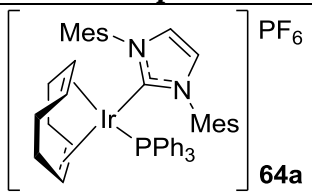 **64a** (0.4 mg, 0.0004 mmol)	DCM (1 mL)	1	25

Substrate	***^{1}H NMR data***[105]
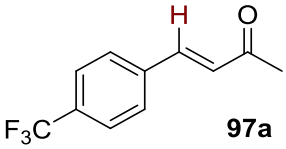 **97a** (86 mg, 0.4 mmol)	**^{1}H NMR** (400 MHz, $CDCl_3$): δ 7.71-7.65 (4H, m, Ar-H), 7.54 (1H, d *J* = 16.3 Hz, Ar-C<u>H</u>=CH), 6.80 (1H, d *J* = 16.3 Hz, CH=C<u>H</u>-CO), 2.43 (3H, s, CO-C<u>H</u>$_3$). Incorporation expected at δ 7.54. Determined against integral at δ 2.43.
Hydrogenation Product	***^{1}H NMR data***[106]
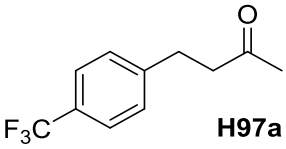 **H97a**	**^{1}H NMR** (400 MHz, $CDCl_3$): δ 7.53 (2H, d, *J* = 8.1 Hz, Ar-<u>H</u>), 7.30 (2H, d *J* = 8.1 Hz, Ar-<u>H</u>), 2.95 (2H, t *J* = 7.5 Hz, C<u>H</u>$_2$), 2.78 (2H, t *J* = 7.5 Hz, C<u>H</u>$_2$), 2.17 (3H, s, CO-C<u>H</u>$_3$). Conversion determined using integrals at δ 2.43 (**D97a**) and 2.17 (**H97a**).

D-Incorporation (%)			***Hydrogenation (%)***		
Run		***Average***	***Run***		***Average***
1	***2***		***1***	***2***	
88	89	89	2	2	2

Substrate	***^{1}H NMR data***[107]
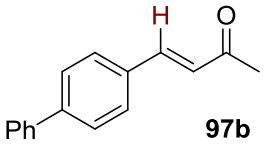 **97b** (89 mg, 0.4 mmol)	**^{1}H NMR** (400 MHz, $CDCl_3$): δ 7.69-7.61 (6H, m, Ar-H), 7.57 (1H, d *J* = 16.3 Hz, Ar-CH=CH), 7.51-7.44 (2H, m, Ar-H), 7.43-7.36 (1H, m, Ar-H), 6.77 (1H, d *J* = 16.3 Hz, CH=CH-CO), 2.41 (s, 3H, CO-CH_3). Incorporation expected at δ 7.57. Determined against integral at δ 2.41.
Hydrogenation Product	***^{1}H NMR data***[59]
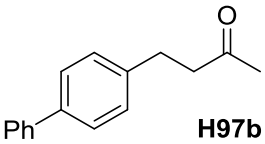 **H97b**	**^{1}H NMR** (400 MHz, $CDCl_3$): δ 7.62-7.59 (2H, m, Ar-H), 7.75-7.53 (2H, m, Ar-H), 7.49-7.44 (2H, m, Ar-H), 7.39-7.34 (1H, m, Ar-H), 7.31-7.28 (2H, m, Ar-H), 2.98 (2H, t *J* = 7.4 Hz, CH_2), 2.83 (2H, t *J* = 7.4 Hz, CH_2), 2.19 (3H, s, CH_3). Conversion determined using integrals at δ 2.41 (**D97b**) and 2.19 (**H97b**).

D-Incorporation (%)			***Hydrogenation (%)***		
Run		***Average***	***Run***		***Average***
1	***2***		***1***	***2***	
81	82	82	2	2	2

Substrate	***^{1}H NMR data***[108]
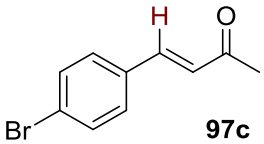 **97c** (90 mg, 0.4 mmol)	**^{1}H NMR** (400 MHz, $CDCl_3$): δ 7.59-7.53 (2H, m, Ar-H), 7.46 (1H, d *J* = 16.5 Hz, Ar-CH=CH), 7.44-7.40 (2H, m, Ar-H), 6.72 (1H, d *J* = 16.3 Hz, CH=CH-CO), 2.40 (3H, s, CO-CH_3). Incorporation expected at δ 7.46. Determined against integral at δ 2.40.
Hydrogenation Product	***^{1}H NMR data***[106]
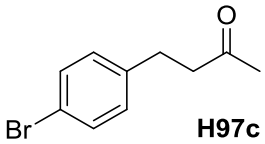 **H97c**	**^{1}H NMR** (400 MHz, $CDCl_3$): δ 7.39 (2H, d, *J* = 8.1 Hz, Ar-H), 7.05 (2H, d *J* = 8.1 Hz, Ar-H), 2.84 (2H, t *J* = 7.2 Hz, CH_2), 2.74 (2H, t *J* = 7.2 Hz, CH_2), 2.14 (3H, s, CH_3). Conversion determined using integrals at δ 2.40 (**D97c**) and 2.14 (**H97c**).

D-Incorporation (%)			***Hydrogenation (%)***		
Run		***Average***	***Run***		***Average***
1	***2***		***1***	***2***	
89	84	87	1	3	2

Substrate	***^{1}H NMR data***[108]
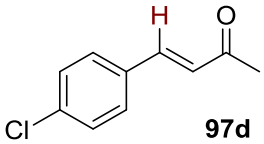 **97d** (72 mg, 0.4 mmol)	**^{1}H NMR** (400 MHz, $CDCl_3$): δ 7.51-7.44 (3H, m, Ar-H and d *J* = 16.1 Hz, Ar-CH=CH), 7.41-7.36 (2H, m, Ar-H), 6.69 (1H, d *J* = 16.3 Hz, CH=CH-CO), 2.39 (3H, s, CO-CH_3). Incorporation expected at δ 7.51-7.44. Determined against integral at δ 2.39.
Hydrogenation Product	***^{1}H NMR data***[109]
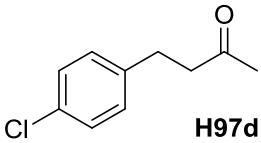 **H97d**	**^{1}H NMR** (400 MHz, $CDCl_3$): δ 7.24 (2H, d, *J* = 8.3 Hz, Ar-H), 7.11 (2H, d *J* = 8.3 Hz, Ar-H), 2.86 (2H, t *J* = 7.2 Hz, CH_2), 2.74 (2H, t *J* = 7.2 Hz, CH_2), 2.14 (3H, s, CH_3). Conversion determined using integrals at δ 2.39 (**D97d**) and 2.14 (**H97d**).

D-Incorporation (%)			***Hydrogenation (%)***		
Run		***Average***	***Run***		***Average***
1	***2***		***1***	***2***	
89	91	90	3	4	4

Substrate	***^{1}H NMR data***[105]
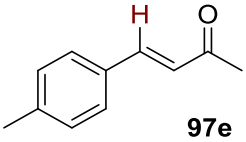 **97e** (64 mg, 0.4 mmol)	**^{1}H NMR** (400 MHz, $CDCl_3$): δ 7.51 (1H, d *J* = 16.1 Hz, Ar-CH=CH), 7.47 (2H, d *J* = 8.0 Hz, Ar-H), 7.23 (2H, d *J* = 8.0 Hz, Ar-H), 6.70 (1H, d *J* = 16.1 Hz, CH=CH-CO), 2.40 (3H, s, Ar-CH_3), 2.39 (3H, s, CO-CH_3). Incorporation expected at δ 7.51. Determined against integral at δ 2.39.
Hydrogenation Product	***^{1}H NMR data***[110]
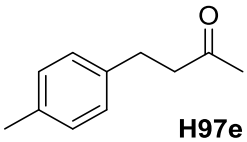 **H97e**	**^{1}H NMR** (400 MHz, $CDCl_3$): δ 7.13-7.08 (4H, m, Ar-H), 2.90-2.83 (2H, m, CH_2), 2.78-2.72 (2H, m, CH_2), 2.33 (3H, s, CH_3), 2.15 (3H, s, CH_3). Conversion determined using integrals at δ 2.39 (**D97e**) and 2.15 (**H97e**).

D-Incorporation (%)			***Hydrogenation (%)***		
Run		***Average***	***Run***		***Average***
1	***2***		***1***	***2***	
68	72	70	1	1	1

Substrate	***^{1}H NMR data***[108]
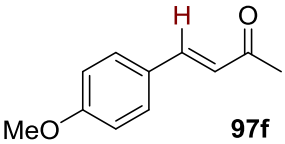 **97f** (70 mg, 0.4 mmol)	**^{1}H NMR** (400 MHz, $CDCl_3$): δ 7.53-7.47 (3H, m, Ar-H and d *J* = 16.0 Hz, Ar-CH=CH), 6.96-6.91 (2H, m, Ar-H), 6.62 (1H, d *J* = 16.2 Hz, CH=CH-CO), 3.86 (3H, s, ArO-CH_3), 2.37 (3H, s, CO-CH_3). Incorporation expected at δ 7.53-7.47. Determined against integral at δ 2.37.
Hydrogenation Product	***^{1}H NMR data***[106]
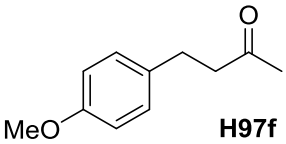 **H97f**	**^{1}H NMR** (400 MHz, $CDCl_3$): δ 7.10-7.08 (2H, m, Ar-H), 6.82-6.80 (2H, m, Ar-H), 3.77 (3H, s, ArO-CH_3), 2.83 (2H, t *J* = 7.5 Hz, CH_2), 2.71 (2H, t *J* = 7.5 Hz, CH_2), 2.12 (3H, s, CH_3). Conversion determined using integrals at δ 2.37 (**D97f**) and 2.12 (**H97f**).

D-Incorporation (%)			***Hydrogenation (%)***		
Run		***Average***	***Run***		***Average***
1	***2***		***1***	***2***	
83	79	81	1	1	1

Substrate	***^{1}H NMR data***[113]
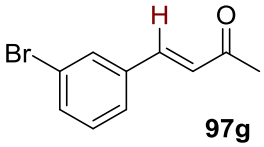 **97g** (90 mg, 0.4 mmol)	**^{1}H NMR** (400 MHz, $CDCl_3$): δ 7.73-7.66 (1H, m, Ar-H), 7.57-7.50 (1H, m, Ar-H), 7.50-7.39 (2H, m Ar-H and d *J* = 16.3 Hz, Ar-CH=CH), 7.28-7.25 (1H, m, Ar-H), 6.71 (1H, d *J* = 16.2 Hz, CH=CH-CO), 2.39 (3H, s, CO-CH_3). Incorporation expected at δ 7.50-7.39. Determined against integral at δ 2.39.
Hydrogenation Product	***^{1}H NMR data***[111]
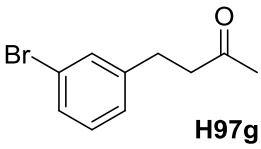 **H97g**	**^{1}H NMR** (400 MHz, $CDCl_3$): δ 7.33-7.31 (2H, m, Ar-H), 7.15-7.10 (2H, m, Ar-H), 2.87-2.85 (2H, m, CH_2), 2.76-2.73 (2H, m, CH_2), 2.14 (3H, s, CH_3). Conversion determined using integrals at δ 2.39 (**D97g**) and 2.14 (**H97g**).

D-Incorporation (%)			***Hydrogenation (%)***		
Run		***Average***	***Run***		***Average***
1	***2***		***1***	***2***	
72	75	74	1	1	1

Substrate	***^{1}H NMR data***[112]
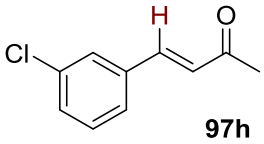 **97h** (72 mg, 0.4 mmol)	**^{1}H NMR** (400 MHz, $CDCl_3$): δ 7.56-7.54 (1H, m, Ar-H), 7.49-7.42 (2H, m Ar-H and d *J* = 16.0 Hz, Ar-CH=CH), 7.41-7.33 (2H, m, Ar-H), 6.73 (1H, d *J* = 16.3 Hz, CH=CH-CO), 2.40 (3H, s, CO-CH_3). Incorporation expected at δ 7.49-7.42. Determined against integral at δ 2.40.
Hydrogenation Product	***^{1}H NMR data***[111]
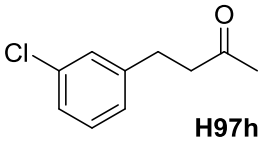 **H97h**	**^{1}H NMR** (400 MHz, $CDCl_3$): δ7.21-7.16 (3H, m, Ar-H), 7.09-7.05 (1H, m, Ar-H), 2.88-2.86 (2H, m, CH_2), 2.76-2.74 (2H, m, CH_2), 2.14 (3H, s, CH_3). Conversion determined using integrals at δ 2.40 (**D97h**) and 2.14 (**H97h**).

D-Incorporation (%)			***Hydrogenation (%)***		
Run		***Average***	***Run***		***Average***
1	***2***		***1***	***2***	
86	80	83	3	3	3

Substrate	***^{1}H NMR data***[113]
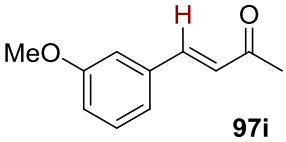 **97i** (70 mg, 0.4 mmol)	**^{1}H NMR** (400 MHz, $CDCl_3$): δ 7.50 (1H, d, *J* = 16.2 Hz, Ar-CH=CH), 7.37-7.30 (1H, m, Ar-H), 7.19-7.13 (1H, m, Ar-H), 7.11-7.06 (1H, m, Ar-H), 7.01-6.94 (1H, m, Ar-H), 6.73 (1H, d *J* = 16.3 Hz, CH=CH-CO), 3.86 (3H, s, ArO-CH_3), 2.41 (3H, s, CO-CH_3). Incorporation expected at δ 7.50. Determined against integral at δ 2.41.
Hydrogenation Product	***^{1}H NMR data***[114]
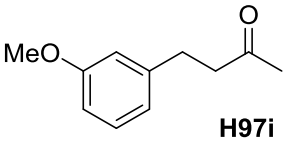 **H97i**	**^{1}H NMR** (400 MHz, $CDCl_3$): δ 7.22-7.17 (1H, m, Ar-H), 6.78-6.73 (3H, m, Ar-H), 3.79 (3H, s, ArO-CH_3), 2.87 (2H, t *J* = 7.6 Hz, CH_2), 2.75 (2H, t *J* = 7.6 Hz, CH_2), 2.14 (3H, s, CH_3). Conversion determined using integrals at δ 2.41 (**D97i**) and 2.14 (**H97i**).

D-Incorporation (%)			***Hydrogenation (%)***		
Run		***Average***	***Run***		***Average***
1	***2***		***1***	***2***	
75	74	75	1	1	1

Substrate	***^{1}H NMR data***[115]
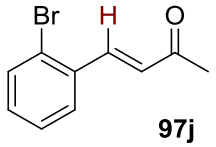 **97j** (90 mg, 0.4 mmol)	**^{1}H NMR** (400 MHz, $CDCl_3$): δ 7.87 (1H, d *J* = 16.3 Hz, Ar-C<u>H</u>=CH), 7.63-7.58 (2H, m, Ar-<u>H</u>), 7.35-7.29 (1H, m, Ar-<u>H</u>), 7.25-7.19 (1H, m, Ar-<u>H</u>), 6.60 (1H, d *J* = 16.3 Hz, CH=C<u>H</u>-CO), 2.40 (3H, s, CO-C<u>H</u>$_3$). Incorporation expected at δ 7.87. Determined against integral at δ 2.40.
Hydrogenation Product	***^{1}H NMR data***[111]
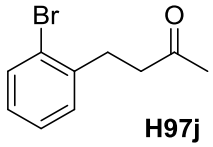 **H97j**	**^{1}H NMR** (400 MHz, $CDCl_3$): δ7.53-7.49 (1H, m, Ar-<u>H</u>), 7.25-7.21 (2H, m, Ar-<u>H</u>), 7.08-7.05 (1H, m, Ar-<u>H</u>), 3.01-2.99 (2H, m, C<u>H</u>$_2$), 2.78-2.75 (2H, m, C<u>H</u>$_2$), 2.15 (3H, s, C<u>H</u>$_3$). Conversion determined using integrals at δ 2.40 (**D97j**) and 2.15 (**H97j**).

D-Incorporation (%)			***Hydrogenation (%)***		
Run		***Average***	***Run***		***Average***
1	***2***		***1***	***2***	
0	0	0	0	0	0

Substrate	***^{1}H NMR data***[116]
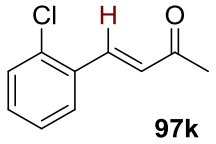 **97k** (72 mg, 0.4 mmol)	**^{1}H NMR** (400 MHz, $CDCl_3$): δ 7.96 (1H, d *J* = 16.4 Hz, Ar-C<u>H</u>=CH), 7.68-7.64 (1H, m, Ar-<u>H</u>), 7.48-7.44 (1H, m, Ar-<u>H</u>), 7.38-7.29 (2H, m, Ar-<u>H</u>), 6.69 (1H, d *J* = 16.4 Hz, CH=C<u>H</u>-CO), 2.44 (3H, s, CO-C<u>H</u>$_3$). Incorporation expected at δ 7.96. Determined against integral at δ 2.44.
Hydrogenation Product	***^{1}H NMR data***[111]
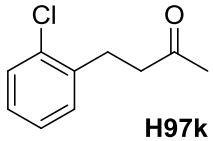 **H97k**	**^{1}H NMR** (400 MHz, $CDCl_3$): δ 7.35-7.31 (1H, m, Ar-<u>H</u>), 7.25-7.21 (1H, m, Ar-<u>H</u>), 7.19-7.13 (2H, m, Ar-<u>H</u>), 3.01-2.99 (2H, m, C<u>H</u>$_2$), 2.78-2.76 (2H, m, C<u>H</u>$_2$), 2.15 (3H, s, C<u>H</u>$_3$). Conversion determined using integrals at δ 2.44 (**D97k**) and 2.15 (**H97k**).

D-Incorporation (%)			***Hydrogenation (%)***		
Run		***Average***	***Run***		***Average***
1	***2***		***1***	***2***	
0	0	0	0	0	0

Substrate	***^{1}H NMR data***[113]
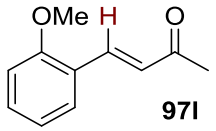 (70 mg, 0.4 mmol)	**^{1}H NMR** (400 MHz, $CDCl_3$): δ 7.90 (1H, d, *J* = 16.5 Hz, Ar-C<u>H</u>=CH), 7.60-7.53 (1H, m, Ar-<u>H</u>), 7.42-7.35 (1H, m, Ar-H), 7.05-6.92 (2H, m, Ar-<u>H</u>), 6.78, (1H, d *J* = 16.5 Hz, CH=C<u>H</u>-CO), 3.92 (3H, s, ArO-C<u>H</u>$_3$), 2.40 (3H, s, CO-C<u>H</u>$_3$). Incorporation expected at δ 7.90. Determined against integral at δ 2.40.
Hydrogenation Product	***^{1}H NMR data***[114]
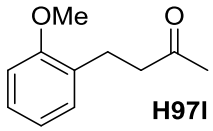	**^{1}H NMR** (400 MHz, $CDCl_3$): δ 7.21-7.12 (2H, m, Ar-<u>H</u>), 6.90-6.83 (2H, m, Ar-<u>H</u>), 3.82 (3H, s, ArO-C<u>H</u>$_3$), 2.89 (2H, t *J* = 7.2 Hz, C<u>H</u>$_2$), 2.73 (2H, t *J* = 8.0 Hz, C<u>H</u>$_2$), 2.14 (3H, s, C<u>H</u>$_3$). Conversion determined using integrals at δ 2.40 (**D97l**) and 2.14 (**H97l**).

D-Incorporation (%)			***Hydrogenation (%)***		
Run		***Average***	***Run***		***Average***
1	***2***		***1***	***2***	
56	32	44	3	2	3

Scheme 2.56 *Investigating the effect of changing the 4-substituent.*

The reactions were carried out following general procedure B and analysed by ^{1}H NMR spectroscopy to confirm the degree of hydrogenation, and the position and degree of deuterium incorporation.

Complex	***Solvent***	***Time (h)***	***Temperature (°C)***
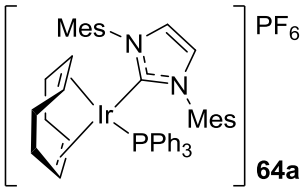 **64a** (0.4 mg, 0.0004 mmol)	DCM (1 mL)	1	25

Substrate	***^{1}H NMR data***[113]
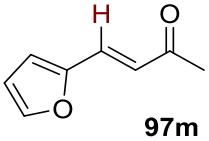 **97m** (54 mg, 0.4 mmol)	**^{1}H NMR** (400 MHz, $CDCl_3$): δ 7.53 (1H, d *J* = 1.7 Hz, Ar-H), 7.30 (1H, d J = 16.0 Hz, Ar-CH=CH), 6.69 (1H, d *J* = 3.2 Hz, Ar-H), 6.65 (1H, d *J* = 16.0 Hz, CH=CH-CO), 6.51 (1H, dd *J* = 3.4 Hz, J = 1.7 Hz, Ar-H), 2.35 (3H, s, CO-CH_3). Incorporation expected at δ 7.30. Determined against integral at δ 2.35.
Hydrogenation Product	***^{1}H NMR data***[117]
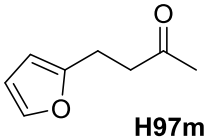 **H97m**	**^{1}H NMR** (400 MHz, $CDCl_3$): δ 7.30-7.28 (1H, m, Ar-H), 6.28-6.26 (1H, m, Ar-H), 6.02-5.98 (1H, m, Ar-H), 2.94-2.91 (2H, m, CH_2), 2.81-2.77 (2H, m, CH_2), 2.17 (3H, s, CH_3). Conversion determined using integrals at δ 2.35 (**D97m**) and 2.17 (**H97m**).

D-Incorporation (%)			***Hydrogenation (%)***		
Run		***Average***	***Run***		***Average***
1	***2***		***1***	***2***	
85	84	85	1	1	1

Substrate	***^{1}H NMR data***[118]
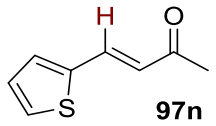 **97n** (61 mg, 0.4 mmol)	**^{1}H NMR** (400 MHz, $CDCl_3$): δ 7.65 (1H, d *J* = 15.8 Hz, Ar-C<u>H</u>=CH), 7.45-7.40 (1H, d *J* = 5.1 Hz, Ar-<u>H</u>), 7.32-7.30 (1H, m, Ar-H), 7.09 (1H, dd *J* = 5.1 Hz, *J* = 3.7 Hz, Ar-<u>H</u>), 6.56, (1H, d *J* = 15.8 Hz, CH=C<u>H</u>-CO), 2.36 (3H, s, CO-<u>CH_3</u>). Incorporation expected at δ 7.65. Determined against integral at δ 2.36.
Hydrogenation Product	***^{1}H NMR data***[109]
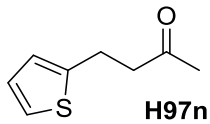 **H97n**	**^{1}H NMR** (400 MHz, $CDCl_3$): δ 7.12-7.10 (1H, m, Ar-<u>H</u>), 6.92-6.89 (1H, m, Ar-<u>H</u>), 6.80-6.79 (1H, m, Ar-<u>H</u>), 3.14-3.09 (2H, m, CH_2), 2.84-2.79 (2H, m, C<u>H_2</u>), 2.16 (3H, s, C<u>H_3</u>). Conversion determined using integrals at δ 2.36 (**D97n**) and 2.16 (**H97n**).

D-Incorporation (%)			***Hydrogenation (%)***		
Run		***Average***	***Run***		***Average***
1	***2***		***1***	***2***	
85	83	84	1	1	1

Substrate	***^{1}H NMR data***[119]
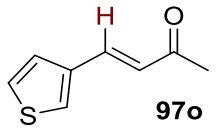 **97o** (61 mg, 0.4 mmol)	**^{1}H NMR** (400 MHz, $CDCl_3$): δ 7.54-7.44 (2H, m, Ar-<u>H</u> & d *J* = 16.2 Hz, Ar-C<u>H</u>=CH), 7.36-7.31 (1H, m, Ar-<u>H</u>), 7.31-7.27 (1H, m, Ar-H), 6.53, (1H, d *J* = 16.1 Hz, CH=C<u>H</u>-CO), 2.36 (3H, s, CO-<u>CH_3</u>). Incorporation expected at δ 7.54-7.44. Determined against integral at δ 2.36.
Hydrogenation Product	***^{1}H NMR data***[120]
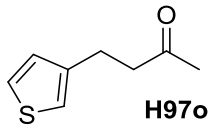 **H97o**	**^{1}H NMR** (400 MHz, $CDCl_3$): δ 7.24-7.20 (1H, m, Ar-<u>H</u>), 6.94-6.89 (2H, m, Ar-<u>H</u>), 2.89 (2H, t *J* = 8.0 Hz, C<u>H_2</u>), 2.73 (2H, t *J* = 8.0 Hz, C<u>H_2</u>), 2.12 (3H, s, C<u>H_3</u>) Conversion determined using integrals at δ 2.36 (**D970**) and 2.12 (**H970**).

D-Incorporation (%)			***Hydrogenation (%)***		
Run		***Average***	***Run***		***Average***
1	***2***		***1***	***2***	
79	79	79	1	1	1

Substrate	***^{1}H NMR data***[121]
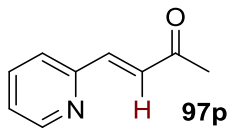 **97p** (73 mg, 0.4 mmol)	**^{1}H NMR** (400 MHz, $CDCl_3$): δ 8.70-8.66 (1H, m, Ar-H), 7.75 (1H, d *J* = 7.7 Hz, ^4J = 1.8 Hz, Ar-H), 7.55 (1H, d *J* = 16.1 Hz, Ar-C<u>H</u>=CH), 7.50 (1H, dt *J* = 7.9 Hz, ^4J = 1.0 Hz, Ar-<u>H</u>), 7.30 (1H, ddd *J* = 7.4 Hz, ^4J = 4.7 Hz, 1.2 Hz, Ar-H), 7.16 (1H, d *J* = 16.1 Hz, CH=C<u>H</u>-CO), 2.43 (3H, s, CO-C<u>H</u>$_3$). Incorporation expected at δ 7.16. Determined against integral at δ 2.43.
Hydrogenation Product	***^{1}H NMR data***[121]
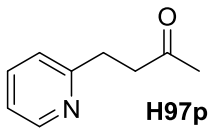 **H97p**	**^{1}H NMR** (400 MHz, $CDCl_3$): δ 8.48 (1H, d *J* = 4.1 Hz, Ar-<u>H</u>), 7.57-7.53 (1H, m, Ar-<u>H</u>), 7.16 (1H, d *J* = 7.7 Hz, Ar-<u>H</u>), 7.09-7.05 (1H, m, Ar-<u>H</u>), 3.05 (2H, t *J* = 7.1 Hz, C<u>H</u>$_2$), 2.93 (2H, t *J* = 7.1 Hz, C<u>H</u>$_2$), 2.16 (3H, s, C<u>H</u>$_3$). Conversion determined using integrals at δ 2.43 (**D97p**) and 2.16 (**H97p**).

D-Incorporation (%)			***Hydrogenation (%)***		
Run		***Average***	***Run***		***Average***
1	***2***		***1***	***2***	
30	34	32	1	0	1

Substrate	***^{1}H NMR data***[122]
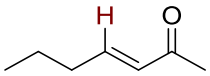 **97q** (45 mg, 0.4 mmol)	**^{1}H NMR** (400 MHz, $CDCl_3$): δ 6.77 (1H, dt *J* = 16.0 Hz, 6.9 Hz, CH_2-C<u>H</u>=CH), 6.05 (1H, dt *J* = 15.9 Hz, ^4J = 1.6 Hz CH=C<u>H</u>-CO), 2.22 (3H, s, CO-C<u>H</u>$_3$), 2.18 (2H, ddd *J* = 7.1 Hz, 6.9 Hz, ^4J = 1.7 Hz, CH-C<u>H</u>$_2$-CH_2) 1.48 (2H, sex *J* = 7.4 Hz, CH_2-C<u>H</u>$_2$-CH_3), 0.92 (3H, t *J* = 7.4 Hz, CH_2-C<u>H</u>$_3$). Incorporation expected at δ 6.77. Determined against integral at δ 2.22.
Hydrogenation Product	***^{1}H NMR data***[123]
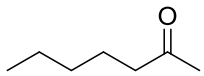 **H97q**	**^{1}H NMR** (400 MHz, $CDCl_3$): δ 2.40 (2H, t *J* = 7.4 Hz, CO-C<u>H</u>$_2$-CH_2), 2.12 (3H, s, CO-C<u>H</u>$_3$), 1.56 (2H, quin *J* = 7.4 Hz, CH_2-C<u>H</u>$_2$-CH_2), 1.34-1.23 (4H, m, C<u>H</u>$_2$), 0.88 (3H, t *J* = 7.1 Hz, CH_2-C<u>H</u>$_3$). Conversion determined using integrals at δ 2.22 (**D97n**) and 2.12 (**H97n**).

D-Incorporation (%)			***Hydrogenation (%)***		
Run		***Average***	***Run***		***Average***
1	***2***		***1***	***2***	
0	0	0	0	0	0

Substrate	***^{1}H NMR data***[124]
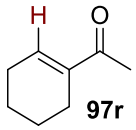 **97r** (49 mg, 0.4 mmol)	**^{1}H NMR** (400 MHz, $CDCl_3$): δ 6.90-6.84 (1H, m, CH_2-C<u>H</u>=C). 2.25 (3H, s, CO-C<u>H$_3$</u>), 2.24-2.15 (4H, m, C<u>H$_2$</u>), 1.67-1.53 (4H, m, C<u>H$_2$</u>). Incorporation expected at δ 6.90-6.84. Determined against integral at δ 2.25.
Hydrogenation Product	***^{1}H NMR data***[125]
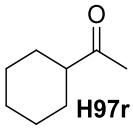 **H97r**	**^{1}H NMR** (400 MHz, $CDCl_3$): δ 2.37-2.30 (1H, m, Cy-C<u>H</u>), 2.14 (3H, s, CO-C<u>H$_3$</u>), 1.90-1.84 (2H, m, Cy-C<u>H$_2$</u>), 1.82-1.77 (2H, m, Cy-C<u>H$_2$</u>), 1.71-1.66 (1H, m, Cy-C<u>H</u>), 1.39-1.19 (5H, m, Cy-C<u>H$_2$</u> & Cy-C<u>H</u>). Conversion determined using integrals at δ 2.25 (**D97r**) and 2.14 (**H97r**).

D-Incorporation (%)			***Hydrogenation (%)***		
Run		***Average***	***Run***		***Average***
1	***2***		***1***	***2***	
0	0	0	0	0	0

Substrate	***^{1}H NMR data***[126]
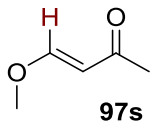 **97s** (40 mg, 0.4 mmol)	**^{1}H NMR** (400 MHz, $CDCl_3$): δ 7.59 (1H, d *J* = 12.9 Hz O-C<u>H</u>=CH), 5.60 (1H, d *J* = 12.8 Hz, CH=C<u>H</u>-CO), 3.73 (3H, s, O-C<u>H$_3$</u>), 2.21 (3H, s, CO-C<u>H$_3$</u>). Incorporation expected at δ 7.59. Determined against integral at δ 2.21.
Hydrogenation Product	***^{1}H NMR data***[127]
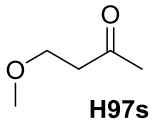 **H97s**	**^{1}H NMR** (400 MHz, $CDCl_3$): δ 3.51 (2H, t *J* = 6.3 Hz, C<u>H$_2$</u>), 3.22 (3H, s, O-C<u>H$_3$</u>), 2.56 (2H, t *J* = 6.3 Hz, C<u>H$_2$</u>), 2.11 (3H, s, CO-C<u>H$_3$</u>). Conversion determined using integrals at δ 2.21 (**D97s**) and 2.11 (**H97s**).

Catalyst Loading 64a	***D-Incorporation (%)***			***Hydrogenation (%)***		
	Run		***Average***	***Run***		***Average***
	1	***2***		***1***	***2***	
(0.4 mg, 0.0004 mmol)	0	0	0	0	0	0
(2.0 mg, 0.002 mmol)	58	57	58	0	0	0

Scheme 2.57 *Investigating influence of the directing group upon olefinic HIE.*

The reactions were carried out following general procedure B and analysed by ^{1}H NMR spectroscopy to confirm the degree of hydrogenation, and the position and degree of deuterium incorporation.

Complex	***Solvent***	***Time (h)***	***Temperature (°C)***
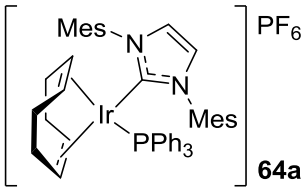 **64a** (0.4 mg, 0.0004 mmol)	DCM (1 mL)	1	25

Substrate	***^{1}H NMR data***[128]
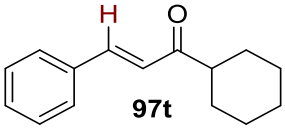 **97t** (86 mg, 0.4 mmol)	**^{1}H NMR** (400 MHz, $CDCl_3$): δ 7.65-7.55 (3H, m, Ar-H and d, *J* = 16.2 Hz, Ar-CH=CH), 7.45-7.37 (3H, m, Ar-H), 6.84 (1H, d, *J* = 16.3 Hz, CH=CH-CO), 2.75-2.62 (1H, m, Cy-H), 1.99-1.89 (2H, m, Cy-H), 1.89-1.81 (2H, m, Cy-H), 1.78-1.70 (1H, m, Cy-H), 1.57-1.19 (5H, m, Cy-H). Incorporation expected at δ 7.65-7.55. Determined against integral at δ 1.78-1.70.
Hydrogenation Product	***^{1}H NMR data***[129]
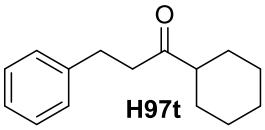 **H97t**	**^{1}H NMR** (400 MHz, $CDCl_3$): δ 7.20-7.15 (2H, m, Ar-H), 7.09-7.07 (3H, m, Ar-H), 2.79 (2H, t, *J* = 7.2 Hz, CH_2), 2.65 (2H, t, *J* = 7.2 Hz, CH_2), 2.25-2.17 (1H, m, OC-CH), 1.70-1.66 (5H, m, Cy-H), 1.28-1.10 (5H, m, Cy-H). Conversion determined using integrals at δ 1.78-1.70 (**D97r**) and 2.25-2.17 (**H97r**).

Catalyst Loading	***D-Incorporation (%)***			***Hydrogenation (%)***		
	Run		***Average***	***Run***		***Average***
	1	***2***		***1***	***2***	
0.1 mol% (0.4 mg, 0.0004 mmol)	97	99	98	28	32	30
0.025 mol% (0.1 mg, 0.0001 mmol)	93	90	92	7	7	7

Substrate	***^{1}H NMR data***[130]
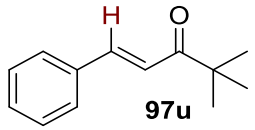 (75 mg, 0.4 mmol)	**^{1}H NMR** (400 MHz, $CDCl_3$): δ 7.66 (1H, d *J* = 15.6 Hz, Ar-C<u>H</u>=CH), 7.59-7.52 (2H, m, Ar-<u>H</u>), 7.42-7.34 (3H, m, Ar-<u>H</u>), 7.11 (1H, d *J* = 15.6 Hz, CH=C<u>H</u>-CO), 1.21 (9H, s, *t*Bu-C<u>H</u>$_3$). Incorporation expected at δ 7.66. Determined against integral at δ 1.21.
Hydrogenation Product	***^{1}H NMR data***[131]
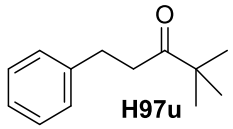	**^{1}H NMR** (400 MHz, $CDCl_3$): δ 7.31-7.28 (2H, m, Ar-<u>H</u>), 7.20-7.17 (3H, m, Ar-<u>H</u>), 2.91-2.86 (2H, m, C<u>H</u>$_2$), 2.82-2.77 (2H, m, C<u>H</u>$_2$), 1.11 (9H, s, *t*Bu-C<u>H</u>$_3$). Conversion determined using integrals at δ 1.21 (**D97u**) and 1.11 (**H97u**).

D-Incorporation (%)			***Hydrogenation (%)***		
Run		***Average***	***Run***		***Average***
1	***2***		***1***	***2***	
93	93	93	11	16	14

Substrate	***^{1}H NMR data***[132]
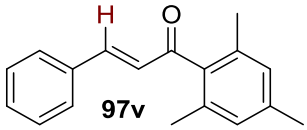 (100 mg, 0.4 mmol)	**^{1}H NMR** (400 MHz, $CDCl_3$): δ 7.53-7.46 (2H, m, Ar-<u>H</u>), 7.41-7.33 (3H, m, Ar-<u>H</u>), 7.21 (1H, d *J* = 16.3 Hz, Ar-C<u>H</u>=CH), 6.96 (1H, d *J* = 16.2 Hz, CH=C<u>H</u>-CO), 6.88-6.86 (2H, m, Ar-<u>H</u>), 2.31 (3H, s, *p*-ArC<u>H</u>$_3$), 2.18 (6H, s, *o*-ArC<u>H</u>$_3$). Incorporation expected at δ 7.21. Determined against integral at δ 2.31.
Hydrogenation Product	***^{1}H NMR data***[133]
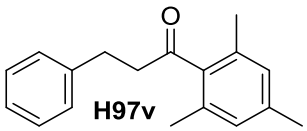	**^{1}H NMR** (400 MHz, $CDCl_3$): δ 7.08 (5H, br s, Ar-H), 6.63 (2H, br s, Ar-H), 2.90 (4H, br s, C<u>H</u>$_2$), 2.20 (3H, s, *p*-C<u>H</u>$_3$), 2.03 (6H, s, *o*-C<u>H</u>$_3$). Conversion determined using integrals at δ 2.31 (**D97v**) and 2.20 (**H97v**).

D-Incorporation (%)			***Hydrogenation (%)***		
Run		***Average***	***Run***		***Average***
1	***2***		***1***	***2***	
87	89	88	1	1	1

Substrate	***^{1}H NMR data***[134]
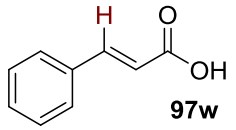 **97w** (59 mg, 0.4 mmol)	**^{1}H NMR** (400 MHz, $CDCl_3$): δ 7.84 (1H, d *J* = 16.0 Hz, Ar-C<u>H</u>=CH), 7.63-7.55 (2H, m, Ar-<u>H</u>), 7.48-7.39 (3H, m, Ar-<u>H</u>), 6.49 (1H, d *J* = 16.0 Hz, CH=C<u>H</u>-CO). Incorporation expected at δ 7.84. Determined against integral at δ 6.49.
Hydrogenation Product	***^{1}H NMR data***[135]
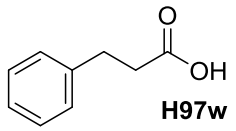 **H97w**	**^{1}H NMR** (400 MHz, $CDCl_3$): δ 7.33-7.30 (3H, m, Ar-H), 7.24-7.22 (2H, m, Ar-<u>H</u>), 3.00-2.96 (2H, m, C<u>H</u>$_2$), 2.72-2.69 (2H, m, C<u>H</u>$_2$). Conversion determined using integrals at δ 6.49 (**D97w**) and 7.24-7.22 (**H97w**).

D-Incorporation (%)			***Hydrogenation (%)***		
Run		***Average***	***Run***		***Average***
1	***2***		***1***	***2***	
0	0	0	18	15	17

Substrate	***^{1}H NMR data***[136]
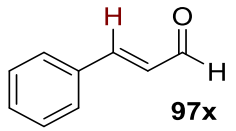 **97x** (53 mg, 0.4 mmol)	**^{1}H NMR** (400 MHz, $CDCl_3$): δ 9.74 (1H, d *J* = 7.7 Hz, CO-<u>H</u>), 7.64-7.56 (2H, m, Ar-<u>H</u>), 7.54-7.43 (4H, d *J* = 16.1 Hz, Ar-C<u>H</u>=CH & m, Ar-<u>H</u>), 6.75 (1H, dd *J* = 15.9 Hz, 7.7 Hz, CH=C<u>H</u>-CO). Incorporation expected at δ 7.54-7.43. Determined against integral at δ 7.64-7.56.
Hydrogenation Product	***^{1}H NMR data***[137]
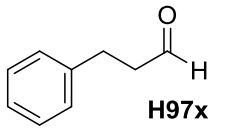 **H97x**	**^{1}H NMR** (400 MHz, $CDCl_3$): δ 9.73 (1H, t *J* = 1.3 Hz, CO-<u>H</u>), 7.24-7.20 (2H, m, Ar-<u>H</u>), 7.18-7.08 (3H, m, Ar-<u>H</u>), 2.87 (2H, t *J* = 7.6 Hz, C<u>H</u>$_2$), 2.69 (2H, td *J* = 7.6, 1.0 Hz, C<u>H</u>$_2$). Conversion determined using integrals at δ 7.64-7.56 (**D97x**) and 7.24-7.20 (**H97x**).

D-Incorporation (%)			***Hydrogenation (%)***		
Run		***Average***	***Run***		***Average***
1	***2***		***1***	***2***	
0	0	0	0	0	0

Substrate	***^{1}H NMR data***[138]
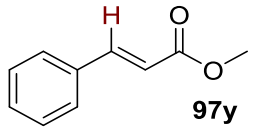 **97y** (59 mg, 0.4 mmol)	**^{1}H NMR** (400 MHz, $CDCl_3$): δ 7.68 (1H, d *J* = 16.0 Hz, Ar-C<u>H</u>=CH), 7.54-7.47 (2H, m, Ar-<u>H</u>), 7.40-7.34 (3H, m, Ar-<u>H</u>), 6.43 (1H, d *J* = 16.0 Hz, CH=C<u>H</u>-CO), 3.79 (3H, s, O-C<u>H</u>$_3$). Incorporation expected at δ 7.68. Determined against integral at δ 3.79.
Hydrogenation Product	***^{1}H NMR data***[139]
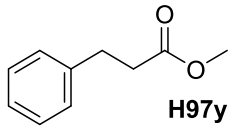 **H97y**	**^{1}H NMR** (400 MHz, $CDCl_3$): δ 7.19-7.40 (5H, m, Ar-H), 3.68 (3H, s, O-C<u>H</u>$_3$), 2.96 (2H, t *J* = 9.0 Hz, C<u>H</u>$_2$), 2.64 (2H, t *J* = 9.0 Hz, C<u>H</u>$_2$). Conversion determined using integrals at δ 3.79 (**D97y**) and 3.68 (**H97y**).

D-Incorporation (%)			***Hydrogenation (%)***		
Run		***Average***	***Run***		***Average***
1	***2***		***1***	***2***	
0	0	0	25	23	24

Substrate	***^{1}H NMR data***[140]
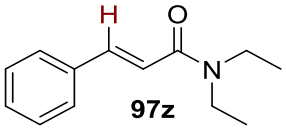 **97z** (81 mg, 0.4 mmol)	**^{1}H NMR** (400 MHz, $CDCl_3$): δ 7.61 (1H, d *J* = 15.4 Hz, Ar-C<u>H</u>=CH), 7.61-7.51 (2H, m, Ar-<u>H</u>), 7.45-7.32 (3H, m, Ar-<u>H</u>), 6.85 (1H, d *J* = 16.4 Hz, CH=C<u>H</u>-CO), 3.58-3.45 (4H, m, N-C<u>H</u>$_2$-CH$_3$), 1.28 (3H, t *J* = 7.2 Hz, CH$_2$-C<u>H</u>$_3$), 1.21 (3H, t *J* = 7.2 Hz, CH$_2$-C<u>H</u>$_3$). Incorporation expected at δ 7.61. Determined against integral at δ 3.58-3.45.
Hydrogenation Product	***^{1}H NMR data***[141]
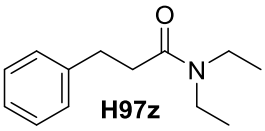 **H97z**	**^{1}H NMR** (400 MHz, $CDCl_3$): δ 7.23-7.19 (2H, m, Ar-<u>H</u>), 7.16-7.09 (3H, m, Ar-<u>H</u>), 3.30 (2H, q *J* = 7.0 Hz, N-C<u>H</u>$_2$-CH$_3$), 3.14 (2H, q *J* = 7.5 Hz, N-C<u>H</u>$_2$-CH$_3$), 2.91 (2H, t *J* = 7.5 Hz, C<u>H</u>$_2$), 2.52 (2H, t *J* = 8.0 Hz, C<u>H</u>$_2$), 1.03 (3H, t *J* = 7.0 Hz, CH$_2$-C<u>H</u>$_3$), 1.02 (3H, t *J* = 6.5 Hz, CH$_2$-C<u>H</u>$_3$). Conversion determined using integrals at δ 3.58-3.45 (**D97z**) and 3.14 (**H97z**).

D-Incorporation (%)			***Hydrogenation (%)***		
Run		***Average***	***Run***		***Average***
1	***2***		***1***	***2***	
82	86	84	4	5	5

Substrate	***^{1}H NMR data***[142]
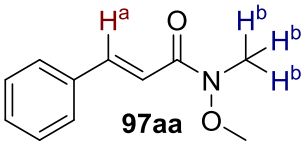 (81 mg, 0.4 mmol)	**^{1}H NMR** (400 MHz, $CDCl_3$): δ 7.76 (1H, d *J* = 15.8 Hz, Ph-C<u>H</u>=CH), 7.63-7.56 (2H, m, Ar-<u>H</u>), 7.45-7.34 (3H, m, Ar-<u>H</u>), 7.06 (1H, d *J* = 15.8 H, CH=C<u>H</u>-CO), 3.78 (3H, s, O-C<u>H</u>$_3$), 3.33 (3H, s, N-C<u>H</u>$_3$). Incorporation expected at δ D^a 7.76, D^b 3.33. Determined against integral at δ 3.78.
Hydrogenation Product	***^{1}H NMR data***[143]
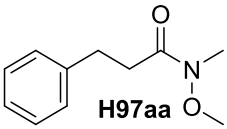	**^{1}H NMR** (400 MHz, $CDCl_3$): δ 7.39-7.12 (5H, m, Ar-<u>H</u>), 3.60 (3H, s, O-C<u>H</u>$_3$), 3.18 (3H, s, N-C<u>H</u>$_3$), 3.00-2.92 (2H, m, C<u>H</u>$_2$), 2.79-2.70 (2H, m, C<u>H</u>$_2$). Conversion determined using integrals at δ 3.78 (**D97aa**) and 3.14 (**H97aa**).

D-Incorporation (%)						***Hydrogenation (%)***		
Run				***Average***		***Run***		***Average***
1		***2***				***1***	***2***	
Da	***Db***	***Da***	***Db***	***Da***	***Db***			
77	6	75	6	76	6	3	3	3

Substrate	***^{1}H NMR data***[144]
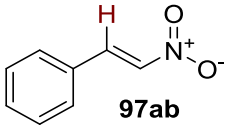 (60 mg, 0.4 mmol)	**^{1}H NMR** (400 MHz, $CDCl_3$): δ 7.99 (1H, d, *J* = 13.8 Hz, Ph-C<u>H</u>=CH), 7.57 (1H, d, *J* = 13.6 Hz, CH=C<u>H</u>-CO), 7.55-7.51 (2H, m, Ar-<u>H</u>), 7.51-7.40 (3H, m, Ar-<u>H</u>). Incorporation expected at δ 7.99. Determined against integral at δ 7.55-7.51.
Hydrogenation Product	***^{1}H NMR data***[145]
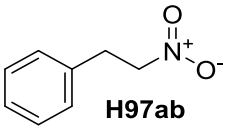	**^{1}H NMR** (400 MHz, $CDCl_3$): δ 7.40-7.25 (3H, m, Ar-<u>H</u>), 7.24-7.17 (2H, m, Ar-<u>H</u>), 4.62 (2H, t, *J* = 7.4 Hz, C<u>H</u>$_2$), 3.33 (2H, t, *J* = 7.4 Hz, C<u>H</u>$_2$). Conversion determined using integrals at δ 7.55-7.51 (**D97ab**) and 7.24-7.17 (**H97ab**).

D-Incorporation (%)			***Hydrogenation (%)***		
Run		***Average***	***Run***		***Average***
1	***2***		***1***	***2***	
82	83	83	4	6	5

Scheme 2.58 *Probing the selectivity between olefinic and aromatic HIE.*

The reactions were carried out following general procedure B and analysed by ^{1}H NMR spectroscopy to confirm the degree of hydrogenation, and the position and degree of deuterium incorporation.

Complex	***Solvent***	***Time (h)***	***Temperature (°C)***
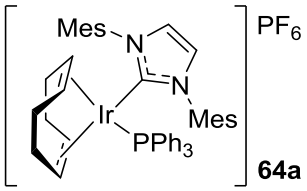 **64a** (0.4 mg, 0.0004 mmol)	DCM (1 mL)	1	25

Substrate	***^{1}H NMR data***[146]
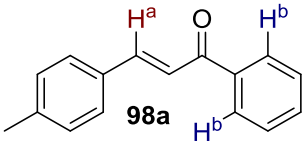 **98a** (89 mg, 0.4 mmol)	**^{1}H NMR** (400 MHz, $CDCl_3$): δ 8.01-7.96 (2H, m, Ar-H), 7.76 (1H, d *J* = 15.7 Hz, Ar-CH=CH), 7.59-7.41 (6H, m, Ar-H & d *J* = 15.7 Hz, CH-CH-CO), 7.22-7.17 (2H, m, Ar-H), 2.36 (3H, s, CO-CH_3). Incorporation expected at δ D^a 7.76, D^b 8.01-7.96. Determined against integral at δ 2.36.
Hydrogenation Product	***^{1}H NMR data***[147]
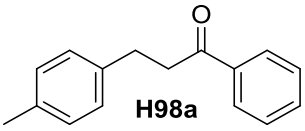 **H98a**	**^{1}H NMR** (400 MHz, $CDCl_3$): δ 8.00-7.97 (2H, m, Ar-H), 7.60-7.56 (1H, m, Ar-H), 7.50-7.46 (2H, m, Ar-H), 7.19-7.12 (4H, m, Ar-H), 3.33-3.29 (2H, m, CH_2), 3.08-3.04 (2H, m, Ar-H), 2.33 (3H, s, Ar-CH_3). Conversion determined using integrals at δ 2.36 (**D98a**) and 2.33 (**H98a**).

D-Incorporation (%)						***Hydrogenation (%)***		
Run				***Average***		***Run***		***Average***
1		***2***				***1***	***2***	
Da	***Db***	***Da***	***Db***	***Da***	***Db***			
84	45	86	46	85	46	4	6	5

Substrate	***^{1}H NMR data***[128]
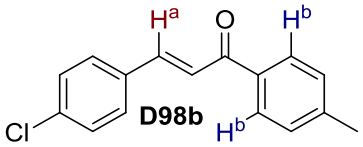 (103 mg, 0.4 mmol)	**^{1}H NMR** (400 MHz, $CDCl_3$): δ 7.95-7.88 (2H, m, Ar-H), 7.73 (1H, d *J* = 15.7 Hz, Ar-CH=CH), 7.59-7.52 (2H, m, Ar-H), 7.48 (1H, d *J* = 15.7 Hz, CH=CH-CO), 7.41-7.33 (2H, m, Ar-H), 7.32-7.26 (2H, m, Ar-H), 2.42 (3H, s, Ar-CH_3). Incorporation expected at δ D^a 7.73, D^b 7.95-7.88. Determined against integral at δ 2.42.
Hydrogenation Product	***^{1}H NMR data***[148]
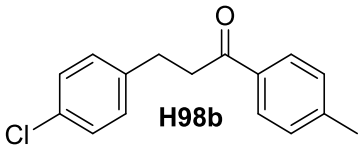	**^{1}H NMR** (400 MHz, $CDCl_3$): δ 7.87-7.84 (2H, m, Ar-H), 7.29-7.21 (4H, m, Ar-H), 7.19-7.15 (2H, m, Ar-H), 3.30-3.21 (2H, m, CH_2), 3.05-2.97 (2H, m, CH_2), 2.40 (3H, s, CH_3). Conversion determined using integrals at δ 2.42 (**D98b**) and 2.40 (**H98b**).

D-Incorporation (%)						***Hydrogenation (%)***		
Run				***Average***		***Run***		***Average***
1		***2***				***1***	***2***	
Da	***Db***	***Da***	***Db***	***Da***	***Db***			
73	6	67	6	70	6	1	1	1

Substrate	***^{1}H NMR data***[128]
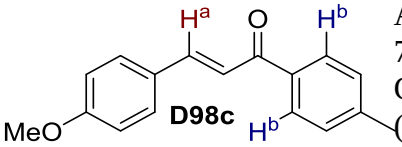 (101 mg, 0.4 mmol)	**^{1}H NMR** (400 MHz, $CDCl_3$): δ 8.00-7.92 (2H, m, Ar-H), 7.80 (1H, d *J* = 15.6 Hz, Ar-CH=CH), 7.66-7.60 (2H, m, Ar-H), 7.44 (1H, d *J* = 15.6 Hz, CH=CH-CO), 7.36-7.30 (2H, m, Ar-H), 7.00-6.93 (2H, m, Ar-H), 3.88 (3H, s, O-CH_3), 2.46 (3H, s, Ar-CH_3). Incorporation expected at δ D^a 7.80, D^b 8.00-7.92. Determined against integral at δ 2.46.
Hydrogenation Product	***^{1}H NMR data***[147]
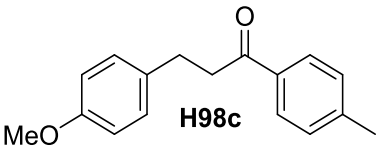	**^{1}H NMR** (400 MHz, $CDCl_3$): δ 7.90-7.86 (2H, m, Ar-H), 7.28-7.24 (2H, m, Ar-H), 7.20-7.16 (2H, m, Ar-H), 6.88-6.85 (2H, m, Ar-H), 3.80 (3H, s, O-CH_3), 3.26 (2H, t *J* = 7.6 Hz, CH_2), 3.02 (2H, d *J* = 7.6 Hz, CH_2), 2.42 (3H, s, Ar-CH_3). Conversion determined using integrals at δ 2.46 (**D98c**) and 3.80 (**H98c**).

D-Incorporation (%)						***Hydrogenation (%)***		
Run				***Average***		***Run***		***Average***
1		***2***				***1***	***2***	
Da	***Db***	***Da***	***Db***	***Da***	***Db***			
95	21	86	20	91	21	1	1	1

Substrate	***^{1}H NMR data***[149]
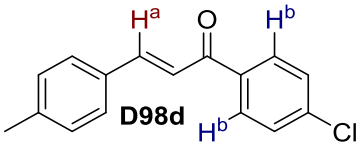 (103 mg, 0.4 mmol)	**^{1}H NMR** (400 MHz, $CDCl_3$): δ 7.98-7.92 (2H, m, Ar-u), 7.78 (1H, d *J* = 15.7 Hz, Ar-C<u>H</u>=CH) 7.56-7.50 (2H, m, Ar-<u>H</u>), 7.48-7.38 (3H, d *J* = 15.7 Hz, CH=C<u>H</u>-CO & m, Ar-<u>H</u>), 7.24-7.19 (2H, m, Ar-<u>H</u>), 2.38 (3H, s, Ar-C<u>H</u>$_3$). Incorporation expected at δ D^a 7.78, D^b 7.98-7.92. Determined against integral at δ 2.38.
Hydrogenation Product	***^{1}H NMR data***[148]
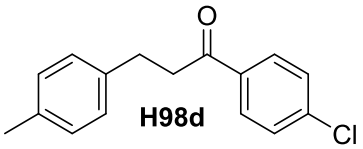	**^{1}H NMR** (400 MHz, $CDCl_3$): δ 7.92-7.88 (2H, m, Ar-<u>H</u>), 7.45-7.40 (2H, m, Ar-<u>H</u>), 7.18-7.11 (2H, m, Ar-<u>H</u>), 7.11-7.07 (2H, m, Ar-H), 3.29-3.24 (2H, m, C<u>H</u>$_2$), 3.07-3.02 (2H, m, C<u>H</u>$_2$), 2.34 (3H, s, C<u>H</u>$_3$). Conversion determined using integrals at δ 2.38 (**D98d**) and 2.34 (**H98d**).

D-Incorporation (%)						***Hydrogenation (%)***		
Run				***Average***		***Run***		***Average***
1		***2***				***1***	***2***	
Da	***Db***	***Da***	***Db***	***Da***	***Db***			
71	71	81	79	77	75	4	3	4

Substrate	***^{1}H NMR data***[150]
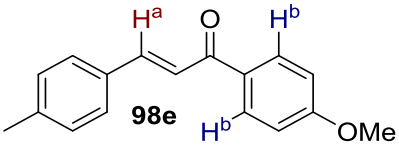 (101 mg, 0.4 mmol)	**^{1}H NMR** (400 MHz, $CDCl_3$): δ 8.06-7.98 (2H, m, Ar-<u>H</u>), 7.77 (1H, d *J* = 15.7 Hz, Ar-C<u>H</u>=CH), 7.55-751 (2H, m, Ar-<u>H</u>), 7.48 (1H, d *J* = 15.7 Hz, CH-C<u>H</u>-CO), 7.24-7.23 (2H, m, Ar-<u>H</u>), 7.00-6.93 (2H, m, Ar-<u>H</u>), 3.87 (3H, s, O-C<u>H</u>$_3$), 2.38 (3H, s, Ar-C<u>H</u>$_3$). Incorporation expected at δ D^a 7.77, D^b 8.06-7.98. Determined against integral at δ 2.38.
Hydrogenation Product	***^{1}H NMR data***[147]
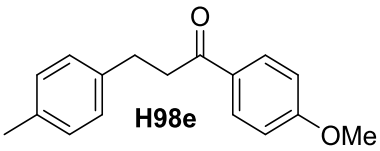	**^{1}H NMR** (400 MHz, $CDCl_3$): δ 8.03-8.00 (2H, m, Ar-<u>H</u>), 7.23-7.16 (4H, m, Ar-<u>H</u>), 6.99-6.92 (2H, m, Ar-<u>H</u>), 3.92 (3H, s, O-C<u>H</u>$_3$), 3.30 (2H, t *J* = 7.7 Hz, C<u>H</u>$_2$), 3.08 (2H, t *J* = 7.7 Hz, C<u>H</u>$_2$), 2.39 (3H, s, Ar-C<u>H</u>$_3$). Conversion determined using integrals at δ 2.38 (**D98e**) and 3.92 (**H98e**).

D-Incorporation (%)						***Hydrogenation (%)***		
Run				***Average***		***Run***		***Average***
1		***2***				***1***	***2***	
Da	***Db***	***Da***	***Db***	***Da***	***Db***			
91	65	86	54	89	60	1	1	1

Substrate	***^{1}H NMR data***[151]
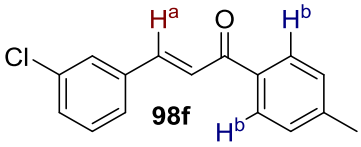 (103 mg, 0.4 mmol)	**^{1}H NMR** (400 MHz, $CDCl_3$): δ 7.96-7.89 (2H, m, Ar-H), 7.71 (1H, d *J* = 15.8 Hz, Ar-CH=CH), 7.64-7.59 (1H, m, Ar-H), 7.55-7.45 (2H, d *J* = 15.8 Hz, CH=CH-CO & m, Ar-H), 7.39-2.26 (4H, m, Ar-H), 2.42 (3H, s, Ar-CH_3). Incorporation expected at δ D^a 7.71, D^b 7.96-7.89. Determined against integral at δ 2.42.
Hydrogenation Product	***^{1}H NMR data***
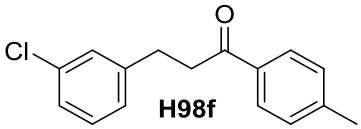	No reference NMR data available, integral for aryl-CH_3 chosen based upon related compound **H98b**. Conversion determined using integrals at δ 2.42 (**D98f**) and 2.40 (**H98f**).

D-Incorporation (%)						***Hydrogenation (%)***		
Run				***Average***		***Run***		***Average***
1		***2***				***1***	***2***	
Da	***Db***	***Da***	***Db***	***Da***	***Db***			
92	10	92	9	92	10	1	1	1

Substrate	***^{1}H NMR data***[151]
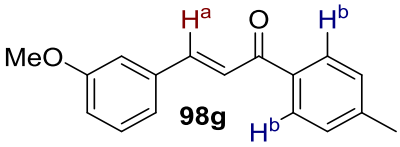 (103 mg, 0.4 mmol)	**^{1}H NMR** (400 MHz, $CDCl_3$): δ 7.96-7.87 (2H, m, Ar-H), 7.74 (1H, d *J* = 15.7 Hz, Ar-CH=CH), 7.49 (1H, d *J* = 15.7 Hz, CH=CH-CO), 7.36-7.26 (3H, m, Ar-H), 7.24-7.20 (1H, m, Ar-H), 7.17-7.11 (1H, m, Ar-H), 6.98-6.91 (1H, m, Ar-H), 3.84 (3H, s, O-CH_3), 2.42 (3H, s, Ar-CH_3). Incorporation expected at δ D^a 7.74, D^b 7.96-7.87. Determined against integral at δ 2.42.
Hydrogenation Product	***^{1}H NMR data***
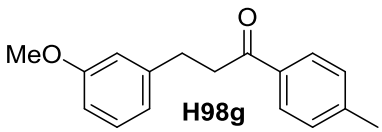	No reference NMR data available, integral for O-CH_3 chosen based upon related compound **H98c**. Conversion determined using integrals at δ 3.84 (**D98g**) and 3.80 (**H98g**).

D-Incorporation (%)						***Hydrogenation (%)***		
Run				***Average***		***Run***		***Average***
1		***2***				***1***	***2***	
Da	***Db***	***Da***	***Db***	***Da***	***Db***			
87	33	86	29	87	31	1	1	1

Substrate	***^{1}H NMR data***[152]
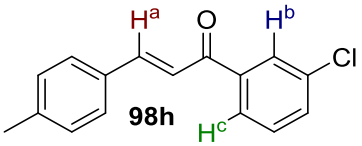 (103 mg, 0.4 mmol)	**^{1}H NMR** (400 MHz, $CDCl_3$): δ 7.98-7.93 (1H, m, Ar-H), 7.88-7.84 (1H, m, Ar-H), 7.78 (1H, d *J* = 15.7 Hz, Ar-CH=CH), 7.55-7.49 (3H, m, Ar-H), 7.44-7.37 (2H, d *J* = 15.7 Hz, CH=CH-CO & m, Ar-H), 7.23-7.18 (2H, m, Ar-H), 2.37 (3H, s, Ar-CH_3). Incorporation expected at δ D^a 7.78, D^b 7.98-7.93, D^c 7.88-7.84. Determined against integral at δ 2.37.
Hydrogenation Product	***^{1}H NMR data***
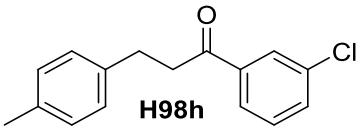	No reference NMR data available, integral for aryl-CH_3 chosen based upon related compound **H98d**. Conversion determined using integrals at δ 2.37 (**D98h**) and 2.34 (**H98h**).

D-Incorporation (%)									***Hydrogenation (%)***		
Run						***Average***			***Run***		***Average***
1			***2***						***1***	***2***	
Da	***Db***	***Dc***	***Da***	***Db***	***Dc***	***Da***	***Db***	***Dc***			
90	86	38	89	85	26	90	86	32	1	1	1

Substrate	***^{1}H NMR data***[153]
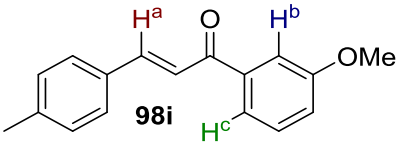 (101 mg, 0.4 mmol)	**^{1}H NMR** (400 MHz, $CDCl_3$): δ 7.78 (1H, d *J* = 15.7 Hz, Ar-CH=CH), 7.61-7.56 (1H, m, Ar-H), 7.55-7.50 (3H, m, Ar-H), 7.45 (1H, d *J* = 15.7 Hz, CH=CH-CO), 7.39 (1H, dd *J* = 7.8 Hz, 7.8 Hz, Ar-H), 7.24-7.24 (2H, m, Ar-H), 7.11 (1H, ddd *J* = 8.0 Hz, ^4J = 2.4 Hz, ^4J = 1.0 Hz, Ar-H), 3.87 (3H, s, O-CH_3), 2.38 (3H, s, Ar-CH_3). Incorporation expected at δ D^a 7.78, D^b 7.55-7.50, D^c 7.11. Determined against integral at δ 2.38.
Hydrogenation Product	***^{1}H NMR data***[154]
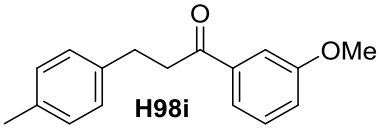	**^{1}H NMR** (400 MHz, $CDCl_3$): δ 7.54-7.52 (1H, m, Ar-H), 7.51-7.48 (1H, m, Ar-H), 3.37-7.35 (1H, m, Ar-H), 7.15-7.08 (5H, m, Ar-H), 3.84 (3H, s, O-CH_3), 3.28-3.24 (2H, m, CH_2), 3.04-3.00 (2H, m, CH_2), 2.32 (3H, s, Ar-CH_3). Conversion determined using integrals at δ 2.38 (**D98i**) and 3.32 (**H98i**).

D-Incorporation (%)									***Hydrogenation (%)***		
Run						***Average***			***Run***		***Average***
1			***2***						***1***	***2***	
Da	***Db***	***Dc***	***Da***	***Db***	***Dc***	***Da***	***Db***	***Dc***			
90	90	15	90	91	16	90	91	16	1	1	1

Substrate	***^{1}H NMR data***[155]
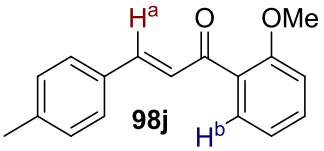 (101 mg, 0.4 mmol)	**^{1}H NMR** (4300 MHz, $CDCl_3$): δ 7.66-7.59 (2H, m, Ar-H & d *J* = 15.8 Hz, Ar-CH=CH), 7.55-7.45 (3H, m, Ar-H), 7.34 (1H, d *J* = 15.8 Hz, CH=CH-CO), 7.26-7.19 (2H, m, Ar-H), 7.10-7.00 (2H, m, Ar-H), 3.92 (3H, s, O-CH_3), 2.41 (3H, s, Ar-CH_3). Incorporation expected at δ D^a 7.66-7.59, D^b 7.55-7.45. Determined against integral at δ 2.41.
Hydrogenation Product	***^{1}H NMR data***
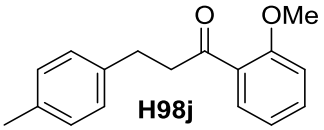	No reference NMR data available, integral for aryl-CH_3 chosen based upon related compound **H98i**. Conversion determined using integrals at δ 2.41 (**D98j**) and 2.32 (**H98j**).

D-Incorporation (%)						***Hydrogenation (%)***		
Run				***Average***		***Run***		***Average***
1		***2***				***1***	***2***	
Da	***Db***	***Da***	***Db***	***Da***	***Db***			
92	94	88	70	90	82	7	1	4

Scheme 2.59 *Examining the influence of ortho-substituents on olefinic HIE.*

The reactions were carried out following general procedure B and analysed by ^{1}H NMR to confirm the degree of hydrogenation, and the position and degree of deuterium incorporation.

Complex	***Solvent***	***Time (h)***	***Temperature (°C)***
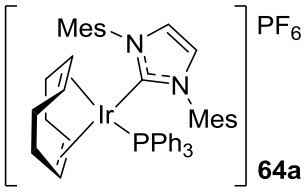 (0.4 mg, 0.0004 mmol)	DCM (1 mL)	1	25

Substrate	***^{1}H NMR data***[156]
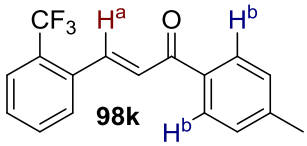 (116 mg, 0.4 mmol)	**^{1}H NMR** (400 MHz, $CDCl_3$): δ 8.10 (1H, d *J* = 15.5 Hz, Ar-C<u>H</u>=CH), 7.95-7.87 (2H, m, Ar-<u>H</u>), 7.84-7.77 (1H, m, Ar-<u>H</u>), 7.74-7.67 (1H, m, Ar-<u>H</u>), 7.62-7.55 (1H, m, Ar-<u>H</u>), 7.52-7.44 (1H, m, Ar-<u>H</u>), 7.40 (1H, d *J* = 15.2 Hz, CH=C<u>H</u>-CO), 7.33-7.26 (2H, m, Ar-<u>H</u>), 2.42 (3H, s, Ar-C<u>H</u>$_3$). Incorporation expected at δ D^a 8.10, D^b 7.95-7.87. Determined against integral at δ 2.42.
Hydrogenation Product	***^{1}H NMR data***
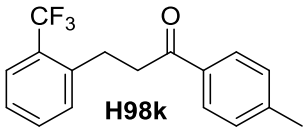	No reference NMR data available, integral for aryl-CH_3 chosen based upon related compound **H98f**. Conversion determined using integrals at δ 2.42 (**D98k**) and 2.40 (**H98k**).

D-Incorporation (%)						***Hydrogenation (%)***		
Run				***Average***		***Run***		***Average***
1		***2***				***1***	***2***	
Da	***Db***	***Da***	***Db***	***Da***	***Db***			
4	68	5	66	5	67	1	1	1

Substrate	***^{1}H NMR data***[151]
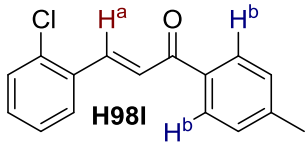 (103 mg, 0.4 mmol)	**^{1}H NMR** (400 MHz, $CDCl_3$): δ 8.15 (1H, d *J* = 15.8 Hz, Ar-C<u>H</u>=CH) 7.95-7.88 (2H, m, Ar-<u>H</u>), 7.76-7.69 (1H, m, Ar-<u>H</u>), 7.46 (1H, d *J* = 15.9 Hz, CH=C<u>H</u>-CO), 7.43-7.38 (1H, m, Ar-<u>H</u>), 7.34-7.25 (4H, m, Ar-<u>H</u>), 2.41 (3H, s, Ar-C<u>H</u>$_3$). Incorporation expected at δ D^a 8.15, D^b 7.76-7.69. Determined against integral at δ 2.41.
Hydrogenation Product	***^{1}H NMR data***[157]
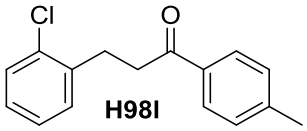	**^{1}H NMR** (300 MHz, $CDCl_3$): δ 7.89-7.86 (2H, m, Ar-<u>H</u>), 7.15-7.37 (6H, m, Ar-<u>H</u>), 3.29 (2H, t *J* = 8.0 Hz, C<u>H</u>$_2$), 3.17 (2H, t *J* = 8.0 Hz, C<u>H</u>$_2$), 2.38 (3H, s, C<u>H</u>$_3$). Conversion determined using integrals at δ 2.41 (**D98l**) and 2.38 (**H98l**).

D-Incorporation (%)						***Hydrogenation (%)***		
Run				***Average***		***Run***		***Average***
1		***2***				***1***	***2***	
Da	***Db***	***Da***	***Db***	***Da***	***Db***			
42	74	46	86	44	80	1	1	1

Substrate	***^{1}H NMR data***[158]
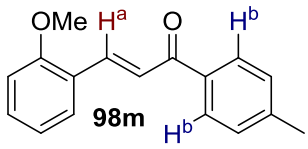 (101 mg, 0.4 mmol)	**^{1}H NMR** (400 MHz, $CDCl_3$): δ 8.09 (1H, d *J* = 15.9 Hz Ar-C<u>H</u>=CH), 7.96-7.88 (2H, m, Ar-<u>H</u>), 7.65-7.56 (2H, d *J* = 15.8 Hz, CH=C<u>H</u>-CO & m, Ar-<u>H</u>), 7.41-7.32 (1H, m, Ar-<u>H</u>), 7.31-7.25 (2H, m, Ar-<u>H</u>), 7.02-6.90 (2H, m, Ar-<u>H</u>), 3.90 (3H, s, O-C<u>H</u>$_3$), 2.44 (3H, s, Ar-C<u>H</u>$_3$). Incorporation expected at δ D^a 8.09, D^b 7.31-7.25. Determined against integral at δ 2.44.
Hydrogenation Product	***^{1}H NMR data***
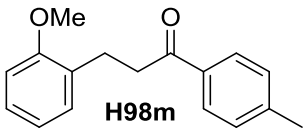	No reference NMR data available, integral for aryl-CH_3 chosen based upon related compound **H98c**. Conversion determined using integrals at δ 2.44 (**D98m**) and 2.40 (**H98m**).

D-Incorporation (%)						***Hydrogenation (%)***		
Run				***Average***		***Run***		***Average***
1		***2***				***1***	***2***	
Da	***Db***	***Da***	***Db***	***Da***	***Db***			
26	9	22	8	24	9	1	1	1

Substrate	***^{1}H NMR data***[151]
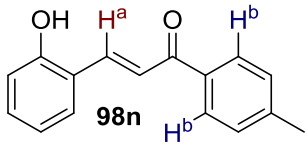 (95 mg, 0.4 mmol)	**^{1}H NMR** (400 MHz, $CDCl_3$): δ 9.12 (1H, s, Ar-O<u>H</u>), 8.16 (1H, d *J* = 15.7 Hz, Ar-C<u>H</u>=CH), 8.07-7.97 (2H, m, Ar-<u>H</u>), 7.87 (1H, d *J* = 15.5 Hz, CH=C<u>H</u>-CO), 7.84-7.78 (1H, m, Ar-<u>H</u>), 7.41-7.34 (2H, m, Ar-<u>H</u>), 7.32-7.25 (1H, m, Ar-<u>H</u>), 7.04-6.97 (1H, m, Ar-<u>H</u>), 6.97-6.89 (1H, m, Ar-<u>H</u>), 2.43 (3H, s, Ar-C<u>H</u>$_3$). Incorporation expected at δ D^a 8.16, D^b 8.07-7.97. Determined against integral at δ 2.43.
Hydrogenation Product	***^{1}H NMR data***[159]
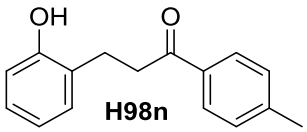	**^{1}H NMR** (400 MHz, $CDCl_3$): δ 8.13 (1H, br s, O-<u>H</u>), 7.89-7.84 (2H, m, Ar-<u>H</u>), 7.25-7.22 (2H, m, Ar-<u>H</u>), 7.12-7.09 (2H, m, Ar-<u>H</u>), 6.92-6.85 (2H, m, Ar-H), 3.42 (2H, t *J* = 6.0 Hz, C<u>H</u>$_2$), 3.02 (2H, t *J* = 6.0 Hz, C<u>H</u>$_2$), 2.40 (3H, s, Ar-C<u>H</u>$_3$). Conversion determined using integrals at δ 2.43 (**D98n**) and 2.40 (**H98n**).

D-Incorporation (%)						***Hydrogenation (%)***		
Run				***Average***		***Run***		***Average***
1		***2***				***1***	***2***	
Da	***Db***	***Da***	***Db***	***Da***	***Db***			
30	21	29	20	30	21	1	1	1

Scheme 2.60 *Fused chalcone substrates for HIE.*

The reactions were carried out following general procedure B and analysed by ^{1}H NMR spectroscopy to confirm the degree of hydrogenation, and the position and degree of deuterium incorporation.

Complex	***Solvent***	***Time (h)***	***Temperature (°C)***
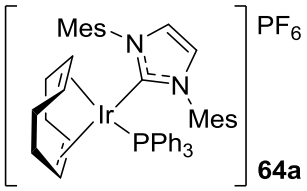 **64a** (0.4 mg, 0.0004 mmol)	DCM (1 mL)	1	25

Substrate	***^{1}H NMR data***[160]
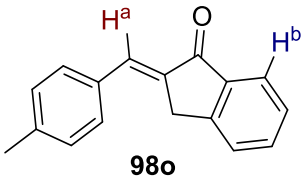 **98o** (94 mg, 0.4 mmol)	**^{1}H NMR** (400 MHz, $CDCl_3$): δ 7.93 (1H, d J = 7.6 Hz, Ar-H), 7.68 (1H, t ^4J = 1.9 Hz, C=CH), 7.65-7.55 (4H, m, Ar-H), 7.47-7.41 (2H, m, Ar-H), 7.29 (1H, d J = 7.8 Hz, Ar-H), 4.04 (2H, d ^4J = 1.9 Hz, CH_2), 2.42 (3H, s, Ar-CH_3). Incorporation expected at δ D^a 7.68, D^b 7.93. Determined against integral at δ 2.42.
Hydrogenation Product	***^{1}H NMR data***[160]
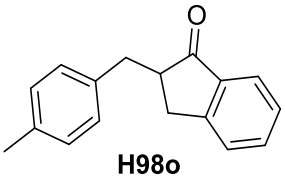 **H98o**	**^{1}H NMR** (400 MHz, $CDCl_3$): δ 7.79-7.75 (1H, m, Ar-H), 7.57-7.54 (1H, m, Ar-H), 7.40-7.38 (1H, m, Ar-H), 7.37-7.34 (1H, m, Ar-H), 7.15-7.12 (2H, m, Ar-H), 7.11-7.08 (2H, m, Ar-H), 3.35 (1H, dd J = 4.3 Hz, ^2J = 14.0 Hz, CH_2), 3.15 (1H, dd J = 7.8 Hz, ^2J = 17.3 Hz, CH_2), 2.97 (1H, dddd J = 4.0 Hz, 4.3 Hz, 7.8 Hz, 10.5 Hz, CH), 2.85 (1H, dd J = 4.0 Hz, ^2J = 17.3 Hz, CH_2), 2.63 (1H, dd J = 10.5 Hz, ^2J = 14.0 Hz, CH_2), 2.32 (3H, s, CH_3). Conversion determined using integrals at δ 2.42 (**D98o**) and 2.32 (**H98o**).

D-Incorporation (%)						***Hydrogenation (%)***		
Run				***Average***		***Run***		***Average***
1		***2***				***1***	***2***	
Da	***Db***	***Da***	***Db***	***Da***	***Db***			
82	2	81	3	82	3	1	1	1

Substrate	***^{1}H NMR data***[160]
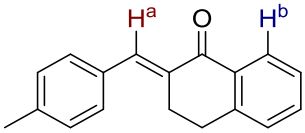 **98p** (99 mg, 0.4 mmol)	**^{1}H NMR** (400 MHz, $CDCl_3$): δ 8.15-8.09 (1H, m, Ar-H), 7.84 (1H, s, Ar-CH-C), 7.52-7.43 (1H, m, Ar-H), 7.38-7.31 (3H, m, Ar-H), 7.26-7.19 (3H, m, Ar-H), 3.15-3.10 (2H, m, CH_2), 2.93 (2H, d *J* = 6.6 Hz, CH_2), 2.38 (3H, s, Ar-CH_3). Incorporation expected at δ D^a 7.84, D^b 8.15-8.09. Determined against integral at δ 2.38.

Hydrogenation Product	***^{1}H NMR data***[160]
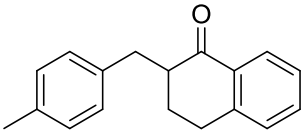 **D98p**	**^{1}H NMR** (400 MHz, $CDCl_3$): δ 8.09-8.05 (1H, m, Ar-H), 7.46-7.74 (1H, m, Ar-H), 7.32-7.26 (1H, m, Ar-H), 7.22-7.18 (1H, m, Ar-H), 7.11 (4H, s, Ar-H), 3.44 (1H, dd *J* = 4.1 Hz, ^2J = 13.9 Hz, CH_2), 2.87-2.96 (2H, m, CH_2), 2.69-2.74 (1H, m, CH), 2.61 (1H, dd *J* = 9.6 Hz, ^2J = 13.9 Hz, CH_2), 2.32 (3H, s, Ar-CH_3), 2.10 (1H, dq *J* = 4.5 Hz, ^2J = 13.3 Hz, CH_2), 1.74-1.81 (1H, m, CH_2). Conversion determined using integrals at δ 2.38 (**D98p**) and 2.32 (**H98p**).

D-Incorporation (%)						***Hydrogenation (%)***		
Run				***Average***		***Run***		***Average***
1		***2***				***1***	***2***	
Da	***Db***	***Da***	***Db***	***Da***	***Db***			
99	99	99	99	99	99	1	1	1

Substrate	***^{1}H NMR data***[161]
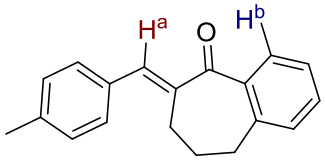 **98q** (105 mg, 0.4 mmol)	**^{1}H NMR** (400 MHz, $CDCl_3$): δ 7.80 (1H, s, Ar-C<u>H</u>=C), 7.77-7.74 (1H, m, Ar-<u>H</u>), 7.48-7.30 (4H, m, Ar-<u>H</u>), 7.24-7.15 (3H, m, Ar-<u>H</u>), 2.88 (2H, t *J* = 6.9 Hz, C<u>H</u>$_2$), 2.60 (2H, t *J* = 6.8 Hz, C<u>H</u>$_2$), 2.37 (3H, s, Ar-C<u>H</u>$_3$) 2.06 (2H, quin *J* = 6.9 Hz, CH_2-C<u>H</u>$_2$-CH_2). Incorporation expected at δ D^a 7.80, D^b 7.77-7.74. Determined against integral at δ 2.37.
Hydrogenation Product	***^{1}H NMR data***[67]
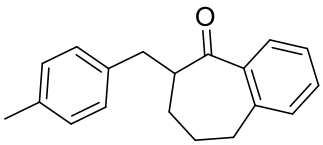 **D98q**	**^{1}H NMR** (400 MHz, $CDCl_3$): δ 7.64 (1H, dd, *J* = 7.6 Hz, ^4J = 1.6 Hz, Ar-<u>H</u>), 7.39 (1H, td, *J* = 7.5 Hz, ^4J = 1.5 Hz, Ar-<u>H</u>), 7.30-7.27 (1H, m, Ar-<u>H</u>), 7.23-7.21 (1H, m, Ar-<u>H</u>), 7.09 (4H, s, Ar-<u>H</u>), 3.28 (1H, dd, ^2J = 13.7 Hz, ^3J = 5.5 Hz, Ar-C<u>H</u>), 3.18-3.10 (1H, m, C<u>H</u>), 3.05-2.91 (2H, m, C<u>H</u>$_2$), 2.73 (1H, dd, ^2J = 13.7 Hz, ^3J = 7.1 Hz, Ar-C<u>H</u>), 2.33 (3H, s, Ar-C<u>H</u>$_3$), 2.05-2.02 (1H, m, C<u>H</u>), 1.94-1.88 (1H, m, C<u>H</u>), 1.72-1.58 (2H, m, C<u>H</u>$_2$). Conversion determined using integrals at δ 2.37 (**D98q**) and 2.33 (**H98q**).

D-Incorporation (%)						***Hydrogenation (%)***		
Run				***Average***		***Run***		***Average***
1		***2***				***1***	***2***	
Da	***Db***	***Da***	***Db***	***Da***	***Db***			
84	11	86	10	85	11	1	1	1

Table 2.10 *Competition reactions between aromatic and olefinic HIE.*

The reactions were carried out following general procedure B and analysed by ^{1}H NMR spectroscopy to confirm the position and degree of deuterium incorporation in both substrate and additive.

Complex	***Solvent***	***Time (h)***	***Temperature (°C)***
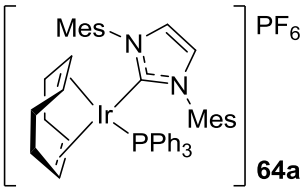 **64a** (0.4 mg, 0.0004 mmol)	DCM (1 mL)	1	25
Substrate	***data***		
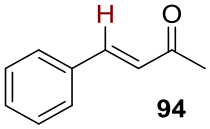 **94** (292.3 mg, 2.0 mmol)	Data was consistent with that reported on page 360.		

Additive	***^{1}H NMR data***[45]
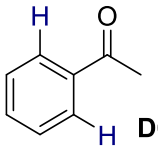 **D61** (48 mg, 0.4 mmol)	^{1}H NMR (400 MHz, $CDCl_3$): δ 7.99-7.95 (2H, m, Ar-H), 7.60-7.56 (1H, m, Ar-H), 7.50-7.44 (2H, m, Ar-H), 2.62 (3H, s, CH_3). Incorporation expected at δ 7.99-7.95. Determined against integral at δ 2.62.

Run	***Incorporation (%)***	
	Substrate	***Additive***
1	82	6
2	83	4
Average	83	5

Additive	*^{1}H NMR data*[162]
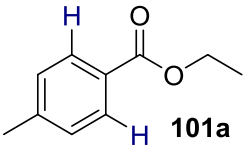 **101a** (66 mg, 0.4 mmol)	**^{1}H NMR** (400 MHz, $CDCl_3$): δ 7.91 (2H, d, *J* = 8.0 Hz, Ar-H), 7.21 (2H, d, *J* = 7.9 Hz, Ar-H), 4.34 (2H, q *J* = 7.1 Hz, O-CH_2), 2.38 (3H, s, Ar-CH_3), 1.36 (3H, t *J* = 7.1 Hz, CH_2-CH_3). Incorporation expected at δ 7.91. Determined against integral at δ 1.36.

Run	*Incorporation (%)*	
	Substrate	*Additive*
1	88	0
2	90	4
Average	89	2

Additive	*^{1}H NMR data*[45]
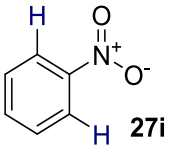 **27i** (49 mg, 0.4 mmol)	**^{1}H NMR** (400 MHz, $CDCl_3$): δ 8.25 (2H, dd, *J* = 7.7 Hz, ^4J = 1.1 Hz, Ar-H), 7.71 (1H, tt, *J* = 7.4 Hz, ^4J = 1.1 Hz, Ar-H), 7.56 (2H, t, *J* = 7.4 Hz, Ar-H). Incorporation expected at δ 8.25. Determined against integral at δ 7.71.

Run	*Incorporation (%)*	
	Substrate	*Additive*
1	80	0
2	88	0
Average	84	0

Additive	*^{1}H NMR data*[45]
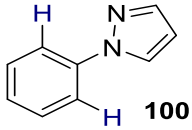 **100b** (58 mg, 0.4 mmol)	**^{1}H NMR** (400 MHz, $CDCl_3$): δ 7.93 (1H, d, *J* = 7.5 Hz, Ar-H), 7.74-7.66 (3H, m, Ar-H), 7.48-7.44 (2H, m, Ar-H), 7.29 (1H, t, *J* = 7.4 Hz, Ar-H), 6.48-6.42 (1H, m, Ar-H). Incorporation expected at δ 7.74-7.66. Determined against integral at δ 6.48-6.42.

Run	*Incorporation (%)*	
	Substrate	*Additive*
1	4	93
2	2	92
Average	3	93

Additive	*^{1}H NMR data*[45]
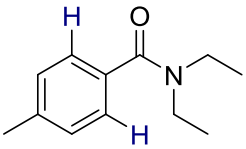 **100c** (77 mg, 0.4 mmol)	**^{1}H NMR** (400 MHz, $CDCl_3$): δ 7.27-7.22 (4H, m, Ar-H), 3.38 (4H, br s, N-CH_2), 2.35 (3H, s, Ar-CH_3), 1.13 (6H, br s, CH_3). Incorporation expected at δ 7.27-7.22. Determined against integral at δ 2.35.

Run	*Incorporation (%)*	
	Substrate	*Additive*
1	0	0
2	0	0
Average	0	0

Additive	*^{1}H NMR data*[45]
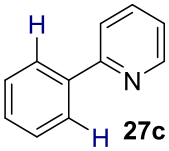 **27c** (62 mg, 0.4 mmol)	**^{1}H NMR** (400 MHz, $CDCl_3$): δ 8.71 (1H, d *J* = 4.7 Hz, Ar-H), 8.02-7.98 (2H, m, Ar-H), 7.79-7.73 (2H, m, Ar-H), 7.52-7.41 (3H, m, Ar-H), 7.26-7.23 (1H, m, Ar-H). Incorporation expected at δ 8.02-7.98. Determined against integral at δ 7.26-7.23.

Run	*Incorporation (%)*	
	Substrate	*Additive*
1	0	0
2	0	0
Average	0	0

Additive	*^{1}H NMR data*[45]
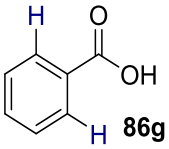 **86g** (49 mg, 0.4 mmol)	**^{1}H NMR** (400 MHz, DMSO): δ 12.93 (1H, br-s, O-H), 8.00-7.88 (2H, m, Ar-H), 7.66-7.56 (1H, m, Ar-H), 7.55-7.44 (2H, m, Ar-H). Incorporation expected at δ 8.00-7.88. Determined against integral at δ 7.55-7.44.

Run	*Incorporation (%)*	
	Substrate	*Additive*
1	22	0
2	23	0
Average	23	0

Scheme 2.61 *Competition between aromatic and olefinic HIE in a single molecule.*

The reactions were carried out following general procedure B and analysed by ^{1}H NMR spectroscopy to confirm the position and degree of deuterium incorporation.

Complex	***Solvent***	***Time (h)***	***Temperature (°C)***
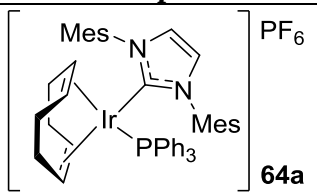 (0.4 mg, 0.0004 mmol)	DCM (1 mL)	1	25

Substrate	***^{1}H NMR data***[163]
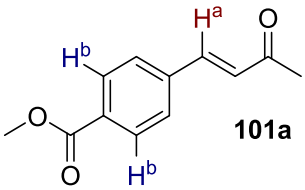 (82 mg, 0.4 mmol)	**^{1}H NMR** (400 MHz, $CDCl_3$): δ 8.10-8.05 (2H, m, Ar-H), 7.65-7.59 (2H, m, Ar-H), 7.54 (1H, d *J* = 16.3 Hz, Ar-C<u>H</u>=CH), 6.80 (1H, d *J* = 16.3 Hz, CH=C<u>H</u>-CO), 3.95 (3H, s, O-C<u>H</u>$_3$), 2.41 (3H, s, CO-C<u>H</u>$_3$). Incorporation expected at δ D^a 7.54, D^b 8.10-8.05. Determined against integral at δ 2.41.
Hydrogenation Product	***^{1}H NMR data***[164]
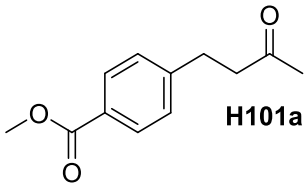	**^{1}H NMR** (400 MHz, $CDCl_3$): δ 7.93-7.89 (2H, m, Ar-<u>H</u>), 7.24-7.20 (2H, m, Ar-<u>H</u>), 3.87 (3H, s, O-C<u>H</u>$_3$), 2.91 (2H, t *J* = 7.5 Hz, C<u>H</u>$_2$), 2.75 (2H, t *J* = 7.5 Hz, C<u>H</u>$_2$), 2.11 (3H, s, CO-C<u>H</u>$_3$). Conversion determined using integrals at δ 2.41 (**D101a**) and 2.11 (**H101a**).

D-Incorporation (%)						***Hydrogenation (%)***		
Run				***Average***		***Run***		***Average***
1		***2***				***1***	***2***	
Da	***Db***	***Da***	***Db***	***Da***	***Db***			
88	2	89	2	89	2	1	1	1

Substrate	***^{1}H NMR data***[163]
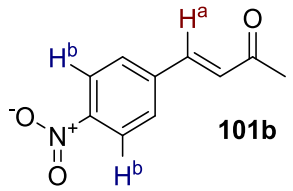 (76 mg, 0.4 mmol)	**^{1}H NMR** (400 MHz, $CDCl_3$): δ 8.33-8.25 (2H, m, Ar-H), 7.75-7.69 (2H, m, Ar-H), 7.56 (1H, d *J* = 16.3 Hz, Ar-CH=CH), 6.84 (1H, d *J* = 16.3 Hz, CH=CH-CO), 2.44 (3H, s, CO-CH_3). Incorporation expected at δ D^a 7.56, D^b 8.33-8.25. Determined against integral at δ 2.44.
Hydrogenation Product	***^{1}H NMR data***[165]
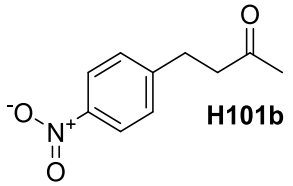	**^{1}H NMR** (400 MHz, $CDCl_3$): δ 8.15-8.10 (2H, m, Ar-H), 7.37-7.31 (2H, m, Ar-H), 3.00 (2H, t *J* = 7.4 Hz, CH_2), 2.82 (2H, t *J* = 7.4 Hz, CH_2), 2.16 (3H, s, CO-CH_3) Conversion determined using integrals at δ 2.44 (**D101b**) and 2.16 (**H101b**).

D-Incorporation (%)						***Hydrogenation (%)***		
Run				***Average***		***Run***		***Average***
1		***2***				***1***	***2***	
Da	***Db***	***Da***	***Db***	***Da***	***Db***			
95	1	95	2	95	2	1	1	1

Substrate	***^{1}H NMR data***[156]
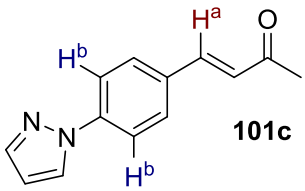 (85 mg, 0.4 mmol)	**^{1}H NMR** (400 MHz, $CDCl_3$): δ 8.00 (1H, d *J* = 2.6 Hz, Ar-H), 7.82-7.75 (3H, m, Ar-H), 7.70-7.63 (2H, m, Ar-H), 7.55 (1H, d, *J* = 16.3 Hz, Ar-CH=CH), 6.75 (1H, d *J* = 16.3 Hz, CH=CH-CO), 6.53 (1H, dd *J* = 2.6 Hz, 1.8 Hz, Ar-H), 2.42 (3H, s, CO-CH_3). Incorporation expected at δ D^a 7.55, D^b 7.82-7.75. Determined against integral at δ 2.42.
Hydrogenation Product	***^{1}H NMR data***
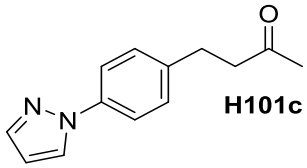	No reference NMR data available, integral for CO-CH_3 chosen based upon related compound **H101b**. Conversion determined using integrals at δ 2.42 (**D101c**) and 2.16 (**H101c**).

D-Incorporation (%)						***Hydrogenation (%)***		
Run				***Average***		***Run***		***Average***
1		***2***				***1***	***2***	
Da	***Db***	***Da***	***Db***	***Da***	***Db***			
0	83	1	87	1	85	1	1	1

Substrate	***^{1}H NMR data***[156]
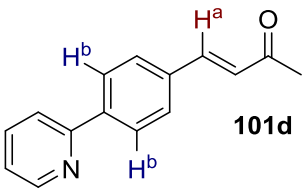 (89 mg, 0.4 mmol)	**^{1}H NMR** (400 MHz, $CDCl_3$): δ 8.74 (1H, dt *J* = 4.8 Hz, ^4J = 1.6 Hz, Ar-H), 8.12-8.03 (2H, m, Ar-H), 7.83-7.75 (2H, m, Ar-H), 7.71-7.65 (2H, m, Ar-H), 7.58 (1H, d *J* = 16.3 Hz, Ar-CH=CH), 7.32-7.24 (1H, m, Ar-H), 6.80 (1H, d *J* = 16.3 Hz, CH=CH-CO), 2.42 (3H, s, CO-CH_3). Incorporation expected at δ D^a 7.58, D^b 8.12-8.03. Determined against integral at δ 2.42.
Hydrogenation Product	***^{1}H NMR data***
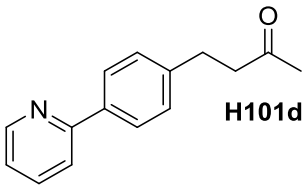	No reference NMR data available, integral for CO-CH_3 chosen based upon related compound **H101b**. Conversion determined using integrals at δ 2.42 (**D101d**) and 2.16 (**H101d**).

D-Incorporation (%)						***Hydrogenation (%)***		
Run				***Average***		***Run***		***Average***
1		***2***				***1***	***2***	
Da	***Db***	***Da***	***Db***	***Da***	***Db***			
0	0	0	0	0	0	0	0	0

Scheme 2.63 *HIE upon Z- enone.*

The reactions were carried out following general procedure B and analysed by ^{1}H NMR spectroscopy to confirm degree of hydrogenation, and the position and degree of deuterium incorporation.

Complex	***Solvent***	***Time (h)***	***Temperature (°C)***
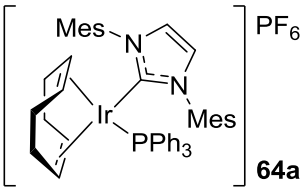 (0.4 mg, 0.0004 mmol)	DCM	1	25

Substrate	***^{1}H NMR data***[166]
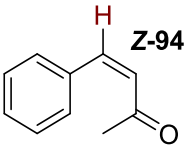 (58.5 mg, 0.4 mmol)	**^{1}H NMR** (400 MHz, $CDCl_3$): δ 7.42-7.29 (5H, m, Ar-H), 6.93 (1H, d *J*= 12.8 Hz Ar-C<u>H</u>=CH), 6.2 (1H, d *J* = 12.6 Hz, CH=C<u>H</u>-CO), 2.13 (3H, s, CO-C<u>H</u>$_3$). Incorporation expected at δ 6.93 Determined against integral at δ 2.13.

Hydrogenation Product	***data***
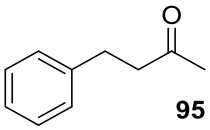	Data was consistent with that reported on page 362.

D-Incorporation (%)			***Hydrogenation (%)***		
Run		***Average***	***Run***		***Average***
1	***2***		***1***	***2***	
0	0	0	1	1	1

Graph 2.7 *Hammett plot for olefinic HIE.*

The reactions were carried out following general procedure C and analysed by ^{1}H NMR spectroscopy to confirm the degree of hydrogenation, and the position and degree of deuterium incorporation. The data for the Hammett plot are summarised in **Table E2.9**.

Complex	***Solvent***	***Temperature (°C)***
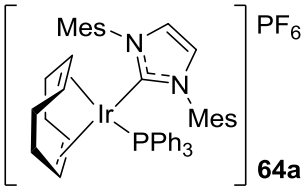 (0.4 mg, 0.0004 mmol)	DCM (5 mL)	25

Substrate	***Data***
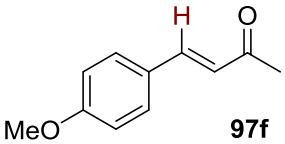 (350 mg, 2.0 mmol)	Data was consistent with that reported on page 370.

Time (sec)	***D-Incorporation (%)***
5	3.8
7	8.6
9	13.3
11	17.3
13	20.6
15	25.2

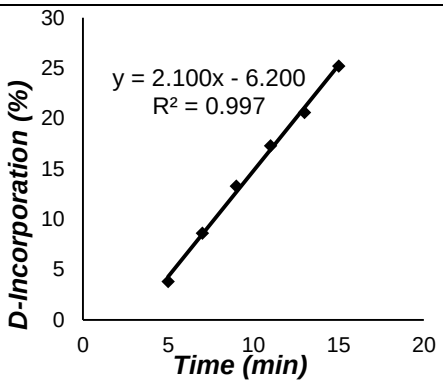

Substrate	***data***
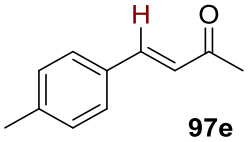 **97e** (320 mg, 2.0 mmol)	Data was consistent with that reported on page 369.

Time (sec)	***D-Incorporation (%)***
5	10
7	12.4
9	17.9
11	21.8
13	25.7
15	30.4

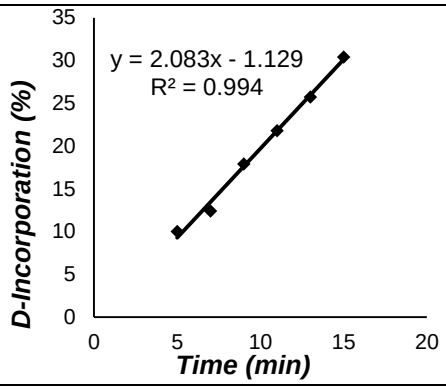

Substrate	***data***
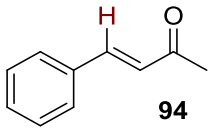 **94** (293 mg, 2.0 mmol)	Data was consistent with that reported on page 362.

Time (sec)	***D-Incorporation (%)***
5	8.9
7	12.3
9	16.9
11	20.5
13	25.0
15	29.4

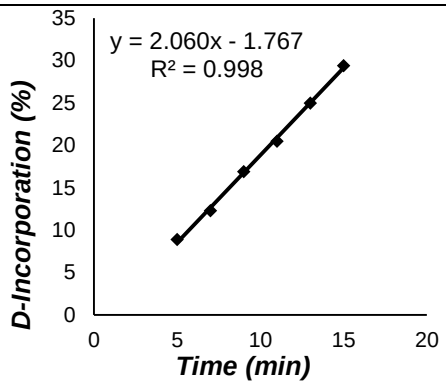

Substrate	***Data***
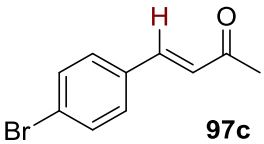 **97c** (450 mg, 2.0 mmol)	Data was consistent with that reported on page 369.

Time (sec)	***D-Incorporation (%)***
5	8.5
7	12.6
9	16.8
11	21.0
13	24.8
15	29.0

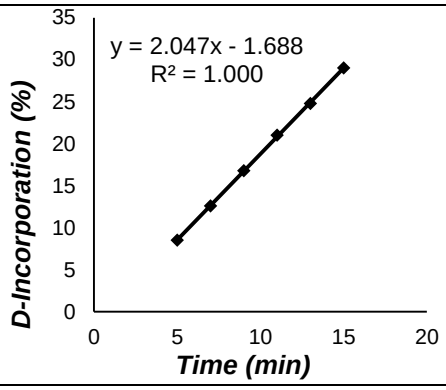

Substrate	***Data***
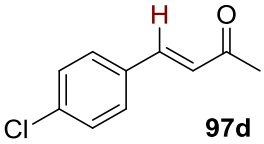 **97d** (360 mg, 2.0 mmol)	Data was consistent with that reported on page 368.

Time (sec)	***D-Incorporation (%)***
5	8.2
7	11.9
9	15.8
11	20.1
13	24.7
15	28.2

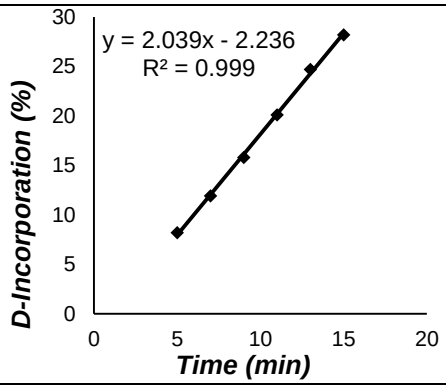

Substrate	***data***
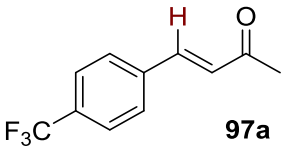 **97a** (430 mg, 2.0 mmol)	Data was consistent with that reported on page 367.

Time (sec)	***D-Incorporation (%)***
5	9.7
7	15.0
9	18.7
11	23.0
13	25.7
15	30.6

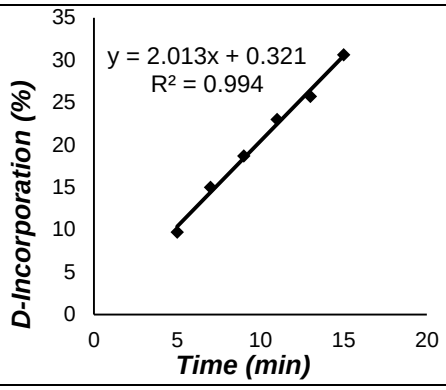

Substituent	v_x/v_H	$log(v_x/v_H)$	σ_p[167]
OMe	1.019	0.0084	-0.27
Me	1.011	-0.0028	-0.17
H	1.000	-0.0045	0
Br	0.994	0.0048	0.23
Cl	0.990	0.0000	0.23
OMe	0.977	0.0100	0.54

Table E2.9

Graph 2.8 *Independent reactions to generate a KIE.*

The reactions were carried out following general procedure B and analysed by ^{1}H NMR specteoscopy to confirm the degree of deuterium (or hydrogen) incorporation.

Complex	***Solvent***	***Temperature (°C)***
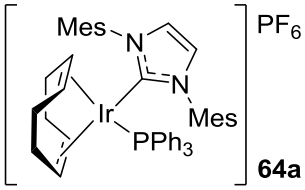 **64a** (0.4 mg, 0.0004 mmol)	DCM (1 mL)	25

Substrate	***Data***
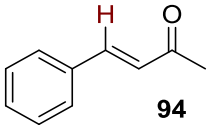 **94** (58.5 mg, 0.4 mmol)	Data was consistent with that reported on page 362.

Time (min)	***D-Incorporation (%)***			
	Run			***Average***
	1	***2***	***3***	
5	38.6	36.7	37.7	37.7
10	56.7	49.8	57.2	54.6

Substrate	***^{1}H NMR data***[168]
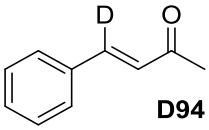 **D94** (58.9 mg, 0.4 mmol)	**^{1}H NMR** (400 MHz, $CDCl_3$): δ 7.62-7.49 (2H, m, Ar-H and d, J = 15.9 Hz, Ar-CH=CH), 7.47-7.39 (3H, m, Ar-H), 6.75 (1H, d, J_{H-D} = 5.2 Hz, CD=CH-CO), 2.41 (3H, s, OC-CH_3). Incorporation expected at δ 7.62-7.49. Determined against integral at δ 2.41.

Time (min)	***H-Incorporation (%)***			
	Run			***Average***
	1	***2***	***3***	
5	11.4	12.4	11.3	11.7
10	16.5	16.0	16.8	16.4

Graph 2.9 *Monitored reactions to generate a KIE.*

The reactions were carried out following general procedure C and analysed by ^{1}H NMR spectroscopy to confirm the degree of deuterium (or hydrogen) incorporation.

Complex	***Solvent***	***Temperature (°C)***
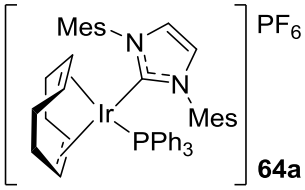 **64a** (2.0 mg, 0.002 mmol)	DCM (20 mL)	25

Substrate	***Data***
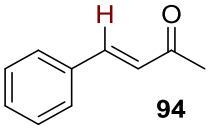 **94** (293 mg, 2.0 mmol)	Data was consistent with that reported on page 362.

Time	***D-Incorporation (%)***
5	22.1
7	40.6
9	57.1

Substrate	***^{1}H NMR data***[105]
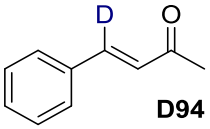 **D94** (294 mg, 2.0 mmol)	**^{1}H NMR** (400 MHz, $CDCl_3$): δ 7.62-7.49 (2H, m, Ar-H and d, J = 15.9 Hz, Ar-CH=CH), 7.47-7.39 (3H, m, Ar-H), 6.75 (1H, d, $J_{H\text{-}D}$ = 5.2 Hz, CD=CH-CO), 2.41 (3H, s, OC-CH_3). Incorporation expected at δ 7.62-7.49. Determined against integral at δ 2.41.

Time	***H-Incorporation (%)***
5	13.8
7	18.3
9	23.0

Scheme 2.66 T*esting olefinic HIE on pharmaceutical agents.*

The reactions were carried out following general procedure B and analysed by ^{1}H NMR spectroscopy to confirm the degree of deuterium incorporation.

Complex	***Solvent***	***Temperature (°C)***
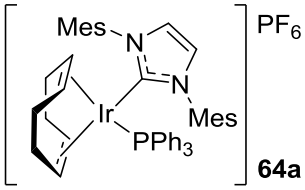 **64a** (0.4 mg, 0.0004 mmol)	DCM (1 mL)	25

Substrate	***^{1}H NMR data***[169]
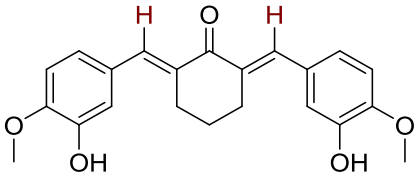 *Cyclovalone* **- 102** (147 mg, 0.4 mmol)	**^{1}H NMR** (400 MHz, $CDCl_3$): δ 7.72 (2H, s, Ar-C<u>H</u>=C), 7.06 (2H, dd *J* = 8.4 Hz, ^{4}J = 2.0 Hz, Ar-<u>H</u>), 6.97 (2H, d ^{4}J = 1.9 Hz, Ar-<u>H</u>), 6.93 (2H, d *J* = 8.2 Hz, Ar-<u>H</u>), 5.80 (2H, s, Ar-O<u>H</u>), 3.90 (6H, s, O-C<u>H</u>$_3$), 2.95-2.88 (4H, m, C<u>H</u>$_2$), 1.86-1.75 (2H, m, C<u>H</u>$_2$). Incorporation expected at δ 7.72. Determined against integral at δ 3.90.

Reaction Time (h)	***D-Incorporation (%)***		
	Run		***Average***
	1	***2***	
3	52	52	52

Substrate	***^{1}H NMR data***[170]
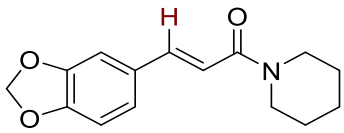 *Ilepcimide* **- 103** (104 mg, 0.4 mmol)	**^{1}H NMR** (400 MHz, $CDCl_3$): δ 7.55 (1H, d *J* = 15.2 Hz, Ar-C<u>H</u>=CH), 7.02 (1H, d ^{4}J = 1.6 Hz, Ar-<u>H</u>) 6.98 (1H, dd *J* = 8.0 Hz, ^{4}J = 1.6 Hz, Ar-<u>H</u>), 6.78 (1H, d *J* = 8.0 Hz, Ar-<u>H</u>), 6.73 (1H, d *J* = 15.2 Hz, CH=C<u>H</u>-CO), 5.97 (2H, s, O-C<u>H</u>$_2$-O), 3.70-7.52 (4H, m, C<u>H</u>$_2$), 1.67-1.59 (6H, m, C<u>H</u>$_2$). Incorporation expected at δ 7.55. Determined against integral at δ 5.97.

Reaction Time (h)	***D-Incorporation (%)***		
	Run		***Average***
	1	***2***	
1	90	92	91

6.4. sp^3 HIE

Scheme 2.67 *First Catalyst Screen for sp^3 HIE.*

The reactions were carried out following general procedure A and analysed by LCMS to confirm the extent of exchange. The position was confirmed through ^{1}H NMR spectroscopy of the highest incorporation result (**Table E2.10**).

Solvent	***Temperature (°C)***	***Time (h)***
DCM (1 mL)	25	3
Substrate	***^{1}H NMR data***[171]	
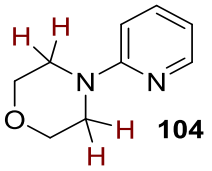 **104** (14.1 mg, 0.086 mmol)	**^{1}H NMR** (300 MHz, DMSO): δ 8.12 (1H, dd *J* = 5.1 Hz, ^4J = 1.5 Hz, Ar-<u>H</u>), 7.54 (1H, ddd *J* = 8.7 Hz, 7.1 Hz, ^4J = 1.5 Hz, Ar-<u>H</u>), 6.81 (1H, d *J* = 8.7 Hz, Ar-<u>H</u>), 6.66 (1H, dd *J* = 7.7 Hz, ^4J = 5.1 Hz, Ar-<u>H</u>), 3.72-3.64 (4H, m, O-C<u>H</u>$_2$), 3.44-3.37 (4H, m, N-C<u>H</u>$_2$). Incorporation expected at δ 3.44-3.37. Determined against integral at δ 6.66.	
	LCMS data	
	Retention time: 0.28 min; Mass ion: 165.1 $(M+H)^+$	

Entry	*Complex*	*D-Incorporation (%)*		
		Run		*Average*
		1	*2*	
1	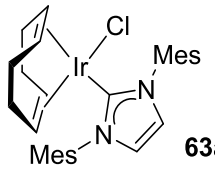 **63a** (1.4 mg, 0.00215 mmol)	0	0	0
2	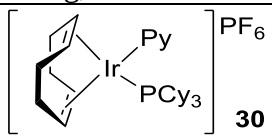 **30** (1.7 mg, 0.00215 mmol)	23	25	24
3	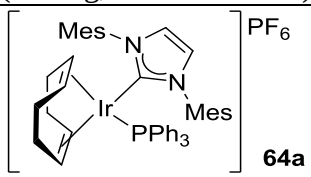 **64a** (2.2 mg, 0.00215 mmol)	87	81	79
4	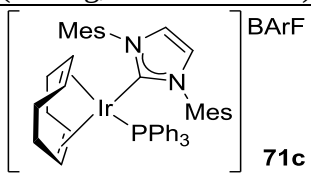 **71c** (3.7 mg, 0.00215 mmol)	88	84	86
5	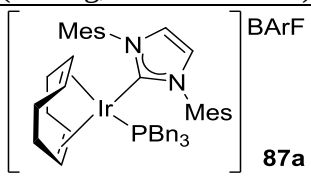 **87a** (3.8 mg, 0.00215 mmol)	83	84	84
6	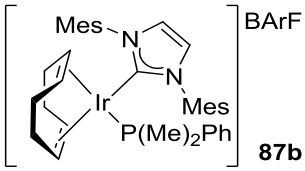 **87b** (3.4 mg, 0.00215 mmol)	78	77	78
7	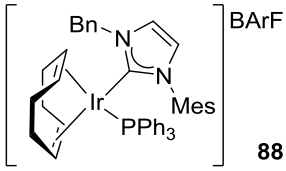 **88** (3.4 mg, 0.00215 mmol)	84	83	84

Table E2.10

Graph 2.11 *Application of Different Solvents for sp^3 HIE.*

The reactions were carried out following general procedure A and analysed by LCMS to confirm the extent of exchange. The position was confirmed through ^{1}H NMR spectroscopy of the highest incorporation result (**Table E2.11**).

Complex	***Temperature (°C)***	***Solvent***	***Time (h)***
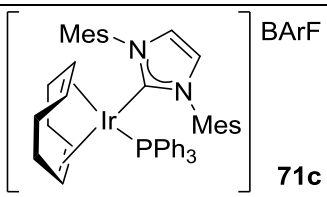 **71c** (7.4 mg, 0.0043 mmol)	25	1 mL	3
Substrate		***Data***	
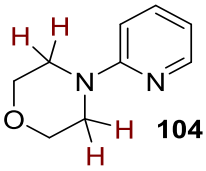 **104** (14.1 mg, 0.086 mmol)		Data was consistent with that reported on page 409.	

Entry	***Solvent***	***D-Incorporation (%)***		
		Run		***Average***
		1	***2***	
1	MeOH	40	41	41
2	IPA	59	56	58
3	*t*amylOH	75	74	75
4	*i*PrOAc	80	72	76
5	*t*BuOAc	92	94	93
6	2-MeTHF	64	73	69
7	CPME	83	83	83
8	MTBE	87	92	90

Table E2.11

Design of experiments delivering the first protocol for morpholine and piperidine HIE

Experimental design was used to assess the effect of varying the catalyst loading, reaction time and solvent volume. As such, 'high' and 'low' values for each of the three variables were chosen. To generate a series of experiments to study optimal conditions within the variable ranges chosen, Design Expert™ software v10.0 (Stat_Ease Inc., Minneappolis, Mn) was used. This generated a *two-level, three-factorial* design containing three centre points, giving 11 experiments in total. The deuterium incorporation of **D104** was used as the response. The reactions were carried out following general procedure A and analysed by LCMS to confirm the extent of exchange. The position was confirmed through ^{1}H NMR spectroscopy of the three centre point results. (**Table E2.12**).

Complex	***Temperature (°C)***	***Solvent***
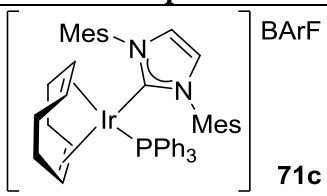	25	DCM
Substrate	***data***	
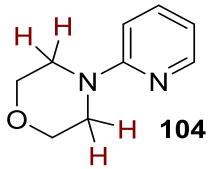 (14.1 mg, 0.086 mmol)	Data was consistent with that reported on page 409.	

Run[a]	***Variable A: Catalyst Loading* (mol%)**	***Amount of 71c (mg (µmol))***	***Variable B: Reaction Time* (min)**	***Variable C: DCM Volume (mL)***	***Response: Incorporation* (%D)**
1 (++-)	1.5	2.2 (1.29)	40	0.5	52
2 (--+)	0.5	0.7 (4.30)	20	2.5	24
3 (+++)	1.5	2.2 (1.29)	40	2.5	94
4 (***)	1.0	1.5 (0.86)	30	1.5	72
5 (-+-)	0.5	0.7 (4.30)	40	0.5	45
6 (***)	1.0	1.5 (0.86)	30	1.5	73
7 (---)	0.5	0.7 (4.30)	20	0.5	30
8 (+--)	1.5	2.2 (1.29)	20	0.5	51
9 (***)	1.0	1.5 (0.86)	30	1.5	69
10 (-++)	0.5	0.7 (4.30)	40	2.5	37
11 (+-+)	1.5	2.2 (1.29)	20	2.5	70

[a] symbol in parentheses indicate points in the design; + high, * mid and – low.

Table E2.12

Runs 4, 6 and 9 represent the centre points of the design. These are employed in order to:

(iii) Assess any curvature in the response of incorporation changes in the variables; and

(iv) Assess the repeatability of the hydrogen isotope exchange reaction.

A response surface was created in the same design program. This generated a half-normal plot inferring that increasing the catalyst loading, reaction time and solvent volume had a positive impact upon the HIE reaction. Furthermore, it indicated the order of significance of each factor; Catalyst Loading >> Reaction Time and Solvent Volume. Additionally, a combined variable of catalyst loading and solvent volume was observed to have a positive impact (**Graph E2.7**).

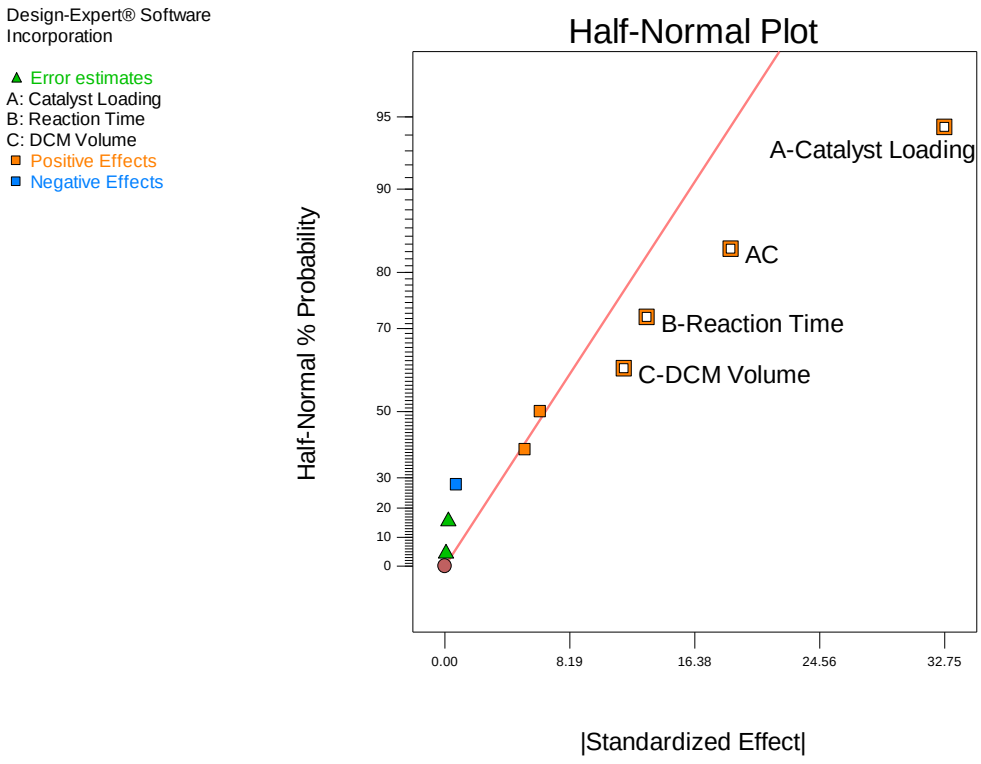

Graph E2.7

Further implementation of the design software generated **Graph E2.8**. By plotting reaction time and catalyst loading at the fixed optimal solvent volume (1 mL) it can be seen that a decrease in catalyst loading and increase in reaction time leads to the optimised conditions (1.0 mol% catalyst, 1 mL solvent, 1 h).

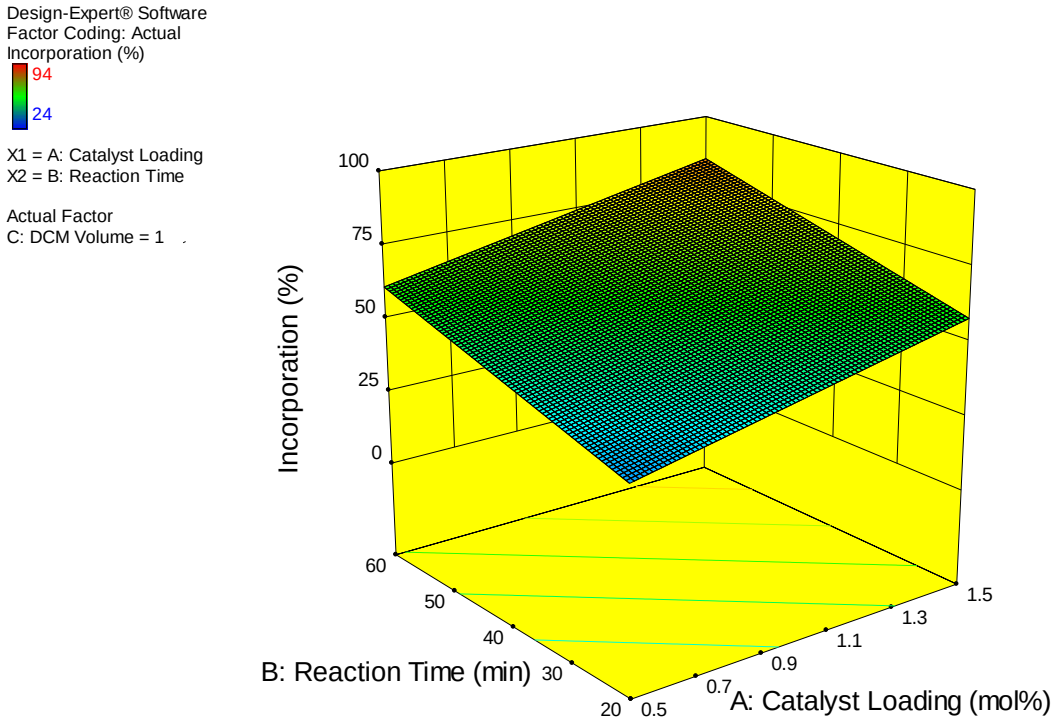

Graph E2.8

Finally, provided below is a graph of Residuals versus Predicted plot. This is a plot of the residuals versus the ascending predicted response values (low incorporation to high incorporation), and tests the assumption of constant variance in the data (**Graph E2.9**).

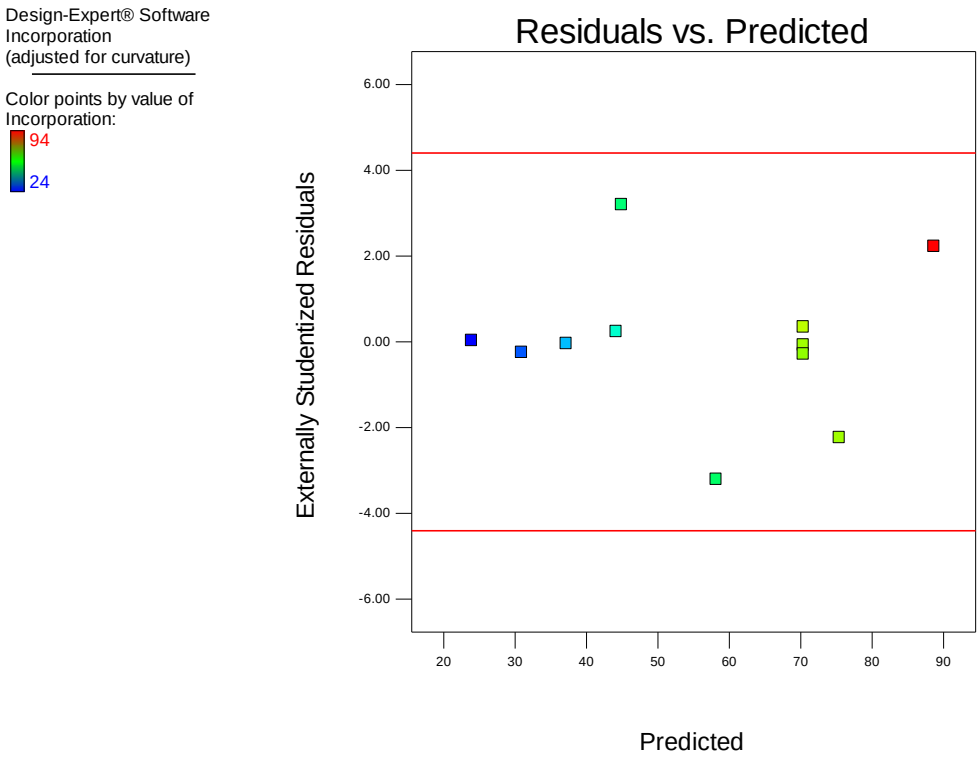
Design-Expert® Software
Incorporation
(adjusted for curvature)
Color points by value of
Incorporation:
94
24
Residuals vs. Predicted
Externally Studentized Residuals
6.00
4.00
2.00
0.00
-2.00
-4.00
-6.00
20
30
40
50
60
70
80
90
Predicted

Graph E2.9

Scheme 2.69 *HIE on morpholine substrates.*

The reactions were carried out following general procedure A and analysed by LCMS to confirm the extent of exchange. The position was confirmed through ^{1}H NMR spectroscopy.

Complex	***Solvent***	***Temperature (°C)***	***Time (h)***
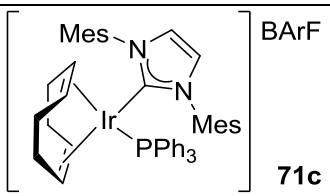 **71c** (1.6 mg, 0.0086 mmol)	DCM (1 mL)	25	1

Substrate	***data***
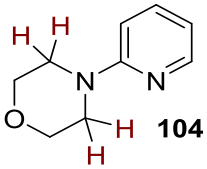 **104** (14.1 mg, 0.086 mmol)	Data was consistent with that reported on page 409.

D-Incorporation (%)		
Run		***Average***
1	***2***	
82	78	80

Substrate	***^{1}H NMR data***[172]
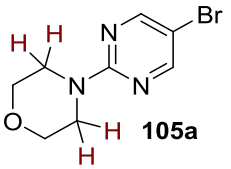 **105a** (14.1 mg, 0.086 mmol)	**^{1}H NMR** (300 MHz, DMSO): δ 8.46 (2H, s, Ar-H), 3.70-3.60 (8H, m, CH_2). Incorporation expected at δ 3.70-3.60. Determined against integral at δ 8.46.
	LCMS data
	Retention time: 2.69 min; Mass ion: 244.1 $(M+H)^+$

D-Incorporation (%)		
Run		***Average***
1	***2***	
94	95	95

Substrate	***^{1}H NMR data***[173]
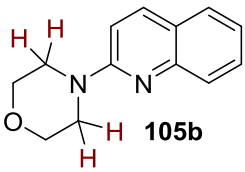 **105b** (18.4 mg, 0.086 mmol)	**^{1}H NMR** (300 MHz, DMSO): δ 8.05 (1H, d *J* = 9.3 Hz, Ar-H), 7.70 (1H, d *J* = 7.9 Hz, Ar-H), 7.61-7.48 (2H, m, Ar-H), 7.28-7.18 (2H, m, Ar-H), 3.76-3.69 (4H, m, O-CH_2), 3.68-3.59 (4H, m, N-CH_4). Incorporation expected at δ 3.68-3.59. Determined against integral at δ 7.28-7.18.
	LCMS data
	Retention time: 0.49 min; Mass ion: 215.1 $(M+H)^+$

D-Incorporation (%)		
Run		***Average***
1	***2***	
94	94	94

Substrate	***^{1}H NMR data***[174]
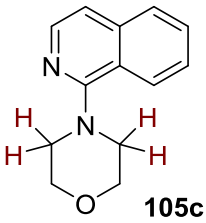 **105c** (18.4 mg, 0.086 mmol)	**^{1}H NMR** (300 MHz, DMSO): δ 8.15-8.08 (2H, m, Ar-H), 7.88 (1H, d *J* = 8.2 Hz, Ar-H), 7.75-7.66 (1H, m, Ar-H), 7.63-7.54 (1H, m, Ar-H), 7.39 (1H, d *J* = 5.7 Hz, Ar-H), 3.90-3.80 (4H, m, O-CH_2), 3.33-3.27 (4H, m, N-CH_2). Incorporation expected at δ 3.33-3.27. Determined against integral at δ 7.39.
	LCMS data
	Retention time: 0.80 min; Mass ion: 215.1 $(M+H)^+$

D-Incorporation (%)		
Run		***Average***
1	***2***	
99	99	99

Substrate	***^{1}H NMR data***[175]
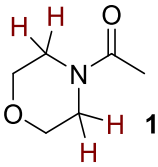 **105d** (11.1 mg, 0.086 mmol)	**^{1}H NMR** (300 MHz, DMSO): δ 3.59-3.48 (4H, m, O-C<u>H</u>$_2$), 3.45-3.36 (4H, m, N-C<u>H</u>$_2$), 1.97 (3H, s, CO-C<u>H</u>$_3$). Incorporation expected at δ 3.45-3.36. Determined against integral at δ 1.97.
	LCMS data
	Retention time: 0.41 min; Mass ion: 130.1 $(M+H)^+$

D-Incorporation (%)		
Run		***Average***
1	***2***	
0	0	0

Substrate	***^{1}H NMR data***[176]
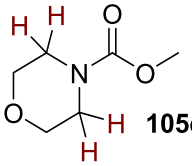 **105e** (12.4 mg, 0.086 mmol)	**^{1}H NMR** (300 MHz, DMSO): δ 3.60 (3H, s, O-C<u>H</u>$_3$), 3.56-3.50 (4H, m, O-C<u>H</u>$_2$), 3.37-3.29 (4H, m, N-C<u>H</u>$_2$). Incorporation expected at δ 3.37-3.29. Determined against integral at δ 3.60.
	LCMS data
	Retention time: 0.92 min; Mass ion: 146.1 $(M+H)^+$

D-Incorporation (%)		
Run		***Average***
1	***2***	
0	0	0

Scheme 2.70 *HIE upon piperidine substrates.*

The reactions were carried out following general procedure A and analysed by LCMS to confirm the extent of exchange, position was confirmed through ^{1}H NMR.

Complex	*Solvent*	*Temperature (°C)*	*Time (h)*
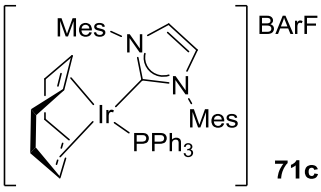 **71c** (1.6 mg, 0.0086 mmol)	DCM (1 mL)	25	1

Substrate	*^{1}H NMR data*[177]
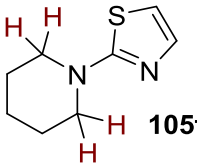 **105f** (14.5 mg, 0.086 mmol)	**^{1}H NMR** (300 MHz, DMSO): δ 7.11 (1H, d *J* = 3.7 Hz, Ar-H), 6.75 (1H, d *J* = 3.6 Hz, Ar-H), 3.45-3.33 (4H, m, N-CH_2), 1.65-1.52 (6H, m, CH_2). Incorporation expected at δ 3.45-3.33. Determined against integral at δ 1.65-1.52. ***LCMS data*** Retention time: 0.67 min; Mass ion: 169.0 $(M+H)^+$

D-Incorporation (%)		
Run		*Average*
1	*2*	
69	73	71

Substrate	*^{1}H NMR data*[178]
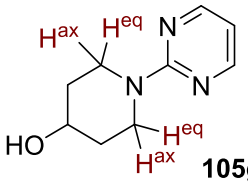 **105g** (15.4 mg, 0.086 mmol)	**^{1}H NMR** (300 MHz, DMSO): δ 8.31 (2H, d *J* = 4.7 Hz, Ar-H), 6.55 (1H, t *J* = 4.7 Hz, Ar-H), 4.64 (1H, d *J* = 4.2 Hz, O-H), 4.24 (2H, ddd ^{2}J = 13.0 Hz, *J* = 5.6 Hz, 4.1 Hz, N-CH_2), 3.72 (1H, oct *J* = 4.2 Hz, O-CH), 3.24 (2H, ddd ^{2}J = 13.0 Hz, *J* = 9.1 Hz, 3.7 Hz, N-CH_2), 1.81-1.70 (2H, m, CH_2), 1.39-1.23 (2H, m, CH_2). Incorporation expected at δ 3.24 axial, 4.24 equatorial. Determined against integral at δ 1.39-1.23. ***LCMS data*** Retention time: 0.72 min; Mass ion: 180.1 $(M+H)^+$

D-Incorporation (%)					
Run				*Average*	
1		*2*			
eq	*ax*	*eq*	*ax*	*eq*	*ax*
84	82	83	83	84	83

Substrate	*^{1}H NMR data*[179]
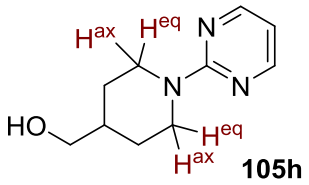 (16.6 mg, 0.086 mmol)	**^{1}H NMR** (300 MHz, DMSO): δ 8.3 (2H, d *J* = 4.7 Hz, Ar-H), 6.53 (1H, t *J* = 4.7 Hz, Ar-H), 4.70-4.58 (2H, m, N-CH_2), 4.40 (1H, t *J* = 5.3 Hz, O-H), 3.33-3.20 (2H, m, O-CH_2), 2.83 (2H, td *J* = 12.7 Hz, 2.7 Hz, N-CH_2), 1.77-1.55 (3H, m, CH_2-CH & CH_2), 1.14-0.95 (2H, m, CH_2). Incorporation expected at δ 2.83 axial, 4.70-4.58 equatorial. Determined against integral at δ 1.14-0.95.
	LCMS data
	Retention time: 0.71 min; Mass ion: 194.1 $(M+H)^+$

D-Incorporation (%)					
Run				*Average*	
1		*2*			
eq	*ax*	*eq*	*ax*	*eq*	*ax*
90	87	88	84	89	86

Substrate	*^{1}H NMR data*[180]
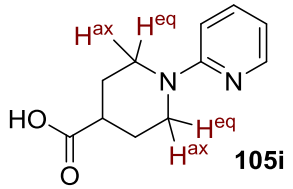 (17.7 mg, 0.086 mmol)	**^{1}H NMR** (300 MHz, DMSO): δ 12.15 (1H, br s, O-H), 8.08 (1H, dd *J* = 5.2 Hz, ^2J = 2.0 Hz, Ar-H), 7.49 (1H, dd *J* = 8.7 Hz, 7.1 Hz, ^2J = 2.0 Hz, Ar-H), 6.80 (1H, d *J* = 8.7 Hz, Ar-H), 6.58 (1H, dd *J* = 7.1 Hz, 5.2 Hz, Ar-H), 4.16 (2H, ddd ^2J = 13.3 Hz, *J* = 4.3 Hz, 3.2 Hz, N-CH_2), 2.92 (2H, ddd ^2J = 13.3 Hz, *J* = 11.5 Hz, 2.9 Hz, N-CH_2), 2.52-2.42 (1H, m, CH), 1.91-1.79 (2H, m, CH_2), 1.61-1.40 (2H, m, CH_2). Incorporation expected at δ 2.92 axial, 4.16 equatorial. Determined against integral at δ 1.61-1.40.
	LCMS data
	Retention time: 0.39 min; Mass ion: 207.1 $(M+H)^+$

D-Incorporation (%)					
Run				*Average*	
1		*2*			
eq	*ax*	*eq*	*ax*	*eq*	*ax*
88	72	86	73	87	73

Substrate	***^{1}H NMR data***[181]
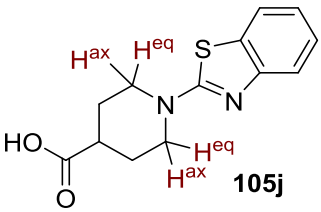 (22.6 mg, 0.086 mmol)	**^{1}H NMR** (300 MHz, CD_3CN): δ 9.05 (1H, br-s, O-H), 7.68 (1H, d *J* = 7.5 Hz, Ar-H), 7.44 (1H, d *J* = 7.5 Hz, Ar-H), 7.28 (1H, td *J* = 7.5 Hz, ^4J = 1.5 Hz, Ar-H), 7.07 (1H, ddd *J* = 7.5 Hz, 7.5 Hz, ^4J = 1.5 Hz, Ar-H), 4.04 (2H, ddd ^2J = 12.6 Hz, *J* = 4.2 Hz, 4.1 Hz, N-CH_2), 3.25 (2H, ddd ^2J = 12.6 Hz, *J* = 11.4 Hz, 3.0 Hz, N-CH_2), 2.62 (1H, tt *J* = 11.1 Hz, 4.0 Hz, CH), 2.07-1.96 (2H, m, CH_2), 1.81-1.64 (2H, m, CH_2). Incorporation expected at δ axial 3.25, equatorial 4.04. Determined against integral at δ 1.81-1.64.
	LCMS data
	Retention time: 2.49 min; Mass ion: 263.1 $(M+H)^+$

D-Incorporation (%)

Run				***Average***	
1		***2***			
eq	***ax***	***eq***	***ax***	***eq***	***ax***
88	79	86	75	87	77

Substrate	***^{1}H NMR data***[182]
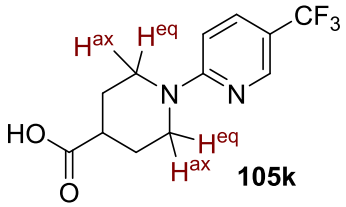 (23.6 mg, 0.086 mmol)	**^{1}H NMR** (300 MHz, DMSO): δ 12.11 (1H, br s, O-H), 8.37 (1H, br s, Ar-H), 7.74 (1H, dd *J* = 9.1 Hz, ^4J = 2.6 Hz, Ar-H), 6.93 (1H, d *J* = 9.1 Hz, Ar-H), 4.27 (2H, ddd ^2J = 13.5 Hz, *J* = 3.8 Hz, 3.8 Hz, N-CH_2), 3.08 (2H, ddd ^2J = 13.5 Hz, *J* = 11.2 Hz, 3.0 Hz, N-CH_2), 2.56 (1H, tt *J* = 11.0 Hz, 4.0 Hz, CH), 1.94-1.81 (2H, m, CH_2), 1.61-1.41 (2H, m, CH_2). Incorporation expected at δ 3.08 axial, 4.27 equatorial. Determined against integral at δ 1.61-1.41.
	LCMS data
	Retention time: 3.19 min; Mass ion: 275.1 $(M+H)^+$

D-Incorporation (%)

Run				***Average***	
1		***2***			
eq	***ax***	***eq***	***ax***	***eq***	***ax***
93	90	92	90	93	90

Substrate	***^{1}H NMR data***[183]
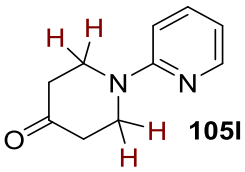 **105l** (15.2 mg, 0.086 mmol)	**^{1}H NMR** (300 MHz, DMSO): δ 8.17 (1H, dd *J* = 4.8 Hz, ^{2}*J* = 1.5 Hz, Ar-H), 7.50 (1H, ddd *J* = 8.6 Hz, 7.4 Hz, ^{4}*J* = 1.5 Hz, Ar-H), 3.73 (1H, d *J* = 7.4 Hz, Ar-H), (1H, dd *J* = 8.6 Hz, 4.8 Hz, Ar-H), 3.89 (4H, t *J* = 7.2 Hz, N-CH$_2$), 2.48 (4H, t *J* = 7.2 Hz, CH$_2$). Incorporation expected at δ 3.89. Determined against integral at δ 2.48.
	LCMS data
	Retention time: 0.34 min; Mass ion: 177.0 (M+H)$^+$

D-Incorporation (%)		
Run		***Average***
1	***2***	
94	92	93

Substrate	***^{1}H NMR data***[175]
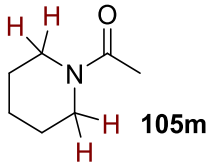 **105m** (10.9 mg, 0.086 mmol)	**^{1}H NMR** (300 MHz, DMSO): δ 3.44-3.27 (4H, m, N-CH$_2$), 1.95 (3H, s, CO-CH$_3$), 1.60-1.33 (6H, m, CH$_2$). Incorporation expected at δ 3.44-3.27. Determined against integral at δ 1.95.
	LCMS data
	Retention time: 1.50 min; Mass ion: 128.2 (M+H)$^+$

D-Incorporation (%)		
Run		***Average***
1	***2***	
0	0	0

Design of experiments delivering the second protocol for piperazine HIE

Experimental design was used to assess the effect of varying the catalyst loading, reaction time and solvent volume. As such, 'high' and 'low' values for each of the three variables were chosen. To generate a series of experiments to study optimal conditions within the variable ranges chosen, Design Expert™ software v10.0 (Stat_Ease Inc., Minneappolis, Mn) was used. This generated a *two-level, three-factorial* design containing three centre points, giving 11 experiments in total. The deuterium incorporation of **D105n** was used as the response. The reactions were carried out according to general procedure A, and are analysed by LCMS to confirm the extent of exchange. The position of exchange was confirmed through ^{1}H NMR spectroscopy of the three centre point results. (**Table E2.13**).

Complex	***Temperature (°C)***	***Solvent***
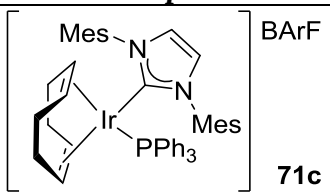	25	DCM
Substrate	***^{1}H NMR data***[184]	
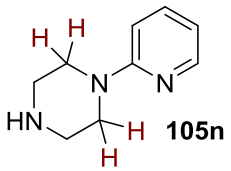 (14.1 mg, 0.086 mmol)	**^{1}H NMR** (300 MHz, DMSO): δ 8.08 (1H, dd *J* = 4.9 Hz, ^{4}J = 2.1 Hz, Ar-H), 7.49 (1H, ddd *J* = 8.7 Hz, 7.1 Hz, ^{4}J = 2.1 Hz, Ar-H), 6.75 (1H, d, *J* = 8.7 Hz, Ar-H), 6.59 (1H, dd *J* = 7.1 Hz, 4.9 Hz, Ar-H), 3.43-3.32 (4H, m, N-CH_2), 2.81-2.70 (4H, m, NH-CH_2). Incorporation expected at δ 3.43-3.32. Determined against integral at δ 2.81-2.70.	
	LCMS data	
	Retention time: 0.37 min; Mass ion: 164.0 $(M+H)^{+}$	

Run[a]	***Variable A: Catalyst Loading* (mol%)**	***Amount of 71c (mg (µmol))***	***Variable B: Reaction Time* (min)**	***Variable C: DCM Volume (mL)***	***Response: Incorporation* (%D)**
1 (***)	3.0	4.5 (2.58)	75	1.5	62
2 (+++)	5.0	7.4 (4.30)	120	2.5	83
3 (+--)	5.0	7.4 (4.30)	30	0.5	48
4 (--+)	1.0	1.5 (0.86)	30	2.5	7
5 (***)	3.0	4.5 (2.58)	75	1.5	62
6 (++-)	5.0	7.4 (4.30)	120	0.5	69
7 (---)	1.0	1.5 (0.86)	30	0.5	5
8 (-+-)	1.0	1.5 (0.86)	120	0.5	10
9 (-++)	1.0	1.5 (0.86)	120	2.5	14
10 (+-+)	5.0	7.4 (4.30)	30	2.5	57
11 (***)	3.0	4.5 (2.58)	75	1.5	64

[a] symbol in parentheses indicate points in the design; + high, * mid and – low.

Table E2.13

Runs 1, 5 and 11 represent the centre points of the design. These are employed in order to:

(i) Assess any curvature in the response of incorporation changes in the variables; and

(ii) Assess the repeatability of the hydrogen isotope exchange reaction.

A response surface was created in the same design program. This generated a half-normal plot inferring that increasing the catalyst loading, and reaction time had a positive impact upon the HIE reaction, with a negligible effect from the solvent volume. Furthermore, it indicated the order of significance of each factor; Catalyst Loading >> Reaction Time >> Solvent Volume (**Graph E2.10**).

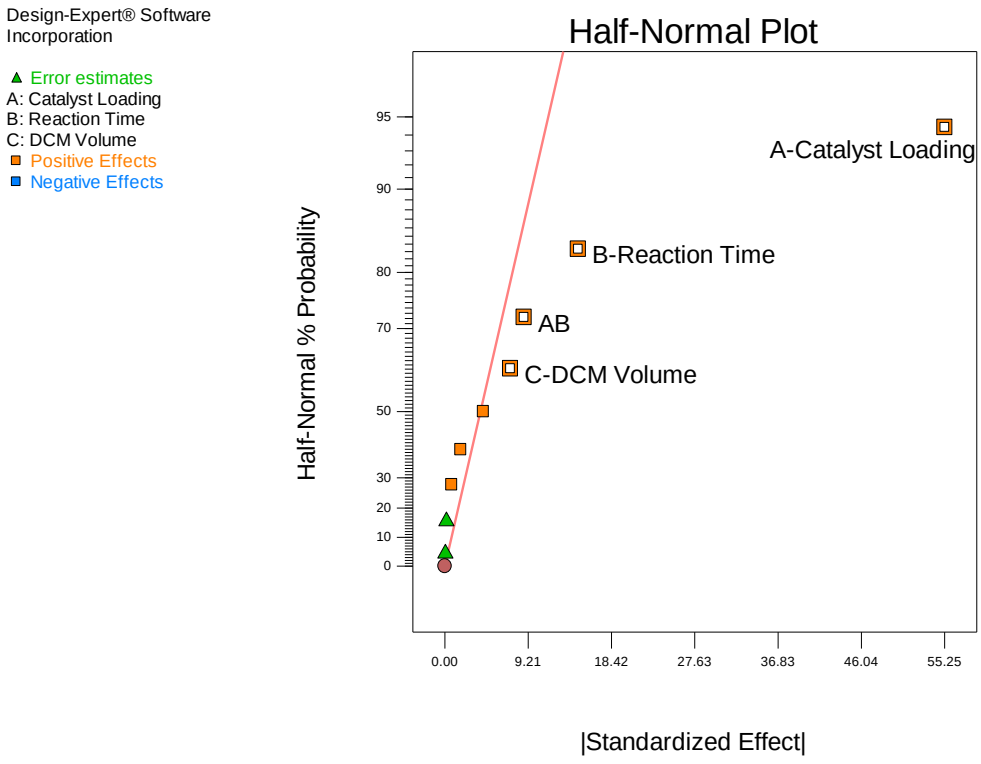

Graph E2.10

Further implementation of the design software generated **Graph E2.11**. By plotting reaction time and catalyst loading at the fixed optimal solvent volume (1 mL), it can be seen that moderately elevated catalyst loading and reaction time leads to the optimised conditions (5.0 mol% catalyst, 1 mL solvent, 3 h).

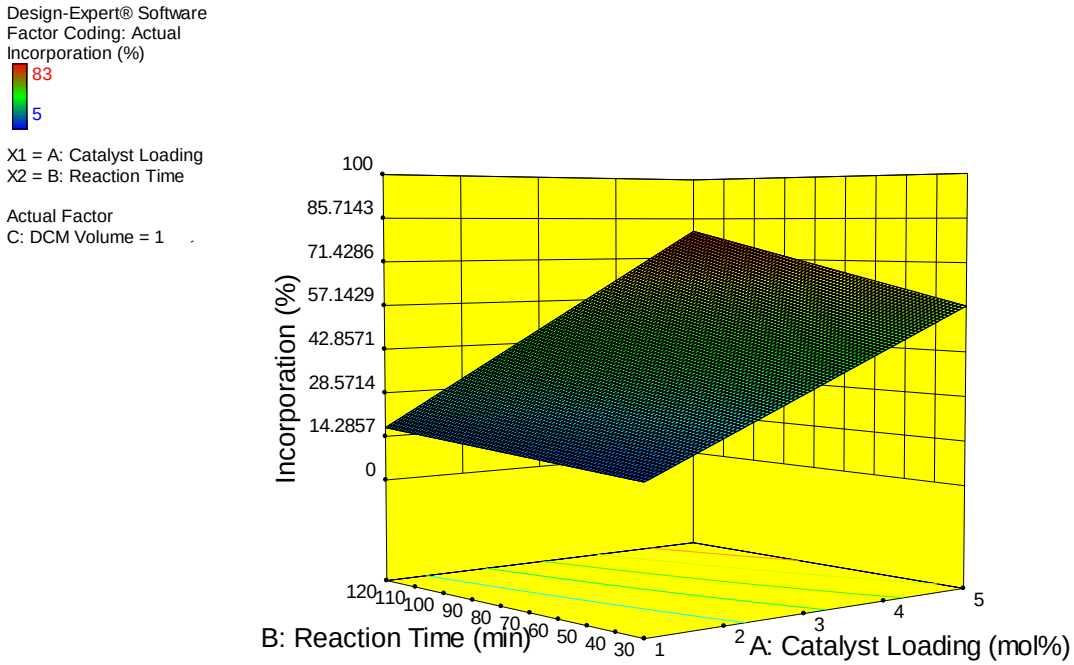

Graph E2.11

Finally, provided below is a graph of Residuals versus Predicted plot. This is a plot of the residuals versus the ascending predicted response values (low incorporation to high incorporation), and tests the assumption of constant variance in the data (**Graph E2.12**).

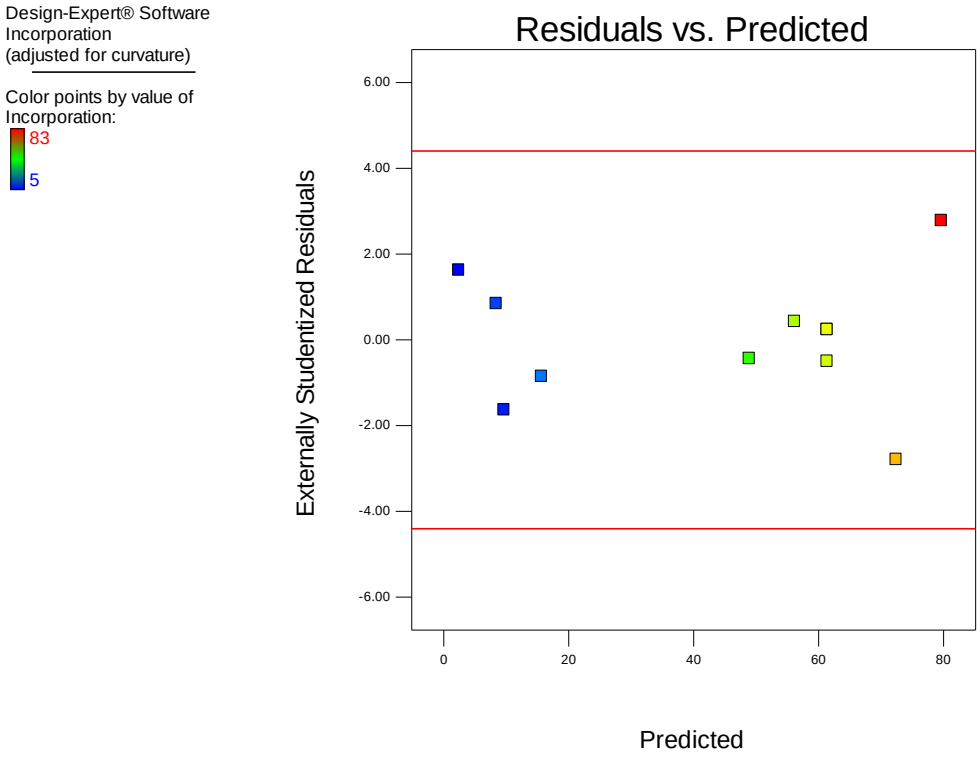
Design-Expert® Software
Incorporation
(adjusted for curvature)
Color points by value of
Incorporation:
83
5
Residuals vs. Predicted
Externally Studentized Residuals
6.00
4.00
2.00
0.00
-2.00
-4.00
-6.00
0
20
40
60
80
Predicted

Graph E2.12

Scheme 2.71 *HIE upon piperazines substrates.*

The reactions were carried out following general procedure A and analysed by LCMS to confirm the extent of exchange, position was confirmed through ^{1}H NMR.

Protocol 1			
Complex	***Solvent***	***Temperature (°C)***	***Time (h)***
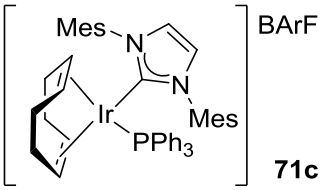 **71c** (1.5 mg, 0.86 µmol)	DCM (1 mL)	25	1

Protocol 2			
Complex	***Solvent***	***Temperature (°C)***	***Time (h)***
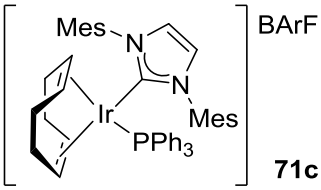 **71c** (7.4 mg, 4.30 µmol)	DCM (1 mL)	25	3

Substrate	***Data***
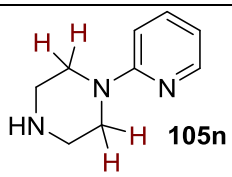 **105n** (14.1 mg, 0.086 mmol)	Data was consistent with that reported on page 424.

Protocol	***D-Incorporation (%)***		
	Run		***Average***
	1	***2***	
1	17	18	18
2	89	89	89

Substrate	***^{1}H NMR data***[185]
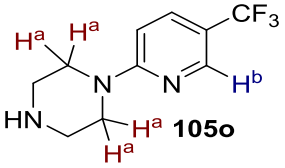 (19.9 mg, 0.086 mmol)	**^{1}H NMR** (300 MHz, DMSO): δ 8.37 (1H, br s, Ar-H), 7.73 (1H, dd *J* = 9.1 Hz, ^{4}*J* = 2.7 Hz, Ar-H), 6.88 (1H, d *J* = 9.1 Hz, Ar-H), 3.59-3.48 (4H, m, N-CH_2), 2.88-2.60 (4H, m, NH-CH_2). Incorporation expected at δ 3.59-3.48. Determined against integral at δ 2.88-2.60.
	LCMS data
	Retention time: 1.12 min; Mass ion: 232.3 $(M+H)^+$

Protocol	***D-Incorporation (%)***					
	Run				***Average***	
	1		***2***			
	D^a	***D^b***	***D^a***	***D^b***	***D^a***	***D^b***
1	11	0	10	0	11	0
2	80	19	77	15	79	17

Substrate	***^{1}H NMR data***[186]
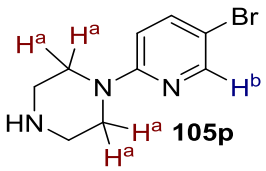 (20.8 mg, 0.086 mmol)	**^{1}H NMR** (300 MHz, DMSO): δ 8.40 (1H, br s, Ar-H), 7.77 (1H, dd *J* = 9.2 Hz, ^{4}*J* = 2.5 Hz, Ar-H), 6.92 (1H, d *J* = 9.4 Hz, Ar-H), 3.64-3.46 (4H, m, N-CH_2), 2.88-2.71 (4H, m, NH-CH_2). Incorporation expected at δ D^a 3.64-3.46, D^b 8.40. Determined against integral at δ 2.88-2.71.
	LCMS data
	Retention time: 2.24 min; Mass ion: 243.0 $(M+H)^+$

Protocol	***D-Incorporation (%)***					
	Run				***Average***	
	1		***2***			
	D^a	***D^b***	***D^a***	***D^b***	***D^a***	***D^b***
1	24	0	23	0	24	0
2	90	30	94	38	92	34

Substrate	***^{1}H NMR data***[187]
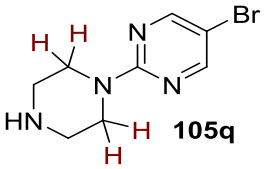 **105q** (20.8 mg, 0.086 mmol)	**^{1}H NMR** (300 MHz, DMSO): 8.46 (2H, br s, Ar-H), 3.89-3.75 (4H, m, N-CH_2), 2.90-2.78 (4H, m, NH-CH_2). Incorporation expected at δ 3.89-3.75. Determined against integral at δ 2.90-2.78.
	LCMS data
	Retention time: 2.24 min; Mass ion: 244.1 $(M+H)^+$

Protocol	***D-Incorporation (%)***		
	Run		***Average***
	1	***2***	
1	7	6	7
2	75	79	77

Substrate	***^{1}H NMR data***[188]
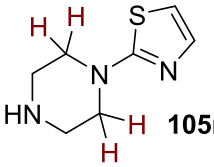 **105r** (14.6 mg, 0.086 mmol)	**^{1}H NMR** (300 MHz, DMSO): δ 7.14 (1H, d *J* = 3.6 Hz, Ar-H), 6.79 (1H, d *J* = 3.6 Hz, Ar-H), 3.36-3.26 (4H, m, N-CH_2), 2.83-2.73 (4H, m, NH-CH_2). Incorporation expected at δ 3.36-3.26. Determined against integral at δ 2.83-2.73.
	LCMS data
	Retention time: 0.29 min; Mass ion: 170.1 $(M+H)^+$

Protocol	***D-Incorporation (%)***		
	Run		***Average***
	1	***2***	
1	29	30	30
2	87	91	89

Substrate	***^{1}H NMR data***[189]
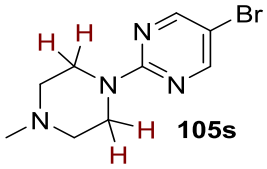 **105s** (22.1 mg, 0.086 mmol)	**^{1}H NMR** (300 MHz, DMSO): δ 8.42 (2H, s, Ar-H), 3.76-3.63 (4H, m, N-CH_2), 2.38-2.29 (4H, m, NMe-CH_2), 2.19 (3H, s, N-CH_3). Incorporation expected at δ 3.76-3.63. Determined against integral at δ 2.19.
	LCMS data
	Retention time: 0.41 min; Mass ion: 259.2 $(M+H)^+$

Protocol	***D-Incorporation (%)***		
	Run		***Average***
	1	***2***	
1	91	92	92

Substrate	***^{1}H NMR data***[190]
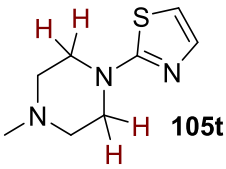 **105t** (15.8 mg, 0.086 mmol)	**^{1}H NMR** (300 MHz, DMSO): δ 7.15 (1H, d *J* = 3.6 Hz, Ar-H), 6.81 (1H, d *J* = 3.6 Hz, Ar-H), 3.43-3.33 (4H, m N-CH_2), 2.46-2.35 (4H, m, NMe-CH_2), 2.21 (3H, s, N-CH_3). Incorporation expected at δ 3.43-3.33. Determined against integral at δ 2.21.
	LCMS data
	Retention time: 0.29 min; Mass ion: 184.1 $(M+H)^+$

Protocol	***D-Incorporation (%)***		
	Run		***Average***
	1	***2***	
1	79	81	80

Substrate	***^{1}H NMR data***[191]
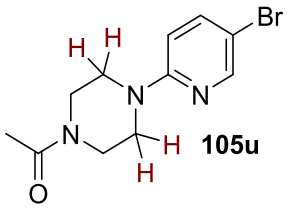 **105u** (24.4 mg, 0.086 mmol)	**^{1}H NMR** (300 MHz, DMSO): δ 8.17 (1H, d ^2J = 2.8 Hz, Ar-H), 7.69 (1H, 1H, dd *J* = 9.1 Hz, ^2J = 2.7 Hz, Ar-H), 6.83 (1H, d *J* = 9.2 Hz, Ar-H), 3.61-3.38 (8H, m, CH_2), 2.01 (3H, s, N-CH_3). Incorporation expected at δ 3.61-3.38. Determined against integral at δ 2.01.
	LCMS data
	Retention time: 2.32 min; Mass ion: 284.2 $(M+H)^+$

Protocol	***D-Incorporation (%)***		
	Run		***Average***
	1	***2***	
1	94	96	95

Regioselectivity could not be assigned by ^{1}H NMR, as such the isotopic distribution from the LCMS analysis is supplied in **Table E2.14**, alongside the mass spectrum of the starting material **105u** and labelled product **D105u Figure E2.1**. This analysis, shows a maximum ion of M+4 (D4), indicative of only four labelling sites instead of the maximum of M+8 (D8) expected if 8 sites were labelled. Using this information and the previous results with **105d**, we are confident that labelling is only directed by the pyridyl group.

Mass ion		284 D0	285 D1	286 D2	287 D3	288 D4	289 D5	290 D6	291 D7	292 D8
Relative abundance (%)	**105u**	47.3	5.4	41.4	5.7	0	0	0	0	0
	D105u	0	0	1.5	10.0	37.2	14.1	32.9	4.3	0

Table E2.14

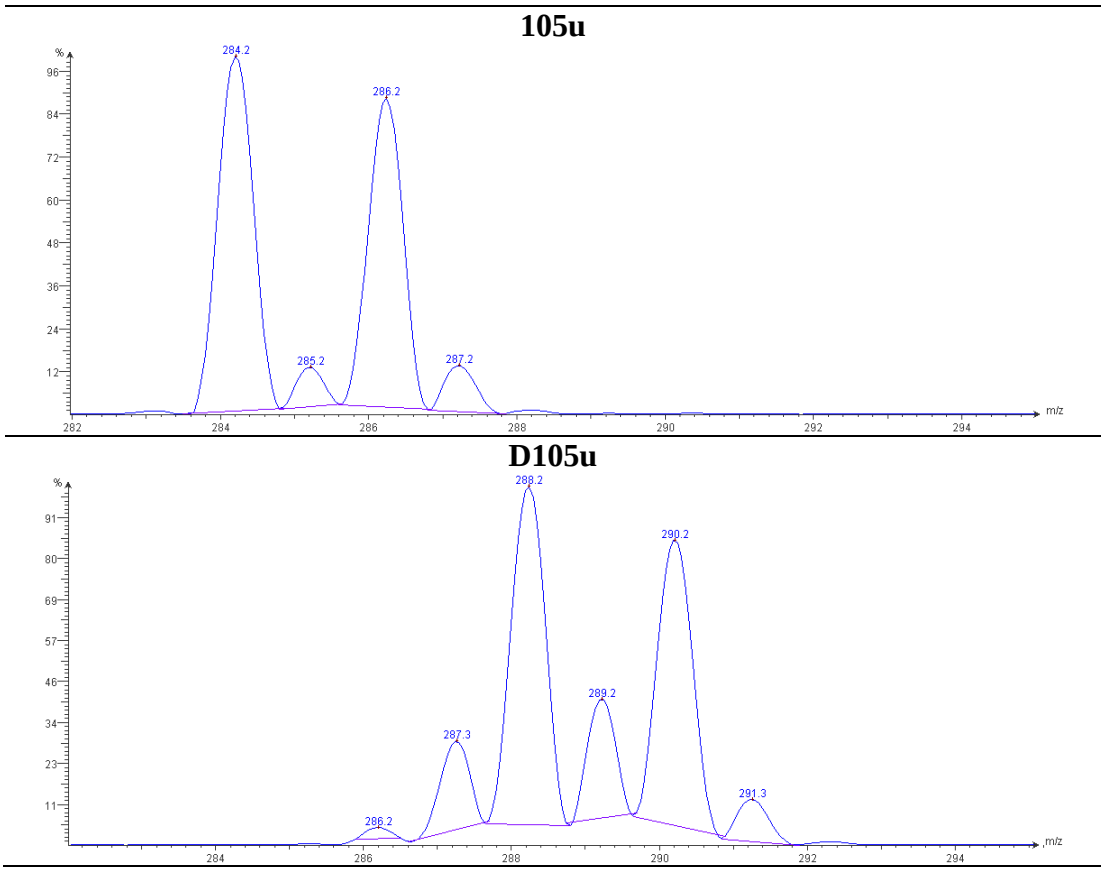
105u
284.2
285.2
286.2
287.2
D105u
286.2
287.3
288.2
289.2
290.2
291.3
m/z

Figure E2.1

Figure 2.14 *NMR studies examining the catalyst deactivation with piperazines.*

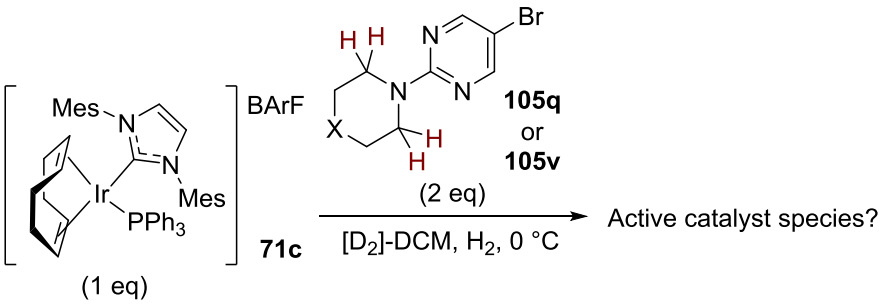

SchemeE2.1

In an oven dried NMR tube, substrate (**105v**: 4.8 mg, 0.02 mmol or **105q**: 4.9 mg, 0.02 mmol), catalyst **71c** (10 mg, 0.01 mmol) and [D_2]-DCM (0.5 mL) were added and the tube capped with a rubber septum. Hydrogen was bubbled through the solution at a constant rate for 5 min to activate the catalyst, and a red to yellow colour change was observed. Following the catalyst activation, the NMR tube was cooled to 0 °C in an ice bath prior to its introduction into the NMR machine. ^{31}P NMR spetrcoscopic experiments were run at 0 °C for to observe changes in the active catalytic species (**SchemeE2.1**).

^{31}P NMR spectroscopic data for the experiments are displayed below (**Figure E2.2**). "Prior to activation" refers to experiments run prior to catalyst activation with H_2, and "activated with H_2" refers to experiments run after catalyst activation with H_2.

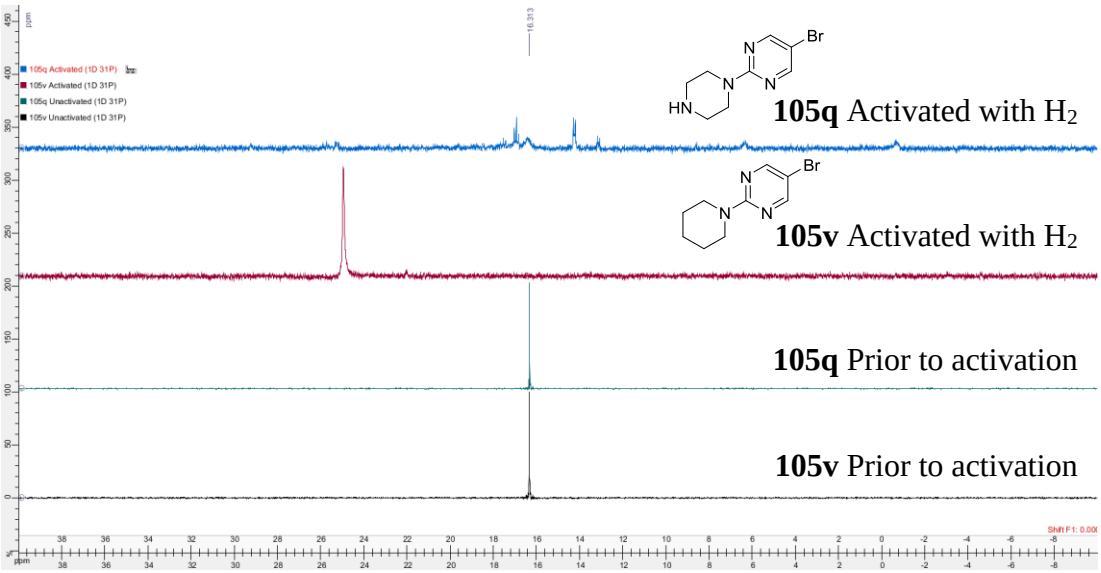

Figure E2.2

Scheme 2.72 *Investigating HIE upon different sized N-heterocycles.*

The reactions were carried out following general procedure A and analysed by LCMS to confirm the extent of exchange. The position was confirmed through ^{1}H NMR spectroscopy.

Protocol 1			
Complex	***Solvent***	***Temperature (°C)***	***Time (h)***
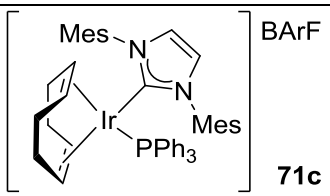 (1.5 mg, 0.86 µmol)	DCM (1 mL)	25	1

Protocol 2			
Complex	***Solvent***	***Temperature (°C)***	***Time (h)***
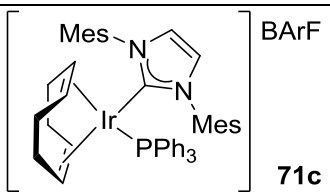 (7.4 mg, 4.30 µmol)	DCM (1 mL)	25	3

Substrate	***^{1}H NMR data***[192]
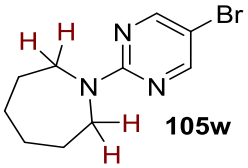 (22.0 mg, 0.086 mmol)	**^{1}H NMR** (300 MHz, DMSO): δ 8.39 (2H, br s, Ar-H), 3.73-3.60 (4H, m, N-CH_2), 1.77-1.61 (4H, m, CH_2), 1.54-1.39 (4H, m, CH_2). Incorporation expected at δ 3.73-3.60. Determined against integral at δ 1.54-1.39.
	LCMS data
	Retention time: 0.29 min; Mass ion: 184.1 $(M+H)^+$

Protocol	***D-Incorporation (%)***		
	Run		***Average***
	1	***2***	
1	49	45	47
2	83	84	84

Substrate	***^{1}H NMR data***[193]
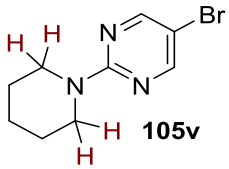 **105v** (20.8 mg, 0.086 mmol)	**^{1}H NMR** (300 MHz, DMSO): δ 8.38 (2H, br s, Ar-H), 3.75-3.62 (4H, m, N-CH_2), 1.66-1.56 (2H, m, CH_2), 1.55-1.43 (4H, m, CH_2). Incorporation expected at δ 3.75-3.62. Determined against integral at δ 1.55-1.43.
	LCMS data
	Retention time: 3.54 min; Mass ion: 242.1 $(M+H)^+$

D-Incorporation (%)		
Run		***Average***
1	***2***	
94	95	95

Substrate	***^{1}H NMR data***[194]
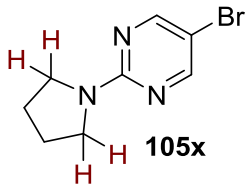 **105x** (19.6 mg, 0.086 mmol)	**^{1}H NMR** (300 MHz, DMSO): δ 8.40 (2H, br s, Ar-H), 3.53-3.38 (4H, m, N-CH_2), 2.01-1.85 (4H, m, CH_2). Incorporation expected at δ 3.53-3.38. Determined against integral at δ 2.01-1.85.
	LCMS data
	Retention time: 2.85 min; Mass ion: 228.1 $(M+H)^+$

Protocol	***D-Incorporation (%)***		
	Run		***Average***
	1	***2***	
1	52	62	57
2	93	94	94

Substrate	***^{1}H NMR data***[195]
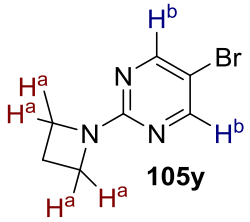 **105y** (18.4 mg, 0.086 mmol)	**^{1}H NMR** (300 MHz, DMSO): δ 8.40 (2H, br s, Ar-H), 4.02 (4H, t J = 7.5 Hz, N-CH_2), 2.30 (2H, quin J = 7.6 Hz, CH_2). Incorporation expected at δ D^a 4.02, D^b 8.40. Determined against integral at δ 2.30.
	LCMS data
	Retention time: 2.30 min; Mass ion: 214.0 $(M+H)^+$

Protocol	***D-Incorporation (%)***					
	Run				***Average***	
	1		***2***			
	D^a	***D^b***	***D^a***	***D^b***	***D^a***	***D^b***
1	0	0	0	0	0	0
2	0	13	0	15	0	14

Scheme 2.73 *Reassessing the catalyst choice for carbonyl directed HIE.*

The reactions were carried out following general procedure A and analysed by LCMS to confirm the extent of exchange. The position was confirmed through ^{1}H NMR spectroscopy of the highest incorporation result (**Table E2.10**).

Solvent	***Temperature (°C)***	***Time (h)***
MTBE (1 mL)	50	3
Substrate	***Data***	
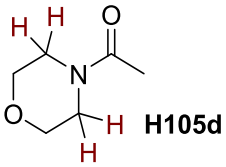 **H105d** (11.1 mg, 0.086 mmol)	Data was consistent with that reported on page 419.	

Entry	*Complex*	*D-Incorporation (%)*		
		Run		*Average*
		1	*2*	
1	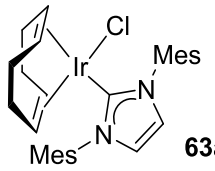 **63a** (2.8 mg, 0.0043 mmol)	0	0	0
2	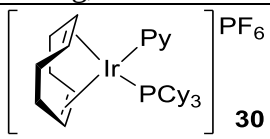 **30** (3.5 mg, 0.0043 mmol)	0	0	0
3	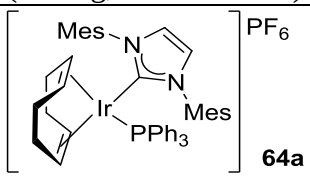 **64a** (4.4 mg, 0.0043 mmol)	0	0	0
4	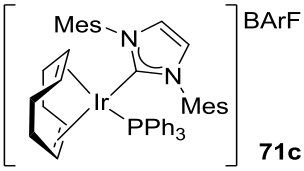 **71c** (7.4 mg, 0.0043 mmol)	12	11	12
5	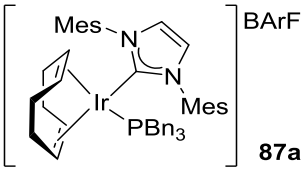 **87a** (7.6 mg, 0.0043 mmol)	91	92	92
6	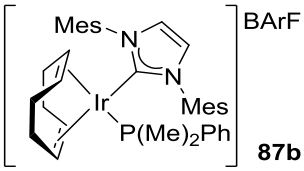 **87b** (6.9 mg, 0.0043 mmol)	62	70	66
7	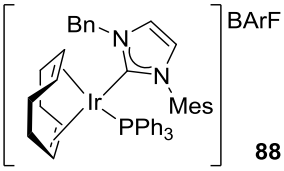 **88** (6.8 mg, 0.0043 mmol)	0	0	0

Table E2.15

Design of experiments delivering the second protocol for carbonyl directed HIE

Experimental design was used to assess the effect of varying the catalyst loading, reaction time and solvent volume. As such 'high' and 'low' values for each of the three variables were chosen. To generate a series of experiments to study optimal conditions within the variable ranges chosen, Design Expert™ software v10.0 (Stat_Ease Inc., Minneappolis, Mn) was used. This generated a *two-level, three-factorial* design containing three centre points, giving 11 experiments in total. The deuterium incorporation of **D105d** was used as the response. The reactions were carried out according to general procedure A and analysed by LCMS to confirm the extent of exchange. The position of exchange was confirmed through ^{1}H NMR spectroscopy of the three centre point results (**Table E2.16**).

Complex	***Solvent***
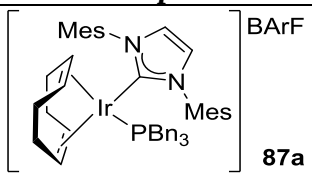 **87a**	DCM (1 mL)
Substrate	***Data***
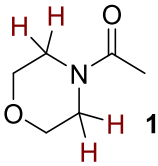 **105d** (11.1 mg, 0.086 mmol)	Data was consistent with that reported on page 419.

***Run*[a]**	***Variable A: Catalyst Loading* (mol%)**	***Amount of 87a (mg (µmol))***	***Variable B: Reaction Time* (min)**	***Variable C: Reaction Temperature (°C)***	***Response: Incorporation* (%D)**
1 (+-+)	5.0	7.6 (4.30)	60	45	62
2 (--+)	1.0	1.5 (0.86)	60	45	7
3 (***)	3.0	4.6 (2.58)	90	35	17
4 (***)	3.0	4.6 (2.58)	90	35	17
5 (++-)	5.0	7.6 (4.30)	120	25	17
6 (+--)	5.0	7.6 (4.30)	60	25	18
7 (---)	1.0	1.5 (0.86)	60	25	4
8 (***)	3.0	4.6 (2.58)	90	35	18
9 (+++)	5.0	7.6 (4.30)	120	45	62
10 (-+-)	1.0	1.5 (0.86)	120	25	3
11 (-++)	1.0	1.5 (0.86)	120	45	7

[a] symbol in parentheses indicate points in the design; + high, * mid and – low.

Table E2.16

Runs 3, 4 and 8 represent the centre points of the design. These are employed in order to:

(i) Assess any curvature in the response of incorporation changes in the variables; and

(ii) Assess the repeatability of the hydrogen isotope exchange reaction.

A response surface was created in the same design program. This generated a half-normal plot inferring that increasing the catalyst loading and reaction temperature had a positive impact upon the HIE reaction, with no effect from altering the reaction time. Furthermore, it indicated the order of significance of each factor; Catalyst Loading > Reaction Temperature >> Reaction Time. Notably, a combination of both reaction temperature and catalyst loading were shown to also positively impact the reaction (**Graph E2.13**).

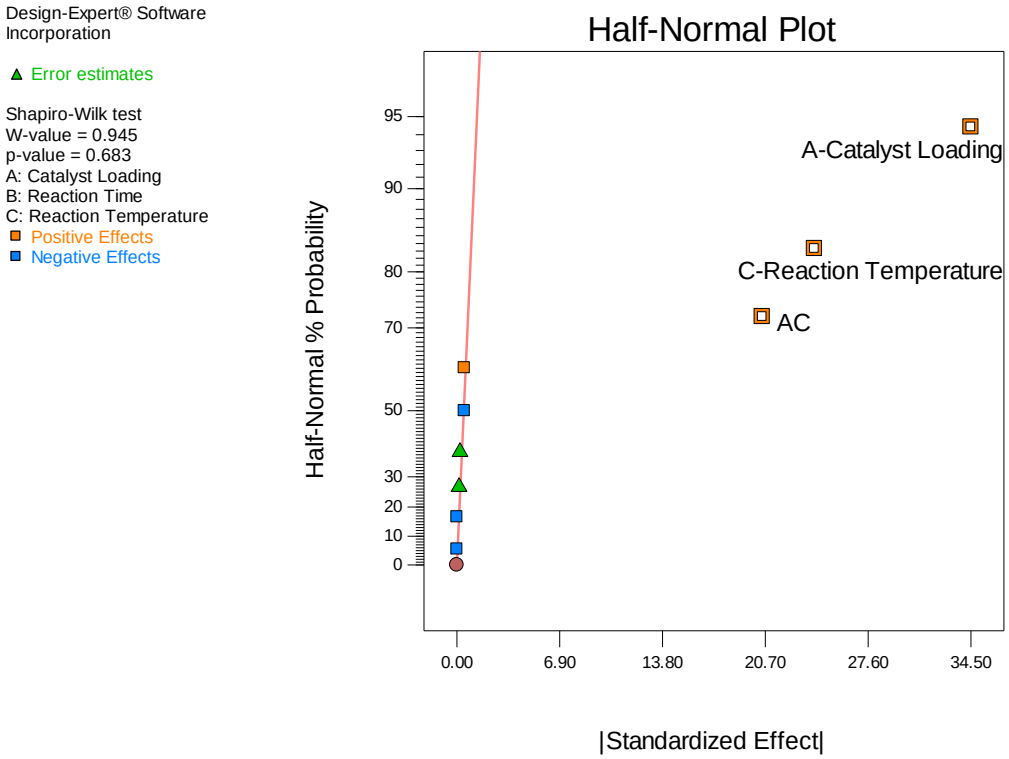

Graph E2.13

Further implementation of the design software generated **Graph E2.14**. By plotting reaction temperature and catalyst loading at the fixed optimal reaction time (1 h), it can be seen that moderately elevated catalyst loading and reaction temperature leads to the optimised conditions (5.0 mol% catalyst, 50 °C, 1 h).

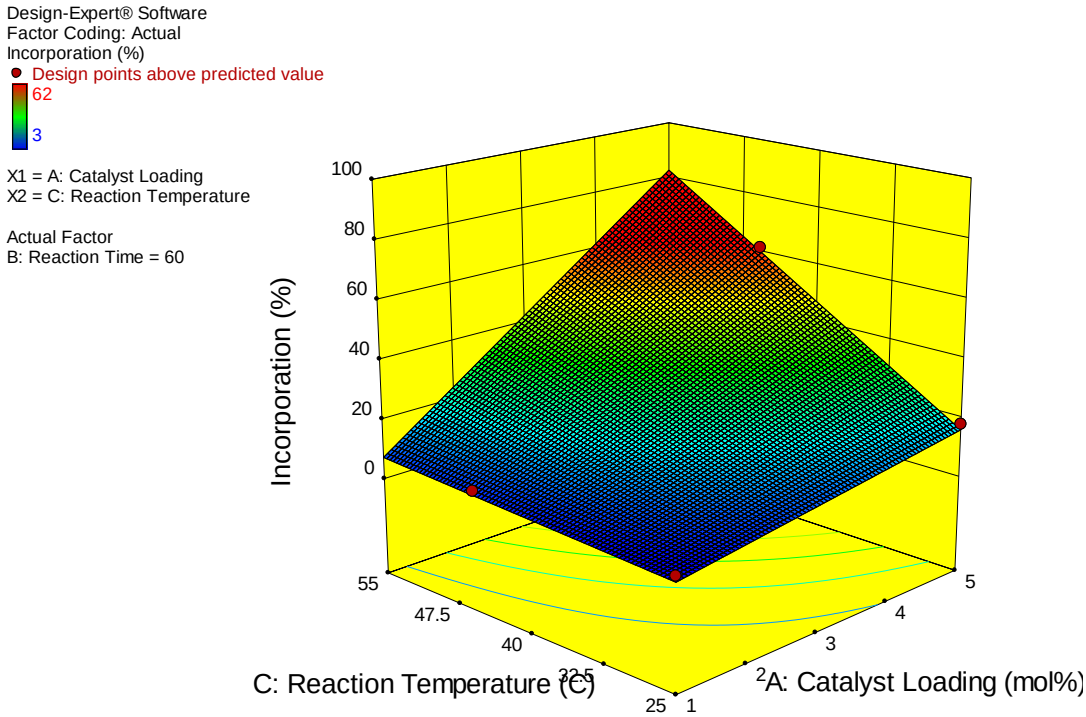

Graph E2.14

Finally, provided below is a graph of Residuals versus Predicted plot. This is a plot of the residuals versus the ascending predicted response values (low incorporation to high incorporation), and tests the assumption of constant variance in the data (**Graph E2.15**). In this case significant clustering of the data points suggests a poor fit for the design. Despite this, the data recovered from the reactions was still used to generate a new protocol for carbonyl directed HIE.

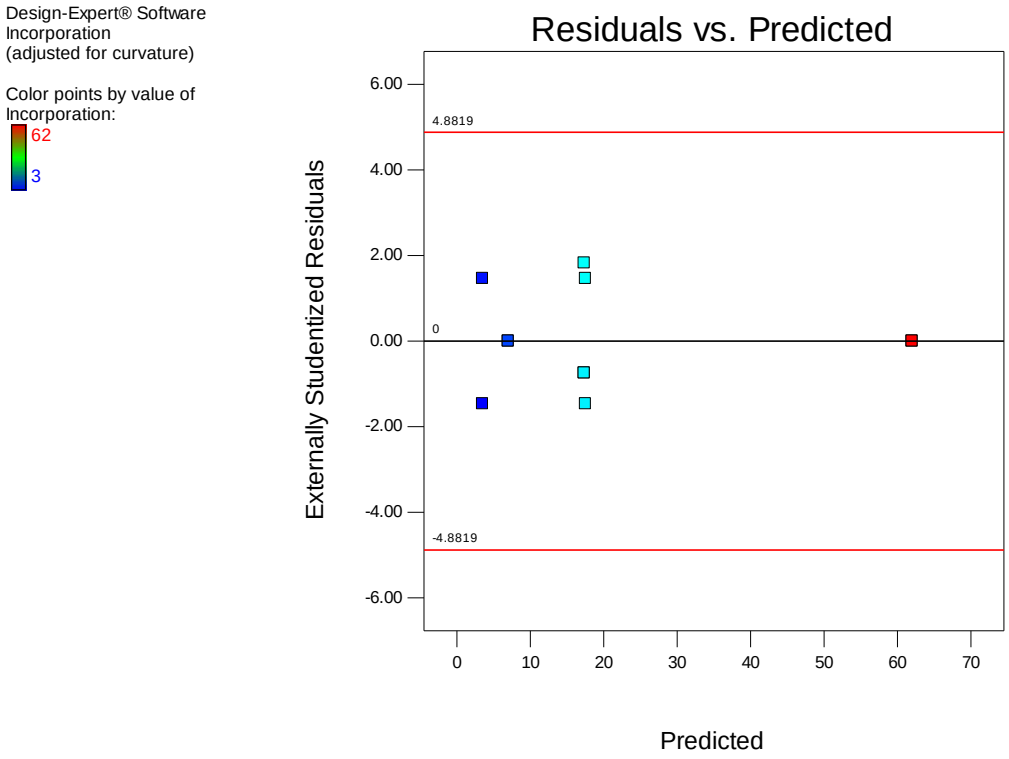
Design-Expert® Software
Incorporation
(adjusted for curvature)
Color points by value of
Incorporation:
62
3
Residuals vs. Predicted
Externally Studentized Residuals
6.00
4.00
2.00
0.00
-2.00
-4.00
-6.00
4.8819
0
-4.8819
0
10
20
30
40
50
60
70
Predicted

Graph E2.15

Scheme 2.74 *sp^3 HIE with carbonyl directing groups.*

The reactions were carried out following general procedure A and analysed by LCMS to confirm the extent of exchange, position was confirmed through ^{1}H NMR.

Complex	***Solvent***	***Temperature (°C)***	***Time (h)***
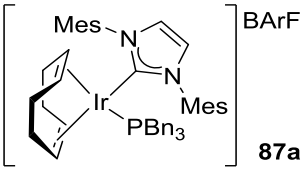 **87a** (7.6 mg, 4.30 μmol)	MTBE (1 mL)	50	1

Substrate	***data***
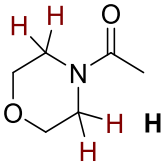 **H105d** (11.1 mg, 0.086 mmol)	Data was consistent with that reported on page 419.

D-Incorporation (%)		
Run		***Average***
1	***2***	
84	80	82

Substrate	***Data***
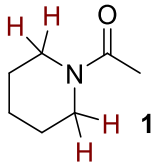 **105m** (10.9 mg, 0.086 mmol)	Data was consistent with that reported on page 423.

D-Incorporation (%)		
Run		***Average***
1	***2***	
60	62	61

Substrate	***^{1}H NMR data***[196]
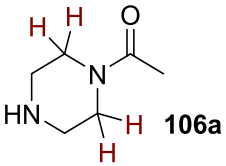 **106a** (11.0 mg, 0.086 mmol)	**^{1}H NMR** (300 MHz, DMSO): δ 3.55-3.51 (2H, m, N-C$\underline{H}_2$), 3.40-3.37 (2H, m, N-C$\underline{H}_2$), 2.83-2.76 (4H, m, NH-C$\underline{H}_2$), 2.04 (3H, s, CO-C$\underline{H}_3$). Incorporation expected at δ 3.55-3.51 & 3.40-3.37. Determined against integral at δ 2.04. ***LCMS data*** Retention time: 0.32 min; Mass ion: 129.1 $(M+H)^+$

D-Incorporation (%)		
Run		***Average***
1	***2***	
0	0	0

Substrate	***^{1}H NMR data***[197]
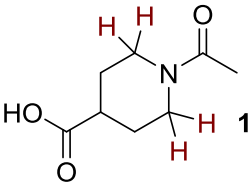 **106b** (14.7 mg, 0.086 mmol)	**^{1}H NMR** (300 MHz, DMSO): δ 3.81-3.68 (2H, m, N-C$\underline{H}_2$), 2.74-2.53 (2H, m, N-C$\underline{H}_2$), 2.39-2.31 (1H, m, C$\underline{H}$), 2.04 (3H, s, CO-C$\underline{H}_3$), 1.87-1.80 (2H, m, C$\underline{H}_2$), 1.52-1.43 (2H, m, C$\underline{H}_2$). Incorporation expected at δ 3.81-3.68 & 2.74-2.53. Determined against integral at δ 2.04. ***LCMS data*** Retention time: 0.55 min; Mass ion: 172.1 $(M+H)^+$

D-Incorporation (%)		
Run		***Average***
1	***2***	
17	18	18

Substrate	***^{1}H NMR data***[198]
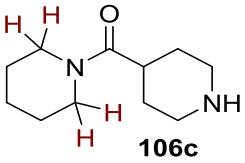 **106c** (16.8 mg, 0.086 mmol)	**^{1}H NMR** (300 MHz, DMSO): δ 3.61-3.50 (2H, m, N-C$\underline{H}_2$), 3.47-3.30 (2H, m, N-C$\underline{H}_2$), 3.20-3.06 (2H, m, N-C$\underline{H}_2$), 2.71-2.53 (3H, m, N-C$\underline{H}_2$ & C$\underline{H}$), 1.75-1.60 (6H, m, C$\underline{H}_2$), 1.59-1.43 (4H, m, C$\underline{H}_2$). Incorporation expected at δ 3.61-3.50 & 3.47-3.30. Determined against integral at δ 1.59-1.43. ***LCMS data*** Retention time: 0.40 min; Mass ion: 211.2 $(M+H)^+$

D-Incorporation (%)		
Run		***Average***
1	***2***	
0	0	0

Scheme 2.75 *Further solvent scope with problematic substrates*.

The reactions were carried out following general procedure A and analysed by LCMS to confirm the extent of exchange. The position was confirmed through ^{1}H NMR spectroscopy.

Complex	***Solvent***	***Temperature (°C)***	***Time (h)***
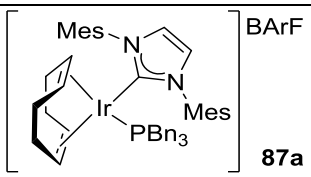 (7.6 mg, 4.30 µmol)	(1 mL)	50	1

Substrate	***^{1}H NMR data***[199]
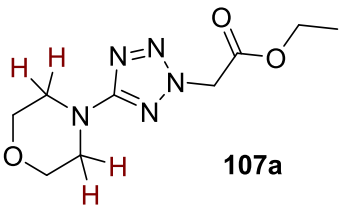 (20.7 mg, 0.086 mmol)	**^{1}H NMR** (300 MHz, DMSO): δ 5.53 (2H, s, N-C<u>H</u>$_2$-CO), 4.19 (2H, q *J* = 7.1 Hz, O-C<u>H</u>$_2$), 3.77-3.63 (4H, m, O-C<u>H</u>$_2$), 3.34-3.29 (4H, m, N-C<u>H</u>$_2$), 1.21 (3H, t *J* = 7.1 Hz, CH$_2$-C<u>H</u>$_3$). Incorporation expected at δ 3.34-3.29. Determined against integral at δ 1.21. ***LCMS data*** Retention time: 2.14 min; Mass ion: 242.1 $(M+H)^+$

Solvent	***D-Incorporation (%)***		
	Run		***Average***
	1	***2***	
t-BuOAc	94	95	95

Substrate	***^{1}H NMR data***[200]
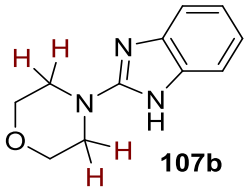 (17.5 mg, 0.086 mmol)	**^{1}H NMR** (300 MHz, DMSO): δ 7.25-7.14 (2H, m, Ar-<u>H</u>), 6.97-6.87 (2H, m, Ar-<u>H</u>), 3.75-3.64 (4H, m, O-C<u>H</u>$_2$), 3.51-3.40 (4H, m, N-C<u>H</u>$_2$). Incorporation expected at δ 3.51-3.40. Determined against integral at δ 6.97-6.87. ***LCMS data*** Retention time: 0.34 min; Mass ion: 204.2 $(M+H)^+$

Solvent	***D-Incorporation (%)***		
	Run		***Average***
	1	***2***	
2-MeTHF	85	89	87

Substrate	***^{1}H NMR data***[201]
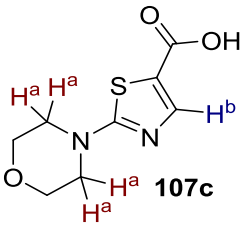 **107c** (18.4 mg, 0.086 mmol)	**^{1}H NMR** (300 MHz, DMSO): δ 7.26 (1H, s, Ar-H), 3.73-3.65 (4H, O-C$\underline{H_2}$), 3.52-3.42 (4H, N-C$\underline{H_2}$). Incorporation expected at δ D^a 3.52-3.42, D^b 7.26. Determined against integral at δ 3.73-3.65.
	LCMS data
	Retention time: 1.47 min; Mass ion: 215.1 $(M+H)^+$

Solvent	***D-Incorporation (%)***					
	Run				***Average***	
	1		***2***			
	D^a	***D^b***	***D^a***	***D^b***	***D^a***	***D^b***
2-MeTHF	91	76	92	75	92	75

Scheme 2.76 *HIE upon non-cyclic substrates.*

The reactions were carried out following general procedure A and analysed by LCMS to confirm the extent of exchange. The position was confirmed through ^{1}H NMR spectroscopy.

Protocol 1			
Complex	***Solvent***	***Temperature (°C)***	***Time (h)***
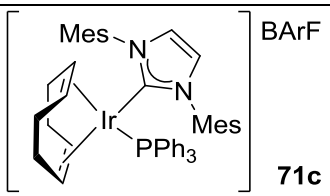 **71c** (1.5 mg, 0.86 μmol)	DCM (1 mL)	25	1

Protocol 2			
Complex	***Solvent***	***Temperature (°C)***	***Time (h)***
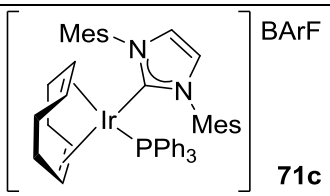 **71c** (7.4 mg, 4.30 μmol)	DCM (1 mL)	25	3

Protocol 3			
Complex	***Solvent***	***Temperature (°C)***	***Time (h)***
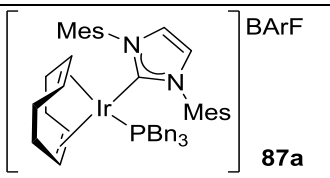 **87a** (7.6 mg, 4.30 μmol)	MTBE (1 mL)	50	1

Substrate	***^{1}H NMR data***[202]
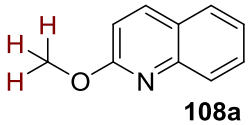 **108a** (13.7 mg, 0.086 mmol)	**^{1}H NMR** (300 MHz, DMSO): δ 8.21 (1H, d *J* = 8.9 Hz, Ar-H), 7.86 (1H, dd *J* = 7.8 Hz, ^4J = 1.6 Hz, Ar-H), 7.78 (1H, d *J* = 8.3 Hz, Ar-H), 7.65 (1H, ddd *J* = 8.4 Hz, 7.0 Hz, ^4J = 1.6 Hz, Ar-H), 7.42 (1H, ddd *J* = 8.1 Hz, 6.9 Hz, ^4J = 1.4 Hz, Ar-H), 7.00 (1H, d *J* = 8.9 Hz, Ar-H), 3.98 (3H, s, O-CH_3). Incorporation expected at δ 3.98. Determined against integral at δ 7.00.
	LCMS data
	Retention time: 3.00 min; Mass ion: 160.1 $(M+H)^+$

Protocol	***D-Incorporation (%)***		
	Run		***Average***
	1	***2***	
1	13	15	14
2	79	80	80

Substrate	***^{1}H NMR data***[203]
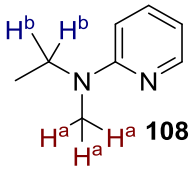 **108b** (11.7 mg, 0.086 mmol)	**^{1}H NMR** (300 MHz, DMSO): δ 8.04 (1H, dd *J* = 4.9 Hz, ^4J = 2.1 Hz, Ar-H), 7.45 (1H, ddd *J* = 8.7 Hz, 7.1 Hz, ^4J = 2.1 Hz, Ar-H), 6.57 (1H, d *J* = 8.7 Hz, Ar-H), 6.50 (1H, dd, *J* = 7.1 Hz, 4.8 Hz, Ar-H), 3.53 (2H, q *J* = 7.1 Hz, N-CH_2), 2.94 (3H, s, N-CH_3), 1.05 (3H, t *J* = 7.1 Hz, CH_2-CH_3). Incorporation expected at δ D^a 3.53, D^b 2.94. Determined against integral at δ 1.05.
	LCMS data
	Retention time: 0.30 min; Mass ion: 137.2 $(M+H)^+$

Protocol	***D-Incorporation (%)***					
	Run				***Average***	
	1		***2***			
	D^a	***D^b***	***D^a***	***D^b***	***D^a***	***D^b***
1	0	0	0	0	0	0
2	93	93	90	90	92	92

Substrate	***^{1}H NMR data***[204]
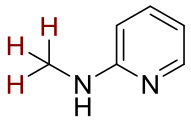 **108c** (9.3 mg, 0.086 mmol)	**^{1}H NMR** (300 MHz, DMSO): δ 7.96 (1H, dd *J* = 5.0 Hz, ^4J = 2.0 Hz, Ar-H), 7.34 (1H, ddd *J* = 8.4 Hz, 7.0 Hz, ^4J = 2.0 Hz, Ar-H), 6.50-6.37 (2H, m, Ar-H), 6.31 (1H, br s, N-H), 2.75 (3H, d *J* = 4.9 Hz, NH-CH_3). Incorporation expected at δ 2.75. Determined against integral at δ 7.34. ***LCMS data*** Retention time: 0.25 min; Mass ion: 109.2 $(M+H)^+$

Protocol	***D-Incorporation (%)***		
	Run		***Average***
	1	***2***	
1	0	0	0
2	33	41	37
3	88	85	87

Substrate	***^{1}H NMR data***[205]
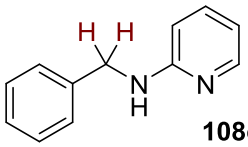 **108d** (15.8 mg, 0.086 mmol)	**^{1}H NMR** (300 MHz, DMSO): δ 7.94 (1H, dd *J* = 4.9 Hz, ^4J = 2.1 Hz, Ar-H), 7.41-7.14 (5H, m, Ar-H), 6.97-6.86 (1H, m, Ar-H), 6.55-6.39 (2H, m, Ar-H), 4.47 (2H, d ^4J = 6.1 Hz, NH-CH_2) Incorporation expected at δ 4.47. Determined against integral at δ 6.55-6.39. ***LCMS data*** Retention time: 0.25 min; Mass ion: 109.2 $(M+H)^+$

Protocol	***D-Incorporation (%)***		
	Run		***Average***
	1	***2***	
1	0	0	0
2	13	17	15
3	96	90	93

Scheme 2.77 *HIE upon FG-activated, non-cyclic, sp^3 positions.*

The reactions were carried out following general procedure A and analysed by LCMS to confirm the extent of exchange. The position was confirmed through ^{1}H NMR spectroscopy.

Protocol 1			
Complex	***Solvent***	***Temperature (°C)***	***Time (h)***
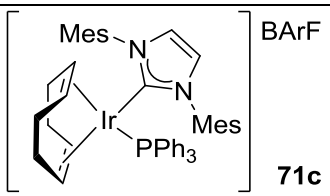 **71c** (1.5 mg, 0.86 µmol)	DCM (1 mL)	25	1

Protocol 2			
Complex	***Solvent***	***Temperature (°C)***	***Time (h)***
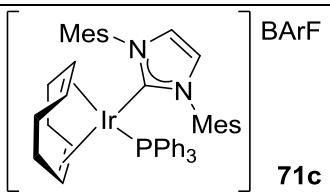 **71c** (7.4 mg, 4.30 µmol)	DCM (1 mL)	25	3

Substrate	***^{1}H NMR data***[206]
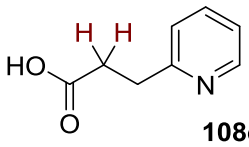 **108e** (13.0 mg, 0.086 mmol)	**^{1}H NMR** (300 MHz, DMSO): δ 12.10 (1H, br s, O-H), 8.46 (1H, dd *J* = 5.1 Hz, ^{4}*J* = 1.9 Hz, Ar-H), 7.68 (1H, dd *J* = 7.7 Hz, ^{4}*J* = 1.9 Hz, Ar-H), 7.26 (1H, d, *J* = 7.9 Hz, Ar-H), 7.19 (1H, dd *J* = 7.7 Hz, 5.0 Hz, Ar-H), 2.96 (2H, t *J* = 7.4 Hz, Ar-CH$_2$), 2.65 (2H, t *J* = 7.4 Hz, CO-CH$_2$). Incorporation expected at δ 2.65. Determined against integral at δ 7.68.
	LCMS data
	Retention time: 0.29 min; Mass ion: 134.1 (M+H)$^+$

Protocol	***D-Incorporation (%)***		
	Run		***Average***
	1	***2***	
1	16	15	16
2	64	66	65

Substrate	***^{1}H NMR data***[207]
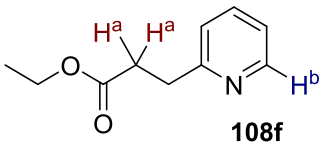 **108f** (15.4 mg, 0.086 mmol)	**^{1}H NMR** (300 MHz, DMSO): δ 8.45 (1H, d *J* = 4.9 Hz, Ar-H), 7.68 (1H, td *J* = 7.7 Hz, ^4J = 1.8 Hz, Ar-H), 7.26 (1H, d *J* = 7.5 Hz, Ar-H), 7.18 (1H, dd *J* = 7.3 Hz, 4.8 Hz, Ar-H), 4.02 (2H, q *J* = 7.2 Hz, O-CH$_2$), 2.99 (2H, t *J* = 7.3 Hz, Ar-CH$_2$), 2.72 (2H, t *J* = 7.3 Hz, CO-CH$_2$), 1.13 (3H, t *J* = 7.2 Hz, CH$_2$-CH$_3$). Incorporation expected at δ 2.72. Determined against integral at δ 1.13.
	LCMS data
	Retention time: 0.46 min; Mass ion: 180.2 $(M+H)^+$

Protocol	***D-Incorporation (%)***					
	Run				***Average***	
	1		***2***			
	D^a	***D^b***	***D^a***	***D^b***	***D^a***	***D^b***
1	0	0	0	0	0	0
2	26	11	20	9	23	10

Table 2.11 *Investigating the selectivity of sp^3 HIE.*

To allow quantification of the substrate and additive remaining after the reaction, each additive **90l-u** and substrate **104** were calibrated against an internal standard through LCMS analysis. The calibration results are detailed previously, apart from **104** and **90u**, which are given below:

Additive	***LCMS data***		
	Retention time (min)		***Mass ion***
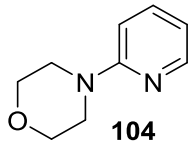 **104**	0.29		165.1 $(M+H)^+$
Mass (mg)	***Area***		***Additive / internal standard***
	Internal standard	***Additive***	
4.1	2500	480	0.192
7.5	3800	1400	0.368
10.3	2800	1300	0.464
14.6	4500	4500	0.711

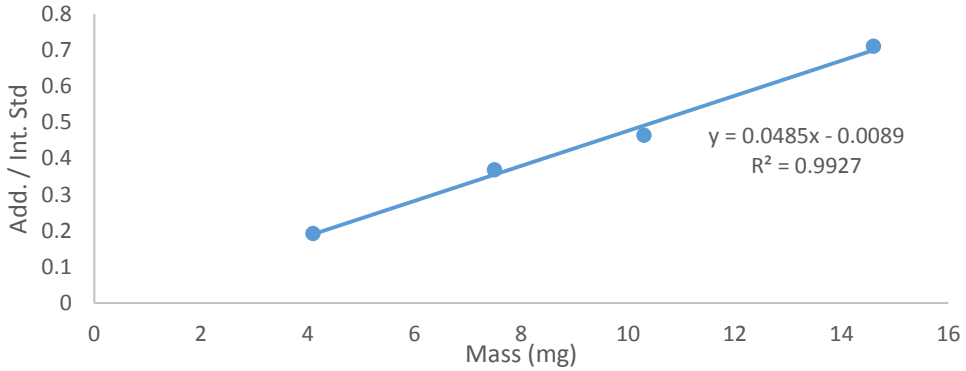

Additive	*LCMS data*		
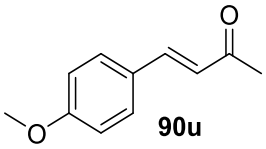 **90u**	*Retention time (min)*		*Mass ion*
	2.58		177.2 $(M+H)^+$
Mass (mg)	*Area*		*Additive / internal standard*
	Internal standard	*Additive*	
3.2	3000	81	0.027
7.3	4200	270	0.064
11.4	4100	390	0.095
15.1	2000	220	0.110

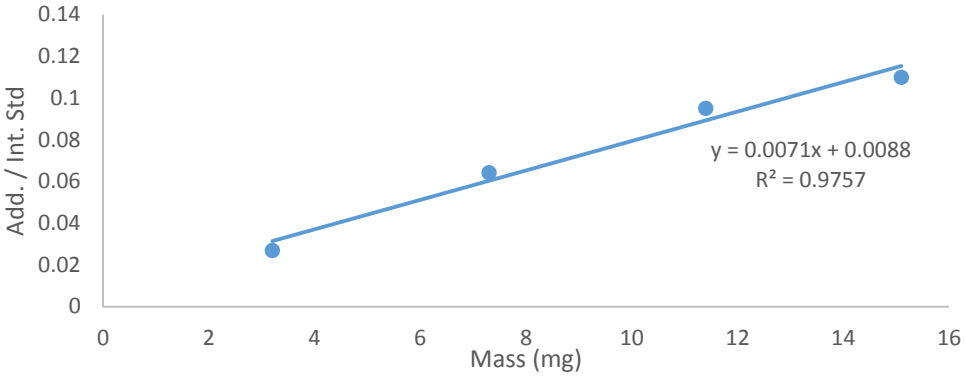

Following calibration, the reactions were carried out following general procedure A, which was modified by adding a stock solution of internal standard **S2** (1 mL of a 10 mg/mL solution) at the end of the reaction, and analysed by LCMS to confirm the extent of exchange and the amount of acid and additive remaining. The position of exchange in additives is assumed from similar known compounds.[45,47]

Internal Standard	*LCMS data*	
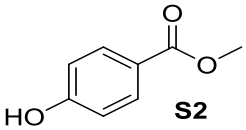 **S2** (10 mg)	*Retention time (min)*	*Mass ion*
	2.09	No mass ion observed

Complex	*Substrate*	*Solvent*	
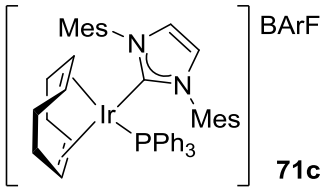 (1.5 mg, 0.86 µmol)	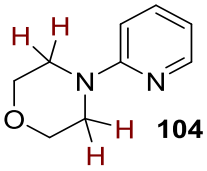 (14.1 mg, 0.086 mmol)	DCM (1 mL)	
		Temperature (°C)	*Time (h)*
		25	1

Additive	*Run*	*Add. yield (%)*	*Add. incorporation (%)*	*Sub. yield (%)*	*Sub. incorporation (%)*
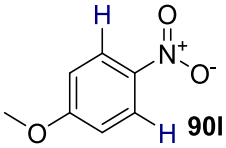 13.2 mg (0.086 mmol)	***1***	90	23	99	92
	2	96	24	93	95
	Average	93	24	96	94

Additive	*Run*	*Add. yield (%)*	*Add. incorporation (%)*	*Sub. yield (%)*	*Sub. incorporation (%)*
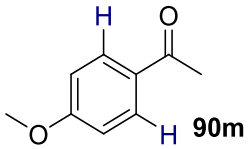 12.9 mg (0.086 mmol)	***1***	95	5	99	94
	2	96	6	99	93
	Average	96	6	99	94

Additive	*Run*	*Add. yield (%)*	*Add. incorporation (%)*	*Sub. yield (%)*	*Sub. incorporation (%)*
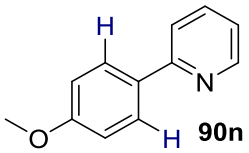 15.9 mg (0.086 mmol)	***1***	99	12	97	0
	2	90	16	93	0
	Average	95	14	95	0

Additive	*Run*	*Add. yield (%)*	*Add. incorporation (%)*	*Sub. yield (%)*	*Sub. incorporation (%)*
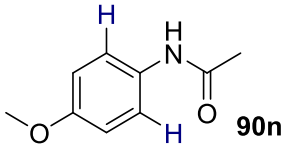 **90n** 14.4 mg (0.086 mmol)	***1***	99	0	93	80
	2	99	0	90	84
	Average	99	0	92	82

Additive	*Run*	*Add. yield (%)*	*Add. incorporation (%)*	*Sub. yield (%)*	*Sub. incorporation (%)*
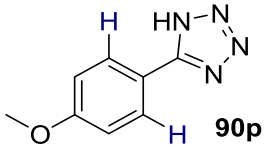 **90p** 15.2 mg (0.086 mmol)	***1***	90	24	99	0
	2	80	25	99	0
	Average	85	25	99	0

Additive	*Run*	*Add. yield (%)*	*Add. incorporation (%)*	*Sub. yield (%)*	*Sub. incorporation (%)*
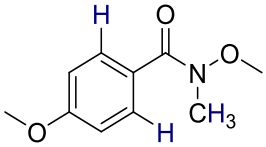 **90q** 16.8 mg (0.086 mmol)	***1***	97	17	95	91
	2	99	17	93	92
	Average	98	17	94	92

Additive	*Run*	*Add. yield (%)*	*Add. incorporation (%)*	*Sub. yield (%)*	*Sub. incorporation (%)*
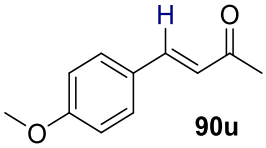 **90u** 16.8 mg (0.086 mmol)	***1***	90	38	90	88
	2	92	32	99	87
	Average	91	35	95	88

Scheme 2.78 *HIE upon substrates containing multiple labelling sites.*

The reactions were carried out following general procedure A and analysed by LCMS to confirm the extent of exchange, position was confirmed through ^{1}H NMR.

Complex	***Solvent***	***Temperature (°C)***	***Time (h)***
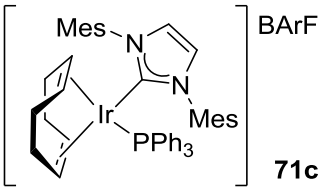 (1.5 mg, 0.86 µmol)	DCM (1 mL)	25	1

Substrate	***^{1}H NMR data***[208]
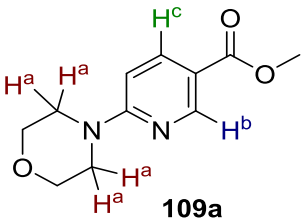 (19.1 mg, 0.086 mmol)	**^{1}H NMR** (300 MHz, DMSO): δ 8.65 (1H, d ^{4}J = 2.5 Hz, Ar-H), 7.96 (1H, dd J = 9.1 Hz, ^{4}J = 2.4 Hz, Ar-H), 6.87 (1H, d J = 9.2 Hz, Ar-H), 3.78 (3H, s, O-CH_3), 3.71-3.64 (4H, m, O-CH_2), 3.63-3.56 (4H, m, N-CH_2). Incorporation expected at δ D^a 3.71-3.64, D^b 8.65, D^c 7.96. Determined against integral at δ 3.78.
	LCMS data
	Retention time: 2.00 min; Mass ion: 223.2 $(M+H)^+$

D-Incorporation (%)								
Run						***Average***		
1			***2***					
D^a	***D^b***	***D^c***	***D^a***	***D^b***	***D^c***	***D^a***	***D^b***	***D^c***
92	4	0	94	5	0	93	5	0

Substrate	***^{1}H NMR data***[209]
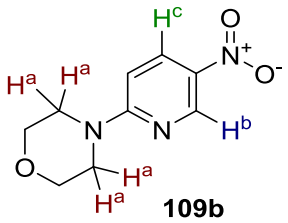 **109b** (19.1 mg, 0.086 mmol)	**^{1}H NMR** (300 MHz, DMSO): δ 8.96 (1H, d ^4J = 2.8 Hz, Ar-H), 8.23 (1H, dd J = 9.6 Hz, ^4J = 2.8 Hz, Ar-H), 6.93 (1H, d J = 9.6 Hz, Ar-H), 3.81-3.59 (8H, m, CH_2). Incorporation expected at δ D^a 3.81-3.59, D^b 8.96, D^c 8.23. Determined against integral at δ 6.93. ***LCMS data*** Retention time: 2.38 min; Mass ion: 210.1 $(M+H)^+$

D-Incorporation (%)								
Run						***Average***		
1			***2***					
D^a	***D^b***	***D^c***	***D^a***	***D^b***	***D^c***	***D^a***	***D^b***	***D^c***
89	90	53	85	91	60	87	91	57

Scheme 2.79, **Graph 2.12** *KIE experiment for sp^3 HIE.*

The reactions were carried out following general procedure A and analysed by LCMS to confirm the degree of deuterium (or hydrogen) incorporation. The position of exchange is assumerd based upon earlier results.

Complex	***Solvent***	***Temperature (°C)***
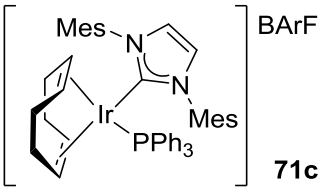 (1.5 mg, 0.86 µmol)	DCM (1 mL)	25

Substrate	***data***
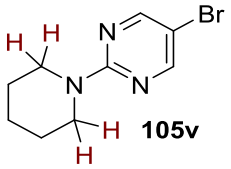 (20.8 mg, 0.086 mmol)	Data was consistent with that reported on page 436.

Time (min)	***H-Incorporation (%)***			
	Run			***Average***
	1	***2***	***3***	
5	31	33	31	32
7	44	46	47	46
9	60	61	61	61

Substrate	***^{1}H NMR data***[168]
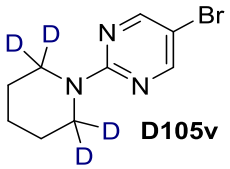 (21.1 mg, 0.086 mmol)	**^{1}H NMR** (300 MHz, DMSO): δ 8.38 (2H, br s, Ar-H), 3.75-3.62 (0.02H, m, N-CH$_2$), 1.66-1.56 (2H, m, CH$_2$), 1.55-1.43 (4H, m, CH$_2$). Incorporation expected at δ 3.75-3.62. Determined against integral at δ 1.55-1.43. ***LCMS data*** Retention time: 3.54 min; Mass ion: 242.1 (M+H)$^+$

Time (min)	***H-Incorporation (%)***			
	Run			***Average***
	1	***2***	***3***	
5	30	31	30	30
7	34	34	34	34
9	39	38	40	39

Scheme 2.80 *HIE on drug substrates.*

The reactions were carried out following general procedure A and analysed by LCMS to confirm the extent of exchange. The position was confirmed through ^{1}H NMR spectroscopy.

Protocol 1			
Complex	***Solvent***	***Temperature (°C)***	***Time (h)***
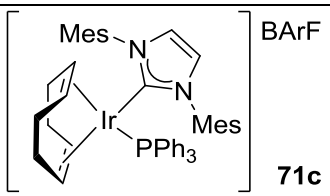 **71c** (1.5 mg, 0.86 μmol)	DCM (1 mL)	25	1

Protocol 2			
Complex	***Solvent***	***Temperature (°C)***	***Time (h)***
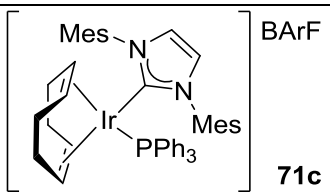 **71c** (7.4 mg, 4.30 μmol)	DCM (1 mL)	25	3

Protocol 2			
Complex	***Solvent***	***Temperature (°C)***	***Time (h)***
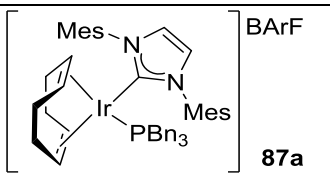 **87a** (7.6 mg, 4.30 μmol)	MTBE (1 mL)	50	1

Substrate	***^{1}H NMR data***[210]
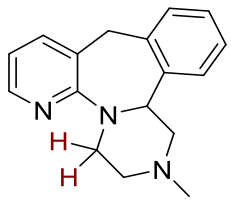 **110** - *Mirtazapine* (22.8 mg, 0.086 mmol)	**^{1}H NMR** (300 MHz, DMSO): δ 8.08 (1H, dd *J* = 4.9 Hz, ^{4}*J* = 1.9 Hz, Ar-H), 7.43 (1H, d *J* = 7.3 Hz, Ar-H), 7.30-7.07 (4H, m, Ar-H), 6.77 (1H, dd *J* = 7.3 Hz, 4.9 Hz, Ar-H), 4.39-4.19 (2H, m, N-CH & Ar-CH$_2$), 3.67 (1H, d ^{2}*J* = 13.5 Hz, Ar-CH$_2$), 3.48-3.36 (2H, m, N-CH$_2$), 2.84-2.66 (2H, m, NMe-CH$_2$), 2.52-2.45 (1H, m, NMe-CH$_2$), 2.36-2.19 (4H, m, N-CH$_3$ & NMe-CH$_2$). Incorporation expected at δ 3.48-3.36. Determined against integral at δ 3.67.
	LCMS data
	Retention time: 0.50 min; Mass ion: 266.3 (M+H)$^+$

D-Incorporation (%)		
Run		***Average***
1	***2***	
94	94	94

Substrate	***^{1}H NMR data***[211]
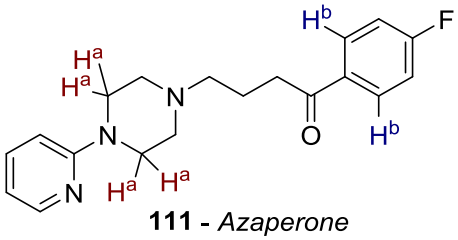 **111** - *Azaperone* (28.2 mg, 0.086 mmol)	**^{1}H NMR** (300 MHz, DMSO): δ 8.15-7.91 (3H, m, Ar-H), 7.49 (1H, ddd *J* = 8.5 Hz, 7.7 Hz, ^{4}*J* = 2.2 Hz, Ar-H), 7.39-7.24 (2H, m, Ar-H), 6.76 (1H, d *J* = 8.6 Hz, Ar-H), 6.60 (1H, dd *J* = 7.7 Hz, 4.8 Hz, Ar-H), 3.43-3.32 (4H, m, Ar-N-CH$_2$), 3.01 (2H, t *J* = 7.0 Hz, N-CH$_2$), 2.45-2.27 (6H, m, CH$_2$ & N-CH$_2$), 1.90-1.77 (2H, m, CH$_2$). Incorporation expected at δ D^a 3.43-3.32, D^b 8.15-7.91. Determined against integral at δ 1.90-1.77.
	LCMS data
	Retention time: 0.38 min; Mass ion: 328.4 (M+H)$^+$

D-Incorporation (%)					
Run				***Average***	
1		***2***			
D^a	***D^b***	***D^a***	***D^b***	***D^a***	***D^b***
98	13	96	12	97	13

Substrate	***^{1}H NMR data***[212]
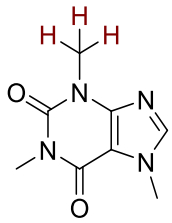 **112** - *Caffeine* (16.7 mg, 0.086 mmol)	**^{1}H NMR** (300 MHz, DMSO): δ 7.98 (1H, s, Ar-H), 3.87 (3H, s, N-CH_3), 3.40 (3H, s, N-CH_3), 3.21 (3H, s, N-CH_3). Incorporation expected at δ 3.40. Determined against integral at δ 3.87.
	LCMS data
	Retention time: 0.92 min; Mass ion: 195.1 $(M+H)^+$

Protocol	***D-Incorporation (%)***		
	Run		***Average***
	1	***2***	
1	41	40	41
2	91	93	92

Substrate	***^{1}H NMR data***[213]
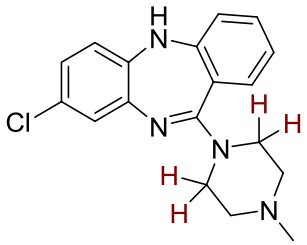 **113** - *Clozapine* (28.1 mg, 0.086 mmol)	**^{1}H NMR** (300 MHz, DMSO): δ 7.37-7.26 (1H, m, Ar-H), 7.22-7.12 (2H, m, N-H and Ar-H), 7.07-6.94 (2H, m, Ar-H), 6.90-6.79 (3H, m, Ar-H), 3.39-3.25 (4H, m, N-CH_2), 2.44-2.31 (4H, m, NMe-CH_2), 2.21 (3H, s, N-CH_3). Incorporation expected at δ 3.39-3.25. Determined against integral at δ 2.21.
	LCMS data
	Retention time: 1.72 min; Mass ion: 327.2 $(M+H)^+$

Protocol	***D-Incorporation (%)***		
	Run		***Average***
	1	***2***	
1	0	0	0
2	11	12	12
3	53	54	54

6.5. Understanding Selectivity in HIE

Graph 2.13 *Eyring-Polanyi plot of HIE upon chalcone derivative* ***98c****.*

The reactions were carried out following general procedure C and analysed by ^{1}H NMR spectroscopy to confirm the position and degree of deuterium incorporation. The rate data for each temperature is given below. This data was obtained over a short reaction time, during which the reaction was considered to be linear.

Complex	***Solvent***
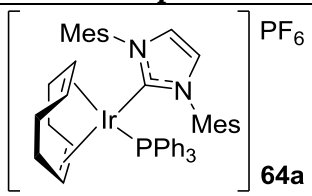 (0.4 mg, 0.0004 mmol)	DCM (5 mL)

Substrate	***Data***
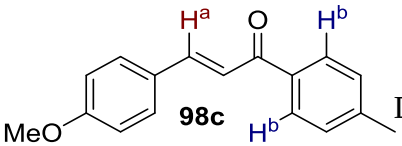 (505 mg, 2.0 mmol)	Data was consistent with that reported on page 384.

-10 °C				
Time	***D-Incorporation (%)***		***Concentration (mmolL^{-1})***	
	D^{a}	***D^{b}***	***D^{a}***	***D^{b}***
7	8.6	1.7	0.366	0.787
9	10.3	1.8	0.259	0.786
11	12.6	2.0	0.350	0.784
13	15.7	2.2	0.337	0.782
15	19.6	2.5	0.322	0.780
25	-	3.5	-	0.772

Table E2.17

0 °C				
Time	***D-Incorporation (%)***		***Concentration (mmolL^{-1})***	
	D^a	***D^b***	***D^a***	***D^b***
7	12.2	2.8	0.351	0.776
9	16.0	3.0	0.336	0.773
11	19.0	3.4	0.324	0.769
13	23.2	3.9	0.307	0.766
15	27.4	4.2	0.290	0.763
25	-	7.2	-	0.742

Table E2.18

10 °C				
Time	***D-Incorporation (%)***		***Concentration (mmolL^{-1})***	
	D^a	***D^b***	***D^a***	***D^b***
7	15.1	2.8	0.340	0.775
9	19.7	3.1	0.321	0.771
11	23.8	3.6	0.305	0.766
13	28.3	4.3	0.287	0.761
15	32.4	4.9	0.270	0.758
25	-	5.3	-	0.729

Table E2.19

17 °C				
Time	***D-Incorporation (%)***		***Concentration (mmolL^{-1})***	
	D^a	***D^b***	***D^a***	***D^b***
7	17.0	3.0	0.332	0.776
9	22.0	4.4	0.312	0.765
11	28.2	5.7	0.287	0.755
13	33.6	6.6	0.266	0.747
15	38.1	8.4	0.248	0.733
25	-	12.3	-	0.702

Table E2.20

25 °C				
Time	***D-Incorporation (%)***		***Concentration (mmolL^{-1})***	
	D^a	***D^b***	***D^a***	***D^b***
7	22.4	4.0	0.302	0.768
9	30.0	5.5	0.276	0.756
11	36.7	8.0	0.250	0.736
13	44.2	9.5	0.231	0.724
15	49.3	12.5	0.212	0.700
25	-	23.0	-	0.616

Table E2.21

The relevant data was then used to obtained the rate constant at each temperature. This was achieved by assuming Michealis-Menten kinetics, in which the rate of product formation is equal to the rate constant and the concentration of substrate catalyst complex in solution.

$$\frac{d[P]}{dt} = k_{cat}[cat{:}\,sub]$$

Furthermore, with a very large excess of substrate in solution (1: 1000, catalyst: substrate) we can assume that the catalyst is always bound to a substrate molecule. Therefore, we observe the maximum rate of reaction and can relate it to the initial catalyst concentration.

$$v_{max} = k_{cat}[cat_0]$$

Temperature (°C)	***$k_{cat\text{-}Da}$ (s^{-1})***	***$K_{cat\text{-}Db}$ (s^{-1})***
-10	0.211	0.0355
0	0.303	0.0750
10	0.358	0.103
17	0.470	0.171
25	0.593	0.345

Table E2.22

The data above was then utilised to form an Eyring-Polanyi plot according to the equation below, and the relevant enthalpy, entropy and activation energy were extracted.

$$\ln\left(\frac{k}{T}\right) = \frac{-\Delta H^{\ddagger}}{R} \cdot \frac{1}{T} + ln\left(\frac{k_b}{h}\right) + \frac{\Delta S^{\ddagger}}{R}$$

Graph 2.14 *Eyring-Polanyi plot of HIE upon different directing group substrates.*

The reactions were carried out following general procedure C and analysed by ^{1}H NMR to confirm the position and degree of deuterium incorporation, and the rate data for each temperature is displayed below. This data was obtained over a short reaction time, during which the reaction was considered to be linear.

Complex	***Solvent***
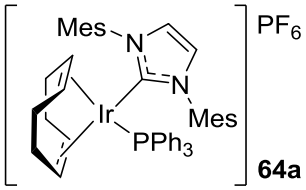 **64a** (0.4 mg, 0.0004 mmol)	DCM (5 mL)

Substrate	***data***
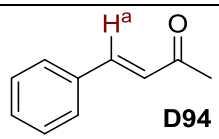 **D94** (293 mg, 2.0 mmol)	Data was consistent with that reported on page 362.
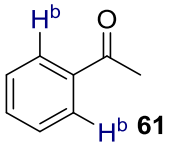 **61** (240 mg, 2.0 mmol)	Data was consistent with that reported on page 395.
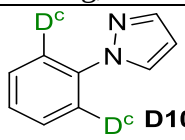 **D100b** (290 mg, 2.0 mmol)	Data was consistent with that reported on page 396.

0 °C				
Time	***D-Incorporation (%)***		***Concentration (mmolL^{-1})***	
(min)	***D^a***	***D^c***	***D^a***	***D^c***
7	2.4	8.3	0.394	0.734
9	3.3	9.7	0.390	0.723
11	4.5	10.7	0.387	0.715
13	6.2	11.4	0.382	0.709
15	7.3	12.4	0.375	0.701

Time	***D-Incorporation (%)***	***Concentration (mmolL^{-1})***
(min)	***D^b***	***D^b***
11	6.6	0.748
15	7.4	0.741
25	8.3	0.734
40	10.0	0.720
60	12.2	0.703

Table E2.23

10 °C				
Time	***D-Incorporation (%)***		***Concentration (mmolL^{-1})***	
(min)	***D^a***	***D^c***	***D^a***	***D^c***
7	6.7	8.7	0.373	0.731
9	8.0	10.3	0.368	0.718
11	9.7	11.4	0.361	0.709
13	11.5	13.0	0.354	0.696
15	13.0	13.9	0.348	0.689

Time	***D-Incorporation (%)***	***Concentration (mmolL^{-1})***
(min)	***D^b***	***D^b***
11	6.0	0.752
15	7.1	0.743
25	8.2	0.734
40	11.2	0.710
60	13.4	0.693

Table E2.24

17 °C				
Time	***D-Incorporation (%)***		***Concentration (mmolL^{-1})***	
(min)	***D^{a}***	***D^{c}***	***D^{a}***	***D^{c}***
7	7.2	10.1	0.371	0.720
9	8.9	11.2	0.364	0.711
11	11.6	12.4	0.354	0.701
13	13.2	14.2	0.347	0.686
15	16.0	15.8	0.336	0.674

Time	***D-Incorporation (%)***	***Concentration (mmolL^{-1})***
(min)	***D^{b}***	***D^{b}***
11	8.2	0.735
15	9.3	0.726
25	11.2	0.711
40	13.5	0.692
60	17.3	0.662

Table E2.25

28 °C				
Time	***D-Incorporation (%)***		***Concentration (mmolL^{-1})***	
(min)	***D^{a}***	***D^{c}***	***D^{a}***	***D^{c}***
7	12.1	13.2	0.352	0.695
9	16.6	15.4	0.334	0.677
11	20.0	17.7	0.320	0.658
13	24.5	20.4	0.302	0.637
15	28.4	22.8	0.286	0.618

25 °C		
Time	***D-Incorporation (%)***	***Concentration (mmolL^{-1})***
(min)	***D^{b}***	***D^{b}***
11	7.9	0.737
15	9.1	0.727
25	12.1	0.704
40	15.0	0.680
60	19.0	0.648

Table E2.26

The relevant data was then used to obtained the rate constant at each temperature. This was achieved by assuming Michealis-Menten kinetics, in which the rate of product formation is equal to the rate constant and the concentration of substrate catalyst complex in solution.

$$\frac{d[P]}{dt} = k_{cat}[cat{:}\,sub]$$

Furthermore, with a very large excess of substrate in solution (1: 1000, catalyst: substrate) we can assume that the catalyst is always bound to a substrate molecule. Therefore, we observe the maximum rate of reaction and can relate it to the initial catalyst concentration.

$$v_{max} = k_{cat}[cat_0]$$

Temperature (°C)	***k_{Da} (s^{-1})***	***k_{Db} (s^{-1})***	***k_{Dc} (s^{-1})***
0	0.100	0.037	0.142
10	0.138	0.050	0.167
17	0.176	0.060	0.218
28 (D^b at 25)	0.330	0.075	0.243

Table E2.27

The data above was then utilised to form an Eyring-Polanyi plot, according to the equation below, and the relevant enthalpy, entropy and activation energy were extracted.

$$\ln\left(\frac{k}{T}\right) = \frac{-\Delta H^{\ddagger}}{R} \cdot \frac{1}{T} + ln\left(\frac{k_b}{h}\right) + \frac{\Delta S^{\ddagger}}{R}$$

Scheme 2.86 *Selectivity investigations with different ring sizes.*

The reactions were carried out following general procedure A and analysed by LCMS to confirm the extent of exchange in each substrate, the labelling position is assumed based upon our previous findings.

Complex	***Solvent***	***Temperature (°C)***	***Time (h)***
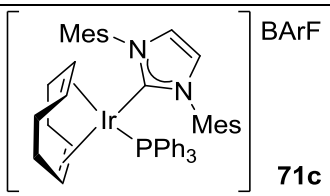 (1.5 mg, 0.86 µmol)	DCM (1 mL)	25	1

Substrate	***LCMS data***
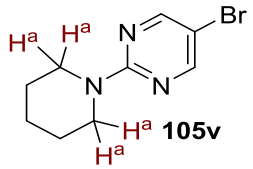 (20.8 mg, 0.086 mmol)	Retention time: 3.54 min; Mass ion: 242.1 $(M+H)^+$
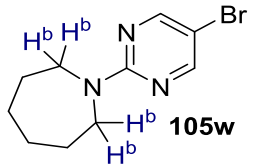 (22.0 mg, 0.086 mmol)	Retention time: 0.29 min; Mass ion: 184.1 $(M+H)^+$

D-Incoporation (%)	
D^a	***D^b***
66	7

Substrate	***LCMS data***
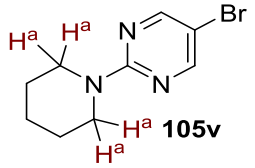 (20.8 mg, 0.086 mmol)	Retention time: 3.54 min; Mass ion: 242.1 $(M+H)^+$
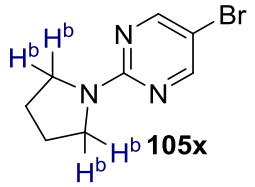 (19.6 mg, 0.086 mmol)	Retention time: 2.85 min; Mass ion: 228.1 $(M+H)^+$

D-Incoporation (%)	
D^a	D^b
85	30

Substrate	***LCMS data***
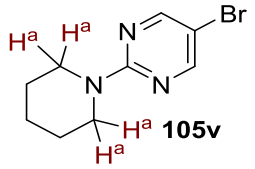 (20.8 mg, 0.086 mmol)	Retention time: 3.54 min; Mass ion: 242.1 $(M+H)^+$
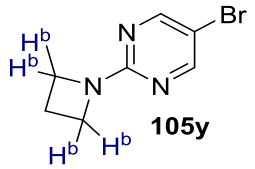 (18.4 mg, 0.086 mmol)	Retention time: 2.30 min; Mass ion: 214.0 $(M+H)^+$

D-Incoporation (%)	
D^a	D^b
80	0

7. References

, [1] Office for National Statistics, **2014**, *Business Enterprise Research and Development*. (http://www.ons.gov.uk/economy/governmentpublicsectorandtaxes/researchanddevelopmentexpenditure/bulletins/businessenterpriseresearchanddevelopment/2014) (last accessed June 2016).
[2] E. M. Isin, C. S. Elmore, G. N. Nilsson, R. A. Thompson, and L. Weidolf, *Chem. Res. Toxicol.* **2012**, *25*, 532.
[3] W. J. S. Lockley, A. McEwen, and R. Cooke, *J. Labelled Compd. Radiopharm.* **2012**, *55*, 235.
[4] P. H. Marathe, W. C. Shyu, and W. G. Humphreys, *Curr. Pharm. Des.* **2004**, *10*, 2991.
[5] T. Toyo'oka, *J. Pharm. Biomed. Anal.* **2012**, *69*, 174.
[6] G. C. Lloyd-Jones, M. P. Munoz, *J. Labelled. Compd. Radiopharm.* **2007**, *50*, 1072.
[7] H. M. T. B. Herath, J. D. McChesney, L. A. Walker, and N. P. D. Nanayakkara, *J. Labelled Compd. Radiopharm.* **2013**, *56*, 341.
[8] J. Sandell, *J. Labelled Compd. Radiopharm.* **2013**, *56*, 321.
[9] P. Beak and R. A. Brown, *J. Org. Chem.* **1982**, *47*, 34.
[10] J. A. Kozocas, J. E. Bupp, M. J. Tanga, J. T. Pluhar, and I. W. Wainer, *J. Labelled Compd. Radiopharm.* **2010**, *53*, 68.
[11] S. Arns, A. Moreau, and R. N. Young, *J. Labelled Compd. Radiopharm.* **2010**, *53*, 205.
[12] C. Than, H. Morimoto, H. Andres, and P. G. Williams, *J. Labelled Compd. Radiopharm.* **1996**, *38*, 693.
[13] J. Atzrodt and V. Derdau, *J. Labelled Compd. Radiopharm.* **2010**, *53*, 674.
[14] Á. Proszenyák, B. Ágai, G. Tárkányi, L. Vida, and F. Faigl, *J. Labelled Compd. Radiopharm.* **2005**, *48*, 421.
[15] H. Sajiki, N. Ito, H. Esaki, T. Maesawa, T. Maegawa, and K. Hirota, *Tetrahedron Lett.* **2005**, *46*, 6995.
[16] J. L. Garnett and R. J. Hodges, *J. Am. Chem. Soc.* **1967**, *89*, 4546.
[17] J. R. Heys, *J. Labelled Compd. Radiopharm.* **2010**, *53*, 716.
[18] C. G. Macdonald and J. S. Shannon, *Tetrahedron Lett.* **1964**, *5*, 3351.
[19] D. Hesk, D. Koharski, S. Saluja, P. McNamara, C. Magatti, D. Cesarz, S. Hendershot, J. R. Jones, *Synthesis and Applications of Isotopically Labelled Compounds, Proceedings of the 6th International Symposium, Philadelphia*, **1998**, Chichester, Wiley.
[20] D. Hesk, C. F. Lavey, and P. McNamara, *J. Labelled Compd. Radiopharm.* **2010**, *53*, 722.
[21] S. L. Regen, *J. Org. Chem.*, **1974**, *39*, 260.
[22] W. J. S. Lockley and D. Hesk, *J. Labelled Compd. Radiopharm.* **2010**, *53*, 704.
[23] M. R. Blake, J. L. Garnett, I. K. Gregor, W. Hannan, K. Hoa, and M. A. Long, *Chem. Commun.* **1975**, *0*, 930.
[24] W. J. S. Lockley, *Tetrahedron Lett.* **1982**, *23*, 3819.
[25] W. J. S. Lockley, *J. Labelled Compd. Radiopharm.* **1984**, *21*, 45.
[26] W. J. S. Lockley, *J. Labelled Compd. Radiopharm.* **1985**, *22*, 623.
[27] S. Chen, G. Song, and X. Li, *Tetrahedron Lett.* **2008**, *49*, 6929.
[28] W. J. S. Lockley, *J. Labelled Compd. Radiopharm.* **2007**, *50*, 779.
[29] G. N. Nilsson and W. J. Kerr, *J. Labelled Compd. Radiopharm.* **2010**, *53*, 662.
[30] R. H. Crabtree, E. M. Holt, M. Lavin, and S. M. Morehouse, *Inorg. Chem.* **1985**, *24*, 1986.
[31] R. Heys, *Chem. Commun.* **1992**, *0*, 680.
[32] J. R. Heys, A. Y. L. Shu, S. G. Senderoff, and N. M. Phillips, *J. Labelled Compd. Radiopharm.* **1993**, *33*, 431.
[33] D. Hesk, P. R. Das, and B. Evans, *J. Labelled Compd. Radiopharm.* **1995**, *36*, 497.
[34] A. Y. L. Shu, W. Chen, and J. R. Heys, *J. Organomet. Chem.* **1996**, *524*, 87.
[35] M. Lavin, E. M. Holt, and R. H. Crabtree, *Organometallics* **1989**, *8*, 99.
[36] A. C. Albeniz, G. Schulte, and R. H. Crabtree, *Organometallics* **1992**, *11*, 242.
[37] G. G. Hlatky and R. H. Crabtree, *Coord. Chem. Rev.* **1985**, *65*, 1.
[38] G. J. Ellames, J. S. Gibson, J. M. Herbert, and A. H. McNeill, *Tetrahedron* **2001**, *57*, 9487.
[39] I. Bauer, H.-J. Knolker, *Chem. Rev.* **2015**, *115*, 3170.
[40] R. P. Yu, D. Hesk, N. Rivera, I. Pelczer, P. J. Chirik, *Nature* **2016**, *529*, 195.
[41] P. W. C. Cross, J. M. Herbert, W. J. Kerr, A. H. McNeill, L. C. Paterson, *Synlett* **2016**, *27*, 111.
[42] P. C. W. Cross, *PhD Thesis, University of Strathclyde*, **2004**.
[43] J. A. Brown, S. Irvine, A. R. Kennedy, W. J. Kerr, S. Andersson, and G. N. Nilsson, *Chem. Commun.* **2008**, 1115.
[44] C. Köcher and W. A. Herrmann, *J. Organomet. Chem.* **1997**, *532*, 261.

[45] J. A. Brown, A. R. Cochrane, S. Irvine, W. J. Kerr, B. Mondal, J. A. Parkinson, L. C. Paterson, M. Reid, T. Tuttle, S. Andersson, G. N. Nilsson, *Adv. Synth. Catal.* **2014**, *356*, 3551.
[46] A. R. Kennedy, W. J. Kerr, R. Moir, M. Reid, *Org. Biomol. Chem.* **2014**, *12*, 7927.
[47] W. J. Kerr, D. M. Lindsay, M. Reid, J. Atzrodt, V. Derdau, P. Rojahn, R. Weck, *Chem. Commun*. **2016**, *52*, 6669.
[48] A. R. Cochrane, S. Irvine, W. J. Kerr, M. Reid, S. Andersson, and G. N. Nilsson, *J. Labelled Compd. Radiopharm.* **2013**, *56*, 451.
[49] W. J. Kerr, M. Reid, T. Tuttle, *ACS Catal.* **2015**, *5*, 402.
[50] F. Lovering, J. Bikker, C. Humblet, *J. Med. Chem.* **2009**, *52*, 6752.
[51] P.O. Stouland, R. G. Bergman, *J. Am. Chem. Soc.* **1988**, *110*, 5732.
[52] L. S. Bennie, C. J. Fraser, S. Irvine, W. J. Kerr, S. Andersson, and G. N. Nilsson, *Chem. Commun.* **2011**, *47*, 11653.
[53] N. Bushby, D. A. Killick, *J. Labelled Compd. Radiopharm.* **2007**, *50*, 519.
[54] L. Yang, H. Huang, *Chem. Rev.* **2015**, *115*, 3468.
[55] E. Vitaku, D. T. Smith, J. T. Njardson, *J. Med. Chem.* **2014**, *57*, 10257.
[56] C. Hansch, A. Leo, R. W. Taft, *Chem Rev.* **1991**, *91*, 165.
[57] R. H. Crabtree, *Chem. Rev.* **2015**, *115*, 127.
[58] K. D. Collins, F. Glorius, *Nature Chem.* **2013**, *5*, 597.
[59] W. J. Kerr, R. J. Mudd, L. C. Paterson, J. A. Brown, *Chem. Eur. J.* **2014**, *20*, 14604.
[60] B. A. Arndtsen, R. G. Bergman, T. A. Mobley, T. H. Peterson, *Acc. Chem. Res.* **1995**, *28*, 154.
[61] K.-H. Kwon, D. W. Lee, C. S. Yi, *Organometallics* **2012**, *31*, 495.
[62] L. Wang, L. Ackermann, *Org. Lett.* **2013**, 15, 176.
[63] T. K. Hyster, T. Rovis, *Chem. Sci.*, **2011**, *2*, 1606.
[64] K. D. Collins, F. Lied, F. Glorius, *Chem. Commun.* **2014**, *50*, 4459.
[65] J. Zhou, J. F. Hartwig, *Angew. Chem. Int. Ed.* **2008**, *47*, 5783.
[66] A. D. Giuseppe, R. Castarlenas, J. J. Pérez-Torrente, F. J. Lahoz, L. A. Oro, *Chem. Eur. J.* **2014**, *20*, 8391.
[67] W. J. Kerr, R. J. Mudd, J. A. Brown, *Chem. Eur. J.* **2016**, *22*, 4738.
[68] C.-T. Hsieh, T. J. Hsieh, M. El-Shazly, D.-W. Chuang, Y.-H. Tsai, C.-T. Yen, S.-F. Wu, Y.-C. Wu, F.-R. Chang, *Bioorg. Med. Chem. Lett.* **2012**, *22*, 3912.
[69] D. Gupta, D. K. Jain, *J. Adv. Pharm. Technol. Res.* **2015**, *6*, 114.
[70] J. R. Heys, C. S. Elmore, *J. Labelled Compd. Radiopharm.* **2009**, *52*, 189.
[71] M. Gómez-Gallego, M. A. Sierra, *Chem. Rev.* **2011**, *111*, 4857.
[72] K. R. Campos, *Chem. Soc. Rev.* **2007**, *36*, 1069.
[73] S.-Y. Zhang, F.-M. Zhang, Y.-Q. Tu, *Chem. Soc. Rev.* **2011**, *40*, 1937.
[74] J.-Q. Li, P. G. Andersson, *Chem. Commun.* **2013**, *49*, 6131.
[75] E. Alexakis, J. R. Jones, W. J. S. Lockley, *Tetrahedron Lett.* **2006**, *47*, 5025.
[76] J. Atzrodt, V. Derdau, W. J. Kerr, M. Reid, P. Rojahn, R. Weck, *Tetrahedron*, **2015**, *71*, 1924.
[77] M. Reid, *PhD Thesis*, University of Strathclyde, **2015**.
[78] W. L. F. Armarego, C. L. L. Chai, *Purification of Laboratory Chemicals*, 7th edition, Butterwoth-Heinemann, **2013**.
[79] W. Kohn, L. Sham, *J. Phys. Rev.* **1965**, *140*, 1133.
[80] R. G. Parr, W. T. Yang, *Density Functional Theory of Atoms and Molecules*, Oxford University Press, **1989**.
[81] Y. Zhao, D. G. Truhlar, *Theor. Chem. Acc.* **2008**, *120*, 215.
[82] M. J. Frisch, J. A. Pople, J. S. Binkley, *J. Chem. Phys.* **1984**, *80*, 3265.
[83] R. Ditchfield, W. J. Hehre, J. A. Pople, *J. Phys Chem.* **1971**, *54*, 724.
[84] D. Andrae, U. Haussermann, M. Dolg, H. Stoll, H. Preuss, *Theor. Chim. Acta.* **1990**, *77*, 123.
[85] F. Weigend, R. Alhrichs, *Phys Chem. Chem. Phys.* **2005**, *7*, 3297.
[86] M. J. Frisch, G. W. Trucks, H. B. Schlegel, G. E. Scuseria, M. A. Robb, J. R. Cheeseman, G. Scalmani, V. Barone, B. Mennucci, G. A. Petersson,H. Nakatsuji, M. Caricato, X. Li, H. P. Hratchian, A. F. Izmaylov, J. Bloino, G. Zheng, J. L. Sonnenberg, M. Hada, M. Ehara, K. Toyota, R. Fukuda, J. Hasegawa, M. Ishida, T. Nakajima, Y. Honda, O. Kitao, H. Nakai, T. Vreven, J. Montgomery, J. E. Peralta, F. Ogliaro, M. Bearpark, J.J. Heyd, E. Brothers, K. Kudin, V. N. Staroverov, R. Kobayashi, J. Normand, K. Raghavachari, A. Rendell, J. C. Burant, S. S. Iyengar, J. Tomasi, M. Cossi, N. Rega, J. M. Millam, M. Klene, J. E. Knox, J. B. Cross, V. Bakken, C. Adamo, J. Jaramillo, R. Gomperts, R. E. Stratmann, O. Yazyev, A. J. Austin, R. Cammi, C. Pomelli, J. W. Ochterski, R. L. Martin, K. Morokuma, V. G. Zakrzewski, G. A. Voth, P. Salvador, J. J. Dannenberg, S. Dapprich, A. D. Daniels, O. Farkas, J. B. Foresman, J. V. Ortiz, J. Cioslowski, D. J. A. Fox, 02 ed, Gaussian, Inc.: Wallingford, CT, **2009**.

[87] Y. Makida, E. Marelli, A. M. Z. Slawin, S. P. Nolan, *Chem. Commun.* **2014**, *50*, 8010.
[88] D. Yang, H. Yang, H. Fu, *Chem. Commun.* **2011**, *47*, 2348.
[89] X. Wang, R.-X. Chen, Z.-F. Wei, C.-Y. Zhang, H.-Y. Tu, A.-D. Zhang, *J. Org. Chem.* **2016**, *81*, 238.
[90] L. Gu, Y. Zhang, *J. Am. Chem. Soc.* **2010**, *132*, 914.
[91] J. Bromilow, R. T. C. Brownlee, D. J. Craik, P. R. Fiske, J. E. Rowe, M. Sadek, *J. Chem. Soc., Perk., Trans. 2* **1981**, 753.
[92] M. Karabacak, L. Sinha, O. Prasad, A. M. Asiri, M. Cinar, V. K. Shukla, *Spectrochim. Acta A* **2014**, *123*, 352.
[93] X. Cui, J. Li, Z.-P. Zhang, Y. Fu, L. Liu, Q.-X. Guo, *J. Org. Chem.* **2007**, *72*, 9342.
[94] D. F. Yu, P. Xing, B. Jiang, *Tetrahedron* **2015**, *71*, 4269.
[95] D. Yang, H. Fu, *Chem. Eur. J.* **2010**, *16*, 2366.
[96] S. Korsager, R. H. Taaning, T. Skydrtrup, *Chem. Eur. J.* **2015**, *21*, 12616.
[97] Y. Yu, L. Zhang, Y. Zhou, Z. Zuhra, *Dalton Trans.* **2015**, *44*, 4601.
[98] T. Leon, A. Correa, R. Martin, *J. Am. Chem. Soc.* **2013**, *69*, 7264.
[99] R. T. Shuman, (Eli Lilly Co), *US5250660 (A)*, **1993**.
[100] S. N. Dighe, H. R. Jdhav, *Tetrahedron Lett.* **2012**, *53*, 5803.
[101] M. Yoshida, Y. Katagiri, W.-B. Zhu, K. Shishido, *Org. Biomol. Chem.* **2009**, *7*, 4062.
[102] S. Hinsberger, K. Huesecken, M. Groh, M. Negri, J. Haupenthal, R. W. Hartmann, *J. Med. Chem.* **2013**, *56*, 8332.
[103] N. Puttaswammy, P. Kumar, M. Al-Ghorbani, P. Vigneshwaran, S. A. Knanum, *J. Med. Chem.* **2016**, *114*, 153.
[104] B. Rao, X. Zeng, *Org. Lett.* **2014**, *16*, 314.
[105] K. R. Buszek, N. Brown, *Org. Lett.* **2007**, *9*, 707.
[106] I. Peňafiel, I. M. Pastor, M. Yus, M. A. Esteruelas, M. Oliván, *Organometallics* **2012**, *31*, 6154.
[107] Y.-F. Chang, Y.-R. Jiang, W.-C. Cheng, *Tetrahedron Lett.* **2008**, *49*, 543.
[108] F. Niu, L. Zhang, S.-Z. Luo, W.-G. Song, *Chem. Commun.* **2010**, *46*, 1109.
[109] J.-J. Cao, F. Zhou, J. Zhou, *Angew. Chem. Int. Ed.* **2010**, *49*, 4976.
[110] Y. Onishi, Y. Nishimoto, M. Yasuda, A. Baba, *Org. Lett.* **2011**, *13*, 2762.
[111] Y.-C. Liu, Z.-L. Wu, *Chem. Commun.* **2016**, *52*, 1158.
[112] L. Wynands, S. Delacroix, A. Nguyen Van Nhien, E. Soriano, J. Marco-Contelles, D. Postel, *Tetrahedron*, **2013**, *69*, 4899.
[113] Z.-X. Du, L.-Y. Zhang, X.-Y. Fan, F.-C. Wu, C.-S. Da, *Tetrahedron Lett.* **2013**, *54*, 2828.
[114] J.-Y. Shang, F. Li, X.-F. Bai, J.-X. Jiang, K.-F. Yang, G.-Q. Lai, L.-W. Xu, *Eur. J. Org. Chem.* **2012**, 2809.
[115] Y. Wang and R. Franzen, *Synlett*, **2012**, 925.
[116] G. Elias, M. N. A. Rao, *Eur. J. Med. Chem.*, **1988**, *23*, 379.
[117] W. Zhu, Y. Yu, H. Yang, L. Hua, Y. Qiao, X. Zhao, Z. Huo, *Chem. Eur. J.* **2013**, *19*, 2059.
[118] X. Li, L. Li, Y. Tang, L. Zhong, L. Cun, J. Zhu, J. Liao, J. Deng, *J. Org. Chem.* **2010**, *75*, 2981.
[119] W. L. Nobles, *J. Am. Chem. Soc.*, **1955**, *77*, 6675.
[120] R. A. Batey, A. N. Thadani, D. V. Smil, *Org. Lett.* **1999**, *1*, 1683.
[121] W. Gao, Z. He, Y. Qian, J. Zhao, Y. Huang, *Chem. Sci.* **2012**, *3*, 883.
[122] M. Bellasoued, J. Atar, M. Bouzid, M. Damak, *Phosphorus, Sulfur Silicon Relat. Elem.* **2010**, *185*, 1886.
[123] R. Mello, J. Martínez-Ferrer, A. Alcalde-Aragonés, T. Varea, R. Acrete, M. E. González-Núňez, and G. Asenio, *J. Org. Chem.* **2011**, *76*, 10129.
[124] S. Liang, G. B. Hammond, B. Xu, *Chem. Commun.* **2015**, *51*, 903.
[125] Y.-F. Wang, Y.-R. Gao, S. Mao, Y.-L. Zhang, D.-D. Guo, Z.-L. Yan, S.-H. Guo and Y.-Q. Wang, *Org. Lett.* **2014**, *16*, 1610.
[126] M. Konkol, H. Schmidt, D. Steinborn, *J. Mol. Catal. A: Chem.* **2007**, *269*, 119.
[127] I. C. Stewart, R. G. Bergman, F. D. Toste, *J. Am. Chem. Soc.* **2003**, *125*, 8696.
[128] M. Rueping, T. Bootwicha, H. Baars, E. Sugiono, *Beilstein J. Org. Chem.* **2011**, *7*, 1680.
[129] M. Chen, J. Wang, Z. Chai, C. You, A. Lei, *Adv. Synth. Catal.* **2012**, *354*, 341.
[130] Y.-D. Shao, X.-S. Wu, S.-K. Tian, *Eur. J. Org. Chem.* **2012**, *8*, 1590.
[131] M. Vellakkaran, M. M. S. Andappan, N. Kommu, *Eur. J. Org. Chem.* **2012**, 4694.
[132] Y. Zhou, X. Li, S. Hou, J. Xu, *J. Mol. Catal. A: Chem.* **2012**, *365*, 203.
[133] K. Nonoshita, K. Maruoka, H. Yamamoto, *Bull. Chem. Soc. Jpn.* **1988**, *61*, 2241.
[134] R. Vilano, M. R. Acocella, A. Scettri, *Tetrahedron. Lett.* **2014**, *55*, 2442.
[135] S. Morrissey, I. Beadham, N. Gatherwood, *Green Chem.* 2009, **11**, 466.

[136] C. Baumert, M. Gunthel, S. Krawczyk, M. Hemmer, T. Wersig, A. Langner, J. Molnar, H. Lage, A. Hilgeroth, *Bioorg. Med. Chem.* **2013**, *21*, 166.
[137] C. Chang, M. Brookhart, *Angew. Chem. Int. Ed.* **2012**, *51*, 9422.
[138] D. S. Gaikwad, D. M. Pore, *Synlett*, **2012**, *23*, 2631.
[139] A. S. Kleinke, T. F. Jamison, *Org. Lett.* **2013**, *15*, 710.
[140] T. Besset, H. Kuhl, F. W. Patureau, F. Glorius, *Chem. Eur. J.* **2011**, *17*, 7167.
[141] M. Szostak, M. Spain, A. J. Eberhart, D. J. Procter, *J. Am. Chem. Soc.* **2014**, *136*, 2268.
[142] D. B. Baker, P. T. Gallagher, T. J. Donohoe, *Tetrahedron* **20013**, *69*, 3690.
[143] S. T. Heller, R. Sarpong, *Org. Lett.* **2010**, *12*, 4572.
[144] S. Marity, S. Manna, S. Rana, T. Naveen, A. Mallick, D. Maiti, *J. Am. Chem. Soc.* **2013**, *135*, 3355.
[145] P. G. Gildner, A. A. S. Gietter, D. Cui, D. A. Watson, *J. Am. Chem. Soc.* **2012**, *134*, 9942.
[146] U. Farid, F. Malmedy, R. Claveau, L. Albers,T. Wirth, *Angew. Chem. Int. Ed.* 2013, **52**, 7018.
[147] Q. Xu, J. Chen, H. Tian, X. Yuan, S. Li, C. Zhou, J. Liu, *Angew. Chem. Int. Ed.* 2014, **53**, 225.
[148] Q. Jiang, T. Guo, Q. Wang, P. Wu, Z. Yu, *Adv. Synth. Catal*, **2013**, *355*, 1874.
[149] M. Y. Wani, A. R. Bhat, A. Azam, D. H. Lee, I. Choi, and F. Athar, *Eur. J. Med. Chem.*, **2012**, *54*, 845.
[150] C. Mahler, U. Muller, W. M. Muller, V. Enkelmann, C. Moon, G. Brunklaus, H. Zimmermann, S. Hoger, *Chem. Commun.*, **2008**, 4816.
[151] M. L. N. Rao, V. Venkatesh, D. N. Jadhav, *J. Organomet. Chem.*, **2008**, *693*, 2494.
[152] A. Kumar, V. D. Tripathi, P. Kumar, L. P. Gupta, Akanksha, R. Trivedi, H. Bid, V. L. Nayak, J. A. Siddiqui, B. Chakravarti, R. Saxena, A. Dwivedi, M. I. Siddiquee, U. Siddiqui, R. Konwar, N. Chattopadhyay, *Biorg. Med. Chem.*, **2011**, *19*, 5409.
[153] J. P. Bradley, T. C. Jarvis, C. D. Johnson, P. D. Mcdonnell, T. A. P. Weatherstone, *Tetrahedron Lett.*, **1983**, *24*, 2851.
[154] T. Zhang, X. Huang, L. Wu, *Eur. J. Org. Chem.* **2012**, *18*, 3507.
[155] Y. Beniyama, K. Matsuno, H. Miyachi, *Biorg. Med. Chem. Lett.*, **2013**, *23*, 1662.
[156] Compound synthesised according to general procedure from: S. N. A. Bukhari, Y. Tajuddin, V. J. Benedict, K. W. Lam, I. Jantan, J. Jalil, M. Jasamai, *Chem. Bio. Drug Des.* **2014**, *2*, 198.
[157] K. Lan, Z.-X. Shan, *Synth. Commun.* **2007**, *37*, 2171.
[158] K. V. Sashidhara, J. N. Rosaiah, A. Kumar, *Synth. Commun.*, **2009**, *39*, 2288.
[159] X. Shang, X. Zhou, Wei, Zhang, C. Wan, J. Chen, *Tetrahedron*, **2015**, *71*, 8187.
[160] T. Ishimaru, N. Shibata, T. Horikawa, N. Yasuda, S. Nakamura, T. Toru, M. Shiro, *Angew. Chem. Int. Ed.* **2008**, *47*, 4157.
[161] J. R. Dimmock, N. M. Kandepu, A. J. Nazarali, T. P. Kowalchuk, N. Motaganahalli, J. W. Quail, P. A. Mykytiuk, G. F. Audette, L. Prasad, P. Perjési, T. M. Allen, C. L. Santos, J. Szydlowski, E. De Clercq, J. Balzarini, *J. Med. Chem.*, **1999**, *42*, 1358.
[162] J. Devlin, W. J. Kerr, D. M. Lindsay, T. J. D. McCabe, M. Reid, T. Tuttle, *Molecules* **2015**, *20*, 11676.
[163] T. Stern, S. Ruckbord, C. Czekelius, C. Donner, H. Brunner, *Adv. Synth. Catal.* **2010**, *352*, 1983.
[164] A. Das, R. Chaudhuri, R.-S. Liu, *Chem. Commun.* **2009**, 4046.
[165] S. A. Van Arman, A. J. Zimmet, I. E. Murray, *J. Org. Chem.* **2016**, *81*, 3528.
[166] M. Egi, M. Umemura, T. Kawai, S. Akai, *Angew. Chem . Int. Ed.* **2011**, *50*, 12197.
[167] C. Hansch, A. Leo, *Substituent Constants for Correlation Analysis in Chemistry and Biology*, Wiley-Interscience, **1979**.
[168] Substrate was prepared through the discussed HIE protocol and purified prior to use by flash column chromatography (EtOAc:Petrol, 20:80).
[169] P.-C. Leow, P. Bahety, C. P. Boon, C. Y. Lee, K. L. Tan, T. Yang, P.-L. R. Ee, *Eur. J. Med. Chem.* **2014**, *71*, 67.
[170] R. Shi, H. Zhang, L. Lu, P. Gan, Y. Sha, H. Zhang, Q. Liu, M. Beller, A. Lei, *Chem. Commun.* **2015**, *51*, 3247.
[171] S. Wagaw, S. L. Buchwald, *J. Org. Chem.* **1996**, *61*, 7240.
[172] N. Boudet, S. R. Dubbaka, P. Knochel, *Org. Lett.*, **2008**, *10*, 1715.
[173] G. Li, C. Jia, K. Sun, Y. Lv, F. Zhao, K. Zhou, H. Wu, *Org. Biomol. Chem.*, **2015**, *13*, 3207.
[174] G.-D. Roiban, G. Mehler, M. T. Reetz, *Eur. J. Org. Chem.*, **2014**, *10*, 2070.
[175] A. Romanens, G. Bélanger, *Org. Lett.*, **2015**, *17*, 322.
[176] M. Distaco, E. Quaranta *Tetrahedron* **2004**, *60*, 1531.
[177] Compound **105f** is commercially available from Fluorochem.
[178] S. R. Katamreddy, A. J. carpenter, C. E. Ammala, E. E. Boros, R. L. Brashear, C. P. Briscoe, S. R. Bullard, R. D. Caldwell, C. R. Conlee, D. K. Croom, S. M. Hart, D. O. Heyer, P. R. Johnson, J. A.

Kasthatus, D. J. Minick, G. E. Peckham, S. A. Ross, S. G. Roller, V. A. Samano, H. R. Sauls, S. M. Tadepalli, J. B. Thompson, Y. Xu, J. M. May, *J. Med Chem.*, **2012**, *55*, 10972-10994.
[179] T. Takayama, T. Shibata, F. Shiozawa, K. Kawabe, Y. Shimizu, M. Hamada, A. Hiratate, M. Takahashi, F. Ushiyama, T. Ol, Y. Shirasaki, D. Matsuda, C. Koizumi, S. Kato (Taisho Pharmaceuticals Co., Ltd), EP2881384 (A1), **2015**.
[180] P. S. Johnson, T. Ryckmans, J. Bryans, D. M. Beal, K. N. Dack, N. Feeder, A. Harrison, M. Lewis, H. J. Mason, J. Mills, J. Newman, C. Pasquinet, D. J. Rawson, L. R. Roberts, R. Russel, D. Spark, A. Stobie, T. J. Underwood, R. Ward, S. Wheeler, *J. Bioord. Med. Chem. Lett.*, **2011**, *21*, 5684.
[181] Compound **105j** commercially available from Enamine.
[182] A. Bouchon, N. Diedrichs, A. Hermann, K. Lustig, H. Meier, J. Pernerstorfer, E. Reissmuller, J. de Vry, M. Mogi, K. Urbahns, T. Yura, H. Jishima, M. Tajimi, N. Yamamoto, H. Yuasa, J. Gupta, Y. Tsukimi, F. Hayashi (Bayer Healthcare), WO2005040119 (A1), **2005**.
[183] M. Presset, N. Fleury-Bregeot, D. Oehlrich, F. Rombouts, G. A. Molander, *J. Org. Chem.* **2013**, *78*, 4615.
[184] E. Brenner, R. Schneider, Y. Fort, *Tetrahedron*, **2002**, *58*, 6913.
[185] M. Keenan, J. H. Chaplin, P. W. Alexander, M. J. Abbot, W. M. Best, A. Khong, A. Botero, C. Perez, S. Cornwall, R. A. Thompson, K. L. White, D. M. Shackleford, M. Koltun, F. C. K. Chiu, J. Morizzi, E. Ryan, M. Campbell, T. W. von Geldern, I. Scandale, E. Chatelain, S. A. Charman, *J. Med. Chem*, **2013**, *56*, 10158.
[186] H. Zimmermann, D. Bruckner, K. Henninger, U. Rosentreter, M. Hendrox, J. Keldenich, D. Land, M. Radke, D. Palsen, A. Kern (Bayer Healthcare), WO2006089664 (A2), **2006**.
[187] A. Thurkauf, *J. Label. Compd. Radiopharm.*, **1997**, *39*, 123.
[188] S. K. Verma, B. N. Acharya, M. P. Kaushik, *Org. Biomol. Chem.*, **2001**, *9*, 1324.
[189] Compound **105s** is commercially available from Apollo Scientific.
[190] C. A. Coburn, M. Maletic, R. Soll, C. Li, Y. Luo, Z. Qi (Merck Sharp & Dohme Corp.), WO2014000178 (A1), **2014**.
[191] C. A. Coburn, M. Maletic, R. Soll, C. Li, Y. Luo, Z. Qi (Merck Sharp & Dohme Corp.), WO2014000178 (A1), **2014**.
[192] R. Heng, G. Koch, A. Schlapbach, M. P. Seiler (Novartis), WO2008034600 (A1), **2008**.
[193] Compound **105v** is commercially available from Fluorochem.
[194] Compound **105x** is commercially available from Fluorochem.
[195] H. Ueno, T. Yamamoto, R. Takashita, R. Yokohama, T. Sugiura, S. Kageyama, A. Ando, H. Eda, A. Eviryanti, T. Miyazawa, A. Kirihara, I. Tanabe, T. Nakamura, M. Noguchi, M. Shuto, M. Sugiki, M. Dohi (Ajinomoto Co. Ltd.), US2015051395 (A1), **2015**.
[196] J. E. Taylor, M. D. Jones, J. M. J. Williams, S. D. Bull, *J. Org. Chem.* **2012**, *77*, 2808.
[197] D. Li, N. Gao, N. Zhu, Y. Lin, Y. Li, M. Chen, X. You, Y. Lu, K. Wan, J.-D. Jiang, W. Jiang, S. Si, *Bioorg. Med. Chem. Lett.* **2015**, *25*, 5178.
[198] H. Bothmann, R. Roncarati, I. Micco, A. Nencini, C. Ghiron (Siena Biotech S.P.A.), WO2007082731 (A1), **2007**.
[199] Compound **107a** is commercially available from AK Scientific.
[200] I. R. Siddid, A. Ibad, M. A. Waseem, G. Watal, *Tetrahedron Lett.* **2016**, *57*, 5.
[201] V. Ladziata, P. W. Glunz, Z. Hu, Y. Wang (Squibb Bristol Myers Co.) W02016010950 (A1), **2016**.
[202] S. Gowtisankar, H. Neumann, M. Beller, *Chem. Eur. J.*, **2012**, *18*, 2498.
[203] Compound **108b** is commercially available from TCI.
[204] D. Wang, D. Kuang, F. Zhang, C. Yang, X. Zhu, *Adv. Synth. Catal.*, **2015**, *357*, 714.
[205] R. Cano, D. J. Ramon, M. Yus, *J. Org. Chem.* **2011**, *76*, 5547.
[206] Y. Yuan, A. A. Zaidi, O. Elbegdorj, L. C. K. Aschenbach, G. Li, D. L. Stevens, K. L. Scoggins, W. L. Dewey, D. E. Selley, Y. Zhang, *J. Med. Chem.*, **2013**, *56*, 9156.
[207] Z.-L. Shen, K. K. K. Goh, C. H. A. Wong, Y.-S. Yang, Y.-C. Lai, H.-L. Cheong, T.-P. Loh, *Chem. Commun.*, **2011**, *47*, 4778.
[208] K. Masashiro, H. N. William, T. Naoki, B. Hiroshi, K. Yasuhiko, I. Nobuhiro (Takeda Pharmaceutical Company Limited), WO2005105802 (A1), **2005**.
[209] A. V. Gulevskaya, B. U. W. Maes, C. Meyers, W. A. Herrebout, B. J. van der Veken, *Eur. J. Org. Chem.*, **2006**, *23*, 5305.
[210] G. J. Kemperman, WO2008125577 (A1), **2008**.
[211] G. P. Migliaccio, S. R. Byrn, *J. Pharm. Sci.*, 1981**,** *70*, 284.
[212] I. L. Martin, J. P. Miranda, N. G. Oliviera, A. S. Fernandes, S. Goncalves, A. M. M. Atunes, *Molecules*, **2013**, *18*, 5251.
[213] A. Leyv-Perez, J. R. Cabrero-Antonino, A. Corma, *Tetrahedron* **2010**, *66*, 8203.